U.S. DEPARTMENT
OF COMMERCE
National Bureau
of Standards

Wind and Seismic Effects

NBSIR 88-3703

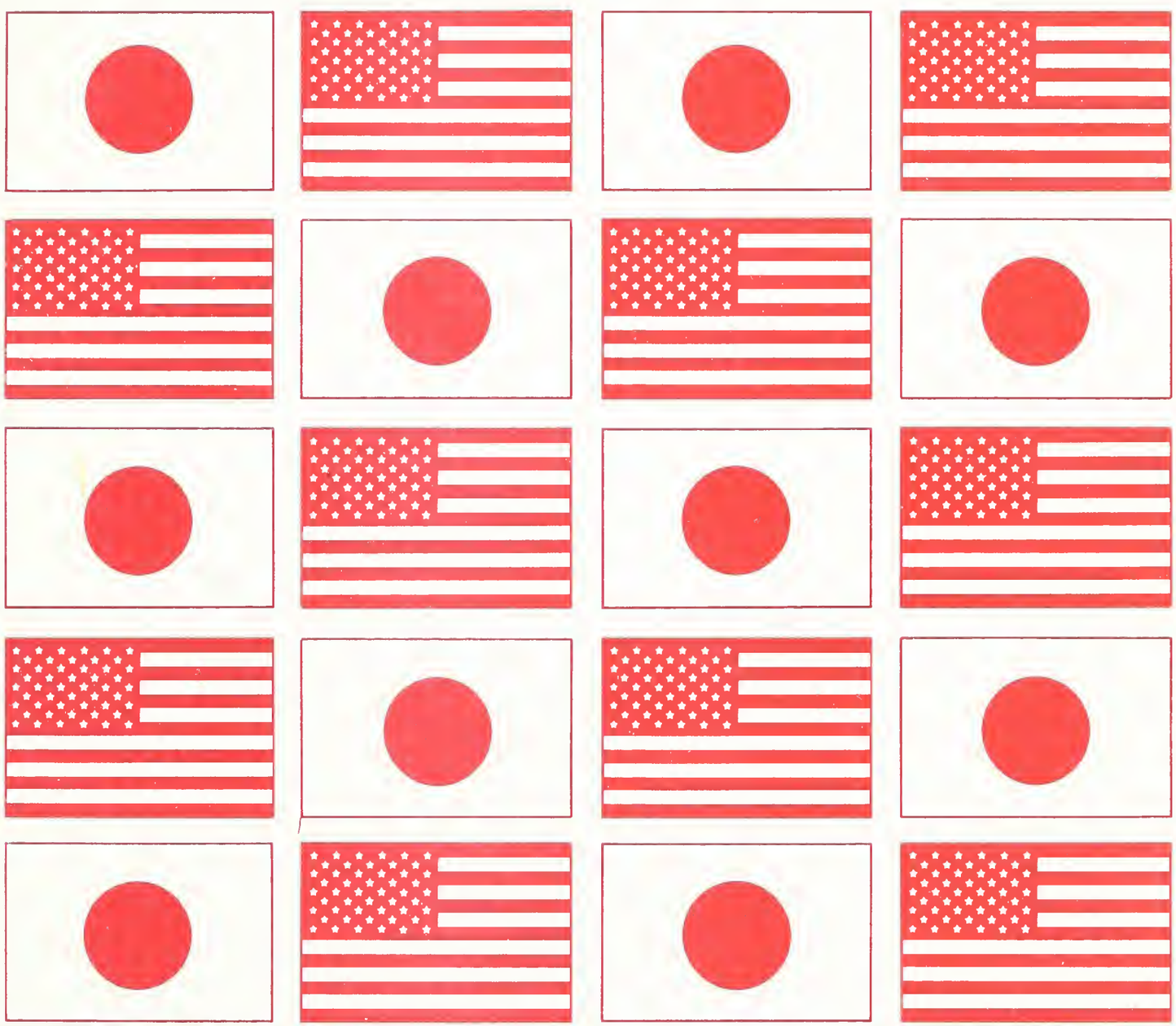

Proceedings of the Nineteenth Joint Meeting

The National Bureau of Standards[1] was established by an act of Congress on March 3, 1901. The Bureau's overall goal is to strengthen and advance the nation's science and technology and facilitate their effective application for public benefit. To this end, the Bureau conducts research and provides: (1) a basis for the nation's physical measurement system, (2) scientific and technological services for industry and government, (3) a technical basis for equity in trade, and (4) technical services to promote public safety. The Bureau's technical work is performed by the National Measurement Laboratory, the National Engineering Laboratory, the Institute for Computer Sciences and Technology, and the Institute for Materials Science and Engineering.

The National Measurement Laboratory

Provides the national system of physical and chemical measurement; coordinates the system with measurement systems of other nations and furnishes essential services leading to accurate and uniform physical and chemical measurement throughout the Nation's scientific community, industry, and commerce; provides advisory and research services to other Government agencies; conducts physical and chemical research; develops, produces, and distributes Standard Reference Materials; and provides calibration services. The Laboratory consists of the following centers:

- Basic Standards[2]
- Radiation Research
- Chemical Physics
- Analytical Chemistry

The National Engineering Laboratory

Provides technology and technical services to the public and private sectors to address national needs and to solve national problems; conducts research in engineering and applied science in support of these efforts; builds and maintains competence in the necessary disciplines required to carry out this research and technical service; develops engineering data and measurement capabilities; provides engineering measurement traceability services; develops test methods and proposes engineering standards and code changes; develops and proposes new engineering practices; and develops and improves mechanisms to transfer results of its research to the ultimate user. The Laboratory consists of the following centers:

- Applied Mathematics
- Electronics and Electrical Engineering[2]
- Manufacturing Engineering
- Building Technology
- Fire Research
- Chemical Engineering[2]

The Institute for Computer Sciences and Technology

Conducts research and provides scientific and technical services to aid Federal agencies in the selection, acquisition, application, and use of computer technology to improve effectiveness and economy in Government operations in accordance with Public Law 89-306 (40 U.S.C. 759), relevant Executive Orders, and other directives; carries out this mission by managing the Federal Information Processing Standards Program, developing Federal ADP standards guidelines, and managing Federal participation in ADP voluntary standardization activities; provides scientific and technological advisory services and assistance to Federal agencies; and provides the technical foundation for computer-related policies of the Federal Government. The Institute consists of the following centers:

- Programming Science and Technology
- Computer Systems Engineering

The Institute for Materials Science and Engineering

Conducts research and provides measurements, data, standards, reference materials, quantitative understanding and other technical information fundamental to the processing, structure, properties and performance of materials; addresses the scientific basis for new advanced materials technologies; plans research around cross-country scientific themes such as nondestructive evaluation and phase diagram development; oversees Bureau-wide technical programs in nuclear reactor radiation research and nondestructive evaluation; and broadly disseminates generic technical information resulting from its programs. The Institute consists of the following Divisions:

- Ceramics
- Fracture and Deformation [3]
- Polymers
- Metallurgy
- Reactor Radiation

[1]Headquarters and Laboratories at Gaithersburg, MD, unless otherwise noted; mailing address Gaithersburg, MD 20899.
[2]Some divisions within the center are located at Boulder, CO 80303.
[3]Located at Boulder, CO, with some elements at Gaithersburg, MD.

Wind and Seismic Effects

PROCEEDINGS OF
THE 19TH JOINT
MEETING OF
THE U.S.-JAPAN
COOPERATIVE PROGRAM
IN NATURAL RESOURCES
PANEL ON WIND AND
SEISMIC EFFECTS

Issued January 1988

Noel J. Raufaste,
EDITOR

Center for Building Technology
National Engineering Laboratory
National Bureau of Standards
Gaithersburg, MD 20899

U.S. DEPARTMENT OF COMMERCE,
C. William Verity, Secretary

National Bureau of Standards,
Ernest Ambler, Director

PREFACE

The U.S.-Japan Cooperative Program in Natural Resources (UJNR) was established in 1964 for the exchange of technical information and experience mutually beneficial to the economics and welfare of both countries. The Panel on Wind and Seismic Effects held its first joint meeting in 1969 in Tokyo, Japan. The joint meeting has been held annually ever since, alternating in Japan and the United States. The Panel is composed of 15 U.S. and 6 Japanese agencies, co-chaired by the National Bureau of Standards and the Public Works Research Institute. Results from this Panel's efforts have impacted building and structure code changes in both countries.

The Nineteenth Joint Meeting was held at the Public Works Research Institute, Tsukuba, Japan, May 12-15, 1987. The Panel featured five themes; 30 technical papers were presented out of the 38 authored manuscripts. Ten Panel task committees promote joint cooperation; they held their meetings during this period.

These proceedings include the program of the Nineteenth Joint Meeting, the Panel resolutions, all technical papers, and the task committee reports.

Partial support to maintain the US Panel was provided by the National Science Foundation, Department of State, Bureau of Reclamation, Department of Navy, Department of Housing and Urban Development, Federal Emergency Management Administration, Nuclear Regulatory Commission, US Geological Survey, and the National Bureau of Standards.

Noel J. Raufaste, Secretary
US Side, Panel on Wind and Seismic Effects

ABSTRACT

The Nineteenth Joint Meeting of the U.S.-Japan Panel on Wind and Seismic Effects was held at the Public Works Research Institute, Tsukuba, Japan, from May 12 - 15, 1987. This publication, the proceedings of the Joint Meeting, includes the program, list of members, Panel resolutions, Panel charter, task committee reports, and technical papers.

Papers were presented to the Panel under five themes. These were:

Theme I - WIND ENGINEERING
Theme II - EARTHQUAKE ENGINEERING
Theme III - STORM SURGE AND TSUNAMI
Theme IV - U.S.-JAPAN COOPERATIVE RESEARCH PROGRAM
Theme V - RESULTS OF RECENT TASK COMMITTEE WORKSHOPS

Subjects covered in the papers presented include:

(1) characteristics of strong winds;
(2) wind loads on structures and design criteria;
(3) earthquake ground motions;
(4) soil liquefaction studies and methods to improve liquefaction resistance;
(5) seismic loads on structures and design criteria;
(6) stress analyses of pipelines during earthquakes;
(7) full-scale seismic experiments;
(8) earthquake hazard reduction program;
(9) use of the microcomputer for earthquake studies;
(10) quantitative evaluation of damage caused by winds and earthquakes;
(11) tsunami research projects;
(12) coordinated masonry building research;
(13) bridge design to resist natural hazards.

KEYWORDS: Accelerograph; bridges; codes; concrete; design criteria; disaster; earthquakes; earthquake hazards; earthworks; geotechnical engineering; ground failures; liquefaction; masonry; pipeline; repair and retrofit; seismicity; standards; storm surge; structural engineering; tsunami; and wind loads.

CONTENTS

CONTENTS

CONTENTS

CONTENTS

PROGRAM FOR 19th JOINT UJNR MEETING

Opening Session

Tuesday - May 12, 1987(10:30 - 12:00)

Conference Hall(8th Floor), Public Works Research Institute

Call to order by Dr. Toshio Iwasaki, Secretary-General, Japan Panel, Director of Planning and Research Administration Department, Public Works Research Institute

Remarks by Mr. Toshio Hirose, Engineer General, Ministry of Construction

Remarks by Dr. W. McPherson, Science Officer, Office of Science and Technology, Embassy of the United States of America

Remarks by Mr. Masayasu Miyabayashi, Director, International Affairs Division, Science and Technology Promotion Bureau, Science and Technology Agency

Remarks by Mr. Shunichiro Kamijo, Chairman, Japan Panel, Director-General, Public Works Research Institute, Ministry of Construction

Remarks by Dr. R. N. Wright, Chairman, U.S. Panel, Director, Center for Building Technology, NEL, National Bureau of Standards, Department of Commerce

Introduction of Japan Panel Members by Japanese Chairman and U.S. Panel Members by U.S. Chairman

Election of Conference Chairman

Adoption of Agenda

Memorial Addresses on the late Dr. T. Okubo by Dr. H. S. Lew and Dr. N. Narita

Adjourn

Commemorating Planting

Group Photograph

Session Program of the 19th Joint Meeting

Tuesday-May 12

Opening Session 10:30-12:00

Lunch 12:00-13:00

*Speaker

International Conference Room

Technical Session 13:00-17:00

Session 1 (Theme II EARTHQUAKE ENGINEERING)

Chairman:S. Kamijo

13:00-13:20 The United States Geological Survey Accelerograph Network in the U.S. -- Operations, Record Processing and Research
A. G. Brady*

13:20-13:40 Estimation on Source Time Function based on Strong Motions and Its Application for Engineering
Y. Kitagawa*, T. Inoue, T. Murota

13:40-14:00 Strong-Motion Instrumentation Program Corps of Engineers
F. K. Chang, R. F. Ballard, A. G. Franklin*

14:00-14:20 Discussion

Session 2 (Theme II EARTHQUAKE ENGINEERING)

Chairman:S. Kamijo

14:20-14:40 Dynamic Behavior of Rock-fill Dam
K. Ohtani*, K. Baba, T. Nakai

14:40-15:00 Comparisons of Dynamic Shear Strength Between Fine Sands and Gravels
N. Matsumoto*, N. Yasuda, M. Okubo, S. Arakawa

15:00-15:20 Discussion

15:20-15:40 Break

Session 3 (Theme II EARTHQUAKE ENGINEERING)

Chairman:S. Kamijo

15:40-16:00 Preliminary Study on Shear Design for RC Piers
H. Shinohara, M. Okahara*, S. Nakatani, K. Taguchi, A. Funakoshi

16:00-16:20 Some Recent Studies on Lifeline Earthquake Engineering in the United States: Experimental and Field Study
T. O'Rourke, J. Isenberg, (L. R. L. Wang*)

16:20-16:40 Some Recent Studies on Lifeline Earthquake Engineering in the United States: Analysis and Design
M. Shinozuka, L. R. L. Wang*

16:40-17:00 Discussion

Reception 18:00-

Wednesday-May 13

Technical Session 9:00-12:00
Session 4 (Theme II EARTHQUAKE ENGINEERING)
Chairman:R. N. Wright

9:00- 9:20 A Review of Base Isolation for Upgrading Earthquake Performance or Building Structures
N. R. Vaidya, R. J. Smith*

9:20- 9:40 Consideration of Earthquakes in Highway Earthworks
Y. Koga*, A. Shimazu, E. Taniguchi

9:40-10:00 Damage, Strengthening, and Retrofit of Bridges
J. H. Gates*

10:00-10:20 Large Scale Model Tests and Analysis of Gravel Drains
S. Iai*, K. Koizumi, S. Noda, H. Tsuchida

10:20-10:40 Discussion

10:40-11:00 Break

Session 5 (Theme IV U.S.-JAPAN COOPERATIVE RESEARCH PROGRAM)
Chairman:R. N. Wright

11:00-11:20 Effect of Number of Loading Cycles and Loading Velocity of Reinforced Concrete Bridge Piers
T. Iwasaki, K. Kawashima*, K. Hasegawa, T. Koyama, T. Yoshida

11:20-11:40 Study of In Situ Testing for Evaluation of Liquefaction Resistance and Occurrence
J. A. Farrar, (R. Ledzian*)

11:40-12:00 Discussion

Lunch 12:00-13:00

Technical Session 13:00-14:00
Session 6 (Theme IV U.S.-JAPAN COOPERATIVE RESEARCH PROGRAM)
Chairman:R. N. Wright

13:00-13:20 U.S.-Japan Coordinated Earthquake Research Program on Masonry Buildings -- Seismic Behavior of Three-Story Full Scale Brick Planar Frame under Cyclic Lateral Loading --
S. Okamoto, Y. Yamazaki*, T. Kaminosono, M. Teshigawara, H. Hiraishi

13:20-13:40 U.S. Coordinated Progam for Masonry Building Research 1986/87
J. L. Noland, (H. S. Lew*)

13:40-14:00 Discussion

14:00-14:10 Break

Task Committee Meetings 14:10-17:00

B:Large-Scale Testing Programs

E:Natural Hazard Assessment and Mitigation through Land Use Programs

H:Soil Behavior and Stability during Earthquakes

I:Storm Surge and Tsunamis

J:Wind and Earthquake Engineering for Transportation Systems

Reception 18:00-

Thursday-May 14

Technical Session 9:00-12:00

Session 7 (Theme I WIND ENGINEERING)

Chairman:S. Kamijo

9:00- 9:20 Mean Wind Force Measurements on the Deer Isle-Sedgwick Suspension Bridge
H. R. Bosch, (C. F. Galambos*)

9:20- 9:40 Field Experiments for Wind Pressure
K. C. Mehta, (C. F. Galambos*)

9:40-10:00 Aerodynamic Chracteristics of Continuous Box Girder Bridges Relevant to Their Vibrations in Wind
N. Narita, K. Yokoyama*, S. Sato, Y. Nakagami

10:00-10:20 On Interpreting Model and Prototype Responses of Suspended-Span Bridges to Wind
R. H. Scanlan, (K. Yokoyama*)

10:20-10:40 Discussion

10:40-11:00 Break

Session 8 (Theme II EARTHQUAKE ENGINEERING)

Chairman:R. N. Wright

11:00-11:20 Experimental Study on Degree of Fixation at Pile Head Joint and Failure Strength of Prestressed High Strength Concrete Piles
Y. Sugimura*, T. Hirade

11:20-11:40 Schemes for Seismic Upgrading of a Major Hospital
J. V. Tyrrell*

11:40-12:00 Discussion

Lunch 12:00-13:00

Session 9(Reports of Workshops) 13:00-14:20

13:00-13:30 Task Committee (C)
H. S. Lew*

13:30-14:00 Task Committee (J)
H. Sinohara*

14:00-14:20 Discussion

14:20-14:30 Break

Task Committee Meetings 14:30-17:00

A:Strong-Motion Instrumentation Arrays and Data

C:Repair and Retrofit of Existing Structures

D:Evaluation of Performance of Structures

F:Disaster Prevention Methods for Lifeline Systems

G:Wind Characteristics and Structural Response

Friday-May 15

Technical Session 9:00-12:00

Session 10 (Theme III STORM SURGE AND TSUNAMI)

Chairman:R. N. Wright

9:00- 9:20 Experimental Investigation on the Damage of Offshore Seawall due to the 1983 Nihonkai-chubu Earthquake Tsunami
K. Tanimoto*, H. Tsuruya

9:20- 9:40 A Summary of the Tsunami History in the United States
H. Meyers*, P. A. Lockridge, J. F. Lander

9:40-10:00 An Estimation of Tsunami Generated by Submarine Landslide
S. Iwasaki*, H. Takahashi

10:00-10:20 Discussion

10:20-10:40 Break

Session 11 (Theme III STORM SURGE AND TSUNAMI)

Chairman:R. N. Wright

10:40-11:00 A Computer Program for Producing Tsunami Travel Time Chart
M. Okada*, M. Ichikawa

11:00-11:20 Numerical Simulation and Experiments on Tsunami run-up
T. Uda*, A. Omata, Y. Yokoyama

11:20-11:40 Discussion

11:40-12:00 Break

Lunch 12:00-13:00

Reports of Task Committees 13:00-15:00

Chairman:S. Kamijo

A:Strong-Motion Instrumentation Arrays and Data
B:Large-Scale Testing Programs
C:Repair and Retrofit of Existing Structures
D:Evaluation of Performance of Structures
E:Natural Hazard Assessment and Mitigation through Land Use Programs
F:Disaster Prevention Methods for Lifeline Systems
G:Wind Characteristics and Structural Response
H:Soil Behavior and Stability during Earthquakes
I:Storm Surge and Tsunamis
J:Wind and Earthquake Engineering for Transportation Systems

15:00-15:20 Break

Adoption of Charter 15:20-15:40

Chairman:S. Kamijo

Adoption of Final Resolution 15:40-16:10

Chairman:S. Kamijo

16:10 Break

Closing Session

Friday-May 15, 1987(16:30-16:50)

International Conference Room

Opening Remarks by Dr. T. Iwasaki, Secretary-General, Japan Panel, Director, Planning and Research Administration Department, Public Works Research Institute

Remarks by Dr. R. N. Wright, Chairman, U.S. Panel, Director, Center for Buildinig Technology, NEL, National Bureau of Standards

Remarks by Mr. S. Kamijo, Chairman, Japan Panel, Director-General, Public Works Research Institute

Closure by Dr. T. Iwasaki

LIST OF MEMBERS

U.S. PANEL ON WIND AND SEISMIC EFFECTS
MEMBERSHIP LIST
1987

Dr. Richard N. Wright, Chairman
Director, Center for Building Technology
National Bureau of Standards
Gaithersburg, MD 20899
(301) 975-5901

Mr. Noel J. Raufaste, Secretariat
Structures Division
Center for Building Technology
National Bureau of Standards
Gaithersburg, MD 20899
(301) 975-5905

Dr. S.T. Algermissen
Office of Earthquake Studies
Branch of Earthquake Tactonics
USGS
Denver Federal Center
Stop 978, Box 25046
Denver, CO 80225
(303) 236-1611

Dr. Celso S. Barrientos
Supervisory Physical Scientist
NOAA/NESDIS
1825 Connecticut Ave., N.W.
Universal Bldg., Rm. 518, E/A132
Washington, DC 20009
(202)673-5400

Dr. Eddie N. Bernard
Director, Pacific Marine Environmental Laboratory
7600 San Point Way, NE
Seattle, WA 98115
(206) 526-6239 FTS 392-6800

Dr. Roger D. Borcherdt
Chief, Branch of Engineering Seismology and Geology
Office of Earthquake Studies, USGS
345 Middlefield Road
Menlo Park, CA 94025
(415) 323-8111 X2755

Dr. A. Gerald Brady
Physical Scientist
Office of Earthquake Studies
U.S. Geological Survey
345 Middlefield Road
Menlo Park, CA 94025
FTS 467-2881
(415) 323-8111 X2881

Dr. John J. Burns, Jr.
Head, Structures Section
Office of Research
U.S. Nuclear Regulatory Commission
Washington, DC 20555
(301) 443-7860

Mr. Lee Butler
Waterways Experiment Station
Office WESCV-2
P.O. Box 631
Vicksburg, MS 39108
(601) 634-2405

Dr. Charles G. Culver
Chief, Structures Division
National Bureau of Standards
Gaithersburg, MD 20899
(301) 975-6048

Dr. A.G. Franklin
Chief, Earthquake Engineering and Geophysics Division
Geotechnical Laboratory
U.S. Army Engineer Waterways Experiment Station
Vicksburg, MS 39180
(601) 634-2658

Mr. G. Robert Fuller
Chief, Standards Branch
Manufactured Housing Construction Standards Division, Room 9156
Dept. of Housing and Urban Development
Washington, DC 20410-8000
(202) 755-6920

Mr. Charles F. Galambos
Chief, Structures Division
Office of Engineering and
Highway Operations R & D
Federal Highway Administration
Department of Transportation
6300 Georgetown Pike
McLean, AV 22101
(703) 285-2087

Mr. James H. Gates
Office of Structures Design
Department of Transportation
1120 N Street
Sacramento, CA 95807
(916) 445-1439

Dr. Michael P. Gaus
Section Head of Critical
Engineering
Division of Emerging and
Critical Engineering Systems
National Science Foundation
1800 G Street, N.W.
Washington, DC 20550
(202) 357-9500

Mr. Peter E. Gurvin
A/FBO, SA-6
Department of State
Washington, DC 20520
(202) 235-3689

Dr. Walter W. Hays
Deputy for Research Application
U.S. Geological Survey
Office of Earthquake Survey
905 National Center
Reston, VA 22043
(703) 648-6711

Dr. William B. Joyner
Geophysicist
Office of Earthquake Studies
Branch of Ground Motion and
Faulting, USGS
345 Middlefield Road
Menlo Park, CA 94025
(415) 323-8111

Mr. Richard W. Kramer
Civil Engineer
Technical Review Staff, D-3210
Bureau of Reclamation
P.O. Box 25007
Denver, CO 80225
FTS 776-8539 or (303) 236-8539

Mr. Richard Krimm
Office of Natural and
Technological Hazards
Federal Emergency Management Agency
Washington, DC 20472
(202) 646-2871

Mr. Paul K. Krumpe
Office of Foreign Disaster
Assistance
Agency for International
Development
Department of State
Washington, DC 20523
(202) 647-9758

Dr. H.S. Lew
Leader, Construction Engineering
Group
Center for Building Technology
National Bureau of Standards
Gaithersburg, MD 20899
(301) 975-6061

Dr. Shih-Chi Liu
Director, Earthquake Hazards
Mitigation Section
1800 G Street, N.W., Rm. 1128
Washington, DC 20550
(202) 357-9780

Mr. Robert MacDonald
Geologic Service Branch
Code D
1630 Bureau of Reclamation
Building 67, Denver Federal Center
Denver, CO 80225
FTS 776-4195 of (303) 236-4195

Dr. Richard D. Marshall
Structural Engineering Group
Structures Division
Center for Building Technology
National Bureau of Standards
Gaithersburg, MD 20899
(301) 975-6071

Dr. Richard D. McConnell
Office of Construction
Veterans Administration
811 Vermont Avenue, NW
Washington, DC 20420
(202) 233-3103

Dr. Francis G. McLean
Chief, Division of Research and Laboratory Services, D-1500
Bureau of Reclamation
P.O. Box 25007
Denver, CO 80225
FTS 776-5981 or (303) 234-3303

Mr. John F. Meehan
Principal Structural Engineer
Research Director
Structural Safety Section
Office of the State Architect
Department of General Services
Sacramento, CA 95805
(916) 445-8730

Mr. Herbert Meyers
Chief, Earth Geophysics
NOAA
325 Broadway
Boulder, CO 80303
(303) 497-6215 or FTS 320-6215

Dr. John B. Scalzi
Program Director, Systems Engineering for Large Structures
National Science Foundation
1800 G Street, NW, Room 1130
Washington, DC 20550
(202) 357-7710

Mr. Joseph T. Schaefer
Chief, Techniques Development Unit
National Severe Storm Forecast Center
National Weather Service, NOAA
601 E. 12th Street
Room 1836
Kansas City, MO 64106
(816) 374-5672

Mr. Robert J. Smith
Department of the Army
Office of the Chief of Engineers
DAEN-ECE-D
Washington, DC 20314-1000
(202) 272-0220

Dr. Lawrence A. Soltis
Supervisory Research Engineer
Engineering Design Criteria
Forest Products Laboratory
Forest Service, Dept. of Agriculture
Madison, WI 53705
(608) 364-5910 or FTS 364-5910

Mr. Joseph Tyrrell
Director, Civil Structural Division
Naval Facilities Engineering Comman
200 Stovall Street
Alexandria, VA 22332
(703) 325-0047

Alternates

Dr. Clifford Astill
Division of Emergency and Critical Engineering
National Science Foundation
1800 G Street, NW, Room 1130
Washington, DC 20550

Mr. Michael Changery
National Climatic Center
Federal Building
Asheville, NC 28801
(704) 259-0765 or FTS 672-0765

Dr. A.J. Eggenberger
Division of Engineering and
Critical Engineering
National Science Foundation
1800 G Street, N.W.
Washington, DC 20550

Mr. Lucian G. Guthrie
Structural Engineer
Office of Chief of Engineers
HQUSACE (DAEN-ECE-D)
Washington, DC 20314-1000
(202) 272-8673

Mr. James Houston
WESCV-Z
P.O. Box 631
Waterways Experiment Station
Vicksburg, MS 39180-0631

Mr. Roger Kenneally
Structures Section
Office of Research
U.S. Nuclear Regulatory Commission
Washington, DC 20555
(301) 443-7860

Mr. Robert R. Ledzian
Senior Staff Assistant for
Research, WO-220
Bureau of Reclamation
Department of the Interior
18th at C Streets, N.W.
Washington, DC 20240
(202) 343-6703

Mr. T.K. Lew
Naval Civil Engineering Laboratory
L51
Port Huenene, CA 93043
(805) 982-5785

Ms. Janina Mirski
Chief, Structures Division
Veterans Administration
811 Vermont Avenue, N.W.
Washington, DC 20420
(202) 389-2394

Mr. Ronald J. Morony
Program Manager
Buildinng Technology Research Staff
Department of Housing and Urban
Development
Washington, DC 20410
(202) 755-0640

JAPAN PANEL ON WIND AND SEISMIC EFFECTS
MEMBERSHIP LIST
1987

Mr. Shunichiro Kamijo, Chairman
Director-General
Public Works Research Institute
Ministry of Construction
Asahi 1-banchi, Toyosato-machi, Tsukuba-gun
Ibaraki-ken 305
Tel. 0298-64-2211

Dr. Toshio Iwasaki, Secretary-General
Director
Planning and Research Administration Department
Public Works Research Institute
Ministry of Construction
Asahi 1-banchi, Toyosato-machi,
Tsukuba-gun, Ibaraki-ken 305
Tel. 0298-64-2211

Mr. Tokunosuke Fujitani
Senior Research Staff
Physical Meteorology Research Division
Meteorogical Research Institute
Meteorological Agency
1-1 Nagamine, Yatabe-machi
Tsukuba-gun, Ibaraki-ken 305
Tel. 0298-51-7111

Mr. Minoru Fujiwara
Head, Bridge Division
Structure and Bridge Department
Public Works Research Institute
Ministry of Construction
Asahi 1-banchi, Toyosato-machi, Tsukuba-gun
Ibaraki-ken 305
Tel. 0298-64-2211

Dr. Sadaiku Hattori
Special Senior Scientist
Building Research Institute
Ministry of Construction
Tatehara 1-banchi, Oh-ho-machi, Tsukuba-gun
Ibaraki-ken 305
Tel. 0298-64-2151

Dr. Masaya Hirosawa
Director
International Institute of
Seismology and Earthquake Engineering Department
Building Research Institute
Ministry of Construction
Tatehara 1-banchi, Oh-ho-machi, Tsukuba-gun
Ibaraki-ken 305
Tel. 0298-64-2151

Dr. Yuji Ishiyama
Head, Planning and Investigation Division
Research Planning and Information Department
Building Research Institute
Ministry of Construction
Tatehara 1-banchi, Oh-ho-machi, Tsukuba-gun
Ibaraki-ken 305
Tel. 0298-64-2151

Dr. Mamoru Katsumata
Head, Seismological and
Volcanology Division
Meteorological Research Institute
Meteorological Agency
1-1, Nagamine, Yatabe-machi, Tsukuba-gun
Ibaraki-ken 305
tel. 0298-51-7111

Dr. Kazuhiko Kawashima
Head, Earthquake Engineering Division
Earthquake Disaster Prevention Department
Public Works Research Institute
Ministry of Construction
Asahi 1-banchi, Toyosato-machi, Tsukuba-gun
Ibaraki-ken 305
Tel. 0298-64-2211

Mr. Yasuyuki Koga
Head, Soil Dynamics Division
Construction Method and Equipment Department
Public Works Research Institute
Ministry of Construction
Asahi 1-banchi, Toyosato-machi, Tsukuba-gun
Ibaraki-ken 305
Tel. 0298-64-2211

Mr. Kiyoshi Kurashige
Head, Typhoon Research Division
Meteorological Research Institute
Meteorological Agency
1-1, Nagamine, Yatabe-machi, Tsukuba-gun
Ibaraki-ken 305
Tel. 0298-51-7111

Dr. Norihisa Matsumoto
Head, Fill Type Dam Division
Dam Department
Public Works Research Institute
Ministry of Construction
Asahi 1-banchi, Toyosato-machi, Tsukuba-gun
Ibaraki-ken 305
Tel. 0298-64-2211

Mr. Tatsuo Murota
Director
Structural Engineering Department
Building Research Institute
Ministry of Construction
Tatehara 1-banchi, Oh-ho-machi, Tsukuba-gun
Ibaraki-ken 305
Tel. 0298-64-2151

Mr. Masatoshi Nagaoka
Head, Second Geographic Division
Geographical Survey Institute
Ministry of Construction
Kitazato 1-banchi, Yatabe-machi, Tsukuba-gun
Ibaraki-ken 305
Tel. 0298-64-1111

Dr. Nobuyuki Narita
Deputy Director-General
Public Works Research Institute
Ministry of Construction
Asahi 1-banchi, Toyosato-machi,
Tsukuba-gun, Ibaraki-ken 305
Tel. 0298-64-2211

Dr. Setsuo Noda
Chief, Earthquake Resistant Structures Laboratory
Structure Division
Port and Harbour Research Institute
Ministry of Transport
3-1-1, Nagase, Yokosuka-shi, Kanagawa-ken 239
Tel. 0468-41-5410

Mr. Keiichi Ohtani
Head, Earthquake Engineering Laboratory
Second Research Division
National Research Center for Disaster Prevention
Science and Technology Agency
3-1, Tennodai, Sakura-mura, Niihari-gun
Ibaraki-ken 305
Tel. 0298-51-1611

Mr. Michio Okahara
Head, Foundation Engineering Division
Structure and Bridge Department
Public Works Research Institute
Ministry of Construction
Asahi 1-banchi, Toyosato-machi, Tsukuba-gun
Ibaraki-ken 305
Tel. 0298-64-2211

Mr. Shin Okamoto
Director
Research Planning and Information Department
Building Research Institute
Ministry of Construction
Tatehara 1-banchi, Oh-ho-machi, Tsukuba-gun
Ibraki-ken 305
Tel. 0298-64-2151

* Dr. Yasushi Sasaki
Head, Ground Vibration Division
Earthquake Disaster Prevention Department
Public Works Research Institute
Ministry of Construction
Asahi 1-banchi, Toyosato-machi, Tsukuba-gun
Ibaraki-ken 305
Tel. 0298-64-2211

Mr. Hiroshi Shinohara
Director
Structure and Bridge Department
Public Works Research Institute
Ministry of Construction
Asahi 1-banchi, Toyosato-machi, Tsukuba-gun
Ibaraki-ken 305
Tel. 0298-64-2211

Dr. Yoshihiro Sugimura
Head, Foundation Engineering Division
Structure Engineering Department
Building Research Institute
Ministry of Construction
Tatehara 1-banchi, Oh-ho-machi, Tsukuba-gun
Ibaraki-ken 305
Tel. 0298-64-2151

Dr. Hiroshi Takahashi
Director-General
National Research Center for Disaster Prevention
Science and Technology Agency
3-1, Tennodai, Sakura-mura, Niihari-gun
Ibaraki-ken 305
Tel. 0298-51-1611

Dr. Katsutoshi Tanimoto
Chief, Breakwaters Laboratory
Hydraulic Engineering Division
Port and Harbour Research Institute
Ministry of Transport
3-1-1, Nagase, Yokosuka-shi, Kanagawa-ken 239
Tel. 0468-41-5410

Dr. Hajime Tsuchida
Deputy Director-General
Port and Harbour Research Institute
Ministry of Transport
3-1-1, Nagase, Yokosuka-shi, Kanagawa-ken 239
Tel. 0468-41-5410

Dr. Takaaki Uda
Head, Coastal Engineering Division
River Department
Public Works Research Institute
Ministry of Construction
Asahi 1-banchi, Toyosato-machi, Tsukuba-gun
Ibaraki-ken 305
Tel. 0298-64-2211

Dr. Hiroyuki Yamanouchi
Head, Structural Dynamics Division
Structural Engineering Department
Building Research Institute
Ministry of Construction
Tatehara 1-banchi, Oh-ho-machi, Tsukuba-gun
Ibaraki-ken 305
Tel. 0298-64-2151

* Mr. Koichi Yokoyama
Head, Structure Division
Structure and Bridge Department
Public Works Research Institute
Ministry of Construction
Asahi 1-banchi, Toyosato-machi, Tsukuba-gun
Ibaraki-ken 305
Tel. 0298-64-2211

* Secretary

HONORARY MEMBERS

Dr. Masami Fukuoka
Professor, Science University of Tokyo

Dr. Shiro Ibukiyama
Vice President, Ohbayashi Road Construction Co., Ltd.

Mr. Mitsuru Nagao
President
New Structural Engineering Ltd.

Mr. Kenji Kawakami
Managing Director
Kubota Inc.

Dr. Kaoru Ichihara
President
Central Consultant Inc.

Dr. Kazuto Nakazawa
President
Civil-Works Research Laboratory

Mr. Yoshijiro Sakagami
Director, Vice-President
Tokukura Construction Co., Ltd.

Dr. Ryuichi Iida
Director
Japan Dam Engineering Center

Dr. Masateru Tominaga
Counselor
Public Works Research Center

LIST OF TASK COMMITTEE MEMBERS

Task Committee	U.S. Side	Japanese Side
A. Strong-Motion Instrumentation Arrays and Data	* A.G. Brady W.B. Joyner A.F. Franklin F.G. McLean H. Meyers	* Hajime Tsuchida Sadaiku Hattori Masaji Ichikawa Yuji Ishiyama Keiichi Ohtani Yasushi Sasaki Hiroyuki Yamanouchi
B. Large-Scale Testing Programs	* H.S. Lew J.B. Scalzi R.J. Smith	* Keiichi Ohtani Yasuyuki Koga Setsuo Noda Shin Okamoto Koichi Yokoyama Hiroyuki Yamanouchi
C. Repair and Retrofit of Existing Structures	* J.B. Scalzi C.F. Galambos P.E. Gurvin H.S. Lew R.D. McConnell R.J. Morony	* Masaya Hirosawa Toshio Iwasaki Shin Okamoto Hiroshi Shinohara
D. Evaluation of Performance of Structures	* G.R. Fuller R.D. McConnell J.F. Meehan J.B. Scalzi R.J. Smith	* Shin Okamoto Yuji Ishiyama Michio Okahara Hiroshi Shinohara Hiroyuki Yamanouchi
E. Natural Hazard Assessment and Mitigation Through Land Use Programs	* S.T. Algermissen A.G. Brady G.R. Fuller R.D. Marshall	* Kazuhiko Kawashima Sadaiku Hattori Toshio Iwasaki Masatoshi Nagaoka Yoshihiro Sugimura
F. Disaster Prevention Methods for Lifeline Systems	* S.C. Liu J.B. Scalzi	* Toshio Iwasaki Kazuhiko Kawashima Tatsuo Murota Setsuo Noda Keiichi Ohtani Yasushi Sasaki
G. Wind Characteristics and Structural Response	* R.D. Marshall C.S. Barrientos C.F. Galambos M.P. Gaus	* Keizo Masamura Tatsuo Hanafusa Tatsuo Murota Nobuyuki Narita Koichi Yokoyama
H. Soil Behavior and Stability During Earthquakes	* A.G. Franklin F.G. McLean R.J. Smith	* Yasushi Sasaki Yasuyuki Koga Norihisa Matsumoto Michio Okahara Yoshihiro Sugimura Hajime Tsuchida

I. Storm Surge and Tsunamis	*C.S. Barrientos	*Takaaki Uda
	E.N. Bernard	Masaji Ichikawa
	L. Butler	Keizo Masamura
	M.P. Gaus	Hiroshi Takahashi
	H. Meyers	Katsutoshi Tanimoto
J. Wind and Earthquake Engineering for Transportation Systems	*C.F. Galambos	*Hiroshi Shinohara
	C.G. Culver	Minoru Fujiwara
	A.G. Franklin	Toshio Iwasaki
	J.B. Scalzi	Kazuhiko Kawashima
		Nobuyuki Narita
		Michio Okahara
		Yasushi Sasaki
		Koichi Yokoyama

*Chairman

LIST OF U.S. PARTICIPANTS

Dr. Richard N. Wright, Chairman
Director, Center for Building Technology
National Bureau of Standards
Gaithersburg, MD 20899

Mr. Noel J. Raufaste, Secretariat
Structures Division
Center for Building Technology
National Bureau of Standards
Gaithersburg, MD 20899

Dr. A. Gerald Brady
Physical Scientist
Office of Earthquake Studies
U.S. Geological Survey
345 Middlefield Road
Menlo Park, CA 94025

Dr. A. G. Franklin
Chief, Earthquake Engineering & Geophysics Division
CEWES-GH Geotechnical Laboratory
U.S. Army Engineer Waterways Experiment Station
Vicksburg, MS 39180

Mr. Charles F. Galambos
Chief, Structures Division
Office of Engineering & Highway Operations R & D
Federal Highway Administration
Department of Transportation
6300 Georgetown Pike
McLean, VA 22101

Mr. James H. Gates
Office of Structures Design
Department of Transportation
1120 N Street
Sacramento, CA 95807

Mr. Robert R. Ledzian
Senior Staff Assistant for Research, WO-220
Bureau of Reclamation
Department of the Interior
18 & C Streets, N.W.
Washington, DC 20240

Dr. H.S. Lew
Leader, Construction Engineering Group
Center for Building Technology
National Bureau of Standards
Gaithersburg, MD 20899

Mr. Herbert Meyers
Chief, Earth Geophysics
National Oceanic and Atmospheric Administration
325 Broadway
Boulder, CO 80303

Prof. R. H. Scanlan
Department of Civil Engineering
Johns Hopkins University
Baltimore, MD 21218

Mr. Robert J. Smith
Department of the Army
Office of the Chief of Engineers
HQUSACE (CEEC-ED)
Washington, DC 20314-1000

Mr. Joseph Tyrrell
Deputy Chief Engineer
Naval Facilities Engineering Command
200 Stovall Street
Alexandria, VA 22332

Prof. L.R.L. Wang
Department of Civil Engineering
Old Dominion University
Norfolk, VA 23508

FORMAL RESOLUTIONS

RESOLUTIONS OF THE NINETEENTH JOINT MEETING
U.S.-JAPAN PANEL ON WIND AND SEISMIC EFFECTS (UJNR)

Public Works Research Institute
Tsukuba Science City, Japan

May 12-15, 1987

The following resolutions are hereby adopted:

1. The Nineteenth Joint Panel Meeting provided an opportunity to exchange valuable technical information which was beneficial to both countries. In view of the importance of cooperative programs on the subject of wind and seismic effects, the continuation of Joint Panel Meetings is considered essential.

2. The following activities have been carried out since the Eighteenth Joint Meeting:

   a. Guest researchers from both countries performed joint research that advanced the state of wind and earthquake engineering.

   b. Technical documents, strong motion records including those from the Mexico Earthquake of 1985, research reports, earthquake damage records and workshop proceedings were exchanged.

   c. Workshops and Planning Conferences were held:

      (a) Planning Conference on Disaster Prevention Methods for Lifeline Systems
      --- Task Committee(F), August, 1986, Charleston, South Carolina

      (b) Third Workshop on Repair and Retrofit
      --- Task Committee(C), May, 1987, Tsukuba

      (c) Planning Conference on Evaluation of Seismic Resistance of Existing Buildings
      --- Task Committee(D), May, 1987, Tsukuba

      (d) Third Bridge Workshop
      --- Task Committee(J), May, 1987, Tsukuba

      The findings promoted improved knowledge for wind and seismic disaster mitigation.

   d. The Coordinated Research Program on Large-Scale Testing of Masonry Structures is currently underway. Research is coordinated by the Joint Technical Coordinating Committee on Masonry Research (JTCCMAR).

3. At the Eighteenth Joint Meeting, a charter was drafted for this Panel on Wind and Seismic Effects as suggested at the 11th UJNR Plenary Conference, December 1985, Tokyo. The charter was approved at the Nineteenth Joint Meeting.

4. The Panel recognizes the importance of the following items:

   a. Translate and disseminate the Japanese MOC "Manual of Repair Methods for Structures Damaged by Earthquakes" to U.S. engineering profession.

   b. Exchange information on application of base isolation and active damping systems.

   c. Collect strong motion data on performance of buried pipeline systems.

   d. Obtain experimental verification of the effectiveness of retrofitting and strengthening methods for structures and soils.

5. The Panel endorses the following workshops proposed by the Task Committees:

   a. Workshop on Strong-Motion Earthquake Observation, Task Committee (A), to be held in the San Francisco area, August 1987.

   b. Fifth Workshop on Repair and Retrofit, Task Committee (C), to be held in conjunction with the 20th UJNR Joint Meeting.

   c. Workshop on Wind Characteristics and Structural Response, Task Committee (G), to be held in the coming year.

   d. Workshiop on Remedial Measure against Liquefaction, Task Committee (H), to be held in conjunction with the 20th UNJR Joint Meeting.

   e. Second Workshop on Storm Surge and Tsunami, Task Committee (I), to be held in conjunction with the 20th UJNR Joint Meeting.

   f. Fourth Bridge Workshop, Task Committee (J), to be held in conjunction with the 20th UJNR Joint Meeting.

   Scheduling for workshops shall be performed by the chairmen of each Task Committee with concurrence of the Joint Panel chairmen. Results of each workshop shall be presented at subsequent Joint Panel Meeting.

6. The Panel recognizes the importance of continued exchange of personnel, technical information, research and recorded data, and methods to mitigate losses from earthquakes and strong winds. The Panel also recognizes the importance of using available large-scale testing facilities in both countries. Thus, these activities should be strengthened and expanded. To facilitate such exchanges, the Panel will continue to encourage them and provide official Panel sponsorship.

7. The Panel recommends that for future Joint Panel Meetings, priority attention be given to the following items:

   a. Task Committee Chairmen should give attention to identifying joint research needs, priorities, development plans, and recommendations for future research programs. Each Task Committee's Chairmen are encouraged to examine their Committee's objectives and to modify the objectives, as appropriate, to meet the need for improved technology.

   b. Task Committee Chairmen should exchange summaries of their Task Committees activities, current and proposed, to the other Task Committees for improved understanding of Panel activities. Task Committee Chairmen should furnish copies of Task Committee correspondence to the Secretariates of both sides.

8. Recognizing that wind and seismic disaster mitigation plans benefit disaster-prone countries worldwide, that many developing countries suffer from natural disasters such as extreme winds, storm surges, earthquakes and tsunamis, and that both the U.S. and Japan have been involved in international technical cooperative programs, the Panel will continue efforts to develop and coordinate projects which provide aid and training to developing countries and maintain the exchange of technical information.

9. The Twentieth Joint Meeting of the UJNR Panel on Wind and Seismic Effects will be held at the Washington D.C. (USA), May 1988. Specific dates, program, and itinerary will be proposed by the U.S. Panel with concurrence by the Japan Panel.

CHARTER OF THE UJNR PANEL ON WIND AND SEISMIC EFFECTS

OBJECTIVES

1) Encourage, develop, and implement the exchange of wind and seismic technology between appropriate United States and Japanese organizations to share scientific and technological knowledge.

2) Develop strong technical links of scientific and engineering researchers between the two countries and encourage exchanges of guest researchers.

3) Conduct joint research in areas of winds and seismic technology including exchange of available research equipment and facilities in both countries. Publish findings from joint research efforts.

4) Conduct cooperative programs to improve engineering design and construction practices and other wind and earthquake hazard mitigation practices. Publish results from cooperative programs.

CURRENT TOPICS AND SUBJECT AREAS OF INTEREST

1) Strong Motion Instrumentation Arrays and Data

2) Large Scale Testing Program

3) Repair and Retrofit of Existing Structures

4) Evaluation of Performance of Structures

5) Natural Hazard Assessment and Mitigation Through Land Use Programs

6) Disaster Prevention Methods for Lifeline Systems

7) Wind Characteristics and Structural Response

8) Soil Behavior and Stability During Earthquakes

9) Storm Surge and Tsunamis

10) Wind and Earthquake Engineering for Transportation Systems

COOPERATIVE ACTIVITIES

1) Conduct annual joint panel meetings alternating locations between the United States and Japan.

2) Publish proceedings of annual meetings and of task committee events.

3) Exchange data and information between both countries.

4) Exchange guest scientists and engineers.

5) Develop cooperative research programs on mitigating the effects of wind and seismic forces on structures. Concerning these programs, exchange available research equipment and facilities in both countries, if necessary.

6) Conduct task committee meetings and workshops in areas identified in "Current Topics and Subject Areas of Interest" to facilitate exchange of technical information.

7) Establish and maintain effective communications between scientists, engineers, and administrators of the two countries.

PANEL MEMBERSHIP

1) Members of the panel are personnel of government agencies designated by the agencies.

2) Other experts may be selected, as temporary members, from appropriate disciplines representing industry, academia, and research organizations.

CHARTER MODIFICATIONS

This Charter may be revised by the concurrence of the US and the Japanese sides.

Theme I

Wind Engineering

Mean Wind Force Measurements on the Deer Isle-Sedgwick Suspension Bridge

By Harold R. Bosch[1]

ABSTRACT

This paper presents the results of a wind tunnel investigation of the Deer Isle - Sedgwick Bridge. The structure studied is a 45 year old suspension bridge located in the State of Maine on the New England coast. Static force measurements were performed on a 1/25 scale section model of this bridge by the Structures Division of the Federal Highway Administration (FHWA). All tests were conducted in the G. S. Vincent Aerodynamics Laboratory at the Turner-Fairbank Highway Research Center (TFHRC). A low-speed wind tunnel with a 6 ft by 6 ft (1.8m by 1.8m) cross section was employed to provide wind velocities up to 40 fps (12.2m/s).

KEYWORDS: Aerodynamics; Drag; Lift; Moment; Stability; Suspension bridge

1. INTRODUCTION

The wind tunnel research reported herein is only part of a larger research program being conducted jointly by FHWA and the Maine Department of Transportation, see reference 1. Work on this project is divided into 4 basic areas:

- Field measurement of wind characteristics at the bridge site and structural response to wind as well as traffic loading.
- Static and dynamic analysis of the structure at each of its various stages of development.
- Wind tunnel testing of section models representing the existing as well as proposed new shapes.
- Development and verification of remedial or rehabilitation measures.

Wind tunnel tests were conducted on a 1/25 scale section model of the Deer Isle-Sedgwick Bridge. The large scaling ratio used permits accurate reproduction of details from the existing bridge cross section. Since the structure has a shape similar to that of the original Tacoma Narrows Bridge and has exhibited significant wind induced response throughout its many years of service, several modifications to the basic bridge section were also evaluated. Section model studies were performed in both smooth flow and simulated large-scale turbulent flow conditions, with wind speeds ranging from 0 to 40 fps (0 to 12.2m/s). RMS response amplitudes were measured for the vertical and torsional degrees-of-freedom to identify regions of aerodynamic sensitivity. Flutter derivatives were computed using damping and frequency measurements obtained from free oscillations of the section model under a variety of wind conditions. Mean lift, drag, and pitching moment forces were obtained for the basic section model and the "best" alternate at several different wind speeds with wind angles of attack ranging from -10 to +10 degrees.

The experimental program outlined above is, in fact, quite comprehensive and research is still underway. The limited space available here does not permit discussion of all the work which has been completed or is underway. Therefore, this paper will concentrate on the investigation and evaluation of mean wind forces. First, a description of the Deer Isle-Sedgwick Bridge will be provided. Next, the test setup, instrumentation, and procedures will be discussed. Test results, in the form of force coefficients, will be presented for the existing shape and Alternate A. Some comparisons will be made between this bridge and the original Tacoma Narrows Bridge. Finally, conclusions will be drawn from the results presented.

2. DEER ISLE-SEDGWICK BRIDGE

The bridge is a girder-stiffened suspension bridge similar in cross section to the original Tacoma Narrows Bridge. As illustrated in figure 1, the structure consists of a main span 1080 ft (329.2m) in length, side spans of 484 ft (147.5m) each, and approach spans of 130 ft (39.6m) each, giving a total length of 2308 ft (703.5m). The structure is symmetrical with two 213 ft (64.9m) high towers. The roadway represents a vertical curve with tangents of 6.5% grade at each end to provide vertical navigational clearance of 85 ft (25.9m) at midspan. The 2-lane roadway itself consists of a 4.5 in (11.4cm) reinforced concrete slab having a width of 20 ft (6.1m). The stiffening girders are 6.5 ft (2.0m) deep and spaced 23.5 ft (7.2m) apart. Spacing of

[1]Federal Highway Administration, HNR-10 6300 Georgetown Pike, McLean, VA 22101

the suspender cables is 28 ft (8.5m). Deck and tower details are presented in figure 2.

3. TEST SETUP

The section model was suspended in front of the wind tunnel nozzle by means of six force transducers, as illustrated in figure 3. Four of these transducers were attached to the laboratory test frame above the test area to measure model lift and moment forces resulting from the wind flow. The two remaining sensors were mounted on the wind tunnel pilasters, located upstream of the test area, for measuring model drag forces. The force transducers consist of stiff cantilever beams with a full strain gage bridge located near each fixed support. This configuration was chosen for its high strain output and small displacement characteristics. Lift and moment sensors were preloaded by the weight of the model itself. To prevent longitudinal or lateral movement of the model during tests, horizontal restraining wires were attached to the end bracket crossbars at the center of gravity of the section. Preloading of the drag sensors was accomplished by attaching restraining wires between the crossbars and the laboratory wall downstream of the wind tunnel nozzle. All wires were tensioned by 2 lb (0.9kg) weights and wire lengths were long to ensure that vertical components do not influence the force measurements.

4. TEST INSTRUMENTATION

Signals from the transducers were routed through shielded cables to an array for instrumentation, as illustrated in figure 4. A set of signal conditioners and amplifiers was used to energize the strain bridge circuitry as well as amplify the incoming analog signals. In addition, the "built-in" low pass filters were used to remove any electronic noise present. Further "cleaning" of the signals was accomplished by passing them through a set of anti-alias low pass filters to eliminate extraneous fluctuations. All analog inputs were monitored through a select switch connected to a digital voltmeter.

To monitor the true wind speed of the wind tunnel, a pitot tube was extended into the flow at the nozzle. This sensor was connected via tubing to a high precision electronic manometer. The manometer provides a digital display as well as an analog output which is proportional to the differential pressure measured.

All conditioned, analog inputs were connected to a high speed, automated data acquisition system (DAS). This DAS was employed to efficiently sample, digitize, and store the experimental measurements onto digital magnetic tape for later reduction and analysis.

5. TEST PROCEDURE

Before starting any measurements, the sensitivity of the force-balance system was adjusted to provide the maximum allowable signals for the anticipated range of applied forces. The system was then calibrated by applying known weights to simulate either drag, lift, or pitching moment forces and recording the analog outputs.

Static force measurements on the section models were taken only under laminar flow conditions. The tests were conducted at wind angles of attack varying from +10 to -10 degrees. For each 1 degree position within this range, the model angle was fixed and force measurements were taken at a series of steady wind velocities ranging from 4 to 26 fps (1.2 to 7.9m/s). At each new velocity, the wind tunnel was allowed to stabilize before measurements were taken. With wind angle and velocity established, the seven data channels were sampled at a rate of 20 cps for a period of 40 to 60 seconds. The DAS was started and stopped manually and the digitized data was recorded automatically in a multiple record file on tape. Periodically, air temperature and barometer readings were taken for later use in correcting the wind tunnel velocity measurements. During testing, the force-balance system was checked for temperature drift and adjusted as necessary.

Force measurements were conducted on the existing cross section and Alternate A only, illustrated in figure 5. Raw data obtained for these two cases was reduced, analyzed, and displayed using the computer system illustrated in figure 6. For each event or tape file, a 20 second window of data was selected for analysis and the mean values calculated for each channel. These "channel means" were then used together with the system calibration factors to determine the drag, lift, and pitching moment forces per foot of section. Drag and lift forces were translated to chord and normal forces using the following:

$$X = D\cos\alpha - L\sin\alpha \qquad (1)$$

$$Z = L\cos\alpha + D\sin\alpha \qquad (2)$$

The orientation of these forces is indicated in figure 7. All forces were then reduced to dimensionless coefficients defined as:

$$C_D = 2D / (\rho V^2 B) \quad (3)$$

$$C_L = 2L / (\rho V^2 B) \quad (4)$$

$$C_M = 2M / (\rho V^2 B^2) \quad (5)$$

$$C_X = 2X / (\rho V^2 B) \quad (6)$$

$$C_Z = 2Z / (\rho V^2 B) \quad (7)$$

6. FORCE RESULTS

6.1 Existing Cross Section

Force coefficients for the existing configuration are displayed graphically in figures 8 through 12. These figures represent a consolidation of all test results obtained within the velocity range 10.8 to 18.6 fps (3.3 to 5.7m/s).

The forces measured exhibit only slight variation throughout the velocity range investigated which supports the view that violation of Reynolds number scaling here will have little effect on test results. The drag coefficients vary from 0.36 to 0.48 over a 20 degree range of wind angle. For a horizontal wind with a mean velocity of 100 mph (161km/h) and 50 mph (80km/h), the respective drag forces are calculated to be 240.4 and 60.1 lb/ft (357.8 and 89.4kg/m) with corresponding pressures of 37.0 and 9.2 psf (1772 and 440pa). In comparison, the AASHTO Bridge Specifications, reference 2, recommends that pressures of 50 and 12.5 psf (2394 and 599pa), be used at the respective velocities and a 0 degree horizontal angle. These figures represent an average drag coefficient of 1.955 for common girder shapes. This coefficient is based upon span depth (d) rather than deck width (B) as demonstrated below:

$$P = D/d = (1/2)\rho V^2 (d/d) C_D$$

$$P = (.5)(.002378)(146.667^2)(1)(1.955)$$

$$P = 50 \text{ psf} \quad (2394\text{pa}) \quad (8)$$

The "equivalent" Deer Isle drag coefficient of 1.446 is somewhat less than the conservative AASHTO value. The minimum and maximum coefficients give pressures of 33.3 and 44.4 psf (1594 and 2126pa), respectively, at the higher velocity. Although the high velocity and high wind angle yield pressures approaching the AASHTO value, it should be noted that this condition is not likely to occur. In point of fact, wind angle tends to decrease as wind speed increases. Figure 13 presents a wind angle envelope developed from data obtained at the Severn Bridge, see reference 3. Such information is frequently used as a guide in the selection of realistic design conditions.

The lift curve for this cross section develops a negative slope in the middle region, -5 to +5 degrees, and flattening of slope near the ends. These are undesireable aerodynamic characteristics since the negative slope indicates a tendency for galloping in vertical modes and flattening means stalling of the deck section at moderate angles of attack. To determine the critical velocity for onset of galloping, the following relationship may be used:

$$2m\zeta\omega + (1/2)\rho VB ((dC_L/d\alpha) + C_D) = 0$$

from figure 9, $(dC_L/d\alpha) = -2.2037/\text{rad}$
from figure 8, $C_D = 0.40$ at $\alpha = 0°$

$$2(74.5)(.015)(.213)(2\pi) + (.5)(.002378)(Vcr)(23.5)(-1.8037) = 0$$

$$Vcr = 40.47 \text{ mph} \quad (65.12\text{km/h}) \quad (9)$$

It should be noted that this computation is for the fundamental vertical mode of the structure with an assumed damping ratio of 1.5 percent. This is particularly important since the critical velocity is directly proportional to the assumed damping and frequency.

The moment curve exhibits a negative slope over nearly the entire range of angles. This characteristic points to the potential for autorotation in torsion and is thus undesireable.

6.2 Alternate A

Force coefficients for this configuration are also presented in figures 8 through 12, representing a consolidation of all test results for wind velocities in the range 5.6 to 25.8 fps (1.7 to 7.9m/s).

It should first be noted that since this model configuration is inherently more stable, it was possible to obtain static measurements over a much wider velocity range than previously. Although there is slightly more variation in the forces with velocity, the total is still considered to be relatively small and, continues to substantiate the view on Reynolds number scaling. In this case, drag coefficients vary between 0.20 and 0.48, with a value of about 0.27 at 0 degrees. This results in a pressure of 25.0 psf (1195pa), which is less than

half the AASHTO value of 50 psf (2394pa) for a velocity of 100 mph (161km/h).

Both the lift and moment curves for this alternate indicate that the aerodynamic characteristics of the bridge can be greatly enhanced by this modification. The slope of the lift curve is positive over the entire range of wind angles. In addition, the moment curve is mostly positive in slope except for large positive angles.

7. DEER ISLE AND TACOMA NARROWS COMPARISON

Since the dramatic collapse of the Tacoma Narrows Bridge in 1940, much effort has been expended to study the aerodynamic stability of long span bridge superstructures. This event is perhaps the best known and most thoroughly documented example of a bridge deck failure due to aeroelastic instability. Wind tunnel studies have been conducted by many organizations including the University of Washington, California Institute of Technology, FHWA, and others resulting in a wealth of experimental information. The cross section of the original Tacoma Narrows Bridge, with stiffening, plate girders 8 ft (2.44m) deep and spaced 39 ft (11.89m) apart, is quite similar to the Deer Isle configuration. The structural similarities together with the availability of extensive aerodynamic data make it possible to compare results obtained for each bridge.

The University of Washington conducted static force measurements on a 1/20 scale section model of the original Tacoma Narrows Bridge, see reference 4. Drag coefficients for this bridge model, designated Aa, have been used here to compute drag pressures for vertical wind angles ranging from -10 to +10 degrees. These pressures are plotted along with the Deer Isle values in figure 14. Review of the results indicates that drag forces are generally equivalent for the two bridges with only slight variation at large positive angles of attack. This small difference is likely due to the smaller depth-to-width ratio of 0.20, unvented curbs, and slightly higher deck position of the Tacoma Narrows section.

Force measurements were also performed on a second Tacoma section model, designated B, which was to the same length scale as the first but with a larger aspect ratio. This model was designed as a "universal model" on which a variety of truss, deck, and plate girder arrangements could be studied. With a depth-to-width ratio of 0.29, version "Bd" of this bridge model more closely approximates the Deer Isle proportions. Therefore, lift coefficients for Model Bd have been used to determine lift pressures for comparison with Deer Isle values. Resulting lift curves for the two bridges are presented in figure 15. Both sets of data clearly demonstrate similar undesireable aerodynamic trends, i.e., flattening of slope at moderate angles and negative slope at small angles.

A review of pitching moment data obtained for each structure also leads to a like conclusion. Both bridge section models exhibit a negative slope in the moment curve over the range of wind angles tested. As noted earlier, this is an undesireable characteristic.

8. CONCLUSIONS

Based upon the results of these force measurements, the following conclusions may be drawn:

- Force coefficients obtained for both the Existing Shape and Alternate A show little variation with change in wind velocity. This supports the view that violation of Reynolds' number criterion in this case will have minimal impact on test results.

- Drag pressures computed for the Existing Shape as well as Alternate A are somewhat less than the conservative AASHTO values. In fact, measurements on the alternate, which is a relatively streamlined cross section, indicate drag forces roughly half those recommended for design.

- The lift coefficient curves obtained for the Existing Shape exhibit a negative slope. This trend generally indicates an undesireable tendency for galloping response in the vertical mode. In addition, there is a flattening of the slope at moderate vertical wind angles which implies potential for stalling of the deck section.

- In a similar fashion, the curves for pitching moment coefficient demonstrate a consistently negative slope. Here, the slope indicates a tendency for autorotation in the torsional mode.

- Force measurements on asymmetric Alternate A, on the other hand, clearly demonstrate that aerodynamic characteristics of the basic cross section can be greatly improved

through simple modification of the shape. In this case, drag is reduced significantly, while lift and moment curves present strongly positive slopes.

- Comparison of the Deer Isle static force results with those obtained by others for the original Tacoma Narrows Bridge illustrates a number of important similarities.

9. REFERENCES

(1) Bosch, H. R., "A Wind Tunnel Study of the Deer Isle - Sedgwick Bridge (Phase I)," Report No. FHWA/RD-87/027, Federal Highway Administration, Washington, D. C., June 1984.

(2) "Standard Specifications for Highway Bridges," AASHTO, Thirteenth Edition, 1983.

(3) Roberts, Sir Gilbert, "Severn Bridge - Design and Contract Arrangements," Proceedings of the Institute of Civil Engineers, Volume 41, pp. 1-58, September 1958.

(4) Farquharson, F. B., et. al., "Aerodynamic Stability of Suspension Bridges with Special Reference to the Tacoma Narrows Bridge," The University of Washington, Engineering Experiment Station, Bulletin Number 116, Part I, June 1949.

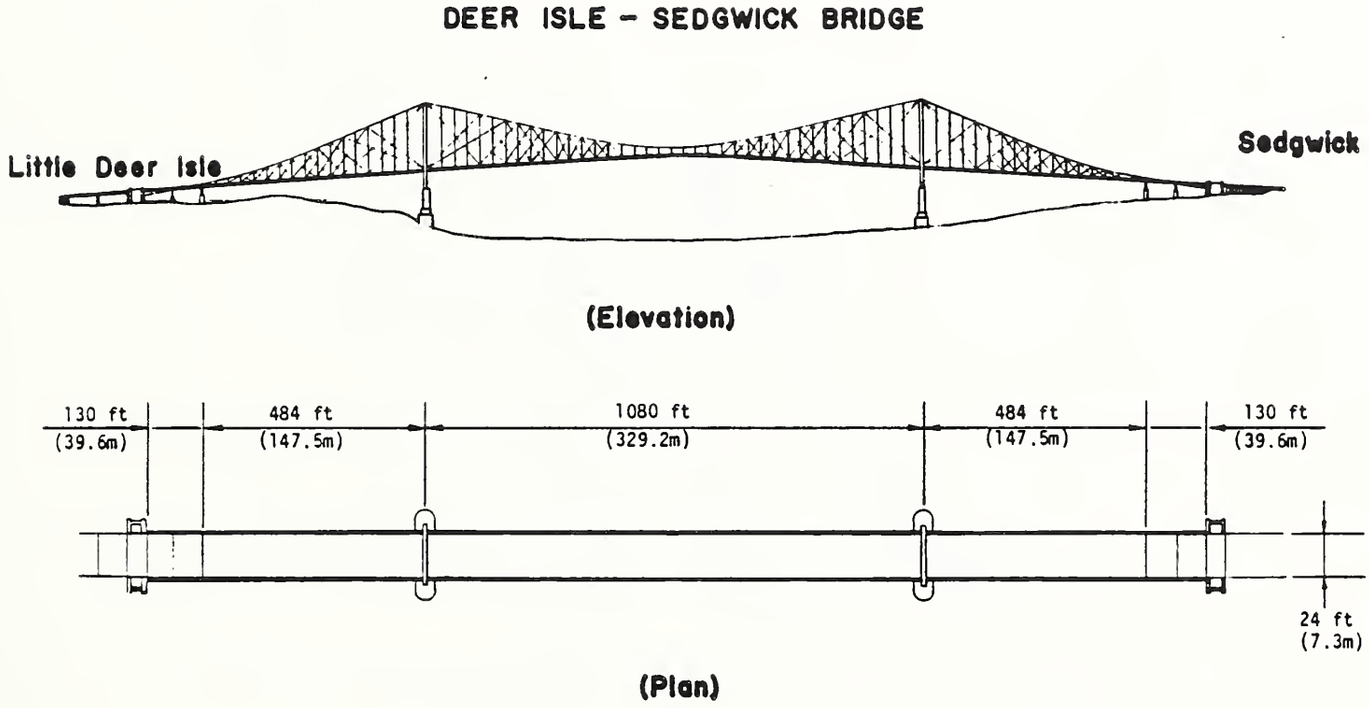

Fig. 1. Deer Isle-Sedgwick Bridge details.

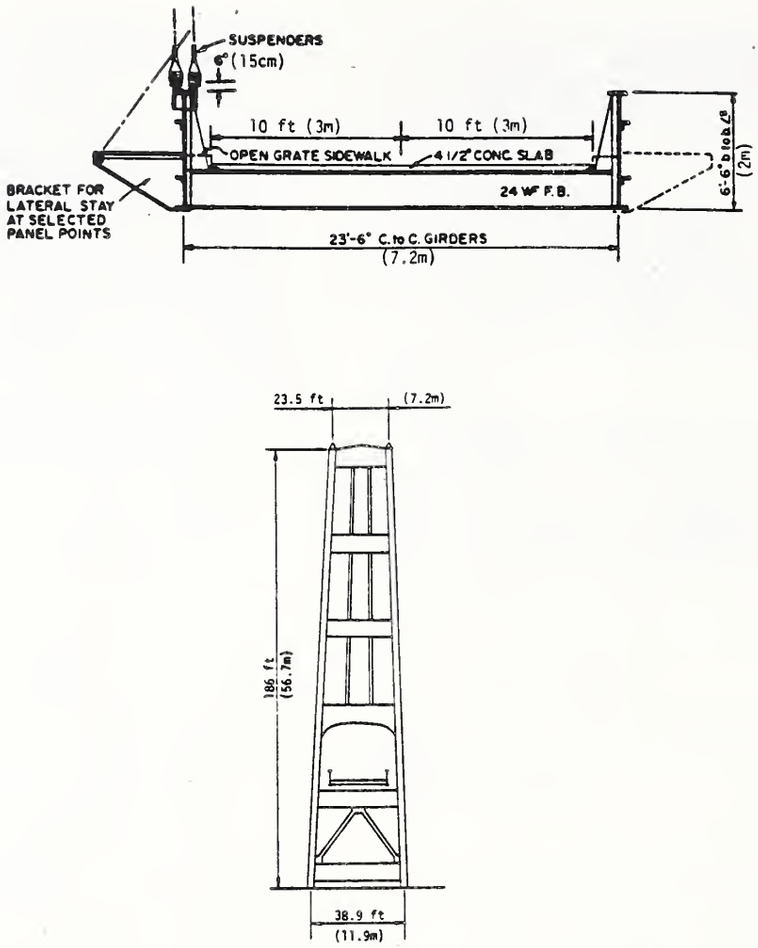

Fig. 2. Bridge deck and tower details.

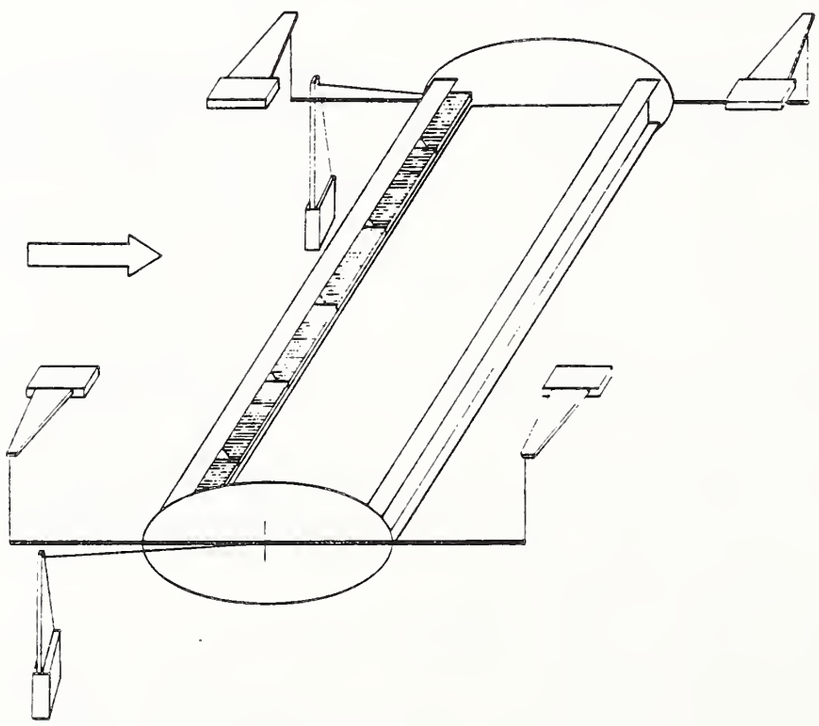

Fig. 3. Force transducer setup.

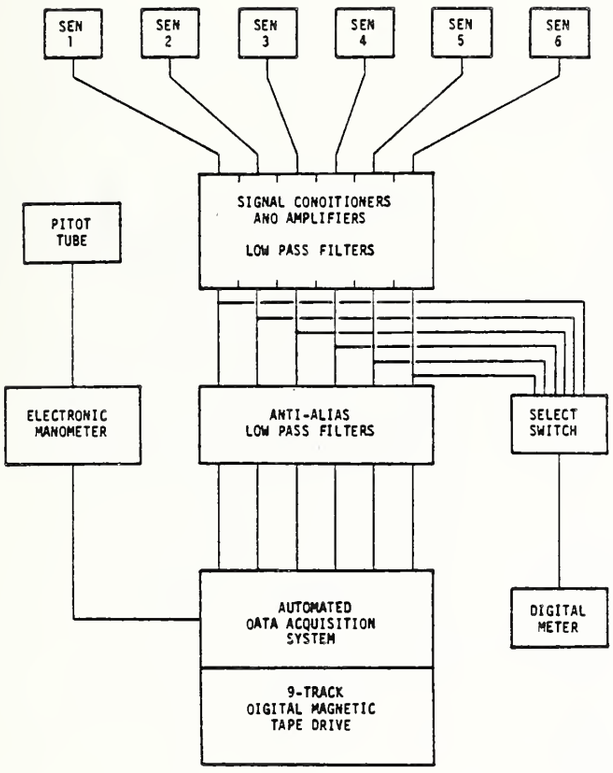

Fig. 4. Instrumentation system.

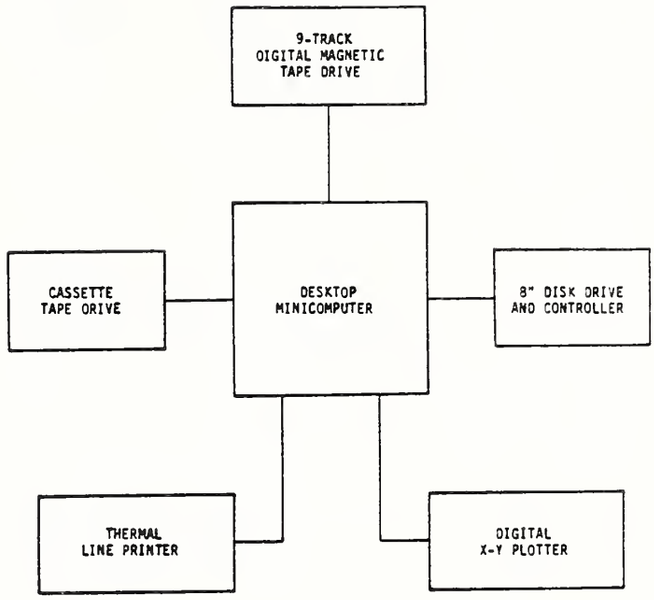

Fig. 6. Data processing system.

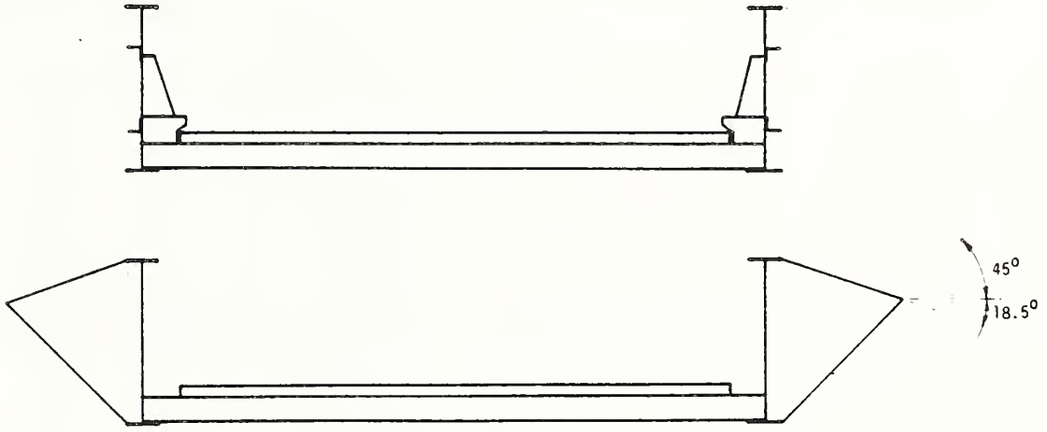

Fig. 5. Existing deck section (top) and Alternate A (bot).

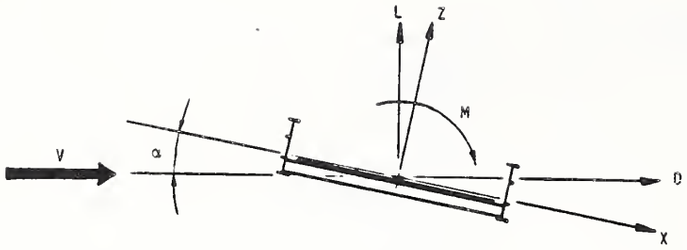

Fig. 7. Orientation of forces.

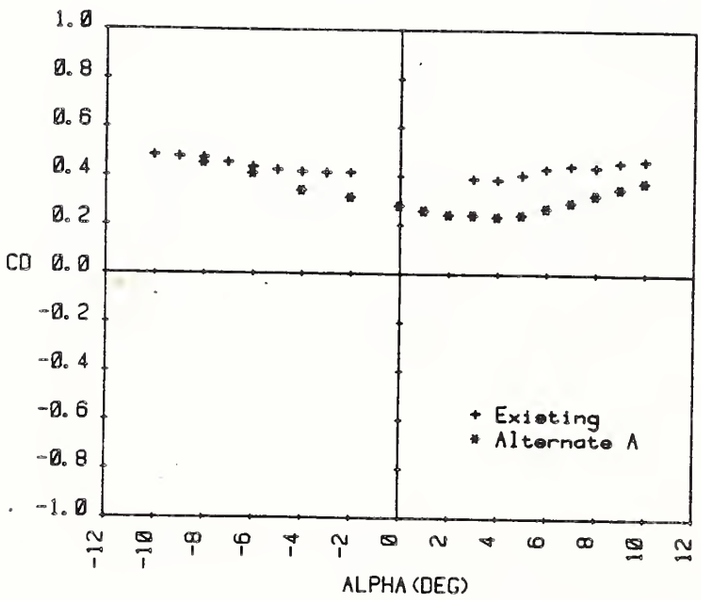

Fig. 8. Drag force coefficient.

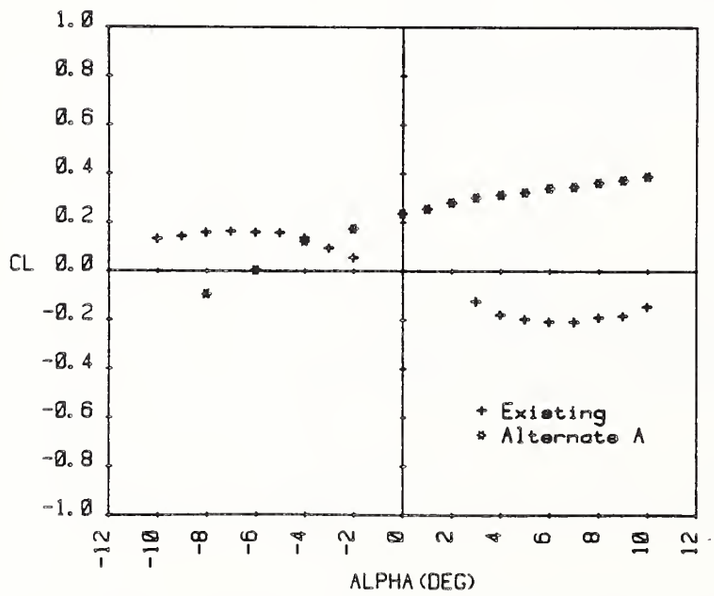

Fig. 9. Lift force coefficient.

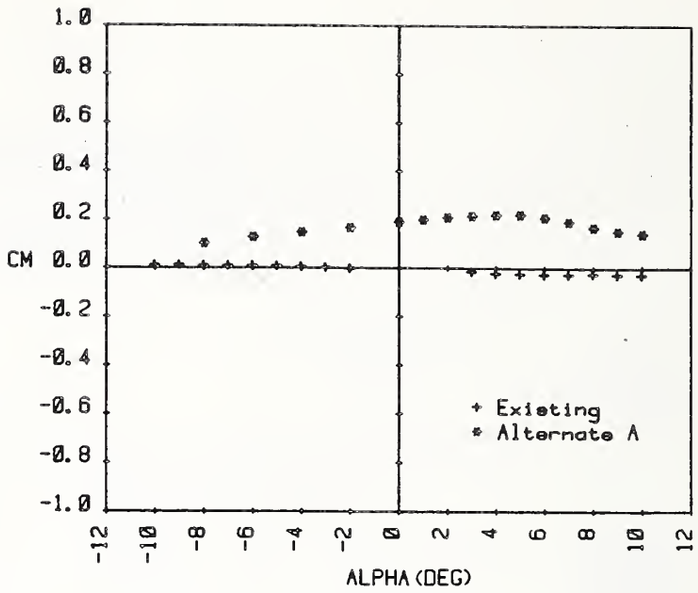

Fig. 10. Moment force coefficient.

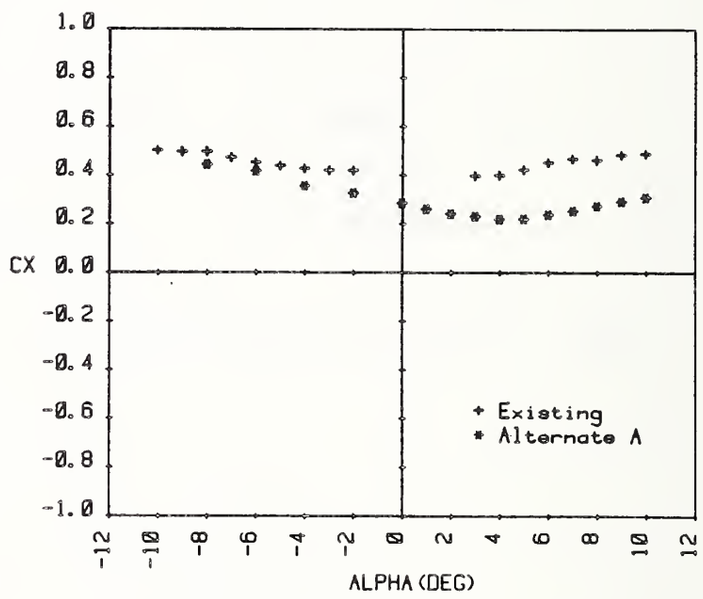

Fig. 11. Chord force coefficient.

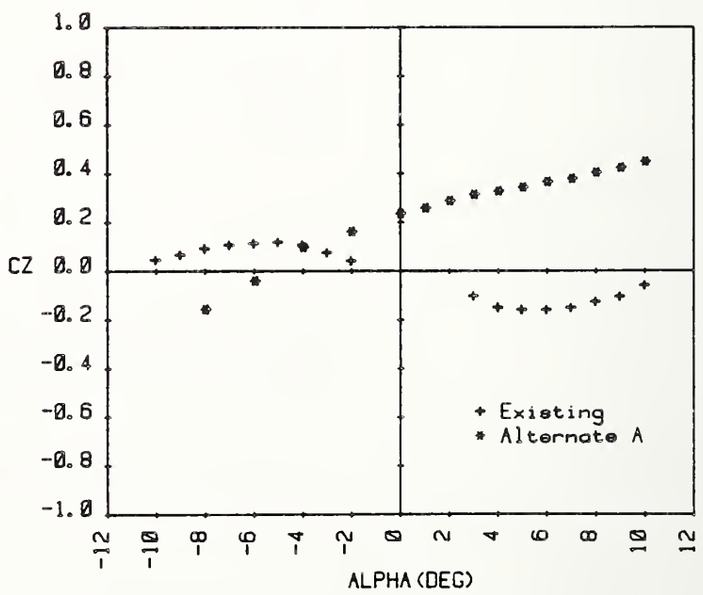

Fig. 12. Normal force coefficient.

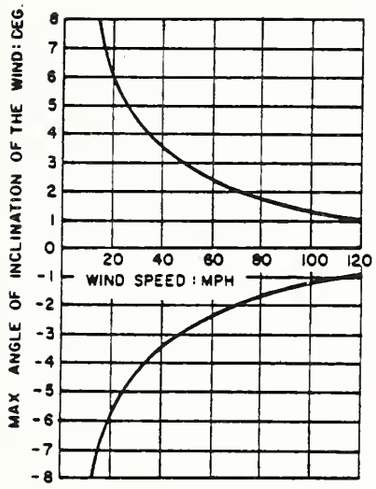

Fig. 13. Wind angle limits - Severn Bridge.

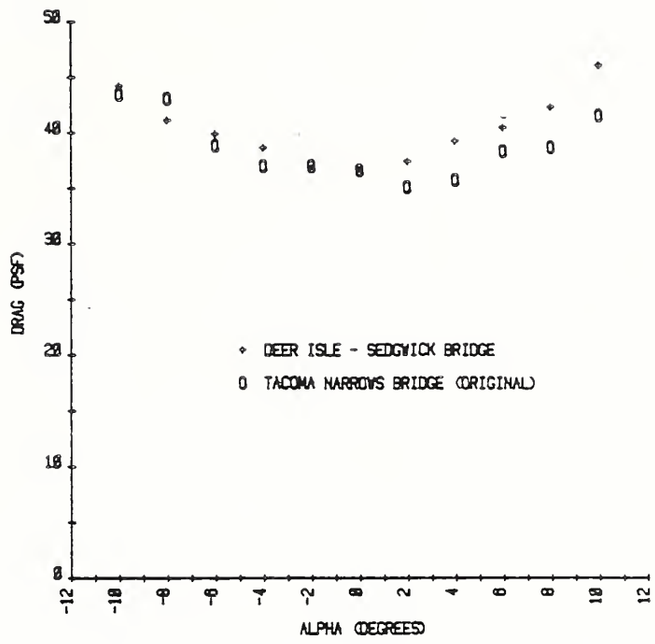

Fig. 14. Drag pressure - Deer Isle and Tacoma.

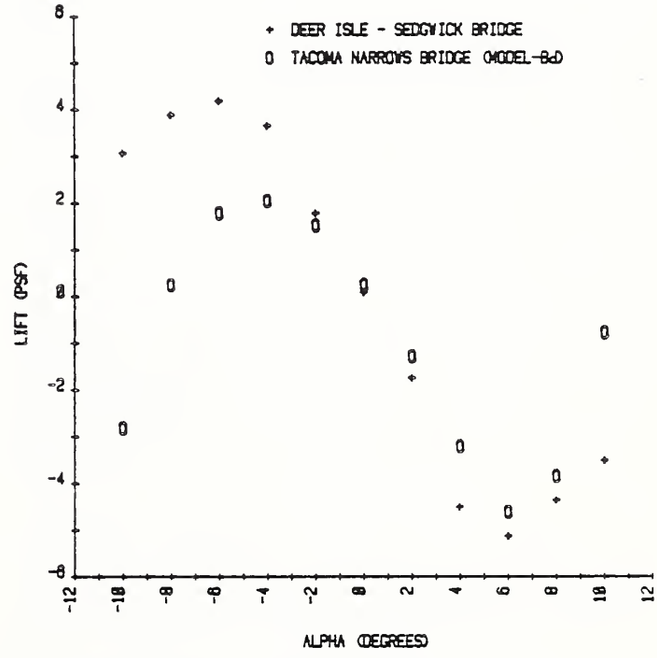

Fig. 15. Lift pressure - Deer Isle and Tacoma.

Field Experiments for Wind Pressure

BY

KISHOR C. MEHTA[1]

ABSTRACT

A project sponsored by the National Science Foundation is underway to collect wind and building surface pressure data in the field. A 30 ft x 45 ft x 12 ft building will be constructed on a concrete pad in flat, open terrain in Lubbock, Texas. The building structure is designed to support on four wheels located in corners of the building so that the building can be rotated on the concrete pad. A 100 ft tall meteorological tower will be instrumented at four levels to measure wind speed and direction. Building surface and internal pressures will be monitored using differential pressure transducers. A computer will control the data acquisition by triggering collection and termination of record. Extra precautions are taken in design of the experiment to collect reliable data in a wind regime that exceeds 20 mph. The paper describes planning of the field site, the instrumentation and the data acquisition system.

KEY WORDS: Building; Field Data; Pressures; Wind

1. INTRODUCTION

Wind-induced damage to buildings and other structures causes significant economic loss in addition to injuries and, at times, fatalities. Continuing urban sprawl increases the population of man-made structures, increasing the potential future cost resulting from wind-induced damage. It is recognized that the bulk of the damage is caused to low-rise ordinary buildings. Enhanced understanding of wind pressures on building surfaces can lead to improved construction of low-rise buildings and has potential of mitigating future damage. Pressure coefficient values that are available in the literature are, to a large extent, determined from wind tunnel tests. A number of full-scale field tests in natural wind environments have been conducted to substantiate wind tunnel test results. Additional field test data can advance understanding of wind pressures on building surfaces and can pave the way for improvement in wind tunnel technology.

A project is underway at Texas Tech University to acquire wind and building surface pressure data in the field. Specific objectives of the National Science Foundation sponsored project are: (1) to acquire a reliable data base for external wind pressures on building surfaces and internal pressures in the building, and (2) to assess the effects of wind direction fluctuations on wind pressures.

The paper describes planning of the field site, the 30 ft x 45 ft x 12 ft building, the meteorological and pressure instrumentation, and the data acquisition system. The experiment will be implemented within the next six months.

2. FIELD TEST FACILITY

The test site is in open terrain on land owned by Texas Tech University in Lubbock, Texas. An aerial view of the site is shown in Figure 1. The site is within a 10-minute drive from the main campus where the research team is headquartered. Lubbock is located on the high plains of Texas. There are no hills or valleys within a 20-mile radius of the city. The terrain is extremely flat, with ground elevation changing approximately 5 ft in a 1000 ft distance. Most of the land surrounding Lubbock is used for agricultural purposes with principal crops of cotton and sorghum. This flat and open terrain eliminates possible anomalies in wind characteristics caused by terrain.

The Lubbock area is an appropriate site for wind pressure experiments in the field because it experiences strong winds many times in a typical year. Table 1 summarizes by month the number of hours of high winds recorded at the National Weather Service station in Lubbock in 1981. The National Weather Service station is within seven miles of the proposed site. Because of the flat and open terrain in the Lubbock vicinity, the winds at the NWS station and the site are of the same intensity. In the wind data shown in Table 2, the wind speed was at least 20 mph for 864 hours, mostly in the spring and fall seasons. The early spring months hold significant promise of frequent strong winds. The open terrain of the proposed site makes it possible to conduct experiments in a relatively simple terrain exposure.

The field test facility is illustrated in Figure 2. The rectangular building with dimensions 30 ft x 45 ft x 12 ft will be placed on a concrete pad. The unique feature of the field facility is placing the building in a circular track so that it can be rotated. The internal structural system of the building is designed to be supported on four wheels, with each wheel located near each corner of the building. A circular railroad track will be embedded in the concrete pad such that the top of the track will be flush

[1]Professor of Civil Engineering, Institute for Disaster Research, Texas Tech University, Lubbock, Texas 79409.

with the concrete surface. Mechanical screw jacks will raise the building and support it on the four wheels. The building will be rotated manually to the desired direction and lowered to let it rest on the concrete. Once a directional position is obtained, the building will be anchored using four anchor bolts. The building will be constructed without architectural features so that the external surfaces will be as smooth and as simple as possible.

Pressures on the building surfaces will be measured at a number of locations using pressure taps. A pressure transducer inside the building will monitor internal pressures. Locations of pressure taps will be selected for each specific data recording event.

The 100-ft tall meteorological tower will be located approximately 150 ft from the building. The tower will be a three-legged truss tower. Wind speeds will be measured at four levels: 100 ft, 60 ft, 33 ft and 12 ft. Wind direction will be measured at two levels: 100 ft and 12 ft. In addition, temperature, barometric pressure and relative humidity will be measured to assess stability of the atmosphere during the data recording period. The speed and direction measuring instruments will be placed on 6 ft long booms. This distance will assure that interference of the tower structure on winds being recorded will be eliminated except for wind direction that comes from the direction of the tower. The wires from the instruments will be brought down to the ground along the tower and transferred to inside the building from underground.

3. INSTRUMENTATION

Two distinct types of instruments are utilized in the project, meteorological and pressure measurement instruments. Horizontal wind speed and wind direction will be measured using a Gill three-cup anemometer and microvane #12002 supplied by Ralph M. Young & Co. One set of these instruments has been acquired and is being tested in the laboratory. One of the tests in the laboratory is the assessment of accuracy with a 250-ft of cable. If the tests of accuracy, linearity and stability are found to be satisfactory, additional instruments will be purchased. No decision has been reached for instruments to measure temperature, barometric pressure and relative humidity.

Pressure taps will be instrumented with differential pressure transducers. One of the important characteristics of the differential pressure transducer needed for this project is the low range of transducer. The full range needed is ±0.5 psi; this low range will provide the desired accuracy of 0.005 psi. Two commercial companies are identified that can supply differential transducers with this low range.

Validyne Engineering Company provides diaphragm type pressure transducer with ±0.5 psi full scale range (model DP45). This is a variable reluctance diaphragm type of transducer. It is rugged with steel housing and can be used for gas or liquid. The range of the transducer can be changed by simply replacing the diaphragm; thus, the transducer is flexible. The disadvantage of this transducer is the cost. It is in the range of $400-$500 per unit.

Omega Engineering, Inc. can provide a 170 series differential pressure transducer with range of ±0.5 psi. The output for this transducer is 35mV ± 2mV. It uses a silicon sensor chip for diaphragm material. Some of its characteristic specifications are: linearity of ±1.5% of full scale output; compensated temperature range of 32 to 122°F; thermal zero effect of ±3 mV; and stability over one year of ±1.5% of full scale output. Suggested cost for this unit is $60 per transducer.

One transducer of each type is purchased. They are being tested in the laboratory for accuracy, stability and suitability for the project. In addition to the instruments mentioned above, calibration equipment for wind speed and differential pressure is being reviewed for acquisition.

A critical item in differential pressure measurement is the reference pressure. Two methods of obtaining reference pressure are being checked: (1) pitot tube with wind vane, and (2) opening below ground surface. Both methods will be implemented in the field. The one that is found to be more stable will be used for reference pressure in differential pressure measurements.

4. Data Acquisition System

Data acquisition will be controlled by a dedicated IBM XT computer which will be housed at the test facility. It is equipped with hard disk, monitor and graphic capabilities. It will be programmed to automatically trigger data collection and termination. In addition, it will be programmed to dump data directly into a Bernoulli box equipped with a 20M byte removable floppy cartridge. This system will be capable of collecting and storing 6 hours of data for 36 channels at the rate of 10Hz for each channel. The data will be collected in digital form using a Metrabyte Dash-8 analog to digital converter. It is planned to collect a 15-minute continuous record, once the collection is triggered by the computer. The computer will monitor wind for one minute and trigger a new data collection if the wind speed is above threshold value. The threshold wind speed will be 20 mph.

The data acquisition system is designed to obtain basic statistical properties such as mean and standard deviation immediately after collection of data. In addition, it will provide time-history plot to spot anomalies in any of the data collection channels. The floppy

cartridge is removable; it will be brought to the Texas Tech campus, where the data will be put on magnetic tape through the Texas Tech computer. Additional analysis of the data will be performed on the main-frame computer on the Texas Tech University campus.

5. Conclusion

This project, sponsored by the National Science Foundation, should provide reliable field data for wind pressure on surfaces of a 30 ft x 45 ft x 12 ft building. Use and analysis of data will depend on the reliability of the data. It is anticipated that wind direction fluctuation and non-stationary winds have potential of providing new knowledge in wind pressures that is not available through wind tunnel testing. Design of the experiment that permits rotation of the building should permit collection of wind pressure data for specific angle of attack. The field site and instruments should be in place within the next six months.

TABLE 1

NATIONAL WEATHER SERVICE HOURLY WIND SPEED DATA FOR LUBBOCK, TEXAS IN 1981

NUMBER OF HOURS BY WIND SPEED RANGE AND MONTH

	Wind Speed Range (mph)			
Month	20-30	30-40	40-50	Totals
January	9	0	0	9
February	27	0	0	27
March	113	25	1	139
April	135	4	5	144
May	153	11	0	164
June	128	3	0	131
July	24	0	0	24
August	2	0	0	2
September	5	0	0	5
October	59	6	0	65
November	82	10	0	92
December	56	6	0	62
TOTALS	793	65	6	864

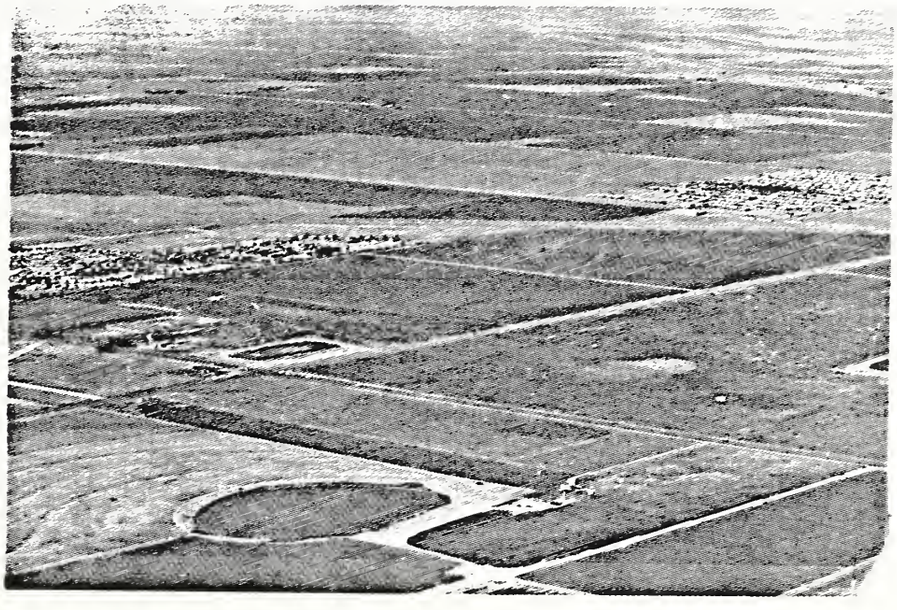

FIGURE 1. AERIAL PHOTOGRAPH OF THE FIELD SITE

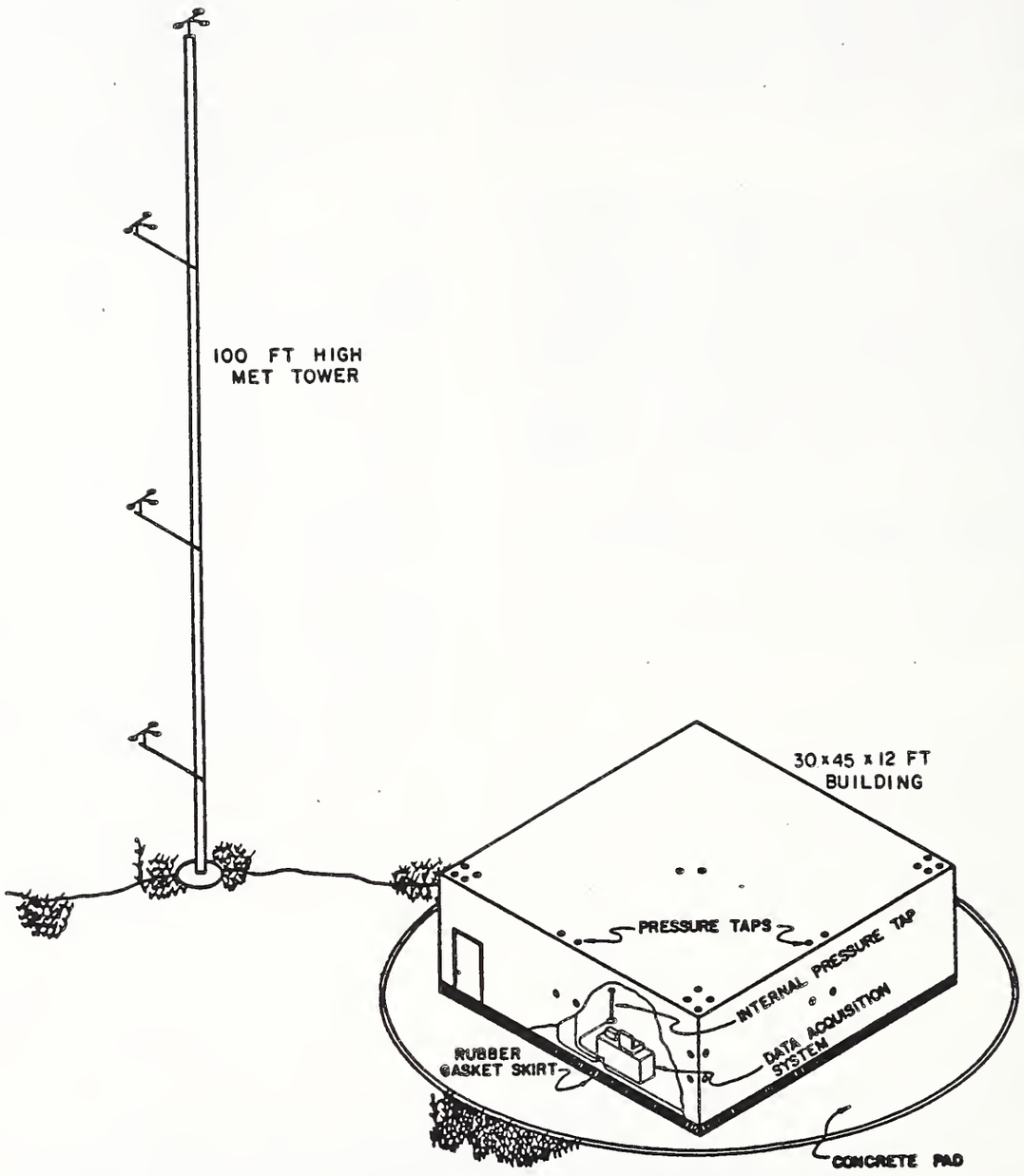

FIGURE 2. FIELD TEST FACILITY

Aerodynamic Characteristics of Continuous Box Girder Bridges Relevant to their Vibrations in Wind

N. Narita,[1] K. Yokoyama,[2] H. Sato[3] and Y. Nakagami[4]

ABSTRACT

The wind tunnel experiments concerning the wind-induced vibrations of continuous box girder bridges are presented in this paper. The vibrations were measured both in smooth and turbulent flow. Their characteristics and the effects of turbulence were investigated and explained in view-point of the aerodynamic damping and the external lift force.

KEY WORDS: Aerodynamic Damping, External Lift Force, Continuous Box Girder Bridge, Wind-Induced Vibration.

NOTATION

B : width of the bridge deck
CL : lift coefficient
D : depth of the bridge deck
f : frequency
fi : natural frequency of i th mode
fr : reduced frequency (= fB/U)
h : displacement of vertical bending vibration
HLh : frequency response function between lift force and heaving motion
Im : imaginary part
Ji : joint acceptance function for i th mode
l : bridge length
m : mass per unit length
Mi : generalized mass of i th mode $(= \int_0^{\ell} m(z)\, \Phi i^2(z)\, dz)$
qi : i th generalized coordinate for h
S : Power Spectral Density Function
U : mean wind speed
Ur : reduced wind speed (= U/(fB) = 1/fr)
u, w : fluctuating wind speed of longitudinal and vertical component
x : axis along the main flow
y : horizontal axis perpendicular to x
z : axis along the bridge axis
δ, δ i : logarithmic structural damping (of i th mode)
δ a, δ ai : logarithmic aerodynamic damping (of i th mode)
ρ : air density,
σ : reduced mass $(= m/(\rho B^2))$,
Φ i : i th mode shape

1. INTRODUCTION

Since the collapse of the Tacoma Narrows Bridge, a great deal of attention has been paid to the wind effects on bridges, resulting in a great number of studies on the subject. These studies have enabled the construction of long-span bridges to take place. However, there is much that remains uncertain concerning the mechanism of the aerodynamic forces and wind-induced vibrations of bridges. This is due to the complexity of the nature of flow around a structure, as well as the complicated configuration of the structure.

In general, structures are apt to vibrate when the product of their natural frequency and their representative length of the section is small compared to the wind speed at the site, and when their mass and damping are small as well. Therefore, research on wind effects is indispensable for construction of long-span bridges, such as suspension bridges and cable-stayed bridges, whose natural frequencies are very small. Since to increase mass is not economical as well as unfavourable due to the reduction of natural frequency, and to increase damping is not practical, the most effective way to reduce wind-induced vibrations is to select the bridge deck section so that it has favourable aerodynamic characteristics as well as sufficient rigidity. Such sections are a truss deck with small solidity ratio and a streamlined box deck which has a large ratio of deck width (B) to depth (D) (say, $B/D > 5$). These bridge deck sections have been applied to most of the long-span bridges.

However, the recent trend of increasing the span length of continuous box-girder bridges presents a new problem. The increased span length decreases the natural frequency of vertical bending mode to values as low as those of cable-stayed girder bridges. To bear the static load by its deck alone, the depth of the bridge section must be larger than that of a suspension or cable-stayed bridge, resulting in a small B/D, which is aerodynamically unfavourable. In Fig. 1 plotted are the changes of the lift slope $(dCF/d\alpha = dCL/d\alpha + CD)$ with B/D [1]. The lift slope, $dCF/d\alpha$, can be considered as a representative value for the aerodynamic admittance and the aerodynamic derivative in the low frequency range (or high wind speed range). The aerodynamic damping would be negative for a bridge deck with small B/D ratio. It may be correctly anticipated that the wind-induced vibrations of such a bridge would be violent.

In the Public Works Research Institute, Ministry of Construction, Japan, several wind tunnel experiments have been coducted concerning the wind-induced vibration of continuous box girder bridges. Among these studies, the followings are described in this paper.

1) the full model test for the proposed bridge design,
2) the sectional model test for the measurement of aero-

[1] Dr. of Eng., Deputy Director General, Public Works Research Institute, Ministry of Construction, Japan.
[2] Head, Structure Division, Structure and Bridge Department, P.W.R.I.
[3] Senior Research Engineer, Structure Division, P.W.R.I.
[4] Engineer, Local Road Division, Road Bureau, Ministry of Construction. (Formerly, Research Engineer, Structure Division, P.W.R.I.)

dynamic damping of box girder bridges, and

3) the single span elastic model test for the measurement of external lift force.

2. FULL MODEL TEST FOR THE PROPOSED BRIDGE DESIGN

The proposed bridge was a four-spanned continuous box girder bridge (150 + 190 + 190 + 150m). B/D changes from 2.2 to 4.1 along th bridge axis. The general view of the bridge is shown in Fig. 2.

The 1/120 full elastic model was constructed in the boundary layer wind tunnel at PWRI, whose test section is 6m wide, 3m high and 27m long. The stiffness of the model was simulated by two steel spines, on which correctly scaled deck segments were mounted. The reduced generalized mass for the first mode $(M1/\int_0^{\ell} \Phi_1{}^2 dz)/(\rho B^2))$ was 32. The logarithmic damping in still air was 0.02 for the first mode, and somewhat smaller for the higher modes. The natural frequencies of the model and the prototype are shown in Table 1.

The vertical vibrational displacement at the midpoint of the center span was measured both in smooth and turbulent flow. The turbulence was generated by spires. The turbulence intensities Iu and Iw were about 12% and 8%, and the integral scales Lxu and Lxw were about 0.8m and 0.3m, respectively. The measured vibrational displacements are shown in Fig. 3.

From the test results, it was found that the proposed bridge had strong possibility of limited amplitude vibrations of 1st mode, 2nd mode, 3rd mode and 5th mode in the low wind speeds, and divergent amplitude vibrations in higher wind speed in smooth flow. On the other hand, the magnitude of limited amplitude vibrations decreased remarkably in the turbulent flow, and the divergent amplitude vibration observed in smooth flow turned to be the less divergent but more random vibration in the turbulent flow.

3. MEASUREMENT OF AERODYNAMIC DAMPING

In general, wind-induced vibrations are caused either by self-excited forces (negative aerodynamic damping) or external forces (approaching turbulence, vortex excitation). When the summation of structural damping and aerodynamic damping is 0 or negative, the aerodynamic instability will take place.

The aerodynamic damping of the box girder bridges was measured in the Low-Speed Wind Tunnel-B of PWRI, whose test section is 1m wide, 2m high and 3m long. The turbulence was generated by the coarse grid whose mesh size is 0.25m and whose bar size is 0.05m. The intensities of the turbulence Iu and Iw are 6.2% and 5.0%, respectively, and the integral scales Lxu, Lxw, Lyu and Lyw are 0.09m, 0.04m, 0.04m and 0.04m, respectively. The measurement was made by the dynamic balance developed at PWRI [2]. The sectional models were shaken in heaving mode with an amplitude of B/100. The cross sections of the tested bridge deck models are shown in Fig. 4. Model A corresponds to the cross section at 1/6 point of the center span of the bridge mentioned in Chapter 2. Model B is a rectangular prism whose B/D = 2. Model C is the typical streamlined box girder for cable stayed or suspension bridges.

The self-excited lift force was transformed into mass-damping parameter as follows.

$$\sigma \delta \alpha = -\mathrm{Im}(HLh) / ((8 \pi fr^2)(0.5 \rho U^2 1)) \qquad (1)$$

In this transformation, the effect of aerodynamic stiffness was neglected, and the uniform mode shape was assumed.

$\sigma \delta \alpha$ of Model A in smooth flow is shown in Fig. 5.1. Positive aerodynamic damping appears in high reduced frequencies ($fr > 0.6$), and then negative damping appears in the lower frequencies ($0.4 < fr < 0.5$). The negative damping corresponds to the limited amplitude vibration observed in the proposed bridge design test. Then the sharp peak of positive damping appears at $fr = 0.23$. The negative damping follows this positive peak. The critical reduced frequency at which the damping turns to negative is about 0.2, which corresponds to the onset of the divergent vibration observed in the proposed bridge design test.

$\sigma \delta \alpha$ measured in the turbulent flow is also shown in the figure. The pattern is similar to that for smooth flow, however, the positive damping peak shifts to the lower reduced frequency and the peak becomes broader in the turbulent flow. It results the decrease of the critical reduced frequency or the increase of the critical reduced wind speed where the aerodynamic damping turns to negative. The aerodynamic damping for the thinner box girder models, whose B/D ratios (3.4 and 4.0) correspond to the cross section at 1/3 and 1/2 point of the center span of the continuous box girder bridge mentioned in Chapter 2, was also measured. Their characteristics were similar to those of Model A. These results suggest that the less divergent but more randam vibration observed in the turbulent flow was caused by the external lift force but not by the negative aerodynamic damping.

In Fig. 5.2. shown is $\sigma \delta \alpha$ of the rectangular prism (Model B). The characteristics of aerodynamic damping of the prism seem similar to those of the box girder bridge (Model A).

These characteristics of $\sigma \delta \alpha$ of the box girder bridge are quite different from those of the streamlined bridge deck (Model C). As is shown in Fig. 5.3, the aerodynamic damping of the steamlined bridge deck is positive both in smooth and turbulent flow. The effect of turbulence on the aerodynamic damping seems negligible for this kind of bridge deck.

4. MEASUREMENT OF THE EXTERNAL LIFT FORCES

Since the aerodynamic damping of the box girder bridge becomes positive in the turbulent flow, the random vibration can be explained by the external lift forces induced by the approaching turbulence or by the vorticies behind the deck. The external lift forces were estimated from the Power Spectral Density Function (PSDF) of the wind-induced vibration of the single span elastic model.

The experiments were made in the Low Speed Wind Tunnel-A in PWRI, whose test section is 2.5m wide, 4m high and 10m long. The three kinds of turbulence were generated by spires and floor roughness. The characteristics of the turbulent flow are shown in Table 2.

The span length, deck width and depth were 1.65m, 0.1m and 0.05m, respectively. The cross section and mass were uniform along the span. The reduced mass and logarithmic structural damping were 33 and 0.01, respectively. The elasticity of the model was provided by the simply supported alminum spine, and the fundamental mode shape of the model was half-sine. The cross sectional shape was similar to the box girder bridge in Chapter 2, except that B/D (= 2.0) is a little smaller.

The wind-induced vibrations were measured both in smooth and turbulent flow. The characteristics of the vibrations (Fig. 6) were similar to those described in Chaper2, however, the effect of turbulence intensity on the rms values of the response was not simple. While the turbulence intensity increases in the order of turbulent flow 1, 2, 3, the rms value around the reduced wind speed 6 increases in the order of 2, 3, 1. The aerodynamic damping estimated from the auto-correlation function of the vibrational displacement suggested that the relatively large responses in the turbulent flow 1 were caused by the small aerodynamic damping.

The PSDF of the reduced generalized force for the first mode was estimated as follows.

$$fSCLCL(f)\,|Ji(f)|^2/l^2 = fSqiqi(f)\,(Mi\,(2\pi fi)^2)^2 / (0.5\,\rho\,U^2\,Bl)^2 / |Hsi(f)|^2 \qquad (2)$$

$$|Hsi(f)|^2 = ((1-(f/fi)^2)^2 + ((\delta i + \delta ai)\,(f/fi)/\pi)^2)^{-1} \qquad (3)$$

The results are shown in Fig. 7. Since the PSDF of the external force has sharp peak in smooth flow, it seems that the primary cause for this force is vortex-excitation. The peak reduced frequency becomes smaller in turbulent flow than in smooth flow. It seems that the turbulence broadens and lowers the peaks of the PSDF when the intensity is not so high (smooth flow, turbulent flow 1 and 2), and that the turbulence increases the power of the external force in case of high intensity (turbulent flow 3).

5. DISCUSSION

The magnitude of the randam vibration of the box girder bridge in turbulent flow is affected by both the external lift force and the aerodynamic damping. In the experiment described in Chapter 3, the lift force on the models at rest was measured in the turbulent flow as well as the aerodynamic damping. The PSDF of the lift force is shown in Fig. 5.1 together with the aerodynamic damping. From the figure, it can be found that the large power of the lift force is associated with the large positive damping.

It may be interesting to note the close correlation between the PSDF of the external lift force and the aerodynamic damping plotted against reduced frequency for the box girder bridges. First of all, the effects of turbulence are similar, namely, turbulence decreases the peak reduced frequency of both the lift force and positive damping, and turbulence broadens their peaks. Secondly, the peak reduced frequencies are almost identical as is shown in Fig. 5.1. These correlations were also observed in case of the rectangular prism whose B/D = 2. As is shown in Fig. 5.2, the peak reduced frequency of the positive damping in smooth flow coindides with the reduced frequency of vortex shedding [3]. The frequency of vortex shedding is identical with the peak frequency of the PSDF of the external lift force. In the turbulent flow, both of these peaks shift to the lower reduced frequency, and they are almost identical as is shown in the same figure. These findings suggest that the vorticies behind the body are the primary factor for both the external lift force and the large positive damping in case of the box girder bridge deck.

The effects of turbulence on the wind-induced vibrations of the continuous box girder bridges are shown schematically in Fig. 8. The Power Spectral Density Function of the external lift force has a sharp peak in case of smooth flow. The turbulence shifts the peak to lower reduced frequency and broadens the peak. The aerodynamic damping has a sharp positive peak in case of smooth flow. The negative damping follows the positive damping at the lower reduced frequency, which corresponds to the onset of galloping. The turbulence shifts the positive damping peak to lower reduced frequency and broadens the peak, which remarkably decreases the reduced frequency for the onset of negative damping. The broad-banded lift force in the turbulent flow is associated with the broad-banded positive damping. This results the less divergent but more random vibration in the turbulent flow.

6. CONCLUDING REMARKS

The wind-induced vertical bending vibrations of continuous box girder bridges have been investigated through the wind tunnel tests. The main findings are as follows.

a. The limited amplitude vibrations in the low wind speed and the divergent amplitude vibrations (galloping) in the high wind speed were observed in case of smooth flow. They were caused by negative damping.
b. The areodynamic damping has a sharp positive peak in case of smooth flow. The negative damping follows the positive damping at the lower reduced frequency, which corresponds to the onset of galloping.
c. The turbulence shifts the positive damping peak to lower reduced frequency and broadens the peak, which remarkably decreases the reduced frequency for the onset of negative damping.
d. The broad-banded positive damping in the turbulent flow is associated with the broad-banded lift force, which changes the galloping into the less divergent but more random vibration in the turbulent flow.
e. The positive aerodynamic damping of the continuous box girder bridges was found to be closely correlated with the external lift force primarily due to the vortex-excitation.

ACKNOWLEDGEMENTS

The authors would like to thank Mr. K. Kanzaki and Mr. M. Fukuda of the Structure Division on PWRI, who prepared for the experiments and processed the experimental data.

REFERENCES

1) T. Mizota and A. Okajima: Experimental Studies of Time Mean Flows around Rectangular Prisms, Proc. of Japan Society of Civil Engineers, Vol. 312, 1981 (in Japanese).
2) T. Okubo, N. Narita and K. Yokoyama: Some Approaches for Improving Wind Stability of Cable-Stayed Girder Bridges, Proc. 4th Int. Conf. on Wind Effects on Bldgs. and Sts., Heathrow, 1975.
3) K. Washizu, A. Ohya, Y. Otsuki and K. Fujii: Aeroelastic Instability of Rectangular Cylinders in a Heaving Mode, J. of Sound and Vibration, 59(2), 1978.

Table 1. Natural frequencies

	1st mode	2nd mode	3rd mode	5th mode
mode	5.6 (Hz)	7.3	9.9	11.2
prototype	0.40	0.57	0.81	0.99

The 4th mode was horizontal bending.

Table 2 Characteristics of the turbulent flow

	Turbulent flow 1	Turbulent flow 2	Turbulent fow 3
Power Exponent	0.12	0.16	0.30
Iu	7.7%	11.4%	20.3%
Iw	5.3%	7.4%	13.0%
Lxu	0.34m	0.35m	0.36m
Lxw	0.15m	0.22m	0.13m

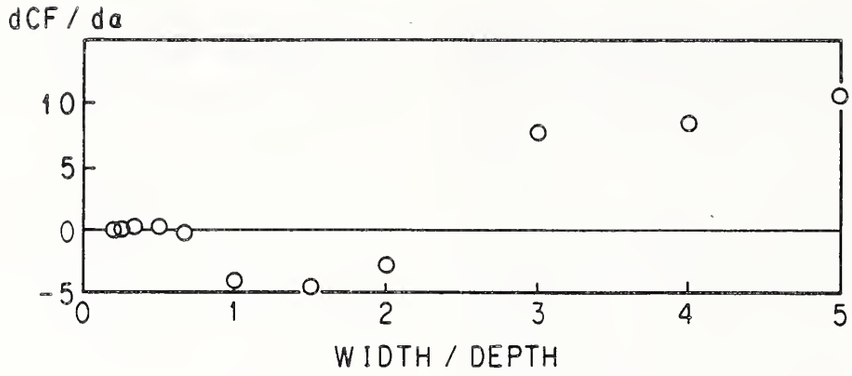

Fig. 1 dCF/dα for rectangular prisms (1)

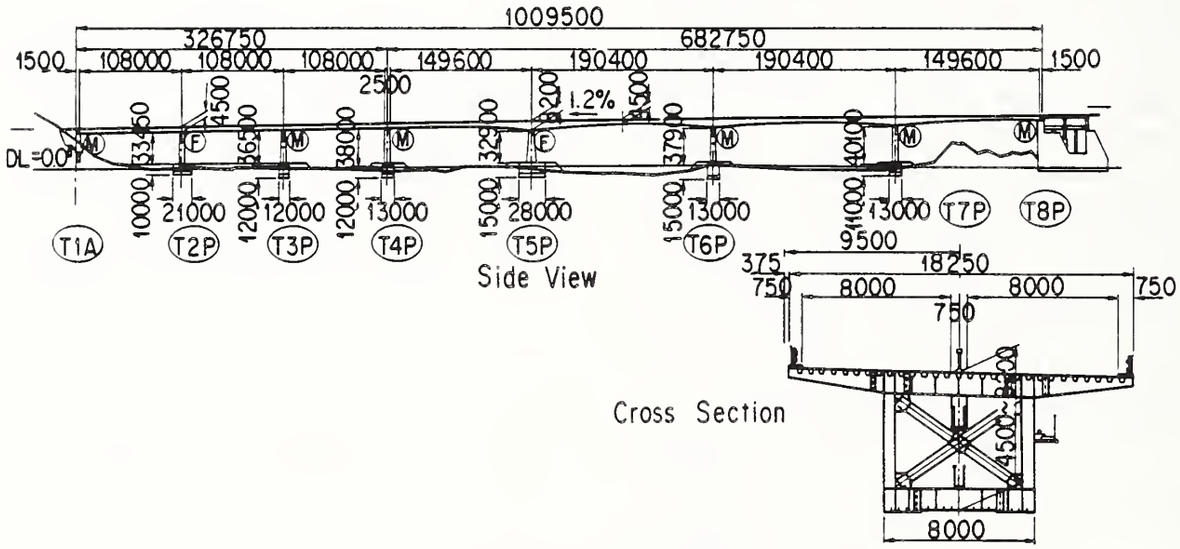

Fig. 2 General view of the proposed continuous box girder bridge

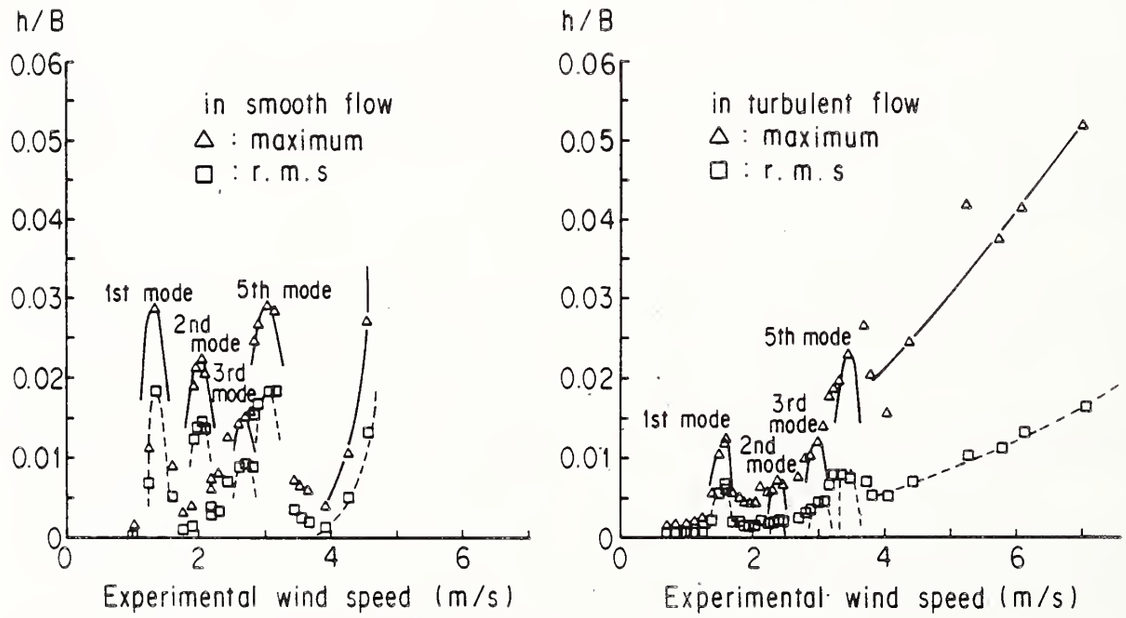

Fig. 3 The vertical displacement at mid-point of the center span

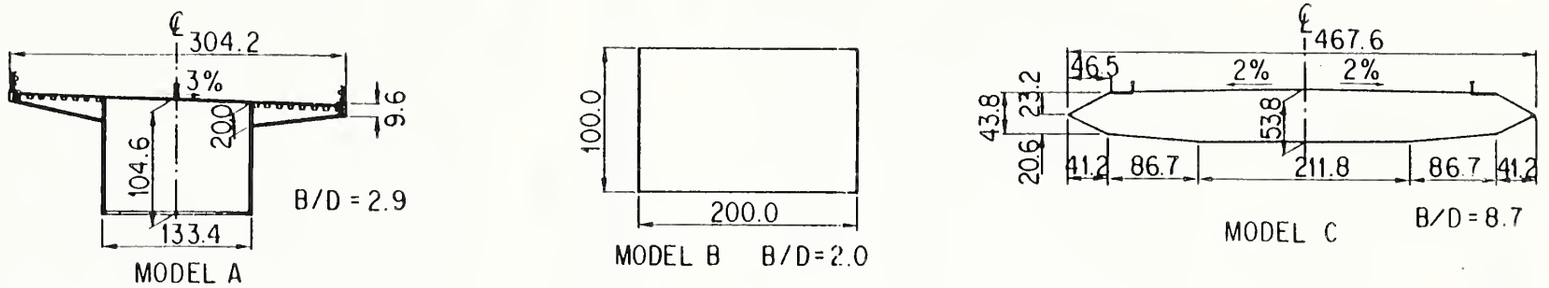

Fig. 4 Cross section of the model

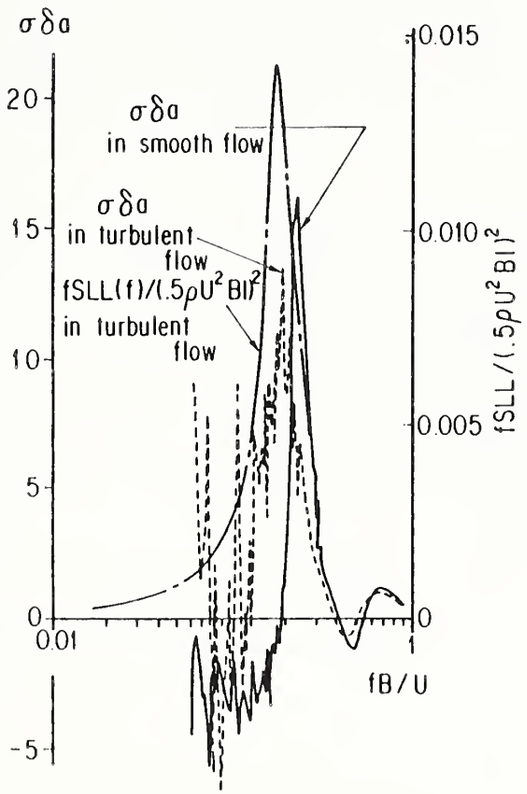

Fig. 5.1 Aerodynamic damping of Model A

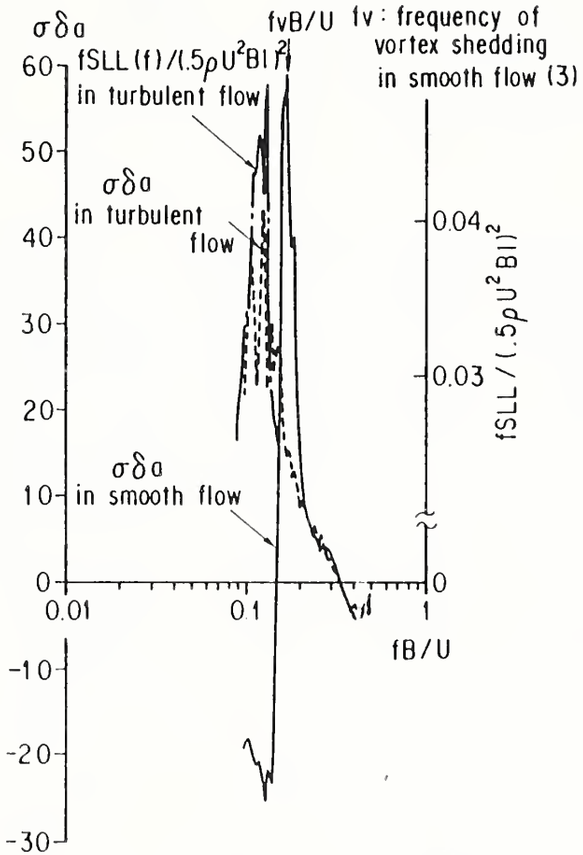

Fig. 5.2 Aerodynamic damping of Model B

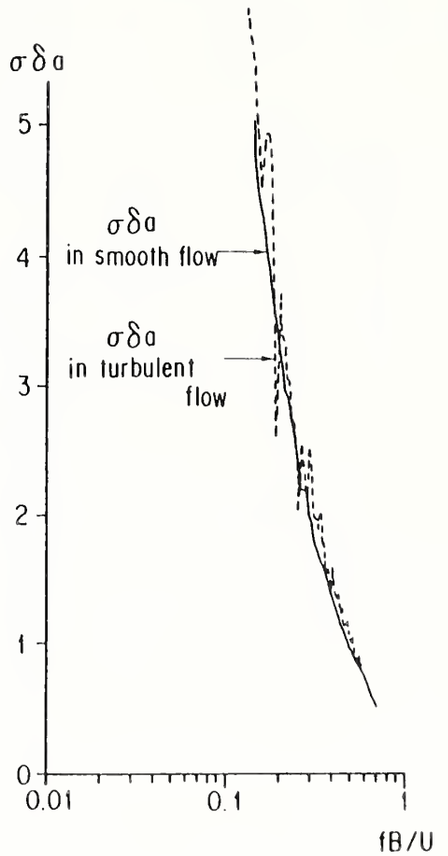

Fig. 5.3 Aerodynamic damping of Model C

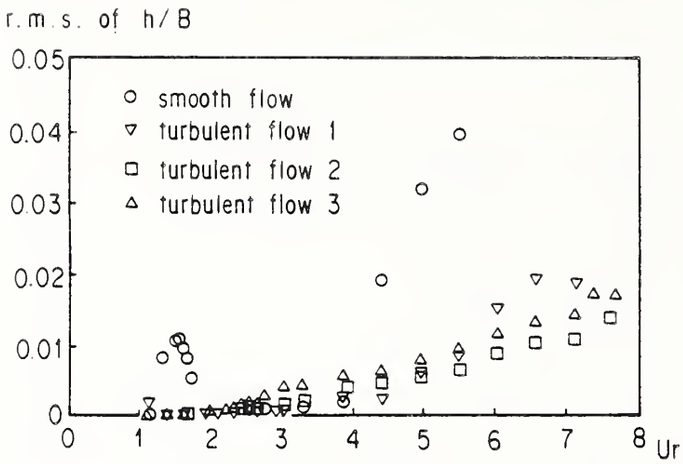

Fig. 6 r.m.s. of wind-induced vibration

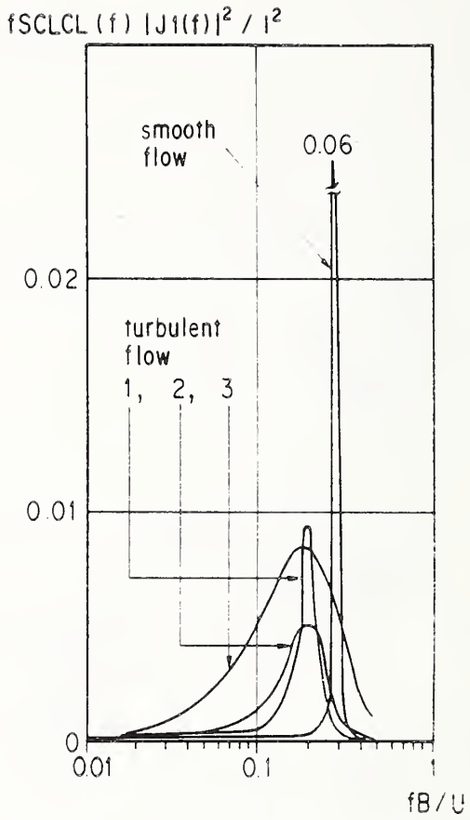

Fig. 7 Generalized external lift force

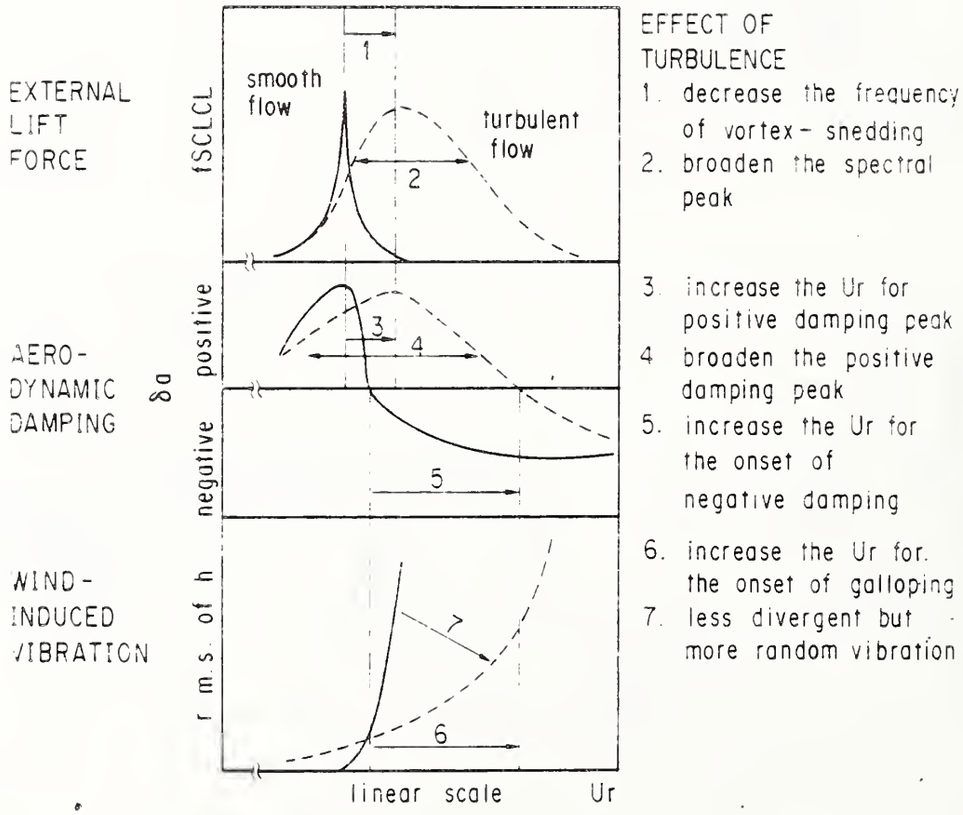

Fig. 8 Schematic Explanation of the wind-induced vibration of the continuous box girder bridges

On Interpreting Model and Prototype Responses of Suspended-Span Bridges to Wind

by

Robert H. Scanlan[1]

ABSTRACT

Aeroelastic models of suspended-span bridges have taken a variety of forms over the last half-century. A prominent engineering tendency over much of that time has been the direct identification of (scaled) model response under wind with expected prototype response. The present paper points out the fact that such direct identification may likely be in error. Since most model action is inevitably at variance with prototype action, *interpretation* of experimental model response is required. Such interpretation is facilitated via a viewpoint that refers to theory. An analytical formulation is employed in which, notably, self-excited aerodynamic effects are recognized through mechanisms like flutter derivatives. Thereafter, by tracing expected specific aerodynamic and structural-dynamic contributions to both prototype and model response, the relation of the latter to the former can be assessed. This process sharpens the value of aeroelastic model tests of bridges.

KEYWORDS

Aerodynamic; Aeroelastic; Bridges; Structural-dynamic; Suspended-span bridges; Wind engineering.

1. INTRODUCTION

In problems of experimental simulation it is invariably of great assistance to establish scaling ratios between the prototype that is to be understood and the physical model that is intended to represent it. When the modeling may be considered as "complete" in all respects, an application of the principles of dimensional analysis alone can often identify those parameter groups that govern the action of the prototype. However, when the physical modeling is "incomplete" in some respects it may become necessary to explore the system under study more thoroughly by first establishing a mathematical model for it and then noting the roles of various nondimensional quantities in the action of the prototype. Thus, even if experiments fall short of complete simulation, the several physical mechanisms involved in them can be studied via partial models for their contributions to the action of the prototype system as a whole.

In the wind tunnel testing of suspended-span bridges, a useful point of view is that no reduced-scale model perfectly duplicates prototype action in all respects. Thus, invoking a mathematical model of the system can help assess the accuracy of inferences drawn from experiment about the prototype. This point of view even enhances the critical interpretation of models initially intended to be "complete." It serves to identify participating mechanisms within the total system.

When constructing a mathematical model of bridge dynamic action under wind it is convenient conceptually to separate off the purely structural part from the purely aerodynamic part. The former is usually adequately described by a set of the eigenmodes and corresponding eigenfrequencies of the prototype, which merely reflect in alternative form its mass and structural stiffness distributions. For the aerodynamic part, some ingenuity has been called for, and this area still comprises a focus for continued effort.

To date, however, the measured steady-state force and moment coefficients of bridge deck sections, their corresponding oscillatory-state flutter derivatives, and the concomitant aerodynamic indicial and admittance functions, have fairly successfully been employed in studying the mechanisms of prototype response to wind. In fact, use of these concepts, usually derived from intentionally abridged, or partial, experiments, has now led to a state of the art in which a critical review of wind tunnel testing practices regarding bridge models can be undertaken. Such a review is given in what follows.

2. THEORY OF PROTOTYPE ACTION

We consider the case of a flexible, suspended-span bridge under high-velocity turbulent wind. The turbulence randomly excites the deck, which responds in a random fashion and also undergoes some degree of aeroelastic interaction, the net spectrum of the attendant response exhibiting peaks at frequencies respectively in the neighborhood of the natural eigenfrequencies of the structure. (The aeroelastic forces may affect the exact values of these frequencies.)

We first consider the interactive forces related to the three degrees of freedom (cf. Fig. 1): h (vertical), α (twist), and p (lateral) of a typical deck section. These actions take the well-known linearized forms [1]:[2]

$$\text{Lift: } L_{ae}=\frac{1}{2}\rho\bar{U}^2B\left[KH_1^*(K)\frac{\dot{h}}{\bar{U}}+KH_2^*(K)\frac{B\dot{\alpha}}{\bar{U}}+K^2H_3^*(K)\alpha\right] \quad (1)$$

$$\text{Moment: } M_{ae}=\frac{1}{2}\rho\bar{U}^2B^2\left[KA_1^*(K)\frac{\dot{h}}{\bar{U}}+KA_2^*(K)\frac{B\dot{\alpha}}{\bar{U}}+K^2A_3^*(K)\alpha\right] \quad (2)$$

$$\text{Drag: } D_{ae}=\frac{1}{2}\rho\bar{U}^2B\left[KP_1^*(K)\frac{\dot{p}}{\bar{U}}+KP_2^*(K)\frac{B\dot{\alpha}}{\bar{U}}+K^2P_3^*(K)\alpha\right] \quad (3)$$

[1] Department of Civil Engineering, Johns Hopkins University, Baltimore, MD 21218.

[2] It should further be noted that an alternate formulation of the aeroelastic forces under random excitation is via the so-called *indicial function* approach [5]. This will not be followed here.

where

ρ = air density

$\bar{U}$ = mean cross-wind velocity

B = deck width

$K = B\omega/U$ = reduced frequency

H_i^*, A_i^* and P_i^* (i = 1, 2, 3) are well-known *flutter derivatives*, experimentally determined functions of K for some specified bridge deck; and it is presumed that h, α, and p are all undergoing sinusoidal oscillation at radian frequency ω. [Figs. 2 and 3, for example, represent representative experimentally obtained plots of $H_1^*(K)$ and $A_2^*(K)$ vs. $2\pi/K$.]

It is worth emphasizing here that the complete flutter derivatives have the form KH_1^*, KH_2^*, etc. and that a pair like $KH_1^*(K)$ is in fact an inseparable product that holds for any given value of $2\pi/K$. Thus, at some mean velocity $\bar{U}$ if the degree of freedom h oscillates according to

$$h = h_1 \sin \omega_1 t + h_2 \sin \omega_2 t \tag{4}$$

then the corresponding self-excited lift force component is

$$L_{ae} = \frac{1}{2}\rho \bar{U}^2 B\left[K_1 H_1^*(K_1)\frac{h_1\omega_1}{\bar{U}}\cos\omega_1 t + K_2 H_2^*(K_2)\frac{h_2\omega_2}{\bar{U}}\cos\omega_2 t\right] \tag{5}$$

where

$K_1 = B\omega_1/\bar{U}$,

$K_2 = B\omega_2/\bar{U}$,

ω_1, ω_2 being the respective radian frequencies of the two oscillation components.

If the deck response components are introduced in terms of the superposition of dimensionless modal contributions $h_i(x)$, $\alpha_i(x)$, $p_i(x)$, then

$$h(x,t) = \sum_i \xi_i(t)\, h_i(x)\, B \tag{6}$$

$$\alpha(x,t) = \sum_i \xi_i(t)\, \alpha_i(x) \tag{7}$$

$$p(x,t) = \sum_i \xi_i(t)\, p_i(x)\, B \tag{8}$$

where $\xi_i(t)$ is the generalized coordinate of mode i. The aeroelastic part of the sectional lift is then

$$L_{ae}(x) = \frac{1}{2}\rho \bar{U}^2 B\left\{\frac{\sum_i K_i H_1^*(K_i)\dot{\xi}_i(t) h_i B}{\bar{U}} + \frac{\sum_i K_i H_2^*(K_i)\dot{\xi}_i(t)\alpha_i(x) B}{\bar{U}} + \sum_i K_i^2 H_3^*(K_i)\xi_i(t)\alpha_i(x)\right\} \tag{9}$$

Analogous forms hold for M_{ae} and D_{ae} from (2) and (3).

Next consider the sectional buffeting terms. These will have the form

$$L_b(t) = \frac{1}{2}\rho \bar{U}^2 B\, L(t) \tag{10}$$

$$M_b(t) = \frac{1}{2}\rho \bar{U}^2 B^2\, M(t) \tag{11}$$

$$D_b(t) = \frac{1}{2}\rho \bar{U}^2 B\, D(t) \tag{12}$$

where L, M, D are respectively the dimensionless random lift, moment, and drag acting on the deck section. Their exact forms will not be specified in the present paper, but may be expected to be experimentally measured results.

We then define the total actions on a deck section to be

$$\text{Lift: } L = L_{ae} + L_b \tag{13}$$

$$\text{Moment: } M = M_{ae} + M_b \tag{14}$$

$$\text{Drag: } D = D_{ae} + D_b \tag{15}$$

This results in the following expressions:

$$L(x,t) = \frac{1}{2}\rho \bar{U}^2 B\left\{\sum_j\left[\left(\frac{K_j H_1^*(K_j) h_j(x) B}{\bar{U}} + \frac{K_j H_2^*(K_j)\alpha_j(x) B}{\bar{U}}\right)\dot{\xi}_j + K_j^2 H_3^*(K_j)\alpha_j(x)\xi_j\right] + L(x,t)\right\} \tag{16}$$

$$M(x,t) = \frac{1}{2}\rho \bar{U}^2 B^2\left\{\sum_j\left[\left(\frac{K_j A_1^*(K_j) h_j(x) B}{\bar{U}} + \frac{K_j A_2^*(K_j)\alpha_j(x) B}{\bar{U}}\right)\dot{\xi}_i + K_j^2 A_3^*(K_j)\alpha_j(x)\xi_j\right] + M(x,t)\right\} \tag{17}$$

$$D(x,t) = \frac{1}{2}\rho \bar{U}^2 B\left\{\sum_j\left[\left(\frac{K_j P_1^*(K_j) P_j(x) B}{\bar{U}} + \frac{K_j P_2^*(K_j)\alpha_j(x) B}{\bar{U}}\right)\dot{\xi}_j + K_j^2 P_3^*(K_j)\alpha_j(x)\xi_j\right] + D(x,t)\right\} \tag{18}$$

The i th generalized coordinate ξ_i responds according to the equation

$$I_i\left[\ddot{\xi}_i + 2\xi_i\omega_i\dot{\xi}_i + \omega_i^2\xi_i\right] = Q_i(t) \tag{19}$$

where I_i is the generalized inertia of the entire bridge structure in the i th mode, ξ_i its damping ratio, and ω_i its circular frequency; the generalized force is

$$Q_i = \int_{\text{deck}}\left[L\frac{\delta h}{\delta\xi_i} + M\frac{\delta\alpha}{\delta\xi_i} + D\frac{\delta p}{\delta\xi_i}\right]dx \tag{20}$$

The explicit form of Q_i becomes

$$Q_i(t) = \frac{1}{2}\rho \bar{U}^2 B^2 \int_{\text{deck}}\left\{\sum_j\left[\left(\frac{K_j H_1^*(K_j) h_j(x) B}{\bar{U}} + \frac{K_j H_2^*(K_j)\alpha_j(x) B}{\bar{U}}\right)\dot{\xi}_j + K_j^2 H_3^*(K_j)\alpha_j(x)\xi_j\right]h_i(x) + \sum_j\left[\left(\frac{K_j A_1^*(K_j) h_j(x) B}{\bar{U}} + \frac{K_j A_2^*(K_j)\alpha_j(x) B}{\bar{U}}\right)\dot{\xi}_j + K_j^2 A_3^*(K_j)\alpha_j(x)\xi_j\right]\alpha_i(x) + \sum_j\left[\left(\frac{K_j P_1^*(K_j) p_j(x) B}{\bar{U}} + \frac{K_j P_2^*(K_j)\alpha_j(x) B}{\bar{U}}\right)\dot{\xi}_j + K_j^2 P_3^*(K_j)\alpha_j(x)\xi_j\right]p_i(x) + L(x,t)h_i(x) + M(x,t)\alpha_i(x) + D(x,t)p_i(x)\right\}dx \tag{21}$$

By carrying out the spanwise modal integrations that take the form

$$G_{r_m s_n} = \int_{\text{deck}} r_m(x)\, s_n(x)\, dx \tag{22}$$

where r, s = h, α, or p; m, n = i or j, the following result can be obtained for the generalized force:

$$\frac{Q_i(t)}{\frac{1}{2}\rho\bar{U}^2B^2}=\sum_j\left[\frac{BK_j}{\bar{U}}\left(H_1^*(K_j)G_{h_jh_i}+H_2^*(K_j)G_{\alpha_jh_i}\right.\right.$$

$$+A_1^*(K_j)G_{h_j\alpha_i}+A_2^*(K_j)G_{\alpha_j\alpha_i}+P_1^*(K_j)G_{p_jp_i}$$

$$\left.+P_2^*(K_j)G_{\alpha_jp_i}\right)\dot{\xi}_j+K_j^2\left(H_3^*(K_j)G_{\alpha_jh_i}$$

$$\left.+A_3^*(K_j)G_{\alpha_j\alpha_i}+P_3^*(K_j)G_{\alpha_jp_i}\right)\xi_j\Big]$$

$$+\int_{deck}[L(x,t)h_i(x)+M(x,t)\alpha_i(x)+D(x,t)p_i(x)]dx \qquad (23)$$

Versions of this result appear in Ref. [2].

It has been assumed in arriving at (23) above that the aeroelastic derivatives do not vary over the span, i.e. that the deck section geometry is uniform spanwise, and that the mean wind velocity is also uniform over the span. When these conditions are not met it is more appropriate to employ the more general eq. (21) for $Q_i(t)$.

3. REMARKS ON THE NATURE OF THE EXCITATION

Based on eq. (23) a number of observations can be made. First, all bridge modes are excited by the turbulence; and, as a general feature of the system, all modes are coupled together in the equations of motion through the medium of the aeroelastic derivatives and the modal integrals (22). The strength of this coupling will thus depend on the relative magnitudes of these terms. The aeroelastic derivatives are functions uniquely of deck cross-sectional geometry, while the modal integrals are consequences of the distributions of mass and stiffness in the bridge structure.

In some of the modes of a structure the deck plays a dominant role, carrying a large percentage of the generalized inertia of the whole system. If the deck structure is uniform over the span in these structures the modal integrals (22) may in such cases be approximately proportional to the well-known conditions of orthonormality between modes. In this situation some of the integrals (22) may approach high ("unit") values while others approach zero values.

An investigation of the first 13 modes of a modern cable-stayed bridge was made as an example, and two items of interest were recorded for each of these modes:

1) the percentage of total bridge generalized inertia concentrated in the deck alone;
2) values of those integrals $G_{r_ms_n}$ (22) in which r = s and n = m, i.e. values dependent on same-mode contributions.

Based on the convention that all generalized inertias I_i were assigned unit value, results for the ratio of deck contribution $(I_i)_{deck}$ to total I_i value, and the integrals $G_{h_ih_i}$, $G_{\alpha_i\alpha_i}$, $G_{p_ip_i}$ are presented in relative units in Table 1. This table serves to identify a) those modes in which prominent deck action is to be expected; b) the character (vertical bending, torsion, or lateral sway) of each mode. Further, it can be expected that for modes with high deck inertia and strong, single-component modal character, the cross-modal integrals (22) will take on less significant values. Some may be negligible.

Arguments of this sort (backed by numerical evaluations) can serve to delineate those modes most likely to participate in wind-induced aeroelastic response. Note that modes 1, 3, 9, 10, 12, and 13 of the example have over 93% of their inertia located in the deck alone, whereas this is quite variable for other modes. Mode 1 clearly has the character of lateral sway; modes 3, 9, 10, 12 are mainly vertical modes; and mode 13 is the first strongly torsional mode. (This mode is particularly likely to pick up wind energy through the agency of the A_2^* coefficients.) For modes like these the deck action represents most of total bridge action. They may be expected to dominate the response.

The possibility that in certain cases the cross-modal integrals (22) may have weak values suggests that on occasion intermodal aeroelastic coupling may not be strong and that in such cases eq. (23) may reduce further to an uncoupled, single-mode form, namely:

$$\frac{Q_i}{\frac{1}{2}\rho\bar{U}^2B^2}=\frac{BK_i}{\bar{U}}\left(H_1^*(K_i)G_{h_ih_i}+A_2^*(K_i)G_{\alpha_i\alpha_i}+P_1^*(K_i)G_{p_ip_i}\right)\dot{\xi}_i$$

$$+K_i^2A_3^*(K_i)G_{\alpha_i\alpha_i}\xi_i \qquad (24)$$

implying the possibility of single-mode aeroelastic response.

If one wishes provisionally to consider single-mode flutter in mode i, either as an actual possibility or as a necessary bounding case, this must imply that, in eq. (19), the mechanical damping term on the left-hand side is to be balanced by the aerodynamic damping terms of the right-hand side. Further, the natural frequency ω_i of the mode is modified to a value $\bar{\omega}_i$ by the aerodynamic stiffness (A_3^*) term. This situation leads first to the frequency modifying relation:

$$\bar{\omega}_i^2=\frac{\omega_i^2}{1+\frac{\rho B^4}{2I_i}A_3^*(K_i)G_{\alpha_i\alpha_i}} \qquad (25)$$

and next to the criterion FC for single-mode flutter instability:

$$FC=\frac{\bar{\omega}_i}{\omega_i}\frac{\rho B^4}{4\xi_iI_i}\left[H_1^*(K_i)G_{h_ih_i}+A_2^*(K_i)G_{\alpha_i\alpha_i}+P_1^*(K_i)G_{p_ip_i}\right]\geq 1 \qquad (26)$$

in which it is understood that $K_i=B\bar{\omega}_i/\bar{U}$.

Finally, the action of wind turbulence may be discussed. First, it has been verified [3] [4] that the presence of turbulence affects the values of the sectional aeroelastic derivatives H_i^*, A_i^*, P_i^*. Hence the values of these quantities as measured under appropriate turbulent conditions should be employed in the analysis. Next, the general action of turbulence is to force all bridge modes into play, as is clear from eqs. (6)–(8), (19), (23). When modes that are more highly damped are excited by the turbulence, their aeroelastic effects couple with others of the system and extract energy from it, effectively delaying the onset of instability. This appears to account for the often observed extension of critical flutter velocities of full-bridge models to higher values under turbulence.

A commonly held view is that two modes—typically a pure bending and a pure torsion—must couple to produce flutter. This phenomenon defines, in fact, the kind of stiffness-controlled "classical" flutter observed in aircraft, where the aerodynamic forces at high speed are large enough to alter two structural frequencies and modes appreciably toward coalescence into a flutter mode. While this type of occurrence is in principle possible

for bridge decks, and is covered by the theory given, by far the greater number of actual occurrences depend upon a single torsional mode becoming intrinsically unstable and "driving" the rest of the system. The mechanism involved in this can immediately be detected by evaluation of the terms in eq. (23), most particularly those involving the A_2^* coefficient, which can lead to negative system damping.

In many cases the question of stability may be regarded as centered therefore on the values taken on by the A_2^* flutter derivative, which typically evolves from negative to positive with increasing values of $U/NB = 2\pi/K$. Modes of higher frequency, corresponding to lower values of U/NB, correspond generally to negative values of A_2^*, whereas lower-frequency modes appropriate positive values of A_2^*, tending toward instability. It is thus quite clear how turbulence, coupling-in many modes that are conducive to greater damping, extends the stability domain.

3.1 The Roles of Different Model Types

Common model types include narrow- and wide-span section, the single-span flexible, and the full-bridge aeroelastic. The roles, results, and interpretations of each can be assessed in light of the theory developed above.

The *narrow-span section model* is the model of choice for most investigations. Tested under laminar flow it yields the primary flutter derivatives and static force coefficients that are usually the most conservative ones. It is usually difficult, however, to test the section model under conditions of properly simulated turbulence. This problem has, however, been approached and largely overcome in recent work [3] [4].

One of the largest open issues is the extent to which prototype action should be inferred from model results. The rigid, spring-supported model can represent only restricted freedoms; and general prototype modal effects therefore cannot be fully duplicated by it. Under these conditions, model response to turbulence will not duplicate that of the prototype.

When the short-span section model is used to acquire section aeroelastic derivatives experimentally it can conveniently be divorced from all but geometric similarity requirements relative to the prototype. Since the aeroelastic derivatives are functions of reduced velocity U/NB only (as with linear-theory derivatives), or of U/NB and response amplitude only (as with problems involving nonlinear theory), the geometric section model need only respect these parameters, and is thus rapid, economical, and relatively simple to test. It most often must be tested in any event, whether or not models of other types are employed.

The section model, with its restricted, rigid modes, can be fitted directly into the general theory outlined above [2]. It can respond essentially in separate components of two distinct prototype modes at a time. When its parameters are employed with the theory, the exact degree to which it meets (or fails to meet) prototype action can be completely assessed, without ambiguity. Its chief role remains, however, in assessing intrinsically aerodynamic and aeroelastic data.

The *wide-span section model* acts in every respect like the narrow-span version but has the added feature of being wide enough to include the integrated spanwise variations of the turbulence effects, both on the net flutter derivatives and on the buffeting response. However, this model must also not be mistaken to have the same response as the prototype. Model action is again restricted essentially to two "pure" prototype modal components. Entry of the modal and other data into the analytical framework given earlier again reveals clearly that model response is not directly equal to scaled prototype response, even in a single mode. This is obvious from the differences that occur in the modal integrals $G_{r_m s_n}$ that appear in eq (22) for the model and prototype. At the same time, the full appreciation of these differences permits correct *interpretation* of model performance under turbulence relative to expected prototype performance.

For example, analysis of model and prototype performance under random inputs [2] can yield the ratio of r.m.s. model response amplitude to expected prototype response in a *single* mode of the latter. This ratio is not unity, even apart from known scaling factors.

The *single-span flexible model* (often realized via the so-called "taut strip" technique) has identical problems to those of the narrow- and wide-span section models, in that it cannot be expected to duplicate prototype modes, full-bridge inertias, or damping. For the simulation of cable-stayed bridges in particular, the fact that it develops a mode or modes of its own is actually a disadvantage, rather than an advantage, since these modes cannot reproduce complex cable-stayed modes. In this respect the wide-span, rigid section model is in fact superior, its "mode" being simpler and more directly adapted to the extraction of flutter derivatives.

The reasoning that leads to use of a single-span, flexible model has often been faulty, to the extent that the effort has been to set up model performance that could be interpreted directly, on a one-to-one scale, as equivalent to prototype performance. Such intended interpretation is illusory. If, in particular, the motivation for a single-span flexible model is to gather in and integrate the spanwise effects of turbulence, then interpretation beyond the one-to-one scale is even more called for, since the model acts differently from the prototype, as seen, again, via the theory outlined earlier.

In particular, referring to the modal integrals (22), these will be vastly different from model to prototype. The deck generalized inertia will not in general duplicate (to scale) full-bridge generalized inertia. Again, only a single (or perhaps two) center-span modes are possible in the single-span flexible model. Inertias and loadings of side spans are not represented. In the case of modern cable-stayed bridges the shapes of the modes realizable by single-span flexible models usually do not conform to prototype modal forms.

The *full-bridge aeroelastic model*, assuming it to be aeroelastically faithful, is the only one with a reasonable chance of directly duplicating prototype performance (to scale) on a one-to-one basis. For this it must be tested under correctly simulated earth's boundary layer winds. Exploiters of such models have encountered the expense, care, and general difficulties involved with them. In particular, their realizable hierarchy of structural vibration modes seldom lines up perfectly, one-for-one, with prototype modes. This line-up may be partially achieved through as many as 10 modes, though rarely. When it is recalled that a wind-critical torsional mode of a modern cable-stayed bridge may be the 13th or 17th mode of the structure, this leaves some open problems.

Other problems of these model types are that they integrate all effects together, permitting less experimental appreciation of specific local mechanisms that may contribute importantly to overall performance.

3.2 General Philosophy of Modeling

Throughout the history of bridge wind-tunnel modeling there has been a tendency on the part of investigators to view the

model as a direct, scaled analog of the prototype. As with any other avenue of investigation, what is objectively discovered may not always conform to preconceptions. In the case of bridge modeling what has been discovered is that the essence of what can be extracted from models is not their performance *per se* but the intrinsic aerodynamic information that they engender, i.e., such data as the static and aeroelastic derivatives, indicial and admittance functions, etc.

The desire to "command" the model into scaled dynamic equivalence to the prototype has led to extensive and needless concern with model structural dynamics, equivalent inertias, artificial rotation points, damping, etc. While no model can duplicate prototype behavior perfectly, as has been argued, numerous attempts continue to be made to bring model performance into such alignment. A much more fruitful approach is to concentrate on exactly what *can* be inferred correctly from model tests. Certainly the static force coefficients and the aeroelastic derivatives are prominent among such items of data. These, coupled with theory, offer a wide range of options regarding the forecasting of prototype performance. This approach allows the aerodynamicist to concentrate attention more upon his principal art and less upon structural dynamics.

When costly attempts are made to encompass the entire problem—both structural and aerodynamic—via a full-bridge aeroelastic model, for example, a large set of parameters, including many structural ones, is "invited" into the problem. Their totality may lessen the validity of conclusions drawn from experiment rather than augment them. A problematic situation that can occur under these circumstances is that a "favorable" but unexplained outcome emerges from the testing. From an engineering viewpoint the cause for this must ultimately be found, but a "global" test, in which too few detailed mechanisms have been explained, may offer a false sense of security.

The analytical and directed experimental approaches outlined in this paper have emphasized the role of theory in discerning the mechanisms responsible for the stability of suspended-span bridges. It should be noted that the theory may be considerably extended [2] beyond the limited scope presented.

4. REFERENCES

1. Scanlan, R. H.: "The Action of Flexible Bridges Under Wind. I: Flutter Theory; II: Buffeting Theory," *Jnl. of Sound and Vibration*, Vol. 60, No. 2, 1978, pp. 187–199 and pp. 201–211.
2. Scanlan, R. H.: "Interpreting Aeroelastic Models of Cable-Stayed Bridges" to appear in *Jnl. EMD, ASCE*, April 1987.
3. Scanlan, R. H. and Huston, D. R.: "Sensitivity of Bridge Decks to Turbulent Wind" *Proceedings* Asia-Pacific Symposium on Wind Engineering, Roorkee, India, Dec. 1985, pp. 167–172.
4. Scanlan, R. H. and Huston, D. R.: "Changes in Bridge Deck Flutter Derivatives Caused by Turbulence" *Dynamic Response of Structures* (Eds.: G. C. Hart and R. B. Nelson) ASCE, 1986, pp. 382–389.
5. Scanlan, R. H.: "Role of Indicial Functions in Buffeting Analysis of Bridges," *Jnl. Struct. Engrg.* ASCE, Vol. 110, No. 7, July 1984, pp. 1433–1446.

TABLE 1

Modal Geometric Integrals and Deck Inertias

Mode No.	Freq. (Hz)	I_i (deck only)	$G_{\alpha_i\alpha_i}$	$G_{h_ih_i}$	$G_{p_ip_i}$
1	0.171	0.992	0.1816 E-07	0.1414 E-11	0.2242 E-06
2	0.188	0.781	0.3354 E-11	0.0896 E-07	0.4358 E-10
3	0.270	0.935	0.3193 E-13	0.2105 E-06	0.2064 E-12
4	0.349	0.890	0.3614 E-12	0.2010 E-06	0.1662 E-11
5	0.389	0.894	0.4876 E-07	0.1685 E-11	0.1975 E-06
6	0.516	0.050	0.7846 E-07	0.3021 E-13	0.0739 E-07
7	0.522	0.062	0.9214 E-07	0.3644 E-13	0.0795 E-07
8	0.552	0.694	0.5313 E-07	0.0729 E-09	0.1317 E-06
9	0.555	0.947	0.1778 E-10	0.2133 E-06	0.4478 E-10
10	0.645	0.975	0.5484 E-14	0.2201 E-06	0.3812 E-13
11	0.696	0.653	0.1239 E-06	0.4637 E-12	0.1130 E-06
12	0.714	0.988	0.2264 E-11	0.2238 E-06	0.1817 E-12
13	0.721	0.955	0.3640 E-05	0.1375 E-12	0.2006 E-08

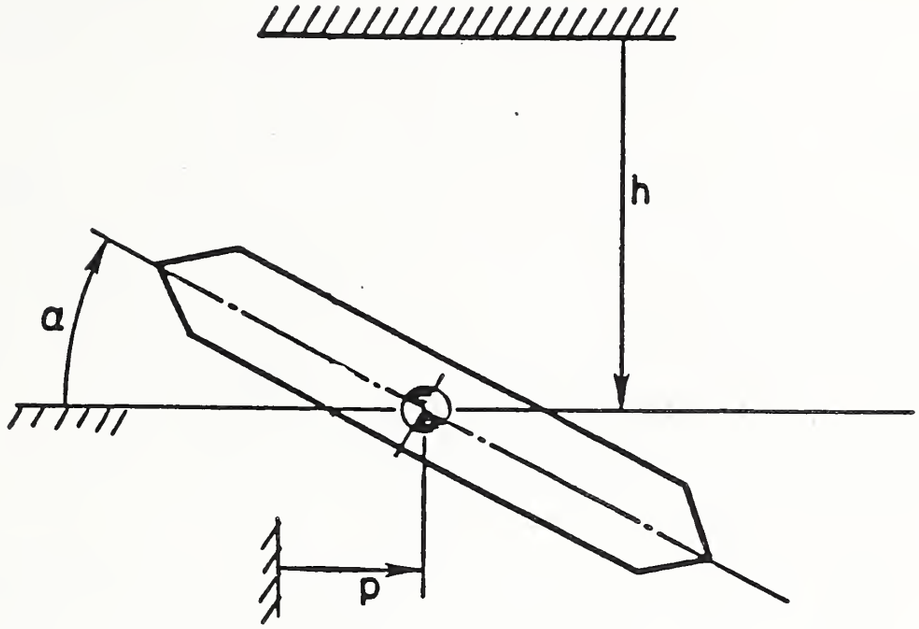

Figure 1.

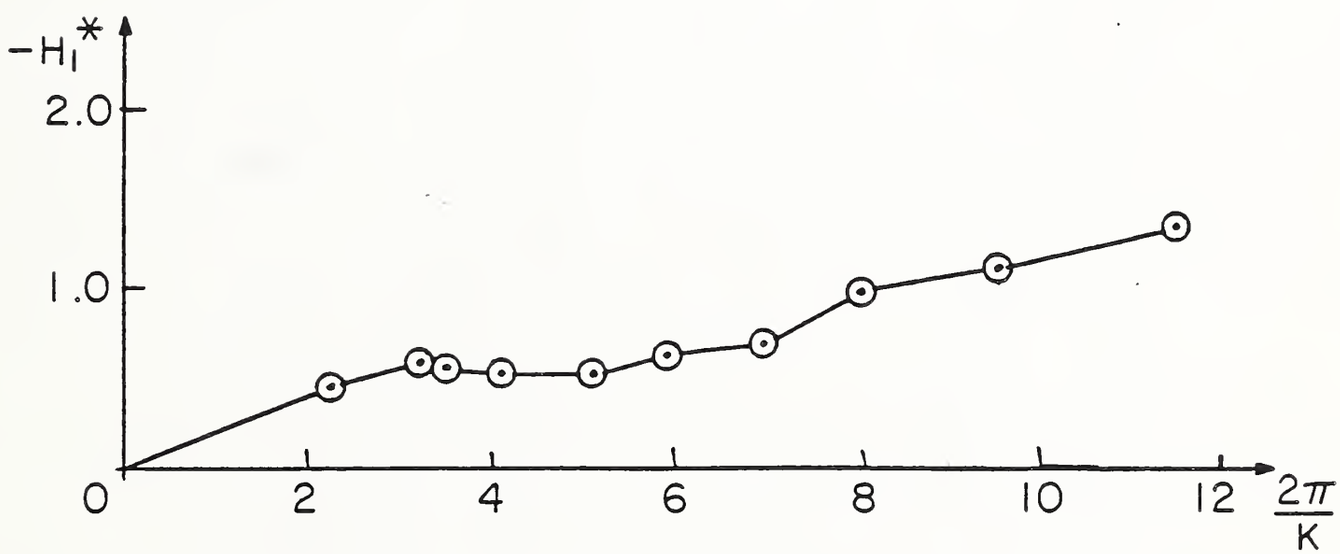

Figure 2.

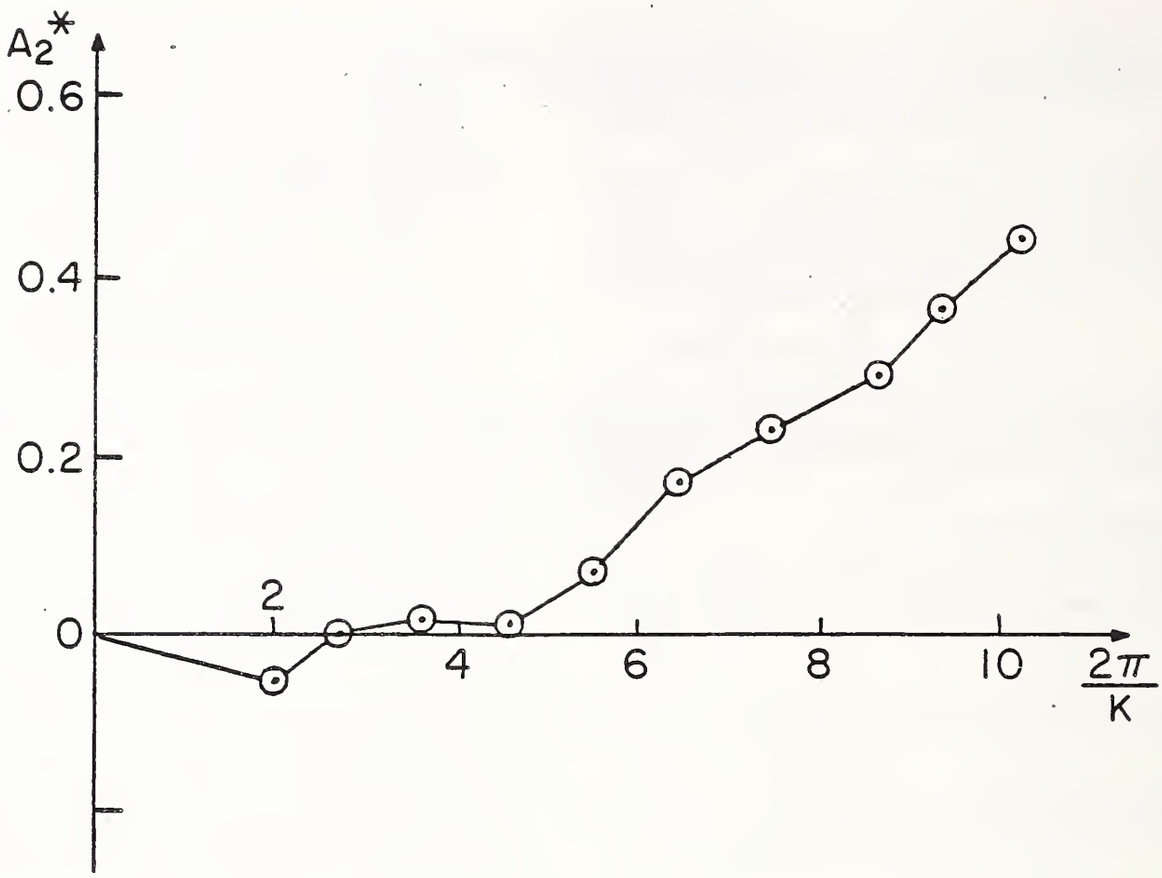

Figure 3.

Theme II

Earthquake Engineering

The United States Geological Survey Accelerograph Network in the U.S.–Operations, Record Processing and Research

by

A. Gerald Brady[1]

ABSTRACT

The United States Geological Survey maintains a strong-motion instrumentation permanent network of accelerographs for recording potentially damaging strong accelerations. At the project level, two projects are responsible for the design, development and operation of the network, and the processing of the resulting ground motion data. Five projects are closely linked to the performance of the network and the processed data. The seven projects, and the relationships between them, are described in terms of their recent accomplishments.

KEYWORDS: Accelerograph; Network; Operation; Data processing.

1. INTRODUCTION

The Branch of Engineering Seismology and Geology, within the Office of Earthquakes, Volcanoes and Engineering, of the U.S. Geological Survey, may be considered to consist of approximately 40 research projects, plus the administrative and data handling projects essential for operation. All research projects are headed in general by Ph.D. scientists. The projects deal with the reduction of earthquake hazard from an understanding of the causative faults, the passage of earthquake-generated strong-motion waves to the surface, and the effect on structures of strong ground motion at the surface. The researchers involved are therefore readily subdivided into geologists, geophysicists and engineers, although there is considerable overlap.

Many measurements of earthquake related phenomena are taken -- continuous in analog or discrete modes for monitoring purposes, and intermittent in analog or discrete modes for specific earthquake occurrences. The strong-motion instrumentation network, characterized by permanently-installed instruments for recording potentially damaging strong accelerations, is one such source of research data. Seven projects are directly related with the development and operation of this permanent network, and with the strong-motion records it produces, while several more projects use some of the more significant record sets for research endeavors that do not form an essential part of their basic project goals. This report describes briefly the two projects that run the network and process the data, together with recent accomplishments. It follows with a description of the five projects whose goals are closely linked to the performance of the primary two.

2. NETWORK PERFORMANCE AND RECORD PROCESSING

2.1 Strong-Motion Instrumentation Network Design, Development and Operations

This network was initiated by the U.S. Coast and Geodetic Survey in 1932 and recorded the first accelerations close to a destructive earthquake on March 10, 1933 (the Long Beach earthquake). At the present time, the network operates in 41 states and in Puerto Rico, and consists of approximately 1000 recording units installed at 600 ground sites, 27 buildings, five bridges, 56 dams, and two pumping plants. Cooperative arrangements for the design, development and operation of many of these installations are in effect with several federal, state, and local agencies, and advisory engineering committees. Cooperative agreements with federal agencies ensure a spread of the network into some regions where the return, in the form of significant records, is not high. The densest parts of the network include the metropolitan and active fault areas in California, followed by the seismically active areas of the remaining western states, Alaska and Hawaii. Arrays of closely spaced sensors, with typical spacing of 100 m, and of less closely spaced sensors (spacing of 1 to 5 km), have been installed in California locations.

Program goals include (1) the recording of potentially damaging ground motions to be used as input by the structural engineering, and geophysical, professions in efforts to reduce the earthquake hazard through a greater understanding, and subsequently, more precise building codes and regulations, and (2) monitoring the earthquake response of civil engineering structures with sensors placed at critical locations. Hopefully, significant, or even damaging, earthquake response would be recorded.

The following recent project activities have been taken in their entirety from the 6-monthly technical summary reports of the National Earthquake Hazards Reduction Program (Ref. 1).

2.1.1 New Instrumentation

Six ground motion stations were established in

[1] U.S. Geological Survey, Menlo Park, CA 94025

the Western United States: three at rock sites in San Francisco including the Golden Gate Bridge abutment, one on the Calaveras fault east of San Jose, and two in western Nevada, at Yerington and Montgomery Pass.

Two four-instrument structural arrays were installed at the Corps of Engineers' John Day and Dalles concrete dams located on the Columbia River between Oregon and Washington. At each structure the instrumentation configuration consists of two accelerographs in the lower gallery, one in the upper gallery, and one on abutment rock.

A 21-channel instrumentation system was completed at a 33-story steel frame building in Los Angeles. The structure is rectangular for the first 12 stories above ground, and is then topped by a 21-story triangular tower. Transducers are located at the basement level, and on the ground, 12th, 13th, and 33rd floors in directions to measure base rocking, two translational modes in each direction, and two torsional modes.

A 15-channel structural monitoring system was installed for the Metropolitan Water District of Southern California on a truss bridge that was recently retrofitted with seismic isolation elastomeric bearings. The bridge has three 180-foot long spans (55 m) that carry a 10-foot diameter (3 m) California Aqueduct water pipe across the Santa Ana River near Riverside. Transducers have been located in the middle of one truss section, at a pier above and below the elastomeric bearing, in the bridge abutment, and in a nearby recorder housing resting on rock.

2.1.2 Recent Earthquake Records

Several hundred earthquake records were recovered during the past six months from instrumentation located in California and Alaska. The following summarizes some of the more important results.

2.2 The National Strong-Motion Network: Data Processing

Data processing of significant records from the strong-motion instrumentation network provides computer-ready corrected accelerograms to the engineering and geophysical research community. Tapes containing this data, and their spectra, are distributed by the National Geophysical Data Center. Reports containing computer plots are distributed by the U.S. Geological Survey. Accompanying data on all records, stations, and recorded events are available on a recently updated database operated on the USGS VAX computer at their Menlo Park Western Region Headquarters (Ref. 2).

In its capacity as data processor for the USGS strong-motion instrumentation network, the project remains current with all recent processing procedures, particularly those in use by other closely associated projects within the USGS. Cooperative processing arrangements have been made in the past with Italy and other countries in Europe, with Chile and other countries in South America, and with Mexico and other countries in Central America.

Local site geology investigations at the strong-motion stations are shared by several projects, but the relevant information from bore holes, and velocity profiles, are intended to be centrally gathered in the section of the database describing the stations (Ref. 2).

2.2.1 Recent project activities

In cooperation with strong-motion network personnel in the Civil Engineering Department of the University of Chile, some of the more distant records of the Chile earthquake (Ms7.8, 3 March 1985) have been digitized and processed. The important records with high amplitudes were processed in Chile. One significant record from Adak, Alaska during the Alaska earthquake (Ms7.7, 7 May 1986) has

Earthquake Date	Magnitude	Location	Records	Peak Acceleration
30 December 1985	5.2	Anchorage, AK	11	Ground .08 g Structure .05 g (Humana Hospital 7th floor)
8 July 1986	5.9	N. Palm Springs, CA	68*	Ground .78 g Structure .12 g (Skinner Dam crest)
13 July 1986	5.3	Offshore off Oceanside, CA	3	Ground .11 g
21 July 1986	6.0	Chalfant Valley, CA	16*	Ground .36 g

*More than 100 aftershock records were obtained from permanent and temporary accelerograph stations following the North Palm Springs and Chalfant Valley earthquakes.

been processed for the U.S. Navy. Two of the California earthquakes in July 1986 produced significant records --North Palm Springs (M5.9, 8 July 1986) and Chalfant Valley, near Bishop, (M6.4, 21 July 1986). A set of 17 records from the North Palm Springs event are being processed, while the most significant records from the Chalfant Valley event are from a downhole array (100 m deep) at Mammoth Lakes.

A user manual and a maintenance manual for the strong-motion database have been prepared, for use by USGS database personnel, even though the database itself is operating at present at its basic level.

3. PROJECTS RELYING ON NETWORK OPERATIONS AND DATA PROCESSING

Three projects rely on the Network Operations project for installation and maintenance of accelerographs performing specific functions. These stations have been incorporated into the permanent network. The projects also rely on the Data Processing project for processing any records forthcoming from the installations.

3.1 National Strong-Motion Network: Engineering Data Analysis

The El Centro Differential Array recorded the 1981 Westmorland earthquake (M5.6, 26 April 1981) and the Hollister Differential Array recorded the 1986 Hollister Earthquake (M5.5, 26 January 1986). These arrays, with station spacing of the order of 100 m, were designed for investigations of differential displacements and their effect on structures with large foundations or widely spaced supports. Differential displacements and spectra, from records of the two events, have been calculated (Ref. 3).

3.2 Experimental Investigations of Liquefaction Potential

This project involves the design and installation of instrumental packages at a chosen site near Parkfield, California, to monitor pore water pressures in buried sand layers, and strong ground motion in a downhole array, during the predicted Parkfield earthquake, should it occur. Four downhole accelerometers will be at depths ranging from 3 to 30 m, in addition to ground level accelerometers. Their installation and maintenance have been coordinated through the Network Operations project and digitizing of any records, including the pore pressure records, will be coordinated through the Data Processing project (Ref. 4).

3.3 Instrumentation of Structures

In the last several years the USGS has established a program where advisory committees, formed in the more seismically active areas of the country, develop lists of structures for possible instrumentation. The recommendations of committees in the San Francisco Bay Region, San Bernardino County, and Los Angeles County, in California, and in Charleston, South Carolina, have resulted in thorough instrumentation of at least one structure in each region (Ref. 5). Further committee recommendations are expected from Orange County, Calif.; Seattle, Wash.; Reno, Nev.; the New Madrid area, Missouri; Boston, Mass.; Anchorage, Alaska; Hawaii; and Puerto Rico.

The well-instrumented structures become part of the permanent network, and any records from future events will be processed accordingly. Records are expected to provide useful information for:

- checking the dynamic model, for the first two modes in each direction, and for torsion and rocking;
- investigating non-linear effects;
- correlating non-linearities and inelastic behavior with damage;
- correlating ground level motion with structural properties and damage;
- the improvement of seismic codes.

4. OTHER SOURCES OF ACCELEROGRAMS

4.1 Strong-Motion Accelerograms of the 3 March 1985 Central Chile Earthquake.

Strong-motion records from the more distant stations during the 1985 Chile earthquake, and records from the significant aftershocks, were digitized and processed by the Data Processing project. The near field records were digitized in Chile. A staff member from the University of Chile visited Menlo Park to assist in the processing. At the completion of all processing, a data tape and report will be prepared (Ref. 6), and the data will be available for use both in Chile, the USGS, and on request.

5. RECENT AND CURRENT RESEARCH PROJECTS USING PROCESSED DATA FROM THE STRONG-MOTION INSTRUMENTATION NETWORK.

5.1 Fundamental Modal Behavior of an Earthquake-excited Bridge

The 1984 Morgan Hill earthquake (M6.1, 24 April 1984) produced a set of acceleration records at the freeway overpass in San Jose, carrying I-280/I-680 across U.S.101, 12 km from the epicenter. Peak accelerations reached 0.1 g at ground level and 0.16 g in the box girder. The integrated displacements at frequencies higher than 3 Hz permit the identification of the fundamental modes and frequencies. The horizontal modes, which include dominant ground level motions up to 90% of deck motions, have frequencies of 3.8

and 3.9 Hz (Ref. 7).

5.2 Differential Ground Displacements

Included in the projects relying on Network Operations and Data Processing, above, is the Engineering Data Analysis project. As described there, data has already been recorded on both the differential arrays. This differential ground motion, were it to occur under the base of an extended structure, would impose direct strains on the structure in addition to those strains from the earthquake loading. The analysis of these records shows that when applied to a simple structure under specific circumstances, these direct strains can be more important than those strains calculated assuming the entire foundation is excited in unison (Ref. 8).

5.3 System Identification in Structural Dynamics

This project develops methods for system identification for use in analyzing the earthquake recordings of instrumented structures. It forms the bridge between the instrumented structures in the strong-motion instrumentation network and the processed records obtained during earthquakes. Preliminary testing of these research methods incorporates the use of the processed records to identify mode shapes and frequencies, and the comparison of these identified characteristics with values from other independent sources.

6. CONCLUSIONS

The research projects within the USGS that are directly involved with the permanent strong-motion instrumentation network of accelerographs and the processing of records form a distinct group in the earthquake hazard reduction program. The basic projects (network operation and data processing) are closely linked to the others in this group (geophysics and engineering problem solving). Although the responsibilities for all projects are clearly delineated, it is clear that the performance of the basic projects is important to the others, while, on the other hand, and in the long term, the basic projects rely strongly on good scientific use of their data.

7. REFERENCES

1. Jacobsen, M. L., and Rodriguez, T. R., 1987. "National earthquake hazards reduction program, summaries of technical reports," Volume XXIII, USGS Open-File Report, in press.

2. Converse, A. M., 1987. User's guide to ESM: a database for strong-motion information: USGS Open-File Report 87-160.

3. Bycroft, G. N. and Mork, P. N., 1987. Differential displacements and spectra for 4 April 1981 Westmorland and 16 January 1986 Hollister earthquakes: USGS Open-File report (in preparation).

4. Holzer, T. L., Bennett, M. J., Youd, T. L., and Chen, A.T.F., 1986, Identification of a site to monitor liquefaction during the predicted 1988 Parkfield earthquake, Cholame Valley, California (abstract): Association of Engineering Geologists Abstracts with Program, Annual Meeting, 29th, San Francisco, p. 51.

5. Celebi, M., and Maley, R. P., 1986. Strong-motion instrumentation of structures in Charleston, S. Carolina, and elsewhere: Proceedings, U.S. National Conference on Earthquake Engineering, 3rd, Charleston, S. Carolina, II, p. 1273-1283.

6. Saragoni, R., Fresard, M., Brady, A. G., Celebi, M. (principle investigator), and Mork, P. N., 1987. Processed Chile earthquake records of 3 March 1985 and aftershocks: USGS Open-file report (in preparation).

7. Brady, A. G. and Celebi, M., 1986. Fundamental modal behavior of an earthquake-excited bridge: U.S. National Conference on Earthquake Engineering, 3rd, Charleston, S. Carolina, III, 2225-2236.

8. Bycroft, G. N., and Mork, P. N., 1987. Differential ground motions and their spectra: in preparation.

Estimation of Source Time Function Based on Strong Ground Motions and Its Application for Engineering

BY

Yoshikazu Kitagawa[1], Takahito Inoue[2]

Tatsuo Murota[3]

ABSTRACT

Dynamic response analysis is applied to earthquake resistant design of structures. It is possible to analyze the dynamic phenomena of structures for the earthquake to the most accurate degree, because the theories and computer programs concerning these analyses have made great progress recently. But the typical observed strong ground motions have been used mostly as "earthquake input". As the number or the nature of those waves are limited as yet, we must take care to use their waveforms for design and a useful method for synthesizing the ground motions has not yet been developed.

In order to use the synthetic ground motions calculated from the fault model as "earthquake input", it is necessary to estimate the characteristics of the source time function correctly. In this paper, we propose the estimation method of the source time function with the observed ground motions by applying the autoregressive(AR) model to the observed ground motions. Further, we apply this procedure to the synthetic waves calculated from the fault model in order to verify this method. As a results, the waveform obtained by using this method corresponds to the source time function of the seismic moment. These results agree with the condition given for the fault model analysis and it is pointed out that this analytical method using the AR model ia available to estimate "earthquake input" for the dynamic response analysis of structures.

KEY WORDS: Source Time Function, Event, Seismic Moment, Fault Model

1. INTRODUCTION

In order to estimate the seismic safety of structures, the dynamic response analysis is applied to earthquake resistant design of structures, and the typical observed strong ground motions have been used mostly as "earthquake input". But as the number or the dynamic properties of those waves are limited as yet, we must take care to use their waveforms for design and a useful method of synthesizing the ground motions has not yet been developed. But recently many trials to have a realistic "earthquake input" have been performed from both a theoretical and observational aspect. They are pseudo-ground motion, superposition of many seismic waves from aftershocks, etc.. Especially in connection with rather long period ground motions, the method of synthesizing the ground motion due to earthquake faulting is applied for engineering. In order to use the synthetic ground motions calculated from the fault model as "earthquake input", it is significant to grasp the characteristics of the source time function correctly. However, the ground motion is strongly affected by the earthquake process itself, the propagating path of the seismic wave, the topography of the ground surface, and the properties of ground surface layers.

In this paper, we propose the estimation method of the source time function with the observed ground motions by using the autoregressive(AR) model for the purpose of estimating the dynamic properties of the ground surface and the seismic wave path. Further, we apply this procedure to the synthetic waves calculated from the fault model in order to verify this method(1).

2. ANALYTICAL METHOD

The inversion method proposed by Kikuchi(2) is one method by which the distribution of events (called strong motion sources) on the fault plane can be estimated. In this method, the parameters for the fault are determined by matching the synthetic waveforms with the observed ones. But, by using a method proposed in this paper the source time function is obtained directly from the observed ground motion. Besides, Nair(3) tries to estimate the source function and the medium response function from the observed ground motion by the AR model, Tomizawa et al.(4) synthesize three-dimensional earthquake ground motion, and Yokota et al.(5) determine the arrival times of P- and S-waves on the

1 Dr. of Eng., Head of Second Earthquake Engineering Division, International Institute of Seismology and Earthquake Engineering, Building Research Institute, Ministry of Construction, Japan.

2 Visiting Researcher of Second Earthquake Engineering Division, International Institute of Seismology and Earthquake Engineering, Building Research Institute, Ministry of Construction, Japan.

3 Director, Structure Department, Building Research Institute, Ministry of Construction, Japan.

prediction system of earthquakes. The outline of this analytical method follows.

In order to estimate the dynamic properties of the ground surface and the seismic wave path, we apply the AR model to the tail part of the observed ground motion which is appeared by the finite discrete time series x_i (i=1,2,....,N). As the tail part, $_t x_i$ (i=L,L+1,....,N; 1≤L≤N), is random data with few non-stationary properties, it is written as

$$ {}_t x_i = \sum_{m=1}^{M} a_m x_{i-m} + \varepsilon_i \quad ; i=L,L+1,....,N \qquad (1) $$

where a_m (m=1,2,....,M) is the AR coefficient and minimusing the average square error, M is the AR order and ε_i is error series. Then in order to determine the suitability of a given AR model, Akaike's final prediction error (FPE)(6) is introduced.

By using the AR coefficient, a_m, obtained in Eq.(1), the estimated value, $_e x_i$, from observed ground motion is represented by the following equation as the linear combination with former values.

$$ {}_e x_i = \sum_{m=1}^{M} a_m x_{i-m} \quad ; i=M,M+1,....,N \qquad (2) $$

This value shown in Eq.(2) includes the dynamic properties of the observation site. Further, the residual time series, e_i, defined by Eq.(3) excludes the dynamic effects of the ground surface and the seismic wave path and includes the much data related to the source characteristics.

$$ e_i = x_i - {}_e x_i = x_i - \sum_{m=1}^{M} a_m x_{i-m} \quad ; i=M,M+1,....,N \qquad (3) $$

If the discrete time series, x_i, shown in Eq.(3) is a deterministic waveform, the error series becomes a white noise process. But as the observed ground motion is the non-stationary random data, the residuals time series shown in Eq.(3) doesn't accept the non-stationary property sufficiently. The non-stationary spike appears in the residuals time series as the non-stationary property is larger in the observed ground motion. The time series, $_r e_i$, which is excluded the non-stationary property from the residuals time series ,e_i, shown in Eq.(3), resembles the stationary gaussian process closely. There is however the non-stationary property of the amplitude which is appeared in Eq.(4)

$$ {}_r e_i = \Phi_i \, {}_s e_i \quad ; i=M,M+1,....,N \qquad (4) $$

where $_s e_i$ is the finite discrete time series with the stationary gaussian process, Φ_i is the weight function which gives the non-stationary property to the amplitude.

By integrating the waveform $_s e_i$ obtained from Eq.(4) shown in Eq.(5), it becomes possible to estimate the source time function as the distribution of events in the fault plane.

$$ \dot{M}_i = \alpha \int {}_s e_i \, dt \quad ; i=M,M+1,....,N \qquad (5) $$

where α is the coefficient including the soil constants at the fault.

Further, when the observed ground motions include the multiple shock sequence, the onset time and the distribution of events in the fault plane are decided from the interval time between events(7).

3. NUMERICAL ANALYSIS

3.1 Analytical model and its characteristics

In order to verify this analytical method, this procedure is applied to the synthetic waves calculated from the fault model. The synthetic waveforms are calculated by using the estimation method developed by Sudo, Kitagawa and Yosimura(8). The used underground structure and fault parameters are shown in Fig.1 and Table 1. The relation between the fault and the observation point(OP-1) is shown in Fig.10 and the epicentral distance is 113 km. The transfer functions of the underground structure obtained by Haskell's method are shown in Fig.2. One is a transfer function between the point source and the ground surface, the other is between the baserock and the ground surface. Both of the transfer functions show a similar property and their predominant frequency is from 2 to 5 Hz. The waveforms of velocity calculated from the fault model with one event, which have the seismic moment shown in Fig.7, are shown in Fig.3 and their fourier spectrum is shown in Fig.4. Besides, this numerical analysis is concerned with the body wave mainly.

In order to estimate the dynamic property of the observation site, it is necessary to select the appropriate AR order and time length of the tail part of the observed ground motion respectively. The reference range of the most appropriate AR order proposed by Akaike(6) is $2\text{-}3\sqrt{k}$(k is number of data). We investigate two cases of the AR order both with the first local minimum of FPE and the lowest value of FPE in that range. Coherence between the observed waveform at point Ⓒ and the waveform applied by the AR model with two cases of the AR order are shown in Fig.5. Regardless of the AR order, the observed wave below 2Hz is regressed by the AR model but the agreement above 2Hz is not so good. Further, coherence between the waveforms obtained from residuals in Eq.(3) and the incident waves at point Ⓐ, Ⓑ are shown in Fig.6(a)(b). The

waveform obtained from the residuals with the first local minimum of FPE of the AR order corresponds with the incident wave at point Ⓑ. On the other hand, the waveform obtained from the residuals with the lowest value of FPE of the AR order agrees with the incident wave at point Ⓐ and the apparent arrival time P and S waves can be measured at the observation point. Judging from Fig.6, as the order of the AR model is higher, the waveform including more source characteristics is obtained from the observed ground motions.

3.2 Property of distribution of events

The waveform obtained from Eq.(5) is shown in Fig.7 as a solid line. When we think that the waveform with the arrival time of S-wave corresponds to the source time function, this waveform shows the earthquake as a single event. As the area of the waveform resembles the seismic moment, the source time function in this figure has 0.66×10^{26} dynecm as the seismic moment. This result agrees with the given condition for analysis shown in Fig.7 as a dotted line. Further, the results of this procedure as applied to the synthetic body and surface waves calculated from the fault model with one event is shown in Fig.8. Its waveform is similar to the waveform shown in Fig.7 and the agreement between the seismic moment obtained in this case and given for analysis is better than in the body wave only.

The results in the case of multiple events are shown in Fig.9. There are two peaks in this source time function. The second peak is smaller than the first peak and the seismic moment of the second event is underestimated more than the given condition for analysis, but the total seismic moment is 0.68×10^{26} dynecm. The interval time between two events is longer than the given condition for analysis because of the Doppler effect. The location and the interval time between two events obtained by using the results at three observation points are shown in Fig.10. These results agree with the condition given for the fault model analysis shown in Table 1.

4. CONCLUSION

In order to obtain the strong ground motion estimation due to realistic earthquake faulting, it is necessary to clarify the source characteristics. In this paper, we propose the estimation method of the source time function with the observed ground motions. For the purpose of excluding the dynamic properties of the ground surface and the seismic wave path, we apply the AR model to the tail part of the observed ground motions. Further we apply this procedure to the synthetic waves calculated from the fault model in order to verify this method. As a result, the waveform obtained by using this method corresponds to the source time function of the seismic moment and these results agree with the condition given for the fault model analysis. It is pointed out that this analytical method using the AR model is available to estimate "earthquake input" for the dynamic response analysis of structures. From now, we plan to investigate in detail by applying this method to the observed ground motion with more complex source condition.

ACKNOWLEDGEMENT

We acknowledge Mr. Toshihide KASHIMA and Miss Yukie TAKASHIMA of Second Earthquake Engineering Division, International Institute of Seismology and Earthquake Engineering, Building Research Institute, Ministry of Construction, Japan kindly much help.

REFERENCES

(1) Y.Kitagawa, T.Inoue : Study on Source Time Function of Strong Ground Motion, Proc.7th J.E.E.S, pp.157-162, 1986, (in Japanese).
(2) M.Kikuchi : Inversion of Complex Body Waves, B.S.S.A, 72, 491, 1982.
(3) G.J.Nair : Estimation of Source Function and Medium Response Function by Autoregressive Method, Phys. Earth Planet. Inter., 32, pp.36-44, 1983.
(4) M.Tomizawa, T.Matsumura, T.Demizu : Synthesis of Three-Dimensional Earthquake Ground Motion by means of Time-Varying Autoregressive Model, Journal of Structural and Construction Engineering, No.349, pp.10-21, 1985, (in Japanese).
(5) T.Yokota, S.Zhou, M.Mizoue : An Automatic Measurement of Arraival Times of Seismic Waves and Its Application to an On-Line Processing System, Bull. Earthq. Res. Inst., Vol.56, pp.449-484, 1981, (in Japanese).
(6) H.Akaike : Fitting Autoregressive Models for Prediction, Ann. Inst. Statist. Math., Vol.21, pp.243-247, 1969.
(7) H.Sato, T.Sato, N.Yamada : Rupture Process of the May 26 1983 Japan Sea Earthquake as Inferred from Strong Motion Accelerograms. Programme Abstr. Seismol. Soc. Japan, No.2, pp.18, 1983 (in Japanese).
(8) K.Sudo, Y.Kitagawa, N.Yoshimura : Strong Motion Estimation due to Realistic Earthquake Faulting, 16th UJNR, 1984.

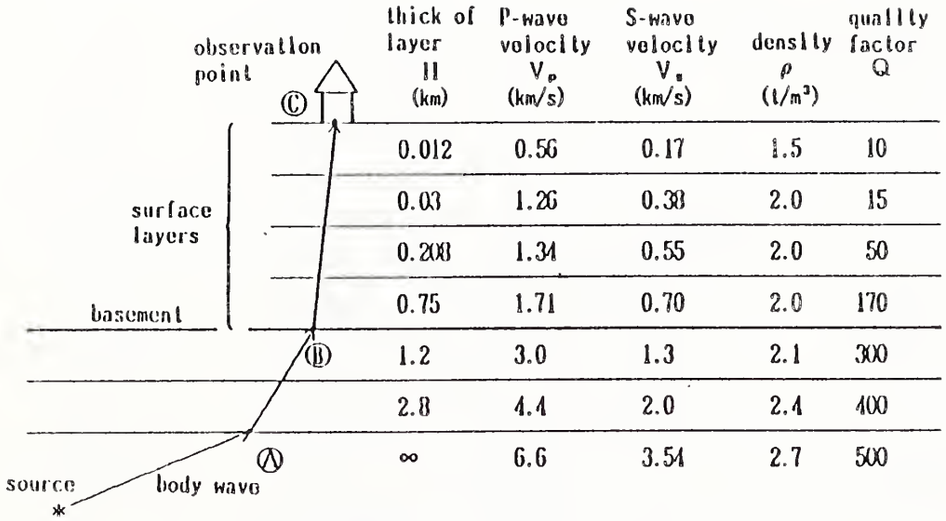

	thick of layer H (km)	P-wave velocity V_p (km/s)	S-wave velocity V_s (km/s)	density ρ (t/m³)	quality factor Q
	0.012	0.56	0.17	1.5	10
	0.03	1.26	0.38	2.0	15
	0.208	1.34	0.55	2.0	50
	0.75	1.71	0.70	2.0	170
Ⓑ	1.2	3.0	1.3	2.1	300
	2.8	4.4	2.0	2.4	400
Ⓐ	∞	6.6	3.54	2.7	500

Fig.1 Model of underground structure

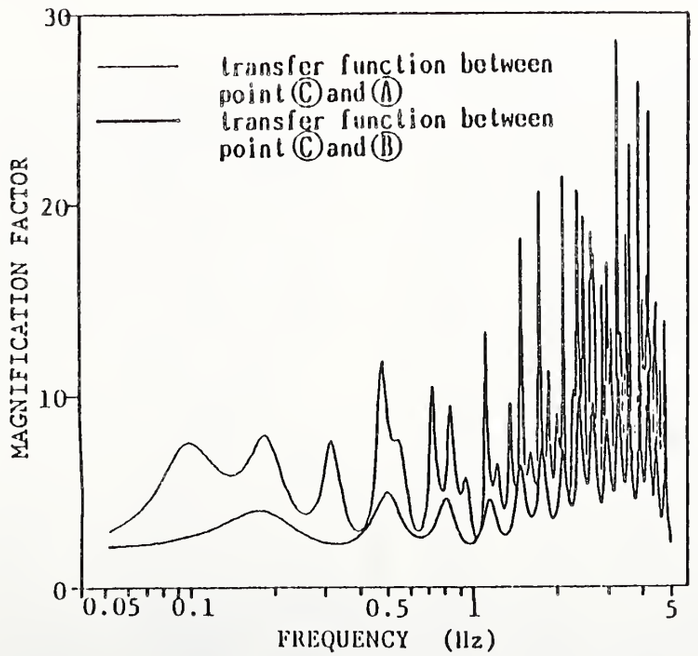

Fig.2 Transfer function of underground structure

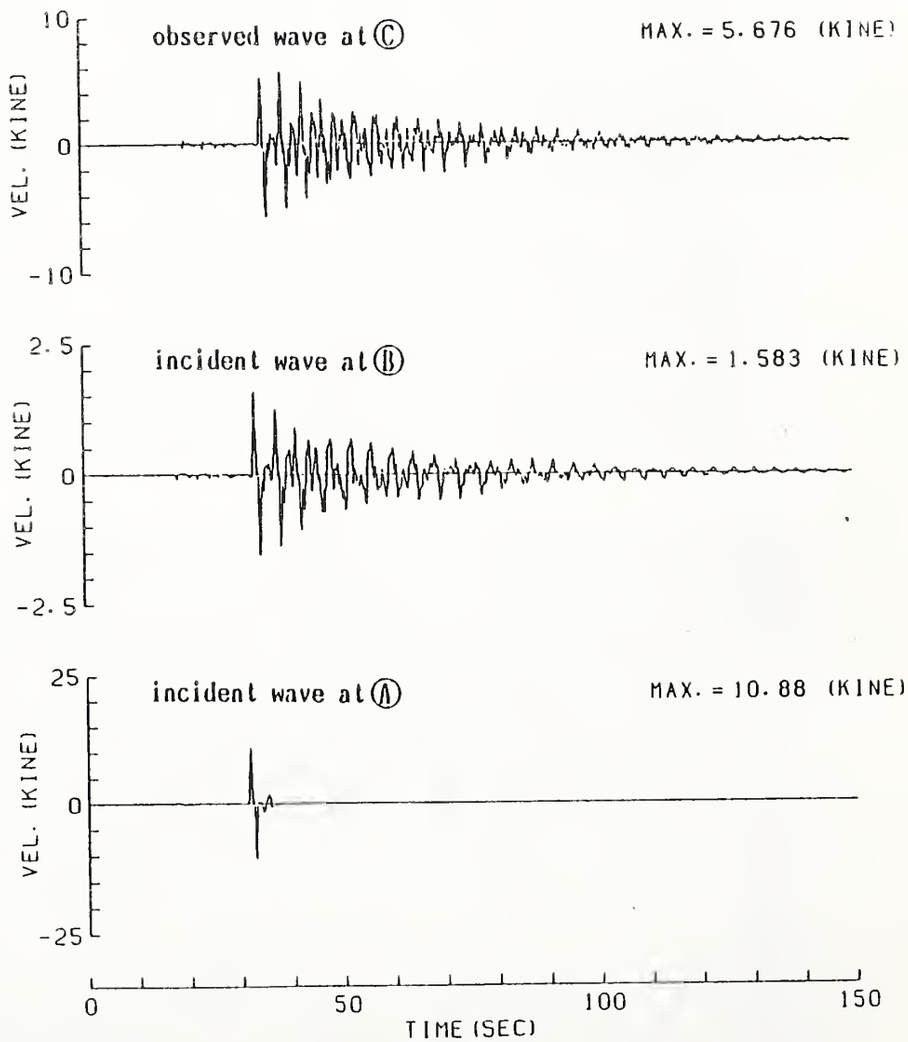

Fig.3 Observed waves calculated from fault model with one event

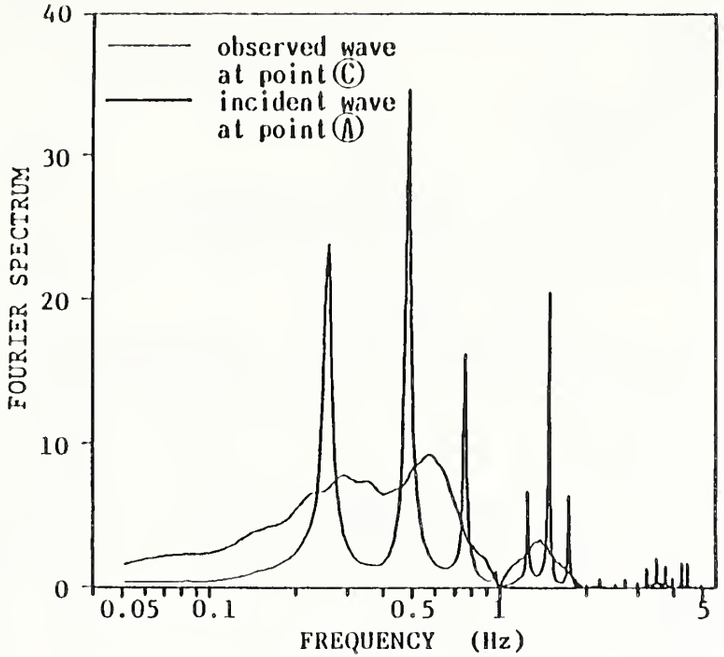

Fig.4 Fourier spectrum

Table 1 Fault parameters

seismic moment	1.0×10^{26}	(dyn cm)
focal depth	8	(km)
dip angle (δ)	100	(deg)
slip angle (λ)	170	(deg)
dislocation (D_0)	100	(cm)
strike	N 80 °W	
rise time	1.0	(sec)
fault length (L)	20	(km)
fault width (W)	10	(km)
rupture velocity	3.0	(km/sec)

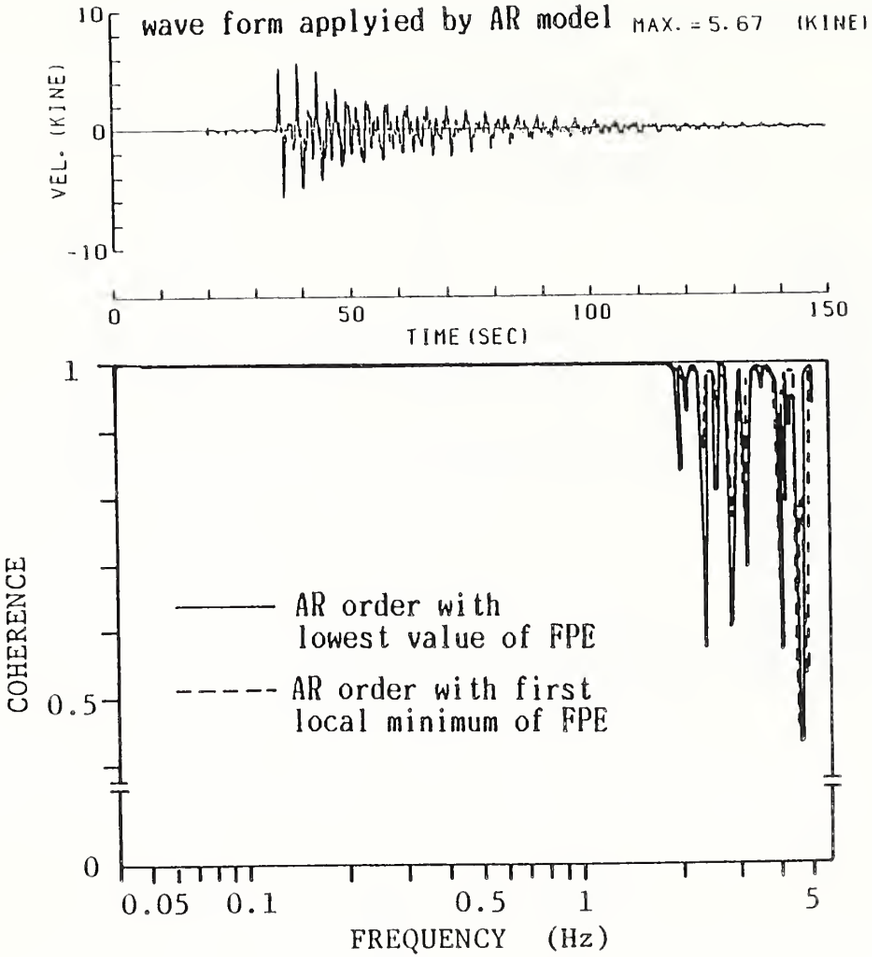

Fig.5 Coherence between observed waves and wave form applied by AR model

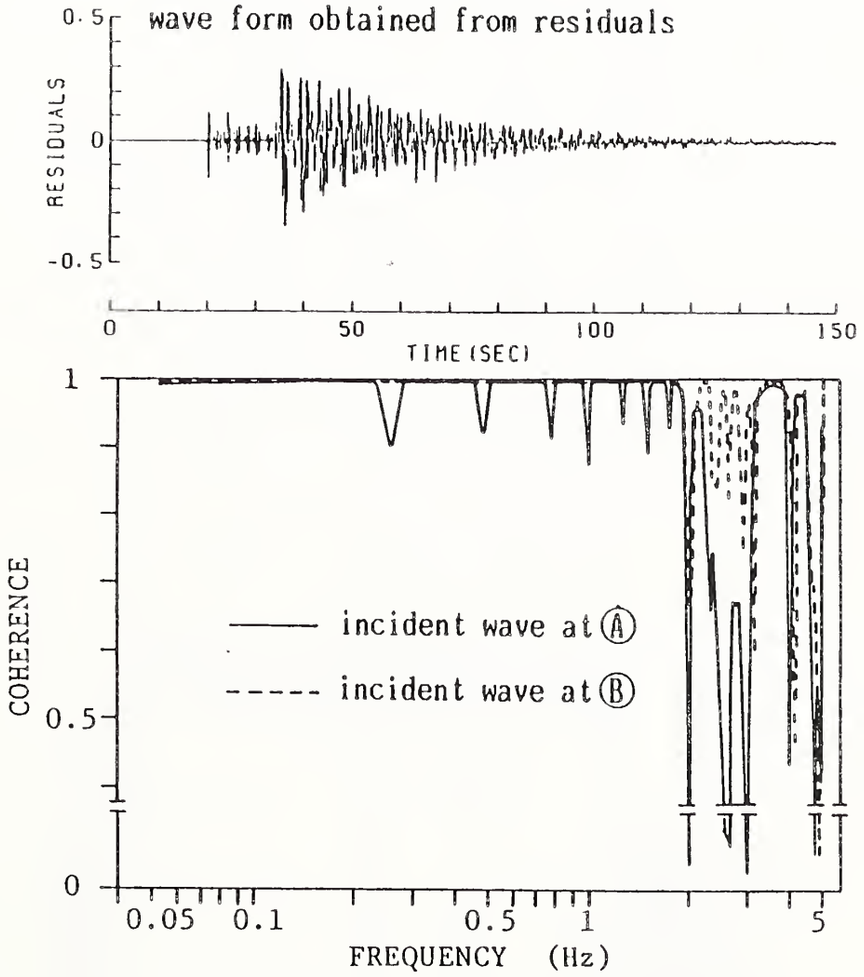

(a) Case of AR order with first local minimum of FPE

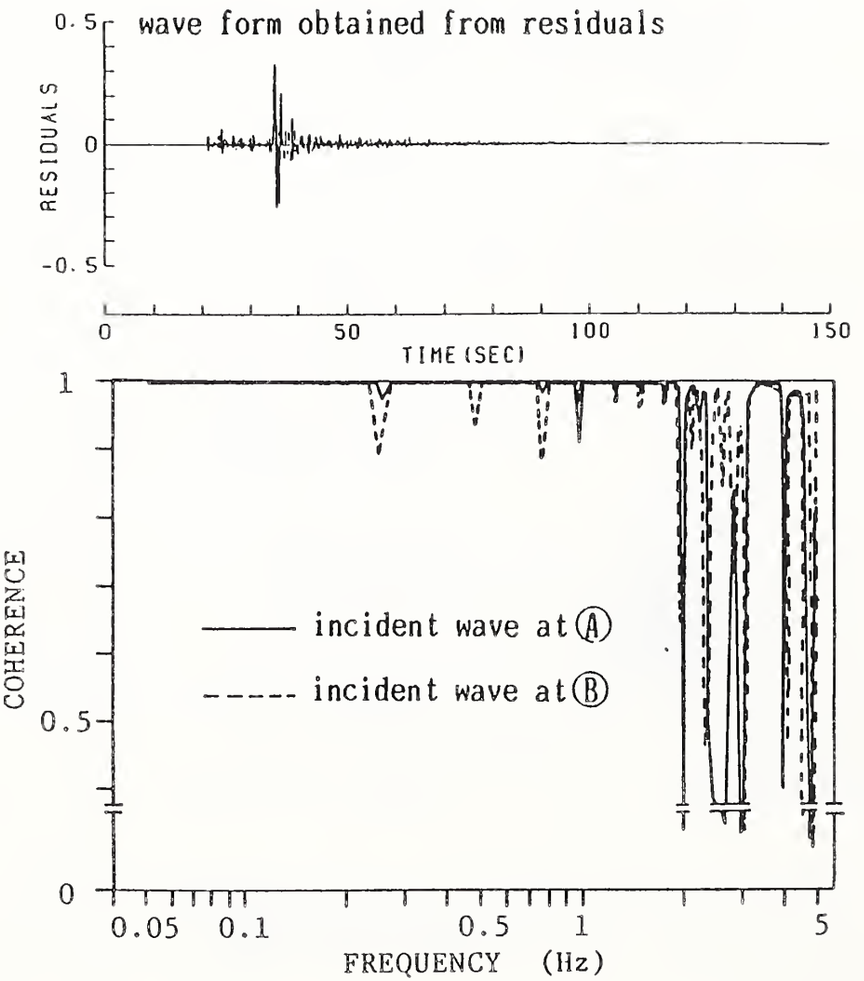

(b) Case of AR order with lowest value of FPE

Fig.6 Coherence between wave form obtained from residuals and incident waves

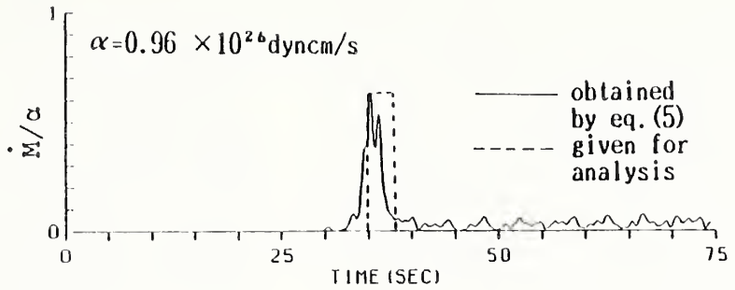

Fig.7 Source time function

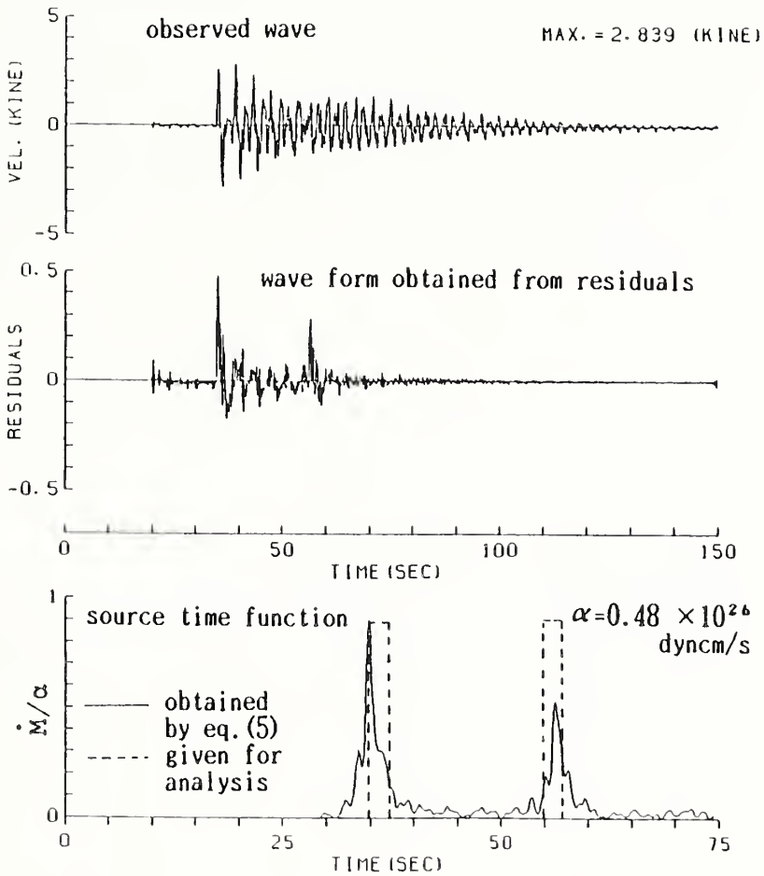

Fig.9 Results in case of two events

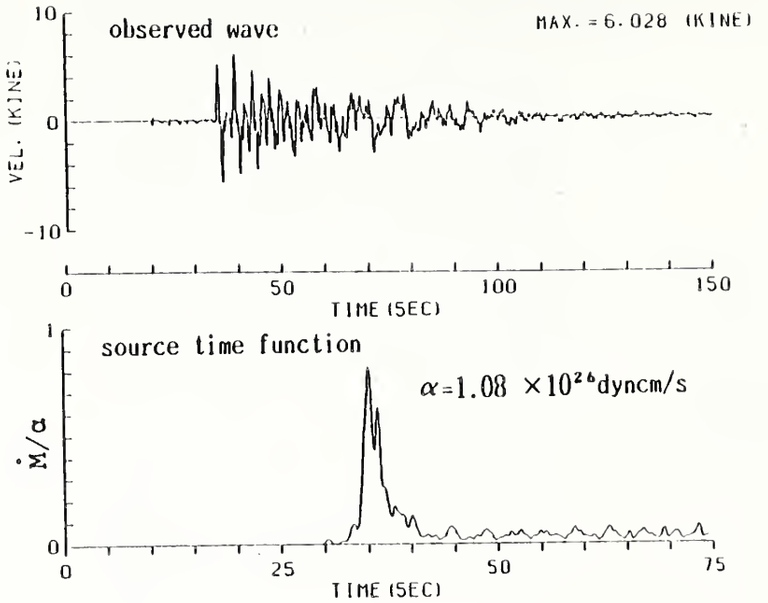

Fig.8 Results after considering body and surface waves with one event

DISTANCE AND INTERVAL TIME BETWEEN EVENTS

EVENT NO.	DISTANCE (km)	INTEVAL (sec)
1		
2	17	20

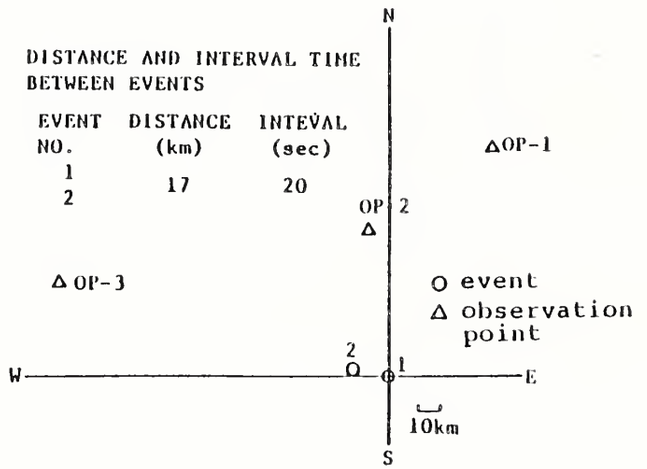

Fig.10 Location of events and observation points

Strong-Motion Instrumentation Program Corps of Engineers

by

F. K. Chang, R. F. Ballard, Jr., and A. G. Franklin[1]

ABSTRACT

The Corps of Engineers Strong-Motion Instrumentation Program was established in 1970 for the purposes of surveillance of seismic safety of Corps structures, provision of performance data, and provision of a data base for earthquake research. The program currently comprises 400 accelerographs, 14 seismic alarm devices, 56 seismoscopes, and 34 peak recording accelerographs at 114 Corps projects in 34 states and Puerto Rico. Responsibility for the program is assigned to the Waterways Experiment Station (WES); installation and maintenance operations are shared by the WES and the U.S. Geological Survey. Significant earthquake records have been obtained in the New Hampshire earthquake of 18 January 1982 and the Borah Peak, Idaho, earthquake of 28 October 1983.

KEYWORDS: Earthquakes; Dams; Instrumentation

1. HISTORICAL BACKGROUND

The Corps of Engineers (CE) Strong-Motion Instrumentation Program (SMIP) was established in 1970 with the primary purpose of surveillance of seismic safety of existing and future Corps structures, such as earth and rock-fill dams, concrete dams, and appurtenant structures. It was also intended to provide a measure of project performance, to provide design and performance comparisons, and to develop a data base for performance predictions and earthquake research. Responsibility for operation of the program was assigned to the U.S. Army Engineer Waterways Experiment Station (WES). Funding was, and continues to be, provided by the individual Corps of Engineer districts on whose projects the instruments are located.

In 1973, an agreement was made with the U. S. Geological Survey (USGS), under which the Seismic Engineering Branch of the USGS undertook the installation and maintenance of all Corps of Engineers (CE) strong-motion instruments. By 1978, the operations were overtaxing the resources of the USGS, and the arrangement was modified. The WES assumed responsibility for installation and maintenance of instruments in the eastern United States, which represents about half of the Corps' instruments. The USGS continues to maintain those instruments in the western United States.

2. GENERAL CRITERIA FOR DESIGN OF INSTRUMENT INSTALLATIONS

Selection of Dams to be Instrumented

General guidance on strong-motion instrument installations is given in the Corps of Engineers' Engineer Manual (EM) 1110-2-1908 (Department of the Army, 1976). In general, all dams in seismic risk zones 3 and 4 of the Seismic Risk Maps (Fig. 1) are required to be instrumented. In other zones, selection of dams to be instrumented takes into account the height, material type, and zoning of the embankment, the type of foundation, whether the embankment is founded on overburden, and the depth to rock. Also, the need for collection of basic data is a consideration. Where there is a likelihood of occurrence of earthquake shocks of sufficient intensity to give useful information, instrumentation is warranted. In questionable cases, the following additional rules are applied:

- Nature of Foundation - If the foundation materials underlying the dam are composed of sands or silty sands that might be subject to liquefaction, the dam should be instrumented.
- Type of Construction - Regardless of seismic risk zone, all hydraulic-fill dams should be instrumented. Rolled earth-fill or earth- and rock-fill dams, being less susceptible to liquefaction, are considered for instrumentation on the basis of other influencing factors.
- Height - Most dams that are more than 100 ft (30 m) high should be instrumented.
- Presence of Known Capable Faults - If the dam is located nearer than 25 miles (40 km) to a known capable fault, it should be instrumented.
- History of Seismic Activity at the Site - If acceleration levels greater than 0.2 g have been recorded in the vicinity of the dam, it should be instrumented.
- Distance from Higher Risk Zone Boundaries - If the dam is located less than 100 miles (160km) from a higher risk zone boundary, it should be instrumented.

[1] U.S. Army Engineer Waterways Experiment Station, Vicksburg, Mississippi

Design of Instrument Arrays

A typical instrument array includes three-component accelerographs at three locations: a free-field location, on the surface of the alluvium a short distance downstream of the dam; on the dam crest, near the center or at the highest section; and on an abutment. On a high dam, additional installations may be made at intermediate locations on the downstream face. Special site conditions may warrant additional free-field or abutment locations. On the other hand, some dams in areas of low seismic risk may have instruments at only one or two locations.

3. INSTRUMENTS USED

Instruments for measuring strong ground motions must be self-contained units. They must be equipped with self-starting devices that will be activated at a prescribed level of seismic activity, and then they must measure and record three components of motion for several minutes. Strong-motion instruments originally approved for use in the Corps' SMIP network included the RFT-250 and RFT-350 Strong-Motion Accelerographs, the SMA-1 Strong-Motion Accelerograph, the PRA-100 Peak Recording Accelerograph, and the Wilmot SR-100 Seismoscope. Manufacture of the RFT Accelerographs has since been discontinued, and those in the network will be replaced by SMA-1 Accelerographs.

Limited demand and controversy over their usefulness have prompted the manufacturers to cease production of the Wilmot Seismoscope. There are 56 seismoscopes still in operation in the network; they continue to be maintained but will eventually be phased out.

The RFT and SMA-1 accelerographs are analog type recorders. Since 1985, the Corps has installed eight DCA-333 digital accelerographs at R. D. Bailey (4 instruments), J. W. Flanagan (3) and Bluestone (1) dams of the Huntington District, Ohio River Division, for the purpose of evaluating their long-term reliability.

As a measure to minimize the need for on-site inspections after earthquakes, seismic alarm devices have been installed on several Corps structures. The seismic alarm device provides a warning when a preset threshold acceleration has been exceeded. The alarm package contains three vertical accelerometers with individual threshold levels commonly set at 0.05 g, 0.10 g, and 0.20 g. After an event, site personnel can readily determine if any of the three threshold levels were reached and how many times the level was exceeded. The alarm devices were designed and fabricated by WES.

4. PRESENT STATUS OF PROGRAM

As of 31 March 1987, the Corps of Engineers had in operation 400 accelerographs, 14 seismic alarm devices, 56 seismoscopes, and 34 peak recording accelerographs (PRA'S), at 119 projects located in 34 states and the Commonwealth of Puerto Rico. A map of instrumented projects is shown in Figure 2, and a tabulation of strong-motion instrumentation is given in Table 1.

5. SIGNIFICANT EARTHQUAKES RECORDED

New Hampshire Earthquake of 18 January 1982

The first instrumental earthquake records representative of seismic activity in the New England area were obtained as a result of the 18 January 1982 Franklin Falls, NH, 4.7 magnitude event, which occurred at latitude 43.5 degrees N, longitude 71.6 degrees W. Thirty-six accelerograms (components) were recorded, digitized, and analyzed (Chang, 1983). The transverse component of the accelerograph record located on the right abutment of Franklin Falls Dam (8 km from the epicenter) recorded a maximum acceleration of 0.55 g, which is the highest value of acceleration ever recorded in the eastern United States. The integrated maximum velocity is 5.59 cm/sec, which is very low in comparison with other earthquake records in the western United States or other earthquake regions.

Mount Borah, Idaho, Earthquake of 28 October 1983

During the M_s 7.3 Mt. Borah earthquake of 28 October 1983, which occurred at latitude 44.0 degrees N, longitude 113.9 degrees W, in central Idaho, nine meaningful strong-motion records (27 components) were recovered on three dams. These were Dworshak Dam (concrete, 330 km from epicenter, 1 record), Lucky Peak Dam (earth, 180 km, 3 records) and Ririe Dam (rock-fill, 179 km, 5 records). Minor damage to the intake structure at Ririe Dam was reported. An analysis of the records was reported by Chang (1985).

ACKNOWLEDGMENT

The tests described and the resulting data presented, unless otherwise noted, were obtained from research conducted under the Strong-Motion Instrumentation Program of the U. S. Army Corps of Engineers by the USAE Waterways Experiment Station. Permission was granted by the Chief of Engineers to publish this information.

REFERENCES

1. Chang, F. K., 1983. "Analysis of Strong-Motion Data from the New Hampshire Earthquake of 18 January 1982," NUREG/CR-3327, U. S. Nuclear Regulatory Commission, Washington, D. C. 20555

2. Chang, F. K., 1985. "Analysis of Strong-Motion Data from the Mount Borah, Idaho, Earthquake of 28 October 1983." Miscellaneous Paper GL-85-12, U.S. Army Engineer Waterways Experiment Station, Vicksburg, Mississippi 39180

3. Department of the Army, 1976. Engineer Manual 1110-2-1908, Instrumentation of Earth and Rock Fill Dams, Part 2 of 2, 19 Nov 1976. Office of the Chief of Engineers, Washington, D.C. 20314

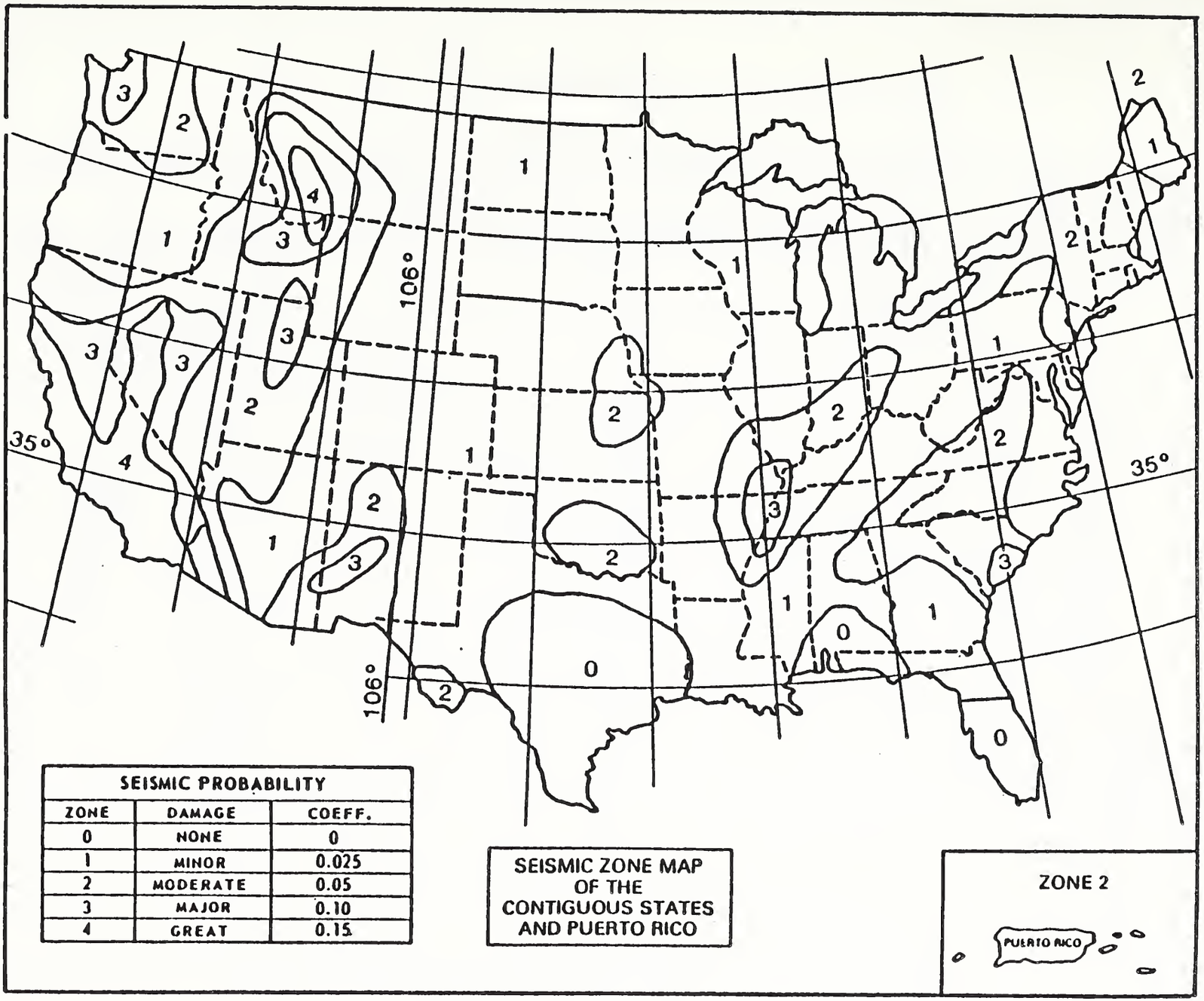

Figure 1. Seismic zone map of the contiguous United States and Puerto Rico

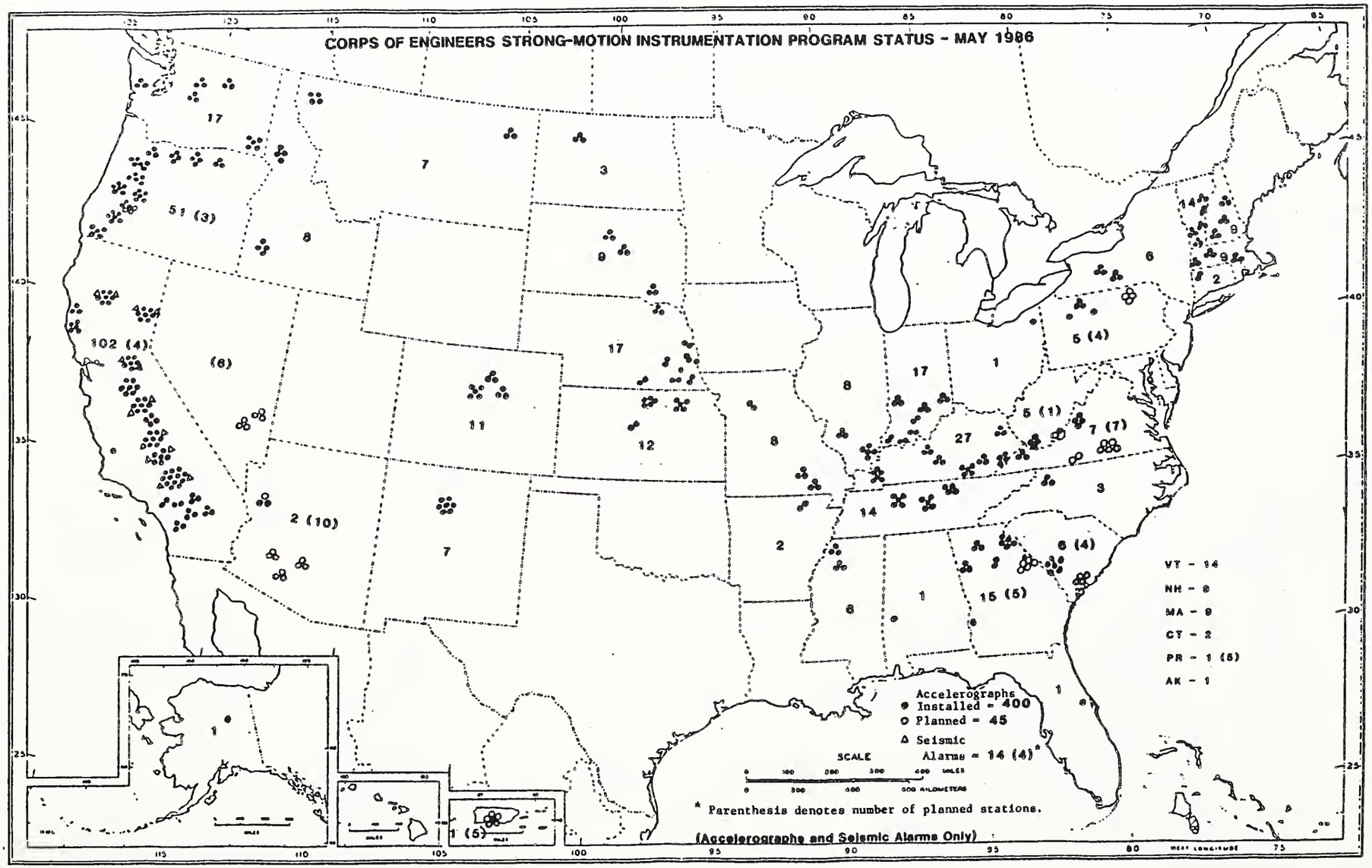

Figure 2. Corps of Engineers Strong-Motion Instrumentation Program Status -- May 1986

TABLE 1

CORPS OF ENGINEERS STRONG-MOTION INSTRUMENTATION PROGRAM STATUS - 31 MARCH 1987

Station No.	Division	District	Project	Type	H (m)	State	Accelerographs		Seismoscopes		Peak Accel.		Seismic Alarm Devices		Serviced By		Coordinates	
							Operational	Planned	Oper.	Plan.	Oper.	Plan.	Oper.	Plan.	USGS	WES	Lat. N	Long. W
	LMVD	St. Louis	Rend Lake	earth	17	IL	3 SMA-1	--	6	--	--	--	--	--	--	X	--	--
			Wappapello	earth	33	MO	3 SMA-1	--	6	--	--	--	--	--	--	X	--	--
	LMVD	Vicksburg	Arkabutla	earth	29	MS	3 SMA-1	--	5	--	--	--	--	--	--	X	--	--
			Sardis	earth	35	MS	3 SMA-1	--	5	--	--	--	--	--	--	X	--	--
	MRD	Kansas City	Harlan County	earth & gravity	32	NE	2 SMA-1	--	--	--	--	--	--	--	--	--	--	--
			Kanopolis	rock-fill	39	KS	2 SMA-1	--	--	--	--	--	--	--	--	--	--	--
			Milford	earth & rock-fill	43	KS	5 SMA-1	--	--	--	--	--	--	--	--	--	--	--
			Truman	earth	40	MO	2 SMA-1	--	--	--	--	--	--	--	--	--	--	--
			Tuttle Creek	earth	47	KS	5 SMA-1	--	--	--	--	--	--	--	--	--	--	--
2253 BCD	MRD	Omaha	Bear Creek	earth	17	CO	3 SMA-1	--	--	--	--	--	--	--	--	--	39.65	105.14
			Big Bend	earth	29	SD	3 SMA-1	--	--	--	--	--	--	--	--	--	--	--
2239 CCD			Cherry Creek	earth	58	CO	3 SMA-1	--	--	--	--	--	--	--	--	--	39.65	104.86
2238 CDD			Chatfield	earth	45	CO	5 SMA-1	--	--	--	--	--	--	--	--	--	39.56	105.06
			Fort Peck	earth	76	MT	3 SMA-1	--	--	--	--	--	--	--	--	--	--	--
			Fort Randall	--	50	SD	3 SMA-1	--	--	--	--	--	--	--	--	--	--	--
			Gavins Point	earth	23	NE	3 SMA-1	--	--	--	--	--	--	--	--	--	--	--
			Garrison	earth & gravel	62	ND	3 SMA-1	--	--	--	--	--	--	--	--	--	--	--
			Oahe	earth	75	SD	3 SMA-1	--	--	--	--	--	--	--	--	--	--	--
			Old Mill Area	rock	--	NE	1 SMA-1	--	--	--	--	--	--	--	--	--	--	--
			Papillion Creek 11	earth	20	NE	2 SMA-1	--	--	--	--	--	--	--	--	--	--	--
			Papillion Creek 20	earth	18	NE	2 SMA-1	--	--	--	--	--	--	--	--	--	--	--
			Salt Creek Dam 2	earth	14	NE	2 SMA-1	--	--	--	--	--	--	--	--	--	--	--
			Salt Creek Dam 17	earth	21	NE	2 SMA-1	--	--	--	--	--	--	--	--	--	--	--
			Salt Creek Dam 18	earth	17	NE	2 SMA-1	--	--	--	--	--	--	--	--	--	--	--
			Federal Bldg., Lincoln	(basement)	--	NE	1 SMA-1	--	--	--	--	--	--	--	--	--	--	--
	NAD	Baltimore	Arkport	earth	36	NY	3 SMA-1	--	--	--	4	--	--	--	--	X	--	--
			Tioga-Hammond	earth & rock-fill	--	PA	--	2 SMA-1	--	--	--	5	--	--	--	X	--	--
	NAD	Norfolk	Gathright	rock-fill	78	VA	2 SMA-1	--	2	--	--	--	--	--	--	X	--	--

(Continued)

TABLE 1 (Continued)

Station No.	Division	District	Project	Type	H (m)	State	Accelerographs Operational	Accelerographs Planned	Seismoscopes Oper.	Seismoscopes Plan.	Peak Accel. Oper.	Peak Accel. Plan.	Seismic Alarm Devices Oper.	Seismic Alarm Devices Plan.	Serviced By USGS	Serviced By WES	Coordinates Lat. N	Coordinates Long. W
	NCD	Buffalo	Mt. Morris	gravity	75	NY	3 SMA-1	--	2	--	--	--	--	--	--	X	--	--
	NED		Ball Mt. Lake	earth & rock	81	VT	3 SMA-1	--	--	--	1	--	--	--	--	X	--	--
			Colebrook R. Lake	earth & rock	66	CT	2 RFT-350	--	--	--	--	--	--	--	--	X	--	--
			Everett	earth	43	NH	3 SMA-1	--	--	--	--	--	--	--	--	X	--	--
			Franklin Falls	earth	54	NH	3 SMA-1	--	--	--	--	--	--	--	--	X	--	--
			Hodges Village	earth	18	MA	3 SMA-1	--	--	--	--	--	--	--	--	X	--	--
			Knightsville	earth	18	MA	3 SMA-1	--	--	--	--	--	--	--	--	X	--	--
			Littleville Lake	earth & rock	51	MA	2 RFT-350	--	--	--	--	--	--	--	--	X	--	--
			Littleville Lake				1 SMA-1									X		
			N. Hartland	earth	38	VT	2 SMA-1	--	--	--	--	--	--	--	--	X	--	--
			N. Springfield	earth	58	VT	3 SMA-1	--	--	--	--	--	--	--	--	X	--	--
			Surry Mt.	earth	28	NH	3 SMA-1	--	--	--	--	--	--	--	--	X	--	--
			Townsend Lake	earth	42	VT	3 SMA-1	--	--	--	--	--	--	--	--	X	--	--
			Union Village	earth	54	VT	3 SMA-1	--	--	--	--	--	--	--	--	X	--	--
	NPD	Portland	Applegate	gravity	74	OR	5 SMA-1	--	--	--	--	--	--	--	X	--	--	--
			Blue River	earth & rock	83	OR	5 SMA-1	--	--	--	--	--	--	--	X	--	--	--
			Bonneville	gravity	60	OR	3 SMA-1	3 SMA-1	--	--	--	--	--	--	X	--	--	--
			Cougar	rock-fill	158	OR	6 SMA-1	--	--	--	--	--	--	--	X	--	--	--
			Dalles L&D	--	40	OR	4 SMA-1	--	--	--	--	--	--	--	X	--	--	--
			Detroit	concrete	137	OR	3 SMA-1	--	--	--	--	--	--	--	X	--	--	--
			Green Peter	concrete	100	OR	2 RFT-350	--	5	--	--	--	--	--	X	--	--	--
			Green Peter				1 SMA-1								X			
			Hills Creek	earth & gravel	93	OR	3 SMA-1	--	--	--	--	--	--	--	X	--	--	--
			John Day L&D		43	OR	4 SMA-1	--	--	--	--	--	--	--	X	--	--	--
			Lookout Point	gravel fill	83	OR	6 SMA-1	--	--	--	--	--	--	--	X	--	--	--
			Lost Creek	earth	104	OR	6 RFT-350	--	--	--	--	--	--	--	X	--	--	--
			Willow Creek	concrete	52	OR	3 SMA-1	--	--	--	--	--	--	--	X	--	--	--
	NPO	Seattle	Chief Joseph	concrete	70	WA	3 SMA-1	--	--	--	--	--	--	--	X	--	--	--
			Howard Hanson	rock-fill	72	WA	3 SMA-1	--	--	--	--	--	--	--	X	--	--	--
			Libby	gravity	136	MT	4 RFT-250	--	--	--	--	--	--	--	X	--	--	--
			Mud Mountain	earth	130	WA	3 SMA-1	--	--	--	--	--	--	--	X	--	--	--
			Wynoochee	concrete	55	WA	3 SMA-1	--	--	--	--	--	--	--	X	--	--	--

(Continued)

TABLE 1 (Continued)

Station No.	Division	District	Project	Type	H (m)	State	Accelerographs Operational	Accelerographs Planned	Seismoscopes Oper.	Seismoscopes Plan.	Peak Accel. Oper.	Peak Accel. Plan.	Seismic Alarm Devices Oper.	Seismic Alarm Devices Plan.	Serviced By USGS	Serviced By WES	Coordinates Lat. N	Coordinates Long. W
2222 DWD	NPD	Walla Walla	Dworshak	concrete	219	IO	4 SMA-1	--	--	--	--	6	--	--	X	--	46.52	116.29
			Lower Granite	earth & gravity	78	WA	5 SMA-1	--	--	--	--	5	--	--	X	--	--	--
			Lucky Peak	earth	104	IO	4 SMA-1	--	--	--	--	--	--	--	X	--	--	--
2767 MCD	NPD	Alaska	Moose Creek, L. Gallery	rock-fill	40	AK	1 SMA-1	--	--	--	--	--	--	--	X	--	64.79	147.18
	ORD	Huntington	Bluestone	concrete	50	WV	1 OCA-31	1 OCA-33	--	--	--	--	--	--	--	X	--	--
			J. W. Flanagan	earth & rock-fill	76	VA	3 OCA-31	--	--	--	--	--	--	--	--	X	--	--
			R. D. Bailey	rock-fill	94	WV	4 OCA-33	--	--	--	--	--	--	--	--	X	--	--
	ORD	Louisville	Brookville	earth & rock-fill	55	IN	3 SMA-1	--	--	--	1	--	--	--	--	X	--	--
			Cagles Mill	earth	45	IN	1 RFT-350	--	--	--	1	--	--	--	--	X	--	--
			Cagles Mill				2 SMA-1									X		
			Cannelton L&O	concrete	47	IN	2 SMA-1	--	--	--	1	--	--	--	--	X	--	--
			Monroe	earth & rock-fill	28	IN	3 SMA-1	--	--	--	1	--	--	--	--	X	--	--
			Newburgh L&O	concrete	33	IN	2 SMA-1	--	--	--	1	--	--	--	--	X	--	--
			Nolin River	earth & rockfill	50	KY	3 SMA-1	--	--	--	1	--	--	--	--	X	--	--
			Patoka	earth & rockfill	26	IN	2 RFT-350	--	--	--	1	--	--	--	--	X	--	--
			Rough River	earth & rockfill	45	KY	3 SMA-1	--	--	--	1	--	--	--	--	X	--	--
			Smithland L&O	concrete	24	IL	2 RFT-350	--	--	--	2	--	--	--	--	X	--	--
			Smithland L&D				3 SMA-1									X		
			Taylorsville	earth & rock-fill	44	KY	3 SMA-1	--	--	--	1	--	--	--	--	X	--	--
			Uniontown L&O	concrete	16	IN	2 SMA-1	--	--	--	1	--	--	--	--	X	--	--
	ORD	Nashville	Barkley	earth & gravity	48	KY	6 SMA-1	--	2	--	1	--	--	--	--	X	--	--
			Center Hill	earth & concrete	76	TN	5 SMA-1	--	2	--	1	--	--	--	--	X	--	--
			Dale Hollow	gravity	61	TN	4 SMA-1	--	2	--	1	--	--	--	--	X	--	--
			J. Percy Priest	earth & concrete	40	TN	5 SMA-1	--	2	--	1	--	--	--	--	X	--	--
			Laurel River	rock-fill	86	KY	3 SMA-1	--	--	--	1	--	--	--	--	X	--	--
			Martin's Fork	concrete	30	KY	4 SMA-1	--	--	--	2	--	--	--	--	X	--	--
			Wolf Creek	earth & concrete	79	KY	5 SMA-1	--	2	--	1	--	--	--	--	X	--	--
	ORD	Pittsburgh	East Branch	earth	56	PA	1 SMA-1	--	--	--	--	--	--	--	--	X	--	--
			Kinzua	earth & gravity	55	PA	3 SMA-1	--	--	--	--	--	--	--	--	X	--	--
			Michael J. Kirwan	earth	25	OH	1 SMA-1	--	--	--	--	--	--	--	--	X	--	--
			Tionesta	earth	47	PA	1 SMA-1	--	--	--	--	--	--	--	--	X	--	--

(Continued)

TABLE 1 (Continued)

Station No.	Division	District	Project	Type	H (m)	State	Accelerographs		Seismoscopes		Peak Accel.		Seismic Alarm Devices		Serviced By		Coordinates	
							Operational	Planned	Oper.	Plan.	Oper.	Plan.	Oper.	Plan.	USGS	WES	Lat. N	Long. W
	SAD	Charleston	Cooper River Rediversion	--	--	SC	--	4 SMA-1	--	--	--	1	--	--	--	X	--	--
2519 BKL	SAD	Jacksonville	Buckman Lock	concrete	15	FL	1 SMA-1	--	--	--	--	--	--	--	--	X	28.51	81.71
			Cerrillos	--	--	PR	1 SMA-1	5 SMA-1	--	--	--	--	--	--	X		--	--
2533 ALO	SAD	Mobile	Allatoona	arch-gravity concrete	66	GA	3 SMA-1	--	--	--	--	--	--	--	--	X	34.163	84.728
2534 BUD			Buford	earth	70	GA	2 SMA-1	--	--	--	--	--	--	--	--	X	34.160	84.074
2537 CRD			Carters	earth & rock-fill	136	GA	3 SMA-1	--	--	--	--	--	--	--	--	X	--	--
			Coffeeville	earth & gravity	27	AL	1 SMA-1	--	--	--	--	--	--	--	--	X	--	--
2537 GLO			Walter F. George Lock & Dam	earth & gravity	45	GA	1 SMA-1	--	--	--	--	--	--	--	--	X	--	--
	SAD	Savannah	Clark Hill	concrete & earth	61	SC	6 SMA-1	--	2	--	2	--	--	--	--	X	--	--
2526 HWD			Hartwell	concrete & earth	73	GA	5 SMA-1	--	1	--	2	--	--	--	--	X	34.35	82.81
2536 RRD			R. B. Russell	concrete & earth	73	GA	1 RFT-350	5 SMA-1	--	--	--	1	--	--	--	X	34.054	82.622
	SAD	Wilmington	John H. Kerr	--	--	VA	--	5 SMA-1	--	--	--	--	--	--	--	X	--	--
			Philpott	--	--	VA	--	2 SMA-1	--	--	--	--	--	--	--	X	--	--
			W. Kerr Scott	earth	45	NC	3 RFT-350	--	2	--	1	--	--	--	--	X	--	--
2301 ADD	SPD	Los Angeles	Alamo	earth	86	AZ	2 SMA-1	1 SMA-1	2	--	--	--	--	--	X	--	34.23	113.60
951 BAD			Brea	earth	27	CA	3 SMA-1	--	--	--	--	--	--	--	X	--	33.89	117.93
108 CND			Carbon Canyon	earth	30	CA	3 SMA-1	--	--	--	--	--	--	--	X	--	33.92	117.84
			Mathews Canyon	--	--	NV	--	3 SMA-1	--	--	--	--	--	--	--	--	--	--
			Painted Rock	--	--	AZ	--	3 SMA-1	--	--	--	--	--	--	--	--	--	--
			Pine Canyon	--	--	NV	--	3 SMA-1	--	--	--	--	--	--	--	--	--	--
969 PRD			Prado	earth	37	CA	3 SMA-1	--	--	--	--	--	--	--	X	--	33.89	117.64
1064 SSD			Salinas	concrete, shale & sandstone fdn.	41	CA	1 SMA-1	--	--	--	--	--	--	--	X	--	35.34	120.50
287 SDD			San Antonio	earth, rock fdn.	49	CA	3 SMA-1	--	--	--	--	--	--	--	X	--	34.17	117.68
949 SPD			Sepulveda	earth	17	CA	2 SMA-1	--	--	--	--	--	--	--	X	--	34.17	118.47
			Tat Momolikot	--	--	AZ	--	3 SMA-1	--	--	--	--	--	--	--	--	--	--
			Whitlow Ranch	--	--	AZ	--	3 SMA-1	--	--	--	--	--	--	--	--	--	--
289 WND			Whittier Narrows	earth	17	CA	2 SMA-1	--	--	--	--	--	--	--	X	--	34.03	118.05

(Continued)

TABLE 1 (Concluded)

Station No.	Division	District	Project	Type	H (m)	State	Accelerographs Operational	Accelerographs Planned	Seismoscopes Oper.	Seismoscopes Plan.	Peak Accel. Oper.	Peak Accel. Plan.	Seismic Alarm Devices Oper.	Seismic Alarm Devices Plan.	Serviced By USGS	Serviced By WES	Coordinates Lat. N	Coordinates Long. W
1010 BKO	SPO	Sacramento	Black Butte	earth	43	CA	2 RFT-250	--	--	--	--	--	2	--	X	--	39.82	122.34
			Black Butte				2 RFT-350								X			
			Black Butte				3 SMA-1								X			
1450 BNO			Buchanan	rock-fill	62	CA	7 SMA-1	--	--	--	--	--	--	--	X	--	37.22	119.98
1017 CYO			Coyote	earth	50	CA	3 RFT-250	--	--	--	--	--	--	2	X	--	39.20	123.18
			Hidden	earth	50	CA	7 SMA-1	--	--	--	--	--	2	--	X	--	--	--
1035 ISO			Isabella	earth	56	CA	5 RFT-250	--	--	--	--	--	2	--	X	--	35.65	118.47
			Isabella				1 RFT-350								X			
			Isabella				6 SMA-1								X			
1484 LSQ			Lake Success	earth	43	CA	6 SMA-1	--	--	--	--	--	2		X	--	36.061	118.92
1133 MKD			Martis Creek	earth fill	35	CA	7 SMA-1	--	--	--	--	--	2	--	X	--	39.326	120.115
1047 NGO			New Hogan	earth & rock	64	CA	2 RFT-250	--	--	--	--	--	2	--	X	--	38.15	120.81
			New Hogan				1 RFT-350								X			
			New Hogan				3 SMA-1								X			
1054 PFO			Pine Flat	concrete	131	CA	3 RFT-250	--	--	--	--	--	--	--	X	--	36.83	119.33
			Pine Flat				1 RFT-350								X			
1098 TMO			Terminus	earth	76	CA	3 RFT-250	--	--	--	--	--	2	--	X	--	36.41	119.00
			Terminus				1 RFT-350	--	--	--	--	--	--	--	X	--	--	--
			Terminus				3 SMA-1	--	--	--	--	--	--	--	X	--	--	--
1216 WSO			Warm Springs	earth	97	CA	5 SMA-1	--	--	--	4	--	--	2	X	--	38.720	123.004
	SWO	Alburquerque	Cochiti	earth	77	NM	7 SMA-1	--	8	--	--	--	--	--	X	--	--	--
	SWO	Little Rock	Clearwater	earth	46	MO	3 SMA-1	--	--	--	--	--	--	--	--	X	--	--
			Norfolk	concrete	71	AR	2 SMA-1	--	--	--	--	--	--	--	--	X	--	--
					TOTAL		400	43	56	0	34	18	14	4				

Comparisons of Dynamic Shear Strength Between Fine Sands and Gravels

By

Norihisa MATSUMOTO[1], Nario YASUDA[2]
Masahiko OHKUBO[3], Shoji ARAKAWA[4]

ABSTRACT

In this paper dynamic shear strength or liquefaction strength of rockfill materials has been investigated by using the large-scale cyclic triaxial testing equipment. The size of saturated columnar specimen is 30-cm in diameter and 60-cm long. The grain size ranges from 0.42mm to 63.5mm.

Tests for twelve specimens of rockfill materials were performed by using the above mentioned equipment in order to study the effects of gradation and density of the materials on the dynamic shear strength.

The followings results are obtained on the dynamic strength of the coarse grained granular materials.

1) The specimen of higher relative density indicates the higher strength against liquefaction in the case of the same grain size distribution.
2) The well graded materials can resist to the cyclic shear stress better than the materials which have smaller uniformity coefficient and the same relative density.
3) The coarse grained materials are stronger against liqueifaction than fine sands.

KEYWARDS: Dynamic Strength, Coarse Grained Granular Materials, Undrained Shear Test

1. INTRODUCTION

A lot of research works have been accumulated on the liquefaction or strength loss of sands during earthquakes. However, available test data of dynamic shear strength for coarse grained granular materials are very limited because the particle size contained in the materials is large and hence the large-scale testing equipment is required.

The authors have developed the large-scale cyclic triaxial testing equipment at Public Works Research Institute of Ministry of Construction to obtain dynamic deformation properties and dynamic shear strength for rockfill materials.

This paper, therefore, describes the test results of effects of grain size distribution and relative density on the dynamic shear strength of saturated rock-fill materials under undrained test condition.

2. GENERAL DESCRIPTION OF TEST

2.1 Large-scale Triaxial Test Equipment

The equipment used for this study is capable of testing 30-cm diameter, 60-cm long specimens. The main features of performances are shown in Table 1. Fig. 1 illustrates the equipment. Friction between loading rod and bearing is minimized by using a ball bearing. The cyclic axial loads are applied by using an electro-hydraulic servo valve. Hydraulic pressure ranges from 120kg f/cm^2 to 180kg f/cm^2. The maximum cyclic frequency is 10Hz for an axial load and 5Hz for an confining pressure.

The two separated sensors shown in Fig. 1, each of which is disk-shaped coil, are used as a displacement transducer for measuring the small range of displacement for the dynamic deformation test. However, the differential-type displacement transducer attached to the outside of a triaxial cell is used in these liquefaction tests.

2.2 Preparation of Specimens and Test Condition

The cyclic triaxial tests (liquefaction test) in this study were performed on rock-fill materials for Sagae Dam which is now under construction in northern part of Japan by the Ministry of Construction. The quality of rock materials consists of mainly dolerite containing pegmatite partially.

Some physical properties of rock materials are shown in Table 2. The grain size distributions of the specimens are illustrated in Fig. 2. Two different gradation curves are adopted and the uniformity coefficient is 12 for A-sample and 7 for B-sample. The maximum particle size of the specimen is 63.5mm, which is less than 1/5 of the diameter of the specimen. This ratio is borrowed from a maximum allowable ratio for the static triaxial tests.

---

1) Dr. of Eng., Head, Filldams Section, Dam Department Public Works Research Institute, Ministry of Construction, Japan
2) Research Engineer, Filldams Section, Dam Department Public Works Research Institute, Japan
3) Engineer, Filldams Section, Dam Department Public Works Research Institute, Japan
4) Research Engineer, Filldams Section, Dam Department Public Works Research Institute, Japan

The materials were placed in six layers, and each layer was compacted with the 33kg f weight electric vibratory rammer which has 950 compaction blows per minutes. The test density was determined from the compaction tests so that relative densities of the materials should be 60, 80, 97% in each gradation.

The procedures of cyclic triaxial tests are as follows

1) The confining pressure of 0.2kg f/cm^2 is applied to the specimen (30-cm in diamater and 60-cm high) and then the vacuum pressure inside the specimen is released.
2) Carbon dioxide (CO_2) of 0.05 kg f/cm^2 pressure is supplied to the specimen for 24 hours in order to fill the air void completely with CO_2 because CO_2 is much easier to dissolve in water than air.
3) After the completion of replacement of air by CO_2, de-aired water of 70 liters is supplied to the sample for 24 hours.
4) Saturation degree of the specimen is investigated by Skempton's B-value and test is carried out about the specimen which B-value is more than 0.96.
5) The burette of 1,000 cc is used for measuring volume change of the sample during the consolidation of about 45 minutes.

The cyclic undrained test is carried out under load-controlled condition of 0.2Hz. The specimen is subjected to the back pressure of 2.0kg f/cm^2 and the confining pressure of 4.0kg f/cm^2, resulting in the effective confining pressure of 2.0 kg f/cm^2.

Shear stress ratio R1 is expressed as the followings

$$R1 = \frac{\tau}{\sigma_{c'}} = \frac{\sigma_d}{2\sigma_{c'}} \quad \cdots\cdots \quad 1)$$

where τ ; cyclic shear stress
σ_d ; cyclic deviatoric stress (single amplitude)
$\sigma_{c'}$; effective confining pressure

The specimen of Toyoura standard sand also prepared after the same manner of coarse grained granural materials.

The digitized test results are recorded by a personal computer through the low-pass filter of 1.0Hz by which the noise is deleted from the measured data. The data aquisition system of the experiment is indicated in Fig.3.

3. TEST RESULTS

Shear stress ratio of cyclic tests ranges from 0.3 to 0.7. This range of values is determined from the dynamic non-linear analysis of 100m high rockfill dam F.E.M. model. Two types of earthquake motions are chosen as an input motion in which maximum acceleration is 250 gals and 350 gals each. The shear stress ratio of whole elements ranges from 0.01 to 1.0 for the former motion and from 0.1 to 0.7 for latter one. The shear stress ratio has a tendency to increase near the slope surface.

Tested results are listed in Table 3. Falling head permeability tests are performed after the saturation of specimens and the permeability coefficients of $2\sim6\times10^{-3}$ cm/sec are observed. Distinct relations were not observed between the permeability and the gradation or the relative density of a specimen.

Typical time histories of load. axial strain and pore water pressure are shown in Fig. 4. Initial relative density of a sample is 97% and shear stress ratio is 0.35. Cyclic frequency of 0.2Hz is determined from the capacity of cyclic triaxial equipment. Fig. 5 is a stress path by axial stress and pore water pressure.

Fig. 6 shows initial liquefaction potential defined as the number when the effective confining pressure becomes 0kg f/cm^2 for the first time The higher the relative density becomes, the larger the number of liquefaction is for A-samples. From this diagram coarse grained granular materials also indicate the liquefaction curves similar to the sands but are much stronger than sands against the same shear stress ratio.

The results of B-samples are also plotted in this figure. B-samples can be liquefied in early stage compared to A-samples for the same relative density at two different levels of about 70% and 90% (see Fig. 7).

Disregarding the rubber membrane penetration to the void of a specimen can lead to the under-estimation of liquefaction potentials. Therefore in the case of the sample of low uniformity coefficient like B-sample, the tested result shows weaker liquefaction strength than real one. Crush of the particle is another reason for low strength of B-sample. Rockfill materials used in this study is easily crushed so B-sample, which uniformity coefficient is smaller than that of A-sample, caused larger volume change by cyclic loads.

The test results of Toyoura standard sand are plotted together in Fig. 7. The relative density ranges from 50% to 80%. It is noticed that coarse grained materials is stronger against liqueifaction than fine sands .

The process of pore water pressure build-up in the specimen is illustrated in Fig. 8. The increase of pore water pressure occurs rather in early stage of liquefaction and gradually approach to zero effective confining pressure for both A-sample and B-sample. Compared to sands, which line is also shown in Fig. 8, the pre pressure build-up of coarse grained granular materials occurs at the early stage of cycles.

The authors plan to investigate the effect of the quality and grain size distributions of rockfill materials on liquefaction potential. And further studies are also required for the dissipation of excess pore pressures to evaluate the safety of rockfill dams subjected to earthquake shaking.

4. CONCLUSIONS

From the previous considerations thae followings can be concluded on the dynamic strength of the coarse grained granular materials.

1) The specimen of higher relative density indicates the higher strength against liquefaction in the case of the same grain size distribution.

2) The well graded materials can resist to the cyclic shear stress better than the materials which have smaller uniformity coefficient and the same relative density.
3) The coarse grained materials are stronger against liqueifaction than fine sands.

Note: This report is based on "N. MATSUMOTO, et. al. –DYNAMIC SHEAR STRENGTH OF COARSE GRAINED GRANULAR MATERIALS, INTERNATIONAL SYMPOSIUM ON EARTHQUAKE & DAMS, 20, MAY, 1987; BEIJING, CHINA".

REFERENCE

1) N. Matsumoto, N. Yasuda, M. Ohkubo – Dynamic Shear Modulus, Damping Ratio, and Poisson's Ratio of Coarse Grained Granular Materials, Vol. 28, No. 11, 1986, Civil Engineering Journal, Japan

TABLE 1

Main features of performances

Specimen size	ϕ30cm x h60cm
Control system	Electro-Hydraulic-Servo
Wave form	Sinusoidal, triangular, and earthquake waves
Axial loading	Maximum loading capacity compression – 20 tf
	Maximum loading capacity extension – 10 tf
	Frequency range 0.2 – 10 Hz
Confining pressure	Max. 15 kgf/cm^2
	Frequency range 0.2 – 5 Hz

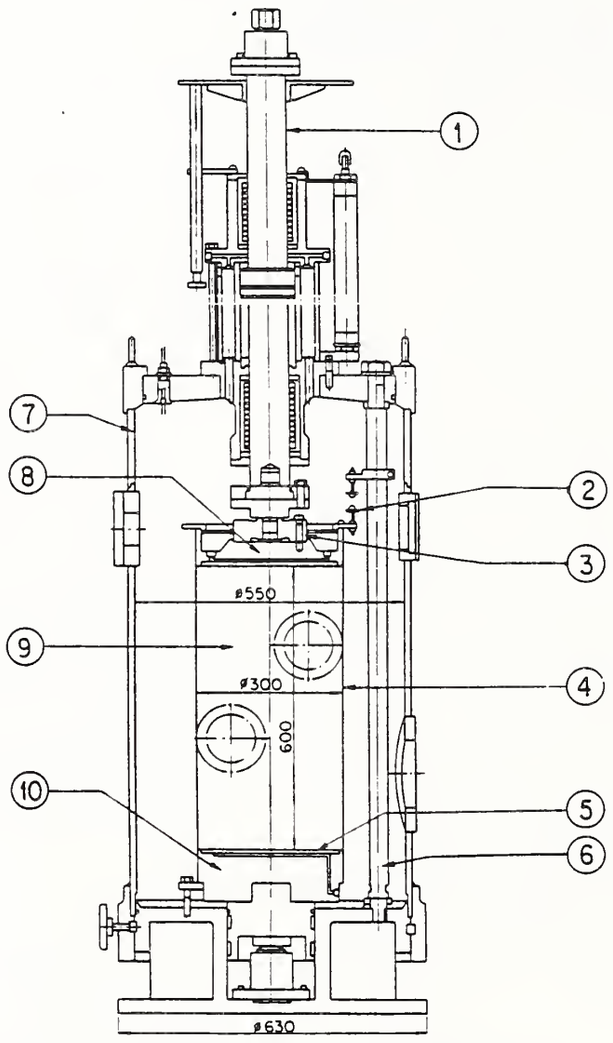

Fig. 1 Cyclic triaxial testing equipment

1. Loading rod
2. Gap sensor
3. Lord cell (Extension & Compression)
4. Rubber membrane
5. Porus metal disk
6. Support
7. Triaxial Cell
8. Loading cap
9. Specimen
10. Pedestal

Table 2 Physical Properties of Materials

		Gravel	Sand
Spefific gravity	Gs	2.509	2.644
Water content	W	2.44 (%) Air-dry	–
Maximum void ratio	e_{max}	0.563	0.905
Minimum void ratio	e_{min}	0.182	0.595
Maximum grain size	d_{max}	63.5 mm	0.42
Coefficient of uniformity	Vc	12 (7)	1.36
Dry density of specimen	r_d	2.024 gf/cm^3	1.538

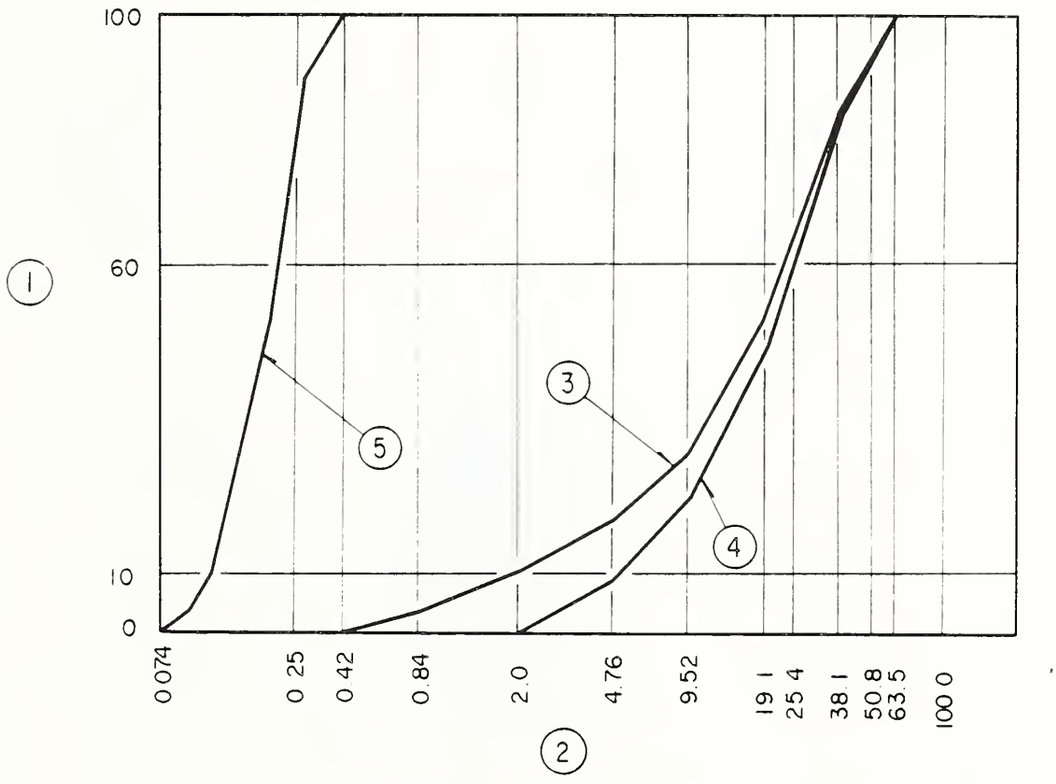

Fig. 2 Grain size distribution curve

1. Percent passing (%)
2. Grain size (mm)
3. A-sample (No. 1 – No. 9)
4. B-sample (No. 10 – No. 12)
5. Standard sand

Table 3 Tested Cases

No. of sample	τ/σ_c'	Dro (%)	e_c	e_{max}	e_{min}	(1) ($\times 10^{-3}$)
1	0.32	60	0.338	0.552	0.248	6.04
2	0.48	60	0.340	"	"	3.10
3	0.65	60	0.345	"	"	4.25
4	0.35	80	0.289	"	"	4.82
5	0.51	80	0.292	"	"	2.46
6	0.67	80	0.288	"	"	5.86
7	0.35	97	0.243	"	"	3.52
8	0.52	97	0.247	"	"	5.54
9	0.68	97	0.245	"	"	2.20
10	0.34	60	0.415	0.669	0.326	5.57
11	0.35	80	0.361	"	"	3.35
12	0.35	97	0.318	"	"	2.00
13	0.26	50	0.739	0.905	0.595	–
14	0.23	60	0.706	"	"	–
15	0.23	80	0.667	"	"	–
16	0.30	80	0.676	"	"	–

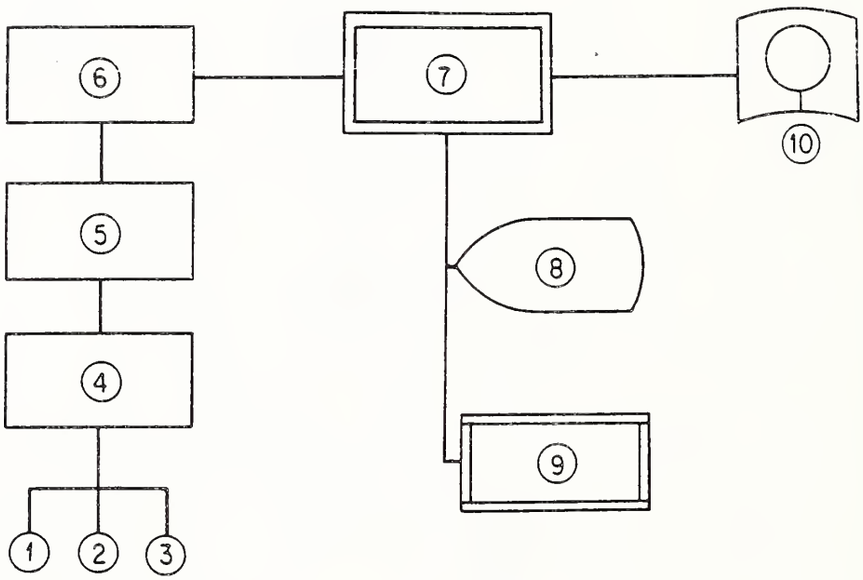

Fig. 3 Data acquisition system

1. Displacement transducer (Cap Sensor)
2. Load cell
3. Pore water pressure meter
4. Amplifier
5. Low-pass filter (1.0 Hz)
6. A/D converter
   (16K words of memory storage for each channel)
7. Personal computer (16 bit)
8. CRT
9. X-Y plotter
10. Floppy disk

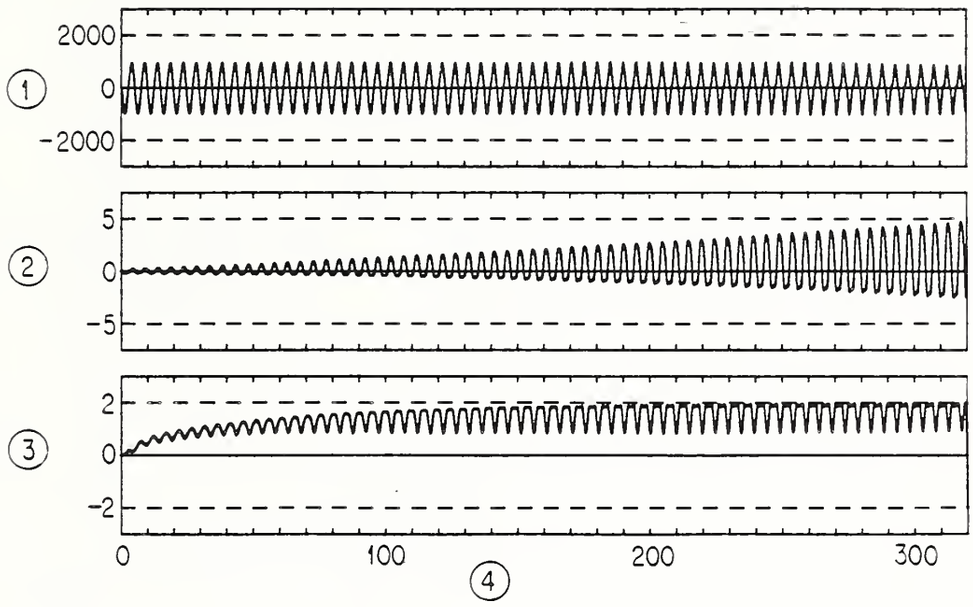

Fig. 4 Time histories of axial load, axial strain and pore water pressure

1. Axial load (kgf)
2. Axial strain (%)
3. Pore water pressure (kgf/cm^3)
4. Time in second

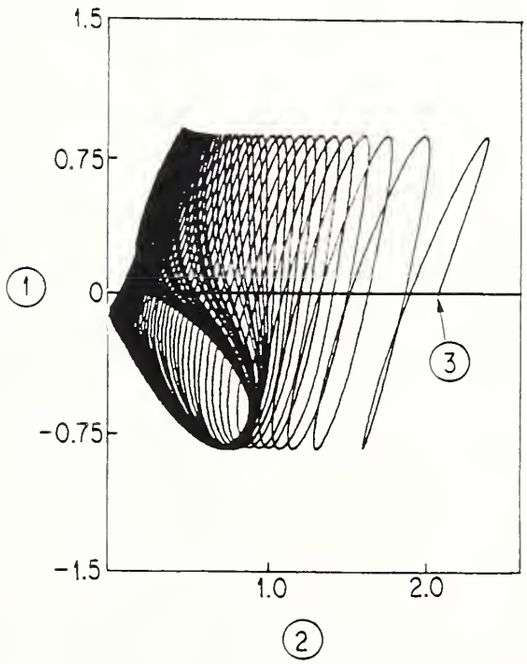

Fig. 5 Stress path of A-sample

1. Shear stress (kgf/cm^2)
2. Effective mean principal stress (kgf/cm^2)
3. Initial stress condition

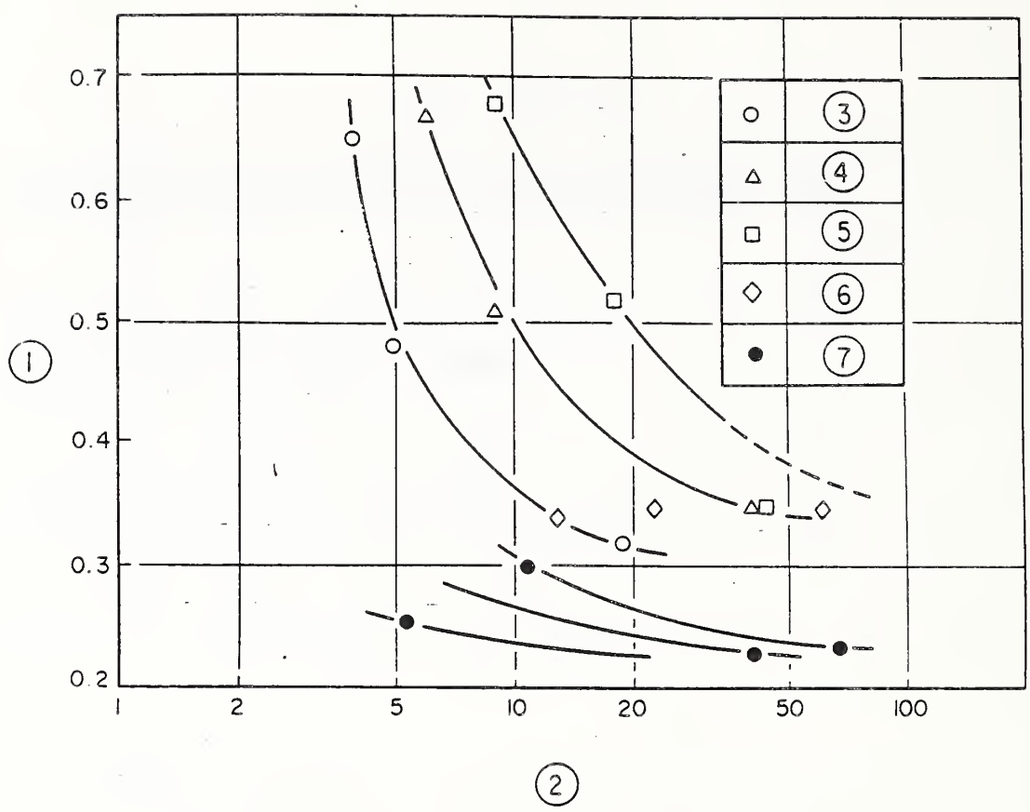

Fig. 6 Liquefaction potential of specimens

1. Shear stress ratio
2. Number of liquefaction
3. A-Sample (Dro = 60%)
4. A-Sample (Dro = 80%)
5. A-Sample (Dro = 97%)
6. B-Sample (Dro = 60% ~ 97%)
7. Toyoura standard sand (Dro = 50% ~ 80%)

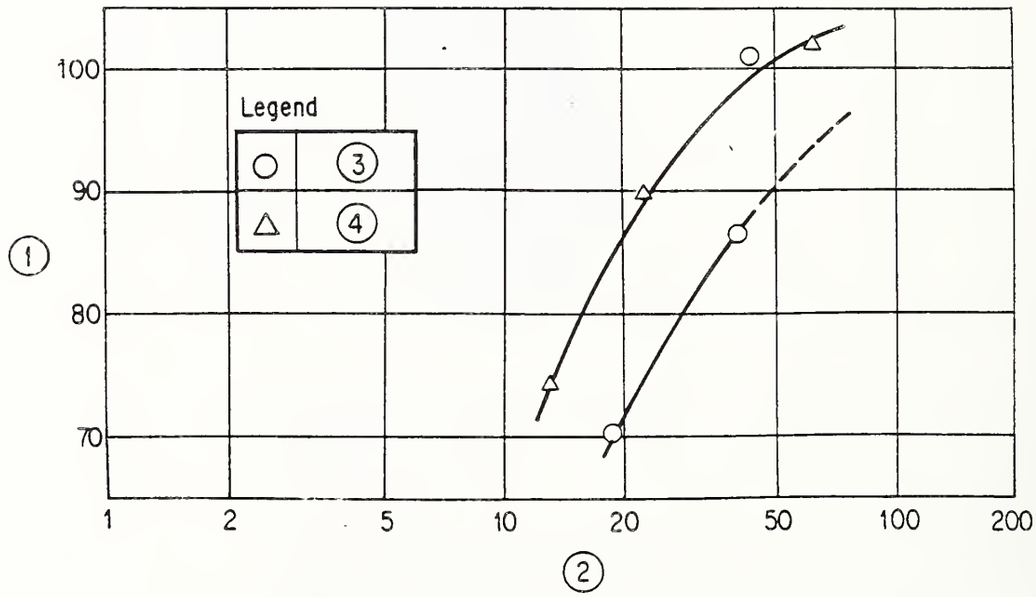

Fig. 7 Comparison of A-Sample and B-Sample on the same relative density

1. Relative density Dr (%)
2. Number of cycles N_L
3. A-Sample (No. 1, No. 4, No. 7)
4. B-Sample (No. 10 ~ No. 12)

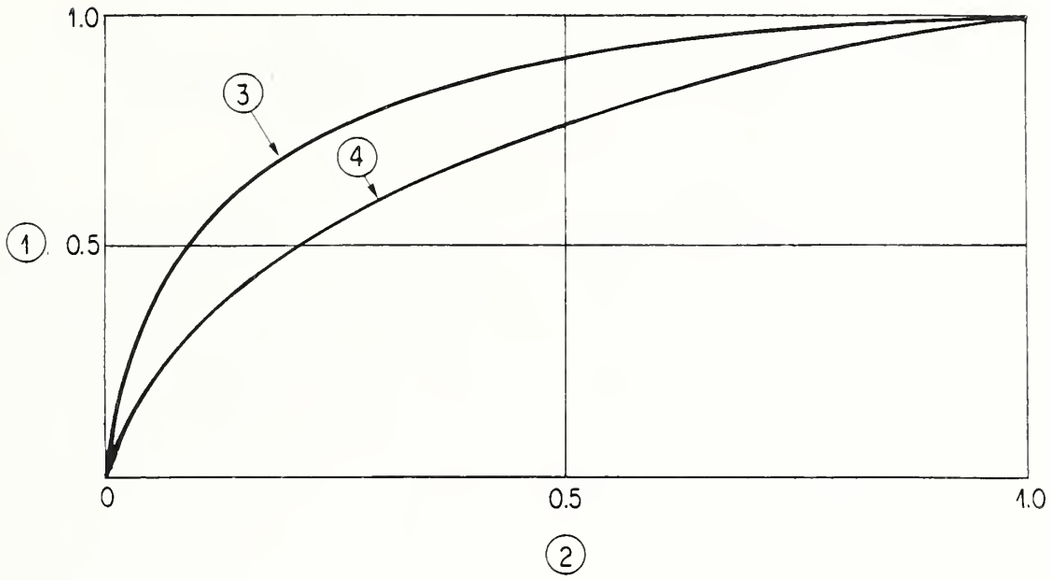

Fig. 8 $N/N\ell \sim \Delta u/\sigma_c$

1. $\Delta u/\sigma_c'$ Pore water pressure
2. $N/N\ell$ $N\ell$; Number of liquefaction
3. A-Sample
4. B-Sample

Preliminary Study of Shear Design for RC Piers

by

Hiroshi Shinohara[1], Michio Okahara[2],
Shouichi Nakatani[3], Keiji Taguchi[4], and Atsushi Funakoshi[5]

ABSTRACT

Earthquakes occur frequently in Japan, and thus the safety for reinforced concrete (RC) columns as well as bridge piers shall be reviewed against bending moments and also against shear force due to seismic load. It is particularly important for RC piers to be designed in such a manner that shear resistance of RC piers will exceed the flexural resistance for preventing brittle collapse. On the other hand, in the design of RC members for the substructure of highway bridges in Japan, no ultimate strength of members is being considered at present.

Therefore, in the present study, the up-to-date state of design methods against shear force to RC members was surveyed on the basis of domestic and foreign design guides and criteria and this design was examined based on data of previous loading tests on RC columns. This report shows the results of survey using the data of previous loading tests, for the design methods being used in various countries as well as the results of the review of both the equation for the shear strength and the required quantity of lateral ties for preventing brittle collapse.

Keywords: Reinforced concrete pier, shear, shear strength, lateral ties and loading tests.

1. INTRODUCTION

In Japan where earthquakes occur very frequently, aseismatic design is considered to be an important problem for not only structures for public facilities but also for various other structures. In the column members for highway bridge piers, axial forces or a bending moment prevails at ordinary times but large horizontal force occurs during earthquakes. The safety of bridge piers must be examined not only against the bending moment but also against shear forces due to the horizontal force that occurs during earthquake. That is, it is known that the RC member shows an excellent deformation performance in case of flexural failure without diagonal cracks but the RC member shows brittle collapse in case of shear failure. For the purpose of preventing this shear failure, it is vitally important for earthquake resistant design that the shear resistance of RC piers will exceed its flexural resistance. Nevertheless, the conventional allowable stress method is still being applied for the design of RC members of the substructure for highway bridges. According to the design rule of this conventional method for shear, it is attempted to limit the average shear stress borne by concrete member to less than the allowable shear stress. Therefore, in the strict sense of the word, the behavior of members subjected to external forces greater than the design loads is not taken into account in present design practice.

On the other hand, there is currently a tendency to adopt the so-called ultimate state design method in the actual design in this country, in which the safety of members is secured by evaluating the variance of load and resistance in ultimate state basing upon probability theory. This tendency is partly seen in the recent revision of the Standard Concrete Specifications (Japan Sciety of Civil Engineers). Namely, the check of safety for failure when subjected to ultimate load is desired even in the design of RC members for substructure of highway bridges.

Therefore, in the present study, the typical design guides and criteria applied in various countries were surveyed and present design methods for shear force were revealed in order to examine the design methods against shear force to column members of RC bridge piers. In addition, the data of previous loading tests for column members were collected and compiled in order to classify failure modes and to review the shear strength. Based on the results, the design method against shear forces acting upon RC bridge piers will be proposed in this report.

2. DESIGN METHODS IN VARIOUS COUNTRIES FOR SHEAR FORCES ACTING ON RC MEMBERS

2.1 General

Design methods for RC members subjected to shear force were studied and compiled by surveying several domestic and foreign design guides, criteria and standards, mainly with respect to the evaluation methods and the structural items related to shear strength.

Design guides, criteria and standards surveyed are:

Standard Concrete Specifications, 1986 (Japan Society of Civil Engineers)
Highway Bridge Specifications, 1980 (Japan Road Association)
ACI Building Code 318-83 (U.S.A.)
AASHTO 1983 (U.S.A.)
BS5400 part 4 (British)
CP110 (British)
CEB/FIP 1978 (Europe)
DIN 1045 (West Germany)

1. Director, Structure & Bridge Department, Public Works Research Institute, Ministry of Construction, Japan.
2. Head, Foundation Engineering Division, Structure & Bridge Department, Public Works Research Institute, Ministry of Construction, Japan
3. Research Engineer, Foundation Engineering Division, Structure & Bridge Department, Public Works Research Institute, Ministry of Construction, Japan
4, 5. Foundation Engineering Division, Structure & Bridge Department, Public Works Research Institute, Ministry of Construction, Japan.

2.2 Comparison of Design Methods in Various Countries

2.2.1 Provisions for Shear Force

Provisions for evaluating methods and structural items relating to the shear strength are compiled in Table 2.1. According to this table, the shear force is resisted by concrete and shear reinforcement, and the required quantity of lateral ties is calculated based on so-called classical truss analogy in every country. Moreover, most provisions have adopted certain forms of the ultimate state design method in order to assure the safety for ultimate strength of members.

2.2.2 Comparison of Shear Strength Evaluation Methods

The principal factors affecting shear strength of concrete are the main reinforcement ratio and axial compressive stress and so on. But these factors are incorporated in design equation slightly differently depending on country.

Characteristic points of these factors are explained below.

(1) Effect of main reinforcement ratio

In most of standards it is considered that the shear strength normally increases as the main reinforcement ratio becomes larger because of the dowelling effect of main reinforcement. BS equation has adopted the correlation between concrete strength and the dowelling effect of main reinforcement, and is different from other standards in that the shear strength borne by the concrete is not increased even if the concrete strength becomes larger where the quantity of main reinforcement is small.

(2) Effect of axial compressive stress

Most of the standards have incorporated only a relatively small effect of axial compressive stress. Especially ACI equation hardly permits an increase in shear strength within the range (5 to 15 kg/cm^2) of stress used for ordinary bridge piers. Also, DIN equation has not incorporated it by the reason that it is of negligible degree. However, CEB equation expects an increase in the shear strength by axial compressive stress.

(3) Influence of effective depth

Some standards consider a decrease of shear strength as scale effect. CEB equation shows no decrease where "d" is over 60 cm.

(4) Effect of lateral ties

The effect of lateral ties is mostly based on the same concept taken from the classical truss analogy in every standard. With respect to the upper limit of the shear strength, the equations of every standard have incorporated provisions based on the crushing of web, but the crushing of the web hardly becomes problematic since the cross section of the actual bridge piers is large.

2.3 Review

Since various factors will affect the shear strength of concrete, the design methods for shear in every standard are slightly different but the concepts of the shear strength of RC members are almost the same. However, these provisions in each country are basically for checking the shear in beam members and not for considering the column members subjected to shear force. Also, though it is known that the shear strength of concrete increases as the shear span ratio decreases, the effect of shear span ratio is currently not considered in the equation for checking shear. It is desirable to make corrections based on the shear span ratio because shear failure of column members occurs frequently in the region where the shear span ratio is small.

3. STUDY OF DESIGN METHODS FOR SHEAR FORCE TO RC PIERS

3.1 Principle of Study

The principle of this study is:

(1) To collect data of previous loading tests on RC column members carried out by various organization in Japan and to compile and classify P-δ relations and failure modes.

(2) To identify the failure modes of RC column members. To classify the failure modes into four kinds of shear failure type, shear flexural failure type, flexural shear failure type and flexural failure type.

(3) For specimens indicated the failure of shear failure type and shear flexural failure type among the failure modes, to survey their region and strength and to review the empirical equation for shear strength.

(4) For specimens indicating the failure of the flexural failure type and the flexural shear failure type among the failure modes, and to survey and review the amount of lateral ties arranged.

3.2 Study Based on Experimental Data

3.2.1 Collection of Experimental Data

Data of loading tests on RC column members were collected under the following conditions:

(1) Cross sectional shape: Only rectangular sections were considered and circular and hollow sections were excluded.

(2) Concrete: Only the normal concrete was considered excluding the specimens of special concrete such as lightweight concrete.

(3) Axial steel material: Only the steel reinforcing bars were considered excluding reinforcement by steel rigid frame, steel plates and PC.

(4) Shear reinforcement: Only lateral ties were considered and spirals and diagonal reinforcing bars were excluded.

(5) Axial compressive stress: Axial compressive stress were considered for the bridge piers excluding specimens with the value over 100 kg/cm^2.

(6) Specimen model: A model as shown in Fig. 3.1 was employed.

The experimental data were collected from 301 specimens tested by the organizations shown in Table 3.1.

3.2.2 Summary of Experimental Data

(1) Relation between maximum mean shear stress and the shear span ratio.

For the experimental data obtained from 301 specimens, the relationship between the maximum

mean shear stress τmax (the value obtained by dividing the maximum load $Pmax$ by column width b times the effective depth d) and the shear span ratio a/d (the value obtained by dividing the column height a by effective depth d) were classified by the tensile reinforcement ratio Pt of column (the value obtained by dividing the cross sectional area As of main tensile reinforcement by column width b times the effective depth d), and the results are shown in Fig. 3.2. From this, it is known that the maximum mean shear stress increases as the shear span ratio a/d becomes smaller and tensile reinforcement ratio Pt becomes larger.

(2) Failure modes

Failure of RC column members due to horizontal forces can be roughly divided into the following forms:

1) Form of shear failure before the flexural yielding of the main tensile reinforcement.
2) Form of flexural failure without the occurrence of diagonal cracks after the flexural yielding of main tensile reinforcement.
3) Intermediate form of failure between (1) and (2) in which the failure occurs as a result of a decrease in strength caused from the diagonal cracks after the flexural yielding of main tensile reinforcement.

In the case of bridge piers, it is said that sufficient flexibility can be maintained if the ratio of ultimate displacement to yield displacement is greater than 4. By taking account of the above, attention was paid to flexural yielding load Py and horizontal displacement $4\text{-}\delta y$ on P-δ curve based on the schematic diagrams of failure modes as shown in Fig. 3.3, and the failure modes were classified into four kinds. Classification and features of these failure modes are shown in Table 3.2.

The experimental data were then classified by the failure mode, and the various indexes were plotted on graphs as shown in Fig. 3.4 to Fig. 3.6. According to these graphs, it is well-recognized that brittle collapse of S type and SB failure type occur considerably in the following regions:

(1) Region with a shear span ratio of a/d <3 (refer to Fig. 3.4).
(2) Region with a relatively large tensile reinforcement ratio Pt (refer to Fig. 3.5).
(3) Region with no or little lateral ties (refer to Fig. 3.6).

3.2.3 Review of the Equation for Shear Strength

Except for the flexural failure type (B type and BS type) among the experimental data, 41 specimens indicated brittle shear failure (S type and SB type). Then, the experimental data from 41 specimens were reviewed by making use of the design equation for shear strength used mostly area in Japan. These equation are shown in Table 3.3. No safety factor for design was taken into account.

Ratio between the maximum mean shear unit stress τcal (=Vc/bd or Vu/bd) calculated by the design equation and the maximum mean shear unit stress τmax (=$Pmax$/bd) obtained from test data was reviewed and compiled.

Among 41 specimens indicated the shear failure type, calculations were made using Eq. (ii) for 28 specimens having no lateral ties, and the results are shown in Fig. 3.7. In addition, calculations were made using Eq. (i) for 41 specimens including those reinforced with lateral ties, and the results are shown in Fig. 3.8. From this, it is apparent that the equation employed for calculating shear strength has underestimated the shear strength in the region where a/d is small. This seems to have occurred because the effect of a/d was eliminated for simplicity and the members to be considered when introducing the design equation though the validity was verified using even the shear span ratio (a/d) as parameter in the empirical equation used for deriving Eq. (ii).

In the same manner, calculations were made using Eq. (v) for 28 specimens not reinforced with lateral ties and Eq. (iv) for 41 specimens including those reinforced with lateral ties, and the results shown in Figs. 3.9 and 3.10. Eq. (v) considers the effect of a/d, but the effect was underestimated in the region of experimental data of $1.0<a/d<3.0$ while the effect was much evaluated in the region of $a/d<1.0$.

As a result of the review stated above, the effect of shear span ratio (a/d) was taken into account by a simple method based on the design equation set forth in the Standard Concrete Specifications, and then the proposed equation for shear strength has been shown in Eq. (3.1)

$$Vu = (4.0 - a/d) \cdot Vc + Vs \quad \ldots\ldots\ldots\ldots (3.1)$$

where, Vc is obtained from Eq. (ii) and Vs from Eq. (iii). Now, comparing the calculated values and experimental values of the maximum mean shear stress, the results as shown in Figs. 3.11 and 3.12 are obtained. As shown in Fig. 3.11, the ratio between experimental value and calculated value was 1.011 in mean value and 24.8% in coefficient of variation.

3.2.4 Review of Reinforcing Effect by Lateral Ties

By identifying the failure modes as shown in Fig. 3.5, a considerably important tendency can be recognized because the failure modes can be classified by the tensile reinforcement ratio and shear span ratio into the region where brittle collapse occurs mostly and the region where failure with a high flexibility occurs. As a sresult, the reinforcing effect of lateral ties on the plane with tensile reinforcement ratio Pt and shear span ratio a/d was qualitatively reviewed by checking the quantity of lateral ties which causes flexural failure with flexibility. In Fig. 3.13, the B type and BS type of failure mode are abstracted and plotted by lateral tie ratio Pw of specimens (=Aw/b·s, where Aw: cross sectional ratio of lateral ties, b: width of column, and S: spacing of lateral ties). From this, it is recognized that flexural failures with flexibility can be bright about even if the lateral ties are not placed at all. This means that it is more rational to arrange the lateral ties on the basis the relation between the tensile reinforcement ratio and the shear span ratio.

3.3 Proposed Design Method for Shear Force to RC Piers

3.3.1 Principle of Design

(1) The shear strength of the column member is to be expressed by the sum of shear strength to be borne by

concrete and shear strength to be borne by lateral ties.
(2) Equaton for shear strength to be borne by lateral ties is to be based on truss analogy.
(3) Equation for the shear strength to be borne by the concrete is to be corrected by the shear span ratio of smaller than 3.
(4) The minimum quantity of lateral ties is to be given by the classification region of shear span ratio and tensile reinforcement ratio.

3.3.2 Checking Position and Others

(1) Checking the shear for RC bridge piers should be made for the maximum shear force at the base of bridge pier.
(2) The shear span ratio should be given by the following formulas (Fig. 3.14):

Shear span: $a=M_{max}/S_{max}$ . . . . . (3.2)

Shear span ratio: a/d . . . . . (3.3)

(3) Tensile reinforcement ratio P_t should be given by the following formula:

Tensile reinforcement ratio: $P_t=A_s/bd$ . . . . . (3.4)

where, A_s: Cross sectional area of tensile reinforcement

3.3.3 Equation for Design Shear Strength

The following equation should be used for calculating the design shear strength:

$$V_u=V_c+V_s \qquad (3.5)$$

where, V_c is given by Eq. (3.6).

In the case of $a/d \geqq 3$:

$$V_c=0.9\beta_d\beta_p\beta_n\sqrt[3]{\sigma_{cd}}\,bd/\gamma_b$$

In the case of $a/d<3$:

$$V_c=0.9\,(4-a/d)\,\beta_d\beta_p\beta_n\sqrt[3]{\sigma_{cd}}\,bd/\gamma_b$$

$$\beta_d=\sqrt[4]{100/d} \leqq 1.5$$

$$\beta_p=\sqrt[3]{100p_t} \leqq 1.5 \qquad (3.6)$$

$$\beta_n=1+2M_o/M_u \leqq 2.0$$

$$\sigma_{cd}=\sigma_{ck}/\gamma_c$$

σ_{ck} : Design compressive strength of concrete

γ_c : Material coefficient of concrete

γ_b : Coefficient of member

V_s is given by Eq. (3.7)

$$V_s=A_w\sigma_{sy}\,d/1.15s \qquad (3.7)$$

A_w : Cross sectional area of lateral ties

σ_{sy} : Yield strength of lateral ties

s : Spacing of lateral ties

3.3.4 Minimum Quantity of Lateral Ties

Quantity of lateral ties should be greater than the values shown in Fig. 3.15.

4. CONCLUSIONS

(1) As a result of surveying various domestic and foreign guides and standards, it has been clarified that many have adopted the ultimate state design method or load coefficient design method. Also, the main trends of reinforced concrete design method in each country have also been clarified.

(2) It has been verified that various guides and standards in every country was applied for the same design method between beam members and column members such as RC piers.

(3) As a result of collecting and compiling the results of loading tests conducted on column members in the past, it has been found that the failure modes can be roughly classified based on the relation between tensile reinforcement ratio and shear span ratio. It has been clarified that the so-called shear failures indicating brittle collapse occur only when the shear span ratio is less than 3 in the case of the load size and sectional shape for normally designed bridge piers.

(4) It has been clarified that the shear strength borne by the concrete varies with the shear span ratio even if the sectional shape is the same, and tends to increase as the shear span ratio becomes smaller. As a consequence, the previous equation for calculating shear strength have been corrected based on the experimental data.

(5) The equation for calculating shear strength and the minimum quantity of lateral ties have been proposed, and should be used when checking the shear in RC bridge piers by ultimate state design method.

Table 2.1 Provisions for the design against shear forces in various countries

Item / Standard	Design system	Basics of checking shear	Check of shear force to be borne by concrete	Check of shear force to be borne by shear reinforcement	Minimum quantity of shear reinforcement
Standard Concrete Specifications, 1986 (Japanese Institute of Civil Engineers)	Ultimate state design method	Checking whether the shear strength is being maintained against diagonal compressive failure of web and flexural shear cracking failure respectively during ultimate loading.	Calculated using calculating equation with compressive strength of concrete, tensile reinforcement ratio, effective depth and axial compressive force as parameters.	Calculated using calculating equation based on classical truss analogy.	More than 0.15% More than 0.2% for columns importance for earthquake resistance.
Specifications for Highway Bridge IV, May 1980 (Japan Road Association)	Allowable stress method	Checking whether the diagonal tensile stress is less than the allowable stress during design load.	Calculated using tables showing allowable shear stress corresponding to the strength of concrete.	Same as above	None
ACI 318-83	Load coefficient design method	Checking whether the shear strength is being maintained against diagonal compressive failure of web and flexural shear cracking failure respectively during ultimate loading.	Calculated using calculating equation with compressive strength of concrete, shear span ratio, axial compressive force and tensile reinforcement ratio as parameters.	Same as above	More than 50 $b_w \cdot s/f_y$. Unit: Pound, in.
AASHTO 1983	Allowable stress method combined with load coefficient design method	Same as above	Same as above	Same as above	Same as above

Item / Standard	Design system	Basics of checking shear	Check of shear force to be borne by concrete	Check of shear force to be borne by shear reinforcement	Minimum quantity of shear reinforcement
BS 5400	Ultimate state design method	Checking whether the shear strength is being maintained against flexural shear cracking failure during ultimate loading.	Calculate using tables showing the maximum shear stresses corresponding to compressive strength of concrete and tensile reinforcement ratio.	Same as above	More than $0.4\ bw \cdot s/0.87fy$ Unit: Pound, in.
CEB/FIP 1978	Same as above	Checking whether the shear strength is being maintained against diagonal compressive failure of web and flexural shear cracking failure respectively during ultimate loading.	Calculated using calculating equation with tensile reinforcement ratio, effective depth and axial compressive force as parameters based on tables indicating the maximum shear stress corresponding to the compressive strength of concrete.	Same as above	More than $Pw\ bw \cdot s$ Unit: Pound, in. Value of Pw (%) Reinforcing rod / Concrete: Equivalent to SR22 / Equivalent to SD41 / Equivalent to SD51 C25–C35: 0.24 / 0.13 / 0.11 C40–C50: 0.30 / 0.16 / 0.13
DIN1045	Same as above	Checking whether the diagonal tensile stress is less than the allowable unit stress in 3 kinds of region classes during design load.	Calculated using tables showing the upper limits of shear stresses classified into 3 regions in response to the compressive strength of concrete.	Same as above	Depending on region class: I) More than 40% of acting shear force. II) Against shear force reduced. III) More than 100% of acting shear force.

Table 3.1 Experimental data collected

Implementing bodies & representative researchers		Year of experiment	Number of specimens
Public Works Research Institute, Ministry of Construction	(Foundation Engineering Division)	FY 1983	26 (33)
"	(")	FY 1984	30 (32)
"	(")	FY 1985	29
"	(Earthquake Engineering Division)	FY 1981 to1985	27
Central Research Institute of Electric Power Industry		FY 1985	6
Metropolitan Expressway Public Corporation	(Miyauchi, Ohkubo)	FY 1978 to 1983	17
Structure Design Office Japan National Railways		FY 1984	43
Taisei Corporation Technical Research Institute	(Akio Ikeda)	FY 1970	30 (38)
Building Research Institute, Ministry of Construction	(Masaya Hirosawa)	FY 1967	6 (14)
Taisei Corporation Technical Research Institute	(Akio Ikeda)	FY 1967	8 (14)
Ohbayashi Corporation Technical Research Institute	(Takeda, Yoshioka)	FY 1970	30
Taisei Corporation Technical Research Institute	(Akio Ikeda)	FY 1970	12 (24)
Chiba Institute of Technology	(Sonobe, Ishibashi)	FY 1967	7 (16)
Tokyo Institute of Technology	(Kiyoharu Kuromasa)	FY 1964	11 (16)
Tokyo University	(Naka)	FY 1963	19 (59)

Table 3.2 Characteristics of failure modes

Failure modes	Characteristics of failure modes
S type	Failure occurs suddenly by a load smaller than flexural yield load P_y with the development of diagonal cracks (called shear failure type).
SB type	Failure occurs suddenly with loads larger than the flexural yield load P_y. Deformation performance is not sufficient, and shear strength suddenly decreases with the displacement of smaller than 4δ. (Called shear flexural failure type.)
BS type	No sudden decrease in shear strength occurs even after the occurrence of diagonal cracks, and this type has the deformation performance of greater than $4\delta_y$. After the occcurrence of flexural yield, diagonal cracks occur frequently with the displacement of 2 to $3\delta_y$. (Called flexural shear failure type.)
B type	Deformation occurs with almost no diagonal cracks up to $4\delta_y$, and the failure occurs at the flexural ultimate load P_u. (Called flexural failure type.)

Table 3.3 Shear strength calculating equation used in the study

1) Shear strength calculating based on Standard Concrete Specifications.

$$V_u = V_c + V_s \quad \text{(i)}$$

where, V_c: Shear strength of column member without lateral ties determined by Eq. (ii).

$$V_c = \tau_c bc \quad \text{(ii)}$$

$$\tau_c = 0.9\beta_d\beta_p\beta_n\sqrt[3]{\sigma_{ck}}$$

$$\beta_d = \sqrt[4]{100/d} \leqq 1.5$$

$$\beta_p = \sqrt[3]{100p_t} \leqq 1.5$$

$$\beta_n = 1 + M_o/M_u \leqq 2.0$$

b : Width of column

d : Effective depth

σ_{ck} : Compressive strength of concrete

V_s : Shear strength with lateral ties determined by Eq. (iii).

$$V_s = A_w\sigma_{sy}d/1.15s \quad \text{(iii)}$$

A_w : Cross sectional area of lateral ties

σ_{sy} : Yielding strength

s : Spacing of lateral ties

2) Shear strength calculating equation proposed by Japan National Railways.

$$V_u = V_c + V_s \quad \text{(iv)}$$

where, V_c : Shear strength of column without lateral ties determined by Eq. (v).

Where $a/d \leqq 2.5$

$$V_c = 3.58\,(a/d)^{-1.166}\,\sigma_{ck}^{1/3}\,(\sqrt{100p_t} + \sqrt[4]{100/d} + \beta_n - 1)bd$$

Where $a/d > 2.5$

$$V_c = 0.94\,(0.75 + 1.4d/a)\sigma_{ck}^{1/3}\,(\sqrt{100p_t} + \sqrt[4]{100/d} + \beta_n - 1)bd \quad \text{(v)}$$

where, $\beta_n = 2M_o/M_u$

$\sqrt{100p_t} \leqq 1.73$

$\sqrt[4]{100/d} \leqq 1.0$

V_s : Shear strength with lateral ties determined by Eq. (iii).

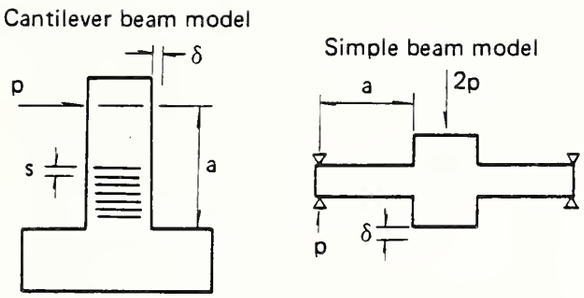

Fig. 3.1 Specimen model

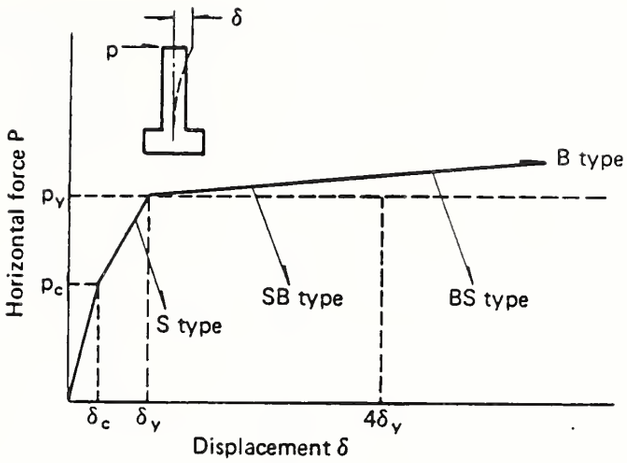

Fig. 3.3 Classification of failure modes by P-δ curve

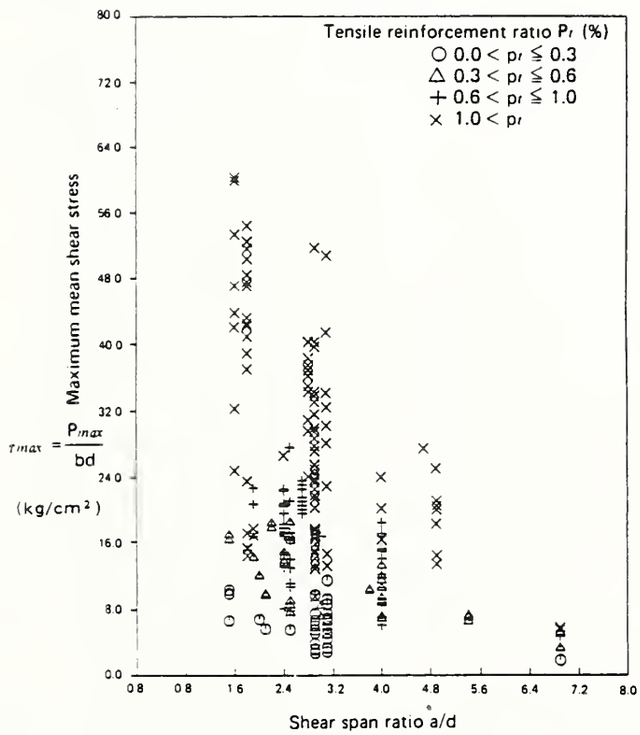

Fig. 3.2 Relationship between maximum mean shear stress and shear span ratio (by tensile reinforcement ratio)

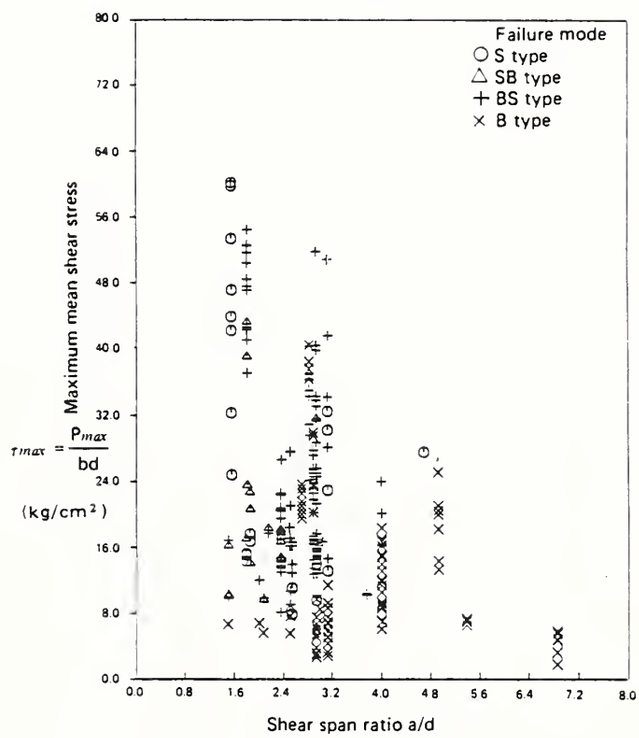

Fig. 3.4 Relationship between maximum mean shear stress and shear span ratio (by failure mode)

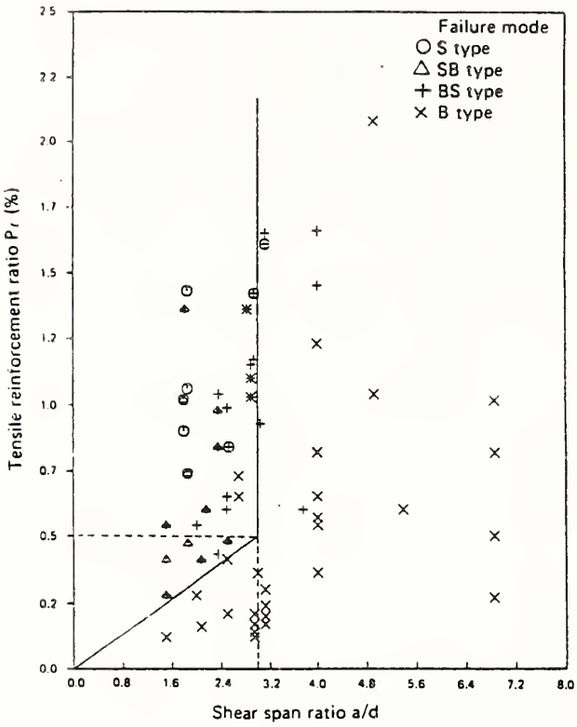

Fig. 3.5 Relationship between tensile reinforcement ratio and shear span ratio (by failure mode)

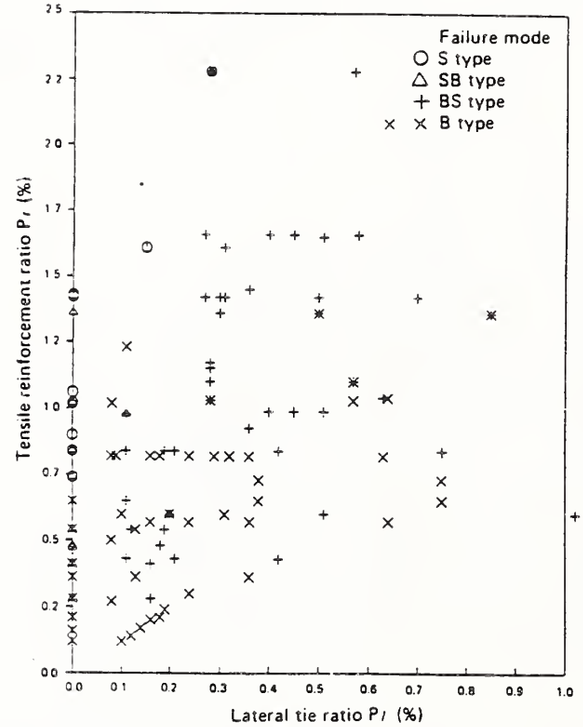

Fig. 3.6 Relationship between tensile refinforcement ratio and lateral tie ratio (by failure mode)

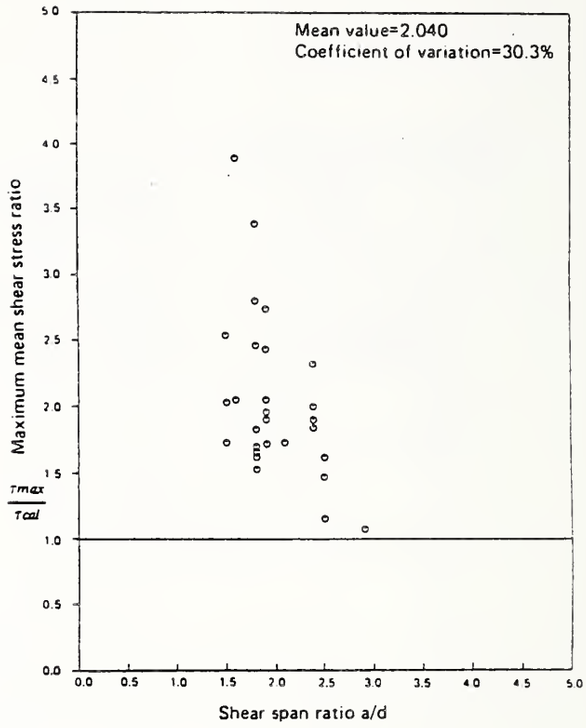

Fig. 3.7 Comparison between experimental values and calculated values based on Standard Concrete Specifications (for 28 specimens)

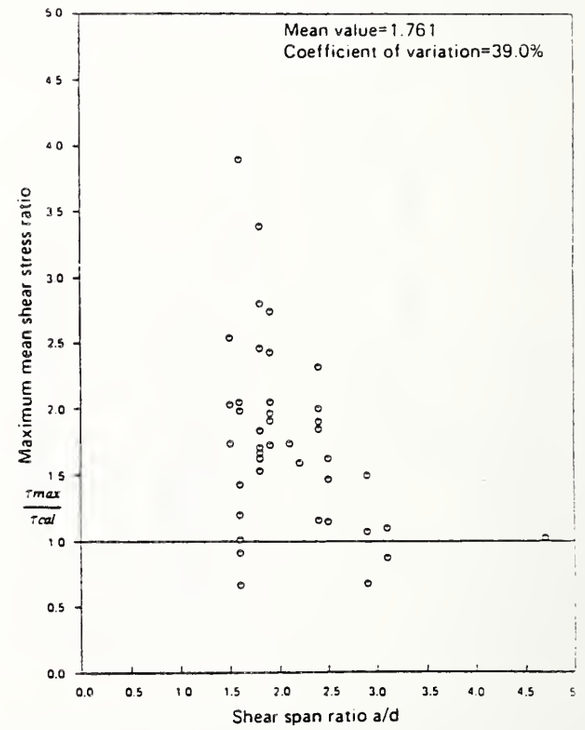

Fig. 3.8 Comparison between experimental values and calculated values based on Standard Concrete Specifications (for 41 specimens)

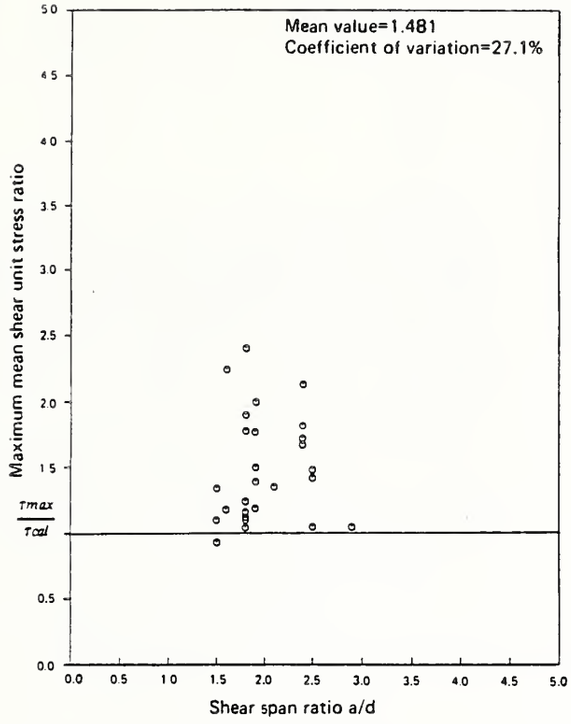

Fig. 3.9 Comparison between experimental values and calculated values on the basis of Japan National Railways' euqation (for 28 specimens)

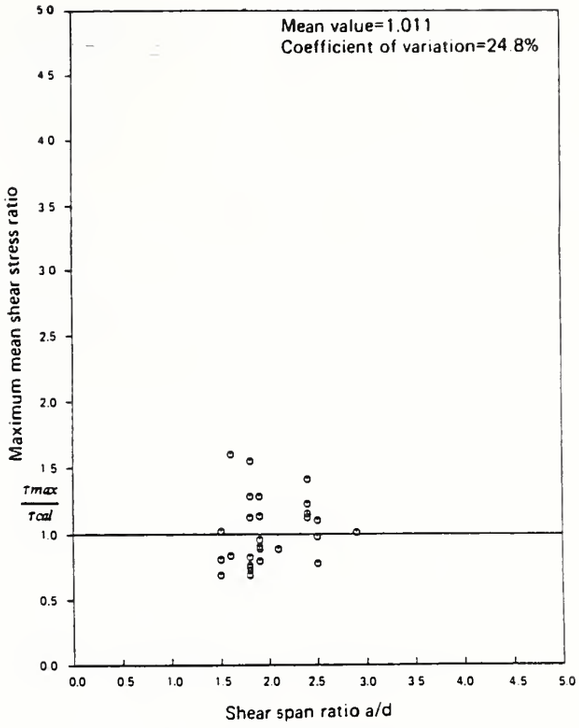

Fig. 3.11 Comparison between experimental values and calculated values based on the proposed equation (for 28 specimens)

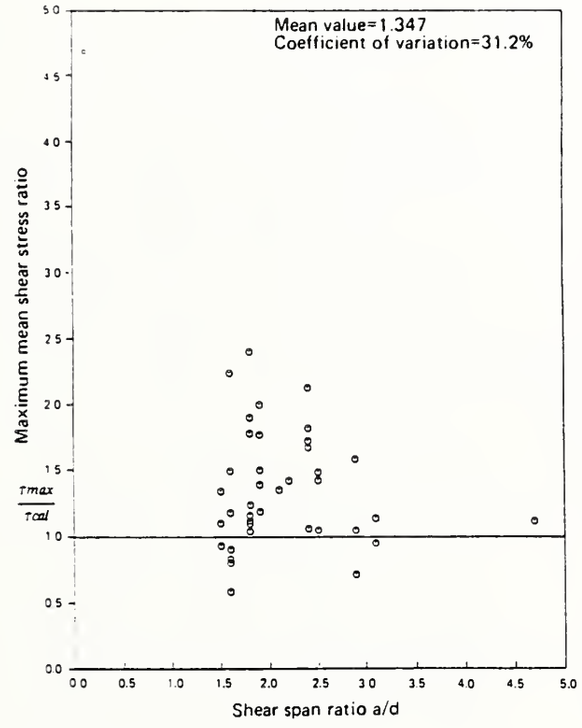

Fig. 3.10 Comparison between experimental value and calculated values on the basis Japan National Railways' equation (for 41 specimens)

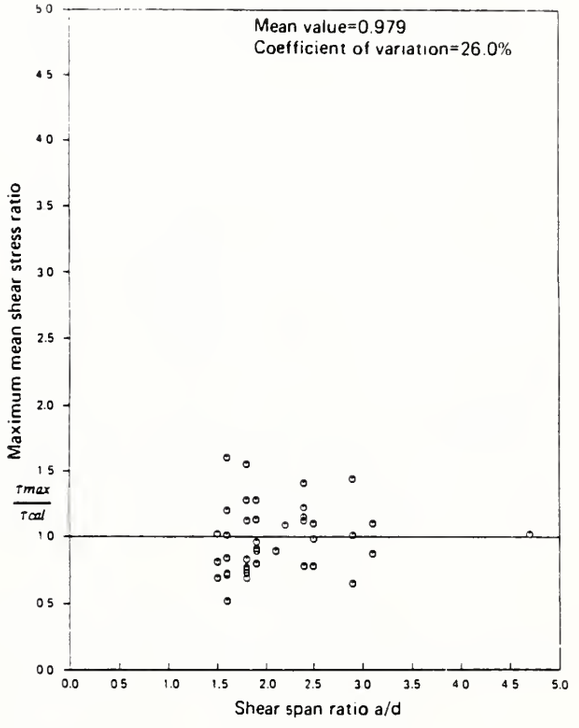

Fig. 3.12 Comparison between experimental values and calculated values based on the proposed equation (for 41 specimens)

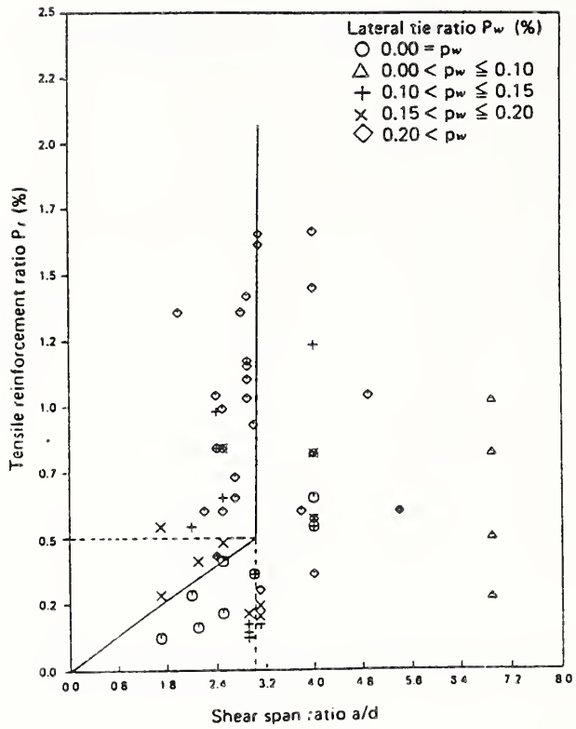

Fig. 3.13 Minimum lateral tie ratio Pw flexural failure type (B type, BS type) specimens

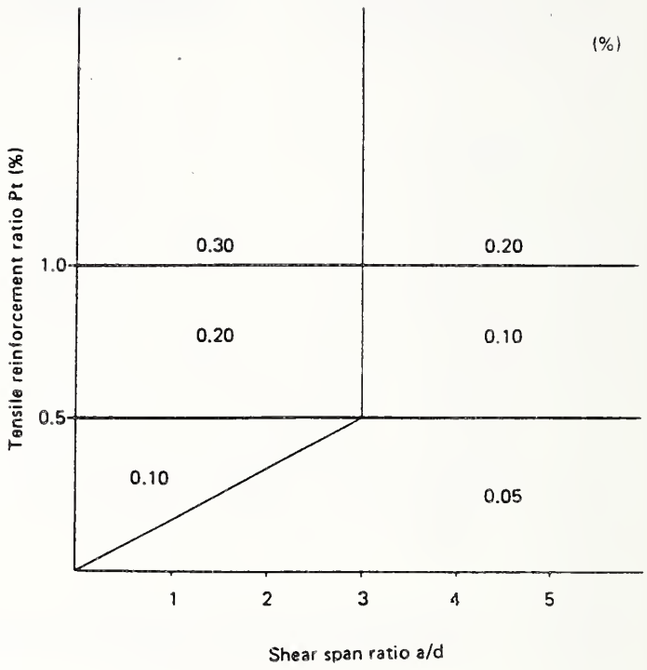

Fig. 3.15 Minimum ratio of lateral ties, Pw (%)

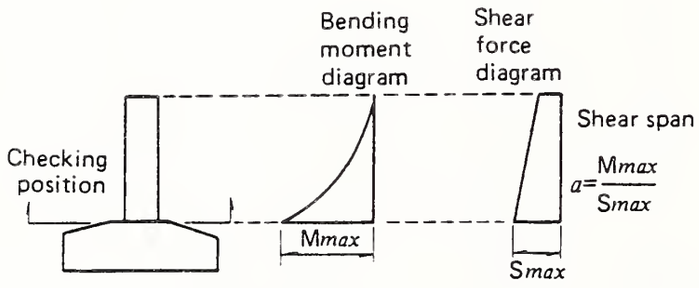

Fig. 3.14 Checking position and concept of a/d

Some Recent Studies on Lifeline Earthquakie Engineering in the United States: Experimental and Field Study

BY

T. D. O'Rourke[1] and J. Isenberg[2]

ABSTRACT

This paper focuses on research pertaining to pipeline systems. It concentrates on experimental and field studies, and begins with a general description of earthquake effects on pipelines. Pipeline response to permanent ground movements is discussed, with a summary of observations during previous earthquakes, a discussion of soil-pipeline interaction models, and a review of previous laboratory experiments, as well as a planned field experiment at a pipeline fault crossing. Pipeline response to traveling ground waves is discussed similarly in terms of previous earthquake observations, soil-pipeline interaction models, and a review of laboratory and field experiments. A summary of experimental trends is given and recommendations are made regarding future research opportunities.

KEYWORDS: Earthquakes; Geotechnical Engineering; Lifelines; Pipelines; Soil-Structure Interaction

1. INTRODUCTION

Lifelines are systems which provide transportation for people, resources, and services, as well as the transmission of electric power, messages, and data. The American Society of Civil Engineers (1) has identified four principal lifeline systems: electric power and telecommunications, gas and liquid fuel, transportation, and water and sewage. The great range of operational criteria as well as the many different mechanical and structural features of lifelines add to their complexity, and make it difficult to characterize research efforts in a truly comprehensive way for all types of lifelines. This paper focuses on research pertaining to pipeline systems. A substantial amount of the lifeline earthquake engineering research in the United States has been devoted to pipelines, principally as a result of the severe damage sustained by pipelines during the 1971 San Fernando (2,3,4) and 1906 San Francisco earthquakes (5,6,7). Research results for pipelines are applicable to gas, liquid fuel, water supply, and sewage systems, as well as various types of cabling and ducts in electric and telecommunication systems.

The paper concentrates on experimental and field studies, and begins with a general description of earthquake effects on pipeline systems. Pipeline response to permanent ground movements is discussed, with a summary of observations during previous earthquakes, a discussion of soil-pipeline interaction models, and a review of previous laboratory experiments as well as a planned field experiment at a pipeline fault crossing. Pipeline response to traveling ground waves is organized in a similar manner with attention to previous earthquake observations, models for soil-pipeline interaction, and laboratory and field experiments.

2. CONCEPTUAL FRAMEWORK FOR PIPELINE EXPERIMENTS

Laboratory and field experimentation for pipeline systems should be integrated within a framework of previous earthquake observations, analytical model development, and applications in practice through appropriate design and siting procedures. A rational plan for research and development includes: 1) characterization of the loading environment, 2) assessment of the loading effects on continuous and jointed pipelines, as well as special valves, pumps, and pressure control devices, 3) experiments designed and organized in conjunction with specific analytical models of soil-pipeline interaction, and 4) the use of experimentally verified models for improvements in siting, design, and risk assessment. Each of these steps is discussed under a subheading which follows.

2.1 Earthquake Loading Environment

Whereas aboveground piping responds to seismic shaking in the same manner as other aboveground structures and equipment, buried piping responds to earthquake motions in such a way as to have nearly the same curvatures and strains as the ground itself. The earthquake response of a buried pipeline depends closely on the static and dynamic deformation, stiffness, and strength of the surrounding soil. An important part of characterizing the earthquake loading environment is a careful assessment of soil properties and deformation patterns, especially when the potential exists for ground failures.

In response to an earthquake, pipelines may be damaged by permanent ground deformation and traveling ground waves. Both effects may have important repercussions on pipeline performance, although damage from traveling ground waves is frequently concentrated in pipelines which have been weakened by corrosion or are constructed of brittle materials such as cast iron or asbestos cement. Permanent ground movements

[1]Cornell University, Ithaca, NY 14853
[2]Weidlinger Associates, Palo Alto, CA 94304

result from irreversible deformations caused by shear failure or volume change, and develop concurrently with or subsequent to seismic shaking. Because permanent movements frequently exceed the peak ground displacements from seismic waves, they should be regarded as conditions of maximum distortion for buried pipelines and cables.

2.2 Assessment of Loading Effects

Three modes of unacceptable performance can be identified for buried pipelines: 1) rupture or excessive deformation of the pipe, 2) excessive rotation at pipeline joints, and 3) pullout or excessive compressive distortion at pipeline joints.

The performance of metallic pipelines, which convey high pressure gas and liquid fuel, depends almost exclusively on the first mode. Modern high pressure facilities are constructed with full penetration butt and longitudinal seam welds, inspected by means of X-ray radiographs or other nondestructive tests of the welds, and composed of mild or high strength steels. There is no well-documented case of a buried or aboveground petroleum or natural gas transmission pipeline constructed according to modern standards having been ruptured by the effects of ground shaking. Large permanent ground deformations associated with landslides, surface faulting, and soil liquefaction are the principal earthquake hazards. Continuous, butt-welded pipelines possess good ductility, and can be deformed well into the plastic range without rupture. Compressive forces, however, may lead to wrinkling and kinking of the pipe wall so that additional deformation of the line tends to concentrate at one location with resulting instability. Permanent ground movements which contribute to high compressive strains in the pipe are therefore undesirable.

Toe areas of lateral spreads and landslides as well as reverse faults are potential locations of large compressive deformation. Pipeline orientation with respect to transverse soil movement also plays an important role in the development of pipeline strain. At fault crossings, a pipeline should be oriented to respond in tension to differential movement. In landslide and lateral spread areas, a pipeline should be oriented parallel to natural topographic contours to promote longitudinal flexure and tensile elongation, thereby minimizing compressive distortion of the line.

Jointed pipelines are subject to all three modes of potentially unacceptable deformation. In some cases, the effects of permanent as well as transient ground deformations may be concentrated at pipeline joints so that their performance under both static and dynamic excitation needs to be understood. Unacceptable performance may result from leakage at a joint without a structural failure such as pullout or material fracture. Joint response to earthquake loads should therefore be evaluated under the conditions of internal fluid pressure that are likely to prevail in the field.

Jointed pipelines are used typically in water trunk and distribution systems, sewage collection systems, and natural gas distribution networks. The great variety of joint types presents a challenge to the experimentalist in deciding which joints to investigate. Many U. S. distribution systems rely on relatively old cast iron pipelines, which were constructed with lead-caulked or cement joints. Because of creep characteristics, lead-caulked joints are likely to show significant differences in behavior for static relative to dynamic loading.

There are a host of valving, pumping, and pressure control devices which also deserve careful evaluation in assessing the earthquake response of pipeline systems. Of special importance are penetrations and connections associated with subsurface and aboveground structures, where locally high concentrations of strain are possible.

2.3 Experiments Guided by Analytical Models

Experiments should be designed and conducted in accordance with analytical models. This is especially true for soil-pipeline interaction, and applies to both laboratory and field experiments.

The use of analytical models as an integral part of the experimental process carries a two-fold advantage. It provides a rational means for interpreting the results; data can be assessed immediately, and potential sources of error can be recognized as well as additional tests or test modifications chosen for further refinement. Coordination with specific models ensures that the testing can be used to verify or change existing analytical procedures. This allows for consistent and systematic improvements in design. With the availability of sophisticated, portable computers and data acquisition systems, it is possible to conduct analytical simulations and testing simultaneously, with real-time comparisons and control of the testing process.

2.4 Improvements in Practice

Experimentation provides a rational basis for selecting analytical models appropriate for design, and of equal importance, for understanding the limitations of these models. In some cases, the uncertainty associated with the performance of a pipeline component can be quantified by probabilistic means for reliability studies. Experiments also point directly to modifications in the materials or configuration of a given component to improve its seismic response. The same experimental methods can be used to substantiate the improved performance.

3. PIPELINE RESPONSE TO PERMANENT GROUND MOVEMENT

3.1 Previous Observations

Large permanent ground movements associated with soil liquefaction, landslides, and surface faulting are the most troublesome sources of potential damage to gas, liquid fuel, and water transmission pipelines. Evidence from the 1906 San Francisco, 1952 Kern County, 1964 Niigata, 1964 Alaska, 1971 San Fernando, 1978 Miyagi-Ken-Oki, 1983 Nihonkai-Chubu, and 1987 Ecuador earthquakes shows an unmistakable correlation between permanent ground movement and buried pipeline damage. Some of the most graphic illustrations of this kind are associated with the 1971 San Fernando earthquake, during which surface faulting and liquefaction-induced lateral spreads and slope movements caused failures in gas transmission and distribution piping (8,9).

Table 1 summarizes the principal causes of permanent ground movement associated with earthquakes. Each category of displacement is described briefly, and specific types of movement within a given category are listed.

Slope instability is a cause of potentially damaging ground movement, with the greatest seismic risks related to slopes showing signs of instability under static conditions. It is unlikely that any pipeline can survive the severe deformation imposed by deep translational and rotational slope failures. If instability involves slumps and relatively shallow slides, slope stabilization may be an effective means of correcting difficulties. Field observations and analytical studies suggest that modern, welded steel pipelines can survive the deformations imposed by relatively shallow and limited slope displacements, provided that the line is oriented perpendicular to the anticipated direction of movement.

In addition to landslides, the principal geotechnical hazards associated with earthquakes are surface faulting and soil liquefaction. Surface faulting is often regarded as the most dangerous source of differential movement, mostly because visible fault displacements have been the subjects of some striking and well-publicized observations. Surface faulting, however, is a relatively rare occurrence. In contrast, soil displacements caused by liquefaction are comparable in magnitude and more widespread. Liquefaction can result in many different types of deformation, including flow failures, lateral spreads, subsidence, loss of bearing, and buoyancy effects.

The most troublesome types of liquefaction-induced movements for a buried pipeline are lateral spreads. Lateral spreads involve the predominantly horizontal movement of competent shallow soils on an underlying liquefied deposit. Maximum displacements are often several feet, and may occur on slopes as gentle as 0.5 to 1.0°.

Assessing liquefaction and landslide hazards for pipelines requires careful attention to geologic features, and may require an assessment of structure, morphology, and topographic characteristics. Two case histories help illustrate the importance of permanent ground movements on pipeline damage.

The first case involves lateral spreading near the Juvenile Hall and Upper Van Norman Reservoir during the 1971 San Fernando earthquake. The information in this example is derived from work by O'Rourke (10). Figure 1a shows a plan view of the bedrock and alluvial sediments surrounding the Upper Van Norman Reservoir. Superimposed on this view are the lateral spread, which occurred at the site, and contours of equal groundwater depth at the time of the earthquake. The soils in the area are chiefly sands, silty sands, and silts, which were laid down in alluvial fans from Weldon and Grapevine Canyons to fill a northeast-trending depression in the bedrock. The location of the lateral spread can be seen clearly as trending northeast of the reservoir between bedrock exposures. The presence of a loose sandy silt and fine sand at a depth of 6 to 9 m with the water table at 3 to 6 m were characteristics that made the site susceptible to liquefaction. The lateral spreading and pattern of ground displacement, however, were controlled by the structure of the bedrock depression and the geomorphic features of the alluvial fans which filled the depression.

Figure 1b shows the mapped ground deformation, with vectors of displacement reported by Youd (11). The maximum soil movement was approximately 1.75 m. Two high-pressure natural gas pipelines were ruptured in the zone of lateral spreading. Both were continuous, girth-welded steel pipelines, with welds dating from approximately 1926 to 1930.

Figure 1c shows the boundary scarps of the lateral spread and vector displacements superimposed on a contour map of the site. There is a clear relationship between the pattern of spreading and the local topography. The lateral spread was confined generally to lower elevations between steeply rising ground to both the northwest and southeast. Moreover, the displacement vectors are nearly perpendicular to the contour lines.

Two earthquakes, which measured 6.1 and 6.9 on the Richter Scale, occurred on March 5, 1987 in the Napo Province of northeast Ecuador. The earthquakes occurred after a month of heavy rains, during which a total of 610 mm of precipitation was measured in the area of the earthquakes. The earthquake epicenters were located near an active volcano, El Reventador. Strong ground shaking triggered rock avalanches and debris slides near the volcano, involving over 100 million m^3 of soil and rock. Landslide material was washed into the surrounding rivers, causing them to swell with mud and debris. The swollen rivers flooded mountain roads and

dwellings, leaving deposits of mud and saturated sediments as deep as 10 m. The flooding and debris slides were responsible for most of the loss of life, which is estimated between 1000-2000 people.

Of major importance is the damage from landslides to the Trans-Ecuadorian Pipeline. The failure of this facility represents the largest single pipeline loss in history. The Trans-Ecuadorian Pipeline is a 660-mm-diameter pipeline, which carries oil 420 km from the Ecuadorian oil fields east of the Andes Mountains to the port of Esmeraldas on the Pacific Ocean. The pipeline was of telescoping design and constructed of X-60 grade steel, ranging in wall thickness from 9.5 to 23 mm. In all locations of damage, the pipeline was constructed as an aboveground facility, supported on 12-m centers by concrete pedestal foundations or double pipe piles with cross beams.

As shown in Figure 2, approximately 10.5 km of the pipeline have been completely destroyed along the north bank of the Coca River east of its confluence with the Salado River. An additional 16 km of the pipeline, east of the Malo River, have been damaged by local debris slides, which have severed the pipeline in at least eight places. Eight km of pipeline west of the Salado River have deformed, with significant distortion and displacement of aboveground pipeline supports.

Loss of the Trans-Ecuadorian Pipeline has deprived the country of 60% of its export revenue. It contributed to a 9% increase in the world price of oil. The lost revenues and cost of reconstruction of this facility are estimated as $1 to $1.5 billion.

3.2 Models for Soil-Pipeline Interaction

The ground movement patterns associated with surface faulting, landslides, and lateral spreading have many characteristics in common. The maximum relative displacements in landslides and lateral spreads are concentrated at the slide margins where movements tend to replicate strike and normal faulting and, thus, may be treated by many of the same modeling techniques that apply for surface faults. O'Rourke, Grigoriu, and Khater (12) point out that, although it is not possible to model with accuracy the soil displacement patterns at all potentially vulnerable sites, it is possible to characterize the worst case conditions which may develop and use these as upper bound estimates of deformation. In general, the most destructive differential soil movements are those which develop abruptly, such that a single-plane or knife-edge model of displacement can be used as an effective and conservative basis for analysis.

Figures 3a and b show a plan view of a pipeline which is intersected by a right lateral strike-slip fault at an angle, β_f. The pipeline is oriented so that fault displacement, d_f, will cause tension in the buried pipeline. It is assumed that sufficient geologic evidence is available to orient the pipeline for tensile deformation. Newmark and Hall (13) analyzed the pipeline deformation as an antisymmetric pattern of circular arcs, with each circular segment spanning the fault centerline and the location of an anchor point. The distance between the fault and the anchor point is known as the anchor length, L_a. Anchors may be caused by bends, tie-ins, and other features which develop substantial resistance to axial movement. Alternatively, the anchor point may represent an effective anchor length, beyond which there is no axial stress imposed in the pipeline from fault movement.

An analytical model was developed by Kennedy, Chow, and Williamson (14) which accounts for increased frictional resistance near the fault crossing and for pipeline bending strains. Figure 4 shows a plan view of pipeline deformation which forms the basis for the Kennedy, Chow, and Williamson model. Only one-half of the antisymmetric pattern of deformation is shown. As in Figure 3, the anchor point represents either a local constraint or the end of the effective anchor length. It is assumed that greater frictional resistance is developed along the curved portion of the pipeline than along adjoining sections because of high horizontal soil pressures resulting from large relative movements between the pipeline and surrounding ground. Kennedy, Chow, and Williamson recommend that the frictional resistance per unit pipe area be taken between 2.4 and 3.3f, where f is the frictional resistance per unit surface area of the pipe. Between the end of the curved portion of the pipeline and the anchor point, the frictional resistance is assumed to be f.

Figure 5 compares the results from both the Kennedy, Chow, and Williamson and the Newmark and Hall models for a case analyzed and reported by O'Rourke, Grigoriu, and Khater (12). The results pertain to a pipeline of X-60 grade steel, buried in granular soil with γ = 19.7 kN/m^3, depth to center of pipe of 1.2 m, and interface friction angle between the pipe and surrounding soil of 27°. The fault displacement, d_f, at a maximum axial pipe strain of 0.03 is expressed as a multiple of the pipe wall thickness, t. It should be pointed out that the maximum axial pipeline strain does not depend on the pipe diameter. The strain depends solely on the axial elongation of the pipeline.

The Kennedy, Chow, and Williamson model can be seen in Figure 5 to give a more conservative result than the Newmark and Hall model, chiefly because of the increased level of frictional resistance along the curved portion of the pipeline. In the figure, the plots are developed for the recommended range of frictional resistance of 2.4 to 3.3f. Over a wide range of

β_f, the Kennedy, Chow, and Williamson model predicts about half the fault movement capacity as the Newmark and Hall model.

Detailed analytical studies of buried pipeline response to fault displacement were performed by Tawfik and O'Rourke (15) with the aid of a computer program developed especially for evaluating pipeline performance for elasto-plastic soil reactions and large plastic strains in the pipeline steel. Their analytical results show that the pipeline deformation differs substantially from a circular arc and that the full value of f does not occur at all locations, as assumed in the Kennedy, Chow, and Williamson and Newmark and Hall models. The analytical results obtained by Tawfik and O'Rourke show strains higher than those predicted under similar conditions by the Newmark and Hall model, and substantially lower than those given by the Kennedy, Chow, and Williamson model.

Given the importance of this type of soil-pipeline interaction for many high pressure transmission pipelines and the wide range in analytical results, it is extremely important to substantiate by experiment the correct modeling assumptions. A major difficulty in conducting an appropriate experiment is the large scale required to comply with the boundary conditions that represent actual pipeline intersections with soil ruptures. Analyses (12) have shown that the effective anchor length of the pipeline required to develop plastic strains in the steel may be several thousand times the pipe wall thickness. Experiments at these scales must be conducted in the field at locations with very special geologic characteristics.

3.3 Laboratory Experiments

Buried pipeline response to large permanent ground movements depends closely on the force-displacement relationships which characterize reactions between the pipeline and surrounding soil. These relationships involve an elasto-plastic response of the soil, which can be represented as a nonlinear or bilinear function. Analytical models for soil-pipeline interaction have evolved from methods which were originally developed to evaluate the lateral and longitudinal soil reactions against deep foundations. Experimental work in the U. S. has focused on characterizing the force-displacement relationships for buried piping subject to longitudinal and lateral displacement with respect to the soil.

Full-scale tests of buried piping with diameters ranging from 25 to 300 mm have been performed in the laboratory (16,17,18) to evaluate the lateral and uplift forces generated by relative movement between pipe and soil as a function of soil density and strength, depth of burial, pipe diameter, and surface roughness of the pipe. The force-displacement relationship has been shown to be modeled by means of a hyperbolic function, or in simplified form as a bilinear representation. Data have been acquired which allow the bilinear relationship to be prescribed as a function of soil density and burial depth (17).

Currently, experimental evidence is lacking for oblique pipeline movement, involving components of both vertical and horizontal displacement with respect to the soil. In addition, data are also absent for characterizing soil restraint for pipelines buried in fine-grained soils such as clay and silt.

Tests have been performed to evaluate the frictional resistance generated by axial movement of a pipe in granular soil (19). These test results tend to corroborate previous experimental evidence for the frictional interface characteristics of deep foundations and retaining walls. Laboratory tests on the flexible joints of ductile iron pipe have been conducted to characterize pullout and rotational capacity (20). On the basis of these tests, the moment-rotation relationship was shown to depend on the properties of the waterproof gaskets provided with the joints.

3.4 Field Experiments

To investigate the performance of pipelines under conditions where permanent ground displacements are critical, a field experiment has been proposed that capitalizes on the predicted recurrence of the 1966 Parkfield earthquake (21) on the San Andreas Fault in Central California. According to the U. S. Geological Survey (22), there is a high probability that a magnitude 6 or greater earthquake will occur there between 1986 and 1993. Seven earthquakes have occurred on this segment of the fault over the last 150 years with an average return period of 22 years. The purpose of the experiment is to study the validity of current models of welded and jointed pipe segments in and adjacent to the surface zone of fault rupture. For welded steel pipe, the critical design parameter is the effective anchor length as defined in Section 3.2. Different analytical approaches lead to significantly different anchor lengths and hence, in some cases, to significantly different designs at fault crossings. For jointed pipelines, it is assumed that ground movement is accommodated almost entirely by relative displacement and rotation at the joints. The Parkfield experiment may show whether the component of fault displacement in the direction of the pipe axis is equal to the joint displacement and, if there are multiple joints in the fault zone, whether they accommodate the fault displacement equally.

To address these and other important issues, both continuous and jointed pipes will be laid in trenches across the fault zone in several different locations along the Parkfield segment. Active instrumentation in the form of strain gages and recording equipment that will be automatically triggered by the earthquake will be relied upon. Joint deformations and rotations

will also be observed visually.

3.4.1 Jointed Pipeline Experiment

The experiments will investigate the relationship between crossing angle and joint deformation and the behavior of joints and pipeline segments just outside the surface fault zone. Ductile iron pipe with rubber gasket joints will be used. Two test beds are illustrated in Figure 6. In each bed, two pipe segments are used in tension and one is in compression. In the narrower bed there will be one joint and no complete segments; in the wider bed there will be two joints and one complete segment. Of course, the actual surface rupture zone does not have distinct boundaries that are shown in the idealized zone of Figure 6. To locate the most likely region of surface rupture and to estimate the width of the rupture zone, we will rely on U.S.G.S. measurements of fault creep which we assume to be premonitory to surface rupture.

According to one simple picture of pipeline response to fault movement, relative displacement along the axis of the pipe is

$$\delta_{rel} = \Delta \cos \theta \qquad (1)$$

where Δ = fault offset and θ = angle of pipe axis with respect to fault strike. For Δ = 100 mm, the joint must accommodate about 100 mm times cos30° = 84 mm, which is close to the allowable for rubber gasket, ductile iron pipe. For θ = 60°, only 50 mm of slip must be accommodated, which should be possible without leakage. What is unresolved by simple theory is how much joint rotation accompanies the fault displacement. The amount by which rotation impairs axial slip capacity can be tested in a laboratory. The Parkfield experiment will show how much joint rotation, if any, actually occurs under the conditions of the test. A second issue is whether, if fault displacement is 100 mm, the pipe segment in compression will fail.

For the jointed pipeline segments, passive instrumentation in the form of markers and viewing ports will be designed to permit visual observations. The viewing port illustrated in Figure 7 will be fitted with a demountable optical device to measure relative displacement and rotation between adjacent segments. Active instrumentation will be in the form of transducers whose active element relies on change of resistance. Three measurements corresponding to two rotations and a displacement in the direction of the pipe axis will be made, leading to a total of 27 active channels.

The effects of fault creep (up to 10 mm/year) will complicate interpretation of measurements, because joint displacement during pre-earthquake creep may reduce capacity to withstand subsequent earthquake displacements. Pipeline response to creep will be monitored at regular intervals so that the condition of the pipe joints at the onset of the earthquake will be known.

3.4.2 Welded Steel Pipeline

The purpose of the welded steel pipeline experiment is to study the mode of deformation and slip between pipe and adjacent soil as a function of distance from the fault zone. As before, we idealize the fault zone as having distinct boundaries. Observations of pipeline behavior will help evaluate how this common oversimplification affects analysis and design. The geometry of the experiment is shown in Figure 8.

According to present estimates, the pipe will not rupture nor will the deformations be concentrated in a narrow zone. Hence it is necessary to measure flexural and extensional components of strain along the length of the pipe using strain gages and an appropriate recording system. Two pipeline segments will be used, one of which will be continuously welded, whereas the other will have joints specially designed to accommodate fault displacement.

Three hypothetical variations of axial strains with distance along the pipe are illustrated in Figure 9. Approximately a dozen measurement points on one side of the fault zone center (west side in Figure 9) will be instrumented. These hypothetical strain data correspond to three different variations of shear stress distribution. Finding out which of these, if any, is correct is a major goal of the experiment. A few measurement points will be provided on the east side to check on symmetry of shear distribution. If the distribution is symmetrical it would imply that the ground displacement is symmetrical about the center point of the pipe, which would be very fortunate.

The experiment provides an excellent opportunity to test the influence of joints on pipeline displacements and strain patterns. The use of joints and special couplings has been recommended as a means of accommodating the vertical and horizontal components of permanent ground movement. Traveling ground waves, however, present a special difficulty for jointed pipelines and it is not known how the repeated displacements from dynamic excitation will be concentrated at the joints nor how it will affect their behavior. At the Parkfield fault crossing, an additional welded steel pipeline will be constructed with joints at the location of expected maximum ground displacement. These will allow for rotation and axial extension to accommodate fault movement. Strain gages will be placed at selected locations which coincide with those on the continuous pipeline so that the joint effects on moment and axial strain distribution can be evaluated.

Ideally, the welded steel pipeline segments should extend beyond the anchor distance calculated

according to current theories. It should also be approximately one-quarter to one-half wavelength long. According to the Newmark-Hall approach (13), the anchor length is about 107 m. This is longer than one-quarter wavelength and slightly less than one-half wavelength. Accordingly, a total length of 214 m represents a reasonable compromise.

Uncertainties arising out of compromises on length of pipeline can be eliminated by introducing a fixed anchor point at the end of the pipe where relative displacement between soil and pipe would be known. So far no reason has been found to require us to introduce artificial constraints, however.

3.4.3 Data Acquisition System

Components of a data acquisition system include strain gages, underground cables, amplifiers, a seismic trigger, recording device, and storage batteries with solar panel for recharging. Ten hz resolution will be achieved. The trigger will be set so as not to activate recording due to creep strains, which will be monitored by periodic on-site visits.

4. PIPELINE RESPONSE TO TRAVELING GROUND WAVES

4.1 Observations in Previous Earthquakes

Extensive empirical studies have been made to measure the performance of pipelines in recent earthquakes. Study of five United States earthquakes (23,24,25) indicates that, where wave effects dominate ground shaking, most leaks in ferrous pipes occur where corrosion has locally reduced pipe wall thicknesses. Bends, tees, and joints are also locations of frequent damage (26). The commonly accepted measure of earthquake damage to underground pipelines is the number of leaks or required repairs per unit length of pipe. Post-earthquake reconnaissance indicates that the promptly appearing damage can be roughly correlated with a measure of ground shaking intensity such as peak acceleration, peak ground strain, or other parameter which characterizes ground motion as due to wave propagation effects. These correlations are useful for predicting damage in future earthquakes and in probabilistic system models.

The most thoroughly studied U. S. earthquake is the 1971 San Fernando event, where ground rupture was responsible for numerous breaks in the northern San Fernando Valley and where wave propagation was responsible for less severe damage in the southern San Fernando Valley. Data on repair frequency compiled by Katayama (27), Figure 10, is correlated with peak acceleration, which enables observations in San Fernando to be compared with Japanese experience. Figure 10 also shows that repair frequency following the 1983 Coalinga, California earthquake agrees reasonably well with the other data (28).

Another possible choice of shaking intensity is ground strain, which can be estimated by subtracting integrated ground motion records that are separated by a known measure of wave speed, such as group velocity. Recent work applying these two methods to data from the San Fernando earthquake is reported in (29) and is illustrated in Figure 11. Other measures of shaking intensity include Modified Mercalli Intensity as applied in (30).

The main obstacle to increasing the data base of damage and repair statistics on the basis of historical earthquakes is lack of reliable data on intensity of local ground shaking. This rules out otherwise useful data from the 1965 Puget Sound, Washington and 1969 Santa Rosa, California earthquakes (31).

It should be noted that the data discussed above come from either Japanese or California earthquakes. The possibility that the data are biased due to ground shaking characteristic of those regions or to other regional anomaly requires further study. It should also be noted that the data represent prompt earthquake damage which appears within several days to several weeks following the earthquake. Detailed study of the San Fernando and Coalinga earthquakes suggests that, in addition to causing prompt damage, earthquakes may accelerate aging of pipeline systems, thus shortening their effective life and permanently increasing maintenance costs.

4.2 Models for Soil-Pipeline Interaction

A summary of the response of pipelines to transient wave effects is presented in (12). A chief assumption of the methods reviewed there is that pipe deformation is assumed to be governed by the strains and displacements of the surrounding soil. This assumption is consistent with field measurements of Japanese researchers (32,33,34,35,36). If it is also assumed that transient ground shaking can be represented by waves of constant shape, then motions at points along various points of the pipeline will differ only by a lag time on an absolute time scale. These assumptions have led to simplified relationships in which axial pipeline strains are directly proportional to the ground velocity and inversely proportional to propagation velocity. Curvatures, usually small, can be related directly to acceleration and inversely to the square of propagation velocity.

Analytical methods for straight pipelines can be grouped into two categories, depending on whether the pipelines are continuous or jointed. The analytical methods of continuous pipelines represent seismic input by specified distributions of ground displacements (37,38) or shearing stresses (39). These distributions are assumed to be sinusoidal over the ground surface and are applied along pipelines at locations which

maximize response. Methods which assume buried pipelines to be rigidly bonded to the soil (40,41,42) lead to expressions for axial and bending strains which depend on the apparent propagation velocity of the traveling ground wave, c, along the pipeline. Rayleigh wave velocity and combinations of dilatational, shear, and Rayleigh velocities are recommended as a basis for c. The American Society of Civil Engineers (ASCE) Committee on Seismic Analysis recommends an apparent wave velocity between 610 and 915 m/sec (43).

The effects of relative displacement between soil and pipeline can be considered by assuming that slip occurs near the ends of the pipeline to mobilize a maximum frictional force per unit pipe length, t_u. Outside the regions of slippage, the pipe and soil move together and, as a result, the pipeline strain coincides with the maximum soil strain, e_g. The maximum slippage length is

$$\ell = e_g EA/t_u \tag{2}$$

in which A is the cross-sectional area of the pipe and E is its modulus.

The maximum frictional force per unit pipe length, t_u, can be obtained from

$$t_u = \frac{\pi}{2} D (1 + K_o) \gamma H \tan\delta \tag{3}$$

where γ is the unit weight of soil, H is depth of the pipe, K_o is the coefficient of earth pressure at rest, and δ is the interface friction angle between the soil and pipe. It follows from this model that the maximum strain in long pipelines for full slip, where $e_a \leq e_g$, is

$$e_a = \lambda t_u/4\,EA \tag{4}$$

and this occurs over a length of pipeline of one-quarter wavelength, λ. Other methods of analysis account for, in addition to peak ground displacement and/or velocity, the shape of the seismic ground waves (37,38). These methods involve solutions of differential equations of equilibrium for specified locations of the seismic waves and can account for effects of slippage between soil and pipe.

Seismic excitation has also been characterized by distribution of shearing stress along pipelines (39). If such a distribution varies sinusoidally, in which t_o is the maximum shearing stress, it is assumed that slip occurs when $t_{(x)}$ exceeds a postulated critical value, t_{cr}, and follows the pattern in Figure 12 for large earthquakes. The maximum stress in the pipeline is

$$\sigma_{max} = \begin{cases} \lambda t_o/2\pi t; \text{ no slip} \\ \lambda t_{cr}/4t; \text{ slip over full length} \end{cases} \tag{5}$$

Static analysis of jointed pipelines provides an upper bound on the relative displacement and rotation in joints (44). The model in Figure 13 idealizes the soil as linearly elastic springs and pipe segments as rigid. If joint forces are neglected and the wavelength is long compared with pipe dimensions, the maximum relative joint displacement and rotation are

$$u_j = \nu L/c_\ell; \qquad \theta_j = aL/c_t^2 \tag{6}$$

where c_ℓ and c_t are longitudinal and transverse components of the apparent wave propagation velocity and L is the length of pipe between joints.

A more refined model of the soil-pipe-joint system is shown in Figure 14 (45). The advances over the model described above are the addition of dampers to represent radiation damping effects of pipe-soil interaction and the addition of springs and dashpots to represent joint behavior. Ground shaking is applied by means of a uniform traveling excitation that propagates with constant amplitude and velocity. Equations of equilibrium incorporate both damping and inertia (38,39,46,47). Reduced models that neglect these terms are used in applications and have been extended to cases of deformable pipe segments (44,48). The most important steps in developing these models are improvements in the joint models, because these are potential weak links, and soil-structure interaction, because this governs the relative displacements transmitted to the pipeline.

Available methods for bends and tees deal with continuous pipelines. The pipelines are composed of elastic linear materials and the soils can be represented by rigid-plastic or elasto-plastic models. Pipe-soil models are illustrated in Figures 15 and 16. In these figures, S and M are shear and moment in the pipe segments, respectively, and Δ^* is the relative displacement between the soil and Element 1. Analyses of these and similar models are in (42,43,49). These methods are based on the assumption that the bend angle does not change, which is unrealistic for bends in thin-wall pipeline. Models of these pipelines should be based on curved thin-wall tubes (50,51), which account for bend flexibility and result in a lower bending moment in the pipe. It can be shown that

$$S_1 = \frac{k_s \Delta^*}{2\bar{\beta}} + \bar{\beta} M; \qquad M = \Delta^* \frac{z\bar{\beta} k^* EI}{r_o \pi} \tag{7}$$

in which Δ^*, S, and M have the same meaning as above, r_o is the bend radius, and $k^* = 1 - 9/(10 + 12\,[4tr\,0/kD)]$. Note that the bending moment, M, varies rapidly with the bend radius, r_o, particularly for small r_o.

4.3 Laboratory Experiments

One aim of laboratory experiments that investigate pipeline response to traveling waves is to develop data on resistance to axial movement of buried pipes. A suite of dynamic and static experiments is reported in (52). In the static tests, a pipe segment was embedded in a soil box and subjected to monotonically increasing axial force. Average values of interface friction were found as functions of depth to diameter ratio; as expected, the maximum frictional resistance varied directly with the burial depth. Subsequently, dynamic tests were performed in a similar test fixture. Hysteresis curves were developed for cyclic loading and dependence of the energy dissipation on frequency and burial depth was measured. A similar series of experiments is reported in (19). In these tests, steel, vitrified clay, and ductile iron pipe materials were subjected to axial and transverse shear loading. In some cases, water was added to the backfill to simulate field conditions. The tests were carried out in a pressurized test fixture to investigate a range of backfill depths. One use of the data developed from such tests is in frictional models of the type described in Section 4.2.

4.4 Field Experiments

There are relatively few field-scale experiments conducted in the U. S. that investigate pipeline response to traveling waves. The experiment that is proposed for the Parkfield area, described above, may provide some useful data, however. This is because there are portions of the welded steel line that are distant from the anticipated zone of maximum surface offset and which may therefore primarily be subjected to shaking from traveling waves. These portions will be instrumented with strain gages and will be within a few hundred meters of strong motion seismographs so that it may be possible to correlate the ground shaking with the pipe response.

A second type of field experiment involves subjecting ductile iron pipe to conditions under which corrosion will proceed at different rates. This test series, conducted by the Ductile Iron Pipe Research Institute, will yield valuable information on corrosion-related damage, which is a major contributor to damage in pipelines subjected to wave propagation effects.

5. CONCLUDING REMARKS

Experimental work in lifeline earthquake engineering should be performed within a conceptual framework of 1) load characterization according to permanent ground deformation and traveling ground waves, 2) assessing the effects of the loading environment on continuous welded pipelines, jointed pipelines, and valving and pressure control devices, 3) experiments performed in conjunction with specific analytical models, and 4) the use of experimentally verified models for improvements in design, siting, and risk assessment. Laboratory research in the U. S. has focused on characterizing the static and dynamic performance of pipeline joints and developing force-displacement relationships for longitudinal and transverse movements of buried piping relative to the surrounding soil. Significant questions exist about the proper analytical assumptions for models of soil-pipeline interaction at locations of earthquake-induced soil ruptures, such as surface faulting and slip at the margins of landslides and lateral spreads. The large-scale effects assocated with this type of problem require field testing at a site with special geologic and seismic characteristics. A test program to resolve design and siting questions about pipeline performance has been planned at a crossing of the San Andreas Fault in Parkfield, California.

ACKNOWLEDGMENTS

This work was partially supported under Research Account No. RF 150-6580A, sponsored by the National Center for Earthquake Engineering Research. The authors also wish to acknowledge the National Science Foundation, ASCE Technical Council of Lifeline Earthquake Engineering, and Earthquake Engineering Research Institute for their support in efforts leading to research reported in this paper.

REFERENCES

1. Technical Committees of the ASCE Council on Lifeline Earthquake Engineering, "Advisory Notes on Lifeline Earthquake Engineering," American Society of Civil Engineers, New York, NY, 1983.

2. Steinbrugge, K. V., E. E. Schader, H. C. Bigglestone, and C. A. Weers, "San Fernando Earthquake February 9, 1971," Pacific Fire Rating Bureau, 465 California St., San Francisco, CA, 1971.

3. Southern California Gas Company, "Earthquake Effects on Southern California Gas Company Facilities," San Fernando, California, Earthquake of February 9, 1971, U. S. Department of Commerce, Vol. II, 1973, pp. 59-64.

4. Subcommittee on Water and Sewerage Systems, "Earthquake Damage to Water and Sewerage Facilities," San Fernando, California, Earthquake of February 9, 1971, U. S. Department of Commerce, Vol. II, 1973, pp. 75-193.

5. O'Rourke, T. D. and P. A. Lane, "A Case Study of Seismic Hazards and Pipeline System Response for San Francisco," Proceedings, Third U. S. National Conference on Earthquake Engineering, Charleston, SC, Vol. III, Aug. 1986, pp. 2167-2178.

6. O'Rourke, T. D., M. D. Grigoriu, and M. M. Khater, "Risk Assessment for Pipelines Subject to Earthquake Movements," Proceedings, Trilateral Summer Workshop on Lifeline

Earthquake Engineering, Taipei, Taiwan, Nov. 1985, pp. 371-389.

7. Trautmann, C. H., T. D. O'Rourke, M. D. Grigoriu, and M. M. Khater, "Systems Model for Water Supply Following Earthquakes," Lifeline Seismic Risk Analysis - Case Studies, Ed. R. T. Eguchi, ASCE, New York, NY, 1986, pp. 30-50.

8. McCaffrey, M. A. and T. D. O'Rourke, "Buried Pipeline Response to Reverse Faulting during the 1971 San Fernando Earthquake," Earthquake Behavior and Safety of Oil and Gas Storage Facilities, Buried Pipelines and Equipment, PVP-Vol. 77, American Society of Mechanical Engineers, New York, NY, 1983, pp. 151-159.

9. O'Rourke, T. D. and M. S. Tawfik, "Effects of Lateral Spreading on Buried Pipelines during the 1971 San Fernando Earthquake," Earthquake Behavior and Safety of Oil and Gas Storage Facilities, Buried Pipelines and Equipment, PVP-Vol. 77, ASME, New York, NY, 1983, pp. 124-132.

10. O'Rourke, T. D., "Geotechnical Considerations for Buried Pipelines," Proceedings, BSSC Workshop on Abatement of Seismic Hazards to Lifelines, BSSC, Washington, D. C., Vol. 5, 1987, pp. 91-106.

11. Youd, T. L., "Ground Movements in the Van Norman Lake Vicinity during San Fernando Earthquake," San Fernando, California, Earthquake of February 9, 1971, U. S. Department of Commerce, Vol. III, 1973, pp. 197-206.

12. O'Rourke, T. D., M. D. Grigoriu, and M. M. Khater, "Seismic Response of Buried Pipelines," Pressure Vessel and Piping Technology, Ed. C. Sundararajan, ASME, New York, NY, 1985, pp. 281-323.

13. Newmark, N. M. and W. J. Hall, "Pipeline Design to Resist Large Fault Displacement," presented at June, 1975 U. S. National Conference on Earthquake Engineering, Ann Arbor, MI, (Paper UILU-ENG-75-2011), pp. 416-425.

14. Kennedy, R. P., A. W. Chow, and R. A. Williamson, "Fault Movement Effects on Buried Oil Pipeline," Journal of the Transportation Engineering Division, ASCE, Vol. 103, No. TE5, May 1977, pp. 617-633.

15. Tawfik, M. S. and T. D. O'Rourke, "Analysis of Pipelines under Large Soil Deformations," Geotechnical Engineering Report 86-1, School of Civil and Environmental Engineering, Cornell University, Ithaca, NY, 1986.

16. Audibert, J. M. E. and K. J. Nyman, "Soil Restraint against Horizontal Motion of Pipes," Journal of the Geotechnical Engineering Division, ASCE, Vol. 103, No. GT10, Oct. 1977, pp. 1119-1142.

17. Trautmann, C. H. and T. D. O'Rourke, Lateral Force-Displacement Response of Buried Pipe," Journal of Geotechnical Engineering, ASCE, Vol. III, No. 9, Sept. 1985, pp. 1077-1092.

18. Trautmann, C. H., T. D. O'Rourke, and F. H. Kulhawy, "Uplift Force-Displacement Response of Buried Pipe," Journal of Geotechnical Engineering, ASCE, Vol. III, No. 9, Sept. 1985, pp. 1061-1076.

19. Merritt, J. L., K. B. Morrill, H. C. Davis, and G. l. Wintergerst, "Tests of Buried Lifelines and Instrumentation/Communication Conduits," Earthquake Behavior and Safety of Oil and Gas Storage Facilities, Buried Pipelines and Equipment, PVP-Vol. 77, ASME, New York, NY, 1983, pp. 273-284.

20. Singhal, A. C. and J. C. Benevides, "Pull Out and Bending Experiments in Buried Pipes," Earthquake Behavior and Safety of Oil and Gas Storage Facilities, Buried Pipelines and Equipment, PVP-Vol. 77, ASME, New York, NY, 1983, pp. 294-303.

21. Brown, R. D. Jr., et al., "The Parkfield-Cholame, California Earthquakes of June-August, 1966--Surface Geologic Effects, Water-Resources Aspects, and Preliminary Seismic Data," Geological Survey Professional Paper 579, U. S. Geological Survey, 1967.

22. Allen, C. R., et al., "A Proposed Initiative for Capitalizing on the Parkfield, California Earthquake Prediction," Board on Earth Sciences, Commission on Physical Sciences, Mathematics and Resources, National Research Council, National Academy Press, Washington, D. C., 1986.

23. Brandow, G. E., "Reconnaissance Report, Imperial County, California Earthquake, October 15, 1979," EERI, El Cerrito, CA, 1980.

24. Isenberg, J., "Role of Corrosion in Water Pipeline Performance in Three United States Earthquakes," Proceedings, 2nd U. S. National Conference on Earthquake Engineering, Palo Alto, CA, Aug. 1979, pp. 683-692.

25. Isenberg, J. and C. E. Taylor, "Performance of Water and Sewer Lifelines in the May 2, 1983 Coalinga, California Earthquake," Proceedings, Symposium on Lifeline Earthquake Engineering: Performance, Design and Construction, San Francisco, CA, Oct. 1984.

26. Isenberg, J., "Water and Sewage Lifelines," Section IV, Advisory Notes on Lifeline

Earthquake Engineering, prepared by the Water and Sewage Committee of the Technical Council on Lifeline Earthquake Engineering, ASCE, New York, NY, 1983.

27. Katayama, T., "Seismic Behaviors of Lifeline Utility Systems - Lessons from Recent Japanese Experience," Journal of Natural Disaster Science, Vol. II, No. 2, Japan, 1980, pp. 1-25.

28. Isenberg, J., "Post-Earthquake Performance of Pipelines in Coalinga," Earthquake Spectra, Vol. II, No. 4, EERI, Oct. 1986, pp. 729-745.

29. Barenberg, M. E., personal communication, 1987.

30. Eguchi, R. T., "Seismic Vulnerability Models for Underground Pipes," Earthquake Behavior and Safety of Oil and Gas Storage Facilities, Buried Pipelines and Equipment, PVP-Vol. 77, ASME, 1983, pp. 368-373.

31. Isenberg, J., "The Role of Corrosion in the Seismic Performance of Buried Steel Pipelines in Three United States Earthquakes," Grant Report No. 6 under NSF Grant Nos. ENV P76-9838 and PFR 78-15049, Weidlinger Associates, Palo Alto, CA, June, 1978.

32. Miyajima, N., J. Miyauchi, K. Shirahawa, and Y. Aono, "An Example of Seismic Design and Earthquake Response Measurement of a Buried Pipeline," Proceedings, U. S. - Japan Seminar on Earthquake Engineering: Research with Emphasis on Lifeline Systems, Tokyo, Japan, Nov. 1978, pp. 177-196.

33. Suzuki, H., "Seismometer Array Observation Along a Gas Pipeline during the Miyagiken-oki Earthquake," Recent Advances in Lifeline Earthquake Engineering in Japan, ASME, New York, NY, 1980, pp. 61-76.

34. Nakamura, M., T. Katayama, and K. Kubo, "Quantitative Analysis of Observed Seismic Strains in Underground Structures," Proceedings, Review Meeting of U. S. - Japan Cooperative Research on Seismic Risk Analysis and its Application to Reliability-Based Design of Lifeline Systems, U. S. National Science Foundation and Japan Society for the Promotion of Science, Jan. 1981, pp. 121-141.

35. Iwamoto, T., N. Wakai, T. Yamaji, and S. Nagao, "Observation of Dynamic Behavior of Buried Ductile-Iron Pipelines during Earthquakes," Earthquake Behavior and Safety of Oil and Gas Storage Facilities, Buried Pipelines and Equipment, ASME, New York, NY, 1983, pp. 285-293.

36. Tsukamoto, K., N. Nishio, M. Satake, and T. Asano, "Observations of Pipeline Behavior at Geographically Complex Site during Earthquakes," Proceedings, 8th World Conference on Earthquake Engineering, Vol. VII, San Francisco, CA, July, 1984, pp. 247-254.

37. Shinozuka, M. and T. Koike, "Estimation of Structural Strains in Underground Lifeline Pipes," Technical Report No. NSF-PFR-78-15049-CU-4, Department of Civil Engineering and Engineering Mechanics, Columbia University, New York, NY.

38. Loh, C. H., A. H. S. Ang, and Y. K. Wen, "Spatial Correlation Study of Strong Motion Array Data with Application to Lifeline Earthquake Engineering," Structural Research Series No. 503, University of Illinois at Urbana-Champaign, IL, Mar. 1983.

39. Nelson, I. and P. Weidlinger, "Role of Coulomb Friction in the Seismic Response of Buried Pipes - General Introduction and Overview," Report No. 18, Weidlinger Associates, New York, NY, Mar. 1982.

40. Newmark, N. M., "Problems in Wave Propagation in Soil and Rock," Proceedings, International Symposium on Wave Propagation and Dynamic Properties of Earth Materials, Albuquerque, NM, pp. 7-26.

41. Sakurai, A. and T. Takahashi, "Dynamic Stresses of Underground Pipelines during Earthquakes," Proceedings, 4th World Conference on Earthquake Engineering, Santiago, Chile, 1969, pp. 150-162.

42. Shah, H. H. and S. L. Chu, "Seismic Analysis of Underground Structural Elements," Journal of the Power Division, ASCE, Vol. 100, No. PO1, July 1974, pp. 53-62.

43. Committee on Seismic Analysis, "Seismic Response of Buried Pipes and Structural Components," ASCE, New York, NY, 1983.

44. Wang, L. R. L., M. J. O'Rourke, and R. P. Pikul, "Seismic Vulnerability, Behavior and Design of Buried Pipelines," Technical Report No. 9, Department of Civil Engineering, Rensselaer Polytechnical Institute, Troy, NY, Mar. 1979.

45. Shinozuka, M., R. Y. Tan, and T. Koike, "Serviceability of Water Transmission Systems under Seismic Risk," Proceedings, 2nd Specialty Conference of the Technical Council on Lifeline Earthquake Engineering, ASCE, New York, NY, 1981, pp. 97-110.

46. Nelson, I. and P. Weidlinger, "Dynamic Seismic Analysis of Long Sequential Lifelines," presented at the Dec. 10-15, 1978 ASME Pressure Vessels and Piping Division Winter Annual Meeting, San Francisco, CA.

47. Wang, L. R. L. and K. M. Cheng, "Seismic Response Behavior of Buried Pipelines," presented at the Dec. 10-15, 1978 ASME Pressure Vessels and Piping Division Winter Annual Meeting, San Francisco, CA.

48. Wang, L. R. L., "Quasi-Static Analysis Formulation for Straight Buried Piping Systems," Technical Memorandum, Department of Civil Engineering, Rensselaer Polytechnical Institute, Troy, NY, July 1978.

49. Goodling, E. C., "Seismic Stresses in Buried Elbows," presented at the Apr. 2-6, 1979 ASCE Convention and Exposition, Boston, MA (preprint 3595).

50. Committee on Gas and Liquid Fuel Lifelines, "Guidelines for the Seismic Design of Oil and Gas Pipeline Systems," ASCE, New York, NY, 1984.

51. Goodling, E. C., "Buried Piping - An Analysis Procedure Update," Earthquake Behavior and Safety of Oil and Gas Storage Facilities, Buried Pipelines and Equipment, Vol. PVP-77, ASME, New York, NY, 1983, pp. 225-237.

52. Wang, L. R. L., "Role and Development of Soil Parameters for Seismic Responses of Buried Lifelines," Earthquake Behavior and Safety of Oil and Gas Storage Facilities, Buried Pipelines and Equipment, Vol. PVP-77, ASME, New York, NY, 1983, pp. 312-323.

Table 1. Principal Causes and Descriptions of Permanent Ground Movement

Cause	Description
Landslides	Mass downslope movements of soil or rock, which may be triggered under static or seismic conditions. Many displacement patterns are possible. Principal forms of movement include 1) rock falls, 2) relatively shallow slumping and sliding of soil, and 3) relatively deep translation and rotation of soil and rock.
Liquefaction	Displacement caused by transformation of saturated cohesionless soils to liquefied state or condition of substantially reduced shear strength. Liquefaction-induced movements include 1) lateral spreading, 2) flow failure, 3) loss of bearing, 4) subsidence, and 5) buoyancy effects.
Faulting	Displacement of adjacent portions of the earth's crust. Movement concentrated in relatively narrow fault zones. Principal types of fault movement include 1) strike, 2) reverse, and 3) normal slip.
Tectonic Uplift and Subsidence	Regional changes in dimension associated with tectonic activity. Generally distributed over large areas.
Vibration-Induced Densification	Settlements and ground cracks arising from a volume loss caused by vibration of dry or partially saturated cohesionless soil; most prominent as a result of earthquake vibrations.

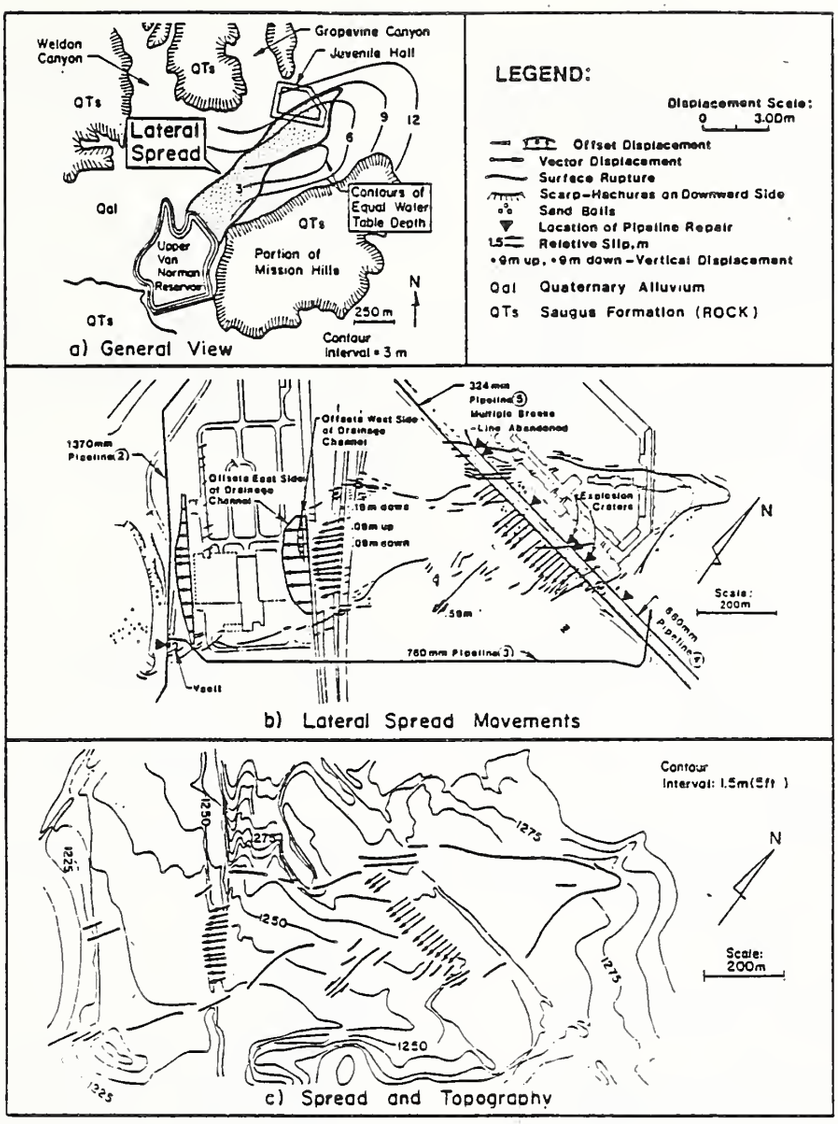

Figure 1. Plan View of Lateral Spread near Upper Van Norman Reservoir after 1971 San Fernando Earthquake (10)

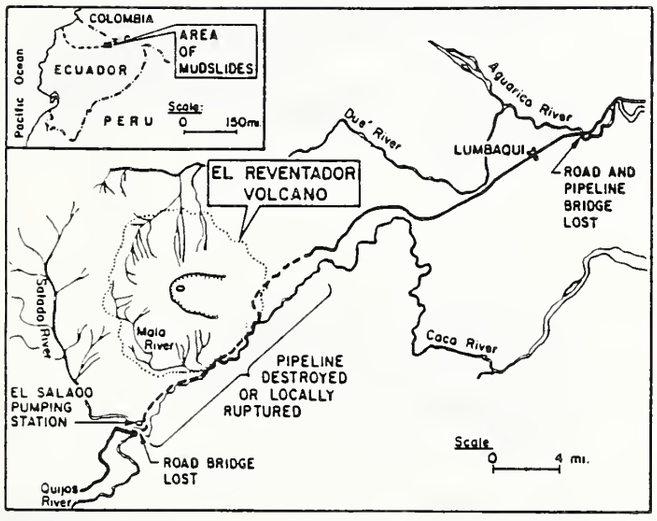

Figure 2. Map Showing Area of Pipeline Damage from 1987 Ecuador Earthquakes

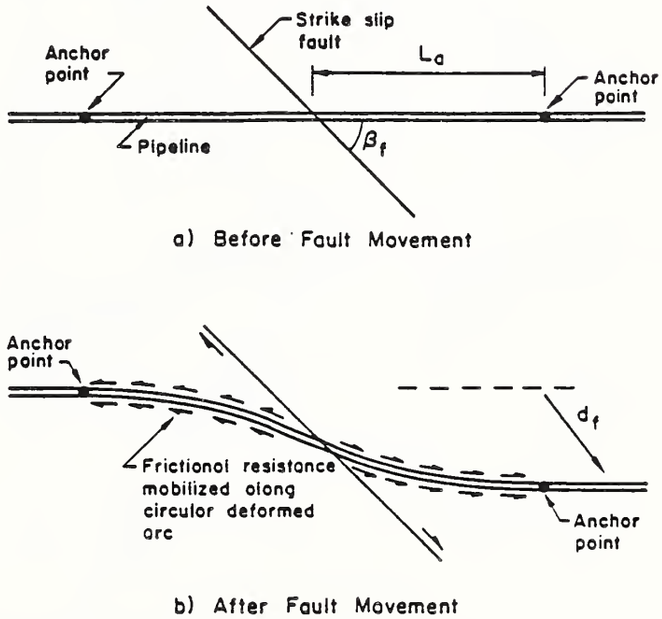

Figure 3. Plan and Cross-Sectional Views of a Continuous Pipeline at a Fault Crossing

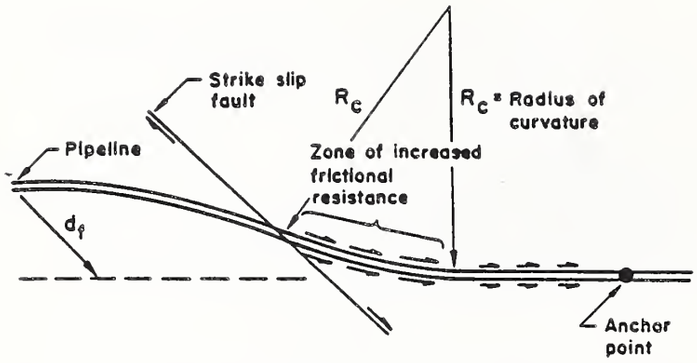

Figure 4. Plan View of Pipeline and Fault Movement as Basis for Kennedy, Chow, and Williamson Model (12)

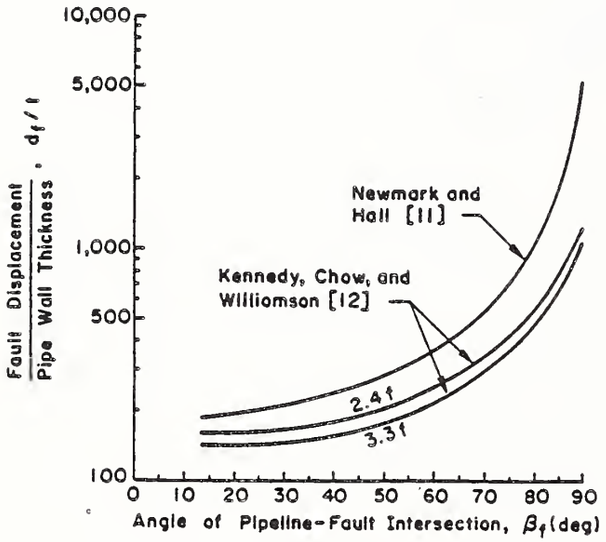

Figure 5. Comparison of Analytical Results for Different Fault Crossing Models (12)

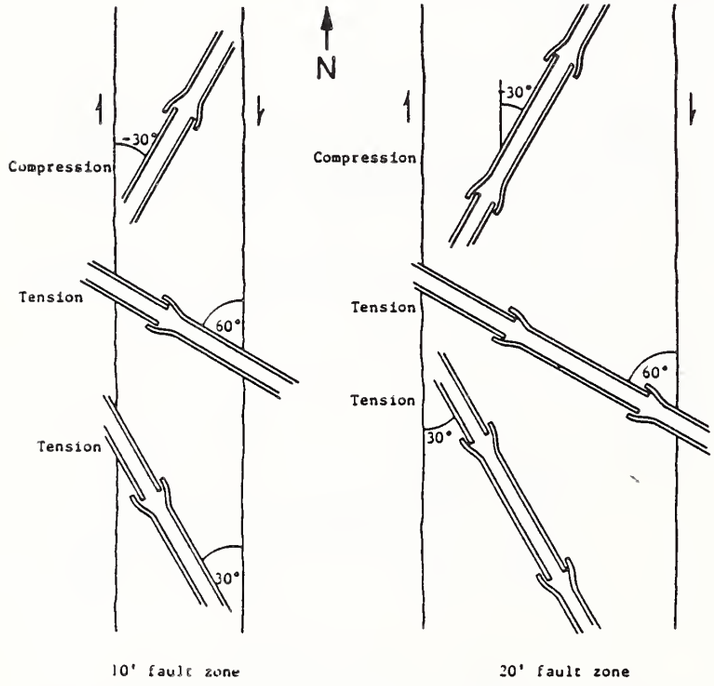

Figure 6. Array of Jointed Pipeline Segments at Various Crossing Angles to Fault Strike; Two Fault Zone Widths Considered

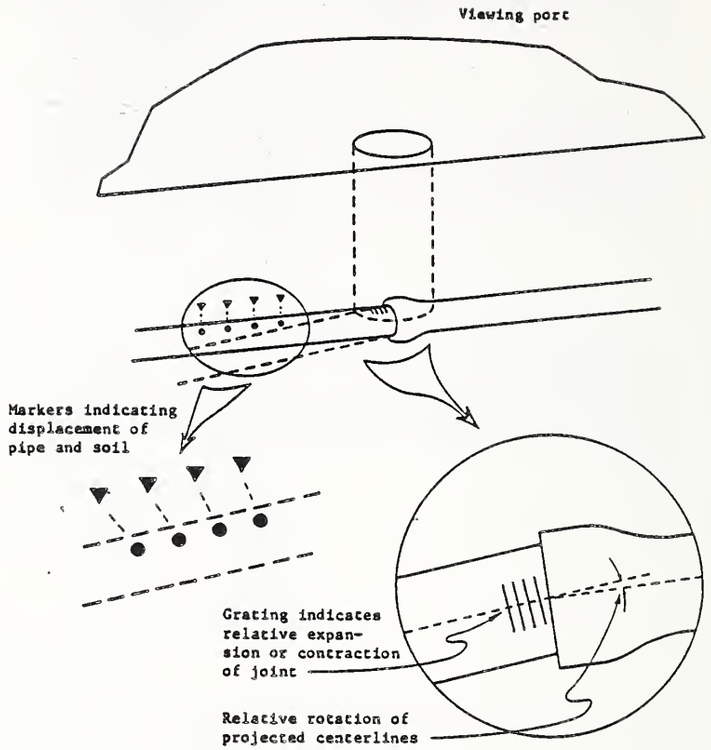

Figure 7. Passive Instrumentation

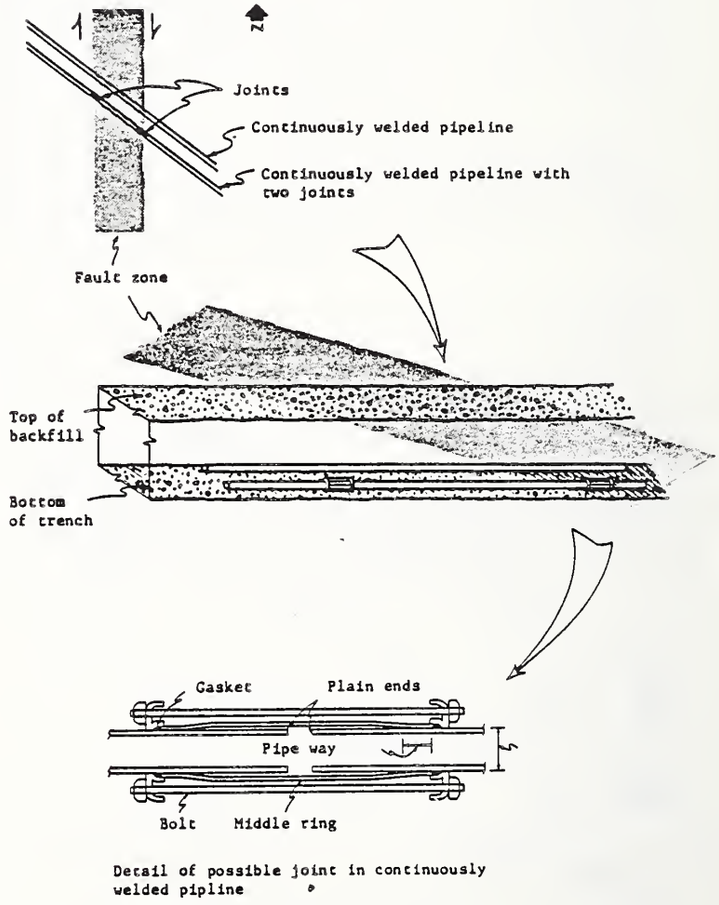

Figure 8. Continuously Welded Pipeline with Two Joints, Laid Adjacent to Continuously Welded Pipeline without Joint

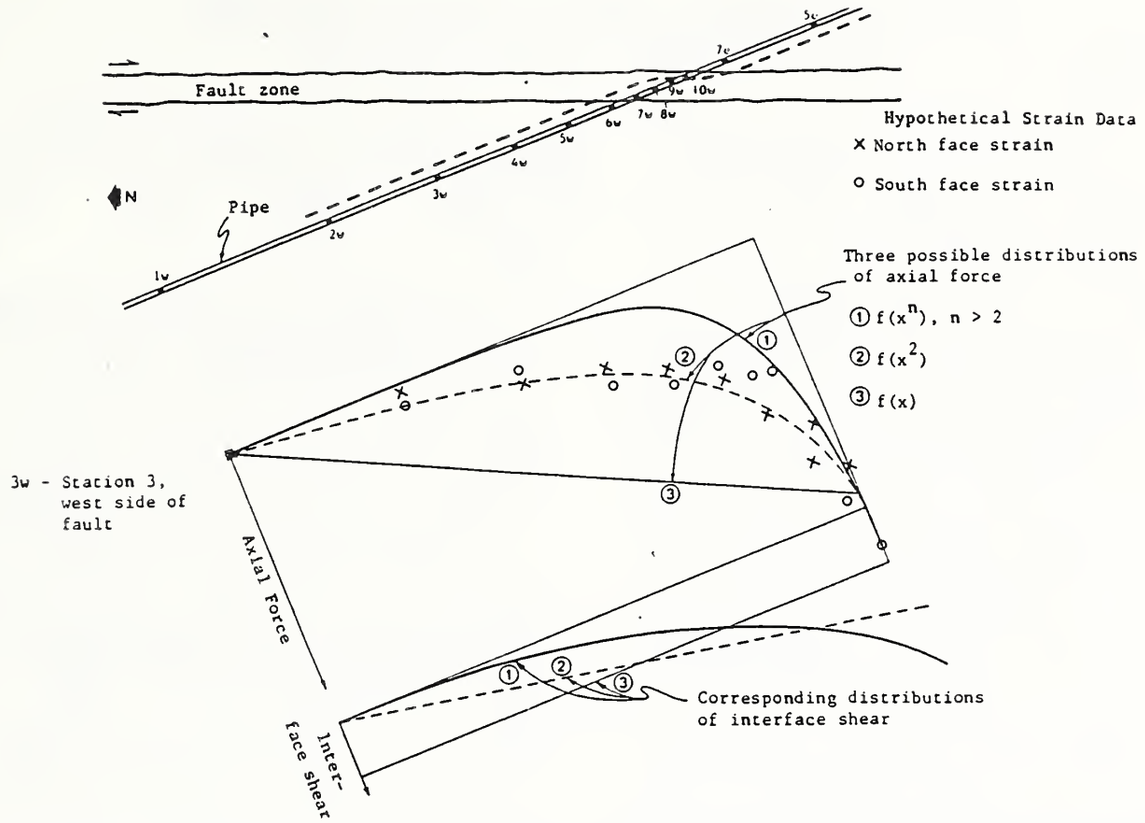

Figure 9. Locations of Strain Measurements, Derived Distribution of Axial Forces, and Corresponding Implied Distribution of Interface Shears for Continuously Welded Pipeline

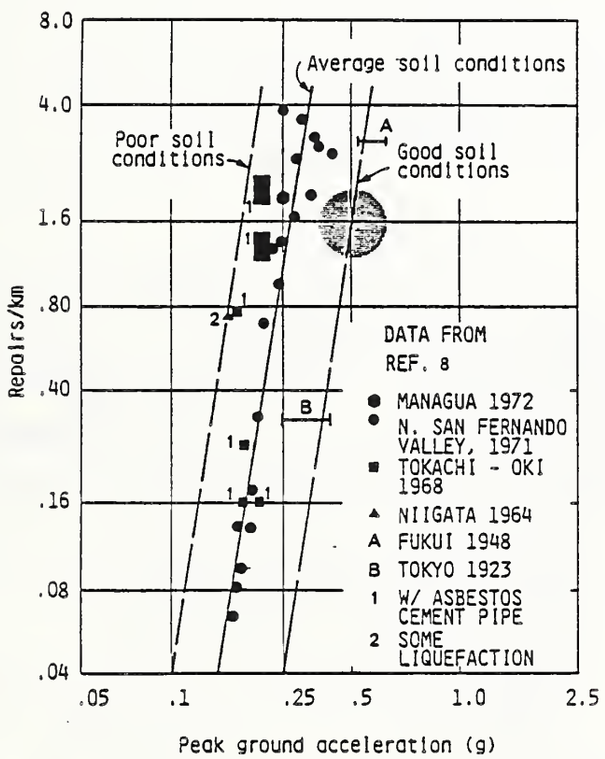

Figure 10. Repairs to Water Distribution Pipelines in Previous Earthquakes (27)

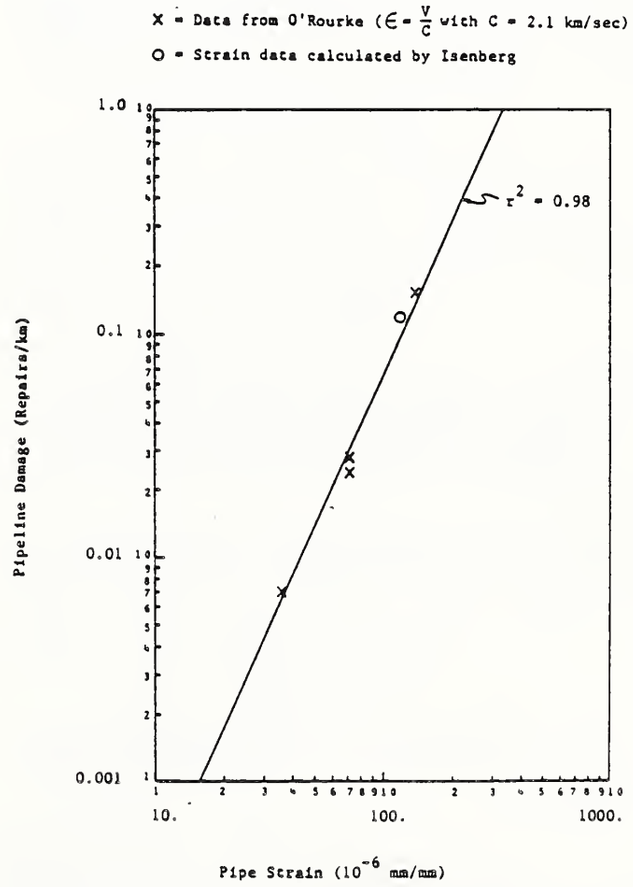

Figure 11. Pipeline Damage vs. Pipe Strain

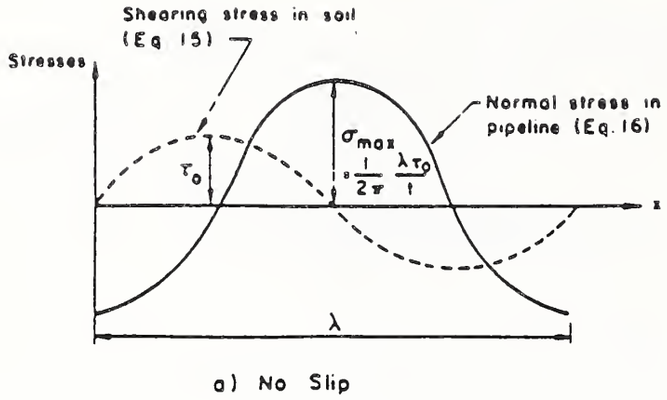

a) No Slip

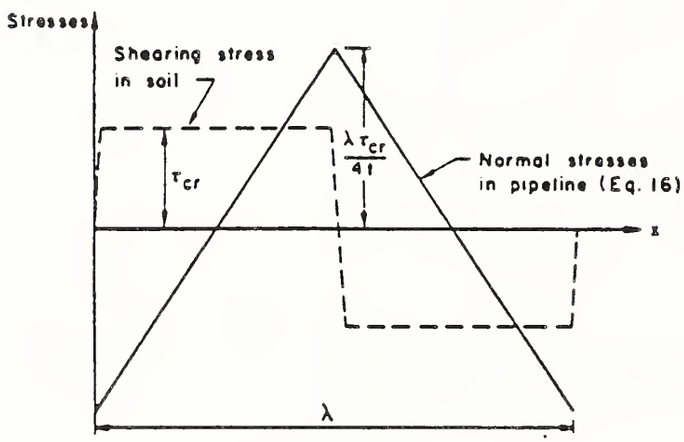

b) Slippage

Figure 12. Stresses in Soil and Pipelines (39)

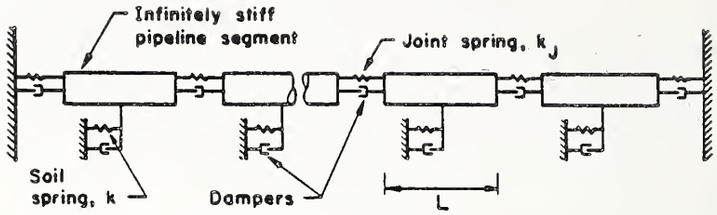

Figure 14. Mechanical Model for a Pipeline with Joints (39)

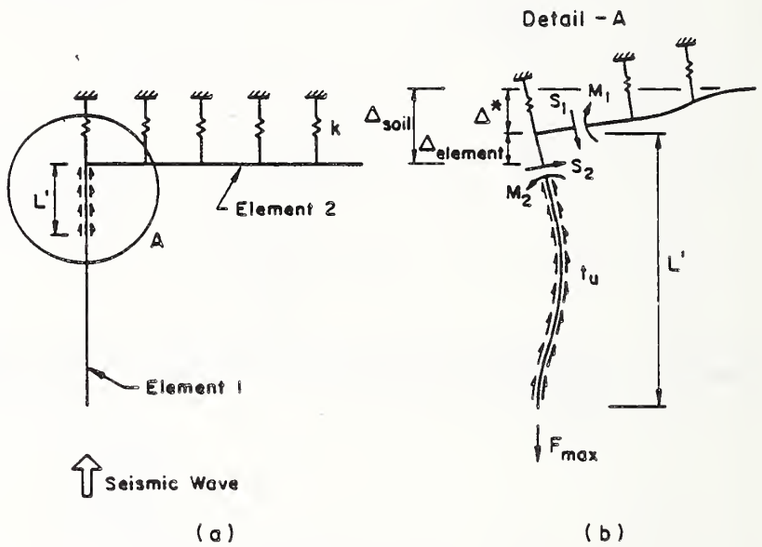

Figure 15. Representation of the Forces, Moments, and Displacements at a Pipeline Bend (12)

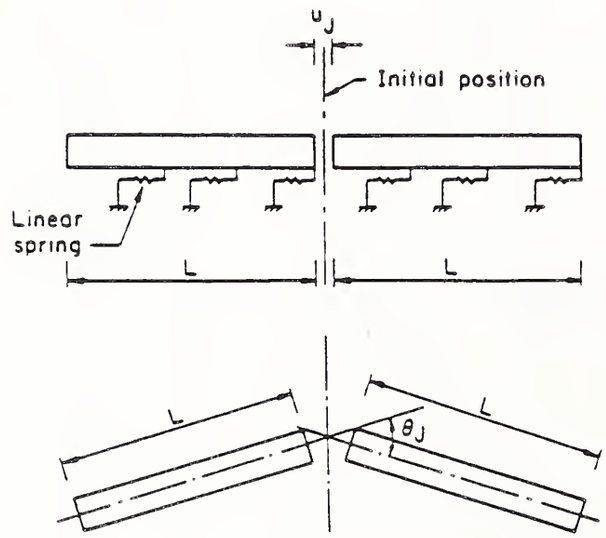

Figure 13. Static Conditions for Pipeline Joint Rotation (44)

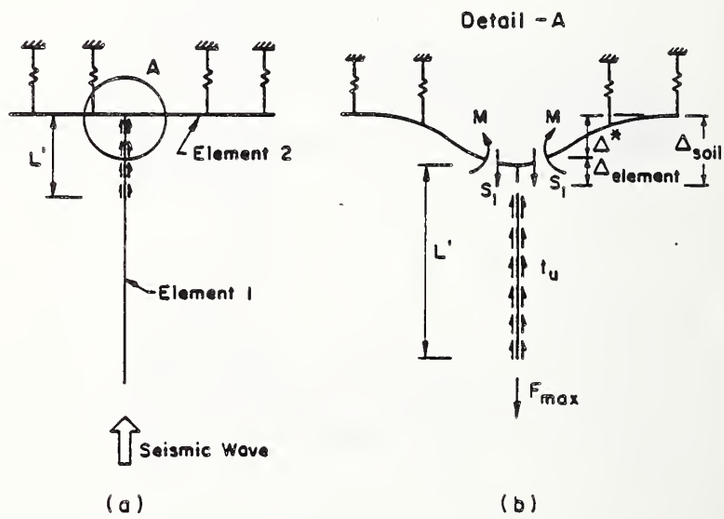

Figure 16. Representation of the Forces, Moments, and Displacements at a Continuous Pipeline Tee (12)

Some Recent Studies on Lifeline Earthquake Engineering in the United States: Analysis and Design

BY

Masanobu. Shinozuka[1] and Leon R. L. Wang[2]

ABSTRACT

This paper reports some recent studies on analysis and design of lifelines in the United States. It consists of two parts: Part A deals with component design and analysis while Part B deals with systems aspects. Dr. Leon R. L. Wang is mainly responsible for Part A, while Dr. Masanobu Shinozuka for Part B. A companion paper written by O'Rourke and Isenberg [A.0] reports on some recent experimental and field studies on lifelines in the United States.

In Part A, the recent developments of component analysis and design of buried pipelines subjected to ground strains or liquefaction induced by seismic shaking (ground wave effects) and large ground movements by several researchers in the United States are reviewed and discussed including work of the authors.

Part B delineates the unresolved issues associated with systems aspects of lifeline earthquake engineering, particularly those of telecommunication transmission facilities network systems, with additional related comments on water transmission pipeline systems. The text in Part B is primarily based on the work performed by Dr. Shinozuka and his associates. Nevertheless, it is hoped that the text describes physical and topological issues that still need to be addressed for the purpose of seismic systems analysis of telecommunications networks.

The results of the studies performed on component design and analysis of lifeline systems as described in Part A of this paper obviously play an important role in determining system survivability and serviceability as described in Part B.

In both parts, emphasis will be placed on those subjects matters that are well suited for joint research between the United States and Japan.

KEYWORDS: Buried Pipeline; Ground Movement; Lifeline; Seismic Shaking; Soil Liquefaction; Telecommunication

PART A: COMPONENT DESIGN/ANALYSIS ASPECTS

A.1. INTRODUCTION

Lifeline systems, which include water and sewer lifelines, oil and gas lifelines, electric power and telecommunication, transmission lines, and transportation lifelines etc. have been damaged heavily by recent earthquakes around the world such as 1971 San Fernando Earthquake, 1976 Tangshan Earthquake, 1978 Miyaki-Ken-Oki Earthquake, and 1985 Mexico City Earthquake and among others. The earthquake damage to these lifelines has recently been receiving more attention because of the impact of these systems upon the populus during and after a major earthquake due to the loss of fire fighting capabilities (water lifeline), disruption of transportation of human and goods (transportation lifeline) and energy (oil and gas lifeline) and possibility of disease (sewer lifeline), etc.

At the present time, scientists, researchers and engineers in the United States, Japan, and other countries are now actively engaged in research for adequate design for all lifeline systems. In the United States, the efforts are represented by several specialty conferences on the subject [A.1 to A.9]. Due to its diversity of the subject, this part of the paper will deal only with the component analysis and design of buried pipelines. The discussions of transportation lifelines, electrical power and communication lifelines etc. are not included.

A.2. HISTORICAL BACKGROUND

The overview of seismic damage of buried pipelines was reported by L. Wang and M. O'Rourke [A.10]. Recently, a comprehensive review on Seismic response of buried pipeline was published by T. O'Rourke et al [A.11] with more than 180 references.

In general, there are three causes of seismic hazards to below-ground lifelines, namely: a) soil straining induced by seismic ground shaking, b) ground movement/rupture and c) soil liquefaction induced by ground shaking.

The major seismic hazards have been observed to come from large ground movement/rupture along fault or soil liquefaction zones. However, their effects are limited to local regions that inherit such potential hazards.

[1]Department of Civil Engineering and Engineering Mechanics, Columbia University, New York, NY 10027, USA

[2]Department of Civil Engineering, Old Dominion University, Norfolk, VA 23508, USA

The effects of wave propagation from seismic ground shaking to the damages of buried straight pipelines located within uniform firm soil have been found to be relatively minor as reported by Isoyama and Katayama [A.12]. The affected area is rather large, however. Without ground failure the damage of buried pipelines occurred mostly at regions where the soil and/or geological conditions change and at joints and junctions [A.13]. Since seismic shaking affects a large area, the design of buried pipeline to seismic shaking is unavoidable.

In this paper, the analysis and design of buried pipeline components for all three conditions will be reviewed and discussed.

A.3. EFFECT OF SEISMIC GROUND WAVES

Under the seismic shaking environment, the response behavior of buried pipelines has been observed to be controlled by the ground displacement/strains, predominantly in the axial direction by Kubo et al [A.14] and the dynamic effects to be negligible by Sakurai and Takahashi [A.15]. To aid the design of buried lifelines, simplified and quasi-static analyses for the response of straight pipelines, bends and junctions to seismic ground waves are discussed. The major assumptions and limitations are that the ground has not failed or liquefied and the traveling wave is constant in speed, shape, and magnitude. Further assumptions or deviation from above conditions will be described at the appropriate subsections dealing with specific components.

A.3.1 Straight Pipelines

Analytical methods for straight pipelines can be grouped into two categories, namely: continuous and jointed pipelines. Continuous pipelines are generally modeled as beams, which are connected to an elastic medium, and their responses can be determined in closed form. On the other hand, numerical solutions are typically required for the analysis of jointed pipelines.

A.3.1.1 Continuous Pipelines

The simplest method to analyze continuous pipelines is based on the assumption that buried pipelines are perfectly bonded to the surrounding soil [A.15, A.16]. In other words, it assumes no relative motion between the pipe and the ground. Thus, as upper bounds, one can take the seismic ground strains as the pipe strains and the seismic ground curvature as the pipe curvatures. This is equivalent to assuming that the pipe has no stiffness and therefore, will follow the ground exactly.

For the analysis and design of continuous pipelines, the upper bound of the axial strain of the pipe, ϵ_p, will be the maximum ground strain, ϵ_g, due to the earthquake:

$$\epsilon_p = \epsilon_g = \pm V_{max}/C_p \qquad (A.1)$$

The upper bound for the maximum curvature of the pipeline, χ_p, will be the maximum ground curvature, χ_g:

$$\chi_p = \chi_g = a_{max}/C_s^2 \qquad (A.2)$$

where V_{max} is the maximum ground velocity and a_{max} is the maximum ground acceleration during a seismic event at the site; C_p and C_s are the longitudinal (compressive) and transverse (shear) wave propagation velocities, respectively, of the controlling environments with respect to the pipeline. If a pipeline with diameter D and the soil move together, the maximum pipeline bending strain ϵ_b is

$$\epsilon_b = \pm\, a_{max}\, D/2\, C_s^2 \qquad (A.3)$$

If a continuous piping system can meet above sets of upper bound criteria (strain and curvature), the pipeline will be adequate against earthquakes that produce ground velocities and accelerations less than the V_{max} and a_{max} in an environment that has ground wave speed greater than the C_p and C_s used in the analysis.

For important projects such as nuclear power plants, the effective apparent wave propagation velocities must be investigated carefully. However, for preliminary design, the wave propagation velocities, C_s and C_p, at the site may be determined by:

$$C_s = \sqrt{\frac{G}{\rho}} \text{ and } C_p = \sqrt{3}C_s \qquad (A.4)$$

where G is the soil shear modulus and ρ the soil mass density.

Note that the effective wave propagation velocity is affected by the characteristics of soil of deeper layers, one should not use the shear modulus of the soil just near or surrounding the pipe. Engineering judgement must be exercised.

The American Society of Civil Engineers's Committee on Seismic Analysis [A.17] recommends an apparent wave propagation velocity between 2000 and 3000 ft/sec (610 to 915 m/sec) for a conservative estimate of pipeline strain. Measurements of apparent propagation velocities by Japanese researchers [A.18] indicate that the recommended values are indeed conservative and that a velocity of 3000 ft/sec (915 m/sec) would be appropriate as a lower bound estimate for most conditions.

One must note that Eq. (A.1) is based on the assumption that pipelines are rigidly bonded to the soil. Under actual conditions, ground wave displacements are transmitted to the pipeline by

means of shear. In the limit, these displacements are constrained by the amount of shear deformation and resistance mobilized at the soil-pipeline interface.

The effects of relative displacement between soil and pipeline can be accounted for by the concept of frictional slippage length [A.19]. If it is assumed that the ground strain ε_g is constant, slip will occur near the ends of the pipeline to mobilize a maximum frictional force per unit pipe length t_u. This condition is illustrated in Fig. 1. The maximum slippage length L_f, is:

$$L_f = 2\ \varepsilon_g\ EA/t_u \qquad (A.5)$$

in which A is the cross-sectional area of pipeline and E is the modulus of the pipeline material.

The maximum frictional force per unit pipe length t_u can be obtained from

$$t_u = \pi D\ (1 + K_o)\ \gamma\ H \tan\ \delta/2 \qquad (A.6)$$

in which ρ is the unit weight of soil, H is the depth of the pipe, K_o is the coefficient of earth pressure at rest, and δ is the interface friction angle between the soil and pipe.

If the pipeline is shorter than twice the maximum slippage length, the maximum pipe strain ε_p would be smaller than ε_g. When seismic waves are considered, it can easily be shown that maximum ε_p occurs for harmonic wave lengths greater than one-half the maximum slippage length. The maximum strain in pipelines for full slip where $\varepsilon_p \leq \varepsilon_g$ is therefore

$$\varepsilon_p \leq \lambda\ t_u/8EA \qquad (A.7)$$

where λ is the wave length.

Other methods of analysis account, in addition to peak ground displacement and/or velocity, for the shape of seismic ground waves [A.20]. The methods involve solutions of differential equations of equilibrium for specified locations of the seismic waves and can account for effects of slippage between soil and pipe [A.20]. It makes use of a conversion factor β_o to estimate the pipe strain by multiplying the free field strain ε_g,

$$\varepsilon_p = \beta_o\ \varepsilon_g \qquad (A.8)$$

The study [A.20] showed that for most cases, β_o is almost 1 (0.98 - 0.99) for straight pipes.

A.3.1.2 Segmented Pipelines

For segmented pipelines, the maximum relative joint displacements and maximum joint rotations become important design parameters in addition to the pipe strains and curvatures.

The methods for the analysis of pipelines with joints are more general than those in the previous subsection since continuous pipes can be viewed as segmented pipes with infinitely stiff joints.

The simplest method for the analysis of jointed pipelines is the static solution [A.21]. It provides an upper bound on the relative displacement and rotation in joints. Figure A.2 shows the model considered in this method. Soil behavior is idealized by linearly elastic springs with stiffness k and the pipe segments are assumed to be infinitely rigid. It is also assumed that joint forces are negligible and the length of seismic waves exceeds significantly the dimension of the pipe segments. According to these assumptions, the maximum relative joint displacement Up, and rotation θ_p are

$$U_p = \varepsilon_g\ L = V_{max} L\ /Cp \qquad (A.9)$$

$$\theta_p = \chi_g\ L = a_{max} L\ /C_s^2 \qquad (A.10)$$

where L is the length of the pipe segment.

If a buried segmented piping system can meet all four sets of upper bounds (pipe strain and curvature; joint displacement and rotation) for a design earthquake, the pipeline will be conservatively safe because in the real case, the pipe strain and relative joint displacement will jointly take-up the imposed ground strain and both the pipe curvature and joint rotation will jointly take-up the imposed ground curvature. One must note that the above conclusions would only be true if one can accurately estimate the maximum ground velocity and acceleration in the region and the seismic wave propagation velocities at the site.

A more realistic representation of the soil-pipe-joint system is shown in Fig. A.3. The equations of equilibrium incorporate both inertia and damping terms [A.22,A.23]. Due to the fact that the dynamic effects to the seismic response of buried pipeline are negligible [A.14], the inertia and damping terms in the dynamic equations of motion have been dropped.

As indicated in Fig. A.3, a pipe segment has axial stiffness (EA/L) and a node at each end. The joints are represented by elasto-plastic joint springs (Fig. A.4). The resistance forces that develop between the soil and the pipe segments are represented by elasto-plastic soil resistance springs. (Fig. A.5) Note that the soil slippage characteristics have been taken into account in the plastic part of the soil spring.

The equations of static equilibrium, obtained from the variation of the total strain energy in the soil-structure interaction system [A.24, A.25] are as follows:

$$[K_{system}] \quad \{X\} = [K_{soil}] \quad \{X_G\} \qquad (A.11)$$

$$2n \times 2n \qquad 2n \times 1 \qquad 2n \times 2n \qquad 2n \times 1$$

where $[K_{system}]$ and $[K_{soil}]$ are the structural system and soil resistance matrices, respectively, $\{X\}$ is the nodal axial displacement vector and $\{X_G\}$ is the ground displacement vector which varies with time.

The solution of pipe motion $\{X\}$ shown in Eq. (A.11) depends on the inputs of the ground motion, $\{X_G\}$. Since $\{X_G\}$ is a function of time, the solution of $\{X\}$ is also a function of time.

Assuming that the wave form of the traveling seismic excitation remains constant over the entire length of the pipeline which consists of n-segments, the inputs of the time-space varying ground motions are:

$$X_{Gi} = \begin{cases} 0 & t-n_i < 0 \\ \Delta_{max} h(t-n_i) & t-n_i > 0 \end{cases} \qquad (A.12)$$

where Δ_{max} is maximum ground displacement input; $h(t)$ is the displacement time function; n_i is the delay time of the seismic wave traveling from the first support to the end node of the i^{th} pipe segment considered as:

$$n_i = \sum_{j=1}^{i} L_j / C_j \qquad (A.13)$$

and C_j is the traveling wave propagation velocity of soil/geological environments surrounding the pipe segment j.

The solution of the system of static governing equations requires the input of ground displacement at an instant of time. The resulting pipeline nodal displacements, X's, are used to determine i^{th} average pipe strain, ε_i and i^{th} relative joint displacement, U_i as:

$$\varepsilon_i = (X_{2i} - X_{2i-1})/L_i \quad \text{and}$$

$$U_i = X_{2i+1} - X_{2i} \qquad (A.14)$$

By comparing these parameters within the earthquake time domain, the maximum values of average pipe strains, ε_p; relative joint displacement, U_p and their corresponding occurrence time and location are determined. Computer solutions and examples can be found in Refs. A.25 and A.26. Several general conclusions can be made through the parametric study:

The effects of pipe segment length on pipe strain and relative joint displacement for three pipe lengths of 10 ft. (3.05 m), 20 ft. (6.10 m), and 40 ft. (12.20 m) were studied using a 20 segment pipeline with elastic joint springs and under a uniform soil environment. It was found that the longer the pipe segment is the larger the pipe strain, and also the larger the relative joint displacement will be. Since the pipe segment length is proportional to the delay time from one end of the pipe to the other end, the longer delay time directly affects the seismic response behavior.

The effects of geotechnical interfaces (change of soil stiffness) and geological interfaces (change wave propagation speeds) were studied. The maximum pipe strain was found to occur near the interface and always in the region with higher soil stiffness. For traveling speed case, the maximum strain was found to occur again near the interface, but in the region with lower traveling speed.

The effects of a number of other parameters on the response of buried pipelines, such as pipe size (diameter), pipe materials, various combinations of soil and joint plasticity, wave propagation velocity, wave forms, duration and magnitude, have been investigated and reported [A.25, A.26]. In general, buried pipelines with longer segment lengths, in regions with lower wave propagation speed, or surrounded by stiff soil (high spring constant) will produce large pipe strains and relative joint displacements. However, soft soil which may slip and soft joint spring which may yield, will reduce both pipe strains and relative joint displacements.

A.3.2 Bends and Junctions

The methods available for the seismic analysis of bends and tees deal generally with continuous pipelines. In most cases, the seismic input is characterized by postulated ground displacement waves [A.19, A.20, A.27]. It is assumed that the pipelines are composed of elastic linear materials and that soils can be represented by rigd-plastic or elasto-plastic models.

A.3.2.1 Bends

Figure A.6 shows the deformation of a bend when the direction of seismic wave propagation coincides with the pipeline referred to as element 1. The deformation of element 1, Δ_e, has two components as shown below

$$\Delta_e = S_1 L_f/EA + t_u L_f^2/2EA \qquad (A.15)$$

where L_f is the effective slippage length, which can be obtained by the following equation:

$$L_f = \frac{4EA\bar{\beta}}{3k}\left(\sqrt{1+\frac{3\epsilon_g k}{2t_u\bar{\beta}}}-1\right) \qquad (A.16)$$

in which $\bar{\beta} = \sqrt[4]{(k/4EI)}$, I is the moment of inertia of the pipe, $k = Dk_s$, and k_s is the modulus of subgrade reaction. The force S_1 at the junction can be approximated by

$$S_1 = \epsilon_g EA - t_u L_f \qquad (A.17)$$

in which $\epsilon_g EA$ is the axial force induced in element 1 when there is no slippage and the soil strain is assumed to be ϵ_g and $t_u L_f$ is the axial force induced in the same element over L_f when slippage occurs.

The soil displacement Δ_s can be approximated conservatively by

$$\Delta_s = \epsilon_g L_f \text{ or } u(\lambda/4) \qquad (A.18)$$

where u is the free field displacement function at quarter wave length.

The force S_1 has been related in Ref. [A.20] to the relative displacement between the soil and element 1 as:

$$S_1 = (3k/4\ \bar{\beta})\ (\Delta_e - \Delta_s) \qquad (A.19)$$

The force S_2 and the bending moment M can be determined by elementary structural analysis as:

$$S_2 = S_1/3 \qquad (A.20)$$

$$M = S_1/3\ \bar{\beta} \qquad (A.21)$$

3.2.2 Tees

Tees can be analyzed by similar approaches. Figure A.7 shows the deformation of a tee when the seismic wave travels along the element 1 without further explanation. The S_1 force and moment are given below:

$$S_1 = (\epsilon_g EA - t_u L_f)/2 \qquad (A.22)$$

in which

$$L_f = \frac{EA\bar{\beta}}{2k}\left(\sqrt{1+\frac{4\epsilon_g k}{t_u\bar{\beta}}}-1\right) \qquad (A.23)$$

and

$$M = S_1/2\ \bar{\beta} \qquad (A.24)$$

The previous methods of analysis are based on the assumption that the bend angle does not change during the seismic excitation. This assumption is not realistic for bends involving thin wall pipelines, for which a more appropriate model should be based on curved thin wall tubes [A.4, A.28]. This type of representation accounts for bend flexibility and results in a substantially lower bending moment in the pipeline. Details can be found in Ref. [A.4, A.28].

A.4. RESPONSE OF BURIED PIPELINE TO GROUND MOVEMENTS

The analysis of pipeline response to ground movements requires input of soil displacement patterns and soil-pipeline interaction resistant characteristics. The pipeline model may be based on continuous beam, jointed beam, shell, or combined beam and shell representations. Because soil and ductile pipe properties are governed by nonlinear stress-strain relationships, the analysis may require complex numerical procedures. The following discusses several analytical studies.

A.4.1 Continuous Pipeline Response to Fault Movements

Analytical treatments of continuous pipeline deformation from fault movement have been developed by several researchers [A.29 to A.34]. This paper briefly discusses some of their developments.

A.4.1.1. Newmark and Hall Model [A.29, A.30]

Fig. A.8 shows a plan view of a pipeline which is intersected by a right lateral strike-slip fault at an angle, β. The pipeline is oriented so that fault displacement Δ_f will cause tension in the buried pipeline. It is assumed that sufficient geologic evidence is available to determine such orientation.

Newmark and Hall [A.30] analyzed the pipeline deformation as an antisymmetric pattern of circular arcs, with each circular segment spanning the fault centerline and the location of an anchor point. The distance between the fault and the anchor point is known as the anchor length, L_a. Anchors may be caused by bends, tie-ins, and other features which develop substantial resistance to axial movement. Alternatively, the anchor point may represent an effective anchor length, beyond which there is no axial stress imposed in the pipeline from fault movement. The pipeline is buried at a depth to centerline H in soil with unit weight γ. The coefficient of at-rest horizontal soil pressure is K_o, and δ is the angle of frictional resistance at the soil-pipeline interface. Using a numerical procedure, relative sensitivity of pipeline response to key parameters were studied. The most important parameters affecting the pipeline's capacity for fault displacement are the angle of crossing β, and the effective anchored length L_a. Increasing β from 50 to 80 degrees increases the capacity for fault displacement by more than a factor of four.

The most favorable angle of crossing is approximate 90°. Increasing of burial depth from 3 to 10 ft (0.9 to 3.3[m]) will decrease the maximum tolerable movement by a factor of four because lower soil resistance from shallower buried depth will allow larger fault movement. Fault displacement capacity increases in direct proportion to wall thickness.

A.4.1.2 Kennedy, Chow, and Williamson Model [A.31,A.32]

The analytical method developed by Kennedy, Chow, and Williamson [A.31,A.32] represents an improvement in model sophistication principally because it accounts for increased frictional resistance near the fault crossing and for pipeline bending strains. It is assumed that greater frictional resistance is developed along the curved portion of the pipeline than along adjoining sections because of high horizontal soil pressures resulting from large relative movements between the pipeline and surrounding ground.

The Kennedy, Chow, and Williamson model gives a more conservative result than the Newmark and Hall model, chiefly because of the increased level of frictional resistance along the curved portion of the pipeline. Because of large deflection is involved, passive soil pressure has been taken into account. Over a wide range of β the Kennedy, Chow, and Williamson model predicts about half the fault movement capacity as the Newmark and Hall model.

Note that in Kennedy et al. and Newmark and Hall models, only axial tensile force at the point of inflection was used for equilibrium and only axial strength of pipe was used for failure criterion. No flexural resistance was considered.

A.4.1.3 Wang and Yeh Model [A.33]

Note that the omission of flexural rigidity of pipe using Newmark and Hall's model [A.29,A.30] and Kennedy et al's model [A.31,A.32] cannot satisfy the equilibrium condition for a pipeline across a "reverse" strike-slip fault that will cause compression in the pipeline. Another assumption in these papers was that the far ends (away from the point of inflection) of the pipeline approach tangentially to the undeformed lines. Actually, the response behavior of buried pipeline at far ends to fault movement should be similar to a beam on an elastic foundation.

To improve the existing results and to generalize the formulations for buried pipelines across any strike-slip faults that may cause either tension or compression failure of the pipeline, Wang and Yeh Model [A.33] included the bending rigidity of pipe, a shear force at the point of inflection of the curved pipe crossing the fault zone and a boundary condition related to a semi-infinite beam on an elastic foundation at some distance away from the fault zone, as shown in Figure A.9. The effects of axial force and bending moment interaction and large deformation will also be included in the analysis. Thus, the problem is two-fold non-linear; geometry non-linearity and material non-linearity. Note that without buckling consideration, the formulations outlined below for buried pipeline across strike-slip faults, can also be applicable to reverse strike-slip with little modifications. In the paper, the design criteria for buried pipeline proposed were (a) the axial stress must be smaller than the yeild strength, of the material and (b) the resulting moment must be smaller than the resisting moment capacity of the pipe section. The influence of the axial forces on the resisting bending moment of a steel pipe can be found in Ref. [A.33].

A series of parametric analyses has been undertaken to study the influence of the fault movement effects on the design of buried pipelines. The general conclusion was that the resisting capacity of buried pipeline to fault movement would be larger for larger crossing angle, smaller buried depth and smaller diameter pipe. However, the study found that the results from earlier studies that were based only on axial stress criterion were unconservative.

A.4.2 Jointed Pipeline Response to Fault Movement

A jointed pipeline can fail by tension in three ways: (a) excessive tensile and bending deformation of the pipe, (b) excessive rotation at a joint, or (c) pullout at a joint. A simplified analytical method for evaluating jointed pipeline response to abrupt soil movement has been developed by O'Rourke and Trautmann [A.34]. As shown in Fig.A.10, the maximum tolerable strike-slip fault displacement d_f can be evaluated as being composed of a critical transverse component d_c and a critical longitudinal component S_L. The value of S_L is given by the displacement pullout capacity of the joint. For many water pipeline with rubber gasket joints, S_L is simply the depth of spigot penetration in the bell end of the adjoining pipe [A.35]. Even when special fixtures are provided to restrain pullout, the axial resistance of the fixtures is generally low compared to the forces developed by permanent soil displacement. Accordingly, S_L can be taken as a conservative limit.

As seen in Fig. A.10, the critical fault movement is defined as:

$$\tan \beta_f = d_c/S_L \qquad (A.25)$$

in which β_f defines the angle of pipeline-fault intersection for which failure may occur by either the transverse or longitudinal components of fault movement.

This value represents the optimal orientation of the pipeline because the fault movement will mobilize the maximum capacities for pullout, rotation, and pipe tension at this angle. For angles larger than the optimal orientation, failure by pipe bending or joint rotation will occur at smaller fault displacements. For angles less than this optimal orientation, failure by joint pullout will occur.

The tolerable fault displacement can be plotted as a function of β_f. Fig.A.11 shows d_f as a function of β_f for various types of jointed pipeline [A.34]. The cross-hatched area in the figure refers to a zone in which cast iron pipeline failure will depend on the location of lead joints relative to the fault centerline. Mechanical joints are shown to fail by pullout at decreasing levels of displacement for $\beta_f < 70$ deg. Extra long, restrained couplings are shown to accommodate potentially as much as 13 in. (330 mm) of abrupt soil movement.

A.4.3 Pipeline Response to Compressive Ground Movement

In previous sections, most studies assumed that the pipeline was oriented to develop elongation in response to ground movements. There are, of course, many instances in which the orientations of potential ground ruptures cannot be determined accurately, and the pipeline may therefore be subjected to compression.

Two modes of deformation can occur when a pipeline is severely compressed. The pipeline may buckle as a beam or it may deform by local warping and wrinkling of its wall.

An analytical investigation of shell buckling [A.36] shows that buried pipelines buckle dynamically under an axial compressive stress and strain very similar to the static buckling stress and strain. The same study demonstrates that the soil stiffness and internal pipe pressure can substantially increase the axial buckling capacity of the pipe.

An experimental study [A.37] indicates that, for a ratio of pipe diameter to wall thickness of 100, local wrinkling occurs at compressive strains between 0.004 and 0.006. Compressive fault displacement will cause strain to accumulate locally at the point of initial wrinkling, thereby leading to a severe concentration of strain at movements considerably less than those causing large tensile strains at fault crossings.

Analytical work has been performed on the problem of beam buckling of pipelines [A.38]. The analyses pertain to conditions in which the tranverse vertical restraint on the pipeline is assumed to be constant and the pipeline is modeled as a linear elastic beam.

Solutions have been presented for two general conditions, pertaining to a pipeline resting on an elastic and rigid foundation.

A.5. PIPELINE RESPONSE IN A SOIL LIQUEFACTION ENVIRONMENT

The performance of pipeline buried in a soil liquefaction zone has not been studied until recently. Preliminary experimental studies have been initiated by Kuribayashi et al. [A.39,A.40] and analytical approaches by Wang and his colleagues [A.41,A.42]. The following discusses briefly these analytical approaches.

A.5.1 Continuous Pipelines

In the liquefiable zone, the seismic waves propagating faster through firm soils along the pipe axis cause an incoherent movement at both edges of the pipe submerged in liquefied mediums. Therefore, a pipeline buried under the liquefied area is subjected to seismic incoherent motions which generate longitudinal and lateral forces on the pipeline. Breaking and buckling are two common pipeline failure modes.

The surrounding soil mediums of the pipe within the liquefiable zone during the earthquake losses shear strength due to seismic waves and the stiffness of the soil foundation varies (decreases) with time within the liquefiable region. The pipe could be considered partially supported until the soil is completely liquefied. This paper proposed a simplified beam-column (buried pipe) model on two time verying strength elastic foundations, one for liquefiable and the other for non-liquefiable zones as shown in Fig. A.12. A finite difference technique involved both temporal and spatial variables is employed to solve the dynamic responses of buried pipelines passing through a soil liquifiable zone which is subjected to an incoherent ground shaking.

For evaluating the dynamic effect of longitudinal incoherent displacement (or strain rate) several moving (loading) speeds applied at the movable end of the pipe are chosen to evaluate their influences on the lateral deflection and axial load of the pipe. Details can be found in Ref.[A.41] and thus will not be repeated.

The results of load response histories showed that the dynamic displacements and axial load of the pipe increase with an increase in the moving speed (strain rate) and thus increase the possibility of dynamic buckling. Since the boundary conditions and the moving speeds do not represent exactly the field conditions, the results can be considered only qualitatively. More studies would be needed to clarify the actual behavior of pipeline passing through soil liquefaction zone.

A.5.2 Pipeline With A Manhole

An experimental research on the responses of buried pipeline including a manhole (Fig. A.13) was carried in saturated sand by Kuribayashi et al. [A.40]. However, no analytical solution has been reported for comparisons. The exact response of a buried pipeline system including manholes in a soil liquefaction environment subjected to seismic shakings is complex and the complete solution for such complex system has not been found.

In a paper, Wang et al. [A.42] proposed to examine analytically both the horizontal and vertical responses of the buried pipeline experiment including a manhole under a soil liquefaction from a realistic but still simple mathematical model. For vertical responses only the static analysis will be applied since the buoyancy force behaves in a static manner. However, for the horizontal responses, a non-linear dynamic analysis including time varying soil spring and damping is proposed. Case studies are carried out to evaluate the response behavior of buried pipelines with and without a manhole. The analytical results are comapred to the experimental results obtained by Kuribayashi et al. [A.40].

Analytical procedure involves critical determination of various influential parameters in the model including: (a) dynamic horizontal water and soil pressures, (b) subgrade reaction forces, and (c) damping characteristics at the structure and soil interface. Unfortunately, the exact values of these parameters are not completely known and assumed values have to be used in the analytical study.

The analytical responses are in general higher than the experimental observation. The discrepancy may be attributed to the sudden change in the parabolic loading case, the approximation of the Rayleigh-Ritz shape function, the under estimation of the damping ratios and finally the omission of the soil-structure-fluid interaction.

A.6 DESIGN CONSIDERATIONS

In the United States, there is no seismic code for buried pipeline design except some guidelines [A.3,A.4]. Some aspects of the lifeline design considerations have been discussed by Wang [A.43].

In the absence of seismic design codes for buried pipelines, several passive design considerations have been used by engineers to reduce seismic damage and minimize hazardous effects. Following are some common engineering practices and recommendations:

1. Redundancy should be built into the distribution system. More smaller pipes should be used in lieu of a single larger pipe to minimize reduction in operation due to breakage of pipes.

2. Blow-off valves should be installed at a location where higher seismic activity is anticipated, such as along a fault line. By this technique, water is led to a nearby reservoir after a blow-off valve fails during an earthquake.

3. Ductile pipe materials such as steel or ductile iron should be used to allow larger pipeline deformations.

4. For segmented pipelines, flexible joints such as rubber gasketed connections should be used to provide for relative joint movements. For anticipated large ground movement, extra long restraining sleeves or 'Bellow Joints' should be used. When feasible, shorter segments which will experience less strain imposed by the ground motion, should be used. Also, relative joint displacements are less for shorter segments.

5. If feasible, consideration should be given to encasing the pipeline in a larger tunnel in order to isolate the pipeline from the seismic ground motion, or to lubricating the pipeline in order to increase the "slippage" between the pipe and the surrounding soil.

A.7. SUMMARY AND CONCLUSION

Part A has summarized the recent developments in component analysis and design of buried lifelines subjected to ground strains or liquefaction due to seismic shaking and ground movements.

To aid in the design of buried pipelines for earthquake loads, various analysis procedures and design considerations for various environments have been reviewed and discussed.

In conclusion, it is important to note that the behavior of buried pipelines is governed by the relative displacements of the ground along the route. Ductility or flexibility to allow buried pipeline movement with the ground is the most important factor for the seismic design of such structures.

PART B: SYSTEMS ASPECTS

B.1. INTRODUCTION

Analytical models appropriate for the network analysis of telecommunication transmission facilities network systems must be developed. Combining these models with those for "exchange office buildings," representative models for the total telecommunication network systems should then be constructed. The utilities equipment may have to be integrated as part of

the total network system. Methods should then be developed to estimate the vulnerability (or equivalently survivability) and the serviceability of such networks. Here, the term "exchange office buldings" is used for simplicity to represent station equipment, switching facilities and related structures including the building which houses them.

The seismic vulnerability indicated the susceptibility of the network to a seismic event (or a sequence of seismic events) and is to be measured in terms of the probability; either the probability of vulnerability or probability of survivability. In estimating such a probability, not only the susceptibility of the transmission facilities network but also those of the exchange office buildings must be taken into consideration. It appears reasonable to model the total network system as a linear graph consisting of vertices and branches in which the vertices represent the exchange office buildings and the branches represent the transmission facilities, typically above- and under-ground transmission cables. Thus, a seismic event could result in the physical damage of the network system equivalent to the removal of the subset (or possibly the entire set) of vertices and branches from the original network. We could postulate that the network has survived an earthquake if all possible pairs of stations retain a minimum level of communication capability. In fact, survivability may be defined in a number of ways. On the one hand, the survival of a network, for example, may require more than one independent path between all the pairs of vertices of the network. On the other hand, in the case of those emergency situations arising from destructive earthquake, we may have to be satisfied (at least immediately after an earthquake), with the following forms of partial connectivity as the definition for network survival: (1) connectivity only among key pairs of stations and (2) a certain percentage of vertex pairs remaining communicable. In developing such criteria, we must have a good understanding of the extent to which and the way in which the communication network system is needed immediately after an earthquake for medical assistance, civil order, fire fighting, and other purposes.

The possible removal of the vertices mentioned above results from damage to the exchange office buildings caused by excessive structural vibrations or structural failures of the buildings housing them due to an earthquake. Similar situations arise when underground water transmission network systems are analyzed for their seismic vulnerability in which, for example, possible failures of pumping stations (these are vertices in that case) need to be taken into consideration. In dealing with telecommunication systems, however, station equipment, switching facilities and the buildings housing them, which as a set are represented by a vertex in the associated linear graph may in turn be modelled as a sub-network. The telecommunication network system, with such sub-networks replacing the vertices, appears to be a more consistent model of the total system and may have to be developed for (1) determining the degree of survivability (or vulnerability) of an existing or proposed system and (2) deriving the optimum designs or improvement strategies on the basis of maximum survivability or minimum vulnerability.

Turning now to the question of serviceability immediately following an earthquake, the quality of service is usually measured in terms of the delay and/or blocking which are obviously dependent upon the post-earthquake states of physical damage and hence functionality of the total network system. Those serviceability criteria appropriate for post-earthquake emergency situations must be developed and evaluated in terms of the probability that the total network system will be able to meet a specified service criterion following an earthquake. Furthermore, study must be made to establish general strategies for restoring the level of service specified by such a criterion if the total network system is damaged to the extent that it cannot satisfy the specified service. The relationship between vulnerability and serviceability is also an interesting subject for future study.

B.2 FAILURE PROBABILITIES OF TRANSMISSION FACILITIES

The first step towards evaluating the survivability and serviceability of a total network system is to assess the probability of failure of various specific items that are classified in the categories of station equipment, switching facilities, building structures and transmission facilities. The transmission facilities, and in particular, the transmission cables and conduits are mainly considered here. The probabilities of failure of those items belonging to the categories of station equipment, switching facilities, building structures and utilities equipment may be evaluated within the context of traditional earthquake engineering which usually deals with building structures and secondary systems attached to it.

Six principal types of transmission media are used for providing transmission channels: (1) open-wire lines, (2) paired cables, (3) coaxial cables, (4) radio, (5) wave guides, (6) optical fibers. For existing urban telecommunication network systems, only media (2) and (3) appear to be important for seismic analyses, at least at this time.

In most cases, underground cables are placed inside conduits and then buried underground.

The conduit system provides physical protection for the cables and also allows new cables to be added inexpensively, although at the expense of an initial cost.

Several potential failure modes of cables (although some of them occur simultaneously) are: (1) rupture of wire conductors, which are the high purity copper, (2) crack, distortion or rupture of insulated materials, whcih are made of wood, pulp, or plastic, (3) rupture of cable sheaths, which are plastic, steel, aluminum, or lead, and (4) rupture of conduit systems which in turn may lead to the cracking, distortion, or rupture of the cables.

Failure mode (1) completely disrupts communication while mode (2) will possibly cause electrical interference (cross-talk) between cable pairs. Modes (3) and (4) will primarily cause water to enter, constituting the principal hazard to which underground cables are subjected since any significant amount of water into the core of pulp-insulated cables will render most of the circuits inoperative. In this regard, a damage matrix displaying physical failure (damage) modes and associated resisting capacities in matrix form should be developed for transmission cables with and without conduits. This is a task similar to the one performed by Kratky et al. [B.1] with respect to the pipes and joints used for water transmission pipelines. Indeed, it is primarily for the construction of these damage matrices that the studies performed in Part A are useful. However, the task of developing such damage matrices for transmission cables appears to be more demanding in terms of the effort to be expended, since little experimental work has so far been systematically performed on these cables and conduits.

After damage matrices are constructed, we must develop damage probability matrices which will indicate the probabilities of a certain type of cables to sustain different levels of damage under various earthquake intensities measured usually in terms of the Modified Mercalli Intensity (MMI) scale. The notion of a damage probability matrix is initially used in [B.2] to describe the general correlation between building damage and earthquake intensity, mainly on the basis of empirical data, supplemented by a dynamic analysis. Figure B.1 illustrates the basic form in which the damage probability matrix is used in [B.2] for a cost-benefit analysis of building structures. A matrix of this form is constructed for each of the alternative design strategies representing the choice of a set of design parameters such as the lateral force requirement associated with a particular seismic zone, materials to be used, structural types to be designed, etc. Furthermore, such a matrix is to be developed on the basis of theoretical analyses and subjective evaluations, as well as the damage statistics collected from past earthquakes. The damage state describes the degree of damage in a qualitative manner with a central damage ratio indicating the (perhaps highly subjective) average ratio of the repair cost associated with each damage state to the cost of building. The numbers in each column indicate the probabilities with which different states of damage will be inflicted upon the building (designed under a particular strategy) by an earthquake of the particular MMI value associated with that column. The reasons why a certain earthquake intensity will not necessarily result in a certain state of damage are, among others: (1) individual buildings, even if they are designed and constructed to meet the same requirements, will have different resistances depending on the skill and idiosyncrasies of the designer and constructor and (2) the individual ground motions, even if they are categorized in the same MMI scale, will obviously be different in detail.

For telecommunications networks involving networks of transmission cables which extend over a wide underground area, a damage probability matrix reflects the uncertainties (a) in the ground conditions, (b) in the way in which the cables are loaded under seismic conditions, and (c) in the resisting capacity of the cables (or in the failure matrices), in addition to the obvious uncertainties surrounding the details of the earthquake ground motion classified in any particular MMI scale. Therefore, such damage probability matrices will generally be developed (a) under each set of ground conditions, (b) for each type of seismic events in which the cables are loaded differently and (c) for each component of the transmission facilities (e.g., coaxial cable with conduit). In previous work [B.3] dealing with water transmission pipelines, the following five types of seismic events were considered the major causes of the physical damage to pipelines: (1) Ground motion associated with the wave propagation; (2) fault movement at the location of a pipe crossing; (3) liquefaction; (4) landslide; and (5) interference with other under- and above-ground structures.

While the Japanese data illustrated in Fig. B.2 indicate that most of the severe physical damage such as severing of cables appears to have resulted from causes (1) and (4) above, those area in the US for which study is intended to be performed, are often surrounded and penetrated by active faults and at the same time possibly include a large number of liquefaction-sensitive locations of significant size. In addition, in telecommunications systems, cables placed underground lead above-ground to central offices, customers' telephone units, etc. much more often than underground water transmission pipelines. Therefore, interference of the underground cables with other under-and

particularly above-ground structures appears to be a serious problem which needs to be investigated. The severing of the coaxial cables near Sendai, Japan due to the relative displacement between the bridge abutment and the ground observed during the 1978 Miyagi-Ken-Oki earthquake, can be considered as typically resulting from such an interference.

The example of a damage probability matrix shown in Fig. B.3 illustrates the possible damage that can occur to an arc welded steel pipe due to the ground motion associated with seismic wave propagation and is used for the analysis performed in [B.3] and [B.4]. However, this matrix can be used only for the case where the damage at the corner of T- and L-shaped pipe joints buried in soft soil is considered. When the locations of possible damage are relatively well defined, either due to the nature of the seismic events (e.g., events (2)-(5) above) or to the stress or strain concentration within the pipes (e.g., at the corner of T-shaped pipe joints as mentioned earlier), a damage probability matrix established for that location along the pipes (or along the cables for telecommunication cables) can be used to estimate the probability of different levels of damage being sustained by the pipes at that location. In Fig. B.3, "A" indicates soft soil conditions and "β" represents a strain concentration factor to multiply the free-field ground strain to obtain the pipe strain. In fact, an underground water transmission system as shown in Fig. B.4 is considered in [B.3, B.4, B.5]. The system is similar to that of the City of Los Angeles, and the area in which it is embedded is divided into a number of square zones. With the aid of a geological map each square zone is assigned a designation: A (soft soil), B (medium soil), C (hard soil) and F (zone where an identifiable fault exists). Actually, an L designation is considered for zones susceptible to liquefaction, but this designation was not assigned to any square zone due to the difficulty of doing so merely on the basis of the geological map used. In this connection, damage probability matrices similar to that given in Fig. B.3, were developed in [B.3] for other seismic events. For example, a damage probability matrix is developed for the segment of pipe that would be embedded in an L zone considering the following: larger scale liquefaction resulting in a severer state of pipe strain will be induced by a more intense earthquake in more liquefaction susceptible soils.

However, in the case of a straight pipe subjected to the ground motion associated with seismic wave propagation, questions such as where along the pipe the damage might occur or how many points per unit length along the pipe are to be considered as potential damage locations, are by no means easy to answer. To resolve these questions, in [B.3] and [B.4], a vulnerability analysis of underground water transmission lifelines was performed under the assumption that the potential damage locations are located along the pipe at an interval of one-half of the seismic wave length. When we have segmented pipes, however, the joints may be the most vulnerable locations.

Following procedures similar to those described above, damage probability matrices for transmission facilities must be developed, and under similar assumptions, they should be used for a vulnerability analysis. In developing the damage probability matrices, the degradation of the structural integrity of the cables and conduits due to corrosion and other aging and wear-out effects must also be taken into consideration.

B.3 ESTIMATION OF SYSTEM SURVIVABILITY

Once the criteria of system survivability (or vulnerability) have been established, the probability of system survivability (or vulnerability) can be obtained by a variety of approaches using damage probability matrices of the system components. Therefore, the damage probability matrices for station equipment, switching facilities, building structures and utilities equipment must also be developed.

In most communication network systems involving electrical and electronic components with their functions defined either on an `on´ or `off´ basis, the methodology of vulnerabiliity analysis is relatively well established. For example, the so-called "naive approach" [B.6] advocates the use of straight forward Monte Carlo simulation techniques in which the success (on) or failure (off) of each component is simulated based on specified probabilities of success and failure, and the resulting network is checked for its connectivity requirements. Repeated trials will then estimate the survivability in terms of empirical probability. The methods that combine analytical and Monte Carlo techniques, such as the functional simulation approach [B.7] and the Moore Shannon approach [B.8] may also be used effectively. The latter method is typically a semi-Monte Carlo approach in the sense that the nubmer of disconnected sub-networks with, say, exactly k elements within the total network, is simulated by Monte Carlo methods and used in an analytical expression to obtain the probability of network connectivity.

For a seismic analysis, however, the telecommunications systems under consideration are subjected to random seismic environments, variable soil conditions, statistical component strength variations, etc., thus resulting in various levels of component damage. Indeed, to make these otherwise unmanageable complications analytically tractable, we have introduced damage probability matrices for each combination of significant parameters. It is

noted here that the recent trend of using fragility curves with engineering confidence statements is an interesting alternative to the use of the damage probability matrix approach.

The vulnerability of the total network system can be estimated by an analytical method similar to that employed in [B.4] (dealing with water transmission lifeline systems) in which the probability that connectivity between a specified vertex and any of the pumping stations will remain intact was defined as the survivability. However, in view of the more complicated connectivity requirements expected for total telecommunications network systems and in the face of the anticipated difficulty of identifying the combined effects of various levels of damage occurring in a number of components in the system, the analytical method developed in [B.4] will require substantial modifications with a possible need for the partial use of Monte Carlo techniques.

B.4 ESTIMATION OF SYSTEM SERVICEABILITY

Every large telecommunications network is based upon the principle of commonly shared equipment. It is this sharing which causes the phenomenon of delay and blocking. To estimate the serviceability of a system, therefore, we must first investigate the average and peak traffic loads under normal operating conditions. Such traffic loading patterns under normal conditions obviously do not apply to post-earthquake emergency situations. In emergency situations, the minimum capacity of the communication system must be maintained for the basic survival requirements of the citizens. The reduced capacity must then be increased by means of installing mobile systems and/or by repair and restoration of the original system. In order to gain empirical insight into the problem of traffic loads, however, normal traffic loading patterns must be known.

A future study would primarily consider those post-earthquake emergency situtations in which the components of the station equipment, switching facilities, building structures, utilities equipment, and transmission facilities, are all subject to possible physical damage and failure. Therefore, the serviceability of the total telecommunications network systems must be analyzed after the vulnerability analysis establishes the lesser state of connectivity that the network systems have deteriorated into, resulting from the damage sustained by these individual components. This task appears to be at most as demanding in terms of analytical and numerical efforts as the serviceability analysis performed on underground water transmission network systems in [B.5]. In [B.5], the vulnerability analysis was performed analytically to produce a sample of degraded networks. On each of these degraded networks, a (nonlinear) flow analysis was performed in the Monte Carlo sense to determine the probability of serviceability defined in terms of remaining levels of flow rate and water pressure at specified vertices for use in post-earthquake fire fighting. Similar approaches appear to be applicable to a serviceability analysis involving telecommunications network systems.

Speaking again of the water transmission system, we might add that, given an earthquake, the earthquake intensity at each potentially critical location of the pipeline is estimated and the damage probability matrix is used accordingly. If the area over which the lifeline system stretches is relatively small compared with the epicentral distance, the earthquake intensity may be considered uniform throughout the area. In this case, the seismic hazard curve given as a function of the earthquake intensity will be convolved with the probabilities of system serviceability (or vulnerability) conditional to various earthquake intensity values in order to derive an estimate of the annual probability of system serviceability (or vulnerability). However, if the spatial variation of the earthquake intensity has to be accounted for, the ensuing analysis becomes more complicated. In [B.4], for example, the empirical attenuation law for the peak ground acceleration (in the surface layer) proposed by Esteva [B.9] was combined with the relationship, also empirical, between the earthquake intensity (MMI) value and peak ground surface acceleration recommended by Gutenberg and Richter [B.10]. This combination produced an expression for the MMI value at the site as a function of the earthquake magnitude M and the hypocentral distance associated with the site. The relationship developed by Kanai [B.11] was also used to estimate the range of the velocity spectrum corresponding to each MMI value, as it is needed to estimate the free field ground strain. These earthquake intensity values can then be used together with the damage probability matrices to produce a sample of degraded networks through the vulnerability analysis. The estimation of the probability of system serviceability then follows. Such a probability of system serviceability, however, is conditional to a particular earthquake with magnitude M originating from a point source or line source or even area source. Appropriate analysis must then be performed to derive an estimate of the annual probability of system serviceability from the conditional probability.

Each step of the procedures described above requires further scrutiny and study in order to reduce the extent of inaccuracy and uncertainty involved. More importantly, we must recognize that these procedures incorporate rather simple models of the bedrock, surface layer, fault movement, etc., and therefore may not be accurate enough to consider all the significant

aspects of free-field ground motion in relation to the structural response analysis. For example, interaction of surface and body waves through lateral inhomogeneities such as dipping layers on the edges of alluvial basins may have to be studied for its effects on the free-field ground motion on or near the ground surface.

B.5 CONCLUSION

The preceeding observations involving telecommunications network systems and water transmission pipeline systems identified the need for further information on a number of critical factors that affect the mitigation of seismic hazards to these systems. Such information is needed in order to develop a more reliable database on which more credible vulnerability and serviceability analyses can be performed. Ultimately, the result of these analyses is expected to provide logical guidelines for more technical measures of seismic hazard mitigation by establishing the design, retrofitting and repair criteria for hardware systems, for evaluating the adequacy of the system's redundancy, and for mapping out strategies for emergency plans and restoration schemes. Even more importantly, such a result provides valuable input to the societal impact analysis that must be performed from a more global point of view. Indeed, the oil pipeline failure due to large-scale landslides during the recent Ecuador Earthquake has inflicted a devastating loss of economy and productivity upon that country. In fact, we have been extremely fortunate that no major earthquakes as large in their scale as those of the New Madrid, Missouri Earthquakes of 1811-1812 and the Charleston, South Carolina Earthquake of 1886, have not struck the Central United States. Energy distribution systems including crude oil, petroleum and natural gas pipeline systems are concentrated in this area from the South and Southwest to densely populated areas of the North and Northeast [B.12]. Physical and functional failures of such energy systems due to seismic events and the resulting disruptions in the supply of energy could produce disasterous consequences of unprecedented scale and magnitude. Such failures would probably be induced by earthquake-triggered large-scale landslides and/or liquefaction. It is about time that we extended the type of analytical procedures described in this paper, applied the results of such procedures for the purpose of mitigating disasters and at the same time continue to identify and work on research issues the resolution of which will greatly alleviate the difficulties associated with mitigation efforts.

ACKNOWLEDGEMENT

The authors wish to acknowledge that most of the works discussed in the paper have been supported by the Earthquake Hazard Mitigation Program of the National Science Foundation over the years. The recent work discussed in Part B was partially supported by Subcontract No. SUNYRF-NCEER-86-3043 under the auspices of the National Center for Earthquake Engineering Research under NSF Grant NO. ECE-867-07591. Dr. Shinozuka wishes to indicate that some of his material is taken from Ref. B.13. Dr. Wang summarizes the results from a large pool of references. Although too many authors and colleagues to be named herein, one should recognize their contributions to the advancement of lifeline component design and analysis as indicated in the references.

REFERENCE

A.0. O'Rourke, T.D., and Isenberg, J., "Some Recent Studies on Lifeline Earthquake Engineering in the United States: Experiment and Field Studies," Proc. of 19th UJNR Meeting, Tsukuba, Japan, May 12-15, 1987.

A.1. ASCE First Speciality Conference on Current State of Knowledge of Lifeline Earthquake Engineering, Los Angeles, CA. August 30-31, 1977.

A.2. ASCE Second Speciality Conference on Current State of Knowledge of Lifeline Earthquake Engineering, Oakland, CA. August 20-21, 1981.

A.3. ASCE Advisory Notes on Lifeline Earthquake Engineering, 1983.

A.4. ASCE Guidelines for Seismic Design of Oil and Gas Pipeline Systems, 1984.

A.5. ASME Publication (PVP-34) on Lifeline Earthquake Engineering-Buried Pipelines, Seismic Risk and Instrumentation, 1979.

A.6. ASME publication (PVP-43) on Recent Advances in Lifeline Earthquake Engineering in Japan, 1980.

A.7. ASME Publication (PVP-77) on Earthquake Behavior and Safety of Oil and Gas Storage Facilities, Buried Pipelines and Equipment, 1983.

A.8. ASME publication (PVP-98-4) on Seismic Performance of Pipelines and Storage Tanks, 1985.

A.9. Building Seismic Safety Council, Proc. of Workshop on Abatement of Seismic Hazards to Lifelines, 1987

A.10. Wang, L.R.L., and O'Rourke, M.J., "Overview of Buried Pipelines Under Seismic Loading," Journal of Technical Councils, ASCE, Vol. 104, No. TC1, 1978, pp. 121-130.

A.11 O'Rourke, T.D., Grigorium, N.D., and Khater, M.M., "Seismic Response of Buried Pipelines," ASME Special Publication, Pressure Vessel and Piping Technology-A Decade of

Progress, 1985.

A.12 Isoyama, R., and Katayama, T., "Seismic Perfomance Evaluation of Water Supply System," Proceedings of Review Meeting of U.S.-Japan Cooperative Research on Seismic Risk Analysis and Its Application to Reliability-based Design of Lifeline System, Honolulu, January 1981, pp. 173-206.

A.13. Kubo, K., and Isoyama. R., "Damage to Buried Utility Pipes in 1978 Miyagi-Ken-Oki Earthquake," Proceedings of the 7th World Conference on Earthquake Engineering, Istanbul, Turkey, Vol. 8, September 1980, pp. 225-232.

A.14. Kubo, K., Katayama T., and Ohashi, M., "Lifeline Earthquake Engineering in Japan," Journal of Technical Council, ASCE, April 1979, pp. 221-238.

A.15. Sakurai, A. and Takahashi, T., "Dynamic Stresses of Underground Pipelines During Earthquakes," Proceedings of 4th World Conference on Earthquake Engineeirng, Chile, 1969, pp. 811-895.

A.16. Newmark, N.M., "Problems in Wave Propagation in Soil and Rock," Proceedings of International Symposium on Wave Propagation and Dynamic Properties of Earth Materials, Albuquerque, New Mexico, 1967, pp. 7-26.

A.17. Committee on Seismic Analysis, "Seismic Response of Buried Pipes and Structural Components," American Society of Civil Engineers, 1983.

A.18. Harada, T., Oda, T., and Shimada, T., "Determination of Apparent Wave Propagation Velocity from Damage Statistics for Buried Pipelines," Earthquake Behavior and Safety of Oil and Gas Storage Facilities, Buried Pipelines and Equipment, American Society of Mechanical Engineers, 1983, pp. 209-216.

A.19. Shah, H.H., and Chu, S.L. "Seismic Analysis of Underground Structural Elements," Journal of the Power Division 100, No. PO 1, American Society of Civil Engineers, July 1974, pp. 53-62.

A.20. Shinozuka, M., and Koike, T. "Estimation of Structural Strains in Underground Lifeline Pipes," ASME Publication PVP-34, Lifeline Earthquake Engineering-Buried Pipelines, Seismic Risk and Instrumentation, 1979, pp. 31-48.

A.21. Wang, L.R.L., "Some Aspects of Seismic Resistant Design of Buried Pipelines", Proc. of ASME 3rd U.S. National Congress of Pressure Vessels and Piping, San Francisco, CA. June 25-29, 1979, PVP-34, pp. 117-131.

A.22. Nelson, I., and Weidlinger, P. "Dynamic Seismic Analysis of Long Sequential Lifelines," Journal of Pressure Vessel Technology, ASME, Vol. 101, No.1, Feb. 1979, pp. 10-20.

A.23. Wang, L.R.L., and Cheng, K.M., "Seismic Response Behavior of Buried Pipelines," Journal of Pressure Vessel Technology, ASME, Vol. 101, No. 1, Feb. 1979, pp. 21-30.

A.24. Wang, L.R.L., "Quasi-Static Analysis Formulation For Straight Buried Piping Systems," Technical Memorandum (SVBDUPS) Project No. 3, Dept. of Civil Engr., Rensselaer Polytechnic Institute, July 1978.

A.25. Wang, L.R.L. and Olabimtan, A, "General Quasi-static Seismic Analysis of Buried Straight Piping Systems," Tech. Rept. LEE-006, School of Civil Eng. & Environmental Science, University of Oklahoma, Sept. 1983.

A.26. Wang, L.R.L., "Design Considerations for Buried Pipelines Under Various Seismic Environements," International Journal of Pipelines, Vol. 5., No. 3, October 1986, pp. 277-287.

A.27. Goodling, E.C. Jr., "Seismic Stresses in Buried Elbows," Presented at the April 2-6, 1979 American Society of Civil Engineers Convention and Exposition, held at Boston, Massachussets (Preprint No. 3595).

A.28. Goodling, E.C., Jr., "Buried Piping-An Analysis Procedure Update," Proceedings of the International Symposium on Lifeline Earthquake Engineeing, Portland, Oregon, American Society of Mechanical Engineers, 1983, pp. 225-237.

A.29. Newmark, N.M., and Hall, W.J., "Pipeline Design to Resist Large Fault Displacement," Proc. U.S. Nat'l Conf. On Earthquake Engineering, Ann Arbor, MI, 1975, pp. 416-425.

A.30. Hall, W.J., and Newmark, M.N., "Seismic Design Criteria for Pipelines and Facilities," Journal of the Technical Councils of ASCE, Vol. 104, No. TC1, Nov. 1978, pp. 91-107.

A.31. Kennedy, R.P., Chow, A.W., and Williamson, R.A., "Fault Movement Effects on Buried Oil Pipeline," Transportation Engineering Journal of ASCE, Vol. 103, No. TE5, Sept. 1977, pp. 617-633

A.32. Kennedy, R.P., Darrow, A.D.C., and Short, S.A., "Seismic Design of Oil Pipeline Systems," Journ. of Tech. Councils, ASCE, TC1, 1979, pp. 119-134.

A.33. Wang, L.R.L., and Yeh, Y.H., "A Refined Seismic Analysis and Design of Buried Pipeline for Fault Movement," International Journal of Earthquake Engineering and Structural Dynamics, Vol. 13., No. 1., Jan-Feb. 1985, pp. 75-96.

A.34. O'Rourke, T.D., and Trautmann, C.H.,

"Earthquake Ground Rupture Effects on Jointed Pipe," Proc. of the Second Specialty Conference on the Technical Council onLifeline Earthquake Engineering, ASCE, Aug. 1981, pp. 65-80.

A.35. Singhal, A.C., "Nonlinear Behavior of Ductile Iron Pipeline Joints," Journal of Technical Topics in Civil Engineering 110, No. 1 American Society of Civil Engineers, May 1984, pp. 29-37.

A.36. Chen, C.C., Ariman, T., and Lee, L.H.N. "Elastic Buckling Analysis of Buried Pipelines under Seismic Loads," Paper presented at the Pressure Vessel and Piping Conference, San Francisco, California, August 1980 (ASME Paper No. 80-C2/PVP-76).

A.37. Bouwkamp, J.G., and Stephen, R.M., "Large Diameter Pipe Under Combined Loading," Journal of the Transportation Engineeirng Division 99, No. TE3, American Society of Civil Engineers, May 1973, pp. 521-536.

A.38. Kyriakides, S., Yun, H.D., and Yew, C.H., "Buckling of Buried Pipelines Due to Large Ground Movements," Earthquake Behavior and Safety of Oil and Gas Storage Facilities, Buried Pipelines and Equipment, New York, American Society of Mechanical Engineers, 1983, pp. 140-148.

A.39. Kuribayashi, E., Kawamura, M., Ieda, R., Aida, M., and Yui, Y., "An Experimental Behavior of Buried Pipes During Liquefaction of Saturated Sandy Soil," Proceedings of the 1985 Pressure Vessels and Piping Conference, ASME Publication, PVP-98-4, June 1985, pp. 34-42.

A.40. Kuribayashi, E., Ieda, R., Kawamura, M., Tsuchiyama, S., and Yamanaka, S., "Behavior of Buried Pipelines with Manholes During Liquefaction (in Japanese)," Proc. of the 21st Annual Meeting of the Japanese Society of Soil Mechanics and Foundation Engineering, Sapporo, Japan, 1986.

A.41. Yeh, Y.H., and Wang, L.R.L., "Combined Effects of Soil Liquefaction and Ground Displacement to Buried Pipeline," Proceedings of the 1985 Pressure Vessels and Piping Conference, ASME publication, PVP, 98-4, June 1985, pp. 43-52.

A.42. Wang, L.R.L., Shim, J.S., and Ishibashi, I., "Response of Buried Pipelines Including Manhole in a Soil Liquefaction Environment," Paper to be presented at 3rd International Conference on Soil Dynamics and Earthquake Engineering," Princeton University, June 22-24, 1987.

A.43. Wang, L.R.L., "Design Considerations for Buried Pipelines Under Various Seismic Environments," International Journal of Pipelines, Vol. 5, No. 3, October 1986, pp. 277-287.

B.1. Kratky, R.J. et al., "Suggested Experiments on Straight Pipes in Air and in Soil," Report No. 9 under NSF Grant No. FR-78-15049, Weidlinger Associates, January 1979.

B.2. Whitman, R.V., et al., "Methodology and Pilot Application," Journal of the Structural Division, ASCE, Vol. 101, No. ST5, May 1975, pp. 1067-1084.

B.3. Shinozuka, M., Takada, S., and Ishikawa, H., "Some Aspects of Seismic Risk Analysis of Underground Lifeline Systems," Journal of Pressure Vessel Technology, Vol. 101, February 1979, pp. 31-43.

B-4. Shinozuka, M., and Koike, T., "Seismic Risk of Underground Lifeline Systems Resulting From Fault Movement," Proceedings of the 2nd US National Conference on Earthquake Engineering, Stanford, California, January 1979, pp. 663-672.

B-5. Shinozuka, M., Tan, R., and Koike, T., "Estimation of Serviceability of Underground Water Transmission Network Systems," Proceedings of the ASCE Specialty Conference on Lifeline Earthquake Engineering, Oakland, California, August 20-21, 1981, pp. 97-110.

B-6. Frank, H., and Chou, W., "Topological Optimization of Comptuer Networks," Proceedings of IEEE, Vol. 60, November 1972.

B-7. Slyke, R.V., and Frank, H., "Network Reliability Analysis: Part I," Network, Vol. 1, 1972.

B-8. Moore, E.F., and Shannon, C.E., "Reliable Circuits Using Less Reliable Relays," Journal of the Franklin Institute, Vol. 262, 1956.

B-9. Esteva, L., "Geology and Predictability in the Assessment of Seismic Risk," Proceedings of the 2nd International Conference of the Association of Engineering Geologists, Sao Paolo, Brazil, 1974.

B-10. Gutenberg, B., and Richter, C.F., Seismicity of the Earth, (NY: Hafner), 1965.

B-11. Kanai, K., Seismological Engineering, (Tokyo: Kyoritsu Press), 1973.

B-12. Coordinating Committee on Energy of the Public Affairs Council, "Vulnerability of Energy Distribution Systems to an Earthquake in the Eastern United States-An Overview," American Association of Engineering Societies, December 1986.

B-13. Shinozuka, M., "Scientific and Engineering Information Needs in Abatement of Scientific Hazards to Telecommunications Systems," BSSC Workshop on Development of and Action Plan for Abatement of Seismic Hazards to Lifelines, Denver, Colorado, November 5-7, 1986.

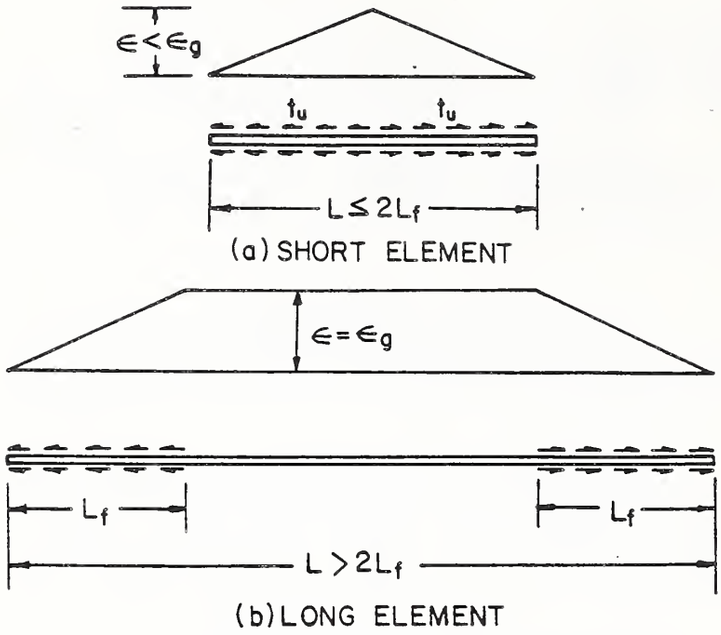

Fig. A.1 Strain in Continuous Pipeline [A.11]

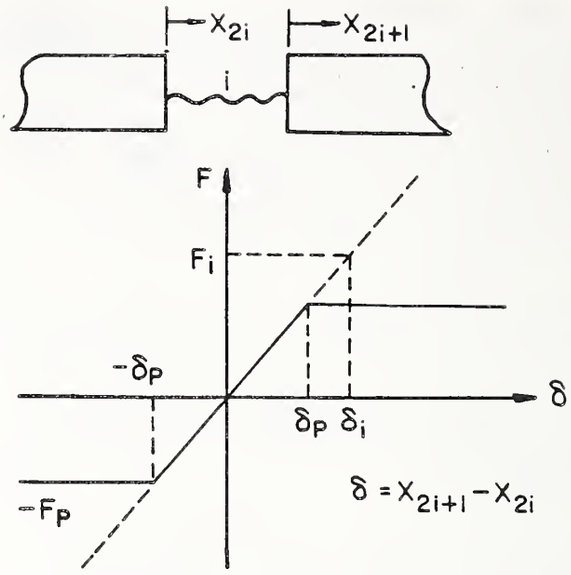

Fig. A.4 Elasto-plastic Joint Spring [A.25]

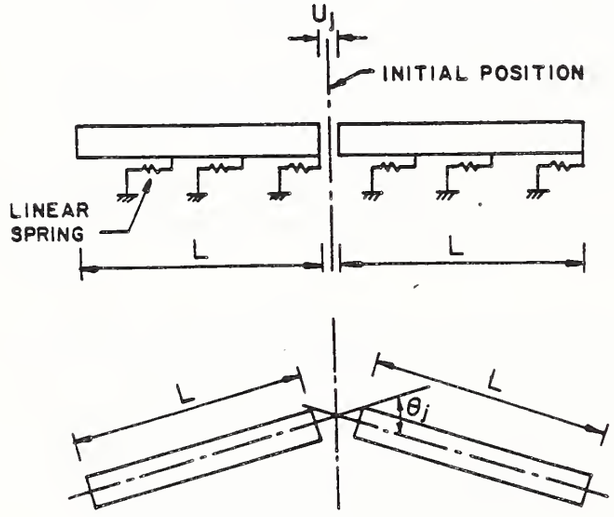

Fig. A.2 Static Joint Rotation [A.21]

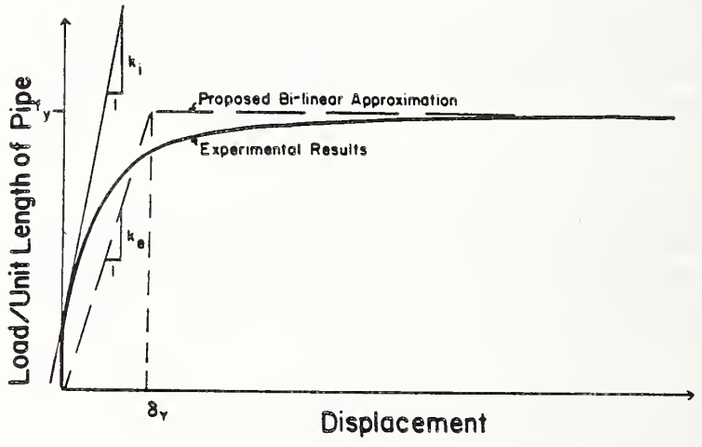

Fig. A.5 Soil Resistant Characteristics [A.25]

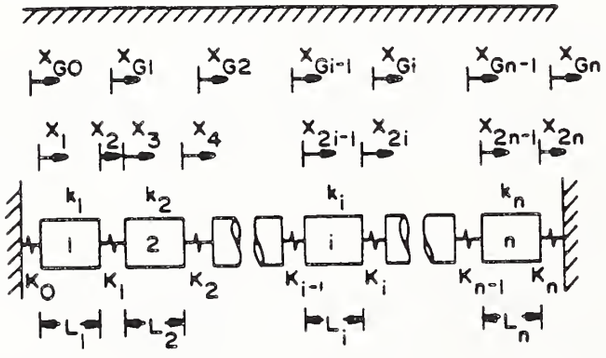

Fig. A.3 A Buried Segmented Piping System Model [A.21]

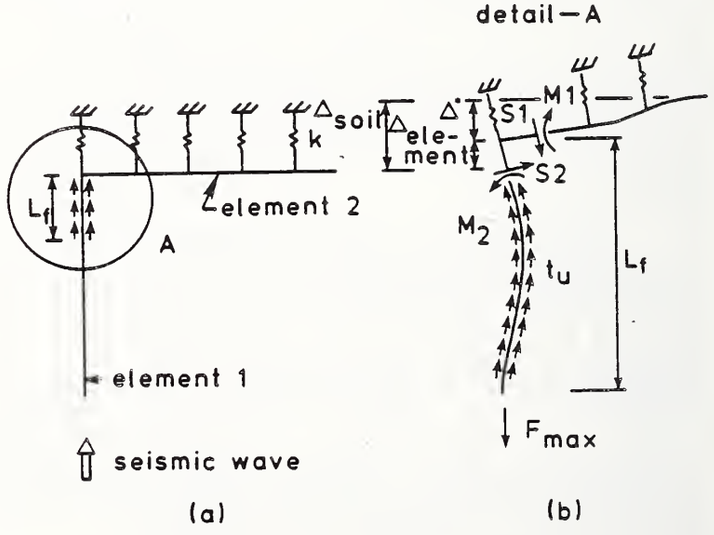

Fig. A.6 Force/Displacement at a Pipeline Bend [A.11]

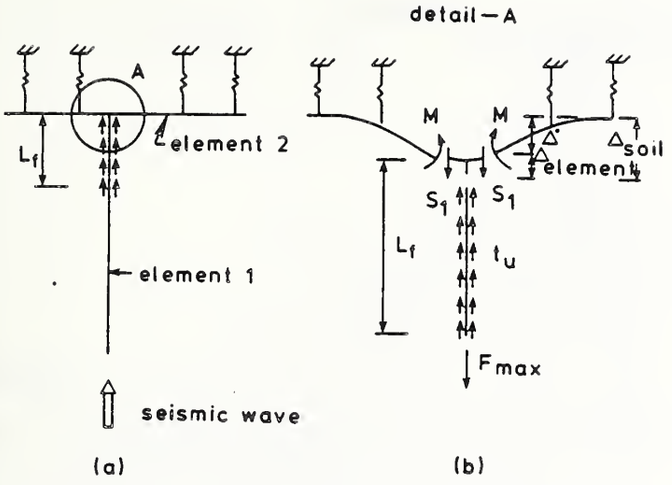

Fig. A.7 Force/Displacement at a Tee Junction [A.11]

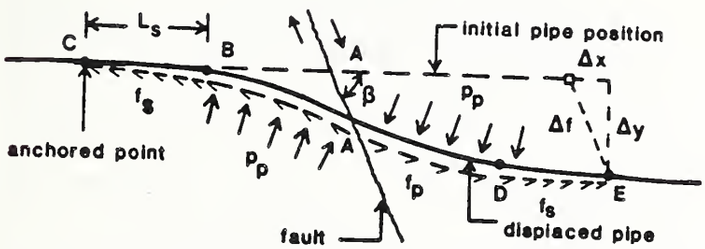

Fig. A.8 Pipeline Response to Strike-Slip Fault Movement-Newmark/Hall/Kennedy's Model [A.29 to A.32]

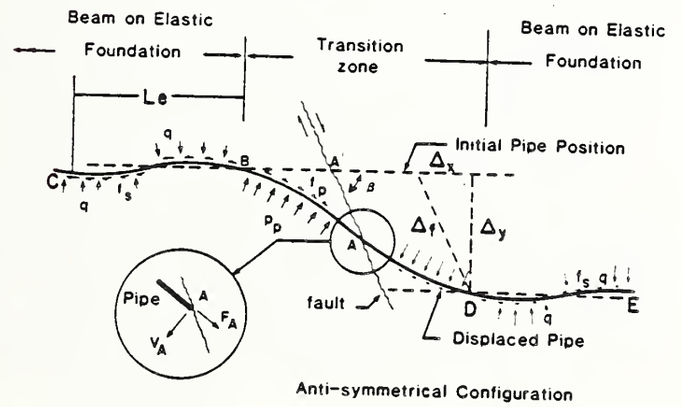

Fig. A.9 Pipeline Response to Fault Movement - Wang and Yeh's Model [A.33]

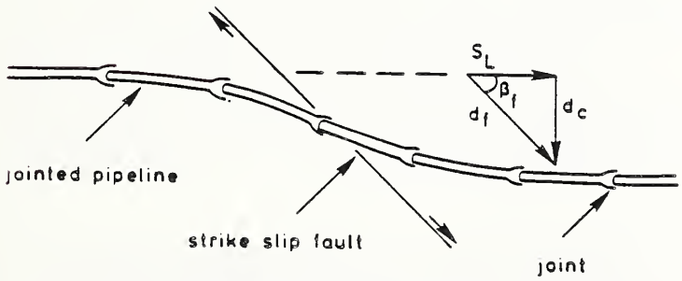

Fig. A.10 Segmented Pipeline Subjected to Strike-slip Fault Movement [A.11]

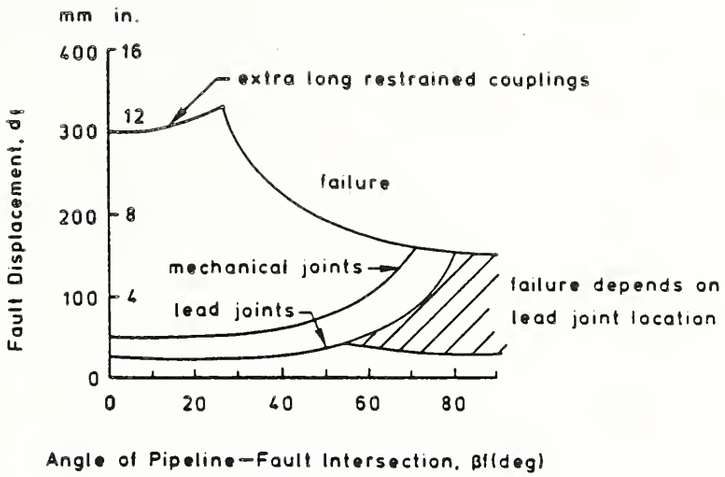

Fig. A.11 Joint Resistance to Fault Movement [A.11]

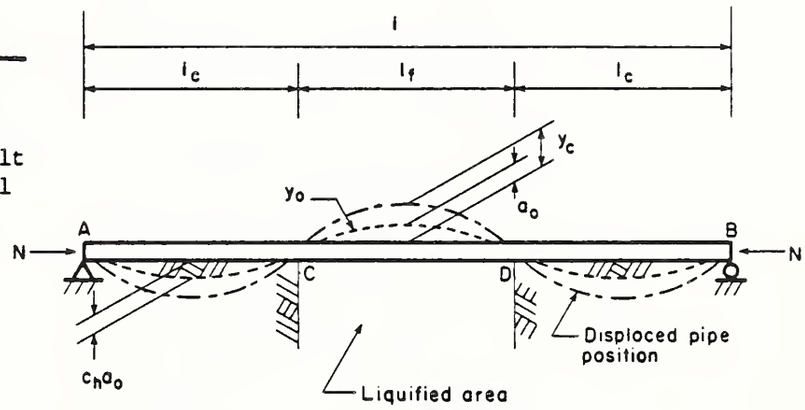

Fig. A.12 Continuous Pipeline in a Soil Liquefaction Zone [A.41]

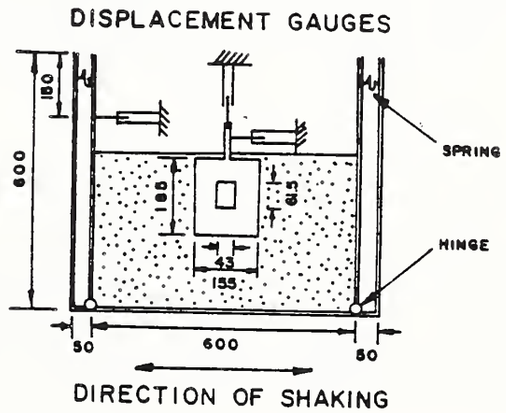

Fig. A.13 Experimental Study of Buried Pipeline with a Manhole in an Soil Liquefaction Environment [A.40]

DAMAGE STATE	CENTRAL DAMAGE RATIO, %	M M INTENSITY			
		VI	VII	VIII	IX
NONE	0				
LIGHT	0.3		P_{DSI}		
MODERATE	5				
HEAVY	30				
TOTAL	100				
COLLAPSE	100				

Fig. B.1 Form of Damage Probability Matrix

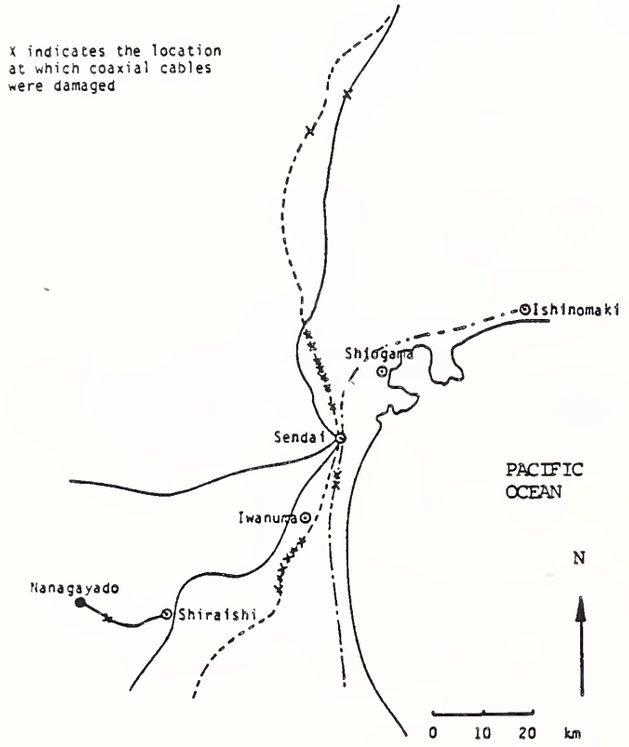

Fig. B.2 Damage Sustained by Inter-city Coaxial Cables Due to the 1978 Miyagi-Ken-Oki Earthquake

I_{MM}	VI	VII	VIII	IX
MINOR	1	0.96	0.18	0
MODERATE	0	0.04	0.71	0.11
MAJOR	0	0	0.11	0.89

Fig. B.3 Damage Probability Matrix for Soil Conditions A and B =3

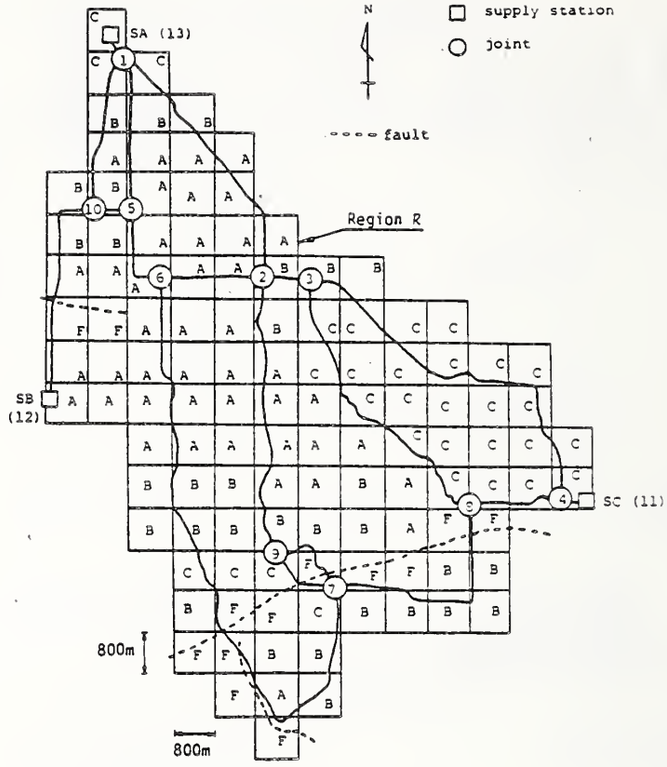

Fig. B.4 Water Distribution System and Simplified Soil Map of Los Angeles

A Review of Base Isolation for Upgrading Earthquake Performance of Building Structures

BY

Dr. Nishikant R. Vaidya[1]
Mr. Robert J. Smith[2]

ABSTRACT

This paper reviews base isolation for upgrading the earthquake performance of building structures. Both new construction and existing structures are considered. Base isolation is a design strategy which attempts to reduce the seismic forces imparted to the building structure and the components housed within the building. This strategy appears to be of particular significance for buildings that are required to be operational through and following a severe seismic event. But, it is not beneficial in all cases. A qualitative criteria for selecting buildings which may be potential candidates are suggested. These criteria may be used in the preliminary stages of building design to screen the types that may benefit from base isolation. Several specific schemes are presented and the manner in which they act to isolate the structure are described. The more prominent isolation schemes use reinforced elastomer bearings which provide isolation in the horizontal direction only. In the more developed schemes (on the basis of use, testing, and analysis) the displacement response is controlled by a friction interface, a lead insert or by special compounding of the elastomer. Design issues revolve around the relatively large displacements and are generally resolved by good detailing. Provided that this is done, it is concluded that base isolation is a sound alternative to traditional methods of aseismic design of building structures.

1. INTRODUCTION

Structural upgrading for the purpose of mitigating effects of earthquakes can consider several alternative solutions. Very broadly they can be fitted into two categories--one is to strengthen the structures and the other is to isolate the structure from the seismic ground motion. Generally, the alternatives are applicable not only in the design stage for new construction but also, if properly detailed, for existing structures. Irrespective of the choice, the solution is more easily adopted for new construction than for existing structures.

Among these alternatives for seismic structural upgrading, the traditional approach has been to add strength and stiffness to the structural systems. Typically, additional bracing and/or shear walls are considered to take the horizontal forces generated from the design seismic event and transmit these forces to the building foundation safely and without significant relative displacements. The seismic forces chosen for design reasonably assure that the building will not collapse in the event of the expected severe earthquake but may be subjected to permanent damage.

In structures of historical significance, the traditional methods may not be the most attractive if they mar the architectural appearance of the facade which must be preserved to elicit at least partially the worth of the facility. For certain mission essential buildings, the intrinsic value dictates that in addition to protecting life, the structure and systems housed therein suffer as little damage as is feasible to reasonably assure the continued operation of the facility through and following the earthquake. Thus, importance of the structure site conditions, seismic potential, and other related issues may prompt consideration of alternate upgrading.

Deviating from the traditional approach then, very broadly two alternative approaches have been considered by the profession to mitigate earthquake effects.

- Reduction of input motion through insulation of the structure, and
- Attenuation of input motion through isolation of the structure.

Insulation takes the form of backpacking or incorporating a trench around the facility and far enough away from it in free-field. Conceptually, the trench intercepts incoming seismic waves and, thus, effects reduction in the input ground motion in the vicinity of the building foundation.

In general, isolation takes the form of supporting the building on a flexible foundation

1. Project Manager, Paul C. Rizzo Associates, Pittsburgh, Pennsylvania.
2. Chief, Structures Branch, U.S. Army Corps of Engineers, Washington, D.C.

such that the seismic ground motions are attenuated as they are imparted to the structure through the isolating mechanism. The general concept is illustrated on Figure 1. Since the isolation mechanism is located at the base of the structure, it is referred to as base isolation. This paper addresses the current methods of base isolation.

In a broad sense, most base-isolation schemes consist of a flexible link between the ground and the supported structure with one or more energy absorbing devices acting either in parallel or in series with the flexible link. Depending upon the scheme, either the flexible link or the energy absorbing device takes on the greater significance. Thus, in the one extreme, attenuation of seismic motion depends primarily on capacity to absorb the seismic energy imparted at the structure/foundation interface; while in the other extreme, the flexible link alone may be designed through a frequency shift to result in a low transmissibility of ground motion.

This paper reviews the criteria for selecting base isolation as a design strategy. Various base isolation schemes are briefly summarized and their anticipated performance described. The information about these schemes has been collected from published literature, technical papers, notes, etc. It is hoped that the information presented here will aid in selecting an appropriate design strategy and evaluating the base isolation systems during the conceptual design stage of a building structure.

2. BASE ISOLATION DESIGN PHILOSOPHY

A general overview of the basic principles of base isolation can be found in texts on earthquake engineering (e.g. Newmark and Rosenblueth, 1971). As this would signify, the concept is not new; its history in seismic applications, which dates back to the early 1900's, has been very aptly described by Kelly (Kelly, 1979). The more recent interest has probably been motivated by several factors, among which the more significant perhaps are, the need for a higher level of earthquake performance of buildings, and equally important, the development of reinforced elastomer bearings which, due to their inherent mechanical properties, have extended the range of applicability of base isolation in earthquake protection of structures. An example of this is the recently completed Law and Justice Center Building in San Bernardino, California. The design of base isolation for this building is illustrated on Figure 2 (Way, 1986).

In this strategy of aseismic design, the entire structure is founded on several bearings which are relatively flexible in the horizontal direction and simultaneously capable of supporting the vertical gravity load of the structure. Isolation from severe ground motions is effected by providing a low horizontal stiffness to the bearings so as to provide a low frequency to the predominant horizontal mode of the structure vibration. Most earthquake ground motion being in the 3 Hz to 10 Hz range is thus effectively filtered and only relatively small accelerations are imparted to the isolated structure. The general principles are illustrated on Figure 3. For simplicity, it is assumed in this figure that the entire structure displaces horizontally on the collection of bearings in a more or less rigid fashion.

Figure 3 shows an idealized response spectrum of earthquake type ground motion. The conventional structure may have predominant periods in the range where the ground motion is amplified. By providing a flexible base, the fundamental period is shifted from T1 to T2 which is outside the range where the ground motion is amplified. Very simply, the principle of base isolation is to effect this shift of the predominant mode of vibration. Indeed, in the extreme case one could support the entire structure on frictionless bearings which then theoretically totally isolate the structure in the horizontal direction. Obviously, the resulting displacements would be significantly large and severe measure to control these displacements would discourage such an approach. Even a nominal shift in the frequency, such as attempted in most base isolation solutions, increases the displacement response to the point where it becomes necessary that some measure to control these displacements be incorporated as an integral part of the base isolation system.

The seismic behavior of base-isolated structures can simply be looked at in terms of the response of damped lower frequency single mass oscillators; and on this basis, compared to the behavior of non-base-isolated structures. But from the practical approach, the similarities end there and the seismic performance of base-isolated structures could be radically different from that of the conventional.

By decreasing the participation of the base-isolated structure in the seismic response, its structural components can be generally designed to remain within the elastic range, and thus decrease the potential for its structural damage during severe earthquakes, (damage which is generally accepted in the conventional seismic design philosophy). But because of this, the isolation bearing becomes the all important structural element sacrificing some of the redundancies inherently present in the conventional design. Details of the structural design need special attention to assure proper vertical and horizontal load distribution to the dispersed and discreet bearing elements. Very broadly then, the design philosophy attempts to relieve the risk to the building structural elements by an approximately equal sharing of the risk by the bearings.

Much has been written and published about base isolation and its strategy of seismic design. A recent workshop (ATC, 1986) on base isolation and passive energy dissipation brought together the current thoughts about the use of these techniques for aseismic design of building structures. Some codes have been proposed for the design of structures using base isolation (SEAONC, 1986, SEAOSC, 1986). Other guidelines present specific design issues that need to be considered (Vaidya and Eggenberger, 1984) if this strategy is chosen. There is still not a complete acceptance of the technique by the profession although it is agreed by most that the principle is sound and is applicable at least to certain types of structures.

The apprehension results, perhaps justifiably so, from the lack of extensive field data on performance of structures constructed on base isolation, (Huang, et. al, 1986). For the most part, current design has to rely rather heavily on the results of analyses using mathematical models and scale model shaker table tests which generate results in a controlled laboratory environment. Indeed, these do not encompass the myriad of variable conditions that will be encountered in the field; and the collection of field data over several years of observed actual performance remains the primary means to refine the technique of base isolation.

But as much as the principal structural element used in the base isolation system, the bearing, is an engineered product admitting to QA/QC with quite a respectable history of use in other applications, some in far more arduous environment, the reliability of the system is perhaps governed more significantly by uncertainties in seismic ground motion on the one hand and the structure response on the other. The former applies to conventional as well as isolated structures. Over the last two decades, a wealth of information has been gathered on the nature of ground motion and the sources of uncertainties in its prediction. As far as the latter, more than conventional structures base-isolated structures lend themselves to a more representative mathematical model for estimating seismic structural response. Isolation is extracted by demanding little participation from the superstructure and the non-structural components in responding to seismic ground motion, thereby reducing the attendant uncertainties in the mathematical model and rendering analytical effort more tractable.

In view of the above and in the spirit of innovation, backed by a wealth of analytical and experimental data, quite a few in the profession appear convinced to consider, evaluate, and use base isolation to mitigate earthquake effects notwithstanding the paucity of specific field performance data.

3. CRITERIA FOR SELECTING BASE ISOLATION

As in any design, diversity forces a choice. Even within the traditional mold, the options for the building system are many and varied. The choice of the optimum solution is generally made in conference with the architect, structural engineer, geotechnical engineer, and the seismologist. As new materials present themselves and eventually get absorbed into construction use, the traditional mold loses significance or at least has to expand its definition to include concepts that these new materials have obviated.

Bearing technology and energy dissipators in the manner of new materials have brought to bear their potential in the design of earthquake resistance. Their successful use in other areas, but nevertheless to mitigate vibration problems in general, is anticipated to increasingly encourage their use in reducing earthquake damage. In this respect, they have expanded the possible options available to the engineer. Depending on one's perspective, their use may be considered as a deviation from the traditional or merely to precipitate an expansion of the traditional role. For the moment, relegating the careful consideration of details to the appropriate engineering phase, which is imperative regardless of the option chosen, the authors prefer to look upon the latter as an appropriate role befitting base isolation.

And in this subset of the overall design task, the first choice is whether the building under consideration should be base isolated; having chosen base isolation, should the designer design his own system or use one of the patented systems? If the use of a patented system is chosen, which system should be selected? Finally, what structural issues specifically related to the base isolation of choice need special attention to reasonably guarantee successful performance of the entire structural system?

Obviously, the design process is dynamic, its elements interacting with one another, extending also to the design tasks prior to the subset being considered here, such as establishing structural design strategy, architectural features, and siting. Both initial and life-cycle costs are an important consideration in the design process also. Previous limited studies (Vaidya and Eggenberger, 1984; Tarics, 1982) have indicated that base isolation can be provided at an equal or lower initial cost. Improved risk is seen to favorably affect life-cycle costs. For these reasons, it is anticipated that base isolation will rather quickly emerge out of the research realm into practice, if it has not already, and the anatomy of the decision (Rigney, 1986) determined predominantly by the deliberation of the engineer. It is to this latter, that this

discussion is addressed and dedicated to facilitate the decision making.

Accordingly, before moving on to the description of the various types of base isolation systems, the following paragraphs are devoted to discussing a procedure that may be used to establish if the concept should be considered in the first place. The need for this first important decision admits the possibility of an inappropriate use of base isolation. Indeed, it should be obvious that base isolation is not a panacea that could provide earthquake protection irrespective of the type and use of the building structure. In some cases, it may be ideally suited; in others it may be only marginally suited; and in still others it may actually degrade the performance of the building. Therefore, the judicious selection of buildings and isolation systems is a major step toward assuring that base isolation will actually enhance the seismic performance and, hence, may be considered as an alternative approach for upgrading structural design.

The following discussion is rather qualitative in nature and should be supplemented with case-by-case quantitative evaluations in the event that on the basis of this qualitative procedure, base isolation cannot be clearly eliminated as a strategy. Without getting too encumbered with specific detail at this point, but keeping in mind that what is being attempted is isolation by detuning, energy dissipation by some damping mechanisms, or usually some combination of the two, the flow chart on Figure 4 presents the basic issues to be considered in the process.

Very broadly, the significant issues to be considered in the decision making are:

- Seismic Zone
- Site Conditions
- Ground Motion
- Lateral Load Resisting Systems
- Physical Dimensions of Structure
- Facility Importance
- Materials of Construction

It is apparent, for example, that low seismic zones may not justify the additional cost of base isolation in reducing the already low seismic risk. In any event, depending upon the building physical dimensions, other loads, such as wind, may govern lateral design. In such zones, conventional techniques for upgrading structural design to earthquake forces may be the preferred approach. For Zone 2 and perhaps Zone 3, reinforced elastomeric pads without additional energy absorption, wind loads permitting, may be a cost effective alternative. While for regions of relatively high seismic risk base isolation with an effective energy dissipation may be the only way to reasonably assure continued operation of the facility through and following a major earthquake.

Site conditions in combination with the seismic zone determines the expected range of ground motion characteristics. This is a step most fraught with uncertainty. If, for example, the likelihood of encountering predominantly low frequency motion is high, the use of base isolation may not be appropriate as detuning may demand that the resulting system have a significantly long period resulting in unrealistic demand for the control of displacement. The use of an energy dissipating system in this case may be more appropriate. The physical dimensions, foundation conditions, and the primary lateral load resisting system may further determine the applicability of base isolation and its type that could lead to an optimum performance. The facility importance and the extent and type of damage that can be tolerated will also impact on whether base isolation should be used.

The following discussion is directed towards screening potential candidates for base isolation. Specific structures should not adopt base isolation nor should they be eliminated as potential candidates solely on the basis of the following criteria. Some quantitative justification is necessary and this can usually be obtained without much technical effort (e.g. Kelly, et. al, 1986). It appears at the outset that base isolation is suitable for the following general situations:

- The site is located in a high seismic zone.
- The structure is not founded on soft soil.
- The building is low to medium height.
- The building has a relatively low shape factor ($H/L \leq 1$).
- The contents of the building are sensitive to high frequency vibration.
- The lateral load resisting system results in a rigid structure.

The flow chart shown on Figure 4 includes only the major steps in the decision process. Several details that must be considered in each step are excluded to preserve simplicity and clarity in the flow chart. Some of these details are discussed in the following paragraphs.

Architectural consideration would lead to the selection of the structural system while siting and site conditions would determine the seismic zone and the seismic coefficient. The procedure envisioned here first performs a preliminary conventional design, say on the basis of UBC (ICBO, 1984) or SEAOC (SEAOC, 1984). For this design, evaluate the dynamic properties, specifically the first mode frequency, structure

mass, and stiffness. Estimate the level of the expected ductility demand in the structural elements in the event of the design earthquake and the maximum credible earthquake. If the ductility demand is acceptably small, then no further consideration of design options is necessary and the conventional design may be refined and the costs evaluated.

Generally, the ductility demand is influenced by the structural system, site seismic potential, and the predominant mode frequency. If the ductility demand is judged to be unacceptable, then either revise the conventional design or consider base isolation.

If the base isolation option is chosen, first estimate the required predominant mode frequency to reduce the seismic coefficient significantly. Establish the stiffness and damping parameters of the base isolation system. If the site soil stiffness is relatively low, about the same magnitude as the required base isolation stiffness, then base isolation may not be appropriate. If the site soils are firm, select and design the base isolation system. Evaluate the isolated structure dynamic parameters and compute system response. If the response is acceptable, refine the structure design and evaluate costs.

Generally, unacceptable response in the base isolated system takes the form of large displacements, and the attendant problems associated with the interface of base-isolated and non-base-isolated components of a building system. If the displacements are unacceptably high, revise the base isolation system design.

As can be gathered from the above discussion, several issues need to be looked at simultaneously. Quantitative values of estimated response of various base isolated structural systems would indeed expedite the process. This work is currently being conducted by the authors. Research work is also being conducted on the influence of site conditions on base-isolated structure response (Constantinou, 1986). When these and other results become available, it is hoped that specific design criteria may emerge. But until then careful evaluation on a case-by-case basis remains the primary means to reasonably assure successful performance of base isolation for earthquake protection of structures.

4. BEARING SYSTEMS

From the brief discussion about the design philosophy and what is being attempted, it follows that the "ideal" base isolation system will perform the following functions.

1. Minimize lateral loads on the structure and minimize the attendant relative displacements.
2. Safely support the vertical load of the structure.
3. Provide restraint against other environmental loads such as wind.

The primary elements of any base isolation system are accordingly, isolation, energy dissipation, and restraint. When mitigation of the earthquake forces are effected predominantly by friction based elements either restricted to the base or dispersed through the structure, the design is sometimes called a passive energy dissipation system. In essence, this may be looked upon as increasing the inherent damping in a structure by enhancing the elements that cause damping in the first place. Thus, very broadly, passive energy dissipation acts in quite a different manner than does isolation. Although these methods are discussed here, their broad scope, applicability, and design variations make it necessary to restrict the discussion to only those types that are located in the base of the structure and in this context are treated much the same as base isolation in which the inevitable means for energy dissipation has taken on the greater significance.

Of the three elements that constitute a base isolation system, restraint assumes a relatively subsidiary role; its use seen as an afterthought to supplement the performance of the former two elements, namely, isolation and energy absorption. Isolation and energy absorption are then the more significant elements engineered into the overall structural strategy, thus deviating from the traditional approach, their main tenet being to reduce the destructive horizontal forces and motions imparted to the structure. Pure isolation attempts to achieve this by detuning, while energy absorption by dissipating the earthquake energy at the structure/foundation interface.

In most currently promoted bearing systems, neither isolation nor energy absorption is solely used at the exclusion of the other; rather, these two elements are combined in a manner to produce synergism and effect the most reduction of destructive horizontal motions. Various combinations have been proposed; some have been actually implemented for aseismic design; several have been tested in a laboratory environment to substantiate their claim at reducing seismic lateral loads; and most have been subjected to mathematical analysis to illustrate their potential. Oversimplifying here only for the sake of clarity, it can be stated that the different ways in which the elements of isolation and energy absorption are combined result in different systems. Consequently, one is not that radically different from another for after all there are only two basic elements to be combined and if we keep this in mind and look at all systems in

this light it is not too difficult to understand the expected performance of each.

The following paragraphs briefly describe the bearing devices and their anticipated performance in isolating the structures they support. A sincere attempt is made here to include all proposed, analyzed, tested and actually used systems. It is only through inadvertency that some may have been missed.

4.1 Plain Elastomer Bearing

The simplest isolation device is a plain elastomer bearing. Due to their inherent properties, elastomers are quite flexible relative to the traditional materials of construction and placed under structures can isolate them from ground motions. Both shear stiffness and compressive stiffness are inversely proportional to the thickness of an elastomer block. In addition, however; the compressive stiffness depends upon the areas of the sides of the elastomer block free to bulge. The disadvantage of plain elastomer bearings is that for the thickness of elastomer required to obtain horizontal isolation the vertical stiffness is relatively low and it is difficult to sustain the gravity loads of the structure without undergoing significant vertical displacements. A three-story school building in Skopje, Yugoslavia uses plain elastomer bearings for isolation (Siegenthaler, 1970).

4.2 Reinforced Elastomer Bearings

The most common base isolation bearings comprise steel-laminated elastomers. These are also most commonly used as bridge bearings. Neoprene and rubber with durometer hardness in the range of 50 to 70 are the more commonly used elastomers for base isolation bearings. Since shear stiffness of the bearing depends upon the total thickness of the elastomer, these bearings retain the horizontal flexibility while their vertical stiffness is significantly increased by the presence of the steel plates. Additionally, the elastomers being non-linear dissipate energy through hysteresis. If no special compounding is used, elastomer bearings of this type provide an equivalent viscous damping of about five percent. Bearings of this type have been used to isolate the structures of a Nuclear Power Station in Cruas, France.

4.3 Reinforced Elastomer Bearings High/Damping Rubber

To reduce the displacement response, it may be necessary to provide means for additional energy dissipation. One way is to specially compound the elastomer such that the bearing in deforming in shear describes a relatively large hysteresis loop thereby dissipating a proportionally larger energy per cycle. High damping elastomer bearings have been implemented under the Law and Justice Center Building in California (Way, 1986).

4.4 Reinforced Elastomer Bearing with External Energy Dissipation Mechanism

Here the performance of the elastomer bearing is supplemented with a mechanical energy dissipator which acts in parallel with the bearing. Plastic deformation of steel beams either in torsion or flexure, extrusion of lead, rubber bumpers are some of the devices proposed to provide energy dissipation. Several specific devices based on the plastic deformation of steel and extrusion of lead have been tested (Skinner et. al, 1975; Skinner et. al, 1977; Stiemer and Chow, 1984). Several of these devices have been included in Bridges in New Zealand (Tyler, 1984).

4.5 Reinforced Elastomer Bearings with Internal Energy Dissipation Mechanism

In this concept, the reinforced elastomer bearing includes a vertical hole in its center which is filled with lead. In undergoing shear deformations, the lead plug deforms plastically in shear and thus results in energy absorption in addition to that provided by the elastomer. The William Clayton Building in Wellington, New Zealand is isolated by bearings of this type (Megget, 1978; Megget, 1984). Additionally, several bridges in New Zealand also use bearings of this type.

4.6 Reinforced Elastomer Bearings with a Frictional Interface

In this concept, a frictional interface is included between the bearings and the structure they isolate (Richli, et. al, 1980). A large seismic event may induce slip of the isolated structure on the frictional interface, thus, dissipating additional energy in friction. In addition to limiting the seismic forces imparted to the structure, the frictional interface also limits the shear deformation of the bearings. Bearings of this type have been used to isolate the structures of the Koeberg Nuclear Power Station in South Africa (Vaidya and Plichon, 1986).

4.7 The Alexisismon (Ikonomou, 1979)

In this concept of base isolation, the functions of supportive vertical load and horizontal isolation are performed separately by two components. A pot bearing carries the vertical load and provides relatively small frictional resistance in the horizontal direction. An elastomer block supplies the horizontal stiffness as a means to provide a restoring force against horizontal displacements. In concept, this may be comparable to the reinforced elastomer bearing with a frictional interface. In action, the

elastomer force here works in parallel with the horizontal frictional resistance. This system has been used to isolate a six-story structure in Greece (Ikonomou, 1979).

4.8 The Resilient-Friction Base Isolator

The resilient-friction base isolator is comprised of a stack of flat steel rings which enclose a central rubber core and if required peripheral rubber cores within the flat rings. Here also, the friction force acts in parallel with the restoring force of the elastomer core. The entire vertical load is supported by the flat rings and the rubber cores only distribute the sliding displacements. A significant amount of analysis and scale model tests (Mostaghel et. al, 1986) have illustrated the potential of this system.

4.9 The Earthquake Barrier System (Caspe, 1986)

This concept relies primarily on sliding friction to provide a force barrier. The barrier physically consists of a friction assemblage with a predetermined friction-slippage level attached to the structure at its base. One suggested assemblage uses two perpendicular sliding rails operating independently. A horizontal diaphragm restrains torsional motion of building columns which are supported by the friction assemblage. Hydraulic dampers or neoprene shear springs may be added in parallel with the friction assemblage to enhance the performance of the barrier systems. Analytical as well as experimental work has been performed on this system (Caspe, 1984).

4.10 Steel Roller Bearings

Steel roller or ball bearings can provide the vertical load carrying function with an independent device used to restrain or limit the horizontal motion. A four-story reinforced concrete frame building in Mexico City is supported on roller bearings. Each bearing consists of 100 one-centimeter diameter steel balls. Horizontal restraints are provided by steel limiting cables (Gonzalez-Flores, 1974). In the event of severe ground motions, the limiting cables may need an additional energy dissipation device.

4.11 The Coil Spring Concept

Perhaps comparable in simplicity to the plain elastomer pads, this concept uses coil springs to mount the structure on the foundation soils. This concept was studied to base-isolate an existing five-story, wood-frame building at the Naval Post Graduate School in Monterey, California (Reed and Kircher, 1986). The disadvantage here is that the horizontal response is strongly coupled with the rocking response of the isolated structure. This concept has been further expanded and studied in the GERB System (Huffmann, 1985).

The above list of isolation devices do not include general geotechnical and structural approaches such as soft soils, sleeved piles, etc. Although in principle these can be categorized as base isolation, the variations here can be numerous and relatively general. Of the devices that have been described above, the reinforced elastomer bearing is the common denominator in the more developed schemes. In terms of the additional damping mechanisms, the reinforced elastomer bearings with the frictional interface, special elastomer compounding, and the internal lead plug appear to be the most developed from the point of view of analysis, confirmatory test, and practical use for the seismic isolation of building structures.

5. STRUCTURAL CONSIDERATIONS

The use of reinforced elastomer bearings is relatively common place in bridges where they have been used primarily to accommodate thermal movements of the bridge deck, and for vibration and noise isolation for buildings and vibrating equipment. Indeed the first such used dates back about 30 years. However, seismic application is relatively recent. Because of the dynamic characteristics of building structures and the ground motions from which isolation is attempted, this application deserves a careful consideration from the point of view of the overall system response.

As mentioned earlier, the structural response of base-isolated structures is significantly different from conventionally founded structures. Vertical load carrying members, such as building columns and load bearing walls, are discreet structural elements tied together horizontally at floor elevations by the floor diaphragms. The lateral loads induced during earthquakes due to the structure mass are transmitted to the foundation by braced frames or shear walls which themselves contain the vertical load carrying elements. Generally, these lateral load resisting elements may also not be continuous but rather discreetly located within the plan dimensions of the building. The floor diaphragms are designed to appropriately collect the distributed inertia forces and transmit them to these discreet lateral load resisting elements. Accordingly, a rigid diaphragm at the base of the building is imperative in transmitting building shears uniformly to the bearings.

Special cases may require close attention to the design of the first floor diaphragm. For example, internal core walls such as those enclosing elevator shafts may be the principal lateral load resisting elements. In such a case, the first floor diaphragm should distribute overturning moments in addition to

the horizontal base shear. In limiting cases of high aspect ratios of such elements, the overturning moment and the resulting tension on at least some bearings may preclude the use of this strategy of aseismic design.

The location and the design of stairs may also require special attention. Stairwell walls may be used for lateral load resistance. These could be a part of the isolated structure but special detail is required in the stair sections traversing the interface between the isolated building and the non-isolated grade outside. Conceptually, a gap of about 15 inches between the building and the perimeter, such as shown for example on Figure 1, can comfortably accommodate the relatively large displacements of the base-isolated structure. Similarly, most utilities and pipes, sewer lines, etc., can incorporate joints to accommodate displacements on the order of 10 to 15 inches.

Nevertheless, most problems of details such as discussed above are just that--problems of good detailing specific to the particular building under consideration and the particular design. Examined rationally, these issues can generally be resolved to satisfaction. In the final design stages, other issues such as the effect on the seismic response due to eccentricity, settlement of foundation soils, effects of vertical and rocking input motion, etc., should be investigated at least for confirmation of the performance of the base isolation. In most cases, these issues are secondary (Vaidya and Plichon, 1986) but depending upon the structure may be of significance.

Specific to the base isolation system, its components namely, the bearing and the energy dissipating device, should be carefully reviewed. Effects of manufacturing tolerances of bearings should be examined. Some tests should be performed on the finished bearings to confirm their mechanical properties. Although elastomers such as neoprene and natural rubber have proven their durability in other applications, the long-term effects of the environment and aging remain controversial. This is perhaps due to the applicability of accelerated aging tests for the performance of the bearings. In any event, this is an important issue particularly because elastomers are known to stiffen with age and lack of movement. Some means of inspection and testing of in-place bearings may be desirable.

Actual experience with systems in place will with time supply required performance data to improve or refine the base isolation systems. Newer applications will perhaps present other issues that have not been thought of, but it appears that most issues can be solved on a rational basis.

6. CONCLUDING REMARKS

This paper has reviewed base isolation as a method for upgrading the earthquake performance of building structures. Both new construction and existing buildings can potentially benefit from it. However, base isolation is clearly not applicable to all situations. The paper discusses criteria for selecting the strategy based upon the site seismic considerations, the use, and the type of building structure. Various base isolation systems currently promoted have been briefly described. Some of these systems are more advanced than others in terms of analytical studies, confirmatory tests, and actual use. Most base isolation schemes use the common element of the reinforced elastomer bearing pad. Additionally, the more successful incorporate a frictional interface, a lead plug, or specially compound the elastomer to provide a healthy hysteresis characteristic to the bearing. This energy absorbing capability controls the relatively large displacements that characterize base isolation schemes.

Design considerations arising due to the particular seismic response characteristics of base-isolated structures are briefly discussed. It is suggested that these are problems of good detailing and just as important here as in the conventional design. Provided that these are paid the attention they deserve, base isolation is a viable alternative to upgrading seismic performance of building structures.

7. REFERENCES

1. Applied Technology Council, 1986, "Proceedings of a Seminar and Workshop on Base Isolation and Passive Energy Dissipation," ATC-17, San Francisco, California.

2. Caspe, M.S., July 1984, "Base Isolation from Earthquake Hazards, An Idea Whose Time Has Come!," Proceedings of the Eighth World Conference on Earthquake Engineering, San Francisco, California, Vol. 5, pp. 1031-1038.

3. Constantinou, M.C. and M.C. Kneifati, 1986, "Effect of Soil Structure Interaction on Damping and Frequencies of Base Isolated Structures," Proceeding of the Third U.S. National Conference on Earthquake Engineering, Charleston, South Carolina.

4. Gonzalez-Flores, M., 1964, "Sistema para Eliminar los Esfuerzos Peligrosos que los Temblores Causan en las Estructuras," Quinto Congreso Mexicano de la Industria de la Construccion, Tijuana, B.C., Mexico.

. Huang, M.J., A.F. Shakal, and J.T. Ragsdale, 1986, "Recorded Motion of a Base Isolated Building During the 1985 Redlands Earthquake," Proceedings, ATC-17, March 12-14, San Francisco, California.

5. Huffmann, G.K, 1985, "Full Base Isolation for Earthquake Protection," Helical Springs and Viscodameyers, Nuclear Engineering and Design 84, pp. 331-338.

7. Ikonomou, A.S., August 1979, "The Alexisismon: An Application to a Building Structure," Proceedings of the Second U.S. National Conference on Earthquake Engineering, Stanford University, California, pp. 443-452.

8. Kelly, J. M., 1982, "Aseismic Base Isolation: Its History and Prospects," World Congress on Joint Sealing and Bearing Systems for Concrete Structures, Publication SP-70, ACI, pp. 549-586.

9. Kelly, T.E., R.L. Mayers, and L.R. Jones, 1986, "Preliminary Design Procedures for Seismic Isolated Structures," Proceedings ATC-17, San Francisco, California.

10. Megget, L.M., July 1984, "The Design and Construction of a Base-Isolated Concrete Frame Building in Wellington, New Zealand," Proceedings of the Eighth World Conference on Earthquake Engineering, San Francisco, California, Vol. 5, pp. 935-342

11. Megget, L.M., December 1978, "Analysis and Design of a Base-Isolated Reinforced Concrete Frame Building," Bulletin of the New Zealand National Society for Earthquake Engineering, Vol. 11, No. 4, pp. 245-254.

12. Mostaghel, N., M. Hejazi, and M. Khodaverdian, 1986, "Response of Structures Supported on Resilient-Friction Base Isolator (R-FBI)," Proceedings of the Third U.S. National Conference on Earthquake Engineering, Charleston, South Carolina.

13. Newmark, N.M. and E. Rosenblueth, 1971, "Fundamentals of Earthquake Engineering," Prentice-Hall, Inc., Englewood Cliffs, New Jersey.

14. Reed, J.W. and C.A. Kircher, 1986, "Base-Isolation of a Five-Story, Wood-Frame Building," Proceedings, ATC-17, San Francisco, California.

15. Rigney, R.B., 1986, "System Selection from an Owner's View or the Anatomy of a Decision," Proceedings ATC-17, San Francisco, California.

16. Siegenthaler, R., 1970, "Earthquake Proof Building Supporting Structure with Shock Absorbing Damping Elements," Schweizerische Bauzeitung, No. 20.

17. Skinner, R.I., J.L., Beck, and G.N. Bycroft, 1975, "A Practical System for Isolating Structures from Earthquake Attack," International Journal of Earthquake Engineering and Structural Dynamics, Vol. 3, No. 3.

18. Skinner, R.I. and G.H. McVerry, June 1975, "Base Isolation for Increased Earthquake Resistance of Buildings," Bulletin of the New Zealand National Society for Earthquake Engineering, Vol. 8, No. 2, pp. 93-101.

19. Stiemer, S.F., F.L. Chow, July 1984, "Curved Plated Energy Absorbers for Earthquake Resistant Structures," Proceedings of the Eighth World Conference on Earthquake Engineering, San Francisco, California, Vol. 5, pp. 967-974.

20. Structural Engineers Association of California, 1984, Seismology Committee, "Recommended Lateral Force Requirements and Commentary."

21. Structural Engineers Association of Northern California (SEAONC), 1986, "Tentative Seismic Isolation Design Requirements," Proceedings, ATC-17, San Francisco, California.

22. Structural Engineers Association of Southern California (SEAOSC), 1986, "Draft Guidelines for the Design of Buildings with Base Isolators," Proceedings, ATC-17, San Francisco, California.

23. Tarics, A.G., 1982, "Cost Consideration of Base Isolation," International Conference on National Rubber for Earthquake Protection of Buildings and Vibration Isolation, Kuala Lampur, Malasia.

24. Tyler, R.G., July 1984, "Developments in Energy Absorbing Devices and the Physics and Engineering Laboratory, DSIR, New Zealand," Proceedings of the Eighth World Conference on Earthquake Engineering, San Francisco, California, Vol. 6, pp. 969-976.

25. "Uniform Building Code," 1979 Edition, International Conference of Building Officials, Whittier, California.

26. Vaidya, N.R. and C.E. Plichon, 1986, "On the Concept of Base Isolation Design in France," Proceedings, ATC-17, San Francisco, California.

27. Vaidya, N.R. and A.J. Eggenberger, January 1984, "Feasibility Evaluation of Base Isolation for the Aseismic Design of Structures," Report to the National Science Foundation, Washington D.C. by D'Appolonia Consulting Engineers, Project No. 82-1365.

28. Way, D and Marshall Law, 1986, "Design and Analysis of a High-Damping Rubber Isolation System" (Case History of the Foothill Communities Law and Justice Center), Proceedings, ATC-17, San Francisco, California.

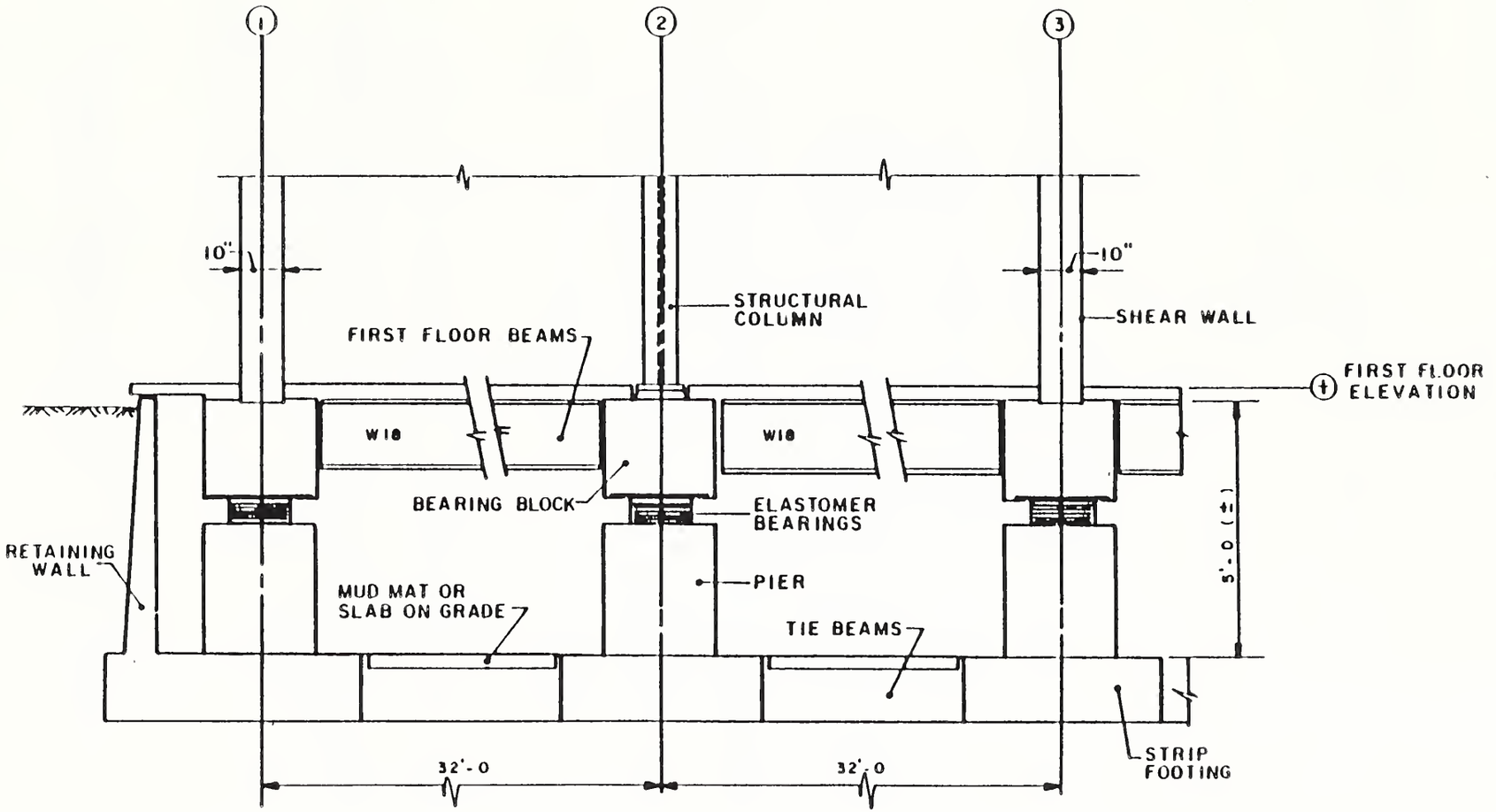

FIGURE 1 – CONCEPTUAL DESIGN OF BASE ISOLATION

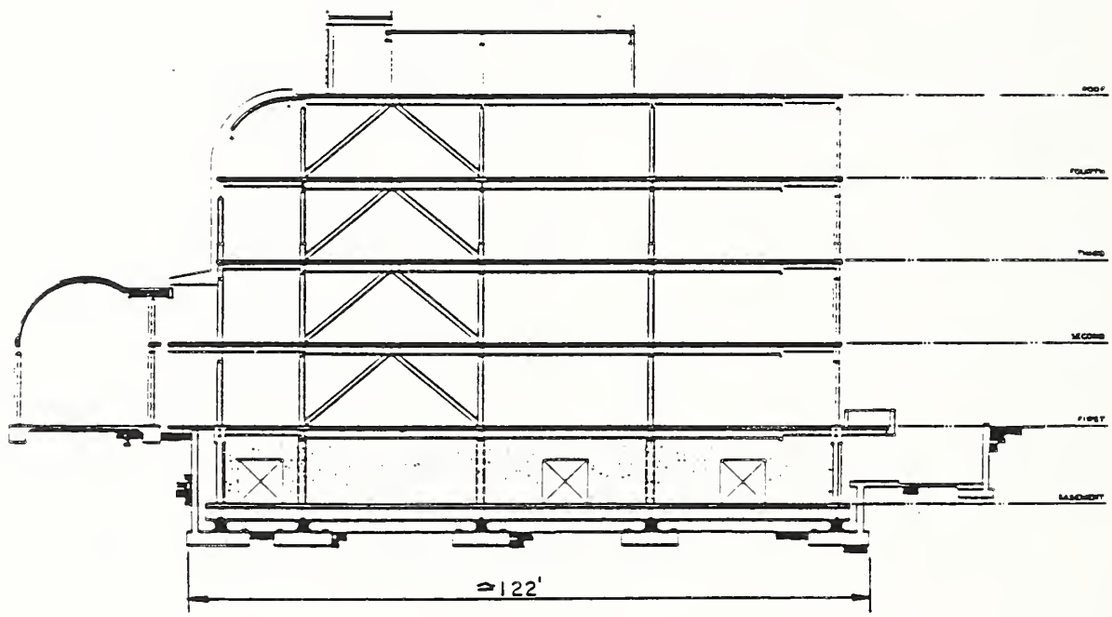

REF. WAY, 1986

FIGURE 2 – BASE ISOLATION DESIGN FOR THE FOOTHILLS COMMUNITY LAW AND JUSTICE CENTER BUILDING

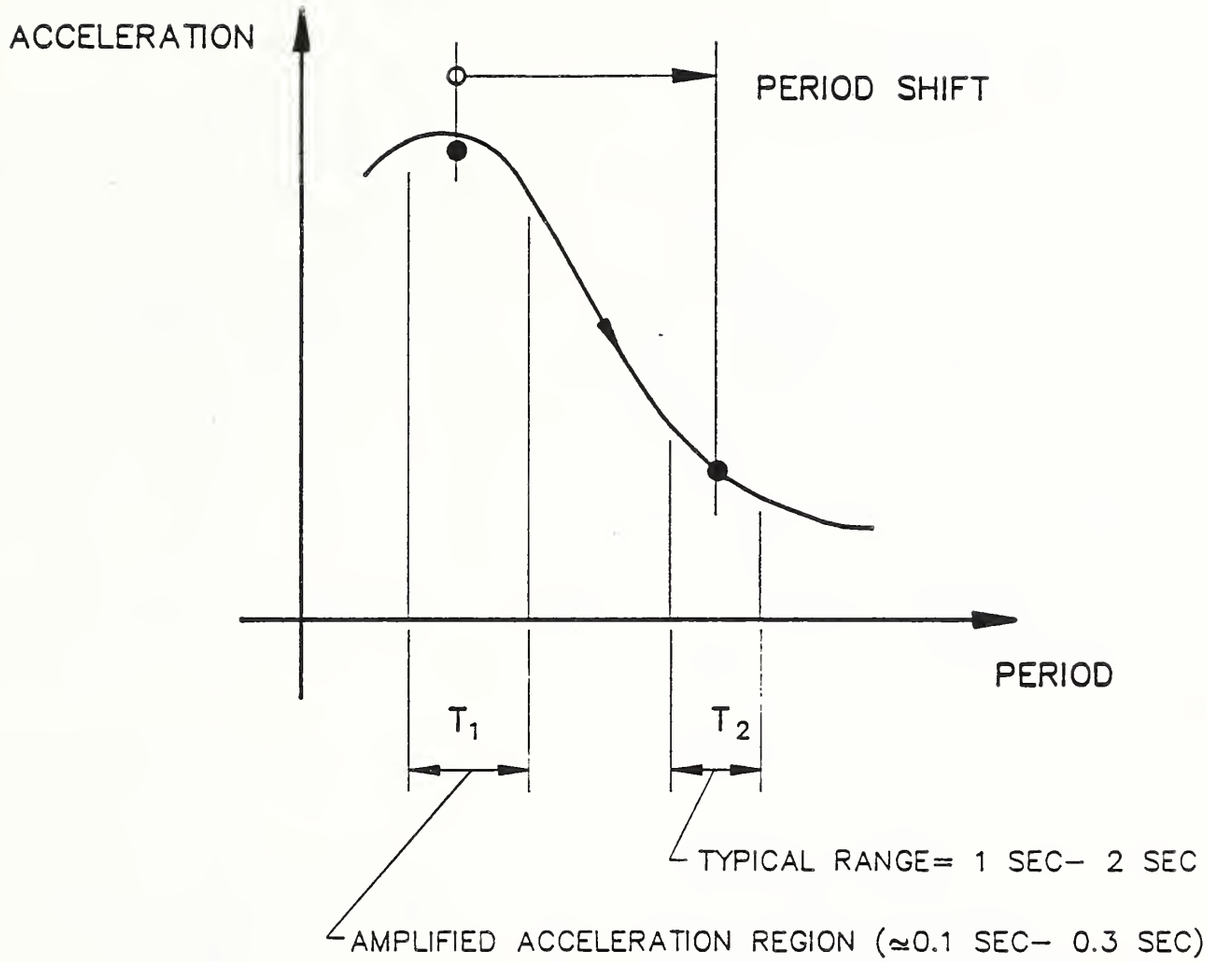

IDEALIZED SEISMIC GROUND RESPONSE SPECTRUM

NOTES:

T_1 = PERIOD OF FIXED BASE STRUCTURE
T_2 = PERIOD OF STRUCTURE ON BASE ISOLATION

FIGURE 3 – PERIOD SHIFT DUE TO BASE ISOLATION

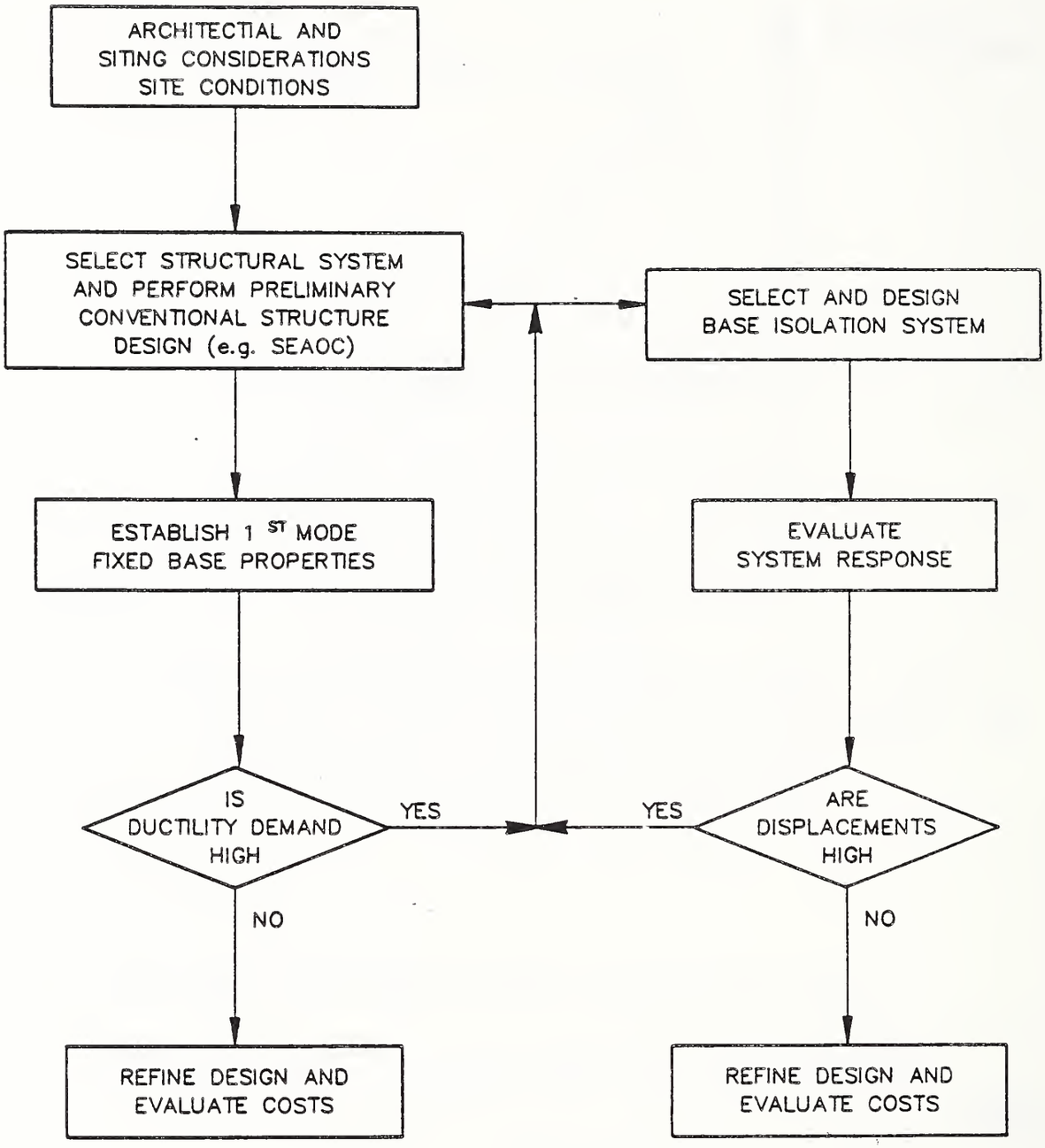

FIGURE 4 – FLOW CHART CRITERIA FOR SELECTING BASE ISOLATION

Consideration of Earthquakes in Highway Earthworks

BY

Yasuyuki Koga 1)
Akiomi Shimazu 2)
Eiichi Taniguchi 3)

ABSTRACT

Earthwork sections in highways such as fills and cuts have been sometimes severely damaged by past earthquakes. It has been usually considered to be fairly easy and economical to repair seismically damaged earthwork sections when damages occurred. However, the required level of earthwork sections has been recently rising because of the large influence and importance of highway earthwork sections in case of their failure.

This paper briefly presents a current practice in highway earthworks against seismic effects mainly on the basis of the recently revised editions of Technical Guideline for Highway Earthwork (Japan Road Association).

KEY WORDS: Highway Earthworks, Seismic Damage, Seismic Design, Seismic Inspection

1. INTRODUCTION

Because of the topography of the country, a large portion of highways in Japan are constructed in mountainous areas in which the topography is steep and the geological and soil property is complex, or in lower land areas whose ground is poor. It can also be said that Japan is in heavily severe condition for the road construction and maintenance because of heavy and frequent rain, snow and earthquakes. Among the total length of highways in Japan exceeding 1.1 million km, structural sections such as bridges and tunnels are only 1,700 km and a large portion of rest consists of earthwork sections. The earthwork sections such as fills and cuts cannot always be assumed to have enough resistance against such natural conditions.

This paper summarizes the viewpoints on the influence of the earthquake in the current technical level of the highway earthworks, which are mainly described in the recently revised edition of Technical Guideline for Highway Earthwork (Japan Road Association).

2. PREVIOUS EARTHQUAKE EXPERIENCE AND DESIGN VIEWPOINTS IN HIGHWAY EARTHWORK SECTIONS

Earthwork structures are one of the earthquake-prone structures among conventional civil engineering structures. Numerous damages occurred in several recent earthquakes in Japan. For example, settlements and cracks of embankments due to the liquefaction of sandy ground occurred in a large scale in the Niigata Earthquake of 1964 and the Nihonkai-chubu Earthquake of 1983 as well. In the Tokachi-oki Earthquake of 1968, the slide of embankments was enlarged because of the soft ground and also the increase of water content of the fill by the rainfall prior to the earthquake. The slides of the embankment constructed on the cuts of mountainous slopes occurred in the Oitaken-chubu Earthquake of 1975 and the Miyagiken-oki Earthquake of 1978. In addition to these examples, slides and rockfalls took place in a large scale in the cuts and natural slopes above the road in the Izu-Oshima-Kinkai Earthquake of 1978. These examples summarize the feature of the damage to the road earthwork sections.

In spite of such a lot of damage examples, no explicit considerations are given in the design of general highway earthwork structures. The reason is described as follows in the Highway Earthquake Essentials (1).

(1) Repairing of earth structures such as cuts and fills is rather easy compared with other structures. In the case of fills, the strength of fills and ground increases as time passes after construction, then the stability increases.

(2) In the fills and cuts of ordinary scale, ordinary soil and geological properties, the standard slope gradient is usually applied, which considers the fill and cut height, and soil classification. Since the standard slope gradient is obtained on the basis of long experiences that the earth structures endured meteorological condition in Japan, such slope gradients are assumed to ensure the stability of the cuts and fills against an external load below some magnitude.

(3) Much is still unsolved about the dynamic soil properties and earth pressures connected with retaining walls, however, it is known from the past experience that retaining walls can functionally stand without particular consideration

1) Head, Soil Dynamics Division, Construction Equipment and Method Department, Public Works Research Institute, Ministry of Construction, Japan
2) Head, Construction Method Division, Construction Equipment and Method Department, Public Works Research Institute, Japan
3) Dr. of Eng., Head, Planning Division, Planning and Research Administration Department (Formerly Senior Research Engineer, Soil Dynamics Division), Public Works Research Institute, Japan

of the seismic effect if the construction is secured. Therefore, no seismic effect is taken account in the design of retaining walls of ordinary size.

But it is desirable to conduct investigations against earthquakes in case of the embankment on a sandy ground which may liquefy during earthquakes, which is high and close to an important structure, or whose damage may probably give a large influence to road traffic and roadside facilities.

Abovementioned is a summary of past experience on seismic effect and fundamental viewpoints on highway earthwork sections up to the present. On the basis of such fundamental viewpoints, a little more concrete viewpoints and calculation formulas for earthquakes are described in the technical guidelines of highway earthworks recently revised.

3. VIEWPOINTS OF EARTHQUAKES IN HIGHWAY EARTHWORK SECTIONS IN THE NEW EDDITION OF TECHNICAL GUIDELINE FOR HIGHWAY EARTHWORK

(1) General and fill slopes

Among the technical guideline for road earthworks recently revised, seismic designing is referred in Technical Guideline for Highway Earthwork -- Countermeasures for Soft Ground (2), Countermeasures for Slope Stability (3), Retaining Wall, Culvert and Temporary Structure (4). Though the expressions of the viewpoint of earthquakes in these technical guidelines are not quite identical, the fundamental viewpoint can be shown as in the flow chart in Fig. 1. This is a simplified version of a flow chart for the highway embankments shown in "Technical Guideline for Slope Stability". Basic ideas hold in other structures. That is, the conditions to be considered in the investigation for the stability of embankments are following three items (3).

(i) Condition for embankment proper

(a) When the height of the fill exceeds the standard values in Table 1.

(b) When the fill material comprises soils with a high water content and a low shearing strength (especially volcanic soils with a high water content).

(c) When the fill material comprises soils with a high water content in which pore pressure tends to increase easily (e.g., soils with a high clay and silt content, volcanic soils).

(ii) Conditions for fill foundation

(a) When the fill foundation is unstable as poor ground and landslide (including liquefiable sandy ground during earthquakes).

(b) When the fill is easily affected by spring water from foundation slope (e.g., partial cut fill section, widened embankment, fill on slope, fill across valley).

(c) When the fill slope may be innundated or the slope toe may be eroded during floods (e.g., fill in ponds and along rivers).

(iii) Influence by the fill failure

(a) When serious damage may be given to adjacent structures in case of failure.

(b) When a long time is needed for repairing work and the road function may be considerably disturbed in case of failure (e.g., fills on slope in mountainous roads without other alternative roads).

The flow in Fig. 1 can be classified into following three cases from investigation items and methods.

(i) None of three conditions above mentioned can be a problem. Standard slope gradients will be used.

(ii) Though the fill and ground condition is not good enough, the influence by th fill failure will be relatively small. Or though the influence by the fill failure is large, such a possibility is small because the fill and ground condition is good. A static stability investigation including a stability analysis is conducted.

(iii) The fill and ground condition is not good enough and the influence on the adjacent structures and road functions by the fill failure is quite large. A static and seismic stability investigation including a stability analysis is conducted.

In a preliminary survey stage the quality of the fill material is estimated considering Table-1 and above case (i). The method to determine the strength of the fill material in the detailed survey stage will be described later in the Chapter 4.

(2) Soft ground (2)

Soft ground is an example of a poor ground condition. When there exists a sandy ground which way liquefy or a clayey ground which may remarkably deform during earthquakes in a section where the influence by the fill failure

is quite large, the investigation for a seismic condition and a proper consideration must be given when needed.

Especially, when the liquefaction phenomenon occurs during earthquakes in a wide area of sandy ground supporting a fill, the bearing capacity for the fill is remarkably reduced and consequently the fill is severely damaged. Therefore it is necessary to estimate the ground condition. The methods used for the estimation varies in the several construction stages from planning to designing.

In the preliminary survey stage with little detailed information of ground soil property, the existence of the ground prone to liquefaction is roughly grasped and the possibility is estimated from the simple information such as micro relief, N-value from the SPT and gradation distribution.

And the investigation method thereafter is to be determined. Subsequently it is evaluated whether the fill is damaged on the basis of soil property obtained from detailed investigation and stability analysis. Countermeasures must be investigated if necessary.

A simplified chart is proposed to judge the possibility of the liquefaction of the ground and the loss of the fill stability on the basis of N-value from the SPT and gradation characteristics without any stability calculation (Fig. 2). This figure shows critical N-value (Ncr) to give failure condition for each soil type against specified seismic coefficient. In the investigation of a specific fill, measured N-values must be compared with critical N-values in Fig. 2 considering the depth and soil kinds. The evaluation of the ground as a whole whether the fill is damaged or not must be done from overall comparison of measured N-values and critical N-values along total depth of the ground. As one of the methods, the stability coefficient for each depth is defined by N/Ncr. It has been recently shown that the average value of the stability coefficient for total depth to be considered has a reasonable correlation with a damage fact. Therefore Fig. 2 can be used a rough estimation. A detailed procedure, though not quite the same as that in the technical guideline, is described elsewhere (5).

Clayey soils generally show less tendency to decrease the shear strength than sandy soils due to vibration. Loss of stability and excessive settlement will occur against static load for a clayey ground where some damage can possibly occur during earthquakes. In other words, if sufficient consideration is given to secure static stability, seismic stability can be generally kept due to the margin to static stability. However, some fills on clayey ground were known to be severely damaged where static stability was assumed not high enough. Therefore seismic stability must be investigated in clayey ground where remarkable damages may occur during earthquakes from detailed results of soil exploration.

The detailed stability analysis method of the fill on poor ground will be described in Chapter 4.

The stability of retaining wall on poor ground must be investigated as well.

(3) Retaining wall (4)

Usually earthquake load is considered for only the retaining walls having height over 8 m from following reasons. Essentially, very few retaining walls have collapsed in past damage examples. Large damages were mostly caused by the collapse of the overall ground which supports retaining walls and fills. Therefore retaining walls of ordinary size will stand against earthquakes without particular seismic calculation if they are carefully designed and constructed under static condition. On the other hand, because the retaining walls over 8 m are considered to exceed the above experience, a seismic calculation is required. Moreover, seismic calculation is also required for the retaining walls over around 5 m when the influence of the collapse of the retaing wall can be large.

(4) Cut slope (3)

Cutting slope is based on past experience more than fill works. Standard slope gradients in Table 2 are generally used as a reference, because natural ground generally consists of complex and inhomogeneous soil layer and it gets less stable due to weathering after construction. In cutting also as in the case of fills, it is necessary not to apply the standard slope gradients in Table 2 but to use such measures as lessing slope gradients depending on three conditions of ground condition, cutting conditions and influence by the failure as in the case of fills.

The investigation procedure of the stability analysis of cutting slopes is similar to that of Fig. 1 for fills. That is, investigation of seismic stability is conducted when the ground or cutting condition is not good enough and the influence by the failure is large.

However, the reliability of stability

calculation for stability investigation of cut slopes is less than that of fill slopes from the above background. Therefore, in the consideration of earthquakes in cut and natural slopes, it is desirable to refer to the past features of landslide disasters during earthquakes and also to consider the countermeasure being effective to the landslide caused by not only earthquakes but other effects. This is because the countermeasure for the rainfall should also be effective to earthquakes to some extent.

Following facts are known from the past earthquake damage to cut and natural slopes.

(i) There are more cases of shallow slope failure and falling rocks in cut and natural slopes than in the rainfall cases.

(ii) The damage ratio is high in the cut and natural slopes where the longitudinal and cross sectional shape is convex. The top of the failure reaches near the ridge.

(iii) Very few damages occur to the slope protection works which (a) considers earth pressure, or (b) closely touches to stable ground, or (c) is flexible, such as lattice walls and cast-in-place concrete crib-works.

(iv) Among the stone and block masonry retaining walls, dry masonry or mortar masonry with steep gradient and thin grout concrete are damaged.

(v) Concrete spraying, mortar spraying, rockfall prevention fences work efficient to some extent.

It is required to refer to the above-mentioned and to estimate the seismic damage possibility and to conduct proper countermeasures of cut slopes.

4. SEISMIC CALCULATION METHOD FOR HIGHWAY EARTH WORK SECTIONS

Following calculation formulas can be used as a reference to conduct a detailed seismic calculation on the basis of soil exploration results.

(1) Fill slope (3)

Following equation can be used to obtain a safety factor for seismic stability, which is based on seismic coefficient method assuming a circular slip surface.

$$F_S = \frac{\Sigma[c\cdot\ell+\{(W-u\cdot b)\cos\alpha-k_h\cdot W\cdot\sin\alpha\}\tan\phi]}{\Sigma(W\cdot\sin\alpha+k_h\cdot W\cdot\frac{h}{r})} \quad \ldots (1)$$

where F_S: Factor of safety,
r : Radius of slip surface,
c : Cohesion of soil,
ϕ : Angle of shear resistance,
ℓ : Length of arc of slip surface cut by each slice,
W : Weight of slice,
u : Pore water pressure,
b : Width of each slice,
k : Design seismic coefficient,
h ; Vertical distance between the center of gravity of each slice and the center of slip circle.
(See Fig. 3)

The Safety factor must be greater than unity in the seismic design of the fill slope.

As to the seismic stability calculation, researches to consider dynamic soil strength are now under way, and dynamic strength characteristics of compacted fill material and weathered residual soils are not well known yet. However, ordinary strength parameters c and ϕ obtained from static tests can be used for ordinary stability analysis, because it is troublesome to do dynamic soil strength tests for fill slopes of ordinary size and the dynamic strength of well compacted fill material is assumed nearly equal to its static strength. Strength parameters can be expressed in terms of effective stress or total stress depending on whether pore pressure against shearing is considered or not. In case of the total stress expression, only the pore pressure from ground water level is considered.

In case of the effective stress expression, the excess pore pressure caused by earthquake vibration is also considered. This situation is summarrized in Table-3.

(2) Fills on soft ground (2)

The estimation of ground strength is important for the fills on soft ground. The expression of soil strength of soft ground varies depending on the soil kinds such as sandy and clayey soils.

1) Sandy ground (liquefiable ground)

At present in Japan, the soil strength of liqueficable ground is mostly expressed in terms of effective stress for stability analysis. The safety factor for fill stability is given by the following equation.

$$F_S = \frac{\Sigma\{c'\cdot\ell+(W-u_o\cdot b-u_e\cdot b)\cdot\cos\alpha\cdot\tan\phi'\}}{\Sigma(W\cdot\sin\alpha+k_h\cdot W\cdot\frac{h}{r})} \quad \ldots . (2)$$

where c',ϕ': Cohesion of soil and angle of shear resistance in terms of effective

stress,

u_o : Pore pressure corresponding to the ordinary ground water,

u_e : Pore pressure generated by the earthquake,

and other notations are the same as those in Eq. (1).

The soil strength of liquefiable ground can also be expressed in terms of total stress, in which the safety factor is calculated by

$$F_s = \frac{\Sigma(\tau_f \cdot \ell)}{\Sigma(W \cdot \sin\alpha + k_h \cdot W \cdot \frac{h}{r})} \quad \cdots\cdots\cdots\cdots \quad (3)$$

where τ_f: dynamic soil strength expressed in terms of total stress.

Calculation by Eq. (2) needs excess pore pressure caused by seismic loading, which is estimated by dynamic shear stress in the ground.

2) Clayey ground

It is considered that the decrease of strength of clayey soils against dynamic loading is not large and on the contrary greater values than static condition can be assumed because of loading rate effect. However, static strength is generally used for stability analysis. That is, the safety factor is obtained from the equation below.

$$F_s = \frac{\Sigma c_u \cdot \ell}{\Sigma(W \cdot \sin\alpha + k_h \cdot W \cdot \frac{h}{r})} \quad \cdots\cdots\cdots \quad (4)$$

where cu: Final undrained shear strength when the consolidation has ended.

(3) Cut slope (2)

As mentioned before stability analyses are not generally performed for the design of cut slopes except the ones in landslide area or old failure area. Stability analyses are conducted for the designing of repairing works of failed slopes. In this case, it is better to do stability analyses assuming not only circular slip surface but other possible shapes of slip surface.

(4) Retaining wall (4)

Retaining walls must be stable in terms of sliding, overturning, bearing capacity of foundation and overall sliding to consist of backfill and foundation against self weight, external load, earthpressure and seismic load (seismic earth pressure and seismic inertia force).

Among these, seismic earth pressures are calculated by applying horizontal seismic inertia force to the wedge in the trial wedge method, in which an arbitary planar slip surface from the toe of the back fill is assumed and the maximum earth pressure obtained from the force polygon of the wedge becomes an active pressure resultant P_A. Seismic inertia force is horizontally applied at the gravitational center of the retaining wall, which is given as K_h/W using design horizontal seismic coefficient K_h and self weight of the retaining wall W. The safety factors and other indices for the stability in seismic stability analyses are as follows:

(i) Safety factor for sliding: $F_s \geq 1.2$

(ii) Stability for overturning: Eccentric distance $|e| \leq B/3$ (B = width of base)

(iii) Bearing capacity of the foundation: $F_s \geq 1.2$

(iv) Overall stability for the sliding including backfill and foundation: the sliding is investigated referring to above Sections (1) and (2).

(5) Seismic investigation for semi-buried road and common utility duct

Besides the conventional earth structures such as fills described up to preceding sections, the aseismity of the semi-buried road constructed at soft ground with high ground water level and common utility duct playing an important role as a life line in a city must be investigated.

(i) Semi-buried road (2)

The stability of the semi-buried road constructed at the site of high ground water level is low even for ordinary buoyant force. The stability for the buoyant force during an earthquake must be confirmed considering the excess pore pressure caused by the liquefaction when it can possibly occur. The safety factor for buoyant force is obtained by following equation.

$$F_s = \frac{W_B + W_S + Q_S}{U_S + U_D} \quad \cdots\cdots\cdots \quad (5)$$

where W_B: Self weight of semi-buried road including pavement and leveling concrete,

Ws: Load by overburden earth above base,

Qs: Shearing resistance of overburden earth above base or frictional resistance between side-

wall of semi-buried road and back fills,

U_S: Buoyant force by the hydrostatic pressure at the bottom of semi-buried road,

U_D: Buoyant force by the excess pore pressure at the bottom of semi-buried road.

The buoyant force U_D is estimated referring to the formula for the common utility duct in the next section.

The safety factor must be greater than 1.2 and 1.0 for static case and seismic case, respectively.

The sidewall is designed as cantilever type retaining wall.

(ii) Common utility duct (6)

There is no experience of the seismic damage to the common utility ducts because they are rather new facilities in Japan. However seismic calculations for the common utility duct are to be conducted at following sites which need precaution from the past experience of the seismic damage to other underground structures:

Soft ground, sections whose ground condition varies steeply, sites where the structure changes or different structures such as are connected vertical ducts, and liquefiable ground.

Except liquefiable ground, the response displacement method is used as aseismic calculations to obtain longitudinal sectional force. Displacement amplifude of the ground and wave length of the ground motion are needed as design seismic input. The former is calculated considering the fundamental period of the surface layer and regional characteristics, and the latter considering the shear wave velocities of the surface layer and bedrock, and fundamental period of the surface layer.

The possibility of the liquefaction is estimated by calculating the liquefaction strength and the liquefaction resistance rate F_L using the method of the highway bridge specification (JRA) on the basis of N-value of the ground and average grain-diameter D_{50}. The excess pore pressure ratio $\Delta u/\sigma v'$ is obtained from F_L and Fig. 7, then the safety factor for floating up is calculated by the equation below.

$$F_S = \frac{W_S + W_B + Q_S + Q_B}{U_S + U_D} \quad \cdots\cdots\cdots (6)$$

where W_S: Weight of overburden earth,

W_B: Self weight of common duct including contained materials and leveling concrete,

Q_S: Shearing resistance of overburden earth,

Q_B: Frictional resistance of sidewall of common utility duct,

U_S: Buoyant force by the hydrostatic pressure at the duct base,

U_D: Buoyant force by the excess pore-pressure at the duct base.

This method is essentially the same as that to obtain excess pore pressure in the stability analysis for the fill. The safety factor for seismic buoyant force must be greater than 1.1.

(6) Design seismic coefficient (2, 3, 4)

The design seismic coefficient for the stability analysis and earth pressure calculation of earth structures must be carefully determined. It is generally calculated by the following equation considering the way to determine one for other civil engineering structures.

$$k_h = \nu_1 \cdot \nu_2 \cdot k_{ho}$$

where k_{ho}: Standard design seismic coefficient, 0.15,

ν_1 : Seismic zone factor,

ν_2 : Ground condition factor.

The factors ν_1 and ν_2 are the same as those used in the Highway Bridge Specification. The important factor ν_3 used in the Highway Bridge Specification is assumed as 1.0 because the earth structure is considered particularly important if a seismic calculation is needed for the structure.

Moreover it may be noticed that the standard design seismic coefficient k_{ho} equals to 0.2 in highway bridges. This is because the road bridge stands above the ground and the response acceleration can get larger than that of fills which is united to the ground.

The design seismic coefficient is not necessarily the maximum response acceleration divided by gravitational accelegration which irregularly fluctuates. This is because the maximum response acceleration occurs only once during the period of earthquake process then if the state to exceed the resistance occurs for a very short period the failure will not occur at once and it is too severe to assume the maximum valve to continue permanently as the seismic coefficient method. This is very important for a material as soil that

does not show a rapid decrease of strength after its failure point. Consequently, the seismic coefficient k_h used for a stability analysis is obtained by reducing the maximum value of assumed seismic motion.

On the other hand, in the sandy ground described in the Section (2)1), it is sometimes required to estimate the excess pore pressure u_e during an earthquake. It is generally estimated from the comparison of seismic shear stress and dynamic shear strength of the ground. The seismic shear stress is roughly estimated from the acceleration at the ground surface. In order to simply express the above shear stress and shear strength, they are generally converted to a shear stress of uniform amplitude and a certain number of cycles. However, the liquefaction strength in the Highway Bridge Specification is represented as the maximum value of shear stress process which changes irregularly. Therefore it is reasonable to compare the above shear strength with the maximum shear stress which is estimated from the maximum acceleration at the ground surface. That is, the seismic coefficient to obtain the excess pore pressure should be the maximum value of the ground motion.

There is no established idea if it is necessary to consider at once the design seismic coefficient and the excess pore pressure mentioned above. One idea sometimes used is to consider the seismic coefficient and the excess pore pressure separately because the peak time of seismic motion and excess pore pressure do not generally coincide.

There are many questions to need future research. They are; (1) if it is reasonable to express the seismic strength of the liquefiable ground through pore pressure, (2) if it is appropriate to consider the seismic coefficient and excess pore pressure separately, (3) how the reference factor of safety should be determined when they are considered separately, and so on.

5. OTHERS

(1) Seismic inspection

So far described is fundamentally based on the several technical guidelines for highway earthwork. Though these guidelines explain the maintenance and administration to some extent, they essentially focus on construction works. On the other hand, it is an important issue how the aseismicity of existing structures should be evaluated when we consider the aseismicity of road earthworks. As regards to this issue, the seismic inspection such road structures as bridges, tunnels, pedestrian overbridges and embankments were conducted in 1986 through a notification by Director-Generals of Road Bureau and City Bureau, MOC. This kind of inspection has been conducted in 1971, 1976 and 1979. The inspection of this time newly handles the fills on steeply inclined ground and at approaching to bridges. The method of the inspection is a basically simple one which considers the topography, the inclination of the foundation, the fill height, the ground condition, the catchment situation, the slope gradient, etc. It is used to judge the aseismicity on the basis of these items, and to extract the sections to need some countermeasures.

(2) Rehabilitation of seismic damage (7)

It is very important to prepare to reduce the damage effect by coping with the damage smoothly and rationally and securing the emergency transportation route. For this purpose, the technical development project by MOC, "Development of rehabilitation technique of seismically damaged structures" has been carried out from 1981 to 1985. As a consequence. "Manual for rehabilitation technique of seismically damaged structures" was published (7). In the part III -- part of Road Facilities of this manual, much is described concerning road fills, natural and cut slopes, common utility ducts, culverts as the reference for rehabilitation.

6. Conclusions

The recent viewpoints of the seismic effect on the highway earthworks were reviewed mainly on the basis of revised technical guidelines for highway earthworks. It has been considered appropriate to cope with the seismic damage by repairing works. But as the socially required level for road functions has been upgraded, the need for concrete evaluation methods, investigation methods and countermeasures of the necessary sections against seismic effect has also been increasing. Therefore techniques to cope with this demand should be much more developed.

Reference

1. Japan Road Association: Highway Earthwork Essentials, 1983 (in Japanese).

2. Japan Road Association: Technical Guideline for Highway Earthwork -- Countermeasures for Soft Ground, 1986 (in Japanese).

3. Japan Road Association: Technical Guideline for Highway Earthwork -- Counter-

measures for Slope Stability, 1986 (in Japanese).

4. Japan Road Association: Technical Guideline for Highway Earthwork — Retaining Walls, Culverts, Temporary Structures, 1987 (in Japanese).

5. Koga, Y. and Matsuo, O.: Simplified procedure to evaluate the stability of embankments on liquefiable ground, 19th Joint Meeting, UJNR, 1987.

6. Japan Road Association: Technical Guideline for Designing of Common Utility Duct, 1986 (in Japanese).

7. Iwasaki T., et al.: Outline of Manual for Repair Methods for Civil Engineering Structures Damaged by Earthquakes, 18th Joint Meeting, UJNR, 1986.

Table 1 Standard Gradients of Cut Slopes

Soil classification		Cutting depth	Gradient
Hard rock			1:0.3 to 1:0.8
Soft rock			1:0.5 to 1:1.2
Sand	Not dense, and poorly graded		1:1.5 to
Sandy soil	Dense	Less than 5m	1:0.8 to 1:1.0
		5 to 10m	1:1.0 to 1:1.2
	Not dense	Less than 5m	1:1.0 to 1:1.2
		5 to 10m	1:1.2 to 1:1.5
Sand soil mixed with gravel or rock masses	Dense, or well graded	Less than 10m	1:0.8 to 1:1.0
		10 to 15m	1:1.0 to 1:1.2
	Not dense, or poorly graded	Less than 10m	1:1.0 to 1:1.2
		10 to 15m	1:1.2 to 1:1.5
Cohesive soil		0 to 10m	1:0.8 to 1:1.2
Cohesive soil mixed with rock masses or cobblestones		Less than 5m	1:1.0 to 1:1.2
		5 to 10m	1:1.2 to 1:1.5

Table 2 Standard Gradients of Fill Slopes

Filling materials	Height of fill (m)	Slope ratio	Remarks
Sand with good grading (SW), gravel, and sand mixed with gravel (GM) (GC) (GW) (GP)	Less than 5m	1:1.5 to 1:1.8	To be applied to fills with sufficient bearing capacity at foundation ground, which are not affected by inundation. Typical unified classes are shown in ( ) for reference.
	5 to 15m	1:1.8 to 1:2.0	
Sand with poor grading (SP)	Less than 10m	1:1.8 to 1:2.0	
Rock masses (including muck)	Less than 10m	1:1.5 to 1:1.8	
	10 to 20m	1:1.8 to 1:2.0	
Sandy soil (SM)(SC), hard clayey soils and hard clay (hard clayey soils and clay of alluvium, loam, etc.)	Less than 5m	1:1.5 to 1:1.8	
	5 to 10m	1:1.8 to 1:2.0	
Soft clayey soils (VH)	Less than 5m	1:1.8 to 1:2.0	

Table 3 Strength Parameters and Pore Pressures to be Used for Stability Calculation in Terms of Total Stress and Effective Stress Methods

	Total Stress Method		Effective Stress Method
Seismic Case	Low Permeability	c_{cu}, ϕ_{cu}, u_o	c', ϕ', u_o, u_e
	High Permeability	c_d, ϕ_d, u_o	

c_{cu}, ϕ_{cu} : Strength Parameters Obtained from CU Test
c_d, ϕ_d : " " " " $\overline{CD}$ "
c', ϕ' : Strength Parameters Obtained from $\overline{CU}$ Test
u_o : Pore Pressure by Normal Ground Water Level
u_e : Pore Pressure Generated by Earthquakes

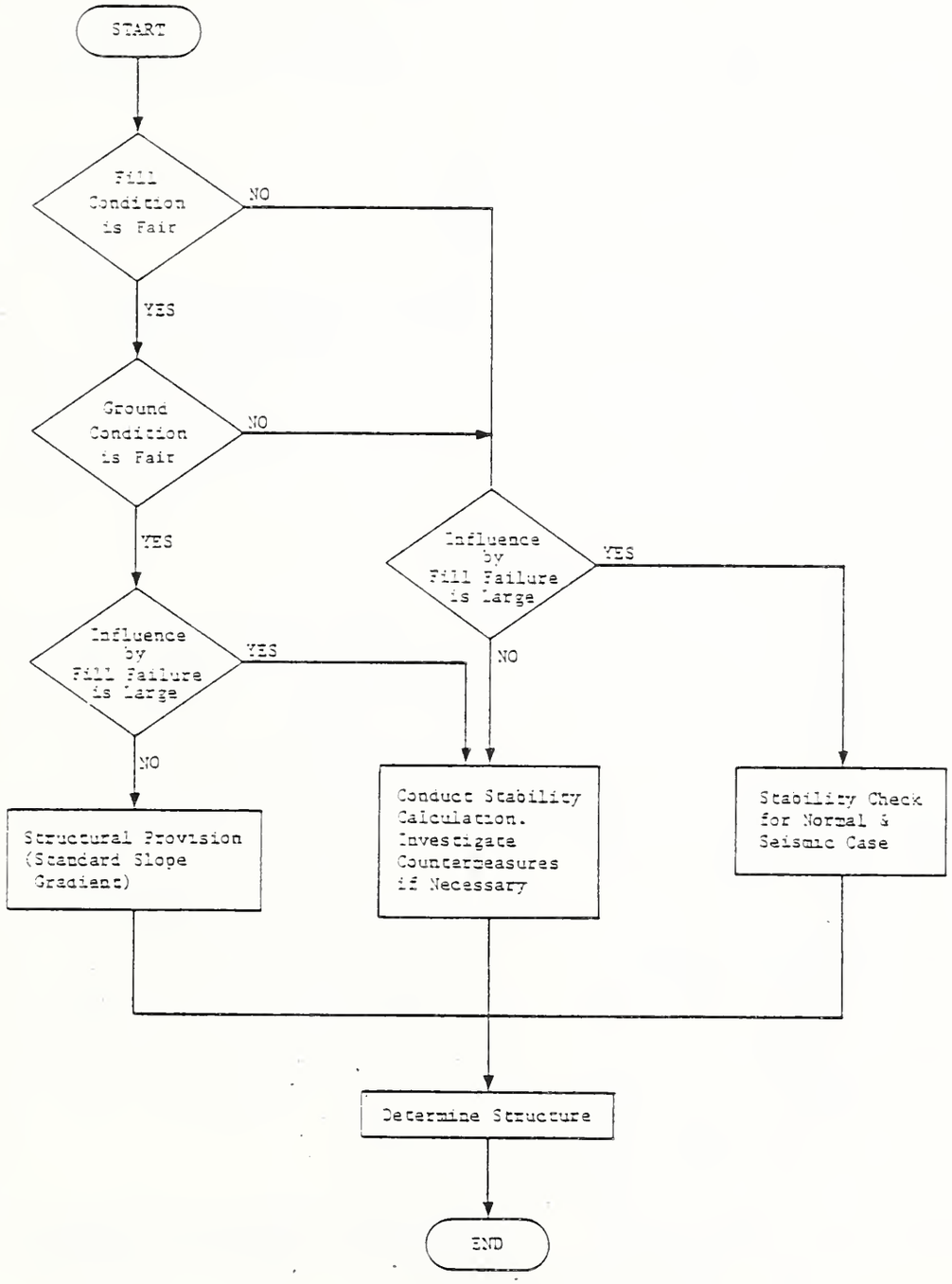

Fig. 1 Flow of Stability Check for Highway Earthworks (Case of Fill Slopes)

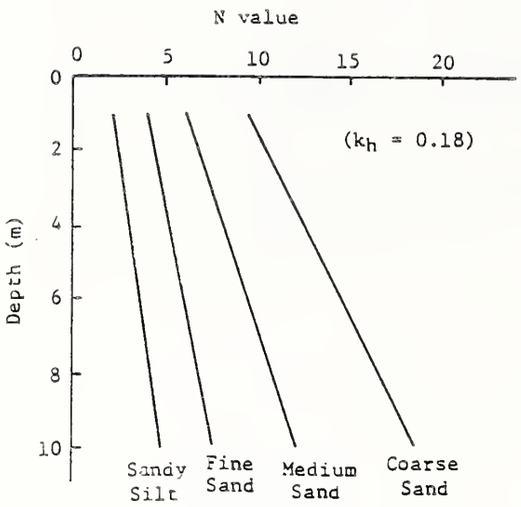

Soil is classified by the description of soil profile or the Table below.

Name	D_{50} (mm)
Sandy Silt	$D_{50} < 0.074$
Fine Sand	$0.074 \leqq D_{50} < 0.25$
Medium Sand	$0.25 \leqq D_{50} \leqq 0.42$
Coarse Sand	$0.42 \leqq D_{50}$

Fig. 2 Critical N Value for Rough Estimation

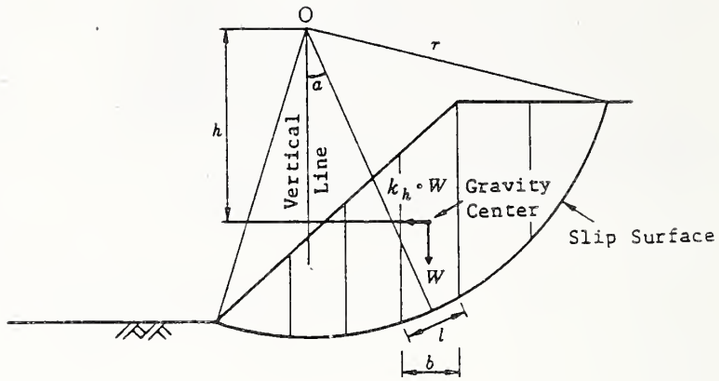

Fig. 3 Seismic Stability Calculation Method by Use of Circular Slip Surface

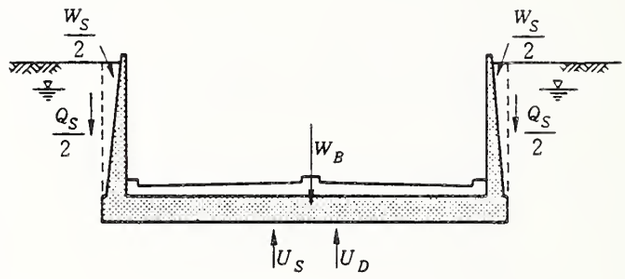

Fig. 4 Forces Acting on Semi-Buried Road

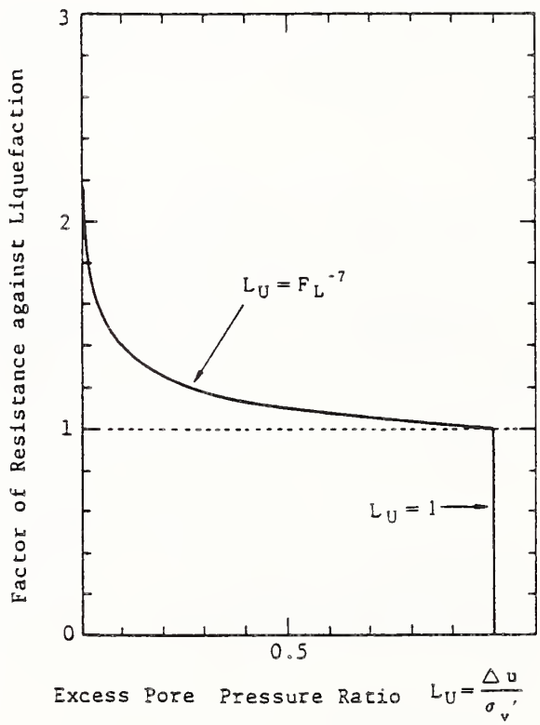

Fig. 5 Relation between F_L and L_U

Damage, Strengthening, and Retrofit of Bridges

BY

James H. Gates 1

ABSTRACT

Earthquake damage to bridges in California since 1932, including the 1971 San Fernando earthquake is summarized. The 1986 damage to a seismically retrofit bridge in the Palm Springs area is described. The completion of the 16 year California project to strengthen and retrofit joints and bearings to increase their seismic capacity is described and plans outlined for the next phase of seismic strengthening and retrofit of columns and substructures of bridges in highly vulnerable seismic areas. Lessons learned from recent earthquakes are summarized.

KEYWORDS: Bridges; Damage; Earthquakes; Retrofit

1. INTRODUCTION

This paper is an extension and update of the previous papers presented at the UJNR in 1983 (5) and 1985 (6) and presents a summary report describing the history of seismic damage to bridges in California and recent efforts in California to strengthening and retrofit of highway bridges to increase their seismic resistance.

1.1 Damage

About 1.5 moderate to large earthquakes have occurred every year in California since 1932. Except for the very damaging 1971 San Fernando earthquake, bridge damage in California has been very limited, especially in the time period before 1971. Since the 1971 San Fernando earthquake, eleven separate earthquakes have been investigated in detail by the California Department of Transportation (CALTRANS) Office of Structures Design, Post Earthquake Investigation Team (PEQIT). Eight formal reports have been written describing these investigations. This paper summarizes the bridge damages observed in California since about 1932, and discusses the implications of the post-San Fernando investigations. The recent damage to a retrofit bridge in the Palm Springs area is also described.

1.2 Retrofit

The task of strengthening seismically deficient joints and bearings is now almost complete for the State owned bridges in California. This paper will present a short summary of the accomplishments of the current retrofit program and a some insights into the future directions of the seismic strengthening of bridges in California.

2. DAMAGE

2.1 Bridge Damage from 1932 to 1971 (18)

In the period from 1932 to 1971 about 26 separate earthquakes with magnitudes of 5.5 or greater occurred in California in regions close to bridge structures. The rate of seismic events in this period average about 1.5 earthquakes per year. At least 1500 bridges were excited by accelerations of 0.35g or more during this period, yet only 33 bridges sustained damage. Of these 33 bridges only 15 bridges required repairs. Total repair costs for this 40 year period has been estimated at $100,000 in 1975 dollars.

Bridges affected in this time period were generally rugged, low short period structures located in rural areas and consisted primarily of stream crossings although in the 1950's some freeway and interchange structures were located close to some events.

Only one bridge was closed to traffic in this time period and this occurred during the 1940 El Centro earthquake when a timber cap slipped off of supporting timber piles. It is interesting to note that a more modern bridge (New River Br. No. 58-05), located at the same location was heavily damaged in the 1979 Imperial Valley earthquake.

Most of the damage to highways recorded in this time period was associated with fill movements and settlement rather than structural damage due to dynamic motions.

2.2 Bridge Damage in the 1971 San Fernando Earthquake (3,19)

The total damage to highway bridges in San Fernando was about $6,500,000 (4). The major damage was concentrated within a narrow region close to and generally within the causitive fault zone of the magnitude 6.6 event.

Two major collapses occurred in this event due to the pulling apart of narrow hinge seats. The route 210/5 Separation (53-1989L) and the

1 Structural Mechanics Engineer, California Department of Transportation, Division of Structures Office of Structures Design, P. O. Box 942874, Sacramento, CA 94274-0001

Northwest Connector OC (53-1985) were both long, tall single column type concrete bridges with several intermediate expansion joints.

The only other complete collapse occurred at the Route 5 (Truck Lane)/405 Separation bridge (53-1548). This bridge was a 335 foot long two span post-tensioned bridge, 38 feet wide on two monolithic columns. The under-reinforced columns broke up so much that the bridge settled to the ground at the bent level.

Damage at several other bridges was heavy enough to require replacement. A total of 6 bridges were eventually completely replaced (including the 3 collapsed bridges). Only the collapsed 2 span portion of the Northwest Connector was replaced and the portions which did not collapse were salvaged and incorporated into the rebuilt structure.

A total of 58 bridges were damaged significantly enough to require restoration work. Damage was highly varied, with about 14 bridges suffering damage over $100,000, 23 bridges with damage between $10,000 and $100,000 and about 21 bridges with minor damage (less than $10,000).

Several important lessons were learned from the evaluation of this damage:

- o Ground shaking in the vicinity of the fault was much larger than expected.
- o Expansion joint seats in continuous bridges were too narrow and were unrestrained.
- o Column members lacked sufficient confinement reinforcement.

As a result of this earthquake, the design force levels for California bridges was increased significantly, the reinforced concrete details were improved, seat widths increased and retrofit of existing bridges was started (4).

2.3 Bridge Damage since 1971

Since 1971 The CALTRANS Office of Structures Design has investigated several earthquakes. Since 1979, formal reports of the most significant of these events have been written:

Date	Magnitude	Location	Bridges Investigated	Bridge Damage Low	Moderate	Heavy
2/21/73	5.7	Oxnard	30-40	5	0	0
8/1/75	6.1	Oroville	98	14	0	0
8/13/78	5.2	Santa Barbara	10-20	3	0	0
8/6/79	5.5	Coyote Lake (11)	15-20	4	1	0
10/15/79	6.4	Imperial Valley (14)	17	3	1	0
1/24/80	5.5	Greenville (13)	8-10	4	0	0
5/25/80	6.7	Mammoth Lakes (15)	17	0	0	0
11/8/80	7.0	Trinidad-Offshore(12)	23	0	0	1
5/2/83	6.5	Coalinga (10)	60	6	0	0
4/24/84	6.2	Morgan Hill (16)	39	0	1	1
7/8/86	5.9	Palm Springs (17)	46	4	3	0

It should be noted that the severity of damage observed since the 1971 San Fernando earthquake is very low and reminiscant of the years before 1971. In spite of this lack of damage, several valuable lessons have been learned.

The effect of earthquakes on various bearing systems is now better known as a result of the investigations of the PEQIT studies. For example the bearings at the Alamo River Bridge, were moved laterally by the Imperial Valley quake of October 15, 1979 (14). The strong shaking at this location lasted only four or five seconds and the total duration was about thirteen seconds. We learned to be very cautious about assuming that keeper plates, bearing plate anchor bolts, keeper plate bolts or welds, and similar details have any significant effect in keeping a bridge superstructure on its supports during a major earthquake. All of the bearings at the end of a span do not always resist horizontal forces simultaneously. Because keeper plates or other devices are not set during construction with exactly the same clearances, only a portion of the bearings will initially resist a horizontal force in one direction.

It is not uncommon for a line of bearings at one end of a span to be damaged to varying degrees after an earthquake. For example the Trinidad-Offshore earthquake on November 8, 1980 (12) provided an example of variable bearing damage at the south abutment of the Fields Landing O.H., when some bearings obviously carried a major portion of the lateral force and others very little load.

Anchor bolts have been placed too close to the edge of the bearing seats in early bridges and causes concrete to spall off and tear out when subjected to horizontal loads. For example in the Coyote Lake earthquake in 1979 (11) the Bent 2 of the 129/101 separation clearly showed this type of damage.

Anchor bolts are frequently threaded below the top surface of the pier or abutment seat. This practice gives results in a reduced area for shear and a greatly reduced resistance to bending and failure generally occurs due to notch sensitivity at the root of thread.

Grout pads under bearing masonry plates have traditionally posed problems during and after construction and have also been one of the main trouble spots in minor quakes. Failure of a grout pad will allow the bearing assembly to move and subject to anchor bolts to combined bending and shear.

Bearing rollers allow normal movements between the sole plate and the superstructure plate. Transverse sliding due to seismic loading takes place on both contract surfaces. Transverse sliding obviously does not start until the horizontal force exceeds the vertical dead load on the bearing multiplied by the coefficient of friction. This action, once initiated, results in repeated impacts on the end keeper plates leading to a progressive bending failure of the plates, as evidenced by bearing damage at the First Street Separation during the Greenville earthquake of January 24, 1980 (13).

We have learned that bridge bearings may not be what they are represented to be on "As Built" plans or maintenance records. Adjustments to bearing details are sometimes made after the initial construction. Sometimes this work may not be of the best workmanship. Records of such work may be inadequate or non-existent. A conservative approach should always be taken both in the original design and in the retrofitting of bridge bearings.

Lastly, it should be noted that even though we see many events which do not cause much damage, or where the strongest motions are not located near any bridges; the threat of heavy damage still exists and a large event is sure to strike a major complex of bridge structures in the future.

2.4 Bridge Damage in the 1986 Palm Springs Earthquake

The Palm Springs earthquake occurred at 2:21 a.m. on July 8, 1986. The epicenter was located approximately 12 miles northwest of Palm Springs, CA. The magnitude was 5.9 ml (Richter). Following the initial shock, many aftershocks were recorded with magnitudes ranging from 3.0 to 4.0. Rupture is assumed to have occurred on the Banning Fault, a branch of the San Andreas Fault.

Bridge damage was limited primarily to the areas of Painted Hills and Whitewater, about 12 miles northwest of Palm Springs. Some damaged houses were found in the area. Palm Springs suffered only minor damage, mainly shattered windows and stock fallen from store shelves. There were rock slides which closed some roads, moderately damaged bridges, downed power lines, some damage to an aqueduct siphon, and serious damage to an electrical substation resulting from the earthquake.

The CALTRANS Structures Design PEQIT Team of Steve Mellon and Mark Imbriani investigated bridge damage in the area on July 9- 11, 1986. The team inspected 46 bridge sites (45 state bridges and 1 county bridge) in Riverside County.

Three bridges were found to have suffered moderate damage and four bridges were slightly damaged. The team discusses the damages to these bridges in detail in their report (17).

Of particular interest is the damage to the Whitewater Overcrossing (Br. No. 56-71). This bridge is located about 8 miles northwest of Palm Springs near the town of Whitewater. It is about 2 miles from the fault and is estimated to have received accelerations in the range of 0.5g.

The superstructure of the bridge is a straight, two span composite steel girder bridge, each span being simply supported with a cast-in-place concrete deck on the girders. The span lengths are 156'-142'. The substructure consists of a single three column concrete bent. Abutments are seat-type with pedestals, bearings and an expansion joint at the roadway level. The total bridge is skewed about 37 degrees. The girders rest on elastomeric bearing pads at all supports. The bridge was strengthened for seismic loads by the addition of steel restrainer cables retrofit in both the longitudinal and transverse directions.

Most of the damage to the structure appeared to be caused by transverse movements. The superstructure, Span 1 at Abutment 1, came to rest 7 inches west of its original position but remained on the pedestal.

At Abutment 1 the concrete was spalled at both corners where the deck overhang came in contact with the abutment backwall. Also on the east side, the overhang impacted the backwall causing a crack in the backwall. Three transverse restrainer cables failed at Abutment 1, along with the original keeper angles on the abutment pedestals. These pedestals were very lightly reinforced and were heavily fractured.

At Bent 2, the cap was lightly cracked on the inside face of both exterior columns.

The Bent 2 metal rail expansion joint sleeve (east side) pulled apart and came to rest misaligned. In order for this sleeve to come apart, it is estimated that the differential longitudinal movement had to be in excess of 4 inches.

At Abutment 3, a single restrainer cable failed. Slight cracking and spalling occurred at the overhang-abutment expansion joint connection, and wingwall/curb joint.

In assessing the damage to the Whitewater Overcrossing the investigation team has offered the following preliminary observations (17):

"The shear capacity of the keeper angle bolts of Abutment 1 was very limited due to lack of confinement by reinforcement steel in the pedestal around these bolts. When the keeper angles failed, the earthquake forces were taken by the cable restrainers. It is estimated that the cable resistance was adequate to withstand the earthquake loads. However, one cable failed at the turnbuckle when a stud stripped out of the coupler because it was inserted only 5/8" into the turnbuckle. It is conjecture that this failure reduced the transverse capacity by 1/3, therefore, overloading the remaining two cables and leading to ultimate failure.

The large transverse offset of the superstructure in this span, as compared to the other spans, is probably due to the sudden energy released when the other two cables broke. The remainder of the retrofit details which included the doweled-in cable stud standard detail and the anchor drum, a bracket bolted to the girder, behaved well, i.e., developed the ultimate strength of the cable.

At Bent 2, the crack in the cap at the inside face of both outside columns is due to lack of reinforcement in this area. The cap obviously was not designed for the earthquake moment developed in this rigid frame during lateral shaking.

At Abutment 3, failure of the restrainer cable was due to the lack of adequate threading of the cable into the coupler (1/2"). As happened at Abutment 1, the stud stripped from the turnbuckle. It is surmised that shaking was subsiding when this connection failed and thus did not overload the adjacent transverse cables as was the case at Abutment 1."

3. RETROFIT

The California retrofit program began almost immediately after the 1971 San Fernando Earthquake (2,7) Projects which were under construction were modified where possible by contract change order to meet increased seismic requirements. This effort was extended to include bridges in the design phase.

The California Department of Transportation identified about 1300 bridges (out of about 13,000) which were primarily deficient in seat width. These unrestrained joints represent the initial focus of the Departments retrofit program. To date about practically all these bridges have been retrofit at a cost of nearly $55 million.

The average California retrofit project consisted of the addition of steel restrainer cables at hinge and expansion joints to prevent spans from collapsing. Force levels were identical to those used on new structures (1). It is expected that the potential for collapse can be minimized even though extensive damage is experienced.

The California design details for restrainer units have evolved to the point where reliable and economical systems are performing satisfactorily under service conditions in the field, although only one installation has been tested by an actual earthquake (17).

Selection of structures for retrofit in California was based on a priority system which takes into account the expected accelerations at the site, the estimated cost to retrofit the structure, the cost of replacement in the event of loss, the length and availability of detours and the average daily traffic as well as other factors which reflect the importance of the bridge in the transportation system.

California developed a simplified restrainer analysis procedure (8,9) which considers many of the non-linear features of multi-hinged bridges, such as expansion joint gaps and the impacting of the superstructure against the abutment fill. This procedure is now used to compute restrainer forces in restrainers in both old and new construction.

The installation of hinge restrainers added a considerable amount of seismic reliability to the California bridge system. There remains however, several weaknesses in various bridges in the network, especially those located in areas of very high seismicity. The task of strengthening columns and substructures will occupy much of our time in the next several years. By applying non-linear analysis techniques it is possible to better predict failure modes and analyze the effects on overall stability when various components fail. Preliminary indications are that by increasing the amount of longitudinal restrainers at joints and strengthening select columns, we can maintain the stability of long tall ramp structures even though considerable damage will occur. Another area for potential strengthening is the addition of infill walls between very weak two column bents.

The task of selection, design and construction of this second phase of retrofit is only just beginning and I hope to be able to keep you informed of our progress on this long range project.

4. REFERENCES

1. "Bridge Design Specifications Manual" Standard Specifications for Highway Bridges Adopted by the American Association of State Highway Bridges, Thirteenth Edition, 1983. With Interim Bridge Specifications through 1985, Washington, D.C., With revisions by The California Department of Transportation, Office of Structures Design, Sacramento, California, August, 1986.

2. Degenkolb, O.H., "Retrofitting Bridges to Increase Their Seismic Resistance", Proceedings of the First Seminar on Repair and Retrofit of Structures. US/Japan Cooperative Earthquake Engineering Research Program. National Science Foundation, University of Michigan, Ann Arbor, Michigan, 1980, Vol 1, pp 109-114.

3. "Field Investigation of Bridge Damage in the San Fernando Earthquake." Bridge Department, Division of Highways, California Department of Transportation, Report of Investigation Team, George G. Fung, Richard J. Lebeau, Eldon D. Klein, John Belvedere, and Adlai F. Goldschmidt, Sacramento, California, 1971.

4. Gates, James H., "California's Seismic Design Criteria for Bridges" Journal of The Structural Division, American Society of Civil Engineers. December, 1976. pp 2301-2313.

5. Gates, James H., "Seismic Resistant Bridge Design in California", UJNR, Proceedings of the 15th Joint Meeting of the U.S.-Japan Panel on Wind and Seismic Effects, Tsukuba, Japan, May, 1983, Paper No. 2-19.

6. Gates, James H., "Earthquake Resistant Bridge Design in California", UJNR, Proceedings of the 15th Joint Meeting of the U.S.-Japan Panel on Wind and Seismic Effects, Tsukuba, Japan, May, 1985, Paper No. 2-7, NBS IR 86-3364, pg 146., May, 1986.

7. Mancarti, G.D., "New Concepts in Earthquake Retrofitting of Highway Bridges". Paper presented at Northwest Bridge Engineers Conference, Boise, Idaho, October, 1981, Updated Sept, 1984.

8. "Memos to Designers", 15-10, Earthquake Design (Commentary), California Department of Transportation, Office of Structures Design, Sacramento, CA, July, 1984.

9. "Memos to Designers", 21-18, Restrainers at Hinges and Bearings California Department of Transportation, Office of Structures Design, Sacramento, CA, December, 1981, Supplement #1, October, 1981, Commentary, February, 1981.

10. "Seismic Report, Coalinga, California Earthquake, May 2, 1983. Caltrans Office of Structures Design, Post Earthquake Investigation Team, James Munro and Eugene G. Klein Jr., 1983.

11. "Seismic Report, Coyote Lake, CA Earthquake of August 6, 1979. Caltrans Office of Structures Design, Post Earthquake Investigation Team, Floyd Mellon, Paul J. Jurach, Richard Hagar, 1979.

12. "Seismic Report, Eureka, CA (Trinidad-Offshore) Earthquake of November 8, 1980. Caltrans Office of Structures Design, Post Earthquake Investigation Team, Frank Semans and Ray Zelinski, 1980.

13. "Seismic Report, Greenville, CA Earthquake of January 24, 1980. Caltrans Office of Structures Design, Post Earthquake Investigation Team, Larry N. Storlie, Frank Semans, 1980.

14. "Seismic Report, Imperial Valley, CA Earthquake of October 15, 1979. Caltrans Office of Structures Design, Post Earthquake Investigation Team, Paul J. Jurach, Larry N. Storlie, George G. Miller and Roy Imbsen (FHWA), 1979.

15. "Seismic Report, Mammoth Lakes Earthquake of May 25, 1980. Caltrans Office of Structures Design, Post Earthquake Investigation Team, Frank Semans, Eugene G. Klein Jr., 1980.

16. "Seismic Report, Morgan Hill, California Earthquake, April 24, 1984. Caltrans Office of Structures Design, Post Earthquake Investigation Team, Richard Land and James Munro, 1984.

17. "Seismic Report, Palm Springs, California Earthquake, July 8, 1986. Caltrans Office of Structures Design, Post Earthquake Investigation Team, Steve Mellon, Mark Imbriani, 1986.

18. "Survey of Past Earthquake Damage to Structures", California Department of Transportation, Bridge Maintenance Engineer, W. J. Jurkovich, File 820.1, February 18, 1975.

19. "The Effect on State Highways of the San Fernando Earthquake, February 9, 1971." State of California, Business and Transportation Agency, Department of Public Works, Submitted Persuant to SB 682, September, 1971.

Large Scale Model Tests and Analysis of Gravel Drains

BY

Susumu Iai*, Katsuhiko Koizumi**, Setsuo Noda***, and Hajime Tsuchida****

ABSTRACT

Performance of gravel drains, installed as one of remedial measures against liquefaction, is studied with large scale model tests. The tests are conducted with a container, set on the shaking table, made of a stack of 64 aluminum rings; the rings of 200 cm in diameter being stacked to the total height of 200 cm. The results of the shaking tests and the analysis indicate a simple design procedure for determining the spacing between the gravel drains.
KEY WORDS: LIQUEFACTION, DRAIN

1. INRODUCTION

Installing gravel drains is one of remedial measures against liquefaction. In general gravel drains can be installed in various shapes, but most of the gravel drains are installed in a columnar shape as shown in Fig.1. The gravel drains are usually installed without vibrations and noises and, therefore, have an advantage over compaction methods when the ground has to be improved near the existing structures.

Performance of gravel drains was first studied by Seed and Booker (1977) [4] by solving a kind of consolidation equations. Several studies followed them [3,6,7]. However, there have never been a large scale model test under horizontal excitations to study the applicability of the equation used by Seed and Booker. Therefore, present study is carried out.

2. LARGE SCALE MODEL TESTS

When the ground shown in Fig.1 is shaken by an earthquake, excess pore water pressure is generated in the soils around gravel drains and, as a result, pore water of the part of the ground bounded by the hexagon in Fig.1 will flow, as indicated by arrows, into a gravel drain. Therefore, it is enough to study the axi-symmetric part of the ground, bounded by the equivalent circle shown in Fig.1, with one columnar gravel drain at its center.

A model of the axi-symmetric part of the ground is made in a container which is set on the shaking table and designed to enforce, in the model ground, pure horizontal cyclic shearing as in the field. This container, shown in Photo 1, is made of a stack of 64 aluminum rings of which diameter and thickness are 200 cm and 2 cm. Between the aluminum rings of 3 cm in height, roller-bearings of 2 mm in diameter are inserted to reduce the friction between the rings. The total height of the stack amounts to 200 cm.

Sands used for the tests are taken from Gaiko district at Akita Port, where liquefaction took place during the 1983 Nihonkai-Chubu-Earthquake. Gravels used for the tests are crushed stones. The grain size accumulation curves are shown in Fig.2. The model ground was made by poring the sand into the water. No

* Senior Research Engineer, Structures Division, Port and Harbour Research Institute
** Member, Earthquake Resistant Structures Laboratory, Port and Harbour Research Institute
*** Ph.D., Chief, ditto.
**** Ph.D., Deputy Director General, Port and Harbour Research Institute

tamping or disturbance was applied. The model of the gravel drain of 60 cm in diameter was constructed with a casing, which was leveled up from time to time as the ground and the drain were constructed. Instruments are deployed in the array configuration in the model as shown in Fig.3 for measuring accelerations, displacements, pore water pressures, settlements, earth pressures, and amount of drained water during the shaking table tests.

3. RESULTS OF THE MODEL TESTS

The shaking table tests are carried out under the conditions shown in Table 1; R-204, R-302, and R-303 are reference tests without a gravel drain and are to be compared with R-502 and R-503, which are the tests with a gravel drain. Among these tests, R-302 and R-502 are of the virgin condition. R-204 is not of the virgin condition in a strict sense but practically can be regarded as of the virgin condition. R-303 and R-503 are carried out after R-302 and R-502, respectively. All the tests are carried out with a sinusoidal input motions of 2 Hz for the duration of 10 seconds.

The shaking table tests resulted the maximum excess pore water pressures shown in Fig.4 for the cases without gravel drains and Fig.5 for the cases with the gravel drain. Comparison of these figures indicates maximum excess pore water pressures in and around the gravel drain are generally smaller than the ones in the ground without a gravel drain when the maximum acceleration of the input motion is about 50 Gals. However, when the maximum acceleration is about 80 Gals, maximum excess pore water pressures around the gravel drain reach the same level as the ones without the gravel drains.

More details on the performance of gravel drain can be understood by the time histories of the excess pore water pressures. The results of the tests at about 80 Gals are shown in Figs.6 and 7, of which values are measured by the instrument at P24 in Fig.2. These results indicate that the gravel drain decreases the rate of generation in pore water pressures and increases the rate of dissipation although the gravel drain fails, at this particular condition, in reducing the maximum value of the excess pore water pressures.

These results qualitatively indicate the effectiveness and the limitation of the performance of gravel drains. The rest of the present paper is devoted to the qualitative evaluation of the performance of gravel drains.

4. BASIC EQUATIONS FOR GRAVEL DRAINS

Seed and Booker analysed the performance of gravel drains by the following equation [4];

$$\frac{\partial u}{\partial t} - \frac{\partial u_g}{\partial t} = \frac{1}{m_v}\cdot\frac{1}{r}\cdot\frac{\partial}{\partial r}\left(\frac{k_s}{\gamma_w}\cdot r\frac{\partial u}{\partial r}\right) + \frac{1}{m_v}\cdot\frac{\partial}{\partial z}\left(\frac{k_v}{\gamma_w}\cdot\frac{\partial u}{\partial z}\right) \qquad (1)$$

in which

- r, z : the radial and verical coordinates
- t : the time coordinate
- u : the excess pore water pressure
- u_g : the excess pore water generated by the cyclic shear under the undrained condition
- k_s, k_v : the coefficients of permeability in the horizontal and vertical directions
- γ_w : the unit weight of water
- m_v : the coefficient of volume compressibility

u_g, in Eq.(1), is given by the following empirical equation [4];

$$\frac{u_g}{\sigma_{vo}'} = \frac{2}{\pi}\cdot\arcsin\left(\left(\frac{N}{N_l}\right)^{1/2\alpha}\right) \qquad (2)$$

in which

σ_{vo}' : the effective vertical stress

N : number of cycles of cyclic shear stress

N_l : number of cycles required to cause initial liquefaction ($u/\sigma_{vo}'=1.0$)

α : an empirically determined constant that has a typical value of 0.7

If we note that $t = N\,f$ = elapsed time of applicating cyclic shear stress of which frequency is f Hz, and $t_l = N_l\,f$ = duration of cyclic shear stress required to cause initial liquefaction, Eq.(2) can be rewritten as follows;

$$\frac{u_g}{\sigma_{vo}'} = \frac{2}{\pi}\cdot\arcsin\left(\left(\frac{t}{t_l}\right)^{1/2\alpha}\right) \qquad (3)$$

Thus

$$\frac{\partial u_g}{\partial t} = \frac{\sigma_{vo}'}{\alpha\pi t_l} \cdot \frac{1}{\sin^{2\alpha-1}\left(\frac{\pi}{2}\cdot\frac{u}{\sigma_{vo}'}\right)\cdot\cos\left(\frac{\pi}{2}\cdot\frac{u}{\sigma_{vo}'}\right)} \qquad (4)$$

The drainage of pore water influences the value of u/σ_{vo}' and thus influences the rate of generation of pore water pressure u_g through Eq.(4).

In order to derive the Eq.(1), Darcy's law and elasto-plastic nature of the skelton, made of sand particles, are implicitly assumed. It is evident, however, that those assumptions are not valid in the state of liquefaction in which the sand particles completely lose their mutual contacts [5]. Some limitations sould exist in the applicability of the Eq.(1). Therefore, the results of the model tests are compared with the computed results by Eqs.(1) and (4).

5. COMPARISON BETWEEN THE EXPERIMENTAL AND ANALYTICAL RESULTS

Among the several constants necessary for the computation by Eqs.(1) and (4), t_l in Eq.(4) was computed for each half cycle of shaking from the time histories of shear stress ratios and the liquefaction resistance curves. The time histories of shear stress ratios are computed by integrating, from the ground surface to the arbitrary depths of the model, the measured time histories of the accelerations multiplied by the density of the model ground. The liquefaction resistance curves of the model ground was obtained by back-fitting the curve to the test results without a gravel drain.

Coefficient of volume compressibility was also obtained by the test results without a gravel drain. Coefficient of volume compressibility, as shown in Fig.8, increases when the excess pore water pressure ratio u/σ_{vo}' increases beyond 0.5. Moreover, once the excess pore water pressure ratio u/σ_{vo}' becomes greater than 0.95, it is difficult to find the one-to-one correspondence between the coefficient of volume compressibility and the excess pore water pressure ratio. These facts indicate that the assumptions of the Darcy's law and the elasto-plastic nature of the skelton can not remain valid in the higher range of the excess pore water pressure ratio because, in this range, significant amount of sand particles lose the mutual contacts. Consequently, the application of Eq.(1) should be limited to the lower range of the excess pore water pressure ratio. In

particular, if the application of the Eq.(1) is limited to the range of $u/\sigma_{vo}' < 0.5$, constant coefficients of volume compressibility and permeability can be used.

Comparison between the experimental and the analytical results without a gravel drain, shown in Figs.9 and 10, confirms the appropriateness of the constants used for the analysis.

Comparison between the results with the gravel drain, shown in Figs.11 and 12, indicates acceptable applicability of Eqs.(1) and (4). Applicability of Eqs.(1) and (4) is confirmed also for the settlements as shown in Fig.13.

Consequently, the applicability of the Eqs.(1) and (4) with the pressure independent constants is confirmed under the condition of $u/\sigma_{vo}' < 0.5$. Therefore, fundamental characteristics of the gravel drains will be studied by using Eqs.(1) and (4) under this condition hereafter.

6. PERFORMANCE OF GRAVEL DRAINS UNDER SINUSOIDAL CYCLIC LOADS

Eqs.(1) and (4) indicate that the pore water pressure ratio u/σ_{vo}' depends on the following dimensionless parameters;

a/b : a ratio characterizing the geometric configuration in which a,b : radii of the gravel drain and the circle of the effective spacing shown in Fig.1,

t_d/t_l : a ratio characterizing the duration of the earthquake shaking in relation to the duration of shaking required to cause initial liquefaction,

$T_l = (k_s \cdot t_l)/(m_v \cdot \gamma_w \cdot a^2)$: a factor charactrizing the duration of earthquake shaking required to cause initial liquefaction in relation to the consolidation properties of the ground,

$R = (8/\pi^2) \cdot (k_s/k_d) \cdot (h/a)^2$: a ratio characterizing the resistance of the drain in relation to the permeability of the sand, in which k_d : the coefficient of permeability of the gravel drain and h : height of the gravel drain,

and

α : a parameter characterizing the shape of the pore water pressure generation curve in Eq.(4).

Among these parameters, there are two parameters which were not used by Seed and Booker [4]. One is T_l which will later be shown a more appropriate parameter than T_d (= T_l t_d/t_l) which was used by Seed and Booker. The other is R which was derived by Yoshikuni and Nakanodo [10] and applied for the analysis of the gravel drains by Tanaka et al [6]. There is another dimensionless parameter characterising the consolidation properties of the gravel drain itself. This parameter has a very minor influence upon the value of the pore water pressure ratio because the time scale of consolidation of gravel drain itself is very small in comparison with the time scale of pore water pressure generation t_l. Therefore, this parameter will not be considered.

Furthermore, the parameter t_d/t_l will be shown to have very minor influence upon the maximum value of the pore water pressure ratio for most of the cases encountered in practice. This fact will be shown at first by using a typical solution of Eqs.(1) and (4). It is noted in Fig.14 that, when the maximum value of u/σ_{vo}' is less than about 0.5, value of u/σ_{vo}' reaches its steady state value before $t = t_l$ (=$0.5t_d$). Therefore, the maximum value of

u/σ_{v0}' is determined only by T_1 and that $(\bar{u}/\sigma_{v0}')_{max}$ is not influenced by the value of t_d/t_1 if $t_d/t_1>1.0$. Similar conclusions can be drawn for various values of a/b, T_1, and R. As shown in Fig.15, the excess pore water pressure ratio reaches 90% of the steady state value of u/σ_{v0}' at the time t_{90}, which is less than $2t_1$ if $(\bar{u}/\sigma_{v0}')_{max}<0.5$. Consequently, the parameter t_d/t_1 has a very minor influence upon the value of $(\bar{u}/\sigma_{v0}')_{max}$ for most of the cases encountered in practice because, for most of the cases, duration of earthquake shaking is greater than about $2t_1$.

Consequently, only four dimensionless parameters determine the maximum value of the pore water pressure ratio; a/b, T_1, R, and α. Therefore, the maximum excess pore water pressure ratio averaged over the horizontal section at the middle level of the ground $(\bar{u}/\sigma_{v0}')_{max}$ can be shown in compact charts as in Fig.16. Conditions used for the computation for Fig.16 are α = 0.7 without vertical permeability in the ground. The computation was carried out by finite element method.

7. DESIGN OF SPACING BETWEEN THE GRAVEL DRAINS AGAINST EARTHQUAKES

Once the simplified solutions shown in Fig.16 have been obtained, spacing between the gravel drains can be determined by the procedure illustrated in Fig.17. As indicated in this figure, there are two important items, besides the constants of the soils, to be provided for determining the spacing; the value of $(\bar{u}/\sigma_{v0}')_{max}$ and the earthquake ground motions.

The value of $(\bar{u}/\sigma_{v0}')_{max}$ can be determined by the stability analysis. However, if the gravel drains are installed in a loosely deposited ground, detailed stability analysis for determining the value of $(\bar{u}/\sigma_{v0}')_{max}$ becomes practically meaningless, because very small errors contained in the liquefaction resistance curve and the shear stress time history has very large influence on the generaion of excess pore water pressures in the ground. It is much more important to give the accurate liquefaction resistance curve and the appropriate shear stress time history.

The value of $(\bar{u}/\sigma_{v0}')_{max}$ apart, the earthquake ground motions observed during earthquakes are very different from each other. Even for the earthquakes of the same magnitudes, there is a great variation in effective duration of the earthquake motions in relation to liquefaction. This fact was revealed by the study by Tokimatsu and Yoshimi (1980) [7]. They define a quantity "c" as a ratio of "cumulative number of equivalent cycles at time t" against " equivalent number of cycles for a whole time history" and, using this quantity, define the effective duration of earthquake motions by the following equation:

$$t_e = 2(t_{c=0.5} - t_{c=0.1}) \qquad (5)$$

in which
t_e : the effective duration of earthquake motions
$t_{c=0.5}$: time at which c = 0.5
$t_{c=0.1}$: time at which c = 0.1

Similar study has been carried out here by using the strong-motion earthquake records obtained by the network of the Port and Harbour Research Institute [9] and redifing the effective duration of earthquake motions t_1^* by the following equation:

$$t_1^* = 2.5(t_{c=0.5} - t_{c=0.1}) \qquad (6)$$

Here, the factor 2.5 (= 2/0.8) was used instead of the factor 2 in Eq.(5) because the factor 2 is

considered as a factor tempered by the engineering judgement.

The results are plotted in Fig.18. These results indicate that there is a trend of increase in the effective duration of the earthquake motions in accordance with the increase in magnitude of the earthquake. However, the scatter contained in the data is so great that it is almost impossible to use the average value of the data if a reliable design is required. For example, if the target earthquake for the design of the gravel drains is of the magnitude of 7.5 or 8, and very reliable design is required, then the wave form of NS component of the strong earthquake motion recorded at Hachinohe Harbour during the 1968 Tokachi-Oki Earthquake (M=7.9) [8], may be considered one of appropriate target earthquake motions, because this wave form has rather short effective duration for liquefaction as shown in Fig.18, in which this earthquake motion is designated as S-252 NS. Ishihara and Yasuda called this wave form "shock type" in the study of liquefaction under irregular loading conditions [2]. It is also widely used for the earthquake resistant design of the structures in Japan.

Once the wave form of the target earthquake is determined, the time history of shear stress ratio is computed by the ground response analysis and the rest of the procedure to obtain the value of t_l is straight forward. At first, the cumulative damage $t/t_l = N/N_l$ is calculated from the time history of shear stress ratio and the liquefaction resistance curve [1]. Secondly, the value of t_l is calculated by the following equation:

$$t_l = 2.5(t_{t/t_l=0.5} - t_{t/t_l=0.1}) \quad (7)$$

in which $t_{t/t_l=0.5}$: time at which $t/t_l = 0.5$

$t_{t/t_l=0.1}$: time at which $t/t_l = 0.1$

Thirdly, influence of the shape of the pore water pressure generation curve is taken into account by redefining the value of t_l as follows:

$$t_l(\text{redefined}) = t_l(N1/N_l)/(NO/N_l) \quad (8)$$

in which $(N1/N_l)$ and (NO/N_l) are, as shown in Fig.19, cummulative damages corresponding to $(u/\sigma_{vo}')_{max}$ obtained from the experiment and the assumed (i.e. Eq.(4) with $\alpha=0.7$) pore water pressure generation curves.

The rest of the procedure shown in Fig.17 with Fig.16 determines the value of a/b.

As an example of the spacing between the gravel drains, consider the case where $(\overline{u}/\sigma_{vo}')_{max} = 0.2$, $k_s = 3\times10^{-2}$ cm/s, $m_v = 3\times10^{-5}$ m^2/kN, $k_d = 10$ cm/s, a = 30 cm, and h = 10 m, and consider that t_l has been already obtained as five seconds by the above-mentioned procedure. Then, $T_l = 55$, and R = 2.7, and from Fig.16, a/b is determined as 0.35 and, therefore, the radius of the circle of the effective spacing is determined as b = 85 cm.

8. CONCLUSIONS

The large scale model tests and the analysis of gravel drains lead to the following conclusions:

(1) The kind of consolidation equations used by Seed and Booker [4] has acceptable applicability in the lower range of the excess pore water pressure ratio (the ratio of excess pore water pressure against the vertical effective

stress). Constants for those equations does not change regardless of the change in the excess pore water pressure if the excess pore water pressure ratio is less than 0.5.

(2) The maximum value of pore water pressure ratio for the gravel drains under sinusoidal cyclic loadings coincides with the steady state value of the pore water pressure ratio for most of the cases encounted in practice. This fact simplifies the design procedure for determining the spacing between the gravel drains.

(3) Resistance of the drain should be considered for designing the spacing between the gravel drains.

(4) The earthquake ground motions used for designing the spacing between the gravel drains sould be carefully chosen.

ACKNOWLEDGEMENT

The authors wish to express their thanks to Mr. K. Mineta, Hokkaido Kaihatsu Consultant, and Mr. T. Yamamoto, Penta Ocean Construction Co., for their works in the experiments and the analysis during their stay in the Port and Harbour Research Institute as visiting researchers. The authors also wish to express their thanks to Mr. M. Kobayashi, Chief of Soil Mechanics Laboratory, Port and Harbour Research Institute, for his works for developing the finite element program.

REFERENCES

1. Annaki,M. and Lee, K.L.(1977) : "Equivalent uniform cycle concept for soil dynamics," Journal of the Geotechnical Engineering Division, ASCE Vol.103, No.GT6. pp.549-564
2. Ishihara, K. and Yasuda, Y. (1975) : "Sand liquefaction in hollow cylinder torsion under irregular excitation," Soils and Foundations, Vol.15, No.1, pp.45-59
3. Ohara, S. and Yamamoto. T. (1986) : "Gravel pile method for preventing liquefaction," Proc. 7th Japan Earthquake Engineering Symposium, pp.727-732
4. Seed, H.B. and Booker, J.R. (1977) : "Stabilization of potentially liquefiable sand deposits using gravel drains," Journal of the Geotechnical Engineering Division, ASCE, Vo.103, No.GT7, pp.757-768
5. Scott, R.F. (1986) : Solidification and consolidation of a liquefied sand column," Soils and Foundations Vol.26, No.4, pp.23-31
6. Tanaka, Y., Kokusho, T., Esashi, Y., and Matsui, I. (1984) : "On preventing liquefaction of level ground using gravel piles," Proc. Japan Society of Civil Engineers, Vol.352 (III-2), pp.89-98 (in Japanese)
7. Tokimatsu, K. and Yoshimi, Y. (1980) : "Effects of vertical drains on the bearing capacity of saturated sand during earthquakes," International Conference on Engineering for Protection from Natural Disasters, Bangkok, pp.643-655
8. Tsuchida, H., Kurata, E., and Sudo, K. (1969) : "Strong-motion earthquake records at the 1968 Tokachi-Oki Earthquake and its aftershocks," Technical Note of the Port and Harbour Research Institute, No.80
9. Tsuchida, H. et al.(1966-1986) : "Annual report on strong-motion earthquake records in Japanese ports," Technical Note of the Port and Harbour Research Institute, No.55-No.519
10. Yoshikuni, H. and Nakanodo, H. (1974) : "Consolidation of

soils by vertical drain wells
with finite permeability,"
Soils and Foundations, Vol.14,
No.2, pp.35-46

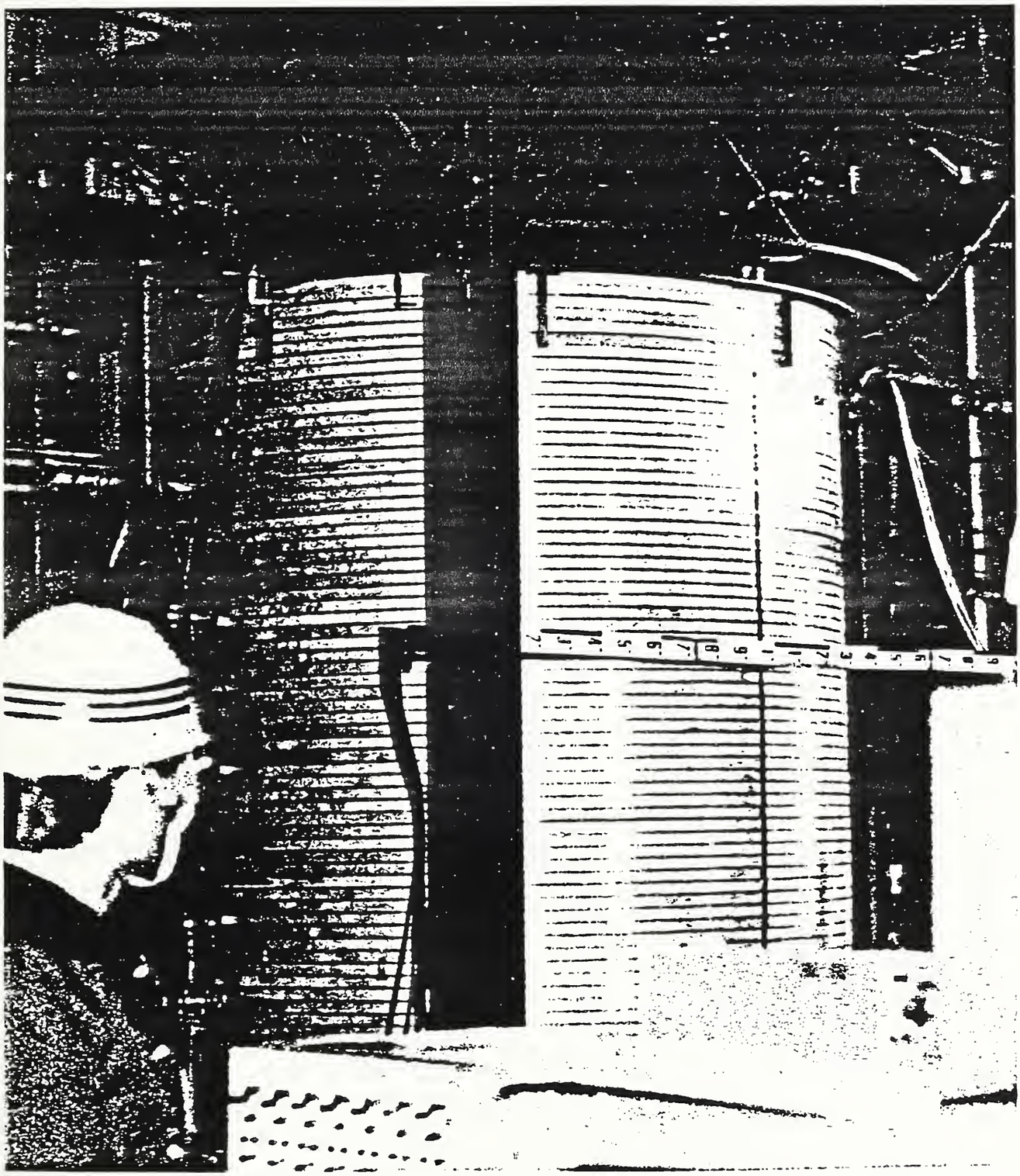

Photo 1 A stack of 64 aluminum rings on the shaking table

Table 1 Conditions for the experiments

Case Number	R-204	R-302	R-303	R-502	R-503
Relative Density (%)	29	31	31	33	35
Acceleration of Shaking Table (Gal)	43	50	81	50	69

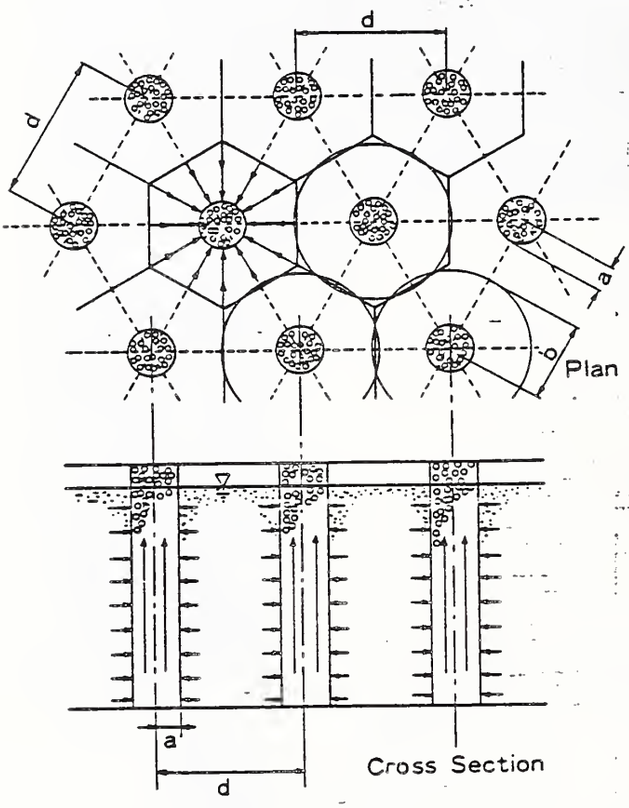

Fig.1 Schematic figure of gravel drains

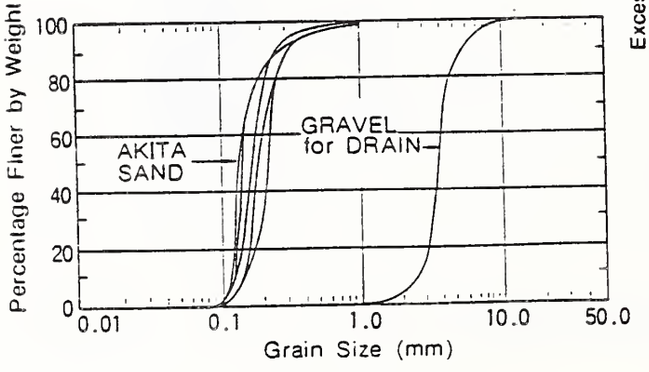

Fig.2 Grain size accumulation curves of the sands and gravels

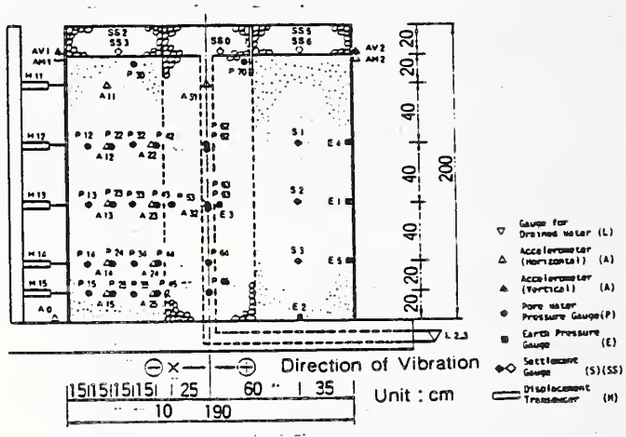

Fig.3 Location of instruments deployed in the model

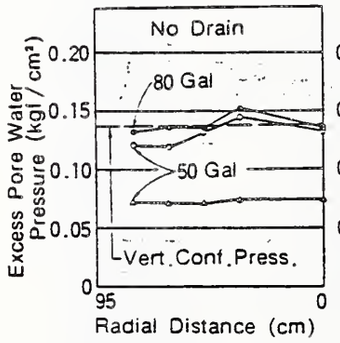

Fig.4 Maximum excess pore water pressures (without a drain)

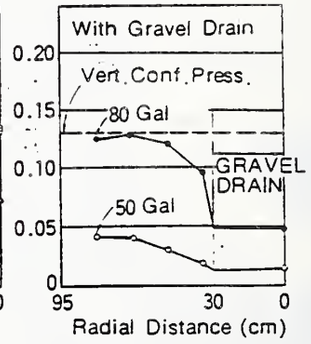

Fig.5 Maximum excess pore water pressures (with a drain)

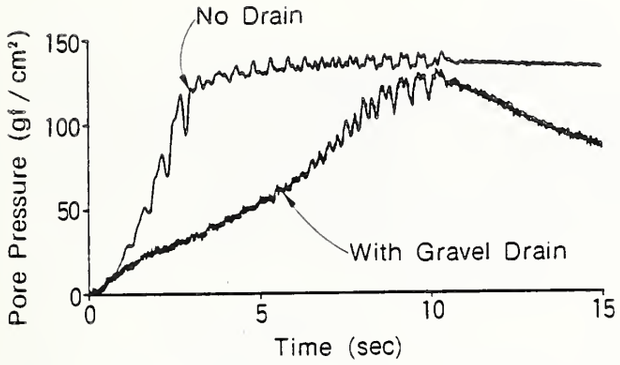

Fig.6 Time histories of the excess pore water pressures at P24 (during the first 15 seconds)

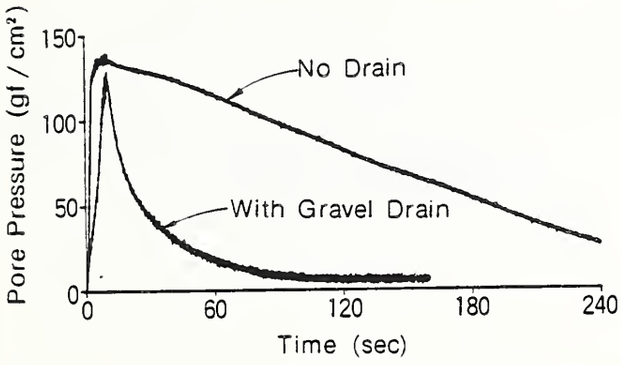

Fig.7 Time histories of the excess pore water pressures at P24 (during the 240 seconds)

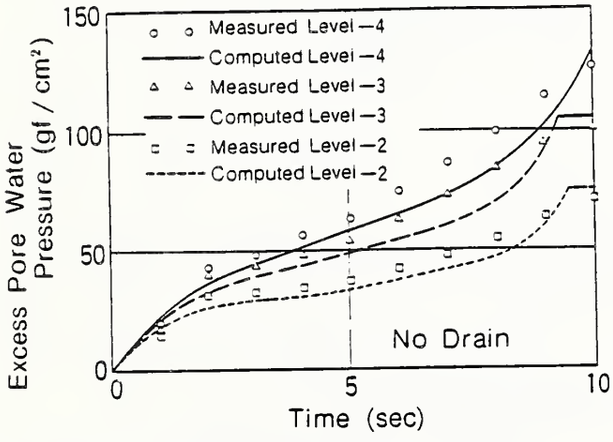

Fig.9 Comparison between the measured and the computed time histories for excess pore water pressures (without a drain)

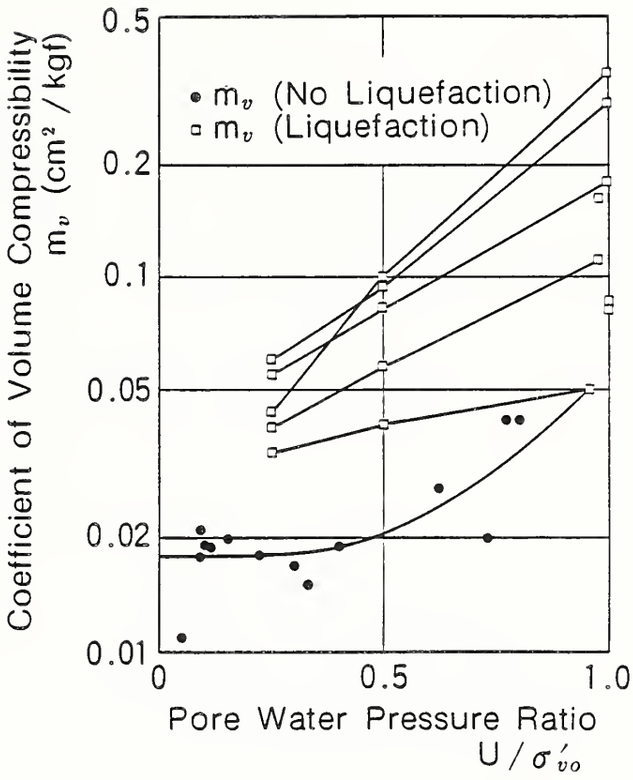

Fig.8 Coefficient of volume compressibility

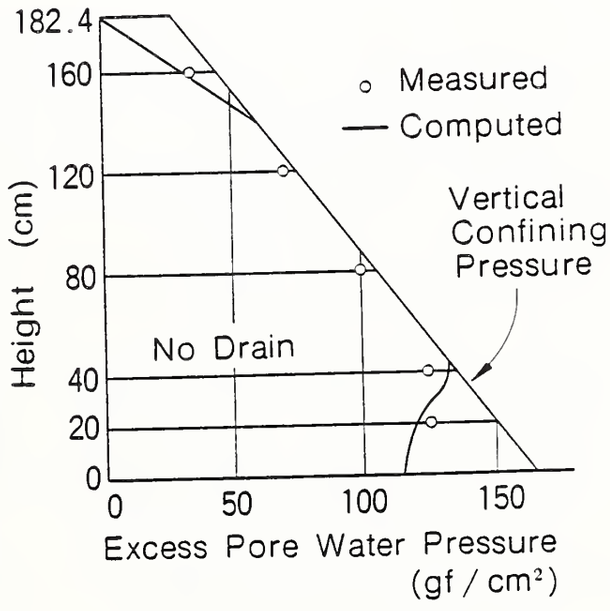

Fig.10 Comparison between the measured and the computed maximum values for excess pore water pressures (without a drain)

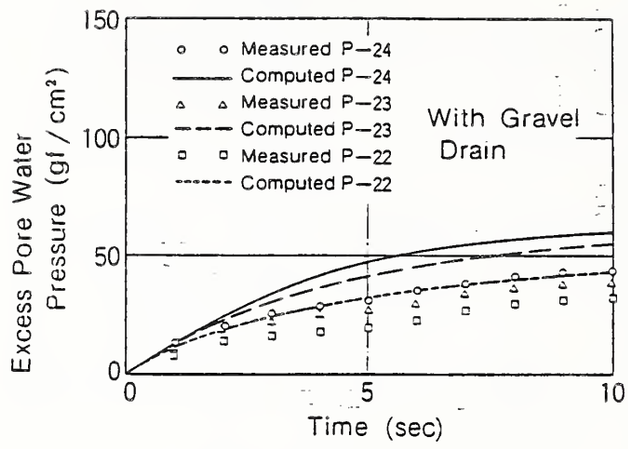

Fig.11 Comparison between the measured and the computed time histories for excess pore water pressures (with a drain)

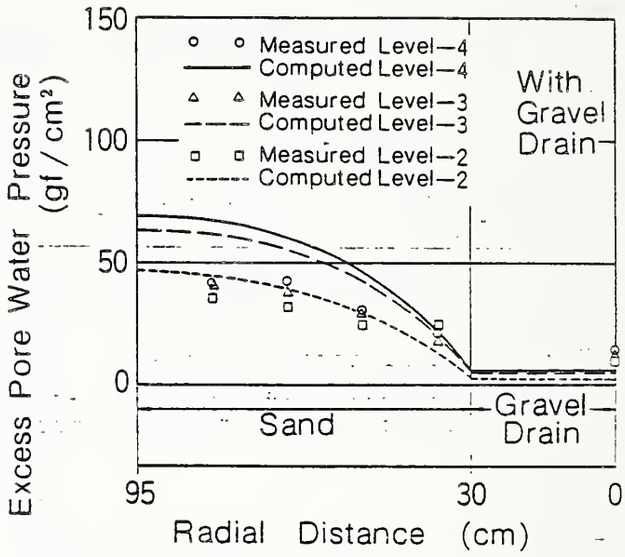

Fig.12 Comparison between the measured and the computed maximum values for excess pore water pressures (with a drain)

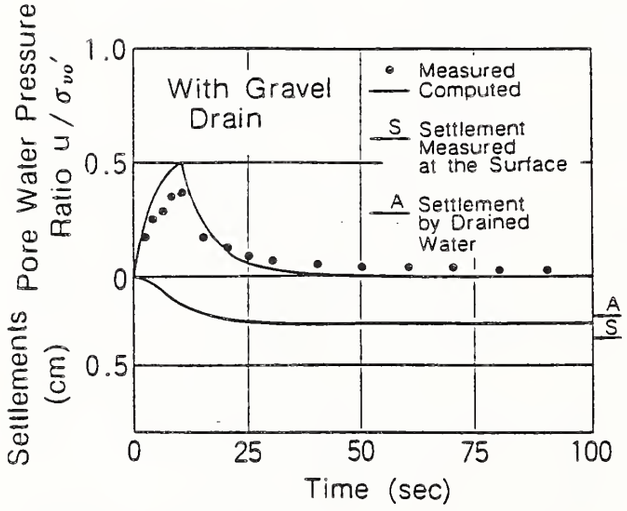

Fig.13 Comparison between the measured and the computed settlements and excess pore water pressure ratio (with a drain)

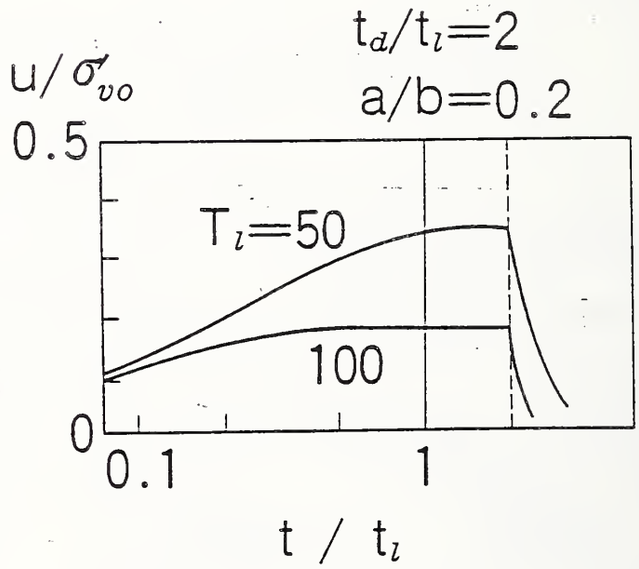

Fig.14 Typical excess pore water pressure change

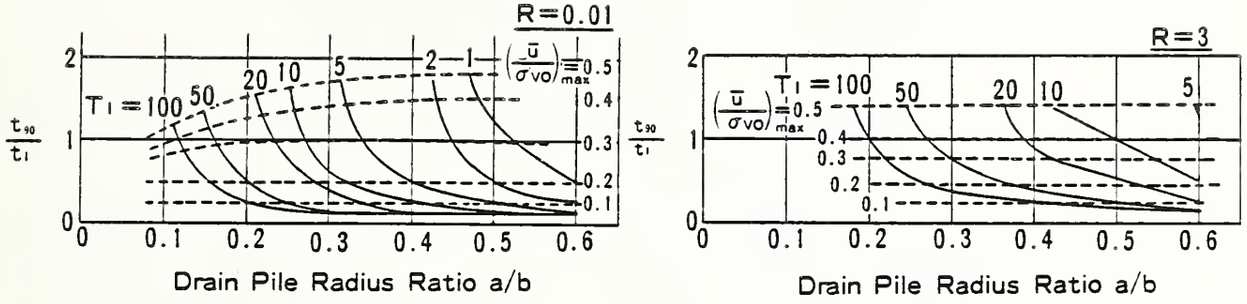

(a) R = 0.01 (b) R = 3

Fig.15 Duration of shaking required to attain the steady state pore water pressures

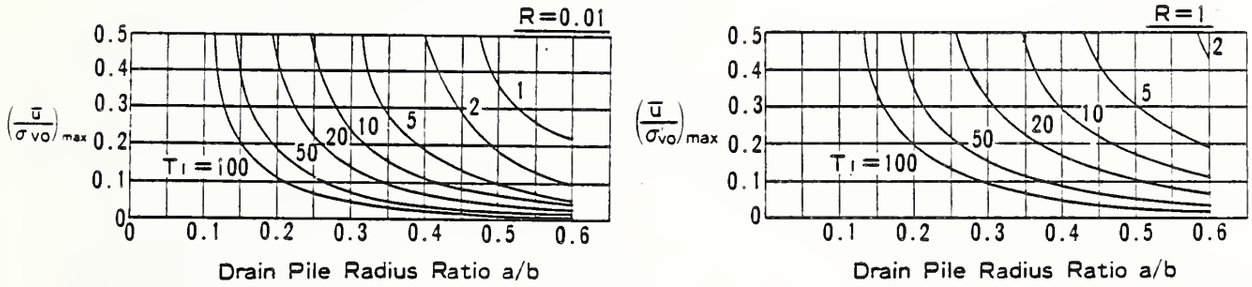

(a) R = 0.01 (d) R = 1

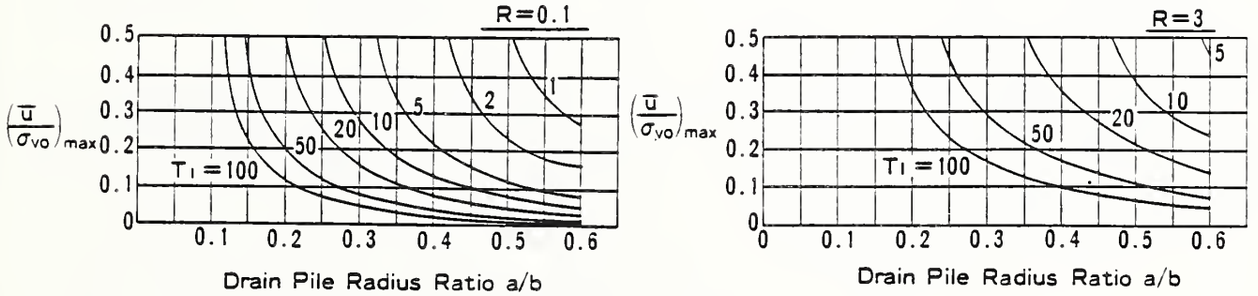

(b) R = 0.1 (e) R = 3

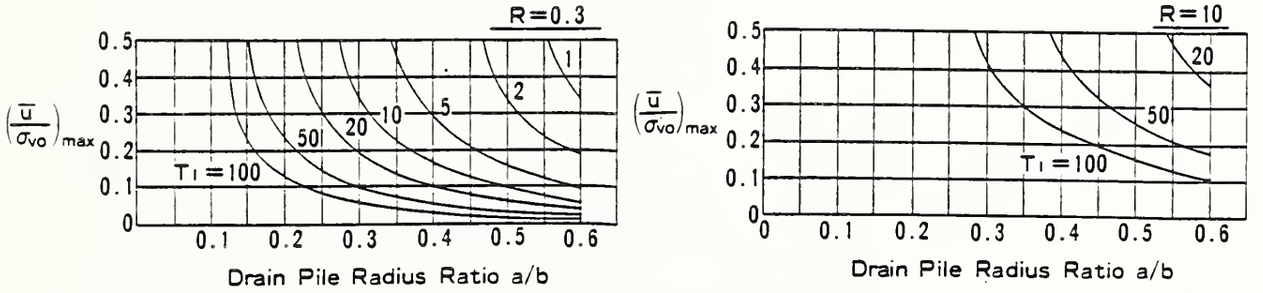

(c) R = 0.3 (f) R = 10

Fig.16 Relation between maximum pore water pressure ratio, time factor, well resistance, and radius ratio

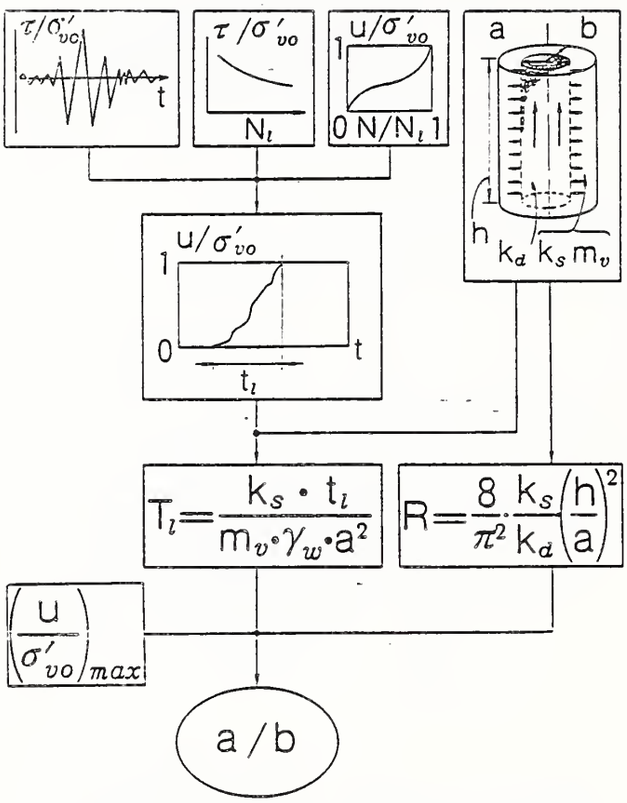

Fig.17 Procedure for determining the spacing between the gravel drains

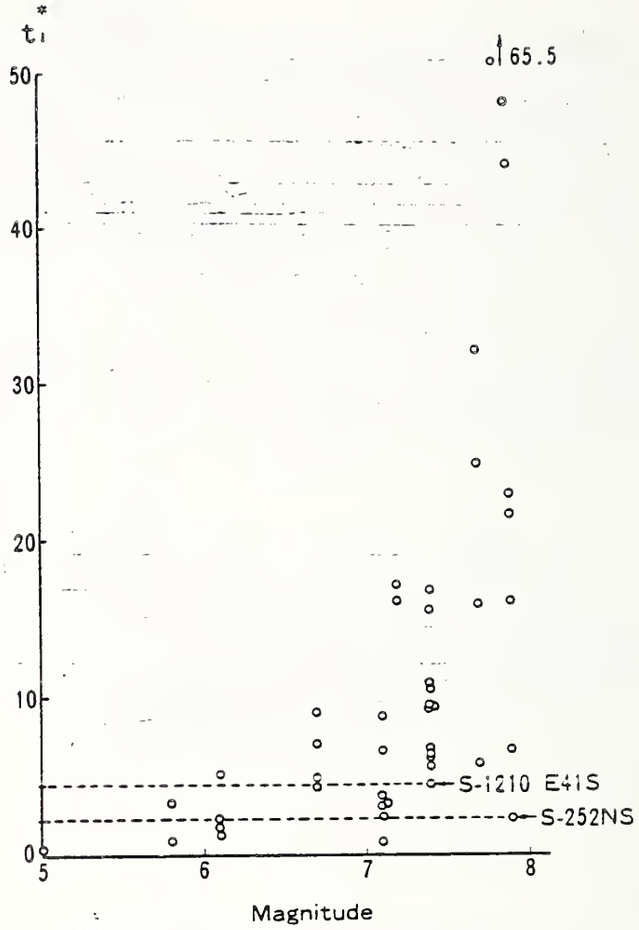

Fig.18 Relation between the magnitude of the earthquake and the effective duration of earthquake motions

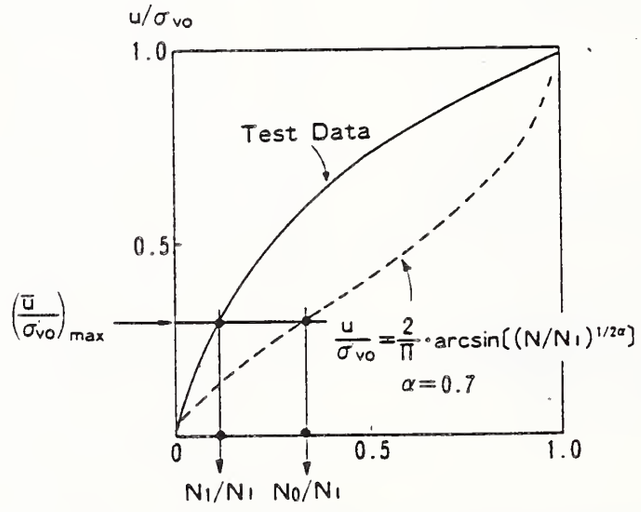

Fig.19 Schematic figure for obtaining correction factors for pore water pressure generation curve

Experimental Study on Degree of Fixation at Pile Head Joint and Failure Strength of Prestressed High Strength Concrete Piles

by

YOSHIHIRO SUGIMURA[1], TSUTOMU HIRADE[2]

ABSTRACT

This paper discusses experimental result of full-scale bending-shear tests for pile-footing joint under various axial load conditions, in order to investigate degree of fixation at pile head joint and ultimate strength of piles. As test specimens, 29 sets in total of prestressed high strength concrete (PHC) piles are used by combining three grades of effective prestress (σ_e=40, 80, 100kg/cm^2) and two kinds of diameter (35cm, 50cm) with six types of joint method. Statically indeterminate loading system is used, i.e., concentrated load is applied at intermediate point between pile head joint and the other pinned supporting point of pile for producing simulated bending moment distribution of pile in the ground by horizontal load.

Conclusions derived from experimental results are classified into the following two categories :

1) Degree of fixation at pile head joint α_r in the range of allowable capacity design is affected significantly by embedding length of pile into footing and axial load. When the ratio of embedding length to pile diameter changes from 0.2 to 1.0, α_r increases from 0.7 to 0.9, and from 0.4 to 0.75 in average, under the conditions with and without axial load, respectively.

2) Final state of PHC pile results in shear failure type, especially in axial load condition, so that it is important to make an effort to keep its ductility in the ultimate capacity design.

Keywords : Bending Shear Test of PHC pile, Fixation Degree at Pile Head, Shear Failure, Aseismic Design of Pile

1. INTRODUCTION

In the earthquake resistant design of pile foundation, it is very important to accumulate information about degree of fixation, i.e., degree of restraint for rotation at pile head and ultimate strength of pile. Theoretical solutions of horizontal resistance of pile are discussed by introducing the concept of degree of fixation at pile head and effect of pile length in the previous paper.[1] In succession, this paper discusses experimental results of full-scale bending-shear tests for joint between prestressed high strength concrete pile and footing under various axial load conditions, in order to investigate degree of fixation at pile head joint and ultimate strength of piles. Some parts of these experiments were already discussed in the previous papers.[2,3]

---

1) Dr. Eng., Head, Geotechnical Engineering Division, Structural Engineering Department, Building Research Institute, Ministry of Construction, Japan

2) Research Assistant, Geotechnical Engineering Division, Structural Engineering Department, Building Research Institute, Ministry of Construction, Japan

2. PREVIOUS STUDIES ON PILE HEAD JOINT UNDER HORIZONTAL FORCE

In the design method of horizontal resistance of pile foundation, it is an important problem of selection that the boundary condition of rotation at pile head is adopted as rigid joint or pin joint. Stress becomes large but displacement is small at pile head in the case of rigid joint. On the other hand, displacement is large but stress becomes small at pile head in the case of pin joint. Therefore, by selecting either of the two, structural designers bring the detail of joint near to the adopted condition in practical design.

Experimental studies on pile head joint under horizontal force have been performed from more than ten years ago,[4~6] and it has been made known that rigidity and strength of pile head joint becomes large for the case of rigid joint. Since the circular notice from the chief of Planning section, Road Bureau, Ministry of Construction was presented in May 1972, and specified that piles and footing should be fixed in principle, design directional to rigid joint has been constituting the main current in the field of road bridge. T. Asama and Y. Adachi explains that the reason why rigid joint is adopted is the most common method in the field of public works and also displacement is an important factor for the case such as bridges,[7,8] although this design guide does not always prohibit pin joint. Therefore, studies on structures in public works,[9~17] wholly in some sense, have been carried out with the intention of rigid joint based on this guide.

In the field of structural design of building foundation, there are some research works according to this guide,[18~20] but philosophy such as design directional to pin joint or design not sharing horizontal force to piles still remains. This situation shows not only variation of design philosophy of pile head joint but indefiniteness of relation between design detail and real behavior of joint. However, taking the opportunity of discovery of earthquake damage of PHC piles due to the Miyagiken-oki Earthquake in 1978, a new look is taken at pile head joint as an important problem. According to the results of survey by the authors,[21,22] earthquake damage type of piles is estimated to be near to rigid joint condition rather than pin joint condition expected in design process, so that condition of pile head joint is an important parameter on earthquake damage of piles. And also, in the supplementary design guide of circular notice from the chief of Building Guidance section, Housing Bureau, Ministry of Construction presented in September 1984, calculation is recommended to get horizontal resistance of pile by considering degree of fixation at pile head.[23] Under such background, experimental studies have been performed actively to investigate degree of fixation at pile head and ultimate strength of piles in the field of building foundation,[24~44] and a trial is made to examine synthetically the past papers on degree of fixation and strength of pile head joint.[45] There appears also in the field of public works, an proposal to make design method more rational by introducing effects of angle of rotation at pile head.[46]

3. DEGREE OF RESTRAINT FOR ROTATION AND DISPLACEMENT FACTOR AT PILE HEAD

The term of degree of fixation at pile head has been often used as the concept showing the rigidity of pile head joint. This is a parameter which shows ratio of fixation of a certain joint at pile head to the case of rigid condition, and is divided broadly into two categories, i.e., degree of fixation to bending moment and degree of fixation to displacement. Here, let examine, the substance of degree of fixation at pile head,

by taking as an example, pile of infinite length of which theoretical solutions were derived in the previous paper.[1] Table 1 shows various degrees of fixation at pile head for the case that boundary conditions are given as bending moment M_0 and angle of rotation θ_0 with known value of inverse of rotational spring k. The numbers in each row in Table 1 show the corresponding references which make mention of degree of fixation based on experimental results. References of the row c) do not always use the same definition expressed in the table, but are classified into the same group because of similarity of phlosophy to degree of fixation.

According to Table 1, degree of fixation to bending moment α_r can be determined directly from the boundary condition at pile head and changes from 0 to 1 when pile head joint changes from pin condition to rigid condition, while degree of fixation to displacement R_{y0} is a fuction including α_r changing from 2 to 1. Besides, if piles are infinite length, the value of R_{y0} changes extremely.[1] Then, α_r and R_{y0} are called as degree of restraint for rotation and displacement factor in strict sense, respectively, and distinguished each other in this paper at need.

The reason of a large number of the references corresponding to the rows c) and d) in Table 1, is related to the fact that cantilever type tests are adopted as the simplest experimental method and investigated test results attaching importance mainly to displacement because rigid joint has been the main current. These are classified into the group of degree of fixation at pile head to displacement, i.e., displacement factor. As mentioned above, it is reasonable to distinguish degree of fixation in a narrow sense, i.e., degree of restraint for rotation from displacement factor.

On the other hand, there are some cases in which degree of restraint for rotation is determined by the definition shown in the row b) based on bending moment from cantilever type tests. But, in this case, it needs the aid of coeffeicient β concerning ground condition.[1] It is reasonable to get degree of restraint for rotation directly from laboratory tests on pile member not through condition of soil deposits. Therefore, the best way is to use the definition of the row a) in Table 1 determined directly from bending moment through staically indeterminate experiment. In the following chapters, only the difference of rotational restraint condition at pile head is discussed by assuming the rotation of footing or foundation beam does not exist.

4. OUTLINE OF EXPERIMENTS

4.1 TEST PROGRAM

Statically indeterminate loading system is used as shown in Fig. 1. The reason is to adopt the method used continuously by the authors,[22] which is capable of getting the degree of fixation directly from bending moment at pile head, and of keeping the similarity of bending moment distribution of pile in the ground due to horizontal force, as mentioned in chapter 3. The loading points B, C and the supporting point A are treated as free for rotation by using Teflon lubricant device support. Footing is fixed to the floor of test room by using the two PC bars.

It is advisable to use alternating cyclic loading system essentially, but one direction cyclic loading system is adopted in these test series, by considering the necessity to avoid the influence of test device used in the previous paper,[22] or difficulty of turnning test specimen round.

Each value of loading step P at the loading point corresponding to allowable, design crack

and design failure bending moment of pile, is calculated for the case that pile head joint is assumed to be rigid joint. And, in principle, after repeating 3 cycles, 5 cycles, and 1 cycle at these loading steps, load is increased to the final failure state. Experiments are performed in two phase test series. In each case, preliminary load corresponding to about one third of allowable load is acted firstly, and after confirming stability of test specimen, main test is started.

4.2 TEST SPECIMENS

Outline of test specimen is shown in Fig. 2, for the case of 20Z'. Structural properties of pile section in phase 1 test series are shown in Table 2 and Fig. 3. And strength of concrete of each specimen and detail of pile head joint are shown in Table 3 and Fig. 4, respectively. Test specimens, 24 in total, are selected by combining pile diameters of 35cm and 50cm, pile grades of A (effective prestress σ_e=40kg/cm^2) and C (effictive prestress σ_e=100kg/cm^2), and axial loads of 0, 30 and 60t.

The detail of joint method in phase 1 test series are as follows. Type X is the most common method that pile cut together with PC bars is buried simply in footing with 10cm depth, and plain concrete is filled inside of pile up to length corresponding to pile diameter. Type Y is the same method as type X except that reinforced concrete is filled inside of pile with a little longer length. Type Z is the method that pile cut leaving PC bars 50 times as long as those diameter is buried in footing with 10cm depth, and covered by steel pipe with concrete outside and filled with plain concrete inside of pile to 40cm long from pile top.

The types of test specimen and strength of materials in phase 2 test series are shown in Table 4 and Table 5, and structural section of pile and detail of pile head joint are shown in Fig. 5 and Fig. 6. In this case, piles in 35cm diameter of grade B (effective prestress σ_e=80kg/cm^2) are used for supplement of phase 1 test series.

The piles were manufactured with separater at the pile end and cut the outer part of PC bars after curing, in order to estimate relaxation of prestress due to cut off of pile head at the job site. Change of prestress during this process was measured by strain gages set up on PC bars and these measured values are listed in Table 4 as the measured effective prestress. Axial load condition is 30t in all the cases.

Similar three types of joint method, i.e., X', Y' and Z' are selected in phase 2 test series, but by using three different embedding length in order to investigate effects of embedding length of pile head in footing. The type X' is the same method as type X in phase 1 test series, but two kinds of embedding length are selected, i.e., 10cm and 35cm, which are called as test specimens 10X' and 35X', respectively. Type Y' is the method pile head in footing is reinforced by rising steel bars and spiral hoops with embedding length of 20cm which is called as test specimen 20Y'. In this case, reinforcing cage is not unified with pile. Type Z' is the similar method as type Z in phase 1 test series, but steel pipe (inner diameter:35.4cm, length:35cm, thickness:0.6cm) is glued to pile with epoxy resin, and 8 anchor steel bars of 35cm bond length (D10-8) are welded to steel pipe. Embedding length are selected as 10cm and 20cm which are called as test specimens 10Z' and 20Z', respectively. In all the specimens in phase 2 test series, plain concrete is not filled inside of pile.

The size of footing and ratio of reinforcement is basically common in phase 1 and phase 2 test series, except that the eight steel bars are bended downward and binded to steel pipe pile for the case of Z' type, and are bended upward around pile surface for the case of Y' type. The shortest distance from the center of pile section to the side of footing is about 1.7 times as long as pile diameter in the case of 35cm pile diameter, and 1.2 times in the case of 50cm pile diameter.

4.3 MEASUREMENT PROGRAM

The following items are measured in common with phase 1 and phase 2 test series.

1) loads at loading points B and C, and reaction force at supporting point A for determination of bending moment distribution of pile

2) displacements at loading points B and C, at supporting point A and at pile head joint E for getting of deflection of pile

3) angle of rotation at pile head

4) angle of rotation of footing

5) strains at pile surface for checking of bending moment distribution of pile

In addition to the above, in phase 1 test series, rosette gages are used to measure three directional strains in pile. And also, in phase 2 test series, measurement points are increased as many as possible, such as displacement for deflection of pile, strains of PC bars for getting bending moment distribution of pile, mold gages and strainmeters of steel bars set in footing to check behavior of joint part, axial load change during test, and strains of PC bars fixing footing to the floor of test room. As an example, measurement location of the case of specimen 20Z' in phase 2 test series is shown in Fig. 7.

5. TEST RESULTS

Figure 8 shows envelope curves of the maximum displacement of pile at virgin loads in phase 2 test series. The maximum displacement of each case is shown by the average of the measured values of the dial gages on the upper surface (D3) and the lower surface (D11) of pile as shown in Fig. 7. Figure 9 shows an example of deflection of pile and strain distribution of pile at each loading step.

It is noticed from these figures that the maximum displacement occurs at the location a little to supporting point A from loading point C and the slight displacement is also observed both at supporting point A and pile head joint E. Initial rigidity in the range of small load is the largest for the case of 35X' in which embedding length is equal to 1B (B:pile diameter) and becomes small as embedding length is short. The maximum strength is the largest for the case of 35X', and becomes smaller in the order of 10Z'>10X' >20Z'>20Y' within the range from 27.3t to 34.9t. And the corresponding displacement of pile is scattering in the range from 2 to 4cm, changing smaller in the order of 35X'>10X'> 10Z'>20Y'>20Z'.

Figure 10 shows the relation between bending moment and displacement at loading point C, and Fig. 11 shows the relation between bending moment and rotation of angle at pile head joint E. Rotation of angle at pile head is calculated from the quantity of pullout at the upper side and push in at the lower side of pile at the end of footing measured by the dial gages (D15, D16), as shown in Fig. 7. But almost all part is consisting of pullout at the upper side and quantity of push in at the lower side is very small. From these figures, linear relation between bending moment and displacement is observed until cracks occur in pile member.

As for rotation of angle at pile head θ_p, the followings are recognized as characteristics around the allowable bending moment of pile member.

1) Under the condition of axial load, θ_p becomes small.

2) As for the effect of joint method, the tendency that θ_p becomes larger in the order Z, Y, X is recognized from the results of phase 1 test series. But in some cases, the order is reversed X and Y. From the results of phase 2 test series, it is remarkable that θ_p becomes smaller as embedding length is longer.

3) When the pile diameter is large, θ_p becomes larger.

4) As for the grade of pile, θ_p becomes larger in the order C, B, A.

6. DEGREE OF FIXATION AT PILE HEAD AT THE ALLOWABLE BENDING MOMENT OF PILE

Figure 12 shows the comparison of the degree of fixation at pile head α_r in each test when the bending moment of pile reaches its allowable value. The abscissa is the ratio between embedding length of pile into footing and pile diameter α_d, and the part of outer steel pipe pile is included in the embedding length for the case of joint type Z. The ordinate is the degree of fixation at pile head, which is corrected to avoid the effect of rotation of footing θ_F and displacement at the point E and A by the following equations (see Fig. 13).

$$\alpha_r = \frac{M_{E'}}{M_{Ef}} \tag{1}$$

$$M_{E'} = M_E - \Delta M_E = M_E - \frac{3EI}{\ell^2}(\ell\theta_F + y_E - y_A) \tag{2}$$

$$M_{Ef} = \frac{1}{2}\left(cP_1 - ab\frac{\ell+a}{\ell^2}P_2\right) \tag{3}$$

in which,

M_E : bending moment at point E determined from the measured values of the loads P_1, P_2 and the reaction force at supporting point R_A

ΔM_E: influence component to the bending moment at point E determined from the measured values of the angle of rotation of the footing θ_F, and the displacements y_E and y_A at points E and A

M_{Ef}: theoretical bending moment at point E corresponding to the conditions of pin support at point A and fixed joint at point E

EI : bending rigidity of pile

a,b,c,ℓ : length of each part of specimen shown in Fig. 13

The following characteristics are derived from Fig. 12.

1) Embedding length of pile into footing is one of the most important influence factor on degree of fixation at pile head α_r, and α_r becomes larger as embedding length is longer. When the ratio of embedding length to pile diameter α_d changes from 0.2 to 1.0, α_r changes from the range of 0.3-0.5 to the range of 0.7-0.8 under the condition without axial load, and from the range of 0.6-0.8 to the range of 0.8-1.0 under the condition with axial load. If α_d is nearly equal to 1, condition of pile head becomes similar to rigid joint.

2) The range of α_r due to the condition with or without axial load has width of about 0.2, respectively, but can be divided clearly into the two groups, i.e., the lower region without axial load and the higher region under the influence of axial load.

3) Degree of fixation at pile head is influenced by the condition if anchor steel bars are unified with pile head or not, even in the case of equal embedding length. If both are welded, degree of fixation becomes large by the bonding effect of anchor steel bars.

7. FAILURE TYPE AND ULTIMATE STRENGTH OF PILE

Test results at the maximum load and failure type of each test are summarized in Table 6, and the final states of test specimen are shown in Fig. 14 and Fig. 15. In almost all the cases, final state results in shear failure of pile except the cases of pile of grade A without axial load which are determined by bending failure (break of PC bars), and also followed by tubular deformation due to circular bending moment, if axial load is large or diameter of pile is large. This phenomenon should be noticed as a specific character of tubular section member, even if this kind of phenomenon is hard to occur in the case of piles in the ground because of confining effect by surrounding soil deposits.

As for footing, comparatively large cracks develop in the case of short embedding length but small or no cracks in the case of long embedding length. And, if embedding part is reinforced by spiral hoops, effect of preventing cracks of footing is exhibited.

Figure 16 shows the comparison between experimental values and analytical values of shear strength of pile. Analytical values are calculated by the following equations, based on the measured values of pile section and strength of materials.

$$_{cal}Q_{cr} = \frac{tI}{S_0}\sqrt{(\sigma_g + 2\phi\sigma_t)^2 - \sigma_g{}^2} \quad (4)$$

$$\sigma_g = \frac{N}{A_e} + \sigma_e \quad (5)$$

in which,

t : thickness of pile (cm)

S_0 : geometrical moment of area of pile expressed by $S_0 = \frac{2}{3}(r_0^3 - r_i^3)$

I : geometrical moment of inertia of pile expressed by $I = \frac{\pi}{4}(r_0^4 - r_i^4)$

N : axial load (kg)

A_e : equivalent area of pile section (cm^2)

σ_e : effective prestress (kg/cm^2)

σ_t : tensile strength of concrete assumed as 7% of compressive strength (kg/cm^2)

r_0 : outside diameter of pile (cm)

r_i : inside diameter of pile (cm)

ϕ : correction factor of shear force assumed to be equal to 0.5

The mean value $\bar{R}$ of ratios of experimental values to analytical values and standard deviation σ are 0.981 and 0.116, respectively, as shown in Fig. 12. It should be noticed that eq. (4) overestimates shear strength of pile in some cases, because analytical values are larger than experimental values. Y. Gotoh and T. Shibata pointed out the accuracy of eq. (4) is slightly inferior to the experimental equation developed by them for estimation of shear strength of reinforced concrete column.[47]

Table 6 shows also the ratios RBM between experimental results and analytical results on the ultimate bending moment of pile. As for M_{uc} in phase 2 test series, all the parameters are the measured values except that tensile strength of concrete of pile is assumed as 7% of compressive strength. In the process of getting M_{uc} in phase 1 test series, catalogued values or initial condition of test are used for the parameters such as yield stress of PC bars, effective prestress and axial load change during test, because those parameters were not measured. It should be noted, therefore, that the accuracy is different in both test series and fairly high values of RBM are observed especially in the case of pile grade A without axial load condition. But, on the whole, the values of RBM less than 1 are recognized in almost all the cases, i.e., shear failure of pile precedes the occurrence of final bending failure. This tendency is more remarkable for the case with axial load

condition than the case without axial load condition.

The importance of design philosophy to avoid the preceding of shear failure of pile will be increasing more and more in earthquake resistant design of pile foundation. Therefore, it is advisable to design leaving sufficient surplus of shear strength of pile, if the eq. (4) is adopted in design process.

8. CONCLUSIONS

Results of bending shear test for pile head joint of prestressed high strength concrete pile are discussed in this paper. The conclusions applicable to practical design of pile foundation derived from these tests are as follows.

1) The important influence factors on degree of fixation at pile head α_r in the allowable capacity design of pile foundation, are the embedding length of pile into footing and the condition with or without axial load, as shown in Fig. 12. When the ratio of embedding length to pile diameter α_d changes from 0.2 to 1.0, α_r increases from 0.7 to 0.9, and from 0.4 to 0.75 in average, under the conditions with and without axial load, respectively, forming increasing curves about 4.2 in width as axial load increases. If pile is embedded to the length corresponding to pile diameter, behavior of pile head joint becomes similar to rigid joint. And if axial load acts, degree of fixation at pile head becomes large entirely. During an earthquake, piles are acted by alternating axial load due to rocking motion of superstructure from the initial condition supporting long term load due to the weight of superstructure. Therefore, degree of fixation of piles located at compression side becomes larger than piles located at pullout side, and shear force is apt to be concentrated to piles in compression side. This effect of axial load will become very important factor for design method of pile foundation.

2) Condition if anchor steel bars into footing are connected with pile or not, is also an important factor on degree of fixation. If anchor bars and pile unified, α_r becomes larger than the case that both are not unified in the range shown in Fig. 12.

3) The ratio α_r is nearly equal to or more than 0.3 and is far from pin condition in any case of joint type used in this study. If pile head is expected as pin condition, it is necessary to develop a certain special joint method separaterly from these joint types.

4) The final state of each test specimen, except some of the piles in grade A without axial load results in shear failure type. Shear span ratios in these tests are scattering in the range from 1.43 to 3.20. This result will be possible to effect ratification of the conclusion of the preceding paper[22] that the boundary of shear span ratio at which shear failure of PHC pile occurs, is nearly equal to 3 for the cases of piles of grade B and C.

Although real shear span ratio of pile in the ground under horizontal force is necessary to investigate separately, this result proves that the examination of shear strength of pile is indispensable factor in earthquake resistant design. And eq. (4) based on elastic theory is apt overstimate the real shear strength of pile. Therefore, improvement such as increase of lateral reinforcement is important for this kind of pile. At least, it is advisable to design leaving sufficient surplus of shear strength of pile, if eq. (4) is adopted in design process.

ACKOWLEDGEMENTS

The experiments in this report were carried by Building Research Institute under the financial and technical support provided the Committee of Pile Head Joint Method (Members of Y. Itoh, K. Imaizumi, K. Inbe, O. Kobayashi, M. Hiraike, M. Fujisawa, N. Mastubara and the authors, phase 1 test series in 1984 to 1985) and the Research Committee of Pile Head Joint Method (Members of K. Ohshima, J. Ohya, T. Okabe, A. Kubota, S. Hayama, M. Yasui and the authors, phase 2 test series in 1985 to 1986) establised in Japan Association for Building Research Promotion. The authors would like to express their thanks to the members of the Committees for the considerable support.

REFERENCES

1) Y. Sugimura : Theoretical Solutions on Horizontal Resistance of Pile by Considering Degree of Restraint for Rotation at Pile Head and Pile Tip (in Japanese), Jour. of Structural and Construction Engineering, Trans. of Architectural Institute of Japan, No.365, pp.132-143, 1986.7

2) Y. Sugimura et al.: Experimental Study on Fixing Ratio of Pile Head Joint and Failure Strength of Prestressed High Strength Concrete Pile (in Japanese), Summaries of Technical Papers of Annual Meeting Architectural Institute of Japan, pp.991-998, 1985.10

3) Y. Sugimura et al.: Experimental Study on Head Joint Method between Prestressed High Strength Concrete Pile and Footing (in Japanese), Summaries of Technical Papers of Annual Meeting Architectural Institute of Japan, pp.1257-1262, 1986.8

4) K. Kokushoh and M. Hirosawa : Strength and Design Method of Pile Head Joint (in Japanese), Soil Mechanics and Foundation Engineering Library 6, Steel Pile, Chapter 3, Japanese Society of Soil Mechanics and Foundation Engineering, pp.171-213, 1969.9

5) K. Tsuno : Tests on Pile Head Joint (in Japanese), PC Pile Handbook, Chapter 36, Association of Concrete Pole and Pile, pp.747-756, 1970.9

6) K. Tsuno : Tests on Pile Head Joint (in Japanese), Prestressed Concrete, Vol.13, No.6, pp.48-54, 1971.12

7) T. Asama and Y. Adachi : Design of Joint between Pile Head and Footing (in Japanese), Douro, pp.76-84, 1972.7

8) Y. Adachi : Rigidity of Joint between Pile Head and Footing (in Japanese) , Doboku Gijutsu Shiryo, Vol.16, No.10, pp8-14, 1974

9) K. Komada and Y. Adachi : On Tests of Joint between Pile Head and Footing (in Japanese), Jour. of the 27th Technical Research Meeting in Ministry of Construction, pp.93-98, 1974

10) K. Komada et al.: On Tests of Joint between Pile Head and Footing, Part 2 (in Japanese), Jour. of the 28th Technical Research Meeting in Ministry of Construction, pp.284-293, 1975

11) K. Komada et al.: On Stress Transfer at Pile Head (in Japanese), Summaries of Technical Papers of the 28th Annual Meeting Japan Society of Civil Engineers, pp.199-200, 1973

12) K. Yahagi et al.: Tests on Fixing Ratio at Pile Head (in Japanese), Summaries of Technical Papers of the 29th Annual Meeting Japan Society of Civil Engineers, pp.264-266, 1974

13) M. Tatsumi and K. Kamemura : A Study of Degree of Fixation at Pile Head (in Japanese), Summaries of Technical Papers of the 30th Annual Meeting Japan Society of Civil Engineers, pp.161-162, 1975

14) K. Komada and Y. Okayama : Experiments on Joint between Pile Head and Footing (in Japanese), Douro, pp.37-41, 1975.6

15) Research Committee on Design of High Strength pile : Report of Tests on Joint between High Strength Concrete Pile and Footing (in Japanese), 40p., 1975.1

16) K. Wada : Design and Tests of Pile Head Joint of Steel Pipe Concrete Pile (in Japanese), Prestressed Concrete, Vol.18, No.1, pp.2-10, 1976.2

17) M. Tazawa et al.: Experiments on Strength of Joint between Steel Pipe Pile and Footing (in Japanese), Taisei Technical Research Report, No.12, pp.149-158, 1979

18) K. Kurihara and H. Takei : Research Development on Joint Method of Pile Head (in Japanese), Technical Research Report of Japan Housing Corporation, No.10, pp.17-32, 1979

19) B. Nakata et al.: Research Development on Joint Method of Pile Head (in Japanese), Summaries of Technical Papers of Annual Meeting Architectural Institute of Japan, pp.1707-1708, 1979.9

20) K. Kurihara : Research Development on Joint Method of Pile Head, Part 2, Case of Steel Pipe Pile (in Japanese), Summaries of Technical Papers of Annual Meeting Architectural Institute of Japan, pp.2067-2068, 1980.9

21) Y. Sugimura and H. Oh-oka : Report on the Damage of Precast Prestressed Concrete Piles during the 1978 Off-Miyagi Prefecture Earthquake (in Japanese), Kenchiku Kenkyu Shiryo, No.31, Building Research Institute, Ministry of Construction, 228p., 1981.7

22) Y. Sugimura et al.: Earthquake Damage and its Reproductive Experiment of Prestressed High Strength Concrete Pile (in Japanese), Trans. of Architectural Institute of Japan, No.340, pp.40-50, 1984.6

23) Y. Sugimura : Earthquake Resistant Design of Building Foundation, Introduction and Commentary on "Design Guide for the Building Foundation against Seismic Force", BRI Research Paper, No.113, Building Research Institute, Ministry of Construction, 43p., 1985.3

24) K. Kokushoh et al. :Experimental Study on Joint of Pile and Footing under Alternative Cyclic Horizontal Force (in Japanese), Summaries of Technical Papers of Annual Meeting Architectural Institute of Japan, pp.2323-2328, 1981.9

25) Association of Concrete Pole and Pile : Technical Report on Countermove of Damage due to the Miyagiken-oki Earthquake (in Japanese), 87p., 1981.11

26) Association of Concrete Pole and Pile : Report on Structural Properties of Precast Concrete Pile (in Japanese), Vol.3, 124p., 1982.7

27) T. Ozawa et al.: Strength and Deformation Characteristics of Prestressed High Strength Concrete Pile Connected with Footing (in Japanese), Summaries of Technical Papers of Annual Meeting Architectural Institute of Japan, pp.1749-1750, 1982.10

28) T. Fukushima et al.: Experimental Study on Bending Characteristics of Pile Head Joint of PC Pile (in Japanese), Summaries of Technical Papers of Annual Meeting Architectural Institute of Japan, pp.2145-2146, 1982.10

29) S. Yamato and M. Takagi : Bending Characteristics of SC Pile Connected with Footing (in Japanese), Summaries of Technical Papers of Annual Meeting Architectural Institute of Japan, pp.2147-2148, 1982.10

30) M. Ohta et al.: Bending and Pullout Tests of Pile Head Joint (in Japanese), Summaries of Technical Papers of Annual Meeting Architectural Institute of Japan, pp.2149-2152, 1982.10

31) H. Satoh et al.: Bending Property of PRC Pile Connected with Footing (in Japanese), Summaries of Technical Papers of the 37th Annual Meeting Japan Society of Civil Engineers, pp.479-480, 1982

32) I. Yamamoto et al.: Ultimate Strength of Joint between Precast Concrete Pile and Footing (in Japanese), Jour. of Fujita Technical Research Division, No.19, pp.115-127, 1983.6

33) Y. Ohnishi et al.: Ultimate Strength of Joint between Pile and Pile-cap on Lateral and Axial Load (in Japanese), Summaries of

Technical Papers of Annual Meeting Architectural Institute of Japan, pp.2727-2730, 1983.9

34) K. Kokushoh et al.: Studies on the Behavior of Pile-Footing Connections under Axial and Lateral Forces (in Japanese), Summaries of Technical Papers of Annual Meeting Architectural Institute of Japan, pp.2731-2738, 1983.9

35) S. Yamato et al.: Studying on Earthquake-Induced Damage of Concrete Pile by Horizontal Load Test with Axial Load under Pile-Head Restrained (in Japanese), Summaries of Technical Papers of Annual Meeting Architectural Institute of Japan, pp.2429-2430, 1984.10

36) T. Saitsu et al.: Proposal of a Joint Method between Pile and Pile-cap (in Japanese), Summaries of Technical Papers of Annual Meeting Architectural Institute of Japan, pp.2439-2440, 1984.10

37) Y. Ohnishi et al.: Ultimate Strength of Joint between Pile and Pile-cap on Lateral Load (in Japanese), Summaries of Technical Papers of Annual Meeting Architectural of Japan, pp.2441-2444, 1984.10

38) H. Akiyama et al.: Experimental Studies on the Steel Pipe Pile Footing Connections under Lateral Forces, Part 1 to Part 3 (in Japanese), Summaries of Technical Papers of Annual Meeting Architectural Institute of Japan, pp.2447-2450, 1984.10

39) H. Akiyama et al.: Experimental Studies on the Steel Pipe Pile Footing Connections under Lateral Forces, Part 4 and Part 5 (in Japanese), Summaries of Technical Papers of Annual Meeting Architectural Institute of Japan, pp.1001-1004, 1985.10

40) K. Kokushoh et al.: Studies on Behavior of Pile-Footing Connections with Steel Socket under Axial and Lateral Forces (in Japanese), Summaries of Technical Papers of Annual Meeting Architectural Institute of Japan, pp.985-988, 1985.10

41) I. Yamamoto and M. Ohta : Strength Properties and Failure Patterns on Joint between Pile and Pile-cap (in Japanese), Summaries of Technical Papers of Annual Meeting Architectural Institute of Japan, pp.989-990, 1985.10

42) H. Ohno et al.: A Study on Behavior of a Cone Shaped Steel Pile Head under Vertical and Horizontal Loading (in Japanese), Summaries of Technical Papers of Annual Meeting Architectural Institute of Japan, pp.999-1000, 1985.10

43) S. Yoshida et al.: Horizontal Load Test on High Strength PC (PHC) Pile (in Japanese), JCI 7th Konference, pp.469-472, 1985.5

44) A. Wada et al.: Study of the Stress Transfer Mechanism in the Pile-Footing Connection under Axial and Lateral Forces (in Japanese), Jour. of Structural and Construction Engineering, Trans. of Architectural Institute of Japan, No.364, pp.111-120, 1986.6

45) I. Yamamoto : Pile Head Joint of Precast Piles (in Japanese), Materials of "Problems on Aseismic Design of Pile Foundation", Panel Discussion on Foundation Engineering, Architectural Institute of Japan, 1985.10

46) T. Asama et al.: Design Method of Pile Foundation by Considering Spring at Pile Head and Horizontal Displacement (in Japanese), Doken Shiryo, No.1715, Public Research Institute, Ministry of Construction, 78p., 1981.8

47) Y. Gotoh and T. Shibata : Shear Strength Estimation for Pretensioned Spun High Strength Concrete Piles (in Japanese), Summaries of Technical Papers of Annual Meeting Architectural Institute of Japan, pp.983-984, 1985.10

Table 1 Comparison of degree of fixation for infinite length pile

Kind of degree of fixation	Boundary condition		Degree of fixation: Equation	Pin	Rigid	References
Degree of fixation to bending moment (Degree of restraint for rotation)	a)	M_0	$\alpha_r = \frac{M_0}{M_{0f}}$	$\alpha_r=0$	$\alpha_r=1$	2), 3)
	b)	$\theta_0=kM_0$	$\alpha_r = \frac{1}{1+EI\beta k}$	$\alpha_r=0$	$\alpha_r=1$	12),15),16),18),20), 25),26),29),39)
Degree of fixation to displacement (Displacement factor)	c)	M_0	$R_{y_0}=2-\alpha_r$	$R_{y_0}=2$	$R_{y_0}=1$	7); 8),13),17),24), 28),30),32),33),41)
	d)	$\theta_0=kM_0$	$R_{y_0} = \frac{1+2EI\beta k}{1+EI\beta k}$	$R_{y_0}=2$	$R_{y_0}=1$	6),12),15),16),25), 26),29),31)

M_0, θ_0: Bending moment and angle of rotation at pile head.

M_{0f} : Bending moment at pile head which is completely fixed.

k : Inverse number of rotational spring at pile head.

Table 2 Properties of pile section (phase 1 series)

Pile Grade B cm	t cm		Standard M_{cr} tm	Standard M_u tm	Equivalent I_e cm^4	Equivalent Z_e cm^3	Design M_{cr} tm	Design M_u tm
35	6	A	3.5	5.3	61540	3517	4.1	6.7
35	6	C	6.0	12.0	63970	3655	6.5	13.9
50	8	C	17.0	34.0	258800	10350	17.9	38.1

Table 3 Properties of test specimen (phase 1 series)

Test No.	Pile F_c	Pile t	Footing F_c	Footing E_c
35AX00	884	64	244	2.45
35AY00	884	64	207	2.52
35AZ00	903	65	178	2.34
35AX30	884	63	247	2.61
35AY30	684	63	233	2.55
35AZ30	903	67	224	2.45
35AX60	884	60	226	2.71
35AY60	884	60	199	2.63
35AZ60	860	65	134	2.68
35CX00	902	65	268	2.44
35CY00	902	65	233	1.86
35CZ00	888	66	194	1.97
35CX30	887	62	204	1.64
35CY30	887	65	212	1.86
35CZ30	888	69	170	1.68
35CX60	886	69	261	2.55
35CY60	886	65	234	2.30
35CZ60	888	65	226	2.12
50CX00	954	83	198	2.32
50CY00	954	84	187	2.41
50CZ00	901	88	175	2.71
50CX60	954	84	177	2.50
50CY60	954	83	223	2.44
50CZ60	901	84	171	2.33

F_c:kg/cm² t:mm E_c:×10³kg/cm²

Table 4 Properties of test specimen (phase 2 series)

Test No.	Thickness t (cm)	Equivalent moment iner. I_e (cm^4)	Effective prestress σ_e (kg/cm²)	Design bending moment M_a (cm)	Design bending moment M_{cr} (cm)
10X'	6.77	65940	87.09	6.67	7.99
10Z'	6.94	66590	86.17	6.67	8.00
20Z'	6.42	64520	95.33	6.91	8.20
20Y'	6.15	63320	94.91	6.83	8.10
35X'	7.75	69260	80.50	6.56	7.94
Standard	6.00	62620	80.00	6.17	7.42

Table 5 Properties of materials (phase 2 series)

Steel		σ_t (kg/cm²)	σ_y (kg/cm²)	E_s ×10⁶
PC bar	9.2	15255	13400	2.11
Footing	D13	6350	4455	2.00
Anchor	D10	5762	3814	2.01

σ_t: Tension σ_y: Yield

F_c: Comp. E_s, E_c: Young's modu.

Concrete		No. (day)	F_c (kg/cm²)	E_c ×10⁵
Pile		49	895	4.08
Footing	10X'	35	228	1.63
	10Z'	35	226	1.61
	20Z'	34	231	1.54
	20Y'	34	235	1.52
	35X'	33	237	1.54

Table 6 Values and failure type at the maximum load

No.	P(t)	Q_E(t)	M_C(tm)	M_E(tm)	RBM*	SSR**	Type
35AX00	17.12	-10.29	10.82	-1.42	1.72	3.01	B
35AY00	21.14	-11.97	14.52	0.25	2.30	3.47	B
35AZ00	24.02	-16.65	8.51	-11.37	1.30	1.95	B
35AX30	28.38	-18.57	11.83	-10.36	1.19	1.82	SB
35AY30	25.36	-16.95	12.00	-8.24	1.20	2.02	S
35AZ30	30.38	-20.70	10.39	-14.35	1.44	1.98	S
35AX60	31.40	-20.63	14.11	-10.53	1.06	1.95	S
35AY60	30.74	-20.61	12.69	-11.95	0.96	1.76	S
35AZ60	34.16	-23.38	11.49	-16.47	1.24	2.01	S
35CX00	31.20	-17.82	19.96	-1.22	1.47	3.20	S
35CY00	28.60	-18.16	13.52	-8.18	0.99	2.13	S
35CZ00	33.00	-21.43	14.93	-10.67	1.10	1.99	S
35CX30	32.58	-20.71	16.10	-8.65	0.98	2.22	S
35CY30	29.62	-19.16	13.08	-9.31	0.80	1.95	S
35CZ30	34.14	-22.50	14.93	-12.09	0.91	1.89	S
35CX60	35.28	-22.90	16.04	-11.34	0.85	2.00	SF
35CY60	32.26	-20.83	15.16	-9.79	0.82	2.07	SF
35CZ60	38.48	-25.67	15.69	-15.01	0.84	1.75	SF
50CX00	65.56	-39.06	40.42	-6.26	1.10	2.07	S
50CY00	61.36	-37.31	34.90	-10.28	0.95	1.85	SF
50CZ00	72.16	-45.54	36.39	-17.69	1.00	1.62	SF
50CX60	74.16	-45.96	39.69	-15.26	0.88	1.75	SF
50CY60	70.20	-44.05	36.29	-16.38	0.80	1.65	SF
50CZ60	83.84	-54.09	38.84	-26.07	0.86	1.43	SF
10X'	28.65	-18.46	14.76	-6.17	0.94	2.12	S
10Z'	29.76	-18.35	14.33	-6.36	0.98	2.34	S
20Z'	27.51	-19.43	10.75	-10.12	0.72	1.77	S
20Y'	27.38	-17.36	12.35	-7.06	0.82	2.20	S
35X'	34.38	-22.95	16.68	-8.58	1.07	2.26	S

*RBM=|Max(M_C,M_E)/M_{uc}| M_{uc}:Analyzed ultimate bending capacity

**SSR=|Max(M_C,M_E)/(Q_E*B)| :Shear span ratio S:Shear

B:Bending SB:Shear-bending SF:Shear and pure bending

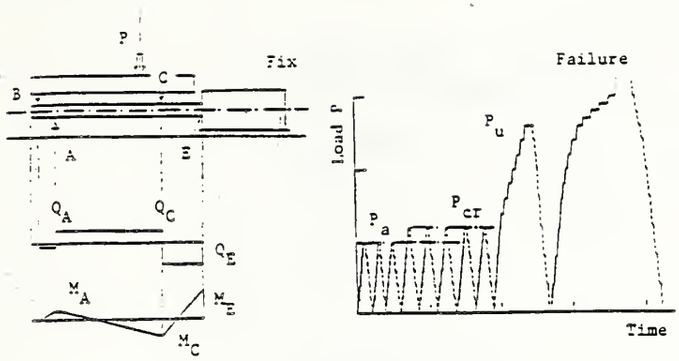

Fig.1 Outline of loading system

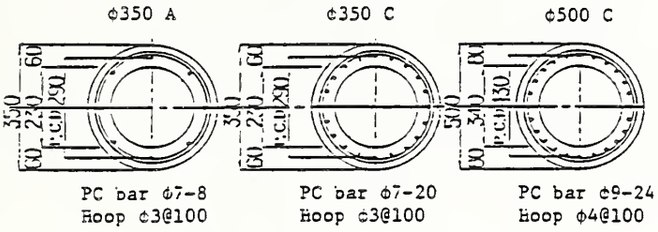

Fig. 3 Pile section (phase 1 series)

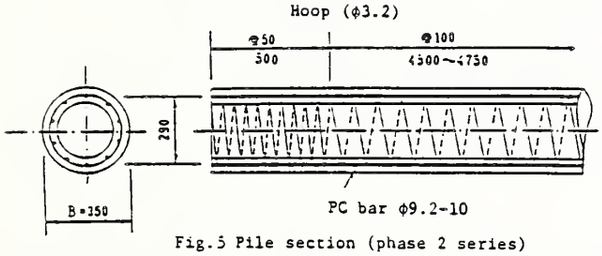

Fig.5 Pile section (phase 2 series)

L:Load cell D:Dial gage for pile FD:Dial gage for footing I:Inclinometer T:Strain gage for PC bars fixed to the floor SG:Strain gage on pile surface PG:Strain gage for PC bar in pile

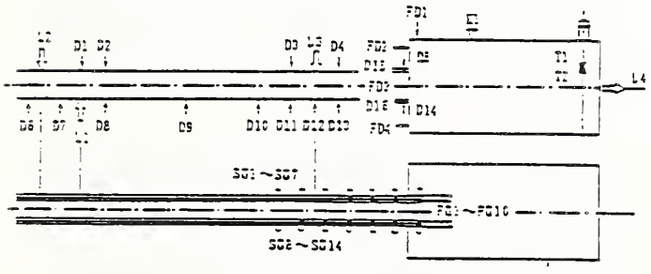

Fig. 7 Location of measurements (case of 20Z')

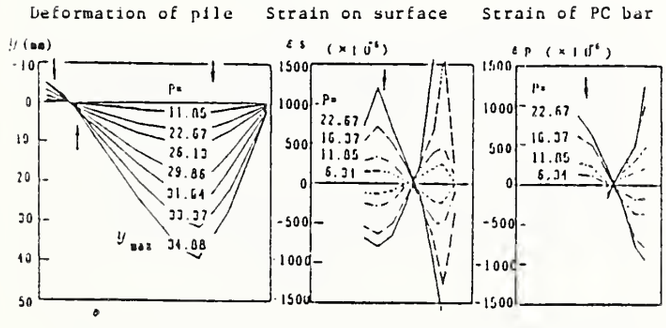

Fig.9 Distribution of displacement and strain of pile (case 35X')

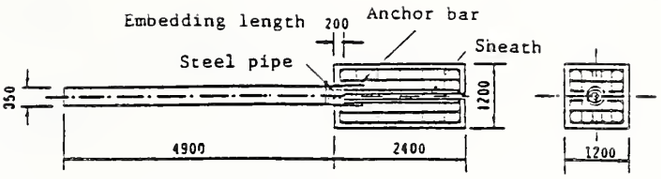

Fig.2 Test specimen (case 20Z')

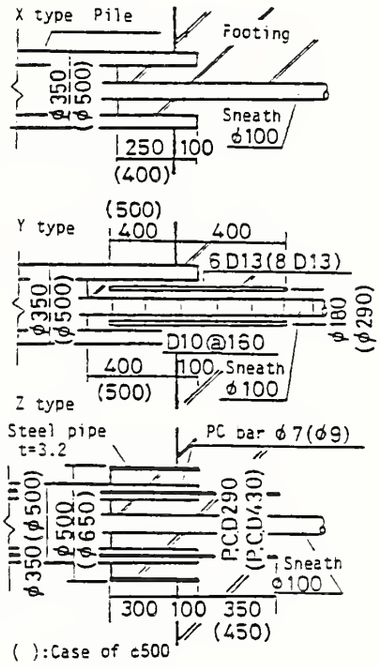

Fig.4 Detail of pile head joint (Phase 1 series)

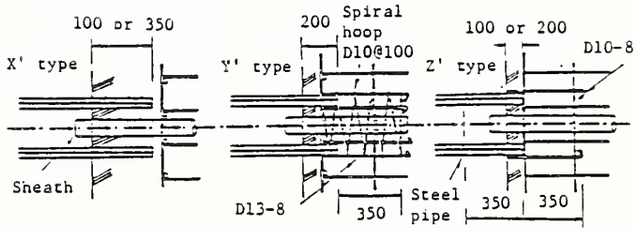

Fig.6 Detail of pile head joint (phase 2 series)

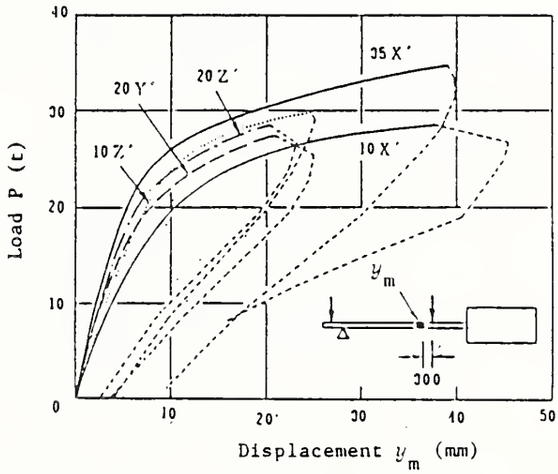

Fig.8 Relation between load and displacement of pile (phase 2 series)

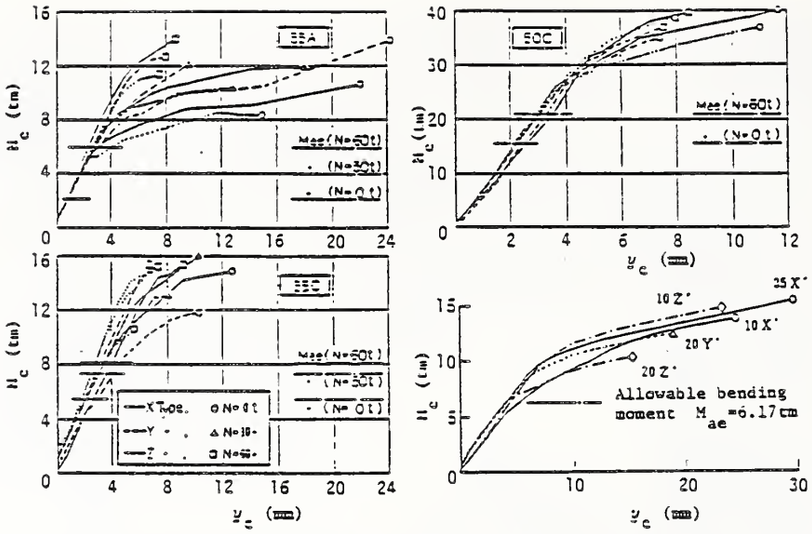

Fig. 10 Relation between bending moment and displacement at loading point C

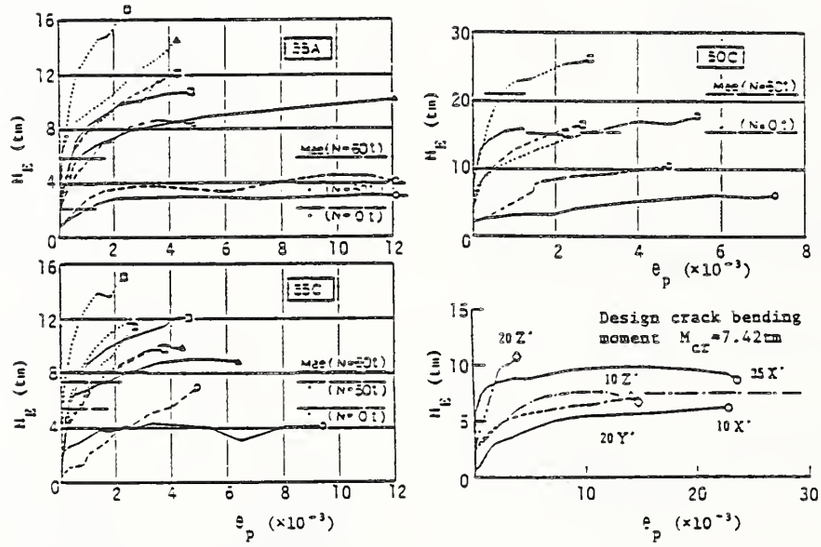

Fig. 11 Relation between bending moment and angle of rotation at pile head

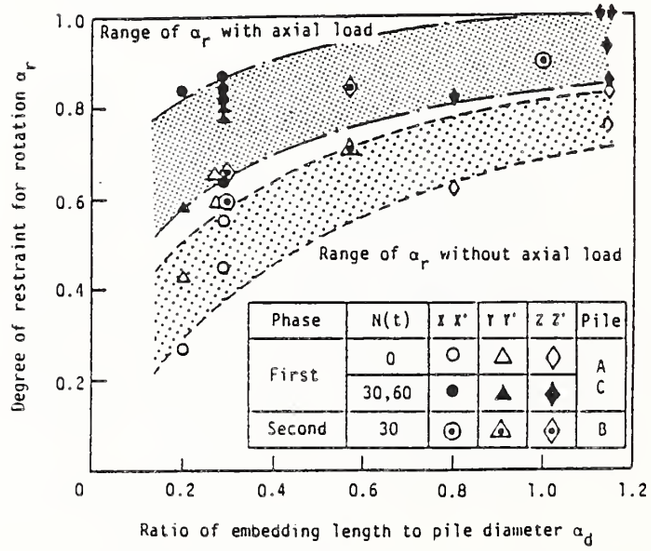

Fig. 12 Degree of restraint for rotation at pile head

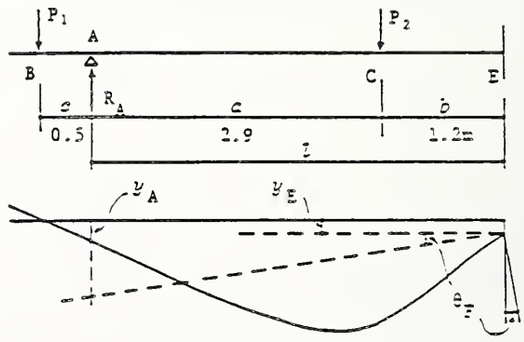

Fig. 13 Correction of bending moment at pile head

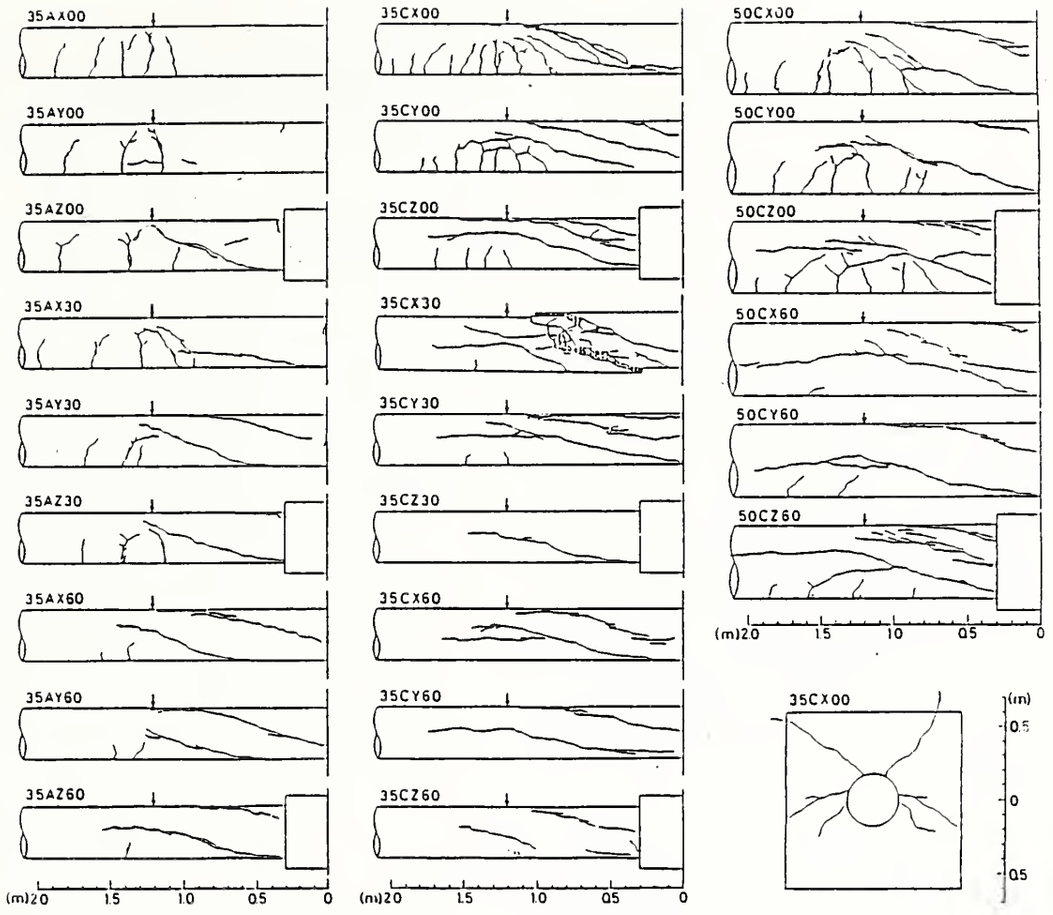

Fig. 14 The final state of cracks of pile (phase 1 series)

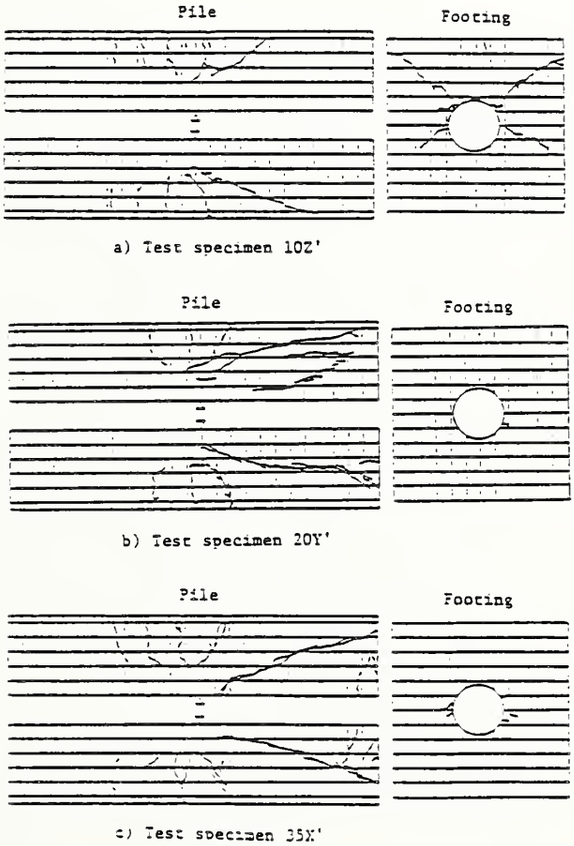

Fig. 15 The final state of cracks of pile (phase 2 series)

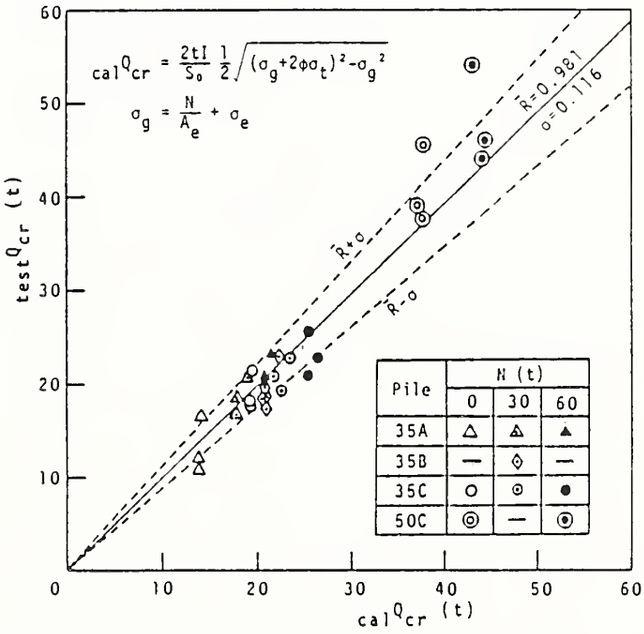

Fig.16 Comparison between experimental and analytical results of shear strength of pile

Schemes for Seismic Upgrading of a Major Hospital

BY

Joseph V. Tyrrell, P.E.[1]

ABSTRACT

Design of the Oak Nolls Naval Hospital was begun in 1965 and construction was completed in 1968. The design was according to the then current criteria which was based on the Uniform Building Code. Earthquake experience in the 1960's created concern for the adequacy of the design codes. The 1971 San Fernando earthquake clearly demonstrated that some existing U.S. structures did not provide a desirable level of seismic safety. Consequently, the U.S. Navy began evaluation of facilities located in areas of high seismic risk. The Oak Nolls Naval Hospital was identified as requiring upgrading and various mitigation schemes were proposed. This paper discussed these schemes.

KEYWORDS: Retrofit; hospital safety; seismic hazard mitigation; upgrading schemes.

1. INTRODUCTION

In the 1960's the Alaska earthquake and other events raised questions regarding the adequacy of design codes. At the same time, accumulating earthquake records indicated that the seismicity of several areas in the United States had been underestimated. In 1966, the first edition of the tri-service design manual contained both increased design criteria and increased estimates of earthquake risk in several locations.

The Naval Facilities Engineering Command had just begun appraising existing structures when the 1971 San Fernando event occurred. This confirmed that there were still deficiencies in the design codes and that certain existing structures were unsafe. Several major hospitals were seriously damaged by the 1971 event. The US Navy's inventory of existing facilities includes a relatively small percentage of high rise or mid-rise structures but hospitals are typically in this category. Because of their importance and the experience of earthquake damage, hospitals were given a high priority in the Navy's investigation.

Of the six naval hospitals investigated, all were found to be be deficient with respect to earthquake safety. Two of these facilities (Bremerton, WA. and San Diego, CA.) have been replaced with new construction. Deficiencies in the hospital at Charleston, SC were relatively minor and upgrading has been completed at a cost of about $100,000. Action has not been taken for the other three hospitals. However, funding was approved for the Oak Nolls hospital located at Oakland, CA. and design completed. Unfortunately, the bids were higher than the available funds and at this time the next step remains to be determined. This paper discusses the existing Oak Nolls structure, the criteria for upgrading, the mitigation schemes considered, and probable reasons for the high bids.

2. EXISTING STRUCTURE

The Oak Nolls Naval Hospital is a nine story, reinforced concrete moment frame with the exterior columns formed as part of precast concrete wall panels. The interior columns and floors were cast in place. The lower four floors are of irregular shape and extend out on three sides from the tower. The tower structure consists of four wings which are offset from the centerline of a central core area (see Figs. 1 & 2). At some places there are discontinuties in the exterior walls where higher levels are supported from a cantilevered floor.

The Oak Nolls structure is supported on piles, some end bearing and some utilizing skin friction. The tops of the piles are at two different elevations depending upon the location. The building was constructed against a hillside. The lowest level is completely below grade and the next higher level is below grade on one side and at grade on the opposite side.

3. DESIGN CRITERIA

The Navy's criteria for lateral force in connection with seismic upgrading of typical buildings is that the capacity of the structure be at least 75% of the demand imposed by an earthquake with an 80% probability of not being exceeded in 50 years. Under this loading, the structure must not collapse. This policy recognizes the fact that there are a large number of

---

[1] Naval Facilities Engineering Command, Consultant in Earthquake Engineering

deficient structures and that it is not economically feasible to provide funds to fully correct all of the deficiencies. The program focuses on structures that are liable to collapse. For essential facilities like hospitals, the target is to provide upgrading so that capacity equals 100% of the demand. A site seismicity study was made and response spectra established for the site (see Fig 3). The preliminary structural investigations utilized the spectra in connection with the 80% /50 year earthquake described above. Analyses were based upon a lumped mass, single degree of freedom model. The structure was also analyzed for the code forces required by Department of Defense criteria. This latter criteria is based upon the Uniform Building Code. The hospital was found to be seriously deficient for both loadings.

4. CONDITIONS FOR UPGRADING

In addition to strengthening to provide sufficient strength and ductility to meet the design criteria, it was determined that it was necessary to maintain full operation of the hospital during construction. This requirement had a major impact on the selection of a structural scheme and significant cost implications. It made it necessary to relocate functions temporarily while work in a given area was completed. Control of noise, dust, and vibration also became a significant issues.

A very detailed phasing plan was drawn up in conjunction with the medical personnel at the hospital. As a result of these requirements, the construction time required was increased from the normal expectation of about 20 months to about 4 years.

5. STRUCTURAL UPGRADING SCHEMES

THe firm of URS/BLUME, San Francisco, CA performed most of the preliminary studies. The following schemes were considered initially:

a. Construct new concrete shear walls normal to the existing walls for both the tower section and the low roofed portion.
b. Add reinforced concrete to increase the shear strength of the exterior walls, walls around the elevator core, and a few selected interior partitions.
c. Construct a very stiff new six story structure in the southwest quadrant (no existing construction in this area), and subsequently a matching structure to replace the existing construction in the northeast quadrant.

The preliminary cost estimates were 10.5 to 11 million dollars (1974) for these schemes. They all involved considerable internal disruption. The third scheme would have allowed relocation of functions from the northeast area to the new southwest area, thus facilitating work in the northeast area. It appeared likely to take longer and be somewhat more expensive. The other two schemes involved exposing a large portion of the occupants to close proximity to construction at one time or another. They also required some reshuffling of functions within the existing space. None were entirely acceptable for the purpose of keeping the facility operational during construction. Consequently, it was decided to explore other possibilities.

6. SECOND GENERATION SCHEMES

The necessity to minimize interference with operations had become the dominant factor influencing design selection. To accomplish this, attention was focused on reinforcement placed at perimeter. This led to the following schemes:

a. A variation of the first scheme with concrete shear walls perpendicular to exterior walls plus reinforcement of the exterior walls.

b. "C" shaped concrete buttresses at the ends of the wings (see Fig 4). The buttresses were to be tied to the existing structure by exterior beams extending along the floors of the tower.

c. Braced steel buttresses at the ends of the wings to be connected in a manner similar to the concrete buttresses.

On closer examination it was apparent that the first of these schemes still required extensive structural work inside the building below the fifth floor in order to carry the reinforcing down to the foundations. Thus this scheme was discarded. The other two schemes also resulted in a similar condition at two of the wings, however, there was much less construction required within the existing building.

Besides the difference in construction techniques, the concrete and steel buttresses also differed in design philosophy. The existing structure was fairly stiff, although much of the initial stiffness would be supplied by elements not intended to take such loading. The concrete buttress envisioned utilization of a typical approach - it would provide even greater stiffness and thus take lateral loads before the vulnerable members. The increase in stiffness would

result in a shorter period and consequently the forces would increase according to the position on the response spectrum.

The steel braced frames were planned to be not quite as stiff as the existing structure. Initially the existing structure would resist most of the lateral force but after a little yielding it would gradually transfer to the new structure. Under the forces associated with a large earthquake, the stiff non-structure elements (exterior walls and partitions) would sustain some yielding. Under a great earthquake there might be structural damage in the original members. The new steel braced frame would remain elastic at all times.

7. SELECTED SCHEME FOR STRENGTHENING

The braced steel buttresses were selected because they cost less and were easier to erect. While the concrete version might have reduced the chance of damage, it was considered unrealistic to prevent any damage because of details of construction and the geometry of the existing structure. The steel buttresses provide the essential requirement for life safety.

The steel design required the new structure to be more flexible than the existing, but also to be stiff enough to quickly pick up the lateral forces when yielding took place in exiting elements. It was found to be feasible to meet these requirements. Additional detail of the steel concept is shown in Figures 5 and 6.

The principal features of the were :

a. Vertical steel braced frames at the end of each of the four wings.

b. Horizontal braced steel diaphragms connected to the existing concrete floors and roof and intended to transfer forces to the new braced frames.

c. Diaphragm chord strengthening for all floors above the fourth floor as well as both shear and chord strengthening of the roof.

d. Drilled caisson foundations supporting the new braced frames and providing for transfer of lateral forces into the ground.

8. ARCHITECTURAL CONSIDERATIONS

One problem with external modification was the fear that the architectural quality of the building would be adversely affected. To overcome this objection, it was planned to provide some architectural treatment. Figure 7 shows one concept. Eventually, it was decided to use a simple, lightweight metal cladding, treated to harmonize with the existing concrete.

9. BASE ISOLATION

For some time the Navy has been considering base isolation treatment to reduce the lateral forces associated with earthquake motions. This method appears to have potential benefits for certain types of construction. To date a project has not been identified. However, proponents of several proprietary systems suggested use for the Oak Nolls hospital. They stated that it could be installed with less disruption to operations and lower cost than conventional strengthening.

After study, this idea was discarded as impractical. A major reason for this decision was the nature of the existing structure. The building is unsymetrical in the first four floors, the center of rigidity is not near the center of mass, the length of piles varies considerably from northeast to southwest, the pile caps are at two different elevations, and the structural details provide very little ductility. The location of the hospital, very close to a major fault, posed the possibility of strong vertical accelerations. Therefore, this application would have taken base isolation into areas outside the framework of experience. Even if the base isolation system worked perfectly, strengthening of the superstructure would have been necessary to avoid severe overstress.

10. FINAL DESIGN AND BID

The final design was prepared by the firm of H. J. Degenkolb Associates, Engineers, San Francisco, CA. They reviewed and reconfirmed the recommendations of the studies. However, it was decided to make some changes since extensive modifications for heating and ventilating, fire protection, and medical improvements had come into the project. Because these items required interior work, it was decided to place the ties and chord strengthening members under the floors inside of the building. These changes further complicated construction and made the phasing plan more difficult.

The bids were about were about 35% above the estimate. This appeared to be attributable to the complexity of the construction which was rooted in the requirement to keep the hospital fully operational during construction. Since additional funds were

not available, the project was deferred. At this time a definite plan of action has not been developed.

11. SUMMARY AND CONCLUSIONS

A number of schemes were investigated and several found to be possible structural solutions for the Oak Nolls hospital. While they were expensive, they were not nearly as costly as building a new hospital of equivalent size and capability. The project was not brought to a successful conclusion because the difficulty and cost of maintaining the hospital operational during construction was under estimated. A suitable upgrading for any given facility is strongly influenced by the nature of its vulnerability and the function served.

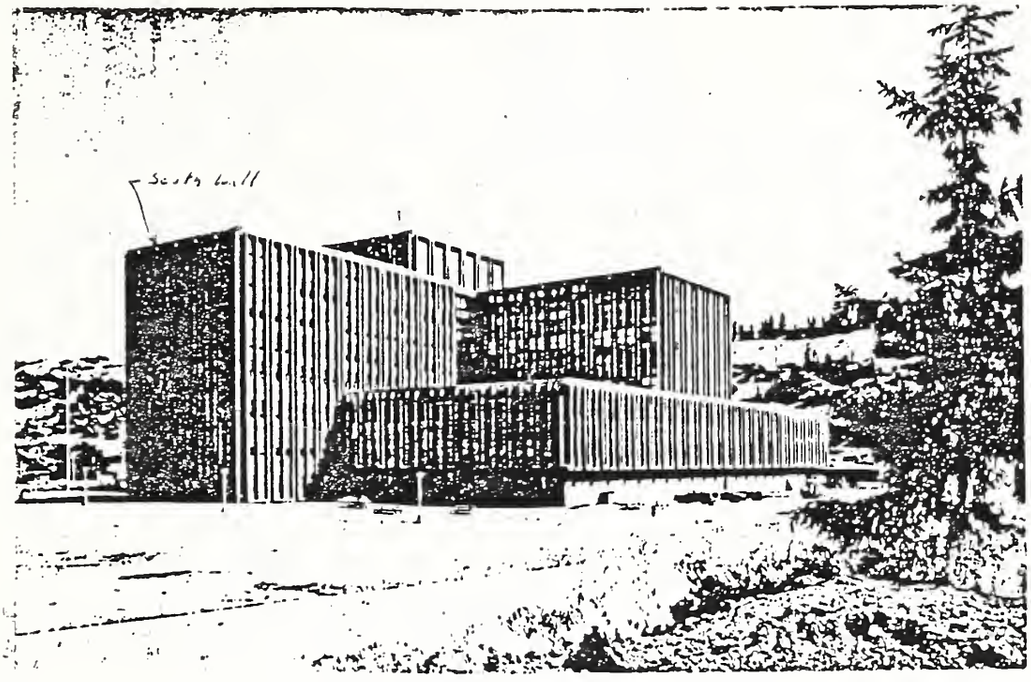

OAKLAND NAVAL HOSPITAL
(VIEW LOOKING NORTH)

FIGURE 1

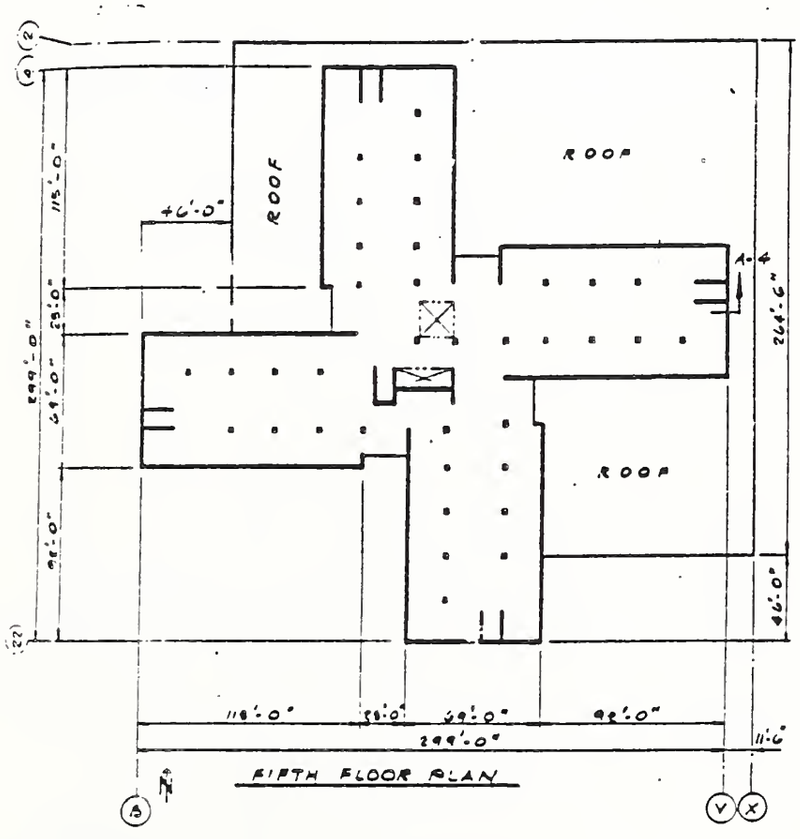

U.S.N. HOSPITAL
OAKLAND, CALIFORNIA

FIGURE 2

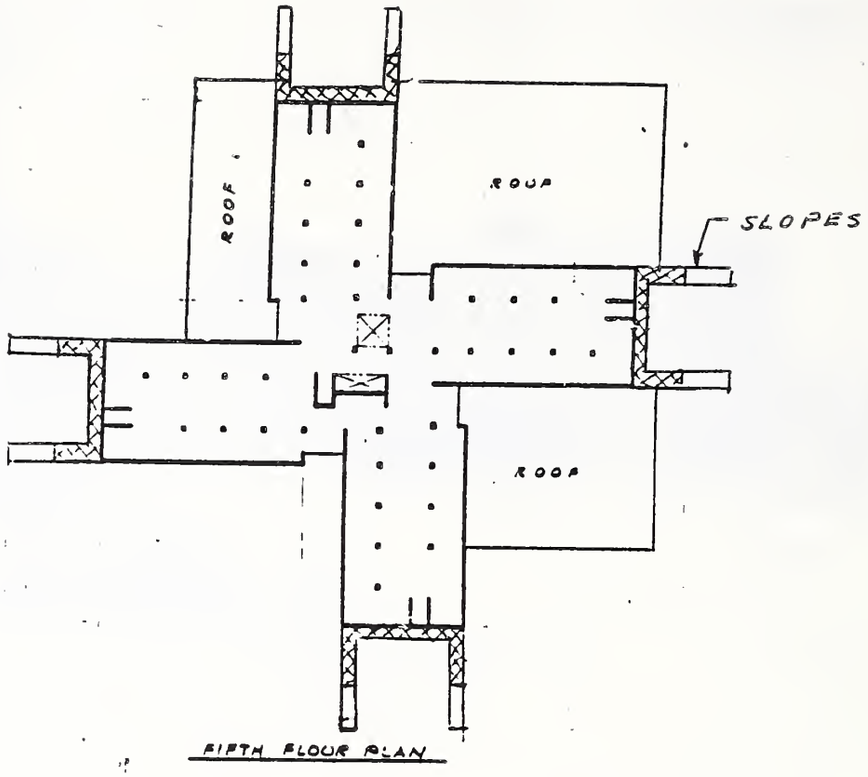

U.S.N. HOSPITAL
OAKLAND, CALIFORNIA FIGURE 4

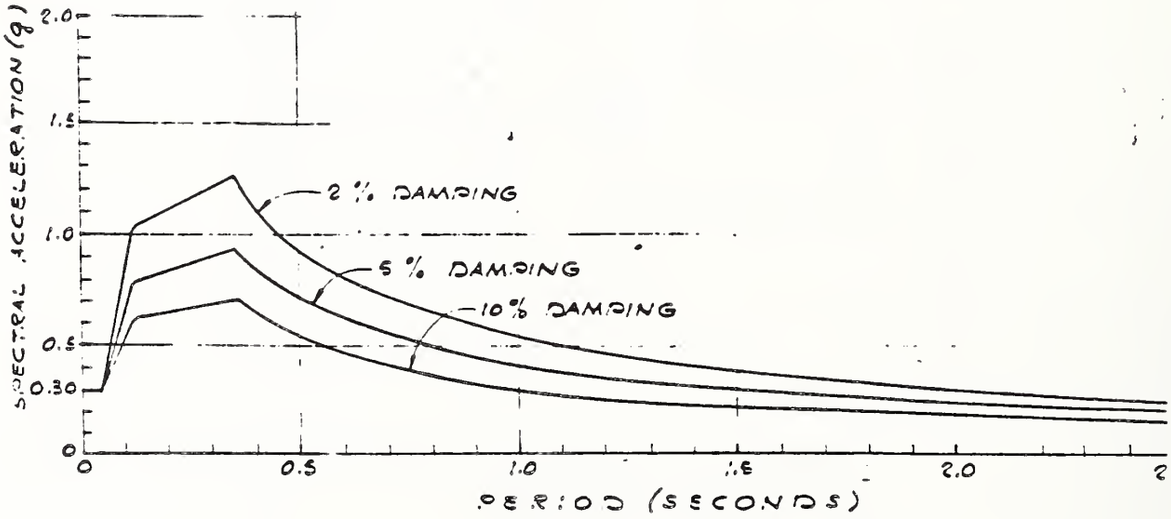

ACCELERATION RESPONSE SPECTRA
FOR EARTHQUAKE WITH 10 % PROBABILITY
OF EXCEEDANCE IN 25 YEARS (B)

USN HOSPITAL
OAKLAND, CALIFORNIA FIGURE 3

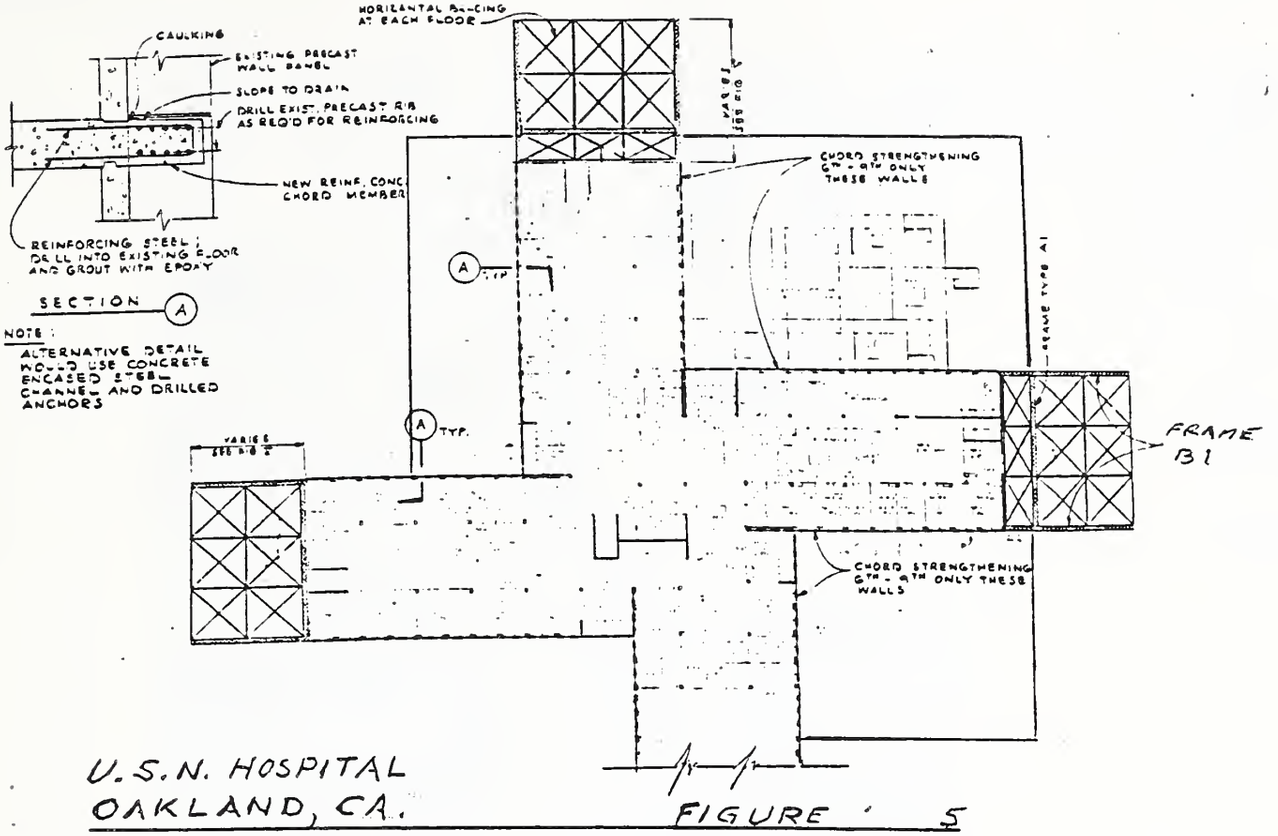

U.S.N. HOSPITAL
OAKLAND, CA.

FIGURE 5

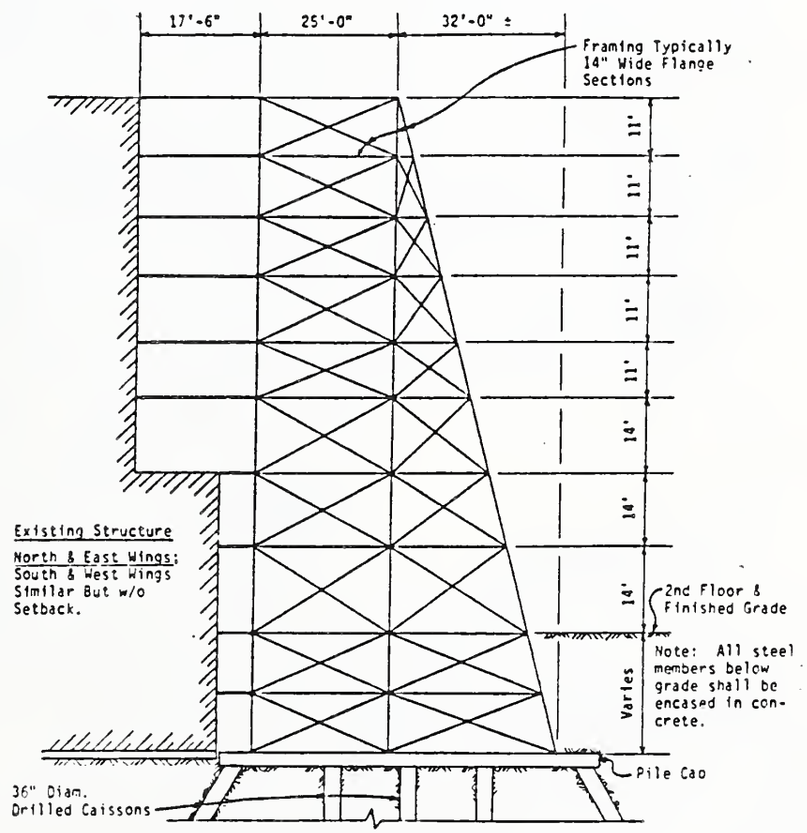

FIGURE 6
BRACED FRAME TYPE B1

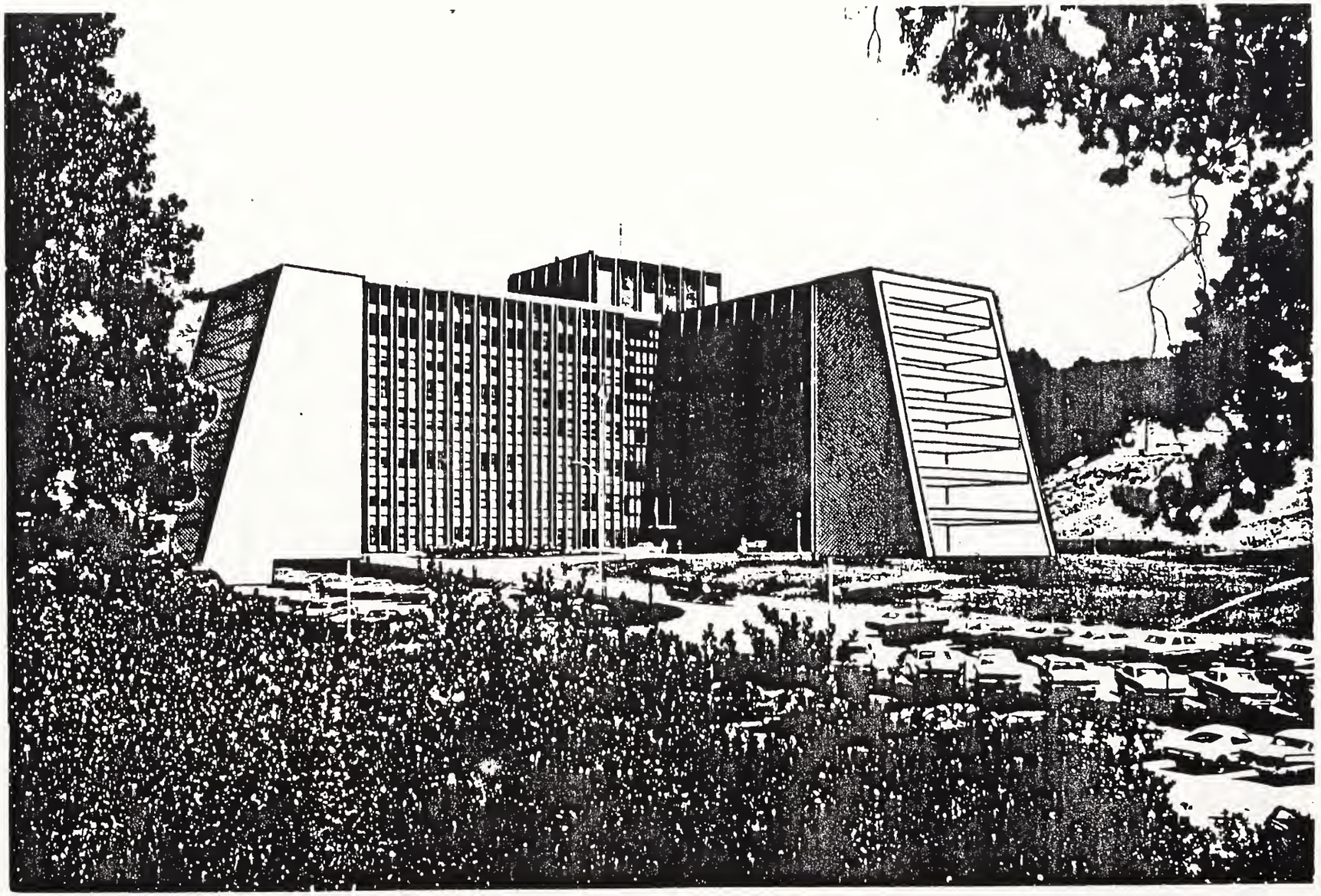

FIGURE 7

PERSPECTIVE VIEW - PROPOSED STRUCTURAL SOLUTION

Theme III

Storm Surge and Tsunami

Experimental Investigation on the Damage of Offshore Seawall due to the 1983 Nihonkai-Chubu Tsunami

BY

Katsutoshi Tanimoto[1] and Hiroichi Tsuruya[2]

ABSTRACT

A tsunami caused by the 1983 Nihonkai Chubu Earthquake (M=7.7) struck the coasts along the Japan Sea. A part of the seawall which was under construction for a future reclaimed land at the outside of Noshiro Port was collapsed by the attack of tsunami.
In this study experiments were conducted on the deformation of the tsunami during the propagation on a continental shelf to the coast. Tsunami forces acting on a vertical wall were also tested under the action of breaking bore to investigate the cause of the damage of the seawalls.
The bottom topography of the sea from the continental shelf to the coast was reproduced in a 163m long wave channel.
From the experiment, the pressure distribution of tsunami in a state of a breaking bore is formulated and it is concluded that the damages of the seawall in Noshiro could be explained well by the present formula.

KEY WORDS: Damage due to Tsunami, Deformation of Tsunami, Bore-type Tsunami, Tsunami Force, Seawall.

1. INTRODUCTION

On 26 May 1983, a tsunami, caused by a seismic disturbance in the offshore of Akita Prefecture at latitude 40°42' and longitude 138°54', struck the coasts along the Japan sea. The tsunami took about one hundred person's lives and brought severe damages over wide area along the Japan Sea. Port constructions such as seawalls and breakwaters were also damaged in various places. For example, the seawall which was under construction for a future reclaimed land at the outside of Noshiro Port was collapsed over 300 meters by the attack of tsunami. The observed period of the tsunami ranged from ten to twenty minutes. A remarkable aspect of this tsunami was that it attacked the northern coasts of Akita Prefecture where the bottom slopes were relatively gentle, in a state of breaking bores with undulations (solitons) succeeding the bore front having a period of about 10 seconds.

[1]Dr. of Eng., Chief of Breakwaters Laboratory, Hydraulic Engineering Division, Port and Harbour Research Institute, Ministry of Transport, Japan.

[2]Chief of Hydrodynamics Laboratory, Marine Hydrodynamics Division, Port and Harbour Research Institute, Ministry of Transport, Japan.

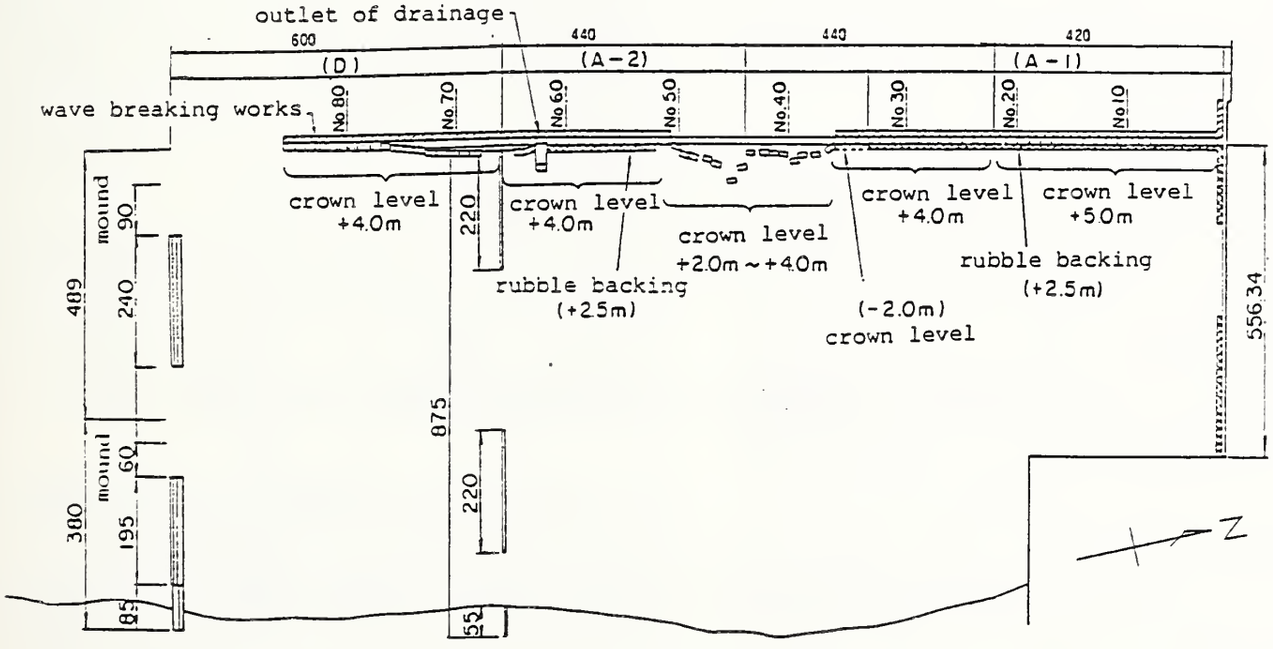

Fig.1 Damage of seawall outside of Noshiro Port

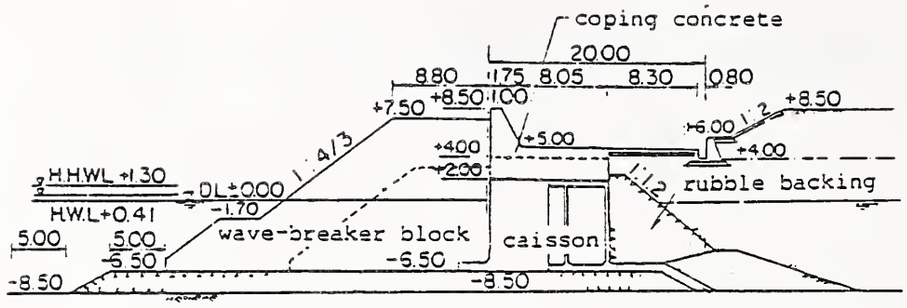

Fig.2 Standard cross section of seawall in the completion (Section A-2)

Fukui et al.[1] investigated the wave pressure of a bore-type tsunami acting on a seawall. They have concluded from the experimental results that both the dynamic pressure at the collision and the continuing pressure after the collision can be represented by linear distributions having the maximum value at the still water level.

On the other hand, Tanimoto[2] has proposed the formula of pressure on a vertical wall due to non-breaking tsunami in a region of relatively large water depth. The formula is a modified one of Goda's formula for the wave pressure on a vertical breakwater on the basis of experimental results so that it can be applied to long waves as tsunamis. In applying these formulae, however, we must previously know how the tsunami attacked to the seawall at Noshiro Port together with its various parameters.

In this study, therefore, experiments were conducted on the deformation of the tsunami during the propagation on a continental shelf to the coast. Tsunami force acting on a vertical wall was also tested under the action of breaking bore to investigate the cause of the damage of the seawalls.

2. DAMAGE OF SEAWALL

The seawall was under construction for a future reclaimed land of the Noshiro electric power plant at the outside of Noshiro Port.

Figure 1 shows the state of the collapse and slide of caissons after the attack of the tsunami. The front seawall facing to the offshore is divided into three parts, namely, A-1, A-2, and D according to the final crest level of the seawall at the completion. Except for the length 200m at the southern part of D, caissons had already been settled.

Figure 2 shows the standard cross section of the seawall at the completion in the part A-2. The dimensions of the caisson are 20m long, 11m wide, and 8.5m deep. The total bottom width including the footing is 12.5m. Only the top levels of the parapet in the parts A-1 and D differ from that in the part A-2. The

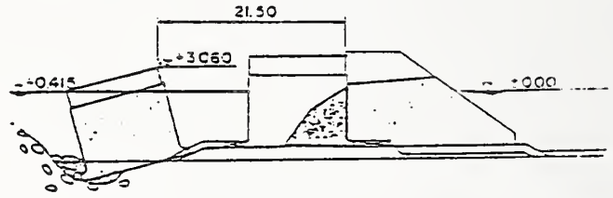

Fig.3 State of sliding of No.68 caisson

concrete cap and the wave dissipating concrete blocks had been constructed to the level +5.0m for the caissons from No.1 to No.21, and +4.0m from No.22 to No.35. The rubble backing had been mounded to the level +2.5m for the caissons from No.1 to No.32, and to the level -2.0m from No.33 to No.35. The caissons in these sections were not damaged. For the caissons from No.36 to No.50, neither the wave dissipating concrete blocks nor the rubble backing had been mounded. And there were various stages of caissons such as that in which sand was packed and only the capping was placed, and that on which the top concrete was constructed to the level +4.0m. The caissons in this section were exceedingly damaged. The caisson No.39, for example, was moved about 38m to the shore side from the initial position and overturned. The caisson No.40 was moved to the shore side about 74m and this was the longest distance among all the damaged caissons.

For the caissons from No.51 to the outlet of drainage, the concrete cap had been constructed to the level +4.0m, and the wave dissipating concrete blocks and the rubble backing (except for the caisson No.51) had also been constructed. In this section no caisson has suffered the damage except for No.51 caisson at the edge of this section.

For the caissons No.63~No.85 in the southern part from the outlet of drainage, the concrete cap and the wave dissipating concrete blocks had been constructed to the level +4.0m. The rubble backing, however, had not been mounded and the caissons except for No.85 was slided over the distance from 0.15m to 21.5m. Figure 3 shows the state of the sliding of the caisson No.68 of which the sliding distance was the maximum within this section.

From the fact in the field above-mentioned, it can be concluded that the sliding or the collapse of a caisson came about mainly in the region where the rubble backing had not been mounded.

3. EXPERIMENTS ON TSUNAMI PRESSURE ACTING ON A VERTICAL WALL

The experiments were conducted in a concrete flume 163m long, 1m wide, and 1.5m deep. The water depth in front of the wave paddle was kept constant at 1m throughout the experiments. The model of sea bottom is started at the distance of 37m from the wave paddle and composed of three slopes. The slope of the most offshore side is 1 on 10 and extended to the horizontal length of 5m. Then, the second slope of 1 on 200 is continued over the horizontal length of 95m and connected to the shore slope of 1 on 20. The scale of the model is 1/200 without distortion. After this the size is described with that in the prototype unless the special notice is given. The offshore water depth on the horizontal bottom corresponds to the depth of 200m in the prototype.

The caisson having the width of 10m and depth of 13m was set at the water depth of 9m. At the front face of the caisson two pressure sensors were equipped (below the still water level 1.4m and 6.3m) to measure the variations of the hydrodynamic pressures of the tsunami. Water elevation was measured at the position 450m offshore from the caisson (station C, water depth is 11.25m).

The periods of the tsunami used in the experiment were 15, 10, and 8 minutes (these periods correspond to 60, 40, and 35 seconds, respectively, in the experiment). The amplitude of tsunami was changed in nine levels for each condition of period. The offshore profile of the tsunami was sinusoidal and the first wave was began to push. The experimental case is summerized in Table 1. The symbol a_0 in the table represents the amplitude of the first wave of the tsunami at the uniform water depth 200m.

Figure 4 shows examples of the water surface elevation (η) and the wave pressure (p) measured during first two waves. In the top figure showing the time history of the water surface elevation at the station C, we can observe that the tsunami approaching to the caisson is greatly deformed into the bore shape having undulations (solitons) from the initial sinusoidal form in the offshore. It is also observed that the reflected bore from the caisson, which is propagating toward the offshore, is superimposed on the incident bore after about 1.5 minutes from passing of the incident bore and that the water surface elevation becomes about twice as much as that

Table 1 Experimental case
(Dimension for model test)

i	T (s)	L (m)	$2a_0$	$2a_0/L$
1/200	60	187.79	9 types	$3.23\times10^{-5}\sim8.52\times10^{-5}$
	40	125.17	〃	$5.91\times10^{-5}\sim2.40\times10^{-4}$
	35	109.51	〃	$1.20\times10^{-4}\sim3.22\times10^{-4}$

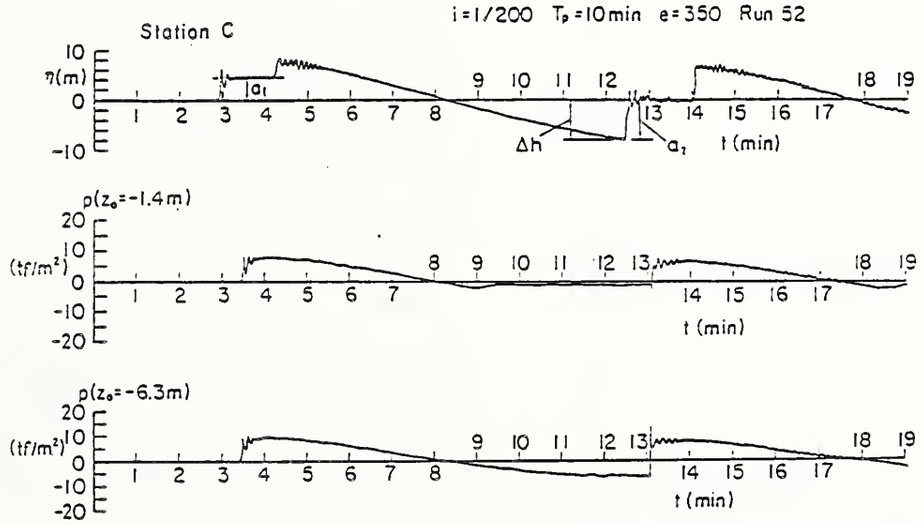

Fig.4 Surface elevation η at station C and pressure p acting on seawall

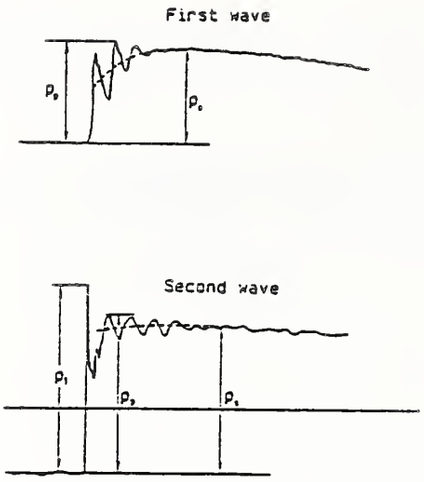

Fig.5 Magnification of pressure signal at 6.3m below still water level

of the leading bore after the overlapping. At the front of the caisson, the reflected bore is to be superimposed on the incident bore without any time difference. Therefore, in the records of pressure, no separation of incident and reflected bores is noticed.

The height of incident bore disregarding undulations is defined as the height from the water level directly before its arrival. As the first bore propagates on a still water, the height a_1 is the height from the still water level. The second bore, however, comes when the water level is extremely lowered by the ebb of the first wave. The difference between the water level and the still water level is represented as Δh_1 ($\Delta h_1 < 0$) and the height a_2 of the second bore is measured from the level Δh_1.

Figure 5 shows the magnified records of pressure measured at 6.3m below the still water level. They correspond to the bottom figure in Fig. 4. Similar to the water elevation, the fluctuations with short periods can be recognized. Especially, the impulsive pressure is generated at the second wave. The time of duration, however, is very short. Therefore, the net momentum of the impulsive pressure is not dominant for the stability of the caisson. Moreover, the impulsive pressure does not appear at the elevation 1.4m below the still water level and it can be thought that the impulsive pressure will act only on a part of the vertical wall. From the above consideration, the impulsive pressure is disregarded. The intensity of pressure due to the action of bore is defined as same way to the height of bore. In the figure, the maximum pressure except for the impulsive one is denoted by p_0, and the maximum pressure for the smoothed record disregarding the undulations is denoted by p_s. In this study, p_s is considered as the representative pressure for the action of bore. When the

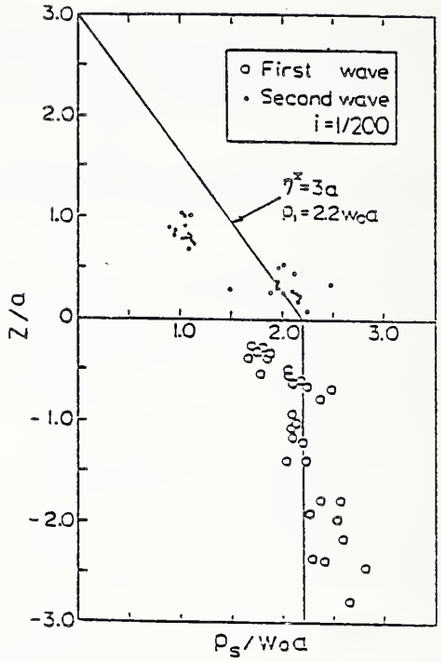

Fig.6 Vertical distribution of bore pressure

bore is accompanied by solitons, the relation $p_0=1.1p_s$ is obtained.

Figure 6 shows the pressure distribution, where w_0 is the specific weight of sea water, a is the height of incident bore and z is the height measured upward from the water level just before the oncoming bore (quasi still water). As the two points of measurement locate below the initial still water level, the data for the first wave distribute only in the negative region of z. For the second wave, on the other hand, all the data distribute in the positive region of z as the water level just before the second bore is lowered and the pressure sensors are exposed to the air. Although the data show some scatter in the figure, the pressure above the quasi still water level decreases as the relative height increases on the average. The pressure below the quasi still water level can be considered to be constant from the viewpoint of the total pressure, although the pressure slightly increases as the relative height decreases. The straight line is drawn by the method of the estimation which will be discussed in Chap. 4.

4. METHOD OF TSUNAMI FORCE ESTIMATION

From the experimental results obtained in Chap.3, the distribution of bore pressure acting on a vertical wall is proposed as shown in Fig. 7. The vertical distance η^* from the quasi still water level and the constant pressure p_1 can be expressed as

$$\eta^*=3.0a_I \quad \cdots\cdots(1)$$

$$p_1=2.2w_0a_I \quad \cdots\cdots(2)$$

where, a_I is the height of the incident bore above the quasi still water level. Notice that the quasi still water level here means that just before the oncoming bore. Therefore, for the second wave in the experiment the water level lowered due to the first ebb must be taken into consideration. When the quasi still water depths h_1 and h_2 before and behind the caisson differ, the difference of the hydrostatic pressure must be considered. In the case of the figure ($h_1 < h_2$), the resultant hydrostatic pressure facing to the offshore direction acts on the caisson. At the bottom of the caisson an uplift acts to the caisson such as $p_u=p_1$ at the edge of the caisson. The buoyancy must be corresponded to the volume just before the attack of the bore as shown in the figure.

The method in estimating a tsunami force presented here is the same as that for the non-breaking tsunami which has already been proposed[2] if the wave height H_I is applied to $2a_I$.

5. INVESTIGATION OF THE CAUSE OF DAMAGE

(1) Critical height of bore against sliding

Figure 8 shows some typical cross sections before the suffering. The cross sections of the damaged caissons are sections III and IV for which the rubble backing were not mounded. The caissons of the section III was slided even if the wave dissipating concrete blocks had been executed.

First of all, we examine that in what condition the sliding of the caisson occurs on the basis of the formula of tsunami force which has already been discussed in Chap. 4. In the investigation the quasi still water depths before and behind the caisson are assumed to be equal ($h_1=h_2$) even for the second wave because the ebb of the first wave continues for relatively long time. It is also assumed that the tsunami force is not affected by the existence of the wave dissipating concrete blocks, since the tsunami force resembles like a hydrostatic pressure. In this situation, the critical height a_c of the oncoming bore against sliding can be expressed as

$$a_c=\frac{\mu W_0+W_0'\tan(\theta+\phi)+1.1w_0h_c^{*2}/B}{\left(1+\frac{h_c^*}{h'}+\frac{\mu}{2}\frac{B}{h'}\right)\times 2.2w_0h'} \quad \cdots(3)$$

where, $h_c^*=\min\{h_c, 3.0a_c\}$, μ the friction coefficient between a caisson and a mound(=0.6), W_0 the weight of a caisson in sea water per unit length (tf/m), w_0 the specific weight of sea water (=1.03 tf/m^3), h_c the height of a caisson from the quasi still water level (m), h' the depth of the bottom of a caisson (m), B the width of a caisson (m), and $\min\{a,b\}$ represents the smaller value of a and b. The second term of the numerator in the right-hand side of Eq.(3) represents the resistance force R against sliding by the rubble backing, namely,

$$R=W_0'\tan(\theta+\phi) \quad \cdots(4)$$

where, W_0' is the total effective weight of the rubble backing above the sliding plane (tf/m), θ the inclination of the sliding plane in degrees, and ϕ is given by the following formula

$$\phi=\tan^{-1}\mu_2 \quad \cdots(5)$$

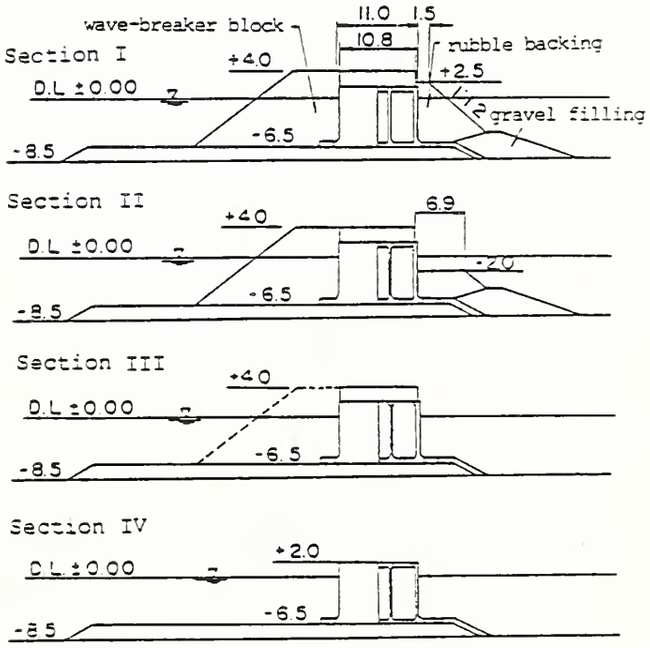

Fig.8 Cross sections of seawalls (under construction)

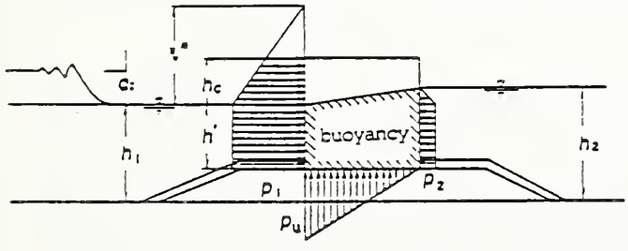

Fig.7 Distribution of tsunami force acting on a caisson

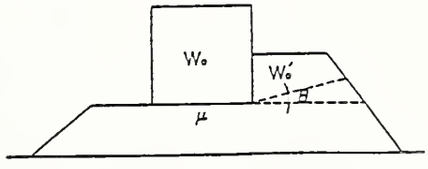

Fig.9 Sliding plane of rubble backing

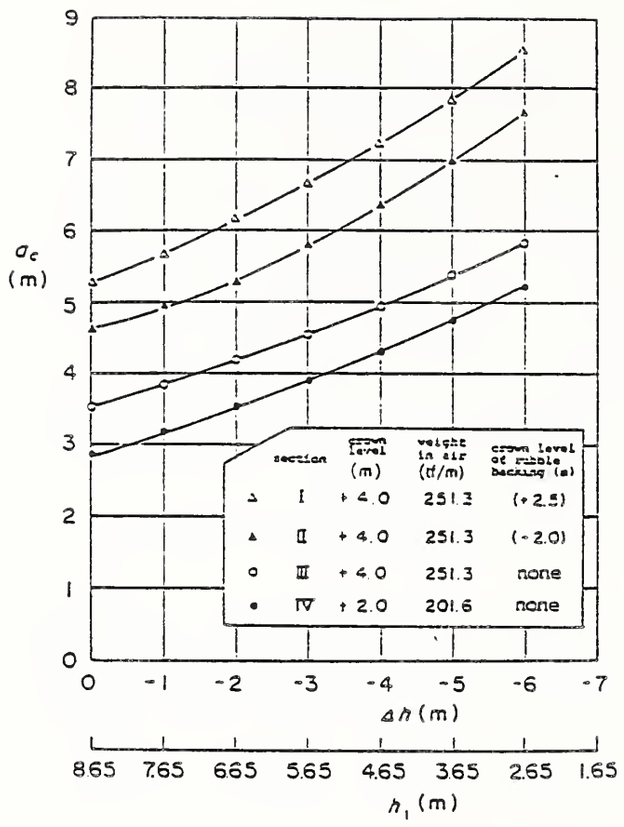

Fig.10 Critical wave height of tsunami for sliding

where, μ_2 is the friction coefficient between the stones (=0.8). Figure 9 shows the sliding plane through rubble backing. The resistance force against sliding in Eq.(4) is given as the minimum value of R for the various values of θ which is detected by the trial and error method. The minimum values for the section I and II in Fig. 8 were obtained when θ equals zero. The effective weight of the rubble backing is calculated by using the unit weights of 1.8 tf/m^3 and 1.0 tf/m^3 for the volumes above and below the water surface, respectively.

Figure 10 shows the calculated result of a_c for the section I~IV by using Eq.(3). In the calculation the astronomical tide level at the attack of tsunami is fixed at -0.15m and the quasi still water level just before the oncoming bore Δh is assumed in the range from zero to -6m (the negative sign represents the decrease of the water level). The weight of the caisson per unit length in air is 251.3 tf/m for the section I~III, and 201.6 tf/m for the section IV.

The critical heights a_c against sliding are 5.3m, 4.6m, 3.5m, and 2.9m for the sections I,II,III, and IV, respectively, when Δh=0. These are the minimum values and the critical height a_c increases as the quasi still water level decreases. The critical height against the overturning can be obtained from same manner, but it is larger than that against sliding. Therefore, the results for the overturning are not presented here.

(2) Inference of the damage condition

We now infer that in what condition the caissons were damaged by applying the results of the field investigation and the experimental study on run-up heights[3].

From the records of the tide gages, we can conclude that the period of the tsunami was about ten minutes. Although an ebb can be recognized at the beginning of the tsunami in the record of the tide gage in Noshiro Port, we regard that the tsunami started from the flood because the deviation of the ebb is very small of the order of 0.2m.

According to the field investigation, the run-up height at the coast around Noshiro Port was 6~7m except near the special topography such as the river mouth. The amplitude of the first tsunami at the offshore of 200m deep, which results in the run-up height of 6~7m on the coast, is deduced as 1.2~1.4m, on the basis of the experimental results, although they are not shown in this paper. As already described, the wave profile is greatly deformed when it propagates on a continental shelf. Again, on the basis of experimental results, the height of first oncoming bore at the water depth of 9m where the seawall exists can be estimated as 2.3~2.6m.

These heights are greater than 1.94m which is the height recorded at the tide station of Noshiro Port. In comparing these results, however, we must keep our mind on the difference of the height between inside and outside of harbor sheltered by breakwaters, the response characteristic of the tide gage well, and the effect of reflected waves. According to the theoretical considerations[5], it is estimated that the ratio of the tsunami heights between inside and outside of the harbor is about 0.5 and the damping ratio of the tide gage well is about 0.8 for the first wave. Consequently, the recorded tsunami height of 1.94m is converted into 4.9m as the height of tsunami outside the harbor. Since this height corresponds to the sum of the incident and reflected waves, the height of incident tsunami can be reasonably considered as the half of 4.9m, namely about 2.5m, which is nearly the same as the deduced height of the first bore mentioned above.

As to the second wave, we assume that the amplitude in the offshore is the same as the first one. This assumption is reasonable because of the results of the numerical calculation for the 1983 tsunami generation and propagation[5]. Then on the basis of the experimental results[4], the quasi still water level Δh lowered due to the ebb of the first wave and the height a_2 of the second bore can

be estimated for the range of the offshore amplitude from 1.2m to 1.4m as follows:

① $\Delta h = -5.2(m)$, $a_2 = 5.0(m)$,
and ② $\Delta h = -5.8(m)$, $a_2 = 6.0(m)$.

When these tsunamis attack the seawalls, their stability can be judged as

1) For the action of the first bore;

$\Delta h=0$, $a_1=2.3\sim2.6<a_c$(Section IV)$=2.9m$.

Therefore, any section is not slided.

2) For the action of the second bore ①;

$\Delta h=-5.2$, $a_2=5.0>a_c$(Section IV)$=4.9m$,
and $<a_c$(Section III)$=5.5m$.

Therefore, only the section IV is slided.

3) For the action of the second bore ②;

$\Delta h=-5.8$, $a_2=-6.0>a_c$(Section IV)$=5.1m$,
$>a_c$(Section III)$=5.8m$,
and $<a_c$(section II)$=7.5m$.

Therefore, the sections IV and III without rubble backing are slided, but section II with rubble backing is not slided.

In fact, the sections IV and III were slided. Therefore, it would be preferable to adopt the larger condition. It thus appears that the first bore of about 2.6m high attacked the seawalls but they were not slided. When the water surface fell down about 5.8m on account of the ebb by the first wave, the second bore of about 6.0m high attacked and the seawalls were damaged.

(3) Deformation of tsunami and its action against seawall under the damage condition

Deformation of the oncoming tsunami and the situation of the action to the seawall under the damage condition are presented below, although the tsunami height is slightly large comparing with the inferred damage condition. Figure 11 shows the water surface elevation measured at various stations without setting the model of the seawall. The water depth becomes shallow from the top of the figure which corresponds to the uniform depth (h=200m) to the bottom one (h = 0m) which corresponds to the shore. The first wave of the tsunami deforms and becomes bore as it propagates to the coast. The site of the seawall locates between the stations B(-8m) and C(-11.25m). At the station C which is slightly offshore from the seawall, the maximum water surface elevation of the first wave arises slightly behind the tip and the value is about 2.6m. At the station B which

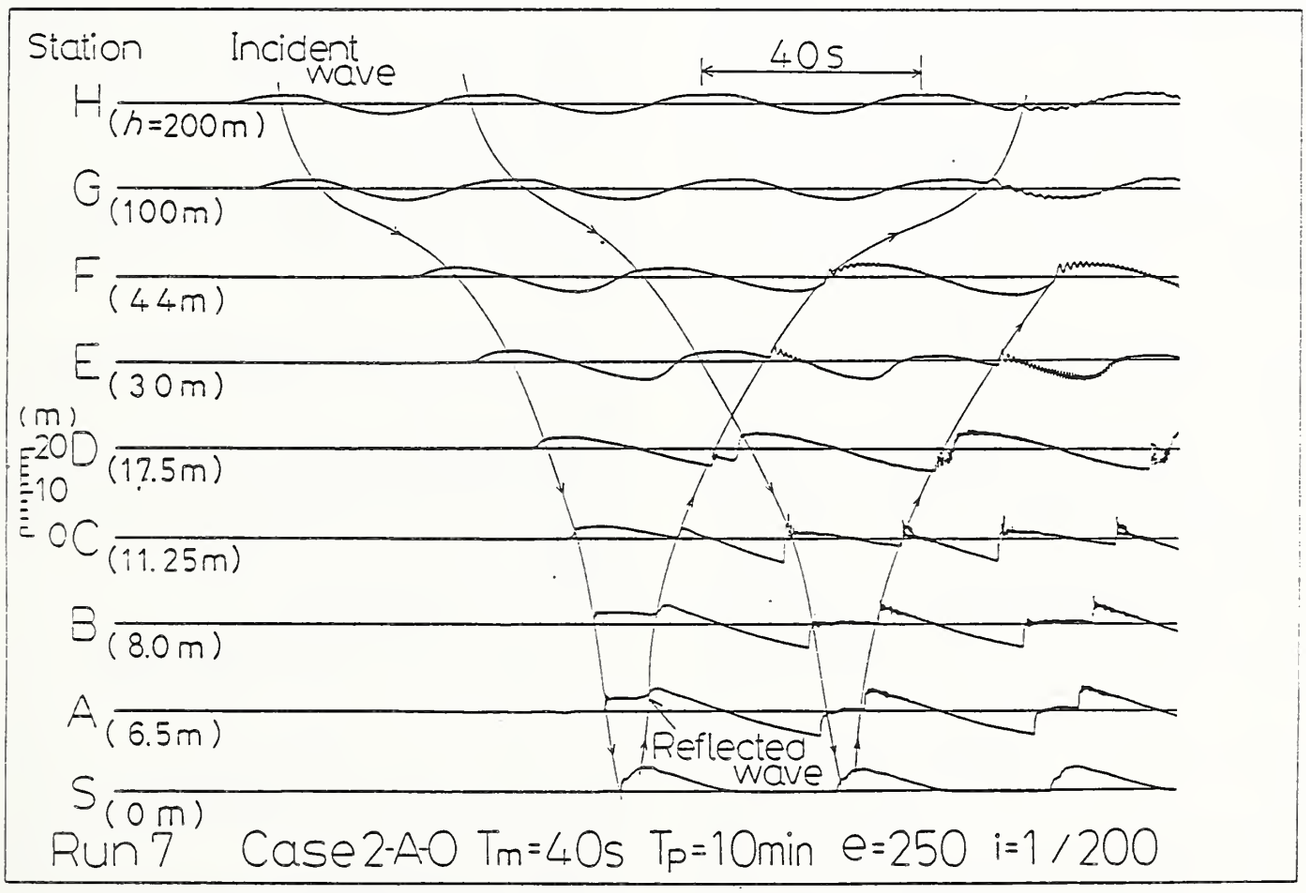

Fig.11 Water surface elevation (without seawall)

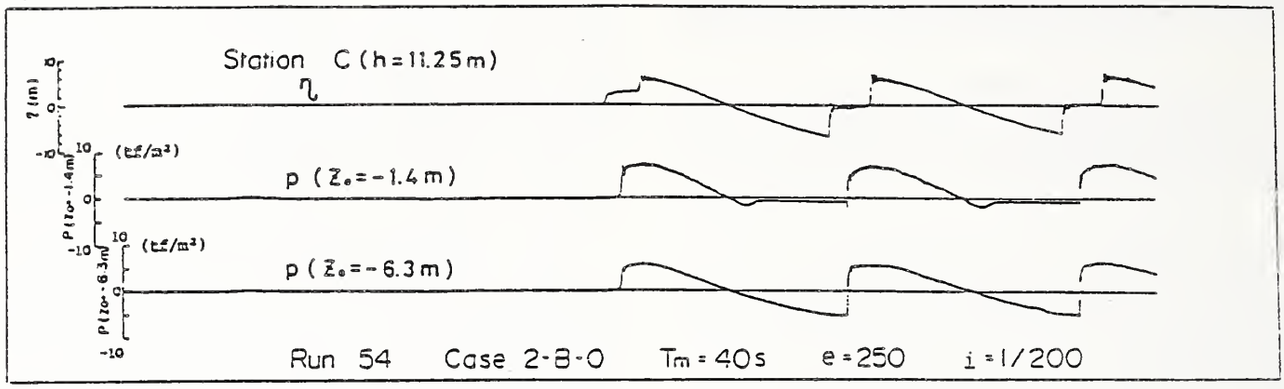

Fig.12 Water surface elevation before seawall and wave pressures acting on vertical wall

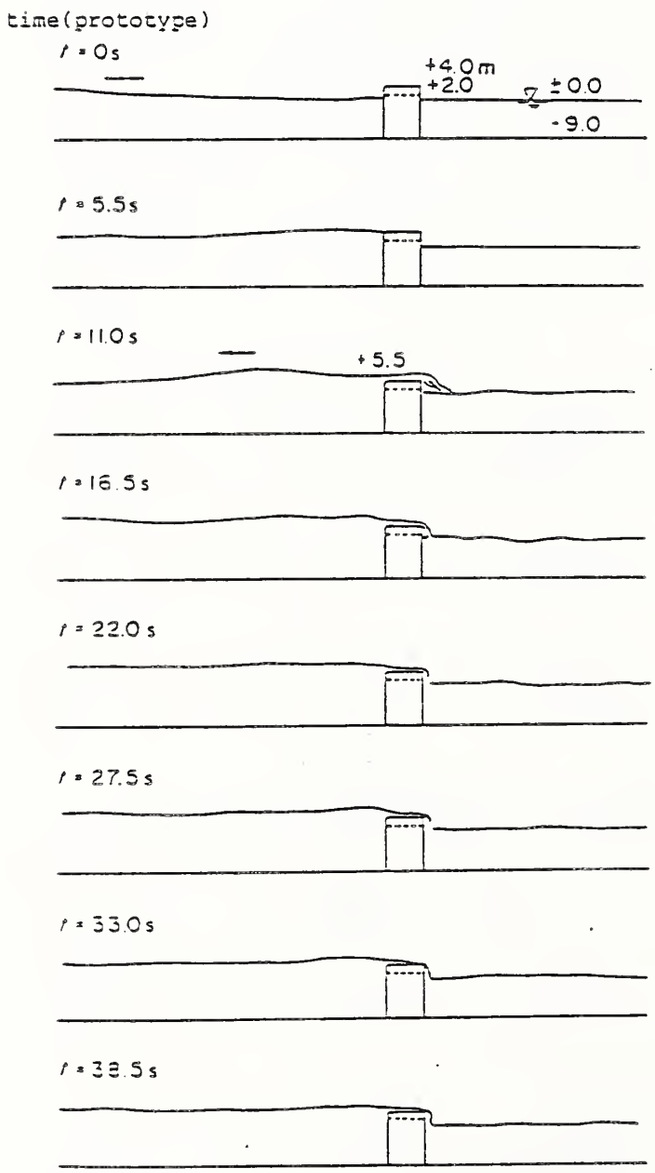

Fig.13 Action of first wave of tsunami on seawall

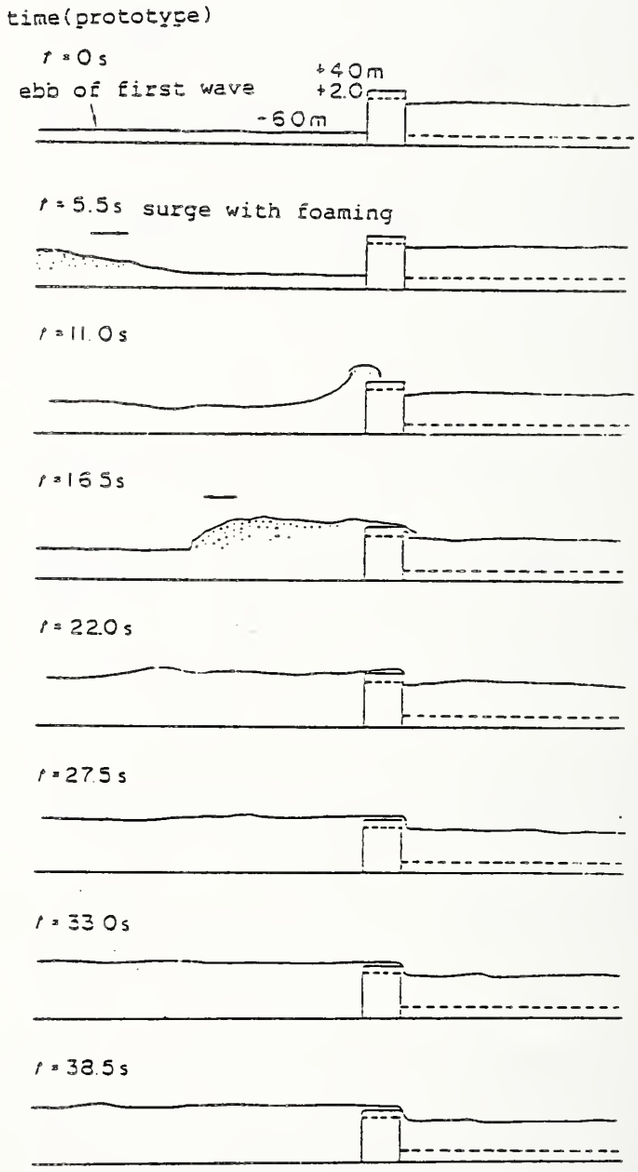

Fig.14 Action of second wave of tsunami on seawall

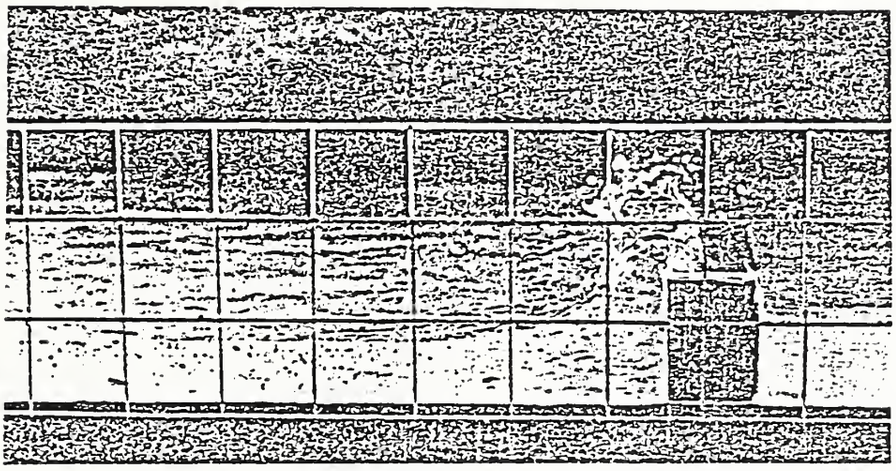

Photo 1 Attack of second bore on seawall

is slightly onshore from the seawall, the small undulations can be recognized at the tip of the first wave. The amplitudes, however, are rather small and the maximum water elevation is about 2.7m.

The second wave at the site of seawall comes out as a distinguished bore when the water surface is extremely lowered by the ebb of the first wave. The lowered water surface level at the station C just before the attack of the second bore is about 5.4m, and 5.2m at the station B. In the record of the second bore, remarkable undulations can be recognized especially at the station C. Among them the second wave is the largest and the wave height is 6m. After the smoothing of the undulations the maximum height of the bore can be read as 6.6m. On the other hand, the amplitudes of undulations at the station B are small and the maximum wave height is only about 1.4m. The maximum height of the bore obtained from the smoothed record of surface elevation is about 5.6m.

Figure 12 shows the water surface elevation at the station C and pressure records measured at the vertical wall when the seawall is settled at the water depth of 9.0m. Comparing with Fig. 11, the reflected waves appear earlier because of the existence of the wall. Therefore, it is slightly difficult to distinguish the incident and reflected waves. If we read the heights of oncoming bore from the record before the reflected bores, the height of the first bore is 2.8m, the lowered water surface level is 7.2m just before the arrival of the second bore, and the smoothed height of the second bore is about 6.5m. If we compare this result with that without the seawall, the bore heights are nearly the same, but the decrease of the water surface just before the second bore is greater when the seawall exists. The reasons are that the formation of a clapotis becomes remarkable by the existence of a vertical wall and the point of measurement is located near the loop.

The above discussion corresponds to the situation that the vertical wall has infinite length. Actually, the length is finite and as the wave length of a tsunami can be considered to be very long, the water surface would not be lowered as in the experiment. Namely, the actual reduction of the water surface can be considered as to exist between that of two cases with and without vertical wall.

Taking the above discussion into consideration, the reduction of the surface water level Δh just before the attack of the second bore in the estimation of the damage state was given as the average of the two.

The large undulations can be recognized at the second bore in the case without the seawall, but they are not remarkable in the case with the seawall. Although the undulations can also be recognized for the pressure, the amplitudes of them are small. The maximum pressure arises some time later from the collision in this case.

Figures 13 and 14 show the situation of the attack of the first and the second waves to the seawall, which are illustrated from the successive photos taken by a motor-driven camera. The time is converted to the prototype value. The overtopping to +4.0m crown level is started within 10 seconds after the oncoming first bore is noticed around the location of 50m in front of the seawall. The height of the overtopping above the crown level is from 1.0m to 1.5m and continues for relatively long time. If the crown level was +2.0m, it would be from 3.0m to 3.5m.

The action of the second wave to the seawall is more rapid and severe. The time interval from the detection of the oncoming bore with foaming around the location of about 50m in front of the seawall to the commencement of overtopping is only 6 seconds. Moreover, the remarkable feature is that the overtopping abruptly happens from the extremely lowered

water level by the ebb of the first wave. At the very initial stage of the action, a relatively high green water is produced (Photo 1). The succeeding overtopping height is, however, not so high of the order of 1.0m above the crown level of +4.0m.

The situation of the attack of the bore-type tsunami on the seawall has been described based on the experimental investigations. Although the cross section and the water depth in the experiments are slightly different from the actual seawall for a reclaimed land of Noshiro Electric Power Plant, the situation is nearly the same. In the experiment, the water surface level behind the seawall at the attack of the second bore is nearly equal to the initial still water level, because the overtopped water cannot return to the offshore side. However, the actual water level behind the seawall would drop considerably comparing with the experiment.

6. SUMMARY

We have described the investigation on the damage of the seawall which was under construction for a future reclaimed land at the outside of Noshiro Port.

In the first place, experiments were conducted to investigate the situation of the attack by the bore-type tsunami and pressures distribution of the tsunami. A formula in estimating the tsunami pressure acting on a vertical wall was obtained.

From the experimental results and the field survey, it appeared that the first bore of about 2.6m high attacked the seawall but it was not slided, and when the water surface was fell down about 5.8m on account of the ebb by the first wave, the second bore of about 6.0m high attacked and the seawall was damaged at last. One of the remarkable features of the bore-type tsunami is that the time variation is extremely rapid. For example, the second bore attacks when the water level is greatly decreased by the ebb of the first wave and shows an abrupt change such that the overtopping begins only within 6 seconds after the detection of the oncoming bore around the locations of about 50m in front of the seawall. Therefore, caissons of the seawall were slided and damaged on account of the great difference of the water levels between before and behind the seawall, because sufficient amount of water could not enter behind the seawall due to the short time.

This paper is revised from that presented in the Proceedings of the 31st Japanese Conference on Coastal Engineering, 1984.

REFERENCES

1) Fukui, Y. et al.: Investigation on tsunami (II), Proc. 9th Japan Conf. Coast. Eng., pp.50~54, 1962, (in Japanese).
2) Tanimoto, K.: On the hydraulic aspects of tsunami breakwaters in Japan, Proc. Int. Tsunami Symp., 1981, IUGG Tsunami Commision, pp.423~435, 1983.
3) Tanimito, K. et al.: Field and laboratory investigations of the tsunami caused by 1983 Nihonkai Chubu Earthquake, Tech. Note Port and Harbour Res. Inst., No.470, 299p., 1983, (in Japanese).
4) Tsuruya, H. et al.: Experimental study on the deformation and run-up of tsunami in shallow water, Proc. 31st Japan. Conf. Coast. Eng., pp.237~241, 1984, (in Japanese).
5) Tanimoto, K. et al.: Field survey and some investigations on the tsunami damage produced by 1983 Nihonkai Chubu Earthquake, Proc. 31st Japan. Conf. Coast. Eng., pp.252~256, 1984, (in Japanese).
6) Tanimoto, K. et al.: Experimental study on tsunami force and investigations of the cause of seawall damages during 1983 Nihonkai Chubu Earthquake, Proc. 31st Japan. Conf. Coast. Eng., pp.257~261, 1984, (in Japanese).

A Summary of the Tsunami History of the United States

BY

Herbert Meyers[1], P. A. Lockridge, and J. F. Lander

ABSTRACT

The National Geophysical Data Center is reviewing its global digital file of available tsunami data for the first time with the ultimate goal of presenting U.S. data in a unified catalog. While some of these data have appeared in separate catalogs in the past, the unified catalog will allow the special characteristics of tsunamis in Alaska, Hawaii, and the West Coast states to be described and compared. Some of the early findings indicate that Alaska is primarily a tsunami-generating region and receives almost no impact from tsunamis generated elsewhere. Hawaii and the West Coast are primarily tsunami-receiving regions and have had little impact from tsunamis generated by local earthquakes. Most of the damage and fatalities from tsunamis in Hawaii in historical times resulted from a single event, the 1946 tsunami originating in the Aleutians. Similarly the most destructive tsunami for both Alaska and the West Coast was the 1964 Gulf of Alaska tsunami.

KEYWORDS: Alaska; Hawaii; Tsunami; West Coast

1. INTRODUCTION

"Tsunami" is customarily defined as a series of waves generated by an impulsive disturbance in the ocean. The definition includes water waves produced by ocean-bottom displacement from earthquakes, landslides, or volcanoes. The National Geophysical Data Center (NGDC) located in Boulder, Colorado is in the process of compiling and reviewing all available data about tsunamis from local or remote sources which have affected the U.S. NGDC's effort in compiling tsunami data is complemented by the efforts of two other components within the National Oceanic and Atmospheric Administration: the Pacific Marine Environmental Laboratory, a research institution; and the National Weather Service, which operates the Pacific and Alaska Tsunami Warning Centers. The following tsunami parameters are included in the tsunami data base at NGDC: (1) information about the cause (e.g., volcanic, earthquake, landslide), location of source, depth and magnitude of earthquake where appropriate, and (2) information about the effects of the tsunami including maximum runup height, tsunami magnitude or intensity[2], local runup, damage, deaths, arrival time, and travel time for each location experiencing the tsunami.

2. SIGNIFICANT FACTS FOR ALASKAN TSUNAMIS

The Gulf of Alaska and the eastern and central Aleutians provide perfect geologic conditions for tsunami generation. The Pacific sea-floor underthrusts the Alaska gulf and peninsula and east and central Aleutian Islands producing large magnitude thrust earthquakes - the kind most frequently associated with tsunami generation. Alaska, like other U.S. coastal areas prone to tsunami damage, has a relatively short and incomplete history. Although reports span 200 years (1788 to present), the record is probably incomplete up to 1900 or later due to low population density in many areas and lack of written tradition by the inhabitants (native Americans, trappers, fishermen).

Since 1788, 34 tsunamis have been reported in the Alaska-Aleutian region. At least six of these tsunamis were caused by landslides in the bays of southeastern Alaska (Lituya and Yakutat Bays). Deep fiords with steep sided glacier valleys and active glaciers make these bays dangerous source areas of giant local tsunamis. These landslides have produced huge waves hundreds of meters high. Three tsunami events in the eastern and central Aleutians have been connected to volcanic eruptions in the area. Table 1 lists the 13 events that are classified as destructive. All of them were caused by local earthquakes. Note that the most significant number of fatalities and damage is from the 1964 tsunami (see Fig. 1).

[2]Tsunami magnitude is defined by Cox and others (1967) as $m = \log_2 H$ where H is the maximum runup height in meters. Tsunami intensity is defined by Solov'ev and Go (1974) as $I = \log_2 \sqrt{2} H$. Maximum runup height is maximum water height above sea level for an event. Local runup is maximum water height above sea level at a specific location for an event.

[1]Chief, Solid Earth Geophysics Division, NOAA, National Geophysical Data Center, 325 Broadway, Boulder, Colorado 80303

More than one-third of the 27 local earthquakes of magnitude 7.5 and greater produced tsunamis in Alaska although most of them had runups of less than one meter (see Fig. 2). Figure 3 shows that although Alaska has had some very destructive events, there are greater risks in other regions of the Pacific such as Japan, South America and Southeast Asia. However, Figure 4 shows that a greater percentage of Alaskan earthquakes above 7.5 result in tsunamis than in other regions except for the west coast of South America. Alaska has experienced relatively little effect from tsunamis generated elsewhere in the Pacific Basin. For example, Alaska has experienced tsunamis from six earthquakes near Japan, but the runups were very small (see Fig. 5). The largest amplitude from such a remotely generated tsunami was 1.8 meters recorded at Attu from the 1960 Chile tsunami.

Of the thirteen destructive tsunamis recorded in Alaska, a few have generated massive tsunamis in the Pacific Basin and have produced extensive damage outside Alaska, particularly in Canada, Hawaii and on the west coast of the United States. Historically, Alaskan tsunamis have not produced damaging waves in Japan, but western Aleutian earthquakes are a potential threat. A summary of the damage that occurred outside the United States from Alaskan tsunamis is shown in table 2. The April 1, 1946 tsunami, generated in the east Aleutian Islands, produced some damage to boats and harbor areas in Chile. The Central Aleutian Island tsunami of Mar. 9, 1957 caused minor damage in El Salvador; and reportedly damaged boats and houses on N.E. Honshu Island, Japan. The Mar. 27, 1964 tsunami, that originated in the Gulf of Alaska, caused $10 million damage in British Columbia, Canada, and caused damage to the oyster and pearl harvest on the Sanriku coast of Japan. Figure 6 shows the locations throughout the Pacific Basin that recorded the 1964 event.

Alaska has significant risks from earthquake generated tsunamis, and from those generated by volcanoes, landslides and icefalls. When seismic gaps are closed by large earthquakes in the Gulf of Alaska, along the Alaskan Peninsula, and in the central Aleutians, massive destructive tsunamis may be generated. This area also has the most apparent potential for producing damaging tsunamis on the West Coast of the United States.

3. SIGNIFICANT FACTS FOR HAWAIIAN TSUNAMIS

The earliest recorded tsunami in Hawaii occurred in 1813. Since that date more than 70 tsunamis have been observed in Hawaii. The Hawaiian record is essentially as complete as possible back to 1837. Unlike other regions of the Pacific, Hawaii receives most of its tsunami damage from distant earthquakes. Hawaii is positioned over a "hot spot" that lies beneath the Pacific plate. The volcanism that is responsible for the formation of the islands themselves is also responsible for the earthquakes that occur there. These smaller magnitude quakes (only one event recorded a magnitude greater than 7.0) are not of the type that produce large tsunamis. In the last 100 years there have been only seven tsunamis produced by local earthquakes, two of which have caused damage. Local earthquakes constitute only a minor tsunami risk (48 deaths) in comparison to tsunamis generated by distant earthquakes (239 deaths).

Hawaii has received tsunami damage from 15 distant earthquakes. At least 63 such other tsunamis generated in every quadrant of the Pacific Basin have been recorded or observed in Hawaii (Fig. 7). Eleven of these have achieved the maximum runup recorded outside their generating areas as they rolled up on the shores of the islands in Hawaii. Figure 8 indicates the maximum runup height recorded in Hawaii from tsunamis generated in regions throughout the Pacific. For example, Hawaii has experienced 12 tsunamis from earthquakes near Japan. The largest runup was 9 meters. However, there are greater risks to Hawaii from earthquakes near Chile or Alaska. Only tsunamis generated in the southwest Pacific whose energy is confined by island chains and the small tsunamis generated along the coasts of North and Central America have not caused damage in Hawaii. Earthquakes near Alaska, Chile and Kamchatka have caused tsunami fatalities in Hawaii. Property losses resulting from tsunamis in Hawaii have been extensive and nearly 400 people have lost their lives. The most damaging events were the April 1946 (see Fig.9) Aleutian event and the May 1960 Chile event (Table 3). Of all the Pacific regions, Hawaii is clearly the most vulnerable to tsunami damage from outside sources.

4. SIGNIFICANT FACTS FOR WEST COAST TSUNAMIS

The Pacific Coast of the United States lies along a plate boundary. However, the Pacific plate is not being subducted beneath the continental plate as in the areas of Alaska, the Aleutians, and South America. Instead the two plates are sliding past each other in a complex system of faults, the most famous of which is the San Andreas Fault. The epicenters of most earthquakes lie on land. For these reasons, the earthquakes on the Pacific Coast of the United States do not produce tsunamis large enough to travel across the ocean basin and be recorded elsewhere. However, the historical records for this area indicate that several earthquakes have produced local tsunamis.

Among the Pacific coast states, California has experienced the greatest number of tsunami events, and is the only one to have had local tsunamigenic (tsunami generating) earthquakes. There were at least 12 incidents of unusual sea movement and flooding related to local earthquakes in the 1800's. The validity of most of these reports is questionable. Destructive

local tsunamis have not been generated in the last one hundred years on the west coast of the United States. The major earthquakes of this century in California have generated only small tsunamis.

There were seven events which caused damage on the west coast of the U.S. (see Table 4). Five of these were remotely-generated tsunamis that caused more that $485 million (in 1980 dollars) in property damage and 16 deaths on the west coast. These events include: the tsunami produced by the Kamchatka earthquake of November 4, 1952 that damaged fishing boats and the harbor at Crescent City; the March 9, 1957 tsunami generated in the Aleutian Islands that smashed ships and damaged docks in San Diego Bay; a magnitude 8.6 earthquake off the coast of Chile on May 22, 1960 that caused damage in Crescent City; the most damaging event by far, the March 28, 1964 tsunami generated in the Gulf of Alaska that caused extensive damage on the coasts of Washington and northern California (see Fig. 10) and the November 1975 tsunami generated by an earthquake in Hawaii that caused minor damage to Catalina Island, California.

Figure 11 shows the maximum runup height in meters recorded on the U.S. West Coast from tsunamis generated in other regions. For example, there were 6 tsunamis reaching the west coast of the U.S. from earthquakes near Japan. None of these produced high runups. There are greater risks to the U.S. west coast from events in Alaska and Chile.

On the east coast of the United States only Puerto Rico and the Virgin Islands have recorded damaging tsunami events. Five tsunamis have been reported there. The event in 1918 killed more than 40 people and caused destruction in Aguadilla, Mayaguez, and Punta Agujereada where the runup reached 6 meters. A tsunami in 1868 in the Virgin Islands killed at least 7 people and did extensive damage to ports and shipping.

5. SUMMARY

A summary of the available data for tsunamis on the shores of the United States is given in table 7. There have been at least 600 deaths and more than $500 million in damage in the past 200 years. Historical records of tsunami events are valuable because they indicate the areas most likely to spawn tsunamis, the size of the earthquakes most likely to generate tsunamis in these areas, and areas most likely to incur the heaviest amounts of damage from tsunamis once they are generated.

Figure 1. Tsunami damage to Seward port facilities from the tsunami of March 27, 1964. The event resulted in more than $280 million (in 1980 dollars) in property damage to Alaska, California, and Hawaii.

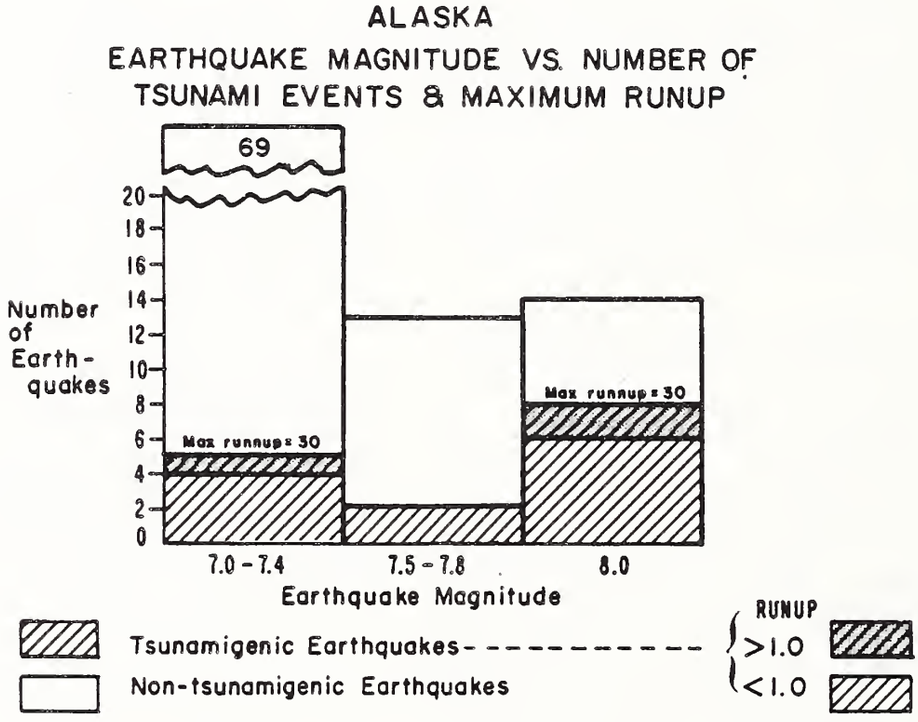

Figure 2. Number of earthquake events of various magnitudes generated on the Alaska coast, number of tsunami events produced by these earthquakes, and maximum runup recorded for events in each magnitude range.

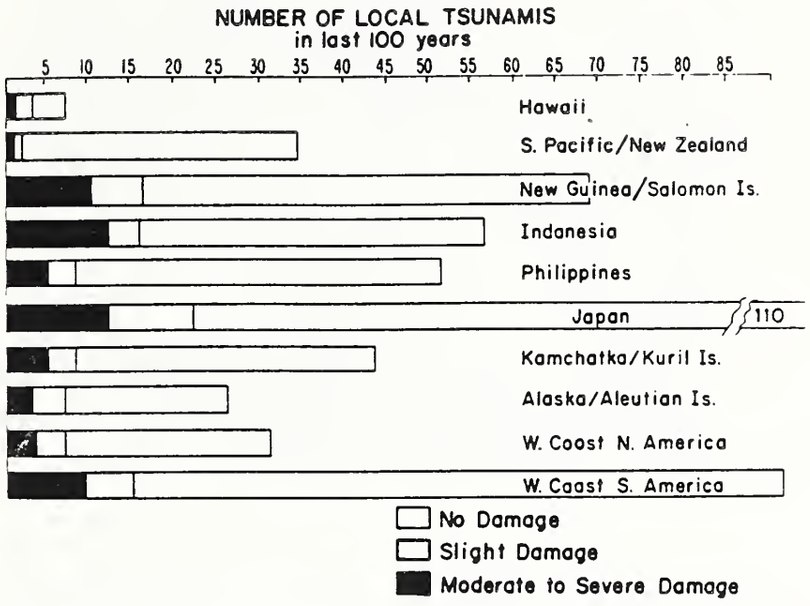

Figure 3. Comparison of the total number of undamaging events, the total number of damaging events, and the number of events that caused at least moderate damage.

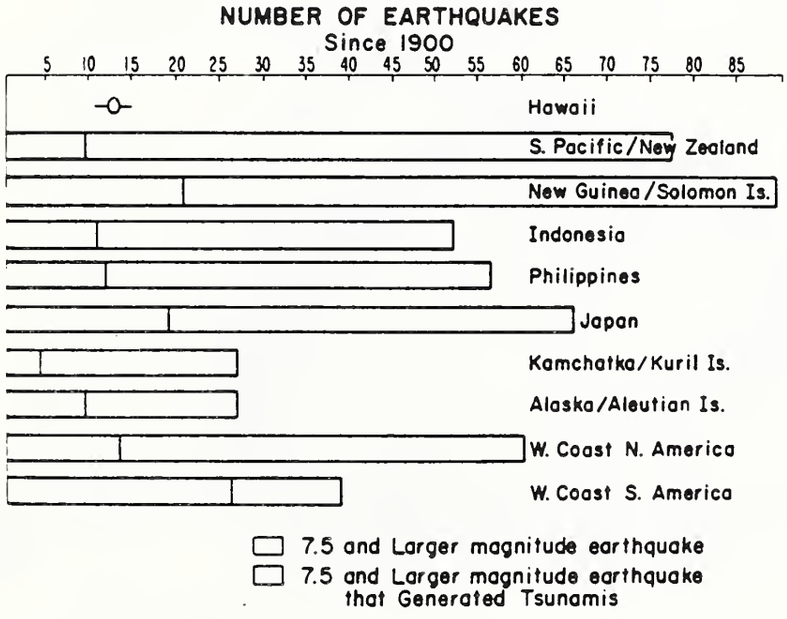

Figure 4. Numbers of earthquakes of magnitude greater than or equal to 7.5 that occurred in each region and number that generated tsunamis in each region.

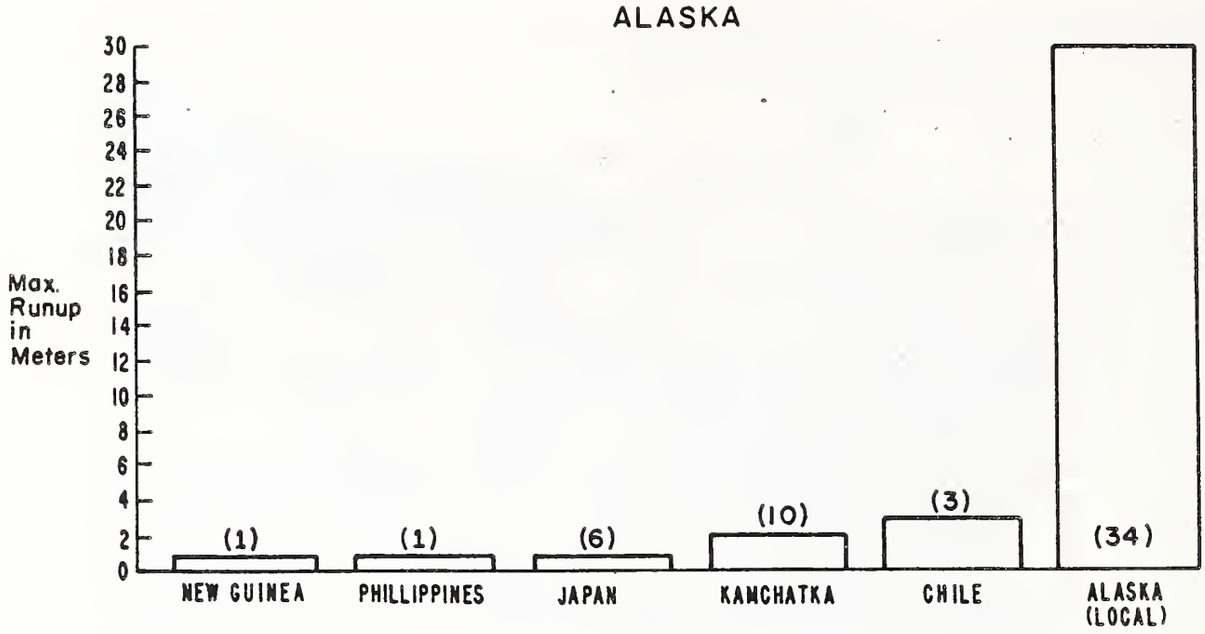

Figure 5. Maximum runup in meters produced on the coasts of Alaska by tsunamis generated in other regions. Numbers in parentheses are total numbers of earthquakes in each source region that generated runups in Alaska.

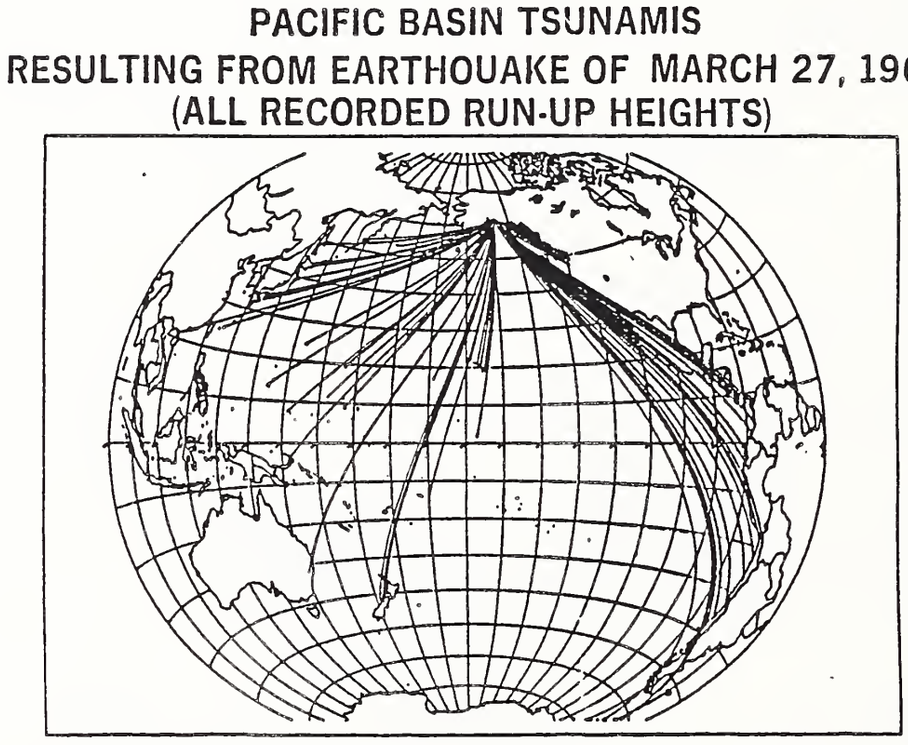

Figure 6. Pacific Basin tsunamis resulting from earthquake of March 27, 1964 (all recorded run-up heights).

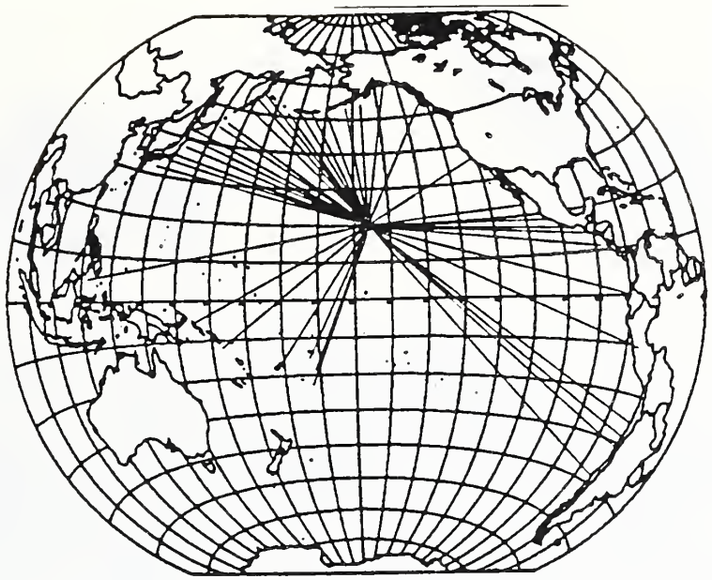

Figure 7. Tsunamis recorded in Hawaii, 1900-1983.

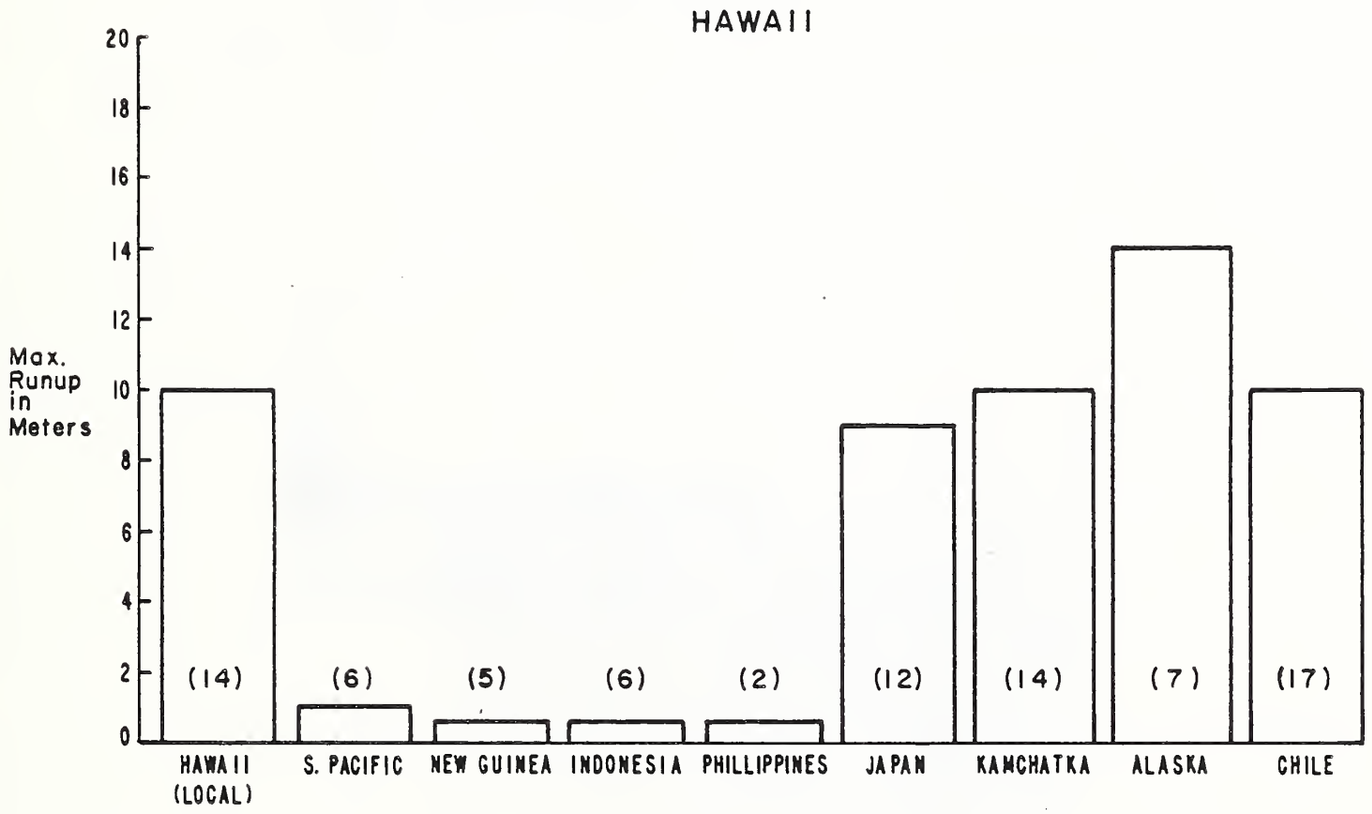

Figure 8. Maximum runup in meters produced on the coasts of Hawaii by tsunamis generated in various source regions of the Pacific Ocean Basin. Numbers in parentheses are total numbers of earthquakes in each source region that generated runups in Hawaii.

Figure 9. A major wave generated by the earthquake of April 1, 1946 in the Aleutian Islands striking the beachfront area at Hilo.

Figure 10a. View of normal conditions at intersection in Crescent City, California.

Figure 10b. View of same area as above showing the damage produced by the tsunami generated by the earthquake of March 27, 1964 in the Gulf of Alaska.

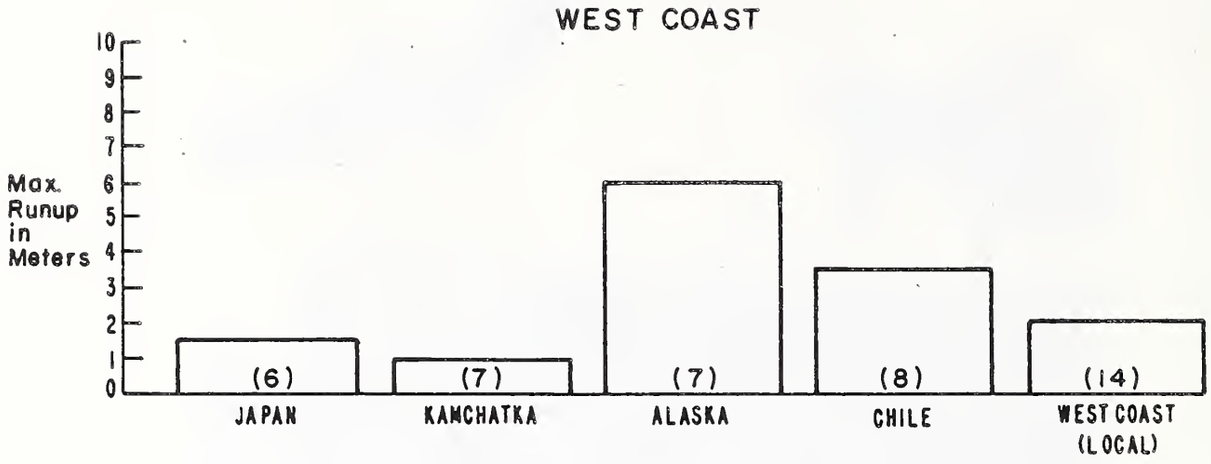

Figure 11. Maximum runup in meters produced on the West Coast of the United States by tsunamis generated in various source regions of the Pacific Ocean Basin. Numbers in parentheses are total numbers of earthquakes in each source region that generated runups on the West Coast.

TABLE 1

SUMMARY OF TSUNAMI DAMAGE IN ALASKA

CAUSE	EVENT DATE	SOURCE REGION	LOCATION OF EFFECT	DAMAGE
T	1788 07 22	GULF OF ALASKA	SHUMAGIN, UNGA AND KODIAK IS.	FLOODING, BUILDINGS WASHED AWAY (SOME)*
L	1845 00 00	GULF OF ALASKA	YAKUTAT BAY	WAVE CAUSED BY GLACIER COLLAPSE (100)
L	1853 00 00	S. ALASKA	LITUYA BAY	(8 CANOES FILLED WITH PEOPLE PERISHED)
T	1878 08 29	E. ALEUTIAN IS.	MAKUSHIN, UNALASKA	VILLAGE DESTROYED
V	1883 10 06	ALASKAN PENINSULA	PORT GRAHAM	FLOODED HOUSES, SHIPS RUN AGROUND
T&L	1899 09 10	GULF OF ALASKA	YAKATAT BAY	SAWMILL DAMAGED, HUTS FLOODED
T	1925 02 23	GULF OF ALASKA	VALDEZ	BOARDWALK TORN UP BY WAVE
L	1936 10 27	S. ALASKA	LITUYA BAY	TWO SMALL BLDGS. DESTROYED
T	1946 04 01	E. ALEUTIAN ISLANDS	UNIMAK IS., ALEUTIAN IS	LIGHTHOUSE DESTROYED (5)
T	1957 03 09	CENTRAL ALEUTIAN IS.	ADAK, UNIMAK, ISLANDS	STRUCTURES, BRIDGES, MOORAGES DESTROYED
T&L	1958 07 09	S. ALASKA	GILBERT INLET, LITUYA BAY	500-M WAVE CAUSED BY LANDSLIDE (2)
T	1964 03 27	GULF OF ALASKA	TOTAL FOR ALL OF ALASKA	$84 MILLION (107)
T	1965 02 03	W. ALEUTIAN ISLANDS	SHEMYA ISLAND	WAREHOUSE, ROAD FLOODED

* Number of deaths in parentheses

Cause Codes
T = tectonic
L = landslide
V = volcano

TABLE 2

DAMAGING EFFECTS OF ALASKAN TSUNAMIS ON AREAS OUTSIDE THE UNITED STATES

EVENT DATE	SOURCE REGION	LOCATION OF EFFECT	DAMAGE
1946 04 01	E. ALEUTIAN ISLANDS	IQUIQUE, ISLA JAUN FERNANDEZ, CHILE	BOATS DAMAGED
1957 03 09	CENTRAL ALEUTIAN IS.	LA UNION, EL SALVADOR	MINOR DAMAGE
		HAKODATE, KUSHIRO, NE. HONSHU, JAPAN	143 HOUSES, 35 BOATS DESTROYED
1964 03 27	GULF OF ALASKA	BRITISH COLUMBIA, CANADA	$10 MILLION DAMAGE
		MISHO, EHIME, SANRIKU, JAPAN	DAMAGE TO PEARL HARVEST
1965 02 03	W. ALEUTIAN ISLANDS	SANRIKU, TOHOKU DIST., WAKAYAMA JAPAN	FLOODING, DAMAGE TO PEARL RAFT

TABLE 3

SUMMARY OF TSUNAMI DAMAGE IN HAWAII

EVENT DATE	SOURCE REGION	LOCATION OF EFFECT	DAMAGE
1835 02 20	SC.CHILE	KAUAI	MODERATE
1837 11 07	S. CHILE	MAUI, HAWAII	174 HOUSES DESTROYED (62)*
1860 12 01	HAWAII	MAUI	WHARF AND HUTS DESTROYED (FEW)
1868 04 02	HAWAII	HAWAII	6 TOWNS DESTROYED (81)
1868 08 13	PERU-N. CHILE	MAUI, HAWAII	SEVERE
1868 10 01	KAHAULOO, PUNA, HAWAII	HAWAII	CHURCH, HOUSES, FLOODED
1869 07 24	HAWAII	HAWAII	HOUSES, SEA BARRIERS DESTROYED
1877 05 09	N. CHILE	HAWAII	$14,000 (5)
1878 01 20	HAWAII	MAUI, OAHU	HOUSES DESTROYED
1901 08 10	SANRIKU, JAPAN	HAWAII	MINOR
1903 11 29	HAWAII	HAWAII	HOUSES WASHED AWAY
1906 08 16	S. CENTRAL CHILE	HAWAII, MAUI	WHARVES DAMAGED
1918 09 08	S. KURIL ISLANDS, USSR	HAWAII	MINOR
1922 11 10	N. CHILE	HAWAII	MINOR
1923 02 04	KAMCHATKA PEN., USSR	HAWAII, MAUI	MORE THAN $1.5 MILLION (1)
1933 03 03	SANRIKU, JAPAN	HAWAII	SOME
1946 04 01	E. ALEUTIAN ISLANDS	HAWAII,OAHU,MOLOKAI,NIIHAU	$36 MILLION (173)
1952 11 05	KAMCHATKA PEN. USSR	OAHU, MAUI, KAUAI, HAWAII	$1 MILLION
1957 03 09	CENTRAL ALEUTIAN IS.	KAUAI, OAHU, MAUI, HAWAII	MORE THAN $8 MILLION
1960 05 22	S. CHILE	ALL OF HAWAII	$75 MILLION (61)
1964 03 27	GULF OF ALASKA	HAWAII, MAUI	$68,000
1975 11 29	HAWAII	HAWAII	$1.5 MILLION (2)

* Number of deaths in parentheses

TABLE 4

SUMMARY OF TSUNAMI DAMAGE ON THE WEST COAST OF THE UNITED STATES

EVENT DATE	SOURCE REGION	LOCATION OF EFFECT	DAMAGE
1812 12 21	S. CALIFORNIA, USA	SANTA BARBARA, CA	SHIP AT ANCHOR DAMAGED
1859 09 24	N. CALIFORNIA, USA	HALF MOON BAY, CA	SCHOONER DAMAGED
1946 04 01	E. ALEUTIAN ISLANDS	SANTA CRUZ, HALF MOON BAY, CA	MINOR DAMAGE (1)*
1957 03 09	CENTRAL ALEUTIAN IS.	LA JOLLA, SAN DIEGO, CA	MINOR DAMAGE
1960 05 22	S. CHILE	WEST COAST	$500,000 DAMAGE
1964 03 27	GULF OF ALASKA	WASHINGTON	$5 MILLION DAMAGE
		OREGON	$0.6 MILLION DAMAGE (4)
		CALIFORNIA	$10.9 MILLION DAMAGE (11)
1975 11 29	HAWAII	CATALINA I., CA	$2,000 DAMAGE

* Number of deaths in parentheses

TABLE 5

SUMMARY OF U.S. TSUNAMIS

	U.S. EVENTS	NON-U.S. EVENTS
EARLIEST OBSERVATION:	1788	1811
TOTAL TSUNAMIS:	63	98
TOTAL TSUNAMIS WITH RUNUP GREATER THAN 1.0 M:	23	19
TOTAL DAMAGING TSUNAMIS:	26	13
TOTAL DEATHS:	>490	130
TOTAL ESTAMATED DAMAGE IN MILLIONS OF U.S. 1980 DOLLARS:	>$480	>$80

An Estimation of Tsunami Generated by Submarine Landslide

by

Sin-Iti Iwasaki[1] & Hiroshi Takahashi[2]

ABSTRACT

On the estimation of heights of tsunamis generated by landslides, the following was found through the laboratory experiment, numerical computaions and linear theory.

(1) In case of tsunamis generated by submarine landslides the maximum wave generating efficiency (wave energy generated by landslides / potential energy loss in the water or the initial potential energy (net. submerged) of the sliding body) is about 10%.

(2) In case of tsunamis due to landslides plunging into the water surface, 8 to 15% of kinematic energy of the sliding body is transformed into the wave energy. And, as indicated (1), about 10% of the potential energy lost in the water is added to the wave energy.

KEY WORDS : efficiency, landslide, tsunami

1. INTRODUCTION

The main cause of tsunamis is submarine earthquakes, but, other causes, landslides and volcanic eruptions, are also thought to generate tsunamis. Especially, submarine landslide-induced tsunamis are not accompanied with so-called foreshocks as in the case of earthquakes and volcanic eruptions. And, tsunamis generated by landslides plunging into the water body can occur inland lakes and reservoirs where normally considered to be safe for such a disasterous giant water waves. Predicting the wave heights for various dimensions and speeds of the slides for site hazard evaluation purposes is of clearly importance.

On the estimation of heights of tsunamis generated by landslides, one of the bases is WIEGEL's(1955) laboratory experiment. One of the conclusions is " about 1% of the initial potential energy (net. submerged) is transformed into the wave energy. " Based on this conclusion, STRIEM&MILOH(1976) calculated the wave height assuming the generated wave is one-dimensional solitary wave. Their submarine landslide model is shown in Fig1. MURTY(1979), using same landslide model and wave system, also apllied WIEGEL's conclusion to the submarine landslide induced tsunami occured on April 27, 1975, in Kitimat Inlet, British Columbia, and showed good agreement with the observation. But, in calculating the solitary wave energy, MURTY commited simple mistake Inversely evaluated efficiency from the combination of the observational data and the correct solitary wave energy is32.2% This value is far from the WIEGEL's conclusion. It is suggested that WIEGEL's result could not be applied simply to all of the landslide-induced tsunami evaluation.

In this paper, both submerged and not submerged landslide induced tsunamis are investigated from the laboratory experiment, numerical computations and linear theory. And, an simple method for tsunami height estimation is presented.

2. RECONSTRUCTION OF THE WIEGEL'S EXPERIMENTAL DATA

The experimental set-up is shown in Fig. 2. Rectangular box allowed to fall freely and wave heights were measured at the sta. 1 and sta. 2. The width of the model basin was nearly equal to the width of the falling box The generated wave could be treated as one-dimensional wave. Parameters were the basin depth d, initial submergence Zo and box weight W. The range of parameters are shown in upper leftside in Fig. 3. In Fig. 3, the ordinate is the initial potential energy (net. submerged) of the falling box (PE) and the abscissa is generated wave enrgy(WE). WE was obtained by the equation (1) under the assumptions that the generated wave had deep water wave characteristics and the effect of dispersion was negligible at the sta. 1.

$$WE = \rho w g^2 H^2 T^2 / 16\pi \qquad (1)$$

where g denotes the gravitational constant, ρw the density of the water, H and T the maximum wave amplitude (trough to crest) and period of the wave measured at the sta. 1, respectively.

In Fig. 3, 1% line of efficiency is added. For large PE, the coincidence of the experimental data and 1% line is rather good, but, for small PE, the efficiency is less than 1% for all of the experimental data.

For explaining this tendency, the concept of Virtual Mass is introduced. When a solid body moves in water in unsteady manner, the water around the body moves with it. This water mass surounding the body is called Added Mass (Virtual Mass). Considering the Virtual Mass, the available potential energy for wave generation is small compared with that estimated by WIEGEL. Virtual Mass depends on the shape and dimensions of the solid body and density of the water. So that, the smaller the PE, the smaller the ratio of available potential energy to PE. It is well explained the discrepancy of the experimental data and 1% line of efficiency for small PE in Fig. 3.

And, introducing the resistant coefficient Cd, the equation of motion for the velocity V of the falling box is

$$(\rho + \rho v) \cdot Vo \cdot dV/dt = (\rho - \rho w) \cdot Vo \cdot g$$

$$+ (1/2) \cdot \rho w V^2 S \cdot Cd \qquad (2)$$

1. Reaearch Worker, 1st Laboratory, Hiratsuka Branch, National Research Center for Disaster Prevention, Japan.

2. Dr. of Science, Director-General, National Research Center for Disaster Prevention, Japan.

where ρ denotes the density of the falling box, $\rho v = Wv/Vo$. Wv the Virtual Mass. Vo the volume of the box and S the square measure of the bottom of the box. Wv is expressed from Fig. 4 taking the horizontal scale of the box L instead of 2a

$$Wv = K1 \cdot \rho w \cdot \pi \cdot L^2 / 4 \qquad (3)$$

In the WIEGEL's experiment. K1=1. 51. Equation (2) can be solved straightforwardly as follows

$$V = \sqrt{\alpha / \beta} \cdot \tanh(\sqrt{\alpha \beta}\, t) \qquad (4)$$

$$\alpha = (\rho - \rho w) \cdot g / (\rho + \rho v)$$

$$\beta = (1/2) \cdot \rho w S \cdot Cd / \{(\rho + \rho v) \cdot Vo\}$$

In the WIEGEL's experimental conditions. the falling box reached the bottom of the basin immediately. Then. the motion of the box can be treated as constant acceleration motion.

$$V = \alpha \cdot t \qquad (5)$$

For convenience in later discussions. physical quantities are written in nondimensional form. Using box horizontal scale L. gravitational constant g and density of the water ρw. velocity. energy and time are nondimensionalized by $\sqrt{gL}$. $\rho w g L^3$ and $\sqrt{L/g}$ respectively.

Taking α as the abscissa in Fig. 5. WIEGEL's experimental data are reconstructed. For small α. the efficiency is less than 1%. but for large α. there are upper limitations depend on Zo and d.

From the linear theoty (KAJIURA. 1963). the wave height η when the box falls with constant acceleration is expressed in terms of time dependent Green's function as follows

$$\eta = -(\alpha / 2\pi) \int_0^t \int Gt|_{\bar{z}=0}\, d\tau\, dx_o \qquad (6)$$

$$Gt|_{\bar{z}=0} = \int_0^\infty (2/\sigma) \cdot \sin\sigma(t-\tau) \cdot \cos m\bar{x} \cdot$$

$$[\cosh\{m(d+Zs)\} - \cosh\{m(d+Zs-AM)\}]$$

$$/\cosh(md)\, dm \qquad (7)$$

where

$$\sigma^2 = m \cdot \tanh(md)$$

$$\bar{x}^2 = (x - x_o)^2$$

$$Zs = Zo - \alpha \tau^2 / 2 \quad ; \quad Zo < 0$$

Integrating (6) numerically. the maximum wave generating efficiency is about 10% when the initial box submergence Zo=0. 0. In the WIEGEL's experimental set-up. the wave energy was calculated only one-side of the falling box. Then. to apply this result to Fig. 3. we must half the value of 10%. The caluculated efficiency is rather high compared with the experimental data. It is indicated that the wave is not developed as expected from the linear theory.

3. NONLINEAR NUMERICAL COMPUTATIONS USING THE BOUNDARY ELEMENT METHOD

In this section. the results of nonlinear computations are compared with the linear theory. In the domain shown in Fig. 6. using the Boudary Element Method. nonlinear numerical computations were made. All the physical quantities were nondimensional. The basic equation for the velocity potential Φ is

$$\Delta\Phi = 0 \quad ; \quad \Omega\text{内} \qquad (8)$$

where Δ denotes the laplacian. Boundary conditions are

$$\partial\Phi/\partial t + (1/2)\{(\partial\Phi/\partial x)^2 +$$

$$(\partial\Phi/\partial z)^2\} + \eta = 0 \quad ; \quad S1\text{上} \qquad (9)$$

$$\partial\Phi/\partial n = nz \cdot \partial\eta/\partial t \quad ; \quad S1\text{上} \qquad (10)$$

$$\partial\Phi/\partial n = 0 \quad ; \quad S2\text{上} \qquad (11)$$

$$\partial\Phi/\partial n = nz \cdot V \quad ; \quad S3\text{上} \qquad (12)$$

where nz denotes the z component of the unit outward normal vector $\tilde{n}$. Equations (9) and (10) are nonlinear.

In this computations. TL=30. 0 and d=16. 0 were fixed. Constant velocity fallings were assumed. The fall began at τ=0 and finished at $\tau = \tau f$. Variables were AM. V and Zo.

According to the linear theory. if the falling velocity is constant. η is expressed as follows with the aid of Green's function (7).

$$\eta = -(V/2\pi) \int_{\substack{\bar{z}=0 \\ \tau=0}} (Gt|_{\substack{\bar{z}=0 \\ \tau=0}} - Gt|_{\substack{\bar{z}=0 \\ \tau=\tau f}})\, dx_o \qquad (13)$$

This integral is independent of V. Then. wave height η is propotional to the constant falling velocity V. Dependence to η of AM and/or Zo is not clear like that.

Fig. 7-1 and Fig. 7-2 are the comparisons of the nonlinear numerical computations and the linear theory. The ordinate is ηmax/V and the abscissa is Zo. Discrepancy between the computations and the linear theory is clear for V≥0. 16 in Fig. 7-1 and for all V in Fig7-2. In the WIEGEL's experiment. the falling body thickness AM=1. 00. Then. it is clear from the Fig. 7-2

that the low efficiency of the experimental data shown in Fig. 5 is due to the nonlinear effect.

4. TSUNAMI GENERATING EFFICIENCY DUE TO THE LANDSLIDES PLUNGING INTO THE WATER BODY.

SLINGERLAND & VOIGHT (1982) presented a empirical formula through the hydraulic studies.

$$\log(\eta max/d) = -1.25 + 0.71 \cdot \log(KE) \quad (14)$$

where ηmax=maximum wave amplitude at a standard distance r/d=4.0 directly in front of a slide. d=average depth offshore from slide site. r=radial horizontal distance from the point of slide impact and KE=nondimensional slide kinematic energy. Laboratory experimental data denoted by black dots shown in Fig. 8. Confidence limits at the 95% level are indicated by dashed line. The back caluculations of slide-induced tsunamis occured in Lituya bay, Alaska and Disenchantment bay, Alaska are also shown in Fig. 8. Informations of both slides are shown in Table. 1

Now, we consider the one dimensional propagation. The energy of solitary wave per unit width is expressed as follows

$$Es = (8/3) \cdot \rho w \cdot g\, d^3\, \gamma \sqrt{\gamma/3} \quad (15)$$

$$\gamma = \eta max/d$$

Then, in the experimental condition, the wave propagated through a 180 arc. The total energy is

$$WE = Es \cdot \pi r \quad (16)$$

And, slide kinematic energy is

$$Ek = (1/2) \cdot \rho s \cdot Vo \cdot Vf^2 \quad (17)$$

where Vo denotes the volume of the slide and Vf the final velocity of the slide. Nondimensional form is

$$KE = Ek/(\rho\, d^3\, g\, d) \quad (18)$$

According to Fig. 8, there is little difference changing the coefficient of log(KE) from 0.71 to (2/3) in the equation (14).

$$\log(\gamma) = -1.25 + (2/3) \cdot \log(KE) \quad (19)$$

Substituting (15) into (16) yields

$$\log(WE) = \log(8\pi/3\sqrt{3}) + \log(\rho w\, g\, d^3) + \log(r) + (3/2) \cdot \log(\gamma) \quad (20)$$

Substituting (19) into (20), after some algebla, we get

$$(WE/Ek) = 0.26$$

It is suggested from Fig. 8 that tsunami generating efficiency is low for the Disenchantment bay slide compared with that for the Lituya bay. The reason of this difference can be considered as follows. The material of the Lituya bay slide was soil (ρ=2.7g/cm^3) but the Disenchantment bay slide was glacier (ρ=1.0g/cm^3). So that, for the case of Lituya bay, the slide generated tsunami even in the water like submerged landslide did. But, for the case of the Disenchantment bay, the glacier did not generate tsunami in the water. To confirm this speculation, we consider the ideal slide whose KE is the same with that of the Disenchantment bay glacier and ρ is the same with that of the Lituya bay slide. The range of KE of the Disenchantment bay glacier varies from 130 to 249 depending on the estimation difference of the final velocity. In Fig. 8, A and B denotes the point of KE=130 and 249 respectively. The efficiency in both cases evaluated by the present method is 15% and 8%. And 10% of the potential energy loss in the water of the ideal slide transformed into the wave energy. Then, the total wave height generated by ideal landslide denoted by $\eta max/d$ comes to 1.30. The points A and B move to the points A′ and B′ as shown in Fig. 8. This values considered to be reasonable compared with the experimental data. It is found that to know the density of the slide is essential to evaluate tsunami height exactly.

5. CONCLUDING REMARKS

On the generation of tsunamis due to landslide, various parameters are concerned. But, for the simple estimation of tsunami height, it is found that the following three parameters, the potential energy lost in the water, kinematic energy and density of the slide, are essential. The tsunami generating efficiency becames large as the initial submergence of the slide becomes small. The maximum generating efficiency is about 10%.

For the case of landslides plunging into the water body, 8 to 15% of kinematic energy of the slide transformed into the wave energy.

REFERENCES

Kajiura, K., The leading wave of a tsunami, Bull. of Earthq. Inst., 41, 535-571, 1963.

Murty, T. S., Submarine slide-generated water waves in Kitimat Inlet, British Columbia, J. Geophys. Res., 84, 7777-7779, 1979.

Saunders, H. E., Hydrodynamics in ship design, Soc. of Naval Architects and Marine Engineers, 1964

Slingerland, R. & B. Voight, Evaluating hazard of landslide-induced water waves, J. of Waterways, Port, Coastaland Ocean Division, ASCE, 108, WW4, 504-512, 1982.

Striem, H. L. & T. Miloh, Tsunamis induced by submarine slumpings off the coast of Israel, International Hydrographic Rev., 53, 41-55, 1976

Wiegel, R. L., Laboratory studies of gravity waves generated by the movement of a submerged body, Trans. Amer. Geophys. Union, 36, 759-774, 1955

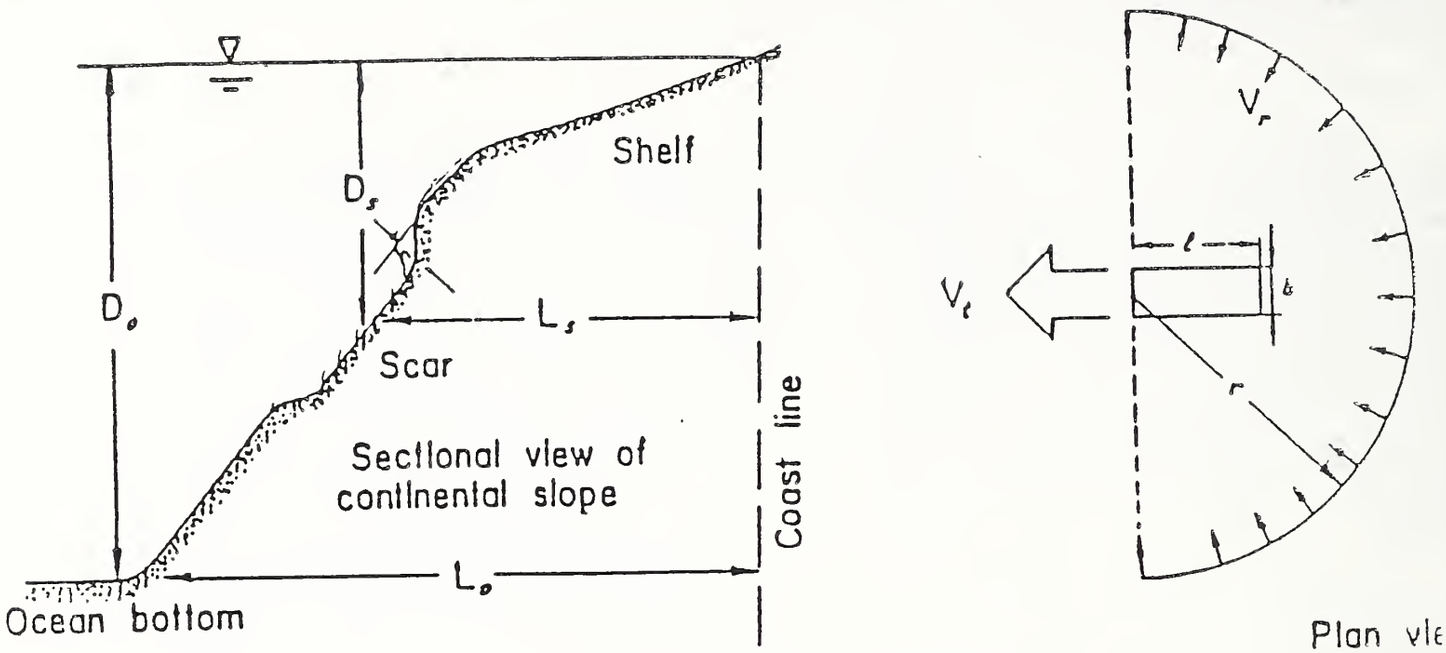

Fig. 1 A model of submarine land slide (after STRIEM & MILOH. 1976)

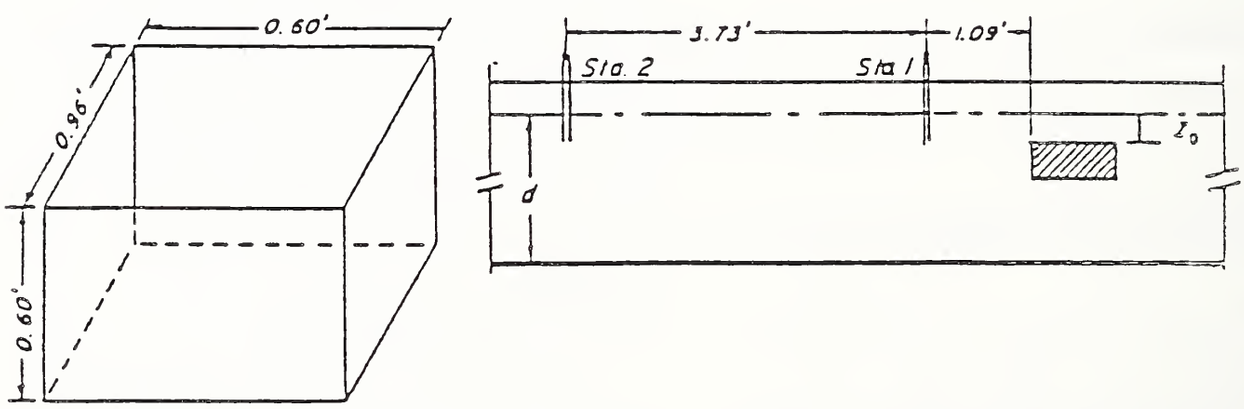

a. Set-up for Series II

Fig. 2 WIEGEL's experimental set-up.

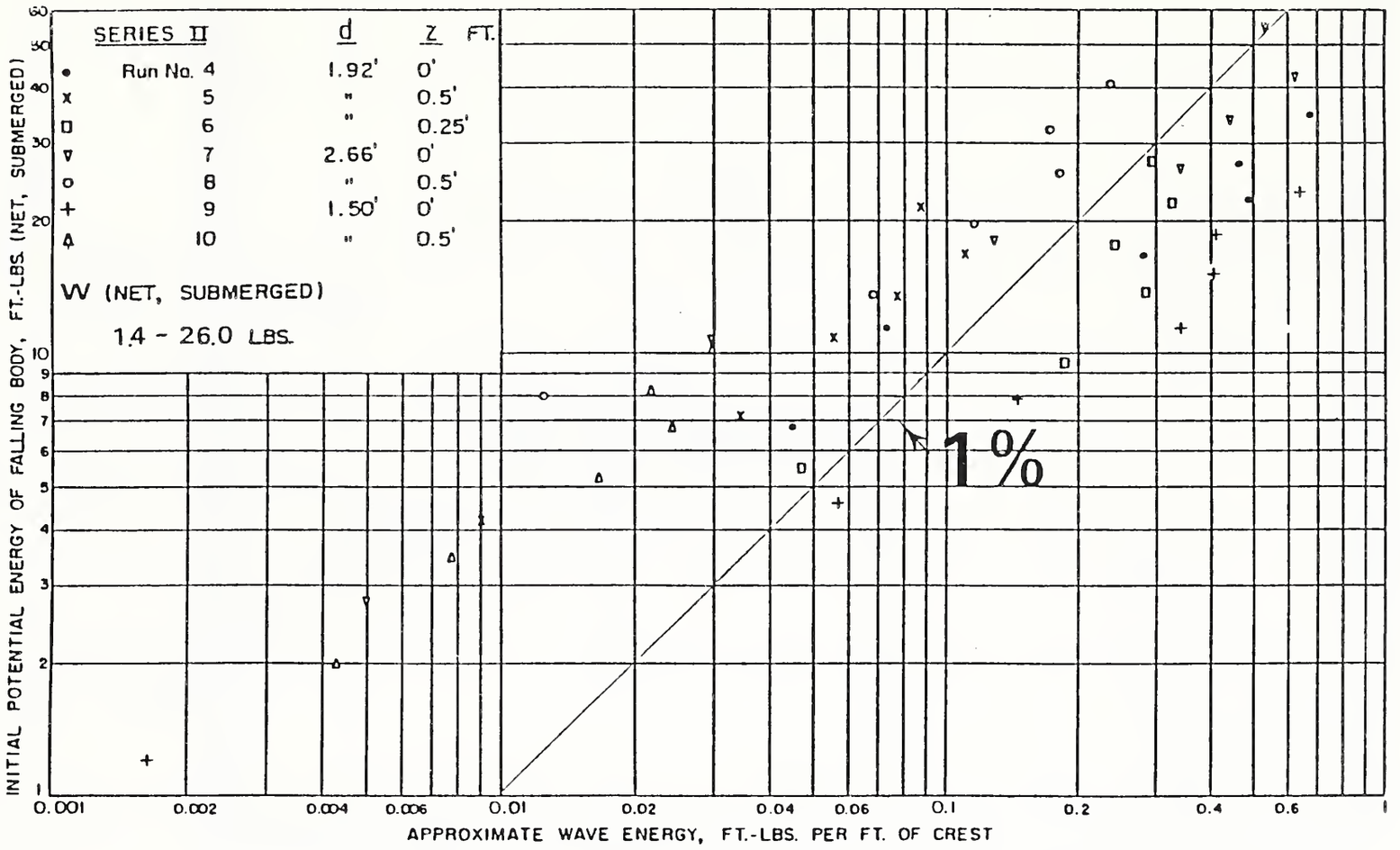

Fig. 3 Relationship between energy of wave disturbance and initial potential energy (net, submerged) of a vertically falling box. 1% line of efficiency is added. (after WIEGEL, 1955)

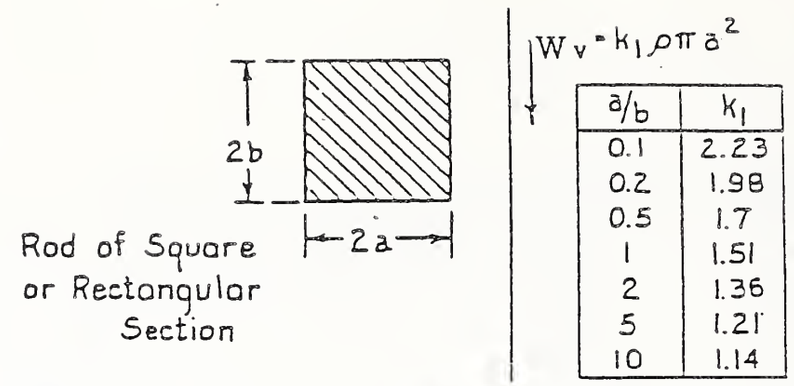

a/b	k_1
0.1	2.23
0.2	1.98
0.5	1.7
1	1.51
2	1.36
5	1.21
10	1.14

Fig. 4 Added Mass Values for two dimensional geometric shape. (after Saunders. 1964)

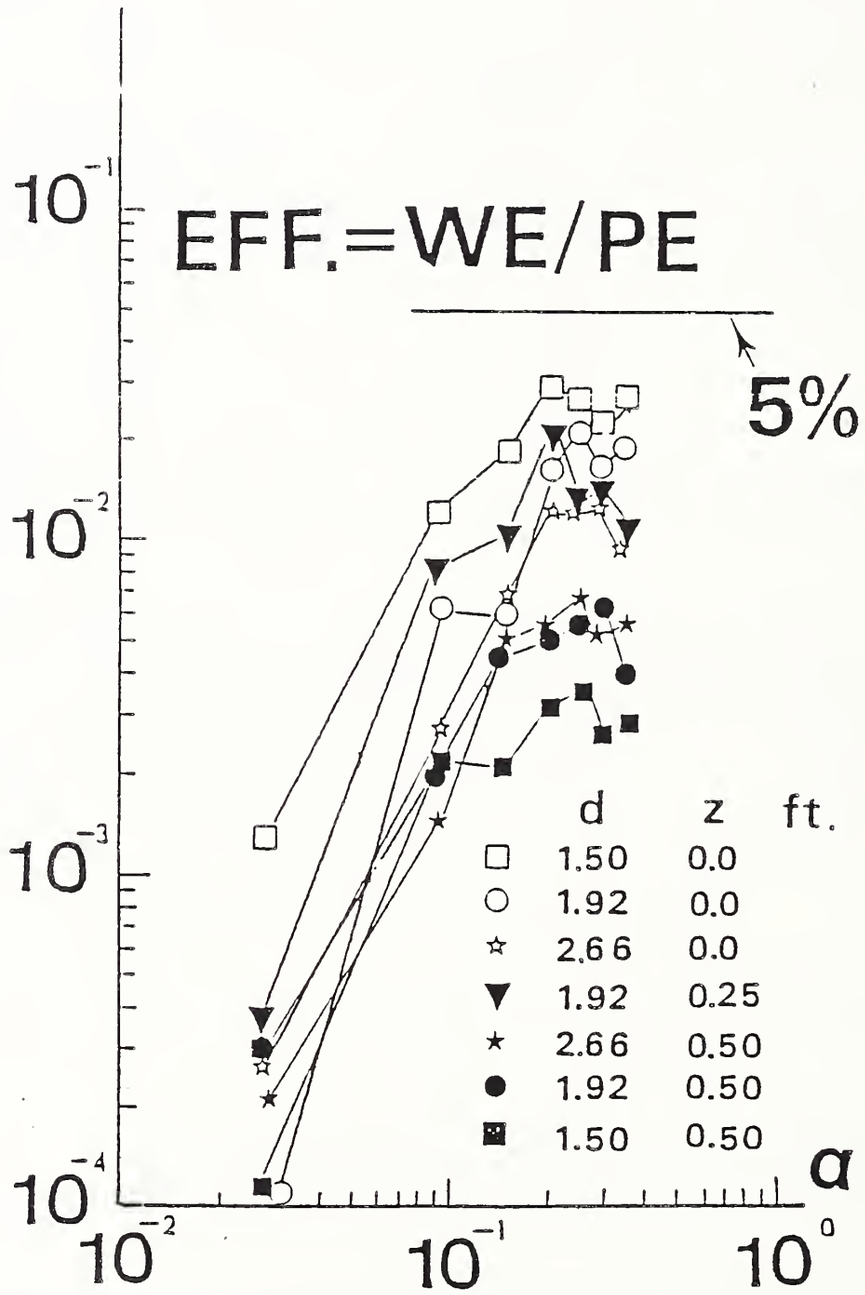

Fig. 5 Reconstruction of the WIEGEL's experimental data in terms of modified acceleration by the concept of the Added Mass. 5% line of efficiency is obtained by the linear theory.

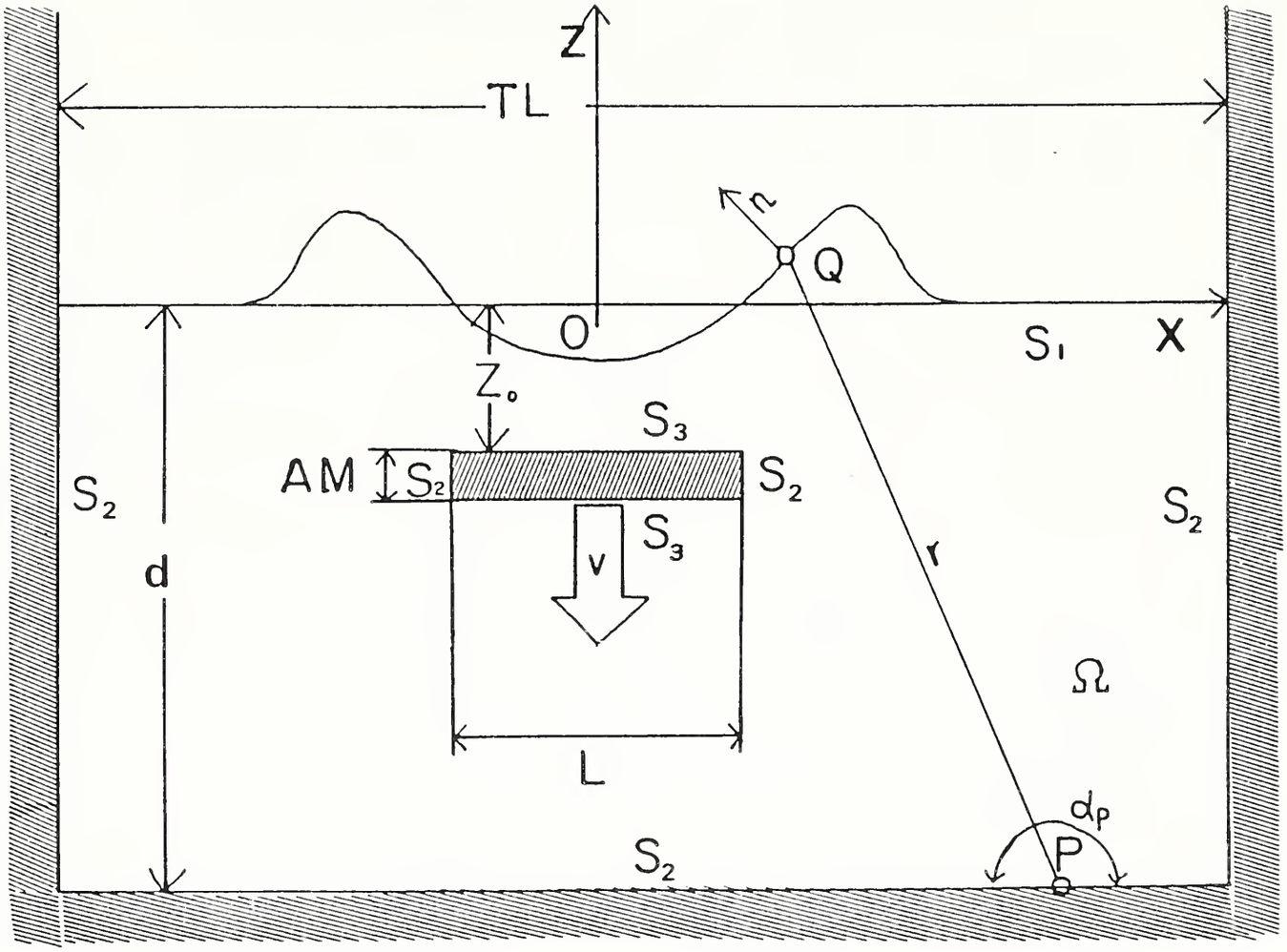

Fig. 6 Schematic view of the domain for numerical computations.

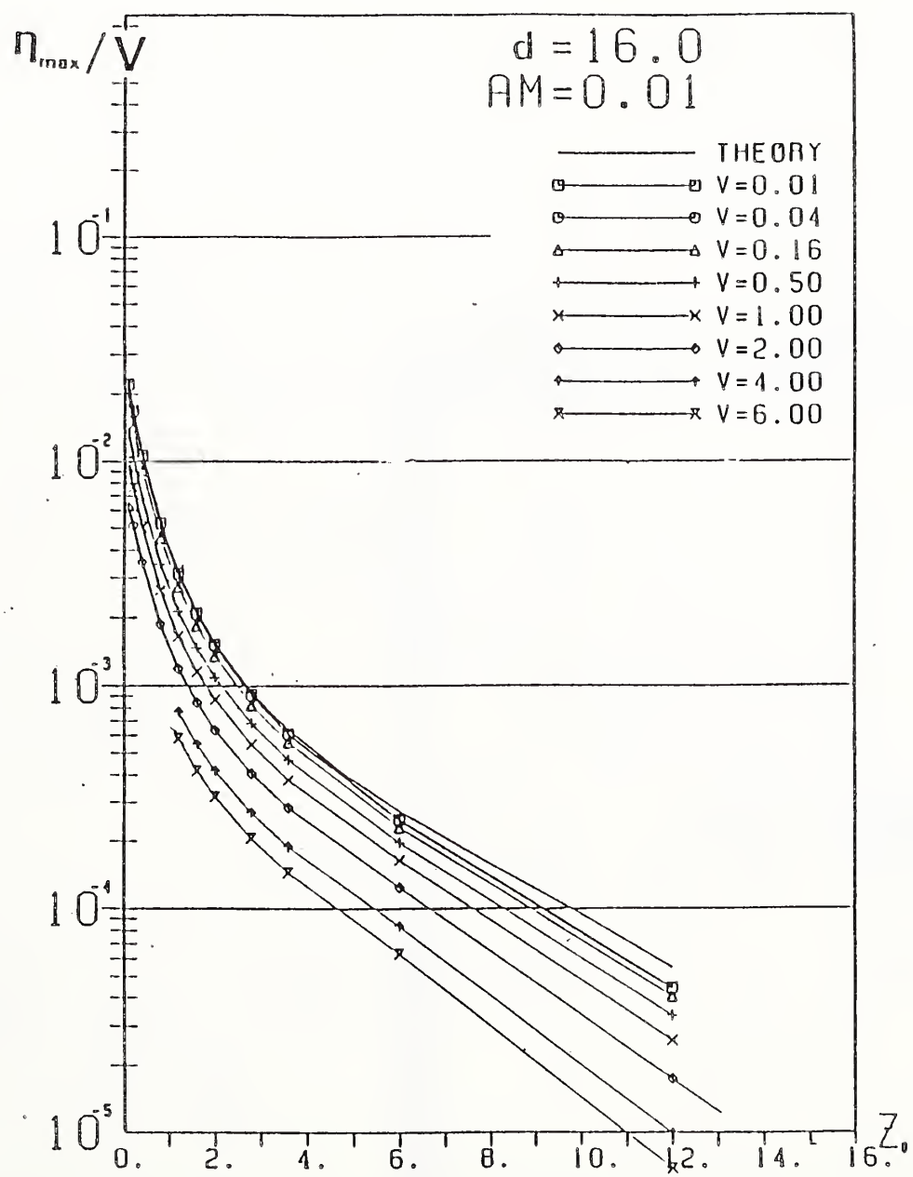

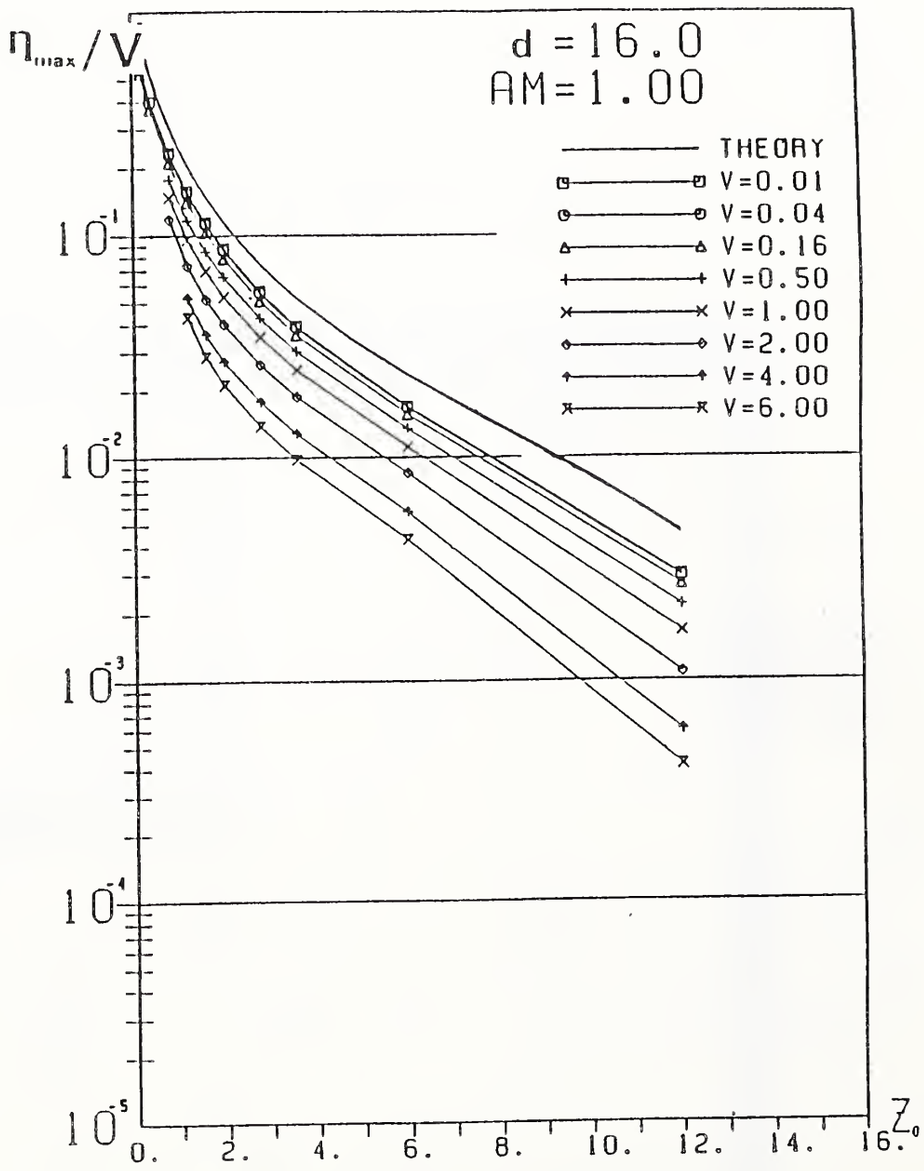

Fig7-1.2 Comparisons of the linear theory and non-linear numerical computations.

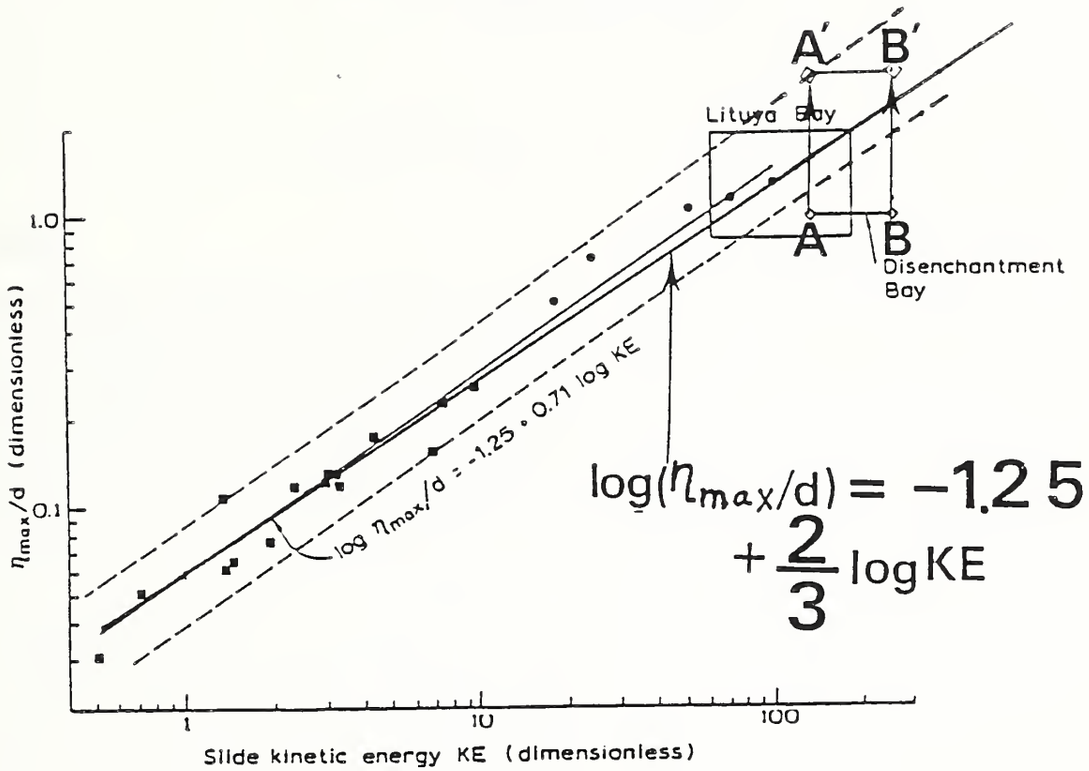

Fig. 8 Relationship of maximum dimensionless wave amplitudes (at r/d=4.0) as function of slide dimension less kinematic energy (after SLINGERLAND & VOIGHT), a little portion is modified.

	Vo (cm^3)	ρ (g/cm^3)	Vf (cm/sec)	d (cm)
LITUYA BAY	3.1×10^{13}	2.7	$5.6\sim6.9\times10^{3}$	1.2×10^{4}
DISENCHANTMENT BAY	2.9×10^{13}	1.0	$6.0\sim8.3\times10^{3}$	8.0×10^{3}

Table. 1

A Computer Program for Producing Tsunami Travel-Time Chart

BY

Masami Okada[1] and Masaji Ichikawa[2]

ABSTRACT

Tsunami travel time chart is used to predict quickly the tsunami travel and arrival time to the objective location or coast. Many charts, prepared for the operational tsunami warning system, were made by hand with much time and labour. We have been developing he software for producing tsunami travel time charts which will be applied in the newly computer system called Tokyo-EPOS, Earthquake Phenomena Observations System, in JMA.

Using various data bases of bathymetry, the travel time is calculated on the triangular grid system on the basis of Huygens' law. The travel time chart is calculated firstly on the fine mesh for small area near tide station or wave source and the results of preceding calculation are adopted as the initial values of travel time for the following computation with a rough mesh covering a wide area. The method of computations is described and a trial production for the north Pacific ocean is shown in this paper.

KEY WORDS : Tsunami, Tsunami Travel Time Chart

1. INTRODUCTION

Tsunami travel time charts are used by tsunami waring systems to provide "real time" predictions of the travel and arrival times of a tsunami, when a large earthquake occurred under the sea bottom. Each travel time chart is centered on a hypothetical center and shows the wave fronts emanating from that center, for which warnings are required. The chart centered on a realistic tsunami wave source is usually compiled after the tsunami arrived along the coast and observed at many tide stations.

In most cases the wave length of tsunami is so long that the wave velocity is given by the square root of the product of the local water depth and gravitational accelerations. Travel time between any two points is given by the integral of reciprocal velocity along the wave ray path. Although there is no problem in hydraulics, it is impossible to calculate theoretically the travel time for the actual bathymetry, because the bathymetry is too complicated. In practical applications, these integrals are carried out numerically.

In ray tracing method, the ray path should be determined prior to the integral of travel time. The amount of spreading of the ray paths is also of interest since it gives a measure of the energy concentrations of tsunami. Nevertheless this method cannot be applied for the operational tsunami travel time chart, because the shadow area in the sea may come out in tsunami propagation map behind islands and shoals. In our software, the tsunami travel time chart is produced by Huygens' construction, which involve the diffraction effect.

2.BATHYMETRIC DATA BASE

We are able to use the ETOPO5 world 5-minute gridded Bathymetric-Topographic data base, which was sent last year from the National Geophysical Data Center, NOAA in USA under the auspices of UJNR and through the courtesy of Deputy Director, J.F.Lander. This data base is very convenient to show the world wide bathymetry, and we should also point out that the values in the file indicate a local average elevation and some of them near the shore lines confuse sea with land. Thus we have revised many valued near shore lines in the northwest Pacific, the region of 20-48°N and 120-152°E.

It is reasonable that the error in the tsunami travel time chart depend on not only the accuracy but also the grid size of the bathymetric data base. We must pay attention to the values in the shallow water in which tsunami propagate slowly. In many cases of calculating the tsunami travel time chart to the tide station located on shore, more fine/small gridded data of bathymetry are

1: Chief, First Research Laboratory, Seismology and Volcanology Division, Meteorological Research Institute, Japan.
2: Dr. of Sci., Former Head, Seismology and Volcanology Divition, Meteorological Research Institute, Japan.

required additionally to represent small topography. We are now compiling the 1-minute gridded bathynetric data bases for the seas adjacent to Japan Islands. Futhermore we are going to prepare very fine gridded data bases (about 500m×500m and about 100m×100m) for about one hundred tide stations on the basis of the bathymetric chart so as to represent adequately the bathymetry of the port and harbour in which the tide station is located. An example of bathymetric data base for small area is shown in figure 1.

3.METHOD

The travel time chart is compiled by using Huygens' construction on the basis of the modified triangular grid system. This method may be complicated and take much more time and memories in computer calculation than the ray tracing one. However the ray tracing method is serious for the operational chart in having the shadow zone behind islands in tsunami propagation map.

The modified triangular grid on Mercator map is shown in figure 2. The values of sea depth are given at apexes of small triangle' and traval time is calculated at all points (squares and circles in figure 2). Each value of the depth is calculated by a simple interpolation in two dimensions from the bathymetic data bases. Considering the grid system, we should remark the difference in distance between the apparent path on the grid and real one. For example the linear length of AE in figure 2 is 0.9 percent shorter than the one on the mesh, that is the connection of AB, BC, CD and DE. The relative discrepancy in distance between two points on the grid is usually less than one percent, except such cases as S to Z' that is start and end points being close. The computational area for tsunami travel time chart is not a rectangle but a parallelogram shown in figure 3.

The local depth in each small triangle is regarded to be linear interpolation of nearly values at three apexes, in calculating the traval time. Then the ray path in a triangle is a part of cycloid curve represented as follow.

$$x = a(\theta - \sin\theta)$$
$$y = a(1 - \cos\theta)$$

The travel time from any point, such as an apex point A or a side point S in figure 2, to the surrounding closely points shown by solid symbols are calculated analytically, assuming that the sea bottom decline uniformly in each small triangle. The travel time T between any two points are given as follow.

$$T = \min_{S} \Sigma \Delta T_i$$

here $S = \Sigma S_i$. S_i is the cycloid path connecting two points on a small triangle, and ΔT_i is the travel time along S_i. The minimum is taken over all possible pathes S on the grid system. Actually we calculate the propagating time from one point to others on the same triangle in the order of arrival time.

It is reasonable that the calculations is carried out on the fine mesh for the coastal area near the tide station and on the rough mesh for the ocean, because the long wave velocity is low in shallow water and the bathymetry is generally more complicated in the coastal area. Thus the travel time chart is compiled on the basis of fine mesh for small area near a tide station or the tsunami source area, and the results of preceding calculations are adopted as the initial values for following computation on a rough mesh covering a wide region. The sckema of computational region is shown in figure 3.

4.TRIAL PRODUCTION

The tsunami travel time chart to Okada tide station, Izu-Oshima island, about 100km south-southwest of Tokyo, is compiled as a trial production by a computer program, named SEIJI in developing. The result of calculation is printed graphically by a line printer, as the present software, is independent from XY-plotter. The chart for the north Pacific ocean is shown in figure 4. Wave source point in calculation is not located on the exact position of the tide station but 250m northwest of the station, because the position of tide station at which sea depth is 0m is considered to be located on land in calculating and no tsunami arrive there. The locations of the centered point and the tide station are shown by the cross +and close circle in figure 1, respectively. The travel time at the hypothetical tsunami source point is supposed to be 50 seconds from tide station, and the time shown in figure 4 is that from tide station.

The computation consist of three step. In the first step, the tsunami travel time chart for the sea on the north of Izu-Ohima island shown in figure 5a was compiled on the basis of small grid of ΔD=200m. Secondly the one for the sea near the district of Kanto and Tokai, central southeast part of Japan, was calculated on the basis of middle grid of ΔD=2000m, whose covering area is shown in figure 5b. The results of these calculation is used in determination of initial values

for the last step in which the calculation was carried out for the north Pacific ocean. Mesh size used in this calculation is 0.25 degree of longitude, and the total number of calculating points is 1,752, 092.

For these calculation we used the computer in our institute, and it take about 30 minutes in CPU time. We cannot compare the computer made charts with the conventional hand-made one, for the conventional tsunami chart from Okada tide station has not been compiled yet. In other case, two kind figures for Japan sea tsunami agree considerably to each other as a whole.

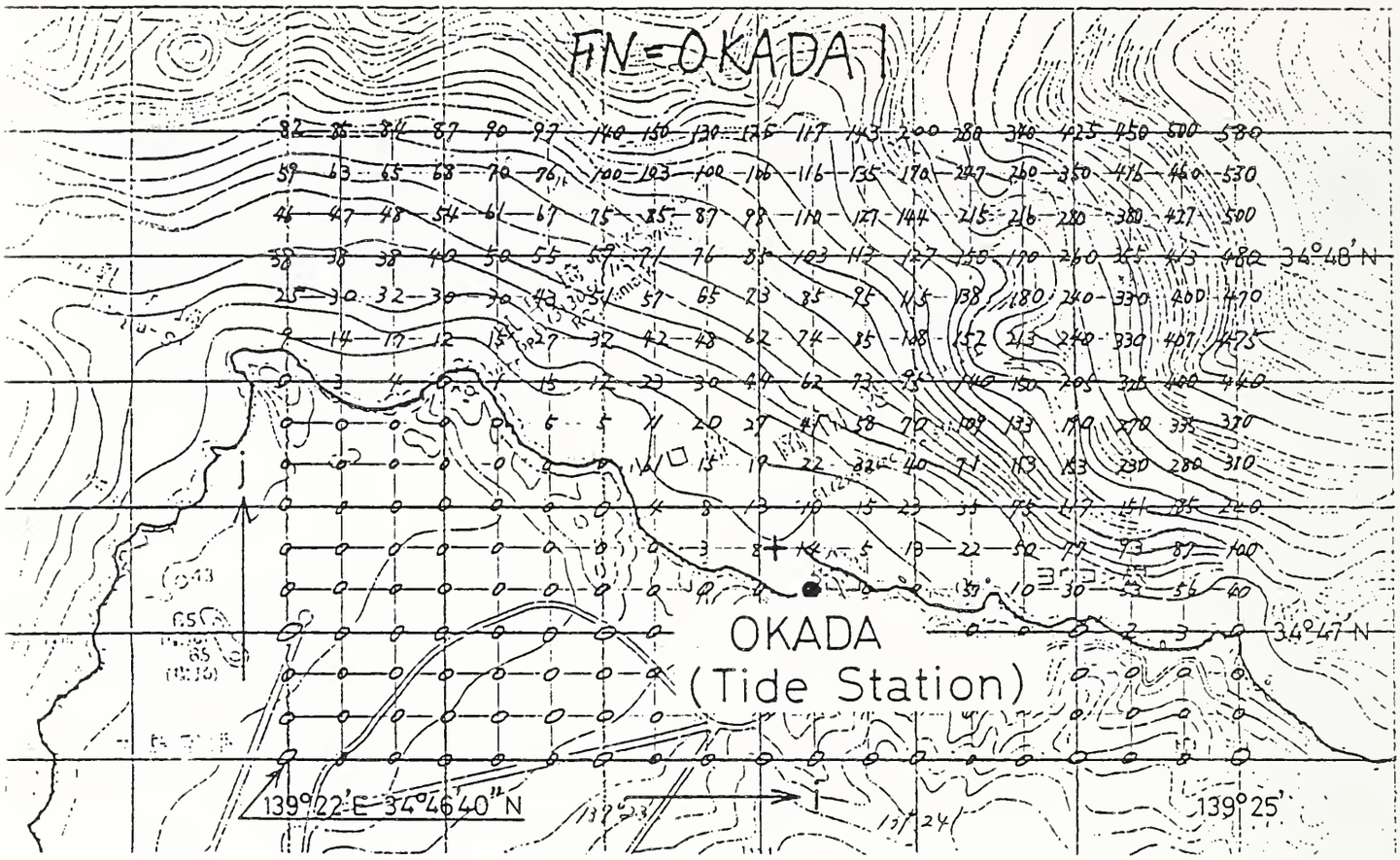

Fig.1. Example of bathymetric data base of small area near Okada tide station, Izu-Oshima. The cross indicates the hypothetical center of the tsunami travel time chart to Okada. Travel time at the point is considered to be 50 seconds from the tide station.

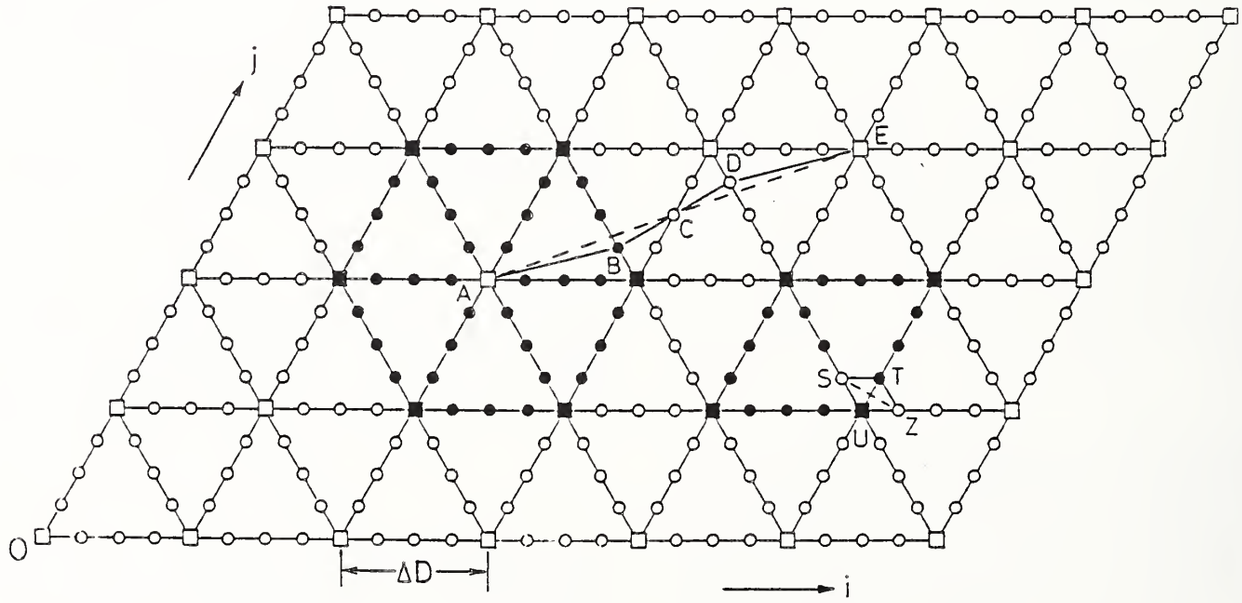

Fig.2. Modified triangular grid system. Sea depth is given at the point of square and travel time is calculate at all points (squares and circles).

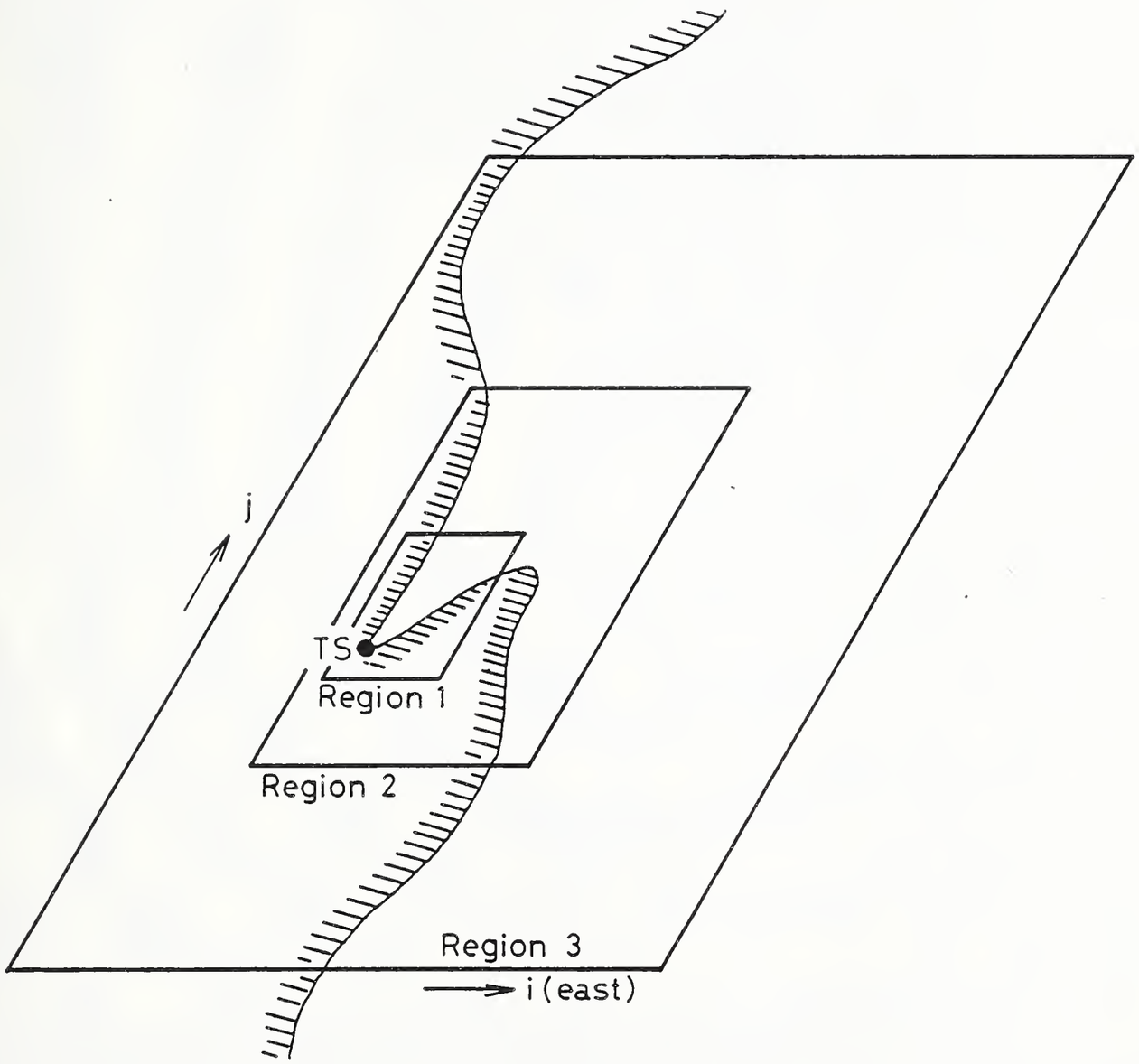

Fig.3. Schematic figure of the computational regions. Tsunami travel time chart to a tide station is firstly produced for the small area on the basis of fine grid, then the preceding results are used as the intial values of computation for the wide region.

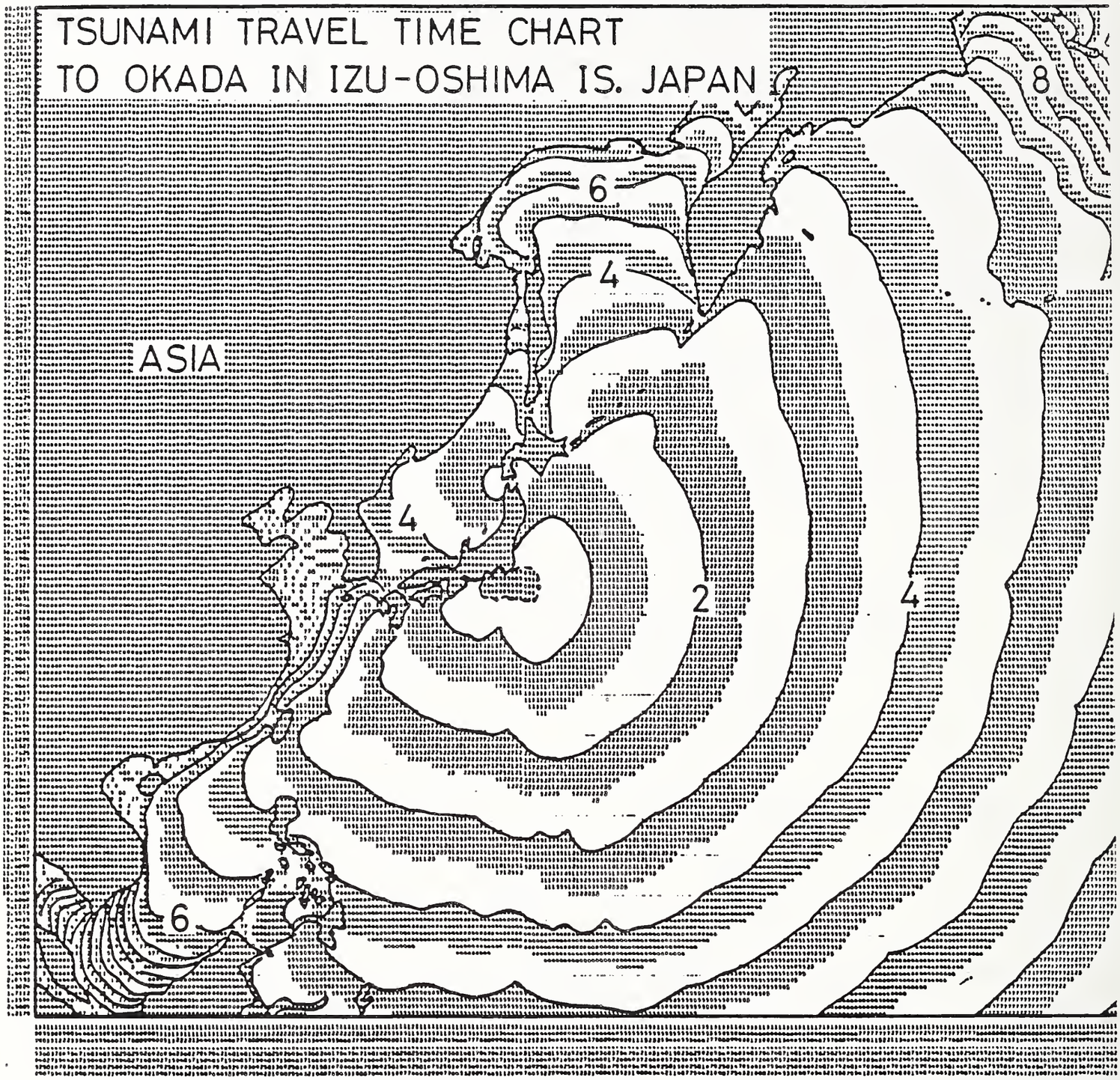

Fig.4 Trial production of the tsunami travel time chart from Okada tide station to the north Pacific ocean. Grid size ΔD is 0.25 degree in longitude.

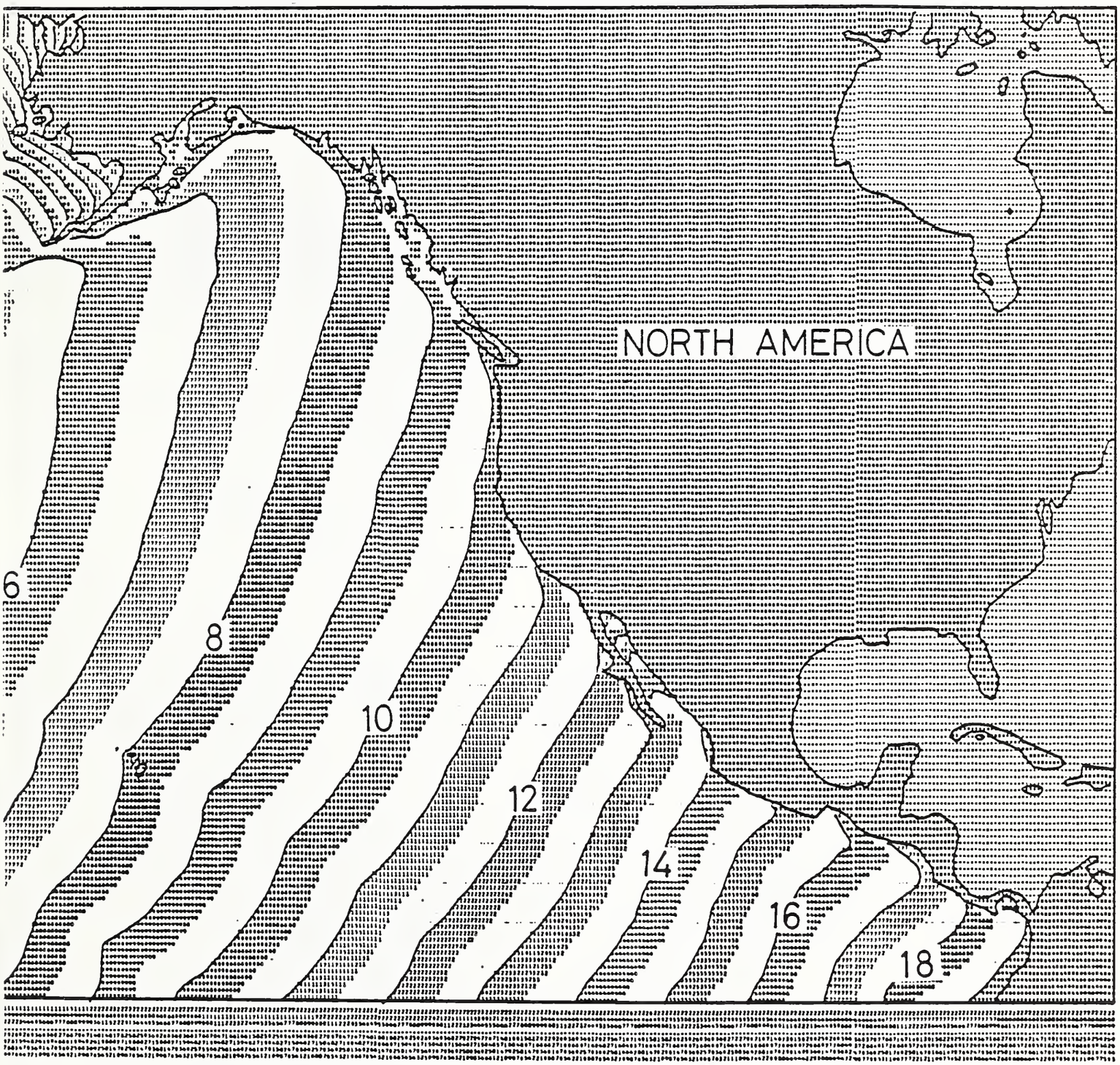
NORTH AMERICA
6
8
10
12
14
16
18

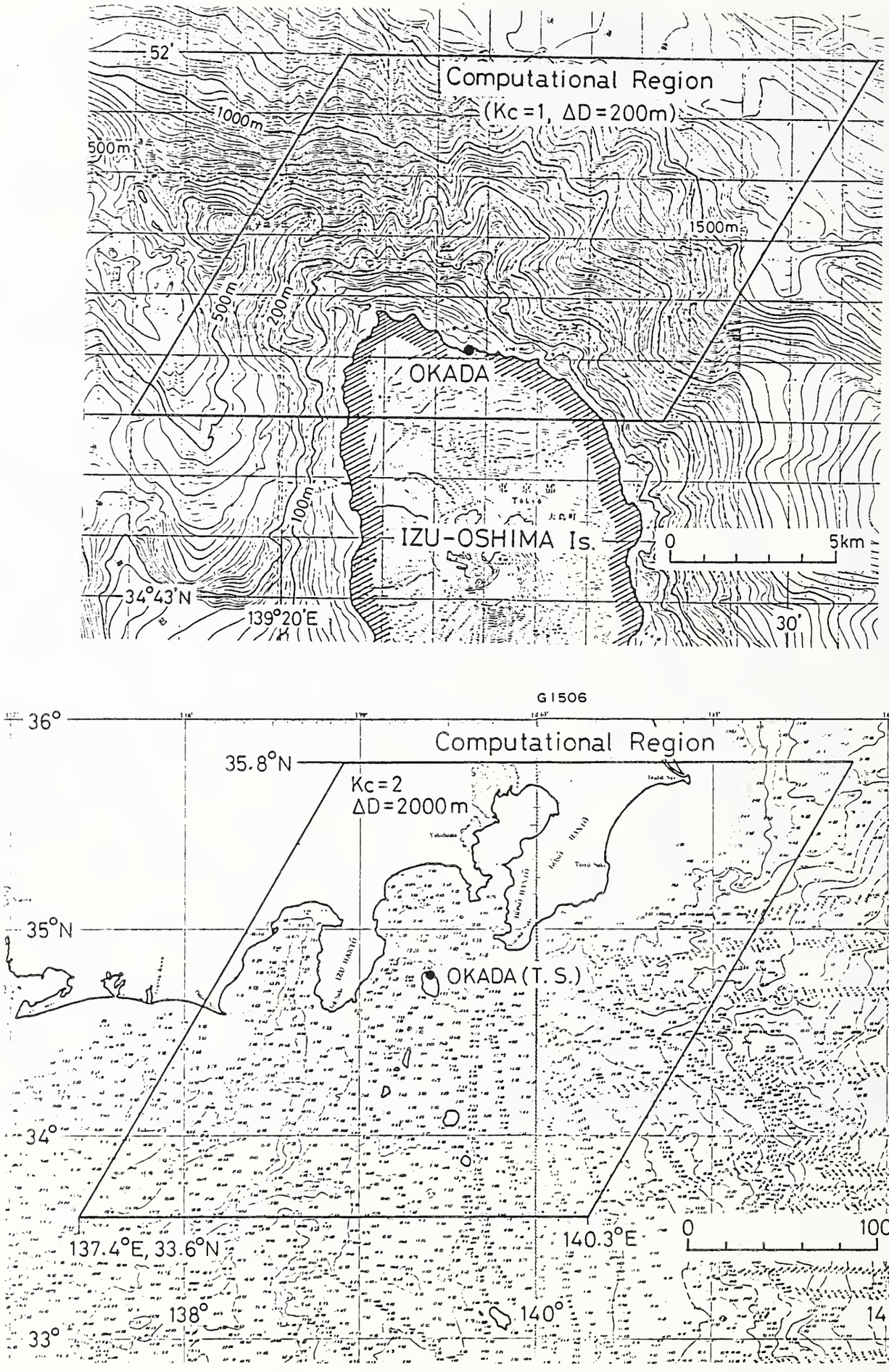

Fig.5 Examples of the computational region. Figures of (upper) and (lower) show the regions used for the first and the second step caluculation of the tsunami travel time chart to Okada, respectively. The one for the third step is the north Pacific ocean.

Numerical Simulation and Experiment on Tsunami Run-Up

by
Takaaki UDA*
Atsushi OMATA **
Yasuhisa YOKOYAMA**

ABSTRACT

Some comparisons are conducted with numerical simulations and experiments on tsunami run-up on the coast where coastal structures or sand dune exist. The numerical simulation model used in this study is quite simple, based on the nonlinear shallow water equation. Temporal and spatial distributions of the water level and velocity are compared.

Consequently it is found that the simple model used in this study has an ability to simulate tsunami movement with enough accuracy in practical use. In the case of the permeable breakwater, which is usually constructed in Japan, detached breakwater can be modelled by the bed level change in one grid.

1. INTRODUCTION

In May, 1983 the coast along the Sea of Japan was damaged severely by a large tsunami caused by the Nihonkai-Chubu Earthquake. After the tsunami various preventive works for future tsunami hazard was proposed. In the planning of these works numerical simulations were carried out in order to predict the critical height of the coastal revetment or the innundated area. Generally there exist sand dunes or shore protection facilities like as the coastal dike or the detached breakwaters along the coastal Japan. Around these structures fluid motion may be considered to be very complicated and simulation model to predict tsunami run-up should also become sophisticated, while usually numerical simulation must be done in wide region along the coast. Therefore for the practical use numerical simulation model should be as simple as possible. Accuracy of the simulation is generally verified only by the comparison with the run-up height of the previous tsunami without the comparison of the distribution of water level or current velocity around the structures in detail based upon the field data. Consequently the effects of the existence of the detached breakwater or coastal dune along the coast are not taken into consideration sufficiently. From this point of view in this study some comparisons are conducted with numerical simulations and experiments on tsunami run-up on the coast where coastal structure or sand dune exist. The numerical simulation model used in this study is quite simple, based on the nonlinear shallow water equation. In the experiments the distributions of water level and velocity are measured with time and space. Temporal and spatial distributions of the water level and velocity are compared with the calculated values.

2. EXPERIMENTS

The experiments were carried out in a fixed-bed wave basin, 30 m long and 5 m wide with 1/100 bed slope. There is a pneumatic type wave generator at the offshore end of the basin(Fig. 1). The sandy beach of uniform slope, coastal dune, coastal revetment and detached breakwater are modelled, and the distributions of water level and velocity were measured with time and space. Locations of various measuring points are shown in Fig. 2.

Each model is of uniform shape in the longshore direction. In the case of detached breakwater permeable and impermeable models are tested. The impermeable one is composed of concrete blocks fixed to the bed to prevent from scattering. The measurements of the water level and the velocity are done by using the capacitance-type wave gauges and the propeller-type current meters set 5 mm above the bottom, respectively.

The solitary wave generated at the offshore end propagated on the bottom slope while changing its profile. At the location 15 m shoreward from the generator the wave front dispersed to form two or three short-period waves and then they broke. Finally the breaking bore was incident to the models.

3. NUMERICAL SIMULATION

The numerical simulation model used in this study is considerably simple, which solves the nonlinear shallow water equation by the leap-frog finite difference method using 5 cm grid and 0.02 sec time intervals. The fundamental equations are as follows:

$$\frac{\partial \eta}{\partial t} + \frac{\partial Q}{\partial x} = 0 \qquad \cdots\cdots(1)$$

$$\frac{\partial Q}{\partial t} + \frac{\partial}{\partial x}\left(\frac{Q^2}{D}\right) + gD\frac{\partial \eta}{\partial x} + \frac{gn^2}{D^{7/3}}Q^2 = 0 \qquad \cdots(2)$$

where h : still water depth
η : displacement above the S.W.L.
D : total water depth ($= h + \eta$)

* Head, Coastal Engineering Division, Public Works Research Institute, Ministry of Construction
** Research Engineer, Coastal Engineering Division, Public Works Research Institute, Ministry of Construction

n : Manning's roughness coefficient
Q : rate of discharge per unit width

Here h takes a negative value on the dry bed, that is the negative vertical distance between the still water level and the ground. For the initial condition wave profile measured just in front of the generator was used. The value of n is assumed to be 0.012, and it was determined empirically in such a way that the difference between measured and calculated run-up height in the case of 1/20 uniform slope is minimal. For the boundary condition of the wave front the method by Iwasaki et al.[1] was used. In their model the wave front is judged by whether value of D is positive or negative. The rate of discharge through the permeable detached breakwater is calculated by

$$\frac{1}{\lambda}\frac{\partial Q}{\partial t}+gD\frac{\partial \eta}{\partial x}+\frac{f}{2\ell}\frac{Q^2}{D}=0 \quad \cdots\cdots(3)$$

where λ : porosity (= 0.5)
ℓ : width of detached breakwater
f : drag coefficient (= 8.6)

4. COMPARISON WITH THE EXPERIMENTAL RESULTS AND THE NUMERICAL SIMULATIONS

The experimental results are compared with the simulations in Fig.3. The simultaneous measurements of the water level and the velocity was difficult because of the large number of the measuring points, so that these measurements were conducted in the repeated experiments with the same physical condition.

In the simulation the mean wave profile measured in front of the generator is used as the initial condition, and therefore this condition is not always the same as the one when the run-up height was measured. This has a considerable large effect on the results because the initial condition is important in the tsunami simulation. In spite of these errors of the initial condition the differences of the run-up height between the experiments and the simulations are less than 10% and they agree considerably well.

The measured and calculated results of water level and velocity are compared in Figs.4 through 8 with regard to 1/20 uniform slope, coastal dune, coastal revetment and detached breakwater, respectively. The spatial profiles of the water level are shown in Fig.9. Time in these figures is measured right after the water level at x =5m starts rising. The reference level of water surface is selected at the still water level in the offshore region and at the dry bed on the beach, respectively. In Figs.4 through 8 the velocity is expressed in the absolute value, because uni-directional current meters were used.

4.1 1/20 uniform slope

The reflected wave in the experiment as shown in Fig.4 has many short-period waves. This simulation can not predict these waves in principle, because the fundamental equation does not include the dispersion term. The phase of the reflected waves in the simulation is faster than that in the experiment, although the cause of this difference is not clearly understood. Both water level and velocity profiles are generally in good agreement, even if wave breaking and mixing at the wave front are neglected. Furthermore the spatial profiles in Fig.9a) also show good agreement each other.

4.2 Coastal dune

The reflected wave in the offshore region as shown in Fig.5 expresses the same result as the one in the uniform slope, while run-up profiles of both water level and velocity agree well. The calculated velocity at P11 on top of the dune is higher than that observed, so that it is considered that the reflected wave at P16 is generated earlier in the simulation. This also causes the phase difference of spatial profile shown in Fig.9b), that is, the profile at t =29 sec in the simulation agrees with the one at t =30 sec in the experiment. These differences are considered to be due to the effects of drag caused by the separation on top of the dune, judging that the velocities at points offshore from P11 located on top of the dune are in good agreement as shown in Fig.5 during the run-up period. Furthermore in Fig.9b) the measured profile of the water surface around on top of the dune is raised higher than that in the simulation. There exist some small differences. However, it is concluded that the run-up motion around the coastal dune can be simulated properly, even if present model is fairly simple.

4.3 Coastal revetment

In this case both water level and velocity are slightly higher on land as shown in Fig.7. Except this small differences the results including spatial profile in Fig.9c) show good agreement between the experiment and the simulation. In the simulation the revetment is treated only as the bed level change in one grid instead of considering the effect of the revetment. Nevertheless it is considered that water motion can be predicted by the model properly, because the separation zone is formed in front of the revetment

4.4 Detached breakwater

The width of the detached breakwater in the model experiment is narrow enough as 5 cm. Therefore the existence of the detached breakwater can be expressed in terms of the bed level change in one grid. The results of impermeable and permeable detached breakwater are discussed, dividedly.

The change of the water level and velocity in

the impermeable detached breakwater is shown in Fig. 7. At the crown of detached breakwater (P5) water level is higher and velocity is smaller in the experiment compared with those in simulation during run-up period. In addition, rapid current movement, keeping shallow water depth, exists continuously at P6 and P7. The initial reflected wave from the slope is generated at around P8 in the simulation, while it is generated at about P15 in the experiment. It is thought that these differences between the experiments and the simulations are caused by errors in estimating water level and velocity at the crown of the detached breakwater during the run-up period. The spatial profile of the water level is shown in Fig. 9d). The difference of the water level between the crown and just shoreward point of the breakwater is large, and thin curret develops on the slope at the initial stage of the wave run-up. In calculating the current over the detached breakwater it is important to take into account the separation of the current at the breakwater.

In case of the permeable detached breakwater the type of the current over the breakwater is different from the impermeable one. The separation of the current is not remarkable at the crown of the breakwater. As a result, it is found that both water level and velocity obtained in the experiment and the simulation (see Fig. 8) have better agreement than that of the impermeable case.

5. CONCLUSION

The numerical simulation was compared with the experimental results on tsunami run-up in the case that some coastal structures and sand dune existed on a coast. It is found that the simple model used in this study has an ability to simulate tsunami movement with enough accuracy in practical use. In the case of the detached breakwater it is important to taken into consideration of the current over the breakwater at the crown of the breakwater. However, in the case of the permeable breakwater, which is usually constructed in Japan, detached breakwater can be modelled by the bed level change in one grid.

REFERENCE

1) Iwasaki, T. and A. Mano : Numerical simulation on 2-dimensional tsunami run-up using Eularian coordinates, Proc. 26th Japanese Conf. on Coastal Eng., pp. 250-254, 1979(in Japanese).

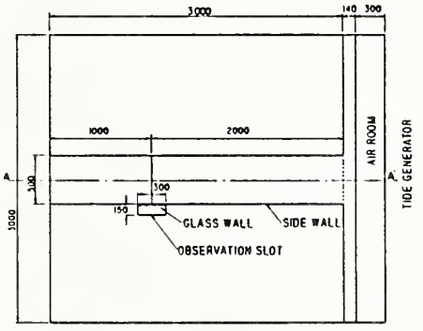

a) plane section

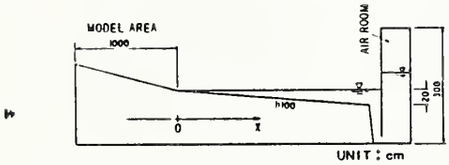

b) cross section (A-A')

Fig. 1 Wave basin

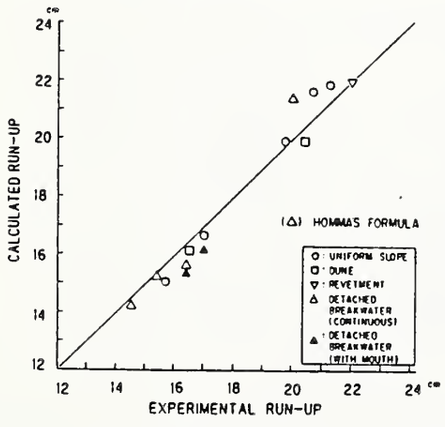

Fig. 3 Comparison of run-up height

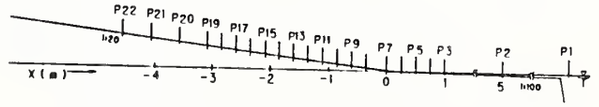

a) 1/20 uniform slope

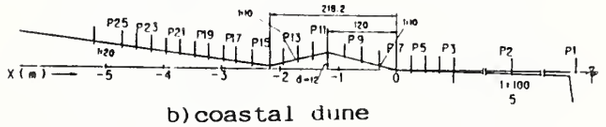

b) coastal dune

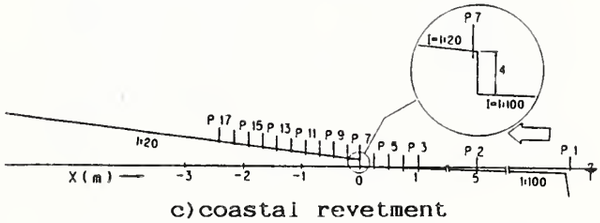

c) coastal revetment

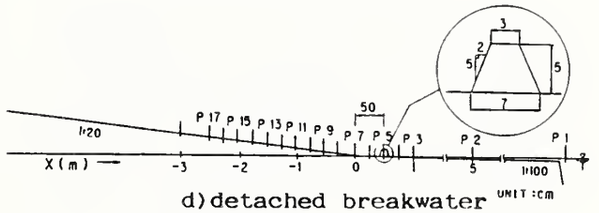

d) detached breakwater

Fig. 2 Models and locations of measuring

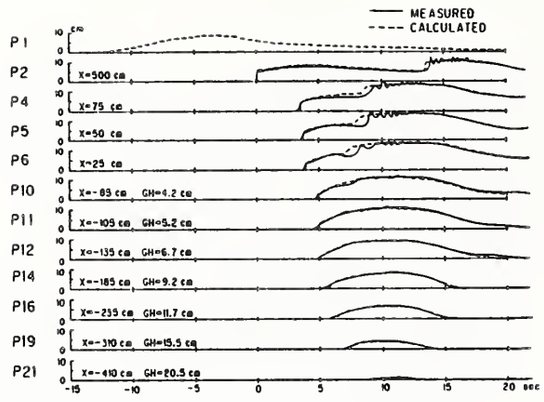

a) water level

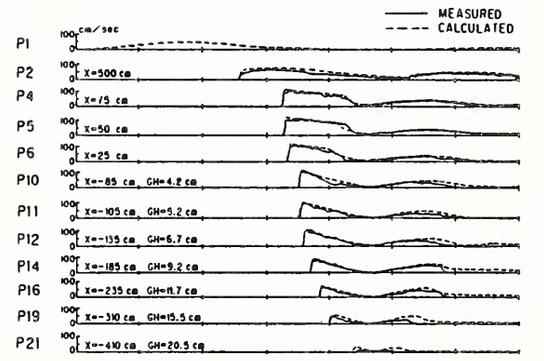

b) velocity

Fig. 4 Time series of water level and velocity (1/20 uniform solpe)

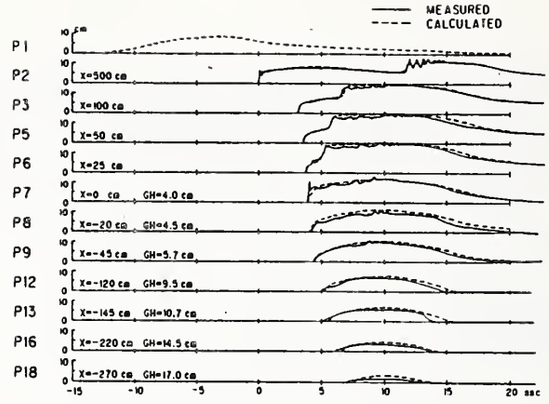

a) water level

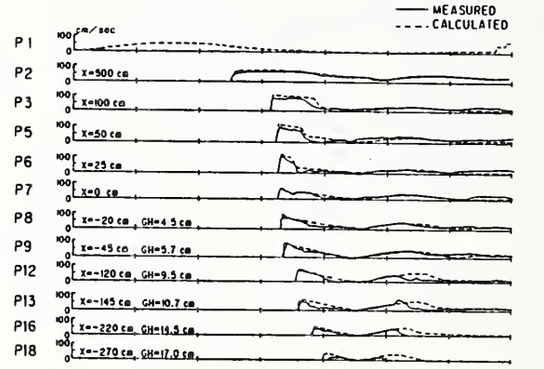

b) velocity

Fig. 6 Time series of water level and velocity (coastal revetment)

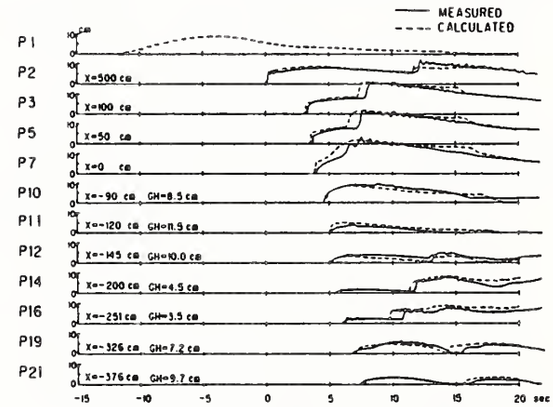

a) water level

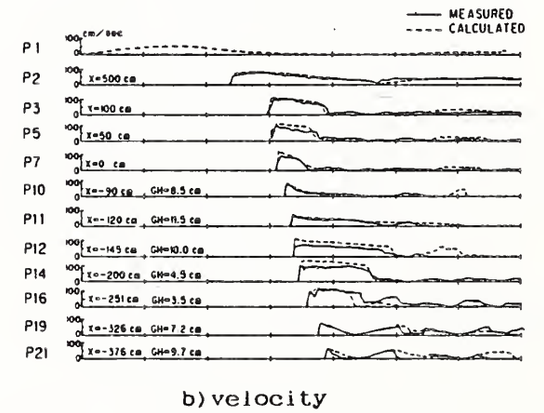

b) velocity

Fig. 5 Time series of water level and velocity (coastal dune)

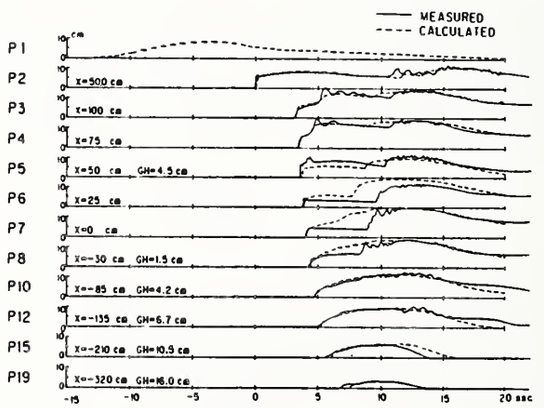

a) water level

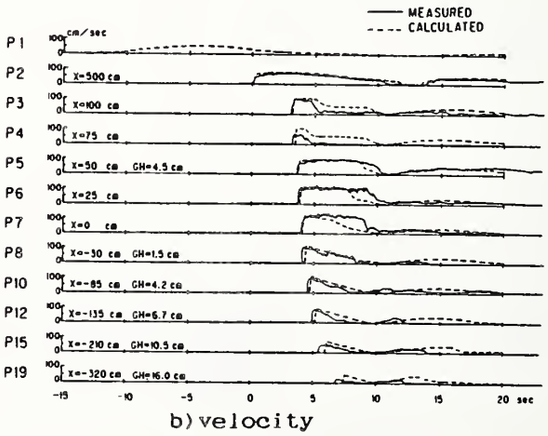

b) velocity

Fig. 7 Time series of water level and velocity (Detached breakwater: impermeable)

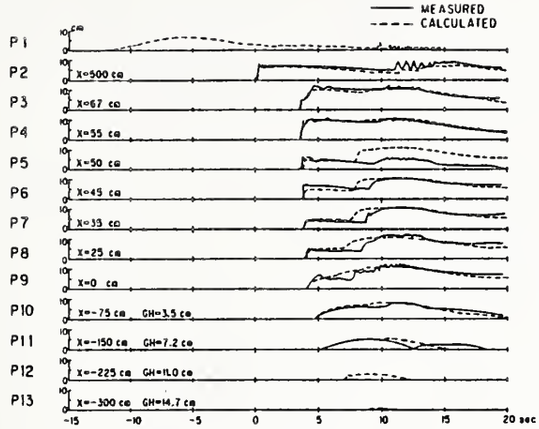

a) water level

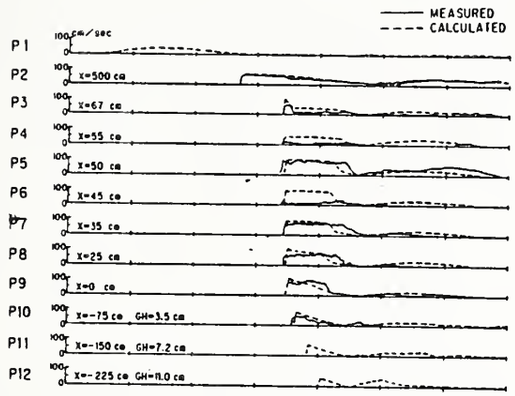

b) velocity

Fig. 8 Time series of water level and velocity
(Detached breakwater: permeable)

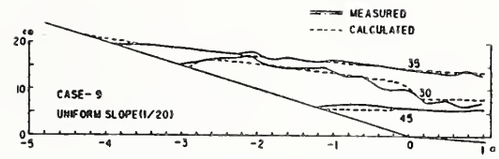

a) 1/20 uniform slope

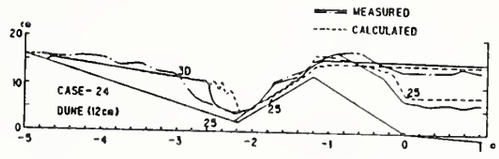

b) coastal dune

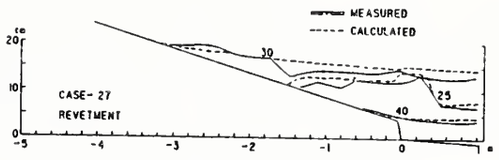

c) coastal revetment

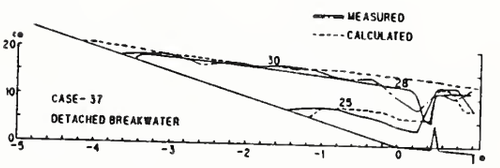

d) detached breakwater (impermeable)

Fig. 9 Spatial profiles of water level

Theme IV

U.S.-Japan Cooperative Research Program

Effect of Number of Loading Cycles and Loading Velocity of Reinforced Concrete Bridge Piers

BY

Toshio Iwasaki[1], Kazuhiko Kawashima[2],
Kinji Hasegawa[3], Tatsuhiko Koyama[4],
and Takeshi Yoshida[4]

ABSTRACT

A series of dynamic loading tests with use of large-scale reinforced concrete bridge piers was conducted to investigate an effect of number of load reversals with the same displacement amplitude as well as an effect of loading velocity. For studying the number of load reversals, seven specimens were subjected to a series of step-wise increasing symmetric displacement with n cycles, in which number of cycles n was varied from 3 to 10 as a parameter to be investigated. For studying the loading velocity, three specimens were subjected to a series of dynamic loading with velocity of 10 cm/sec and 100 cm/sec.

It was understood from the study that although deterioration of the specimen progresses, as a general trand, in accordance with increase of the number of inelastic loading cycles, for specimens which failed in flexure, effect of the number of loading cycles between 3 and 10 is less significant at the loading desplacement smaller than or equal to the displacement at which the maximum load was developed. It was also found that deterioration of the specimen subjected to dynamic loading of 10 cm/sec takes place earlier by an amount of approximately 1 δ_y than that subjected to dynamic loading of 100 cm/sec.

KEY WORDS: Bridge Pier, Dynamic Loading Test, Reinforced Concrete Structure, Seismic Design

1. INTRODUCTION

In the past, number of highway bridge have suffered damages due to extreme earthquakes. Reinforced concrete bridge piers supporting superstructures are quite susceptible to damage from strong ground motions. This fact became evident during the Miyagi-ken-oki Earthquake of 1978, when numerous reinforced concrete bridge piers designed by the traditional elastic approach suffered severe damages[1]. Such evidence clearly showed the importance to study inelastic behavior with energy dissipation of reinforced concrete bridge piers under severe ground motions.

Various investigations have been made to study inelastic behavior of reinforced concrete bridge piers subjected to strong earthquakes, and specimens simulating reinforced concrete bridge piers have been tested under various loading conditions such as static and dynamic cyclic loading, earthquake-like loading[2)~9)]. In almost all the test, however, loads were step-wise increased monotonically up to failure, in which at each step several cycles of symmetrical loading reversals with the same displacement amplitude were carried out. Although number of loading cycles at each step may have a significant effect on the test results, little is known about the effect of load reversals on the mechanism of inelastic behavior of reinforced concrete bridge piers. Because structural response amplitude also highly depends on the number of response cycles[10)], it is inevitable to study such effects in order to apply the dynamic loading test data for practical seismic design of reinforced bridge piers which are to be subjected to earthquake ground motion.

1 Dr. of Engr., Director, Earthquake Disaster Prevention Department, Public Works Research Institute, Ministry of Construction, Japan
2 Dr. of Engr., Head, Earthquake Engineering Division, Earthquake Disaster Prevention Department, Public Works Research Institute, Ministry of Construction, Japan
3 Research Engineer, ditto
4 Assistant Research Engineer, ditto

Furthermore, althougl the seismic effects to bridge piers are dynamic, in almost all the past tests the specimens were subjected to static loading from a limitation of loading facilities.

This study presents a series of dynamic loading test results of large-size reinforced concrete bridge pier models subjected to different number of load reversals with the same displacement amplitude and different loading velocities. Effect of number of loading cycles and loading velocities on strength and energy dissipating capacity is presented in terms of comparison of hysteresis loop, accumulated energy dissipation and equivalent damping ratio.

2. TEST SPECIMENS AND EXPERIMENTAL SET-UP

2.1 Effect of Number of Loading Cycles

Seven large-size reinforced concrete specimens simulating cantilever piers of bridges as shown in Fig. 1 and Table 1 were used for studying the number of load reversals. Specimen number presented show those used to identify specimens in a series of dynamic loading tests conducted at the Public Works Research Institute[11]. The cantilever pier was framed into a massive reinforced concrete footing which was anchored to a test floor by means of post tensioned rods. The common characteristics over the seven specimens are the cross section of 50 cm x 50 cm, main reinforcement ratio of 2.03 % with use of 40 SD30 bars(deformed bar) with diameter of 13 mm, and tie reinforcement ratio of 0.1 % with use of 9 mm diameter SR24 bars (plain bar) placed at 25 cm intervals. The layout of tie bars depends on the Japanese practice in accordance with the Specifications for Design of Highway Bridges. The tie bars were lapped at least 60 mm. They used portland cement with uni-axial compression strength ranging from 319 to 340 Kg/cm^2, and agregates with the maximum grain size of 10 mm. Effective pier heights h from bottom to the center of loading point were taken as parameter to be investigated as 2.5 m (P-10, P19 and P-20), 1.752 m (P-17 and P-20) and 1 m (P-18 and P-20) so that the shear-span ratio, which is defined as a ratio between effective height h and effective width d (width-covering depth), becomes 5.4, 3.8 and 2.2, respectively.

2.2 Effect of Loading Velocity

For studying the effect of loading velocity, three reinforced concrete cantilever specimens as shown in Fig. 2 were used. They have the same characteristies on the cross section of 80 cm x 40 cm, effective pier hight h of 2.4m, main reinforcement ratio of 0.87 % and tie reinforcement ratio of 0.08 %. Main reinforcements of 22 SD30 bars (deformed bars) with diameter of 13 mm were placed on only two sides which sustained tension and compression during loading, and no reinforcements were placed on the other two sides. Tie reinforcements with use of 9 mm diameter SR24 bars (plain bars) were placed at 20 cm intervals. They used portland cements with uni-axial compression strength ranging from 311 and 385 kg/cm^2, and agregates with the maximum grain size of 10 mm.

3. LOADING CONDITIONS

The specimens were loaded at the cantilever tip as shown in Fig. 3 by means of an electro-hydraulic dynamic actuator with loading capacity of ±125 tf, max. stroke of ±125 mm and max. loading velocity of 1 m/sec. Extensive electric instrumentation was used to measure and record the basic deformation parameters such as strains of main and tie reinforcements as well as the displacement and acceleration at the loading point.

Although a compression stress of about 5 to 20 Kg/cm^2 is generated in the piers with ordinary shape and height due to the dead weight of superstructure, it was disregarded in the test.

For studying the number of load reversals specimens were subjected to a series of stepwise increasing symmetric displacement cycles as shown in Fig.4. At each step, n cycles of loading with the same displacement amplitude was carried out, in which number of cycles n was varied from 3 to 10 as a parameter to be investigated. The loading velocity was taken as 25 cm/sec over each step. The step-wize was determined by increasing the displacement in each step by a displacement ductility factor of one. The yield displacement δ_y corresponding to one ductility factor was defined as the displacement at loading point at which reinforcing bars at the extreme

tension fibre firstly reached yield strain.

A number of strain guages were placed on the two longitudinal reinforcing bars on each side to the loading direction, and the averaged strain of the two reinforcing bars , which were placed at the foot of pier, was used to determine the yield displacement. The yield strain of reinforcement was assumed as 1800μ oased on a number of tensile test of the specimens.

It should be noted in the study of number of load reversals that in specimen P-18, slips between footing and test floor were developed duing the 2 δ_y loading due to inadequate anchoring of the specimen to the floor. Therefore, the 2 δ_y loading was subsequently carried out again, and these data were treated as those for 2 δ_y loading.

For studying the loading velocity, the same loading procedure as above was used, in which number of cycles n was assumed as 10, and loading velocity V was varied as 10 cm/sec and 100 cm/sec.

Because the force detected by means of a load-cell equiped in the dynamic actuator represents total force applied to the specimen including an inertia force associated with masses of the specimen and the loading jig, the lateral force P which actually loaded to the specimen was calculated assuming that the inertia force along the cantilever pier distributes in an inverted-triangle shape with the inertia force at the foot being zero.

4. EFFECT OF NUMBER OF LOADING CYCLES

4.1 Failure Mode

Figs. 5,6 and 7 show failure modes of the model piers with emphasis on cracks and spalling-off of cover concrete as well as elongation, buckling and cut of reinforcements. Failure modes on the side perpendicular and pararell to the loading direction are presented here for the specimens with shear-span ratio of 5.4 and 3.8, and those with shear-span ratio of 2.2, respectively, so that progress of failure mode be clearly observed.

The specimens with shear-span ratio of 5.4 and 3.8 failed clealy in flexure. By increasing loading displacement, flexural cracks were firstly formed on the side near foot, and spalling-off of cover concrete at the critical flexural region followed. Progress of significant flexural cracks finally penetrated the critical section causing break up of the concrete core, and inelastic buckling of main reinforcement either outwards between two adjacent tie bars or sideways were progressively developed. It should be noted here that pull-out of main reinforcement from footing was developed due to loss of bond caused by load reversals in the anchorage, which, in turn, caused rotation at the foot and contributed to the pier displacement significantly. Eventually cut of main reinforcement was developed which critically deteriorated the load and stiffness.

In comparison, the specimens with shear-span ratio of 2.2 failed in shear. By increasing loading displacement, diagonal shear cracks were firstly developed on the side, and break up of the concrete core accompanying complete spalling-off of the cover concrete brings to final degradation of the stiffness.

In all the above-descibed failure modes, increase of the number of loading cycles n clearly accelerates failure in accordance with increase of loading displacement. For example, the specimen with shear-span raio of 5.4, which were subjected to three reversals at each loading step, suffered spalling-off of cover concrete only at a region 30 cm from the foot even after the loading with displacement amplitude of 8 δ_y, while the same specimen subjected to ten reversals at each loading suffered much severe spalling-off of cover concrete at a region 40 cm from the foot after the 5 δ_y loading.

Table 2 showed an effect of number of loading cycles for flexural failure in terms of number of longitudinal reinforcement which were cut due to cyclic inelastic buckling. No longitudinal reinforcements were cut in the specimens which failed in shear. It is apparent that the number of loading cycles is of significant factor affecting the ultimate failure mode of flexural cantilever piers associated with cut of main reinforcement.

Fig. 8 shows strains induced in the tie bars of the specimens with shear-span ratio of 2.2. Although failure of concrete made unable to measure the strain of tie bars for larger loading displacements, it is apparent that increase of number of loading cycles brings increase of strains developed in tie bars. It should be noted that tie bar at 50 cm from foot (mid-height of the pier), which were subjected to ten reversals at each step, already yielded even at 2 δ_y loading displacement.

4.2 Strength and Deformation Capacity

The behavior of the test specmens was firstly studied from continuous plots of hysteresis loop of the load vs. displacement at the loading point. Fig. 9 shows comparisons of the envelopes of the hysteresis loops.

For the flexural specimens with shear-span ratio of 5.4 and 3.8, effect of the number of loading cycles varies in accordance with loading displacement. For loading dispacement smaller than or equal to 4 δ_y for specimens with h/d = 5.4 and 3 δ_y for specimens with h/d = 3.8, the envelopes of hysteresis loop seem almost independent of the number of loading cycles. It should be noted here that the critical displacments 4 δ_y (h/d = 5.4) and 3 δ_y (h/d =3.8) correspond to those at which the maximum loads were achieved. This implies that for flexural specimens the number of loading cycles has less significant effect on the envelopes of hysteresis loop until the maximum load is developed. However after these displacements, a significant drop in load can be observed in the envelopes in accordance with increase of the number of loading cycles. Especially, as was previously discussed, drops in load associated with cut of longitudinal reinforcements critically depend on the number of loading cycles.

On the other hand, for the specimens with shear-span ratio of 2.2, which failed in shear, more significant changes of envelope of hysteresis loop in accrdance with the number of loading cycles are observed ,i.e., for loading displacement larger than $\delta_y \sim 2\delta_y$, the envelope of the specimen subjected to ten reversals is much smaller in load than that of the specimen subjected to three reversals. It should be, however, noted that there is some doubts as to whether the difference observed in the comparison of envelops can be entirely attributed to the effect of number of loading cycle, because of the slips developed in specimen P-18 between footing and test floor during 2 δ_y loading. As was described in the preceding chapter, as a consequence the P-18 specimen was totally subjected to 20 load reversals with 2 δ_y displacement, and this might cause appreciable deterioration of the specimen. However, since progress of break up of the concrete core accompanying yielding of tie bars is pronounced in shear specimens, it is considered reasonable that effect of number of loading cycle is more pronounced in shear specimens than in flexural specimens although the difference observed in Fig. 9 (c) is not necessarily entirely caused by the effect of number of loading cycles.

Table 3 summalizes the yield load P_y, max. load P_u, yield displacement δ_y and ultimate displacement δ_u for seven specimens. Only averaged values developed between in positive and in negative loading directions are presented in Table 3. For specimens with shear-span ratio of 5.4 and 3.8, the max load Pmax is almost free from the number of loading cycles , which, in turn, shows that a ratio of the max. load to the yield load , P_u/P_y, is also almost independent of the numben of loading cycles. For specimens with shear-span ratio of 2.2, the max. load P_u when subjected to three inelastic revesals is only 8% larger than that subjected to ten inelastic reversals, i.e., effect of number of loading cycles in terms of the max. load P_u is not necessarily significant as anticipated from clear difference which was observed in the envelope of hysteresis loop presented in Fig. 9 (c).

In comparison, the ultimate displacement δ_u of the specimens which failed in flexure significantly varies in accordance with the number of loading cycles, which, in turn, affects the ductility factors, i.e., a ductility factor obtained from the tests using three inelastic revesals for the same displacement amplitude is 36% and 19% larger than those from ten inelastic reversals tests for specimens with shear-span ratio of 5.4 and 3.8, respectively. Therefore the number of loading cycles have to be well examined

when the ductility factors obtained with different test procedures are to be compared. The ductility factor for specimens with shear-span ratio of 2.2 does not, however, show significant changes with respect to the number of loading cycles.

4.3 Energy Dissipating Capability

An area surrounded by a hystersis loop as shown in Fig.10 represents an amount of energy dissipated during that loading reversal, and hence, accumulating the energy dissipation during each loading reversal, total amount of energy dissipated in the specimen during the loading test may be calculated. Since the accumulated energy dissipation so obtained is lager in those specimens which experienced larger number of loading cycles, direct comparisons of the accumulated energy dissipation do not represent the energy dissipation capability of the specimens. Therefore, the accumulate energy dissipations calculated for the specimens which were subjected to three and five cycles of inelastic reversals for each loading step were multiplied by a factor of 10/3 and 10/5, respectively, so that the accumulated energy dissipation be compared on the basis of the same number of loading cycles of ten. Fig.11 represents the accumulated energy dissipation thus obtained.

As anticipated from the previous discussions, the accumulated energy dissipation significantly decreases with increasing the number of loading cycles not only in the specimens which failed in flexure but those in shear. It should be noted, however, that such decreases of the accumulated energy dissipation with respect to increase of the number of loading cycles become apparent at the loading displacement larger than about 4 δ_y, 3 δ_y, and 2 δ_y for the specimens with shear-span ratio of 5.4, 3.8 and 2.2, respectively. It should be reminded from Fig.9 that those loading displacements almost correspond to the loading displacement at which the maximum load was developed. Therefore it may be considered that effects of the number of loading cycles on capability of energy dissipation are less significant until the maximum load was developed, and that it progressively becomes significant after the maximum load. Total amount of accumulated energy dissipated during the test for the specimens which were subjected to three load reversals is approximately 50% larger than that for the specimens which were subjected to ten load reversals.

Energy dissipation capability was also studied in terms of an equivalent hysteretic damping ratio h_e which is defned as

$$h_e = \frac{1}{2\pi}\frac{\Delta W}{W} \quad \cdots\cdots (1)$$

in which W is an energy dissipated during one load reversal and W is an elastic energy as defined in Fig 10. Fig.12 shows variations of the equivalent hysteretic damping ratio h_e with respect to the displacement amplitude of cyclic loading. As a general trend, the equivalent damping ratios increase with increasing the loading displacement, take a peak value of approximately 0.2 at 4 δ_y (h/d=5.4 and 3.8) and 0.12 ~ 0.16 at 2~3 δ_y (h/d=2.2), and progressively decrease to a value of about 0.15 (h/d=5.4 and 3.8) and 0.1(h/d=2.2). The effect of number of loading cycles can be observed in the decreasing path after h_e takes the peak value, i.e., h_e decreases promptly in the specimens which were subjected to larger number of loading cycles.

5. EFFECT OF LOADING VELOCITY

5.1 Failure Mode

Fig.13,14 and 15 compare failure modes observed on the side surface perpendicular to the loading direction. Progresses of the flexural failure in the three specimens are essentially the same with those observed in Fig. 5 and 6 , i.e, by increasing loading displacement, flexural cracks were firsty formed, and spalling-off of cover concrete at the critical flexural region followed. Subsequently, significant flexural cracks penetrated into concrete core, and even cuts of main reinforcement were developed. It should be noted, however, that the spalling-off of cover concrete was initiated at 4 δ_y for the specimen with loading velocity of 10 cm/sec, while it was initiated at 5 δ_y for two specimens with loading velocity of 100 cm/sec.

It was also observed that cuts of main reinforcements were developed during 6 δ_y loading displacement for the specimen with

loading velocity of 10 cm/sec, while they were developed during the 7 δ_y loading displacement for the two specimens with loading velocity of 100 cm/sec. Table 4 shows the effect of loading velocity in terms of loading displacements where spalling-off of cover concrete and cut of main reinforcement were initiated. It is clear from these evidence that failure is likely to develop promptly in specimen subjected to loading velocity of 10 cm/sec with an amount of approximately 1 δ_y as compared with the specimens subjected to loading velocity of 100 cm/sec.

5.2 Strength and Deformation Capacity

Fig.16 shows the hysteresis loops of the load vs. displacement at the loading point, and Fig.17 shows the comparison of first excursion of hysteresis loops. The hysteresis loops between three specimens show the same behavior for displacement smaller or equal to 4 δ_y, which implies that the effect of loading velocity is less significant for that displacement. However, beyond loading displacement of 5 δ_y, specimen subjected to loading velocity of 10 cm/sec shows appreciable drop in load as compared with the specimens subjected to the loading velocity of 100 cm/sec. The shape of hysteresis loop is also lean in the specimen subjected to loading velocity of 10 cm/sec. Such a prompt deterioration of the specimen with loading velocity of 10 cm/sec is clearly brought by the prompt progress of flexural failure as described in the preceding section.

Fig.18 shows comparison of load vs. displacement relation of the specimen in terms of envelopes of the hysteresis loop. As was auticipated from the above discussion, the maximum load was developed at 2 δ_y on + side and 4 δ_y on - side for loading velocity of 10 cm/sec, while it was developed at 4 δ_y on + side and 4 ~ 5 δ_y on - side for loading velocity of 100 cm/sec. This shows that the maximum loads are developed at larger loading displacement in accordance with increase of loading velocity, which implies that stable load vs. displacement hysteresis can be credited in the loading with higher loading velocity.

Table 5 summalizes the load and displacement performance of the three specimens.

5.3 Energy Dissipating Capability

Figs.19 and 20 show comparison of energy dissipation and equivalent hysteretic damping ratio h_e for the three specimens. It is clear in these comparison that difference of the energy dissipation and equivalent hysteretic damping ratio in accordance with loading velocity is less significant for loading displacement smaller than or equal to 4 δ_y. However beyond this displacement, the energy dissipation and equivalent damping ratio take larger value in loading velocity of 100 cm/sec than in loading velocity of 10 cm/sec.

It should be noted here that the loading displacement of 4 δ_y almost corresponds to the displacement where the load begins to decrease after taking the maximum load P_u.

6. CONCLUDING REMARKS

In an attempt to study effects of number of inelastic loading cycles and loading velocity on strength and energy dissipating characteristics of reinforced concrete bridge piers, a series of dynamic loading tests with use of ten large-size specimens was conducted by varying the number of inelastic loading cycles from three to ten and by varying the loading velocity as 10 cm/sec and 100 cm/sec. Shear-Span ratio of the specimens was 5.4, 3.8 and 2.2 for the study of number of loading cycles, and 6.8 for the study of loading velocity. Based on the test results presented, the following conclusions may be deduced :

1) Effect of number of loading cycles

i) As a general trend, deterioration of the specimen progresses in accordance with increase of the number of inelastic loading cycles with regardless of flexural failure or shear failure.

ii) However, for specimens with shear-span ratio of 5.4 and 3.4 which failed in flexure, effect of the number of loading cycles between 3 and 10 is less significant for the loading displacement smaller than or equal to the dispacement at which the maximum load was

developed. Within this loading displacement, the envelope of hysteresis loop, acumulated energy dissipation, equvalent hysteretic damping ratio and the maximum load are less significantly affected by the number of inelastic loading cycles. However, over this displacement, deteriorations of the specimen becomes significant in accordance with number of inelastic loading cycles. Especially, deterioration of the specimen associated with cut of main reinforcement due to cyclic inelastic buckling critically depends on the number of loading cycles.

iii) For the specimens with shear-span ratio of 2.2, which failed in shear, the effect of number of inelastic loading is much significant as compared with the flexural specimens. The envelope of hysteresis loop shows significant drop in load at displacements larger than $\delta_y \sim 2\ \delta_y$.

2) Effect of loading velocity

i) Deterioration of the specimens in terms of loading displacements at which spalling-off of cover concrete and the maximum load P_u were developed takes place earlier in specimen subjected to loading velocity of 10 cm/sec than those subjected to loading velocity of 100 cm/sec with an amount of approxinately $1\ \delta_y$.

ii) Effect of loading velocity on energy dissipating capability in terms of accumulated energy dissipation and equivalent damping ratio are less significant for loading displacement smaller than or equal to $4\ \delta_y$. However beyond this displacement, energy dissipation capability is appreciably larger in the specimens subjected to loading velocity of 100 cm/sec than in the specimen subjected to loading velocity of 10 cm/sec.

REFERENCES

1) Okubo, T. , Ohashi, M. , Iwasaki,T. , Kawashima, K. and Tokida, K. : Damage Features of Civil Engineering Structures due to The Miyagi-ken-oki Earthquake of 1978, 11th Joint Meeting, Wind and Seismic Effect, UJNR, Tsukuba, Japan, 1979.

2) Park, R. and Blakeley, R.W.G. : Seismic Design of Bridges, RRU Bulletin 43, National Roads Board, 1979

3) Yamamoto, T., Ishibashi, T., Otsubo, M., and Kobayashi, S. : Experimental studies on Seismic Resistance of A Pier with Reinforcement Terminated in A Tension Zone, Proc. of JSCE, Vol.348, V-1, 1984.

4) Ohta, M. : A Study on Earthquake Resistant Design for Reinforced Concrete Bridge Piers of Single- Column Type, Report of the Public Works Research Institute, Vol. 153, 1980 (in Japanese).

5) Ikeda, S., Eya, S. and Yamaguchi, T. : Behavior of Reinforced Concrete Cylindrical Columns under Reversed Cyclic Loadings, Trans. of the Japan Concrete Institute, 1986.

6) Mutsuyoshi, H., Machida, A. and Tsuruta, K. : Predicting the Nonlinear Earthquake Response of Reinforced Concrete Structures in Consideration of Strain Rate Effect, Proc. of Japan Society of Civil Engineers, vol. 366, V-4, 1986.

7) Park, R., Kent, D.C. and Sompson, R.A. : Reinforced Concrete Members with Cyclic Loading, Proc. of ASCE, vol. 98, No.9ST7, 1972.

8) Krawinkler, H. and Popov, E. : Hysteresis Behavior of Reinforced Concrete Rectangular and T-Beam, 6 WCEE

9) Gulkam, P. and Sozen, M. : Inelastic Response of Reinforced Concrete Structures to Earthquake Motions, ACI Journal, 1974.

10) Kawashima, K. and Aizawa, K. : Earthquake Response Spectra Taking Account of Number of Response Cycles, Earthquake Engineering and Structural Dynamics, Vol. 14, 1986.

11) Kawashima, K., Hasegawa, K. Koyama, T. and Yoshida, T. : Experimental Investigation on Dynamic Strength and Ductility of Reinforced Concrete Bridge Piers, Part I, No.2232 of the Technical Memorandum, Public Works Research Institute, Ministry of Construction, 1985.

Table-1 Specifications of Test Specimens for Studying Number of Load Reversals

Shear-Span Ratio h/d			5.4			3.8		2.2	
Number of Loading Cycles n			10	5	3	10	3	10	3
Specimen			P-10	P-22	P-19	P-17	P-20	P-18	P-21
Cross-section		[cm]	50 x 50	50 x 50	50 x 50	50 x 50	50 x 50	50 x 50	50 x 50
Effective Height h		[cm]	250	250	250	175	175	100	100
Main Reinforcement	Material and Diameter	[mm]	SD30,13	SD30,13	SD30,13	SD30,13	SD30,13	SD30,13	SD30,13
	Reinforcement Ratio	[%]	2.03	2.03	2.03	2.03	2.03	2.03	2.03
Tie Bar	Material and Diameter	[mm]	SR24, 9	SR24, 9	SR24, 9	SR24, 9	SR24, 9	SR24, 9	SR24, 9
	Reinforcement Ratio	[%]	0.1	0.1	0.1	0.1	0.1	0.1	0.1
Concrete (Portland Cement)	Max. Grain Size of Aggregate	[mm]	10	10	10	10	10	10	10
	Cylinder Strength	[kg/cm²]	319	320	340	328	324	334	321
Loading Velocity		[cm/sec]	25	25	25	25	25	25	25

Table-2 Number of Longitudinal Reinforcement Cut During Cyclic Loading

Shear-Span Ratio h/d	5.4			3.8		2.2	
Number of Loading Cycles n	10	5	3	10	3	10	3
1 ~ 5 δy	0	0	0	0	0	0	0
6 δy	1	0	0	0	0	0	0
7 δy	3 (4)	0	0	6	0	0	0
8 δy	7 (11)	2	0	6 (12)	0	0	0

Table-3 Comparison of Load and Displacement Performance

Shear-Span Ratio h/d			5.4			3.8		2.2	
Number of Loading Cycles n			10	5	3	10	3	10	3
Load	Yield Load Py	[t]	11.6	10.9	10.9	15.9	15.5	27.6	27.7
	Maximum Load Pu	[t]	16.8	16.7	16.6	24.2	24.6	39.1	42.7
	Pu/Py		1.45	1.53	1.52	1.52	1.59	1.42	1.54
Displacement	Yield Displacement δy	[cm]	1.30	1.30	1.30	0.75	0.75	0.39	0.39
	Ultimate Displacement δu	[cm]	9.26	11.45	12.59	5.92	7.08	2.02	1.99
	δu/δy		7.1	8.8	9.7	7.9	9.4	5.2	5.10

Table-4 Comparison of Failure Modes

Loading Velocity V		10cm/sec	100 cm/sec	
Specimen		P-37	P-38	P-39
Initiation of Spalling-off of Cover Concrete	+ side	4 δy	6 δy	6 δy
	− side	5 δy	5 δy	5 δy
Number of Main Reinforcement Cut during Londing	1 ~ 5 δy	0	0	0
	6 δy	4	0	0
	7 δy	−	11	11

Table-5 Comparison of Load and Displacement Performance

Loading Velocity		10cm/sec	100 cm/sec	
Specimen		P-37	P-38	P-39
Load	Yield Load Py [t]	7.1	8.1	6.3
	Maximum Load Pu [t]	8.4	9.0	9.0
	Pu / Py	1.18	1.11	1.43
Displacement	Yield Displacement δy [cm]	0.91	0.85	0.84
	Ultimate Displacement δu [cm]	5.7	5.7	7.5
	δu / δy	6.3	6.7	8.9

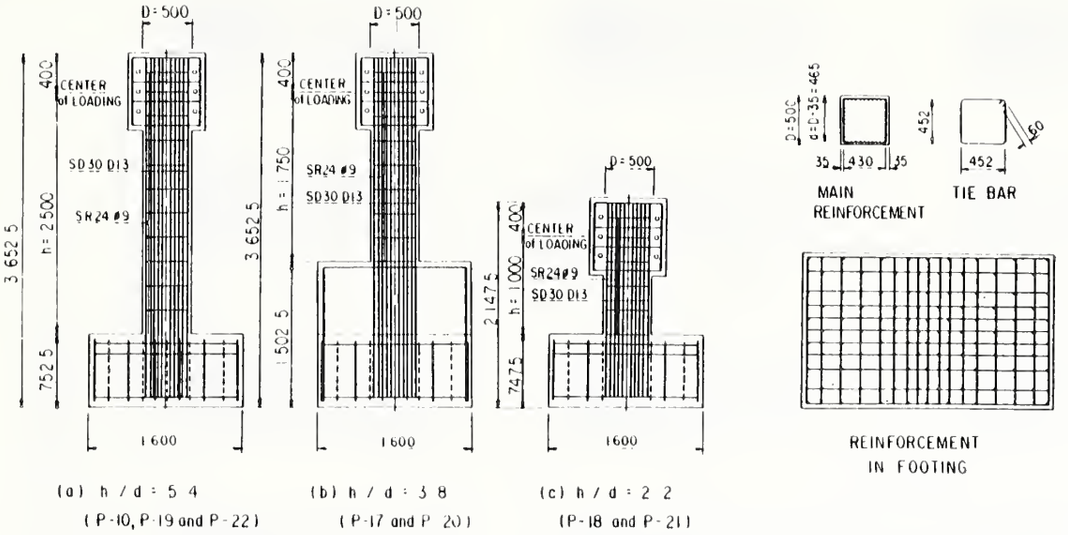

Fig. 1 Test Specimens for Studying Number of Load Reversals

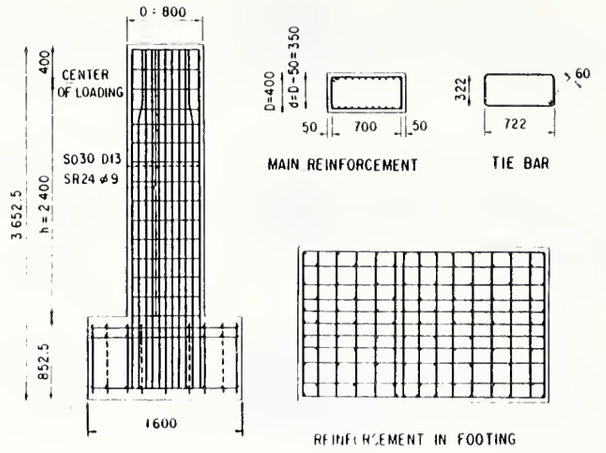

Fig. 2 Test Specimens for Studying Loading Velocity

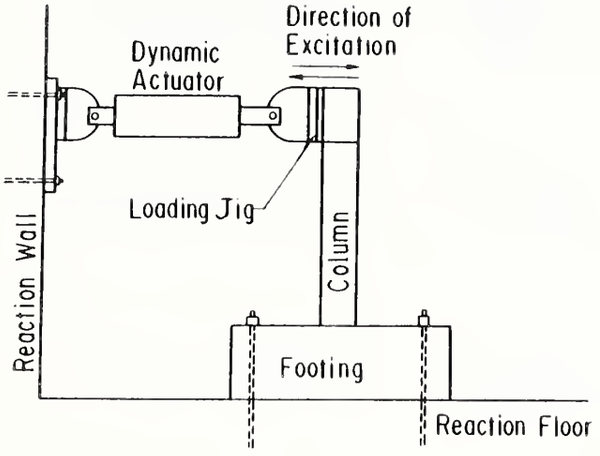

Fig. 3 Experimental Set-up

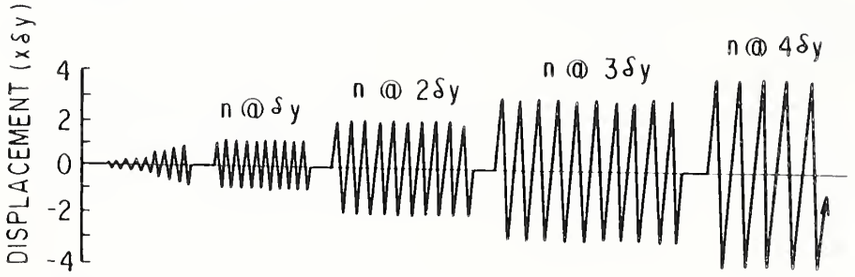

Fig. 4 Step-wise Increasing Symmetric Loading Displacement with n Reversals

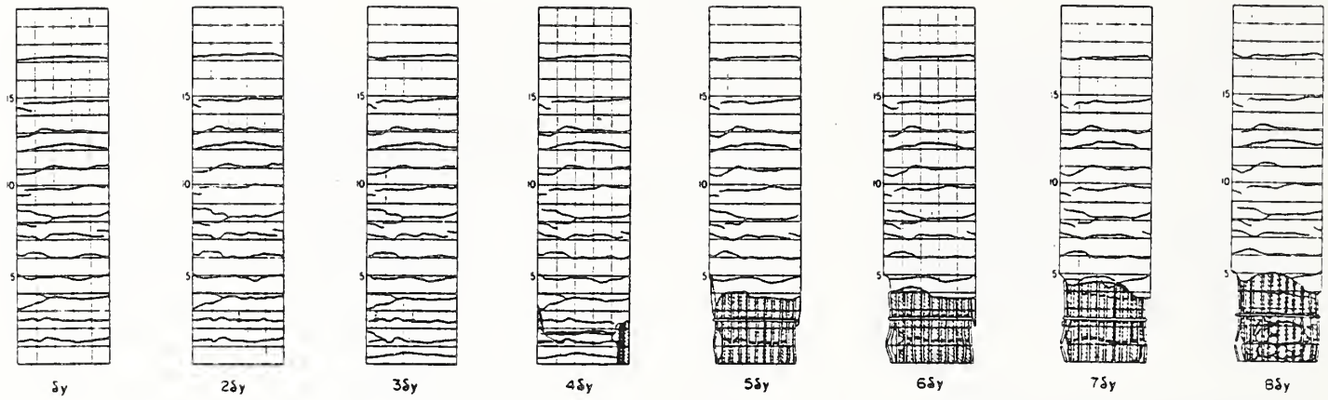

(a) Number of Loading cycle n=10

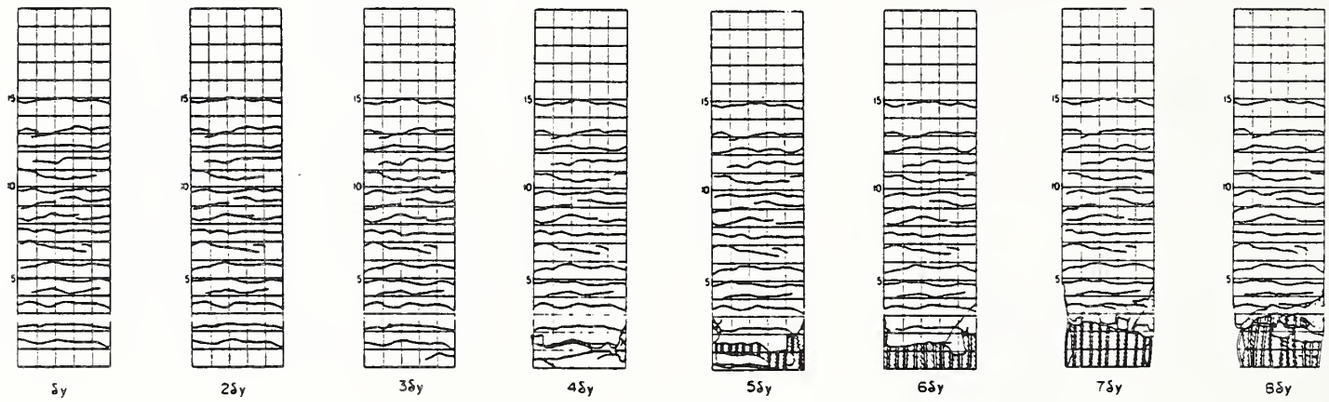

(b) Number of Loading cycle n=3

Fig. 5 Failure Mode for Specimen with h/d=5.4

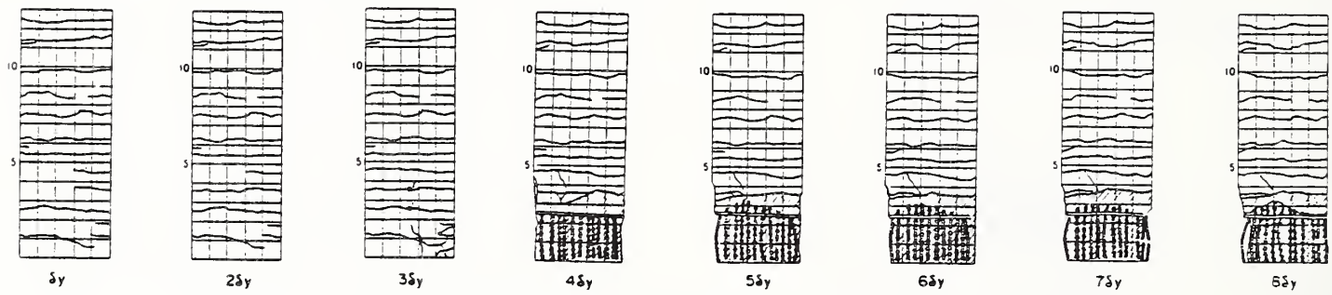

(a) Number of Loading cycle n=10

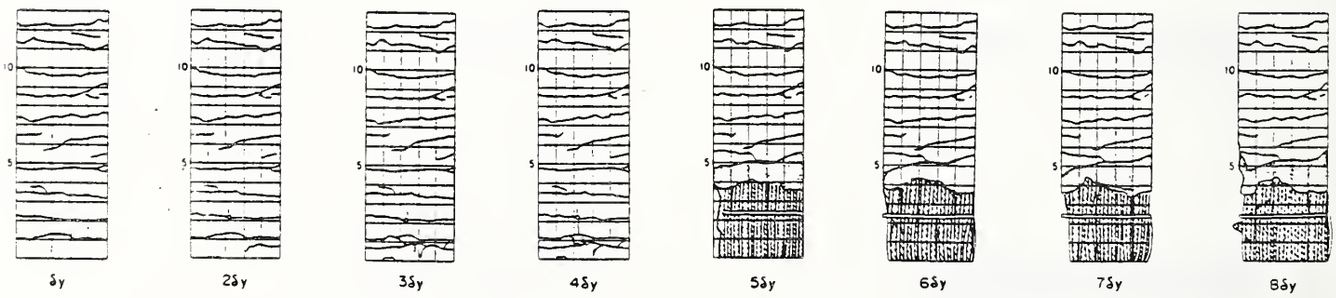

(b) Number of Loading cycle n=3

Fig. 6 Failure Mode for Specimen with h/d=3.8

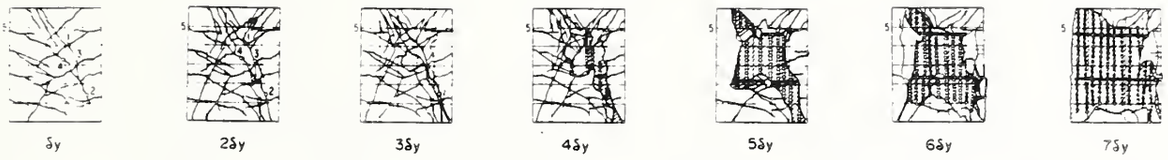

(a) Number of Loading cycle n=10

(b) Number of Loading cycle n=3

Fig. 7 Failure Mode for Specimen with h/d=2.2

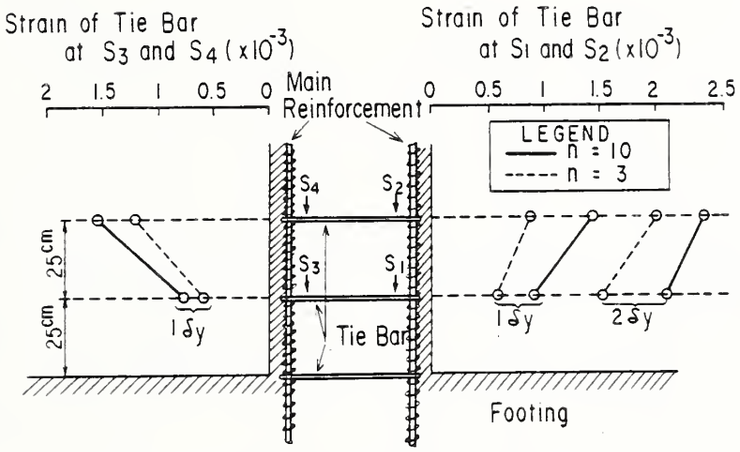

Fig. 8 Strains Induced in Tie Bars

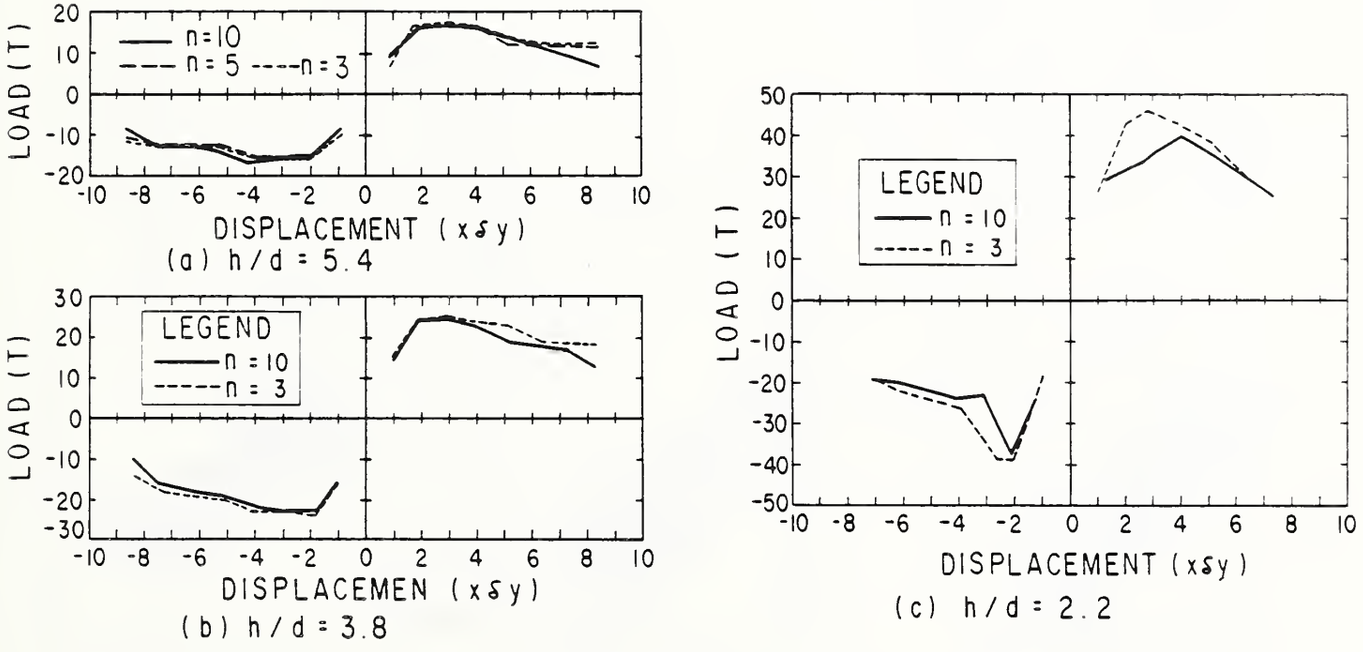

Fig. 9 Comparison of Envelope of Hysteresis Loops

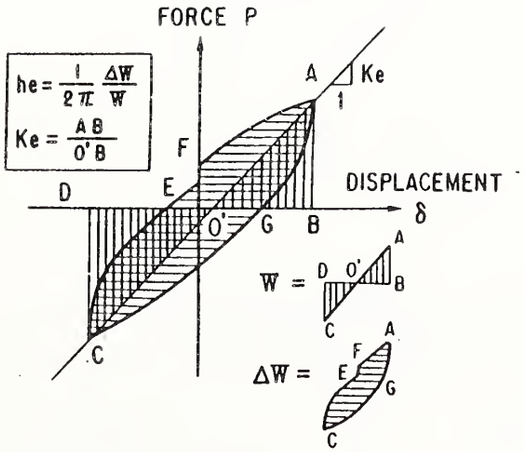

Fig.10 Definition of Equivalent Hysteretic Damping Ratio

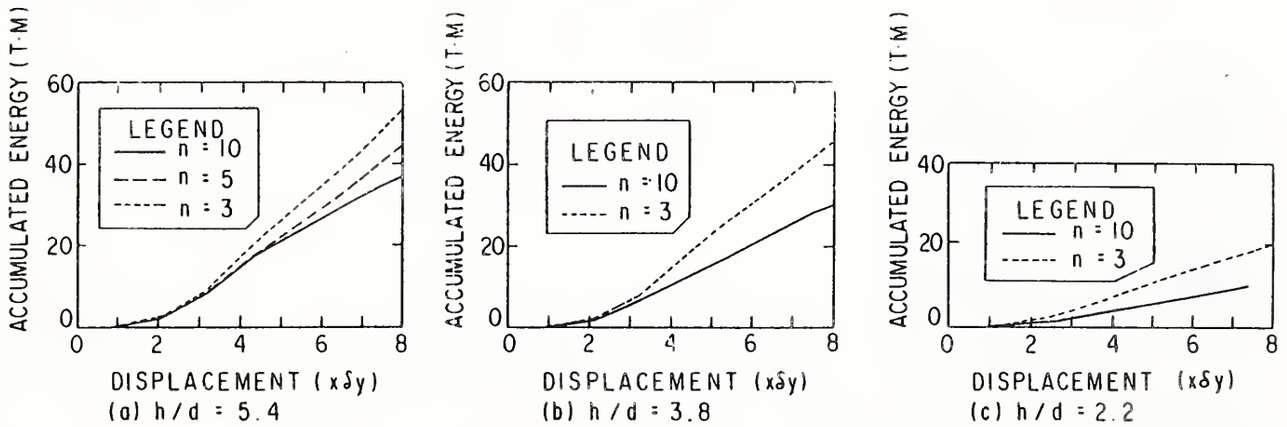

Fig.11 Comparison of Accumulated Energy Dissipation

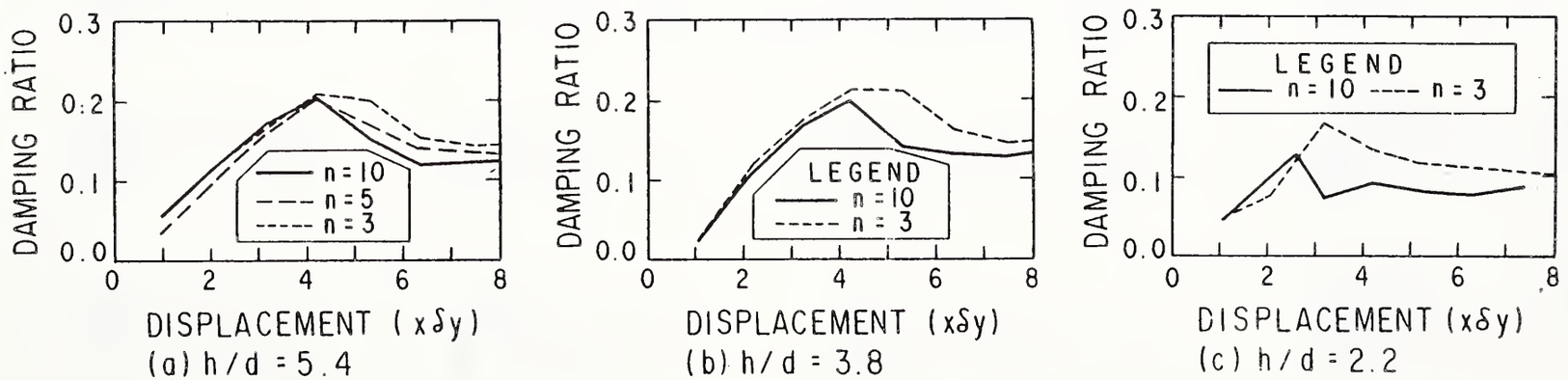

Fig.12 Comparison of Equivalent Hysteretic Damping Ratio

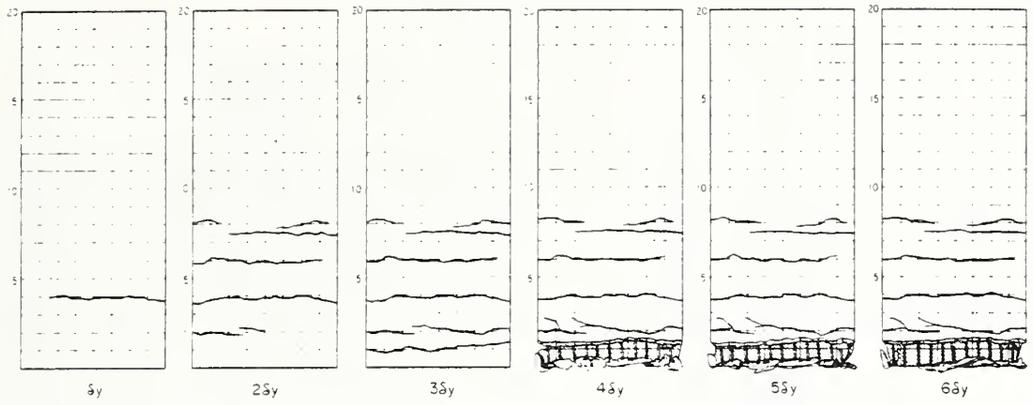

Fig.13 Failure Mode for Specimen with Loading Velocity V=10cm/sec (P−37)

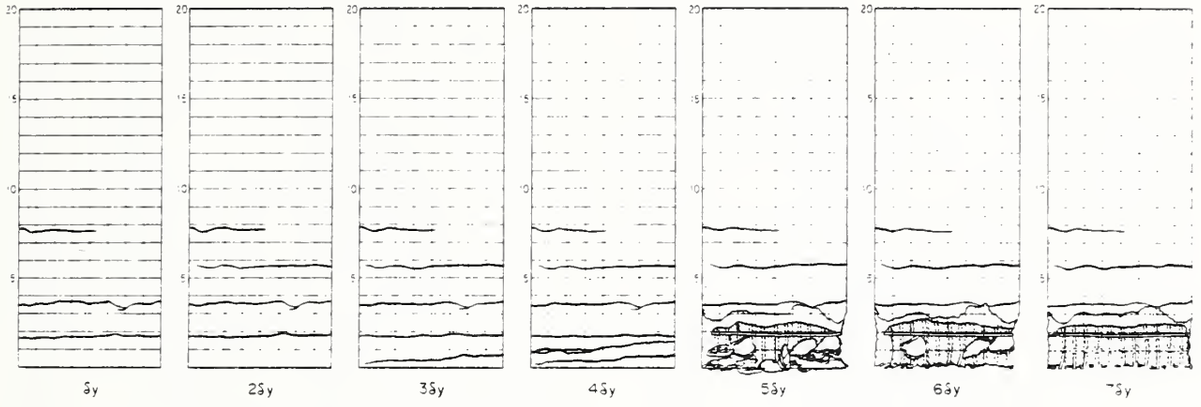

Fig.14 Failure Mode for Specimen with Loading Velocity V=100cm/sec (P−38)

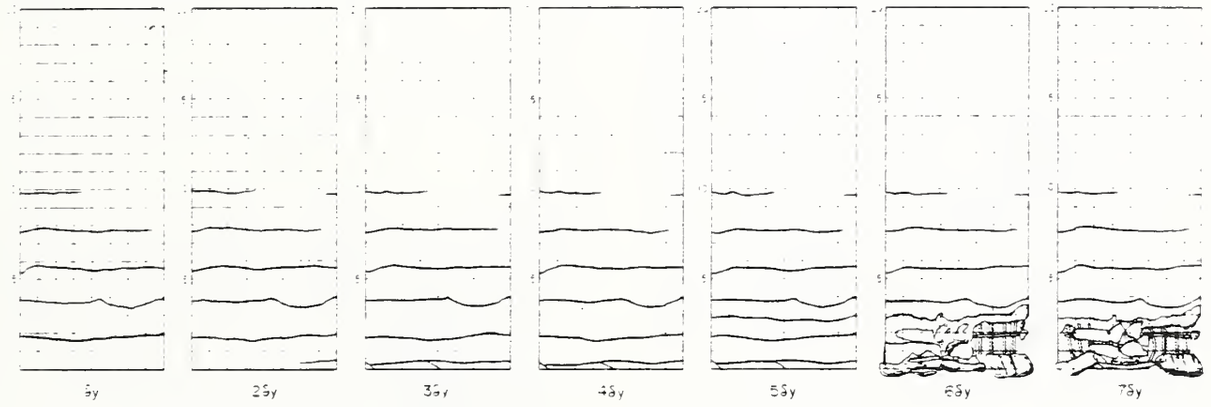

Fig.15 Failure Mode for Specimen with Loading Velocity V=100cm/sec (P−39)

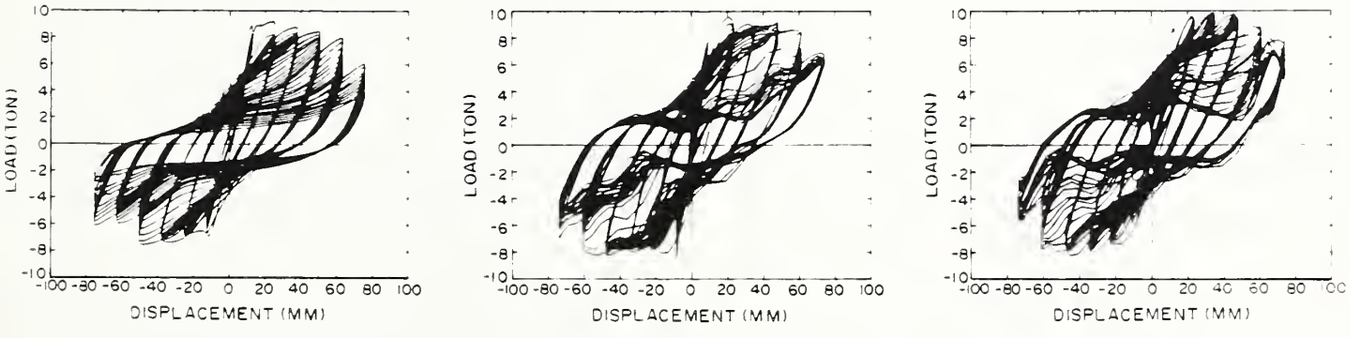

(a) V=10cm/sec (P−37) (b) V=100cm/sec (P−38) (c) V=100cm/sec (P−39)

Fig.16 Comparison of Hysteresis Loops

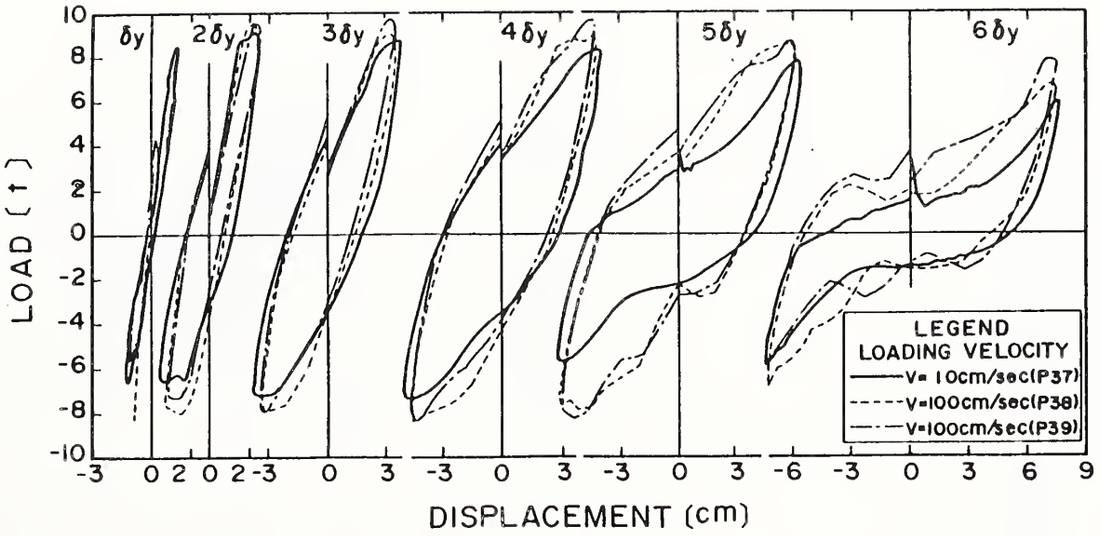

Fig.17 Comparison of First Excursion of Hysteresis Loops

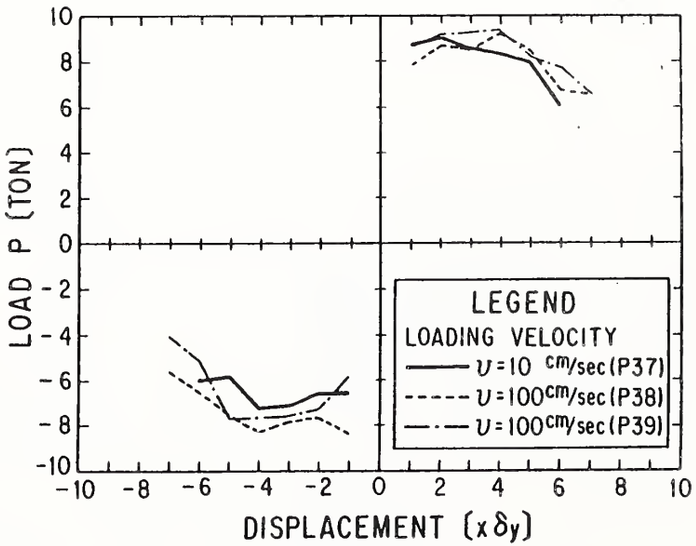

Fig.18 Comparison of Envelope of Hysteresis Loops

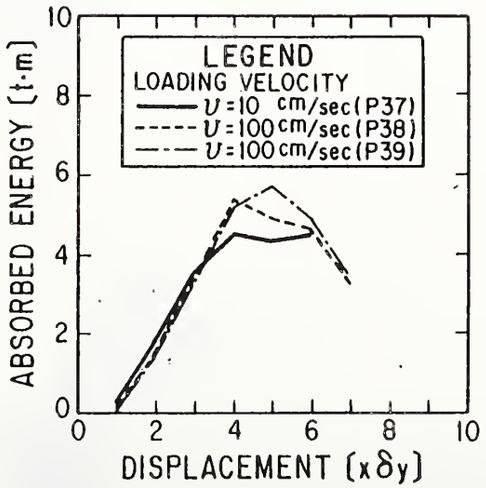

Fig.19 Comparison of Energy Dissipation

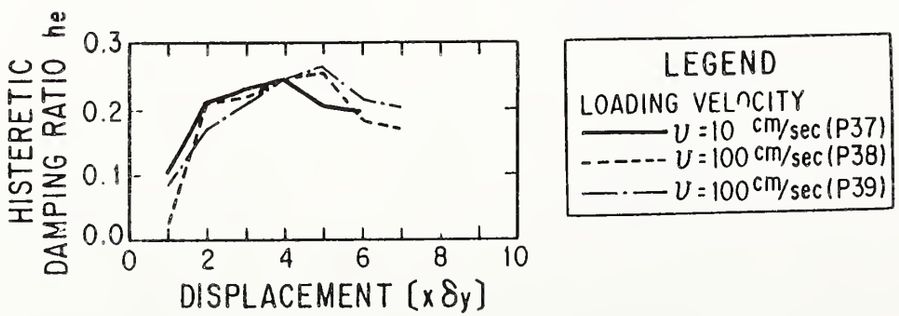

Fig.20 Comparison of Equivalent Hysteretic Damping Ratio

Study of In Situ Testing for Evaluation of Liquefaction Resistance and Occurrence

Jeffrey A. Farrar[1]

ABSTRACT

Analysis of penetration testing for liquefaction resistance evaluations performed at field liquefaction sites in Japan is described. The study reviews results of standard penetration, cone penetration, and vibrocone tests performed in October and November of 1983 at six field study sites which exhibited evidence of liquefaction in Akita and Niigata, Japan. Standard penetration test data with energy measurements and corrections to account for sampler dimensions are analyzed using N1 and Japanese simplified methods, and factors of safety against liquefaction are compared. Mechanical cone penetration test data are analyzed according to methods proposed by Seed and Olsen. A method to evaluate liquefaction resistance from cone penetration testing by using the state parameter is developed and evaluated. Flat plate dilatometer tests were performed at three liquefaction sites in the Hachiro-Gata Lagoon area of Japan. Dilatometer tests were performed using quasistatic and dynamic advancement techniques, and ability to predict liquefaction occurrence is evaluated. Vibrocone testing and its ability to quantify cyclic strength is evaluated. Findings of the report indicate additional case study data from silty sand sites and with differing loading conditions are required to further proof test relationships.

KEYWORDS: Cone Penetration; In Situ Testing; Standard Penetration; Vibrocone

1. INTRODUCTION

The purpose of this report is to investigate various in situ testing techniques for evaluation of liquefaction occurrence in Japan. The current report is an extension of U.S.-Japan cooperative studies initiated in 1983 with fieldwork. This report focuses on the cone penetration (CPT) and flat plate dilatometer (DMT) tests but also addresses the use of standard penetration (SPT) and vibrocone penetration (VCPT) testing. Data obtained in a comprehensive field study performed in 1983 at six study sites are reviewed, and a field study with the DMT was performed. Results of these studies have developed valuable case history information on various methods of geotechnical testing and will improve our ability to accurately predict occurrence of earthquake liquefaction.

From the results of the 1983 field study, several important papers have been published to date. However, there is yet no evaluation of the CPT test from the data collected. Several researchers have recently published papers on the use of CPT for liquefaction resistance evaluation, but lack case history validation. Results of the U.S.-Japan 1983 field data can be used to check these methods. Another new in situ test, the DMT, has recently become very popular among geotechnical groups. Laboratory chamber testing in sands has indicated that the instrument may have good potential for evaluation of liquefaction. To date, only one field liquefaction study site in the U.S. has been investigated. In this study of the DMT, three locations in the Hachiro-Gata Lagoon were investigated by quasistatic and dynamic advancement techniques.

1.1 Background Information

A comprehensive field study was performed to investigate in situ testing techniques in October and November 1983 in Akita and Niigata prefectures. Three sites from each prefecture were selected for study, with two sites showing evidence of liquefaction and one site showing none. As shown on Fig. 1, the Niigata sites were affected by the 1964 Niigata earthquake of Richter magnitude 7.5 and Akita sites were affected by the 1983 Nihonkai-Chubu earthquake of Richter magnitude 7.7. According to strong motion seismographs in areas nearby study sites, maximum ground accelerations of 0.17 and 0.16 g were used in analyses of data for Akita and Niigata sites, respectively.

Study sites in Akita were labeled sites A, B, and C. The sites are all located in the Hachiro Gata Lagoon area as shown on Fig. 2. The Hachiro-Gata area is reclaimed land surrounded by protective dikes. Site A is located on the approach to Gomyoko bridge at dike station WC 15+553. This location experienced serious lateral spreading of the approach fill. Site B is located at dike station FD 6+900 where there was a slope failure of the dike and numerous sand boils. Site C is located at dike station WC 0+580 where no damage was experienced.

Study sites in the Niigata area were labeled D, E, and F (Fig. 3). Site D is the Kawagishi-Cho apartment building site which is famous for the rotational movement of apartment buildings. Ishihara and Koga (1) have documented soil conditions at the site through SPT, CPT, and undisturbed sampling. Site E is on the left bank of the Showa Ohashi bridge where extreme damage to the bridge and surrounding ground mass was experienced. Site F is on the right bank of the Showa-Ohashi bridge site where no damage occurred. Analysis of the Showa-Ohashi bridge damage was performed by Iwasaki, et al. (2).

---

[1] Supervisory Civil Engineer, U.S. Department of the Interior, Bureau of Reclamation, Division of Research and Laboratory Services, Geotechnical Branch, Denver, Colorado.

The field study at these study sites was probably one of the most intensive of its kind to date. A listing of the testing performed at each study site is given in Table 1. Some of the tests performed included SPT with energy measurements, CPT, Swedish dynamic cone, Swedish weight sounding, piezocone, vibrocone, and other dynamic cone tests. Borings and soundings were generally spaced at distances of 2 m from one another. Soil types present at the sites are summarized on figure 4. The sites are almost completely comprised of clean fine to medium sands.

Following the field investigations, OYO Corporation compiled the sounding and laboratory data obtained from the study in a report dated March 1984. Presentation of SPT energy measurements and vibrocone results were made by Sasaki, et al. (3), at the meeting of the U.S.-Japan Panel on Wind and Seismic Effects (UJNR) in May 1984. Results of SPT measurements were documented by Kovacs, et al. (4), in National Bureau of Standards report dated August 1984. With additional data on SPT energy made available, Seed reevaluated the SPT data base to refine the N1 method (5). At the UJNR meetings of May of 1985 and 1986, Sasaki, et al. (6, 7), presented papers refining the vibrocone test. On August 17-20, 1985, the UJNR group sponsored a workshop on in situ testing with results soon to be published. Ohya and Iwasaki (8) presented a paper which concentrated on the dynamic penetration testing and its correlation with liquefaction resistance. In this paper, relationships were proposed for a ratio of static penetration from the CPT to dynamic penetration from the Swedish dynamic cone or automatic ram sounding test to predict liquefaction.

Several approaches to liquefaction resistance evaluations from CPT testing have evolved over the past 10 years. Many initial proposals were not very refined and sometimes depended on extensive site-specific correlation with the SPT test. In 1985, both Robertson (9) and Ishihara (10) proposed relationships with normalized cone tip resistance and cyclic strength. Both methods were felt to only be applicable to clean, low compressibility sands as an increase in fines or more compressible minerals such as micas would greatly reduce cone resistance. At the ASCE specialty conference on in situ testing, Seed (11) proposed a similar relationship based on refined SPT-CPT correlation. Only two case history sets of information were available to validate the proposed method. The method included correlations to account for fines content.

Some researchers have argued that the cone appeared to be too insensitive to stress-fabric effects which are beneficial to liquefaction resistance. Olsen (12) presented a method which incorporates normalized tip and sleeve resistance to evaluate liquefaction strength. This method was developed for the electric cone with a sleeve directly behind the tip. The difficulty with this method is that sleeve data must be accurately determined. In cohesionless soils, sleeve resistance is typically one-tenth of the tip resistance; and additional accuracy of less rugged, independent load-cell electric cones is required for the method.

Researchers working on the Beaufort Sea drilling islands developed a correlation of state parameter to normalized cone resistance to study failures. The concept of the state parameter was presented by Been and Jeffries (13) in 1985. The state parameter measures the distance or position of a sand in given void ratio stress condition to a reference steady-state line. The steady-state line is the same as defined by Castro and Poulos and originally proposed in the critical void ratio concept of Casagrande. The advantage to this approach is that many significant engineering parameters such as static stress - strain behavior can be correlated to the state parameter. In addition, positive values of the state parameter are indicative of collapse potential of sand structure under existing stress conditions resulting in very large strain development in loading events such as earthquakes. Recently, Been, et al. (14), have determined a correlation of normalized cone tip resistance with state parameter by determining steady-state lines for sands used in cone chamber tests.

In this report, each of the concepts for CPT evaluation of liquefaction will be studied. Depending on the results, more in-depth studies will be made. Conclusions regarding the general applicability of the methods will be made.

An additional study was performed with the flat plate dilatometer (DMT) testing device to gain valuable case history experience with the instrument. The Public Works Research Institute arranged for a field study with this device which took place in the Hachiro Gata Lagoon area during October 29 through November 1, 1986. The DMT test has been discussed by Marchetti (15) who developed the test in the mid-1970's. In 1982, Marchetti (16) discussed the possible use of the test for liquefaction evaluations. Robertson (17) proposed a correlation of the horizontal stress index to cyclic stress ratio. Based on discussions at the UJNR workshop on in situ testing and with users and manufacturers of the DMT, the differences between dynamic and quasi-static insertion were also evaluated to see if sensitive sands could be identified.

2. DISCUSSION

2.1 SPT Simplified Methods

Two methods of evaluation of liquefaction resistance using the SPT find widespread usage. In Japan, Iwasaki and Tatsuoka, et al. (18), have developed a method whose basis is in a large quantity of undisturbed sample testing to

develop a correlation between cyclic strength for 20 cycles of equivalent loading ($R1_{20}$), SPT N value normalized for overburden pressure effects, and particle size expressed in terms of mean particle diameter (D_{50}).

In the U.S. Seed (5) and coworkers developed a method which separates liquefaction and nonliquefaction from observed field performance data on a plot of cyclic stress ratio and SPT N1 value normalized to a stress level of 1 ton/ft^2. The method also distinguishes for fines content in sands. Neither method is applicable for low-plasticity silts or gravelly soils.

When studying previous liquefaction sites, the most difficult task is to determine the actual zones of liquefaction. Since SPT testing is the most widely accepted method of evaluating liquefaction, it will for the basis for testing cone penetration and other methods for their ability to predict liquefaction. As a result, the SPT analysis must be carefully performed to evaluate zones of liquefaction.

Results of SPT analysis using both SPT techniques by Ohya and Iwasaki (8) are shown on Fig. 5. On this figure, liquefied and critical zones where factor of safety is close to 1 are shown. Inspection of these plots indicate there is good agreement among the methods in their predictions. One will also notice, however, that the two methods diverge at high and low factors of safety. This trend has been identified in the past by others. The divergence at large factors of safety could possibly be explained by loosening of undisturbed samples of dense sands during the sampling process, thereby reducing the $R1_{20}$ strength.

The analysis of factor of safety by the Seed N_{160} method was reperformed to incorporate energy corrections and corrections for sampler barrels in accordance with the 1984 report. Calculations for this analysis are summarized on Table 2. The boring logs used for this analysis were reported by OYO Corporation in March 1984. To estimate the induced cyclic stress ratio at the depth of interest, the simplified equation proposed by Seed was used. To simplify calculations, a single unit weight of 120 lb/ft^3 was used and the reduction factor r_d was the equation proposed by Iwasaki (18). SPT N values obtained with the ASTM sampler were increased to account for larger inside barrel diameter by using the recommendation by Kovacs (4). The factor of 20 percent is probably too large for low blow count soils, and a factor of 10 percent is probably more appropriate. After conversion for sampler size, the N value was then adjusted to an energy level of 60 percent using the equation proposed by Seed and Kovacs (4, 5). At each field study site, only several energy data points were available at depths of greater than 30 ft. Where energy data were available, they were directly applied to the N value obtained; and an average value was used for the remainder of the boring. At site E, energy data were not available; but the same operator and drill rig previously used at site D were again used. At site F, no data could be assumed; therefore, Japan average energy was used (4). Corrections for rate and borehole size, as recommended by Seed (5), were not used as it was felt that they were purely speculative and probably overemphasized.

After conversion to N_{60}, the value was then normalized to an overburden pressure of 1 ton/ft^2 using the following equation for the factor C_N;

$$C_N = (\sigma_v')^n = (\sigma_v')^{-0.5} \qquad \text{Equation 1}$$

with σ_v' (vertical effective stress) in ton/ft^2

The graphic C_N values proposed by Seed (1984) were not used as it requires prejudging the relative density of the deposit. The values of C_N using the above equation are median points of those from the two curves recommended by Seed.

After obtaining values of N_{160} along with fines content information, cyclic strength was determined by visual examination of the N_{160} chart. If fines were present, increased strength was interpolated from the curves for various ranges of fines contents. In some cases, the cyclic strength was estimated as infinite following concepts of limiting shear strain potential.

The resulting change in factor of safety from both SPT methods is shown on figures 6 and 7. Factors of safety from the Japanese method were not recomputed but scaled graphically from the report by Ohya and Iwasaki. It can seen that, at lower factors of safety, the agreement is now better between the two methods in most cases. This can be attributed to the higher energy level (68 percent) delivered in Japan. Correction to the N_{60} value results in an increase of the N value. Remaining differences at a low factor of safety can be attributed to slightly higher cyclic strength observed in the Japan undisturbed sample test data due to consolidation of loose sands.

2.2 Analysis of 1983 Field Data Using the Q_{c1} Method

The method presented by Seed (11) is refined correlation of cyclic stress ratio to normalized cone penetration resistance (Q_{c1}). The effects of particle size on the correlation were inferred by refining the Q_c/N versus D_{50} data base to incorporate energy consideration on the SPT value and then using the SPT data base to develop the relationship. In this approach, the N value should be normalized to the 60-percent energy level to check the Q_c/N_{60} versus D_{50} relationship. Using Q_c/N_{60} and D_{50}, the Q_{c1} method could be extended to silty sands by inferring fines content from D_{50}; and dividing lines separating occurrence of liquefaction were developed. The chart for clean sands is very

similar to the charts proposed by Robertson and Ishihara (9,10). Seed compared this approach to case history data at the Niigata Kawagishi-Cho apartment site [Ishihara and Koga (1)] and the Imperial Valley study sites in the U.S. [Youd (19)]. Additional field performance data from this study will assist in validating this method.

In the 1985 UJNR workshop on in situ testing, Ohya and Iwasaki presented evidence that the ratio of Q_c to dynamic blow count N_d from the Swedish dynamic penetration test could be used to predict occurrence of liquefaction. Larger ratios of Q_c/N_d had indicated increasing possibility of liquefaction. In this study, the Q_c/N_{60} ratio was also studied for this effect. A comparison of Q_c/N_{60} versus D_{50} particle size is shown on figure 8. On the figure, points which did or did not liquefy according to SPT N_{160} analysis are appropriately marked. From this plot, there is no consistent trend in liquefaction occurrence; and there is wide scatter among the data.

Begemann friction mantle cone (ISSMFE M2 penetrometer) tests were performed at each of the study sites. Tip resistance data, Qc, were normalized for overburden pressure effects using the same correction factor C_N as used in the N_{160} analysis. It should be noted that this normalization proposed by Seed (11) is not in accordance with findings presented by Jamiolkowski (20), who recommended the n exponent of equation 1 to be -0.72 with σ_v' in kg/cm^2. As with the SPT analysis, a single unit weight of 120 lb/ft^3 is used with all stress computations.

A dependent analysis of occurrence of liquefaction was performed to evaluate the Q_{c1} method. At each SPT depth interval, Q_{c1} values were averaged. Plots of Q_{c1} and cyclic stress ratio were made on the proposed chart, and points which did or did not liquefy from SPT prediction could be marked. A summary of dependent data is given in Table 3, which also shows the average friction ratio in the SPT interval. All of the values are less than 2.5 percent, which is the common borderline dividing sands and sand-silt-clay mixtures using the Begemann friction mantle cone. For electrical cones, this value will be different. The Q_{c1} method should not be used for liquefaction assessment using the Begemann cone if higher friction ratios are obtained.

A summary chart, Fig. 9, shows that liquefaction occurrence is accurately predicted at the sites. From the individual charts for each site the cyclic strength was determined by visual inspection, taking into account the percentage of fines and D_{50} particle size. The cyclic strength and factor of safety for the Q_{c1} data are summarized in Table 4 and factor of safety is plotted on Figs. 6 and 7 for comparison to SPT methods. The Q_{c1} factor of safety compares very well with SPT methods. It is interesting to note that, at site A, liquefaction is predicted to greater depth using the Q_{c1} method. This may possibly reflect on the greater uncertainty of overburden pressure corrections for the SPT at shallow depths.

Results of the study of the Q_{c1} method indicate that the method is very suitable for evaluation of liquefaction resistance for clean sands. Since no sample is obtained in the test, the friction cone should always be used to check friction ratio. Further field evidence is required to evaluate silty sands and sand deposits which have been subject to larger cyclic stress ratios. Additional study is also required for sands of varying compressibilities due to varying mineralogies.

2.3 Evaluation of Olsen's CPT Method of Liquefaction Assessment

A method of liquefaction resistance evaluation using normalized cone and friction sleeve data from the CPT test was proposed by Olsen (1984). By incorporating normalized sleeve resistance, sensitive soils can be detected. The CPT tip resistance is relatively insensitive to stress history effects, such as overconsolidation, and some aging effects, such as slight cementation. The sleeve is more sensitive to effects, such as overconsolidation.

Olsen developed a soil characterization chart that identifies sensitive, normally consolidated, and overconsolidated behavior. The advantage of this method is that it may also identify sensitive silts and silt-sand mixtures which are potentially liquefiable. Normalization of the tip resistance Q_c uses the same form as previous sections of this report; but the exponent n in equation 1 varies with soil type, and an iterative process is used. Sleeve friction is normalized by dividing by the effective overburden pressure, since it is a measure of remolded strength. Using SPT-CPT and laboratory cyclic stress ratios, stress ratio contours of liquefaction resistance strength were drawn on the characterization chart.

The relationship developed by Olsen was developed for electric cone testing with friction sleeves located immediately behind the tip. The sleeve friction measured by the Begemann friction mantle cone is located further back behind the cone tip. The sleeve has a shoulder or bearing surface at its base and, therefore, measures higher levels of sleeve friction. DeRuiter (21) states that the electric friction is, on the average, only one-half of Begemann mechanical friction values. In electric cone testing with subtraction-type cones, the sleeve friction can be in error as much as ± 0.3 ton/ft^2, making it difficult to obtain accurate friction readings.

For this study, the Begemann cone data were normalized for a qualitative comparison with

Olsen's chart to evaluate if use of such a chart was feasible for mechanical cones. The exponent n to obtain the correction factor to normalize Q_c was taken as -0.72, since practically all of the soils were clean sands. Friction sleeve data were not reduced to be more comparable to electric cone friction values. Normalized tip and sleeve resistance data points are summarized in Table 3. A summary plot with data points for all six sites is shown on the soil characterization chart on Fig. 10. On Fig. 11, data from site B are plotted on the characterization chart, which contains the contours of cyclic strength. Beside the data points on this figure, the SPT N_{160} cyclic strength values are shown.

From review of the figures, it is evident that the Begemann friction values are higher than the electrical data. It is possible that the cyclic stress ratio contours and characterization zones could be shifted to the right to make Olsen's method applicable to the Begemann cone. The general trend of liquefiable data points lying on the sensitive side of the normally consolidated zone confirm the concepts of this method. Dense dilative sands fall in the overconsolidated zone.

Overall, conclusions regarding this approach are that the method in concept is fundamentally correct. Possibilities exist to modify this relationship for mechanical cones. The benefit of this approach is that it may be able to identify sensitive silts and sand-silt mixtures and eventually apply cyclic strength estimates. For now, if sensitive sands with fines or silts are identified by the method, laboratory testing may be required. Disadvantages to the method are its log-log relationship, which makes resolution difficult. Also, sleeve friction measurement is more sensitive and subject to error.

Since accurate conversions of mechanical to electrical cone data cannot be made, electrical cone data are required from case history sites in clean sands, sands with fines, and silts to validate the method.

2.4 Evaluation of the State Parameter for Liquefaction Assessment

The state parameter (ψ) proposed by Been and Jefferies (13) is simply a convenient method to develop a common referencing system which can quantify static stress - strain behavior of sands and eventually sand-silt mixtures. The concept of the state parameter is shown on Fig. 12. The unique reference line is the steady-state line which is fairly easily measured on remolded contractive specimens. The state of the soil is expressed as a function of mean normal stress and void ratio. Soils, whose position is the below the steady-state line with a negative value of state parameter, will exhibit dilatant behavior in shear. Soils, whose state lies above the steady-state line with a positive value of state parameter, are contractive in shear. The contractive condition indicates potential collapse of structure with extremely large deformations. Contractive soils are rare in natural deposits; but if identified, they can exhibit extensive deformation upon earthquake or additional static loading. Been and Jeffries (13) have related the state parameter to angle of phase transformation, drained peak angle of shearing resistance, dilation rate, and decrease in peak to steady-state friction angle.

In a currently unpublished paper, Been, et al. (14), have determined the steady-state lines for all of the sands used in CPT chamber testing and have found a unique relationship to Q_c normalized to mean effective confining pressure and the state parameter in clean sands. The initial correlation developed is shown on Fig. 13. Additional study is needed to determine the relationship for silty sands.

In this study, it was desired to calculate the state parameter for qualitative comparison to liquefaction resistance. The equation proposed by Been, et al. (14), to determine the state parameter from Qc is as follows:

$$\psi = -.092 \ln\left[\left(\frac{Qc - I_1}{I_1'} + 17\right)/31\right] \quad \text{Equation 2}$$

where I_1 and I_1' are the first total and effective stress invariants (mean normal stress). In equation 2, stress is expressed in kPa. Calculation of state parameter requires knowledge of the value of K_o (ratio of in situ vertical to horizontal stress). Based on results of DMT tests to be presented later in this paper, a K_o value of 0.6 was assumed for liquefied sites and 1.0 for nonliquefied sites. The state parameter was calculated for all Q_c values.

Average state parameter values in SPT depth intervals are summarized in Table 4. Inspection of these data reveals extremely low state parameter values in a low cone bearing zone from 5.0 to 6.5 m in depth at site B. Liquefaction sites D and E had more moderate values of the state parameter.

The state parameter for the zone present in site B is very close to being a contractive value; but if the equation for state parameter is examined, it is found that extremely low values of tip resistance would be required to indicate a contractive condition. In fact, the tip resistance may approach zero since the sand structure collapses away from the cone.

Results of this analysis indicate that moderately dilative sands are subject to level ground liquefaction and resulting excessive deformations. In order to develop a correlation in terms of the state parameter, the Q_{c1} versus

cyclic strength relationship was used. Q_{c1} values for clean sands from the chart proposed by Seed were converted to state parameter values by assuming K_o = 0.5 with typical sand unit weight and ground-water location at the ground surface. Then, state parameter points calculated in SPT intervals were plotted with liquefaction occurrence as predicted by the SPT N_{160} method noted. The results are shown on Fig. 14.

The results indicate that the majority of the liquefied data points fall in the proper position, with exception of two near-surface data points at sites B and C and a point at site D at 7.3 m with high cone bearing. At site C, there was no evidence of liquefaction. As discussed earlier, shallow blow counts from the SPT are more difficult to evaluate due to uncertainty of pressure normalization. Also, erratic energy transmission is a problem with the SPT at shallow depths. It is highly probable that the cone can better estimate near-surface liquefaction occurrence.

The effect of deriving a state parameter versus cyclic strength correlation based on K_o = 0.5 conditions will have a similar effect as the N_1 method, which disregards varying K_o in pressure correction of the N value. In equation 2, the state parameter is most sensitive to the Q_c value and less sensitive to mean normal stress, since the tip resistance is typically two orders of magnitude larger than mean normal stress levels. At higher K_o values, the dominant increase in Q_c will cause a more negative value of state parameter to be estimated if K_o = 0.5 conditions are assumed. This will result in predicted increase in cyclic strength, which is appropriate for liquefaction studies. However, the K_o = 0.5 assumption would overestimate the dilational tendency for static stress - strain behavior predictions.

In conclusion, there seems to be a relationship between the state parameter and occurrence of liquefaction. Further study should be performed to evaluate the effects of higher K_o values on the state parameter and its ability to predict liquefaction. Since it is difficult to determine field K_o values, a K_o = 0.5 assumption is appropriate for young alluvial soils which are typical subjects of liquefaction studies. The shortcoming of the method is that relationships still need to be developed for silty sands and silts. Additional studies are required to test sand in a contractive condition and sands which contain fines. The benefit of this approach for clean sand at this time is that static stress - strain behavior of the soil can also be estimated. As with the Q_{c1} method, there is no sample obtained, so the method should only be applied with friction ratios of less than 2.5 percent and gradation of the sand should be checked to be sure the fines content is less than 10 percent.

2.5 Analysis of Flat Plate Dilatometer Test Results

The flat plate dilatometer test (DMT) was introduced by Marchetti in the mid 1970's. Marchetti (15) presented a summary of the equipment and data reduction procedures in the ASCE Geotechnical Journal. The DMT consists of a flat blade-shaped penetrometer with a 60-mm circular expandable membrane located on the face of the blade. The blade is usually quasi-statically advanced at 20-mm/s at 20-cm intervals, while thrust pressure at the surface is recorded. At each 20-cm increment, pressure is released from the rods and the membrane is expanded. Two readings are obtained at each interval:

- First, an internal pressure to lift the membrane into an approximately planar condition
- Second, an internal pressure to extend the membrane approximately 1.1 mm into the soil

The two readings are obtained in about 30 seconds. After subtraction of inertial pressures required to expand the membrane freely in air, values of P_0 and P_1 are obtained from the first and second readings, respectively. Based on the two readings, three index parameters are determined as follows:

Material or Deposit Index, Id $$I_d = \frac{P_1 - P_0}{P_1 - U_o}$$

Lateral Stress Index, Kd $$K_d = \frac{P_0 - U_o}{\sigma'_{vo}}$$

Dilatometer Modulus, Ed $$E_d = 34.7\ (P_1 - P_0)$$

The material index is used to determine the soil type. It represents the normalized difference between 1-mm expansion pressure, P_1, and contact pressure, P_0, which is the measure of soil rigidity. Since soil classification is based only on rigidity, some errors in estimated soil type may exist. The horizontal stress index is related to lateral earth pressure at rest. The dilatometer modulus is a numerical solution for $(E/1 - \mu^2)$ when expansion is modeled as loading of a circular area in an elastic half space. The modulus obtained must be empirically related to soil modulus since drainage conditions and disturbance vary.

Dilatometer parameters have been related to K_o, ϕ', S_u, P'_c, E_{25} (sand), and E (clays). The soil friction angle in sands is now based primarily on thrust data and bearing capacity analysis [Schmertmann (22)]. Based on initial

chamber tests in normally consolidated and prestressed sands, Marchetti (16) felt that the instrument was more sensitive to prestress than the CPT and proposed it as a viable method for evaluation of liquefaction potential. Marchetti proposed that K_d values of less than 1.5 would indicate sands at relative densities of less than 60 percent and that resistance to liquefaction in terms of cyclic strength may be roughly proportional to $K_d/10$. A most recent paper showing additional chamber test results in sands was presented by Baldi, et al. (23). Robertson (17), after consideration of chamber test data and a relationship between relative density and liquefaction resistance proposed by Christian and Swiger (24), proposed a correlation between the K_d and liquefaction resistance. After attending the 1985 UJNR workshop on in situ testing, DMT users felt there may be some relationship of liquefaction to the change in K_d with static and dynamic advancement. In this study, both the effects of static and dynamic driving and Robertson's method will be analyzed.

On October 29 through November 1, 1986, the Public Works Research Institute, Ministry of Construction, Japan, performed a series of nine soundings using DMT and CPT testing in the Hachiro Gata Lagoon area. DMT equipment was supplied by the Bureau of Reclamation for this study. Six soundings were located in sites B and C of the 1983 field study. An additional site A' was located near the Gomyoko Bridge at dike station WC 13+620 where the dike had settled up to 1 m, and approximately 6 m of banking soil were available for testing. CPT and SPT data were available for site A' from previous investigations. At each site, a cone penetration test using a Dutch mantle cone (ISSMFE penetrometer M1) was performed to evaluate any change in soil conditions since the dikes were rehabilitated after 1983. The rebuilding did not include subsurface densification.

At each site, dynamic and static DMT tests were performed to evaluate effects on the K_d index. Static DMT tests were advanced with a portable cone penetration machine which used anchors to develop additional reaction. Thrust pressure to quasi-statically advance the DMT was measured at the surface with CPT hydraulic pressure gauges. At site B, the pressure gauges malfunctioned and a second sounding with the DMT blade was performed. The Swedish automatic ram sounding equipment was used to dynamically advance the DMT. This device uses a chain cam mechanism to lift and drop the hammer so that consistent energy is applied. The 63.5-kg hammer is dropped from 50 cm. The DMT blade was driven with CPT rods for 20 cm, and the number of blows were recorded for each increment. On the two dynamic soundings at sites B and C, the hammering action loosened the wire contact at the base of the sensing disk at about 7 and 5 m, respectively; and the soundings were terminated. No other specific equipment problems occurred.

The completed sounding numbers, test site, test type, and depths are listed below:

Sounding No.	Site	Test type	Depth
86-1-2	B	Quasi-static	15 m
86-1-3	B	Dynamic	7 m
86-2-2	A'	Quasi-static	8 m
86-2-3	A'	Dynamic	7 m
86-3-2	C	Quasi-static	5 m
86-3-3	C	Dynamic	4 m

DMT data were reduced using IBM PC Basic program DILLY4 distributed by GPE, Inc., the U.S. distributor of the DMT. The program provides tabular output of all parameters and a graphic output of strength, stress, and modulus values. Computer data reduction used methods recommended by Schmertmann (22) for plane strain friction angle and K_o. For the dynamic soundings, the thrust data from the adjacent static tests were input instead of trying to convert the number of blows to thrust.

Summary graphs which contain pertinent data from both quasi-static and dynamic tests on one graph for each site are shown on Figs. 15, 16, and 17. Cone penetration data from the 1983 field studies and the current study are plotted in terms of Q_{c1} for sites B and C are shown on Figs. 18 and 19. From Fig. 18, it can be seen that Q_{c1} has increased to a depth of 5 m since 1983. Below 5 m, the same zone of low cone bearing sands exists with little increase in Q_{c1}. At site C, it can be seen that Q_{c1} has increased over a depth of 2.5 to 5 m.

At site A', the DMT summary graph (Fig. 16) indicated an interbedded deposit of silty sands and sands with highly erratic data. Cone tip resistance data also indicated soils with fines. Data from site A' were not included in the analysis of liquefaction resistance. It will be included when additional gradation and cone data from the previous borings can be analyzed.

The effects of dynamic driving of the DMT in loose and dense sands can easily be distinguished from the summary graphs. Dynamic driving causes an increase in material index and friction angle and a decrease in horizontal stress index and modulus. Of interest for liquefaction potential is the decrease in K_d. At site B, dynamic driving resulted in reducing K_d to below 1 in critical liquefied zones. At site C, the reduction in K_d is also apparent; but values remained above 2. In an attempt to quantify this reduction, the ratio of dynamic to static K_d were analyzed. At site C in dense sand, a 60 percent reduction of K_d occurred at

3 to 4 m in depth. At site B, an 80-percent reduction in K_d occurred at a depth of 5 to 6 m in loose sand. However, a 90-percent reduction in K_d occurred at 4 to 5 m at site B where normalized cone bearing was significantly higher. Additional checks of dynamic and static K_d ratios resulted in no correlation to liquefaction resistance. The only conclusion that can be drawn is that, if dynamic K_d is less than 1, liquefaction seems highly likely.

The quasi-static K_d values were then compared to Robertson's method. K_d values were averaged in the 1983 SPT intervals. Using the SPT factor of safety as a guide, K_d values in zones which had liquefied at site B could be plotted on the proposed relationship by Robertson on Fig. 19. These data confirm a limiting K_d value of 4.2 at cyclic stress ratio of 0.18. At site C, the K_d value varied considerably in the SPT interval; and a bar was used to show the nonliquefied zone. Since Q_{c1} had increased in 1986, the Q_{c1} cyclic strength was used to show increased strength of the deposit. This approach indicates the K_d versus cyclic strength line may increase more sharply than proposed by Robertson. Additional field performance data will be needed to confirm the K_d relationship at higher cyclic stress ratios.

In conclusion, the field tests at Hachiro Gata have resulted in a better understanding of the DMT in sands. Major changes can occur between static and dynamic DMT tests to the point where dynamic driving should be discouraged in loose and dense sands alike. It is doubtful that a useful correlation between dynamic and static K_d values and liquefaction resistance can be developed. Robertson's proposed correlation works well, but additional information will be needed at higher levels of cyclic loading and in dense sands at low levels of cyclic loading.

Since material index is not necessarily a good indicator of soil type, there may also be questions regarding fines contents in the soils tested.

2.6 Comments on the Static and Dynamic Penetration Resistance

So far on this project, there have been four types of static dynamic comparisons of penetration resistance attempted. The ratio of cone resistance to SPT resistance was shown on Fig. 10 to be highly erratic. Likewise, K_d ratios obtained in this recent study do not show consistent trends. Ohya and Iwasaki (1985) showed some success in correlating CPT Q_c to the Swedish dynamic penetration N_d value. However, there is also considerable scatter among the data; and the relationship could not be correlated to quantify cyclic strength. Sasaki and others at the Public Works Research Institute have shown the vibrocone to have good success, at least in a qualitative sense. If any method of a static to dynamic comparison methods stands a chance of success, it seems to be the vibrocone.

Recent efforts to quantify the decrease in cone penetration resistance, D, from the VCPT with cyclic strength are summarized by Sasaki, et al. (7). In Table 4, the most recent version of the equation expressing cyclic strength ($R1_{20}$) versus decrease in cone resistance and effective overburden pressure was used to calculate strength. The D value was obtained for the study sites from plots shown in Sasaki, et al. (3). A review of Table 4 indicates that liquefaction would not have been predicted at any of the study site SPT intervals.

Review of the decrease in resistance diagrams indicates a general trend of reduction of D with depth. In current field use, the force on the cone tip is being measured at the ground surface. As a result, friction buildup on the rods is influencing the penetration resistances. The recent modification to incorporate effective overburden pressure into the strength equation may compensate for this effect; but it is possible that friction buildup occurs at different rates for the static and dynamic soundings which are performed independently. If this is the case, the static and dynamic components of D may have to be adjusted separately. Static Q_c can be compared to CPT Q_c data and friction can be evaluated; but the only solution to evaluating the effect on vibratory Q_c is to locate a load cell within the tip or just above the vibratory section.

A second problem with the correlation is the use of cyclic strength data from undisturbed samples obtained the field. The sampling process has a tendency to densify loose sand. Trimming and reapplication of confining stresses may further densify the sand. The converse effect can occur with dense sands. As a result, there is a general flattening of the cyclic strength versus D curve. On Fig. 21, the two equations proposed for the vibrocone are plotted on a cyclic strength versus D diagram. Also plotted on the diagram are the SPT N_{160} cyclic strength data and D value summarized in Table 4. In the area of 100- to 60-percent reduction (1 - D = 0.0 to 0.4), SPT strength data for a given D value seem reasonable. At smaller values of D or as 1 - D approaches 1, there is considerable scatter. The point of lower cyclic strength in this area originate from deeper zones at liquefied sites where friction has reduced the magnitude of decrease. If the friction problem is solved, it may be possible to develop the anticipated trend line shown on the figure.

To summarize, two recommendations can be made to improve VCPT performance. First, the effects of rod friction must be omitted or determined accurately. Second, either of the three approaches which follow could be taken to develop the cyclic strength correlation; laboratory chamber studies of sands of known cyclic

strength, field cyclic strength determinations on sands which are frozen prior to sampling; or correlations to accepted in situ testing techniques such as Iwasaki - Tatsuoka, N_{160}, or Q_{c1} approaches. In order to extend the prediction into sands containing fines, it may be helpful to add a friction sleeve to the static penetrometer system to assist in identifying these materials.

3. CONCLUSIONS

Comparisons of liquefaction resistance evaluation techniques using the SPT, CPT, DMT, and vibrocone have been performed with the data obtained from the 1983 U.S.-Japan cooperative field study sites and a field study performed in 1986. Pertinent conclusions regarding the methods considered along with recommendations for further study are as follows:

a. SPT data were reanalyzed to incorporate energy and sampler corrections using the N_{160} method proposed by Seed (5) and compared to the Iwasaki, et.al. (18), method. The methods agree very well with only slight differences at low factor of safety. At a large factor of safety, the methods diverge due to the limiting shear strain concept of the N_{160} method.

b. CPT data were analyzed using the Q_{c1} method proposed by Seed (11). Results of an SPT dependent analysis and independent Q_{c1} factor of safety comparisons show the method was very reliable and suitable for use in liquefaction analysis. Additional field performance comparisons in silty sands and sands subjected to higher levels of cyclic loading are required.

c. CPT data were analyzed for a qualitative comparison to the method proposed by Olsen (12). The method in concept is fundamentally correct, but modifications would be required to develop the relationship for mechanical cones.

d. CPT data were analyzed and a method developed to evaluate liquefaction resistance using the state parameter proposed by Been and Jeffries (1985). The method should have comparable accuracy as the Q_{c1} method and has the additional benefit of estimating static stress - strain behavior in shear. Additional study will be required to evaluate prestress effects and extend the correlation to silty sands.

e. A series of six DMT soundings were performed by the Public Works Research Institute at the Hachiro Gata Lagoon area during October and November of 1986. Comparisons of static and dynamic K_d values did not indicate a trend correlated to liquefaction resistance. Static K_d values were compared to the method proposed by Robertson (1984) with favorable results, additional studies of silty sands and sands subjected to higher levels of cyclic loading are required.

f. Of all static-dynamic penetration techniques, the vibrocone test has the best potential for accurate prediction of liquefaction resistance. Equipment or calculation methods need to be improved to overcome rod friction effects. The correlation of penetration decrease to cyclic strength requires further study.

4. ACKNOWLEDGMENT

This study was made possible by a science award for foreign specialists by the Science and Technology Agency, Japan. The host agency was the Public Works Research Institute, Ministry of Construction, Japan. Special thanks are extended to Drs. Sasaki and Iwasaki for their interest and assistance with this study. Also, thanks are extended to Matsumoto and Kondo of the Ground Vibration Division, PWRI, for assistance in field DMT testing and data reduction.

The Bureau of Reclamation approved my detail and supplied DMT testing equipment to perform this study.

5. REFERENCES

(1) Ishihara, K., and Y. Koga, "Case Studies of Liquefaction in the 1964 Niigata Earthquake," Journal of the Japanese Society for Soil Mechanics and Foundation Engineering, vol. 21, No. 3, September 1981.

(2) Iwasaki, T., K. Tokida, and S. Yoshida, "Investigation on Seismic Resistance of Grounds at Showa Bridge Damaged During the Niigata Earthquake," Technical Memorandum No. 1591, Public Works Research Institute, Ministry of Construction, Japan.

(3) Sasaki, Y., K. Kutara, T. Iwasaki, H. Miki, Y. Itoh, K. Kaminaga, W. D. Kovacs, L. A. Salomone, J. A. Farrar, "U.S.-Japan Cooperative Research on In-Situ Testing Procedures For Assessing Soil Liquefaction (No. 1)," Proceedings of the Sixteenth Joint Meeting, U.S.-Japan Panel on Wind and Seismic Effects, UJNR, Washington, D.C., May 15-18, 1984.

(4) Kovacs, W. D., and L. A. Salomone, "Field Evaluation of SPT Energy Equipment, and Methods in Japan Compared with the SPT in the United States," NBSIR 84-2910, National Bureau of Standards, Center for Building Technology, Gaithersburg, Maryland, August 1984.

(5) Seed, H. B., K. Tokimatsu, L. F. Harder, and R. M. Chung, "The Influence of SPT Procedures in Soil Liquefaction Resistance Evaluations," Report No. UCB/EERC-84/15, College of Engineering, University of California, Berkeley, California, October 1984.

(6) Sasaki, Y., Y. Koga, Y. Itoh, T. Shimazu, and M. Kondo, "In-Situ Test for Assessing Liquefaction Potential Using Vibratory Cone Penetrometer," Proceedings of the Seventeenth Joint Meeting, U.S.-Japan Panel on Wind and Seismic Effects, UJNR, Tsukuba, Japan, May 21-24, 1985.

(7) Koga, Y., Y. Sasaki, Y. Itoh, and O. Matsuo, "Field Investigation of Seismically Damaged Sites by Use of Vibratory Cone Penetrometer," Proceeding of the Eighteenth Joint Meeting, U.S.-Japan Panel on Wind and Seismic Effects, UJNR, Washington D.C., May 12-15, 1986.

(8) Ohya, S., T. Iwasaki, and M. Wakamatsu, "Comparative Study of Various Penetration Tests in Ground that Underwent Liquefaction During the 1983 Nihonkai-Chubu and 1964 Niigata Earthquakes," Proceedings of the First U.S.-Japan Workshop on In Situ Testing Methods for Evaluation of Soil Liquefaction Susceptibility, San Francisco, California, August 17-20, 1985 (unpublished).

(9) Robertson, P. K., and R. G. Campanella, "Liquefaction Potential of Sands Using the CPT," Journal of the Geotechnical Engineering Division, American Society of Civil Engineers, vol. 111, No. 3, March 1985.

(10) Ishihara, K., "Stability of Natural Deposits During Earthquakes," Proceedings, Eleventh International Confrence on Soil Mechanics and Foundation Engineering, vol. 1, August 1985.

(11) Seed, H. B., and D. DeAlba, "Use of SPT and CPT Tests for Evaluating the Liquefaction Resistance of Sands," ASCE specialty conference on the Use of In Situ Tests in Geotechnical Engineering, Blacksburg, Virginia, June 1986.

(12) Olsen, R. S., "Liquefaction Analysis Using the Cone Penetrometer Test (CPT)," Proceedings of the Eighth World Conference on Earthquake Engineering, San Francisco, California, July 1984.

(13) Been, K., and M. G. Jeffries, "A State Parameter for Sands," Geotechnique, vol. 35, No. 2, 1985.

(14) Been, K., J.H.A. Crooks, D. E. Becker, and M. G. Jeffries, "State Parameter Interpretation of the Cone Penetration Test in Sands," submitted for publication in Geotechnique, March 1985.

(15) Marchetti, S., "In Situ Tests by the Flat Dilatometer," Proceedings of the Geotechnical Division, American Society of Civil Engineers, vol. 106, No. GT3, March 1980.

(16) Marchetti, S., "Detection of Liquefiable Sand Layers By Means of Quasi-Static Penetration Tests," Proceedings of the Second European Sysposium on Penetration Testing, Amsterdam, May 24-27, 1981.

(17) Robertson, P. K., and R. G. Campanella, "The Flat Plate Dilatometer Test for Liquefaction Assesment," Soil Mechanics Series No. 79, Department of Civil Engineering, University of British Columbia, Vancouver, 1984.

(18) Tatsuoka, F., S. Iwasaki, K. Tokida, S. Yasuda, M. Hirose, T. Imai, and M. Kon-no, "Standard Penetration Tests and Soil Liquefaction Potential Evaluation," Soils and Foundations, JSSMFE, vol. 20, No 4., December 1980.

(19) Youd, T. L., and M. J. Bennett, "Liquefaction Sites, Imperial Valley, California," Journal of the Geotechnical Engineering Division, American Society of Civil Engineers, vol. 109, No. 3, March 1983.

(20) Jamiolkowski, M., G. Baldi, R. Bellotti, V. Ghionna, and E. Pasqualini, "Penetration Resistance and Liquefaction of Sands," Proceedings of the Eleventh International Conference on Soil Mechanics and Foundation Engineering, San Francisco, California, 1985.

(21) deRuiter, J., "Electric Penetrometers for Site Investigations," Journal of the Soil Mechanics and Foundations Division, American Society of Civil Engineers, vol. 97, No. SM2, February 1971.

(22) Schmertmann, J., "A Method for Determining the Friction Angle in Sands from the Marchetti Dilatometer Test," Proceedings of the Second European Symposium for Penetration Testing, vol. 2, Amsterdam, May 1981.

(23) Baldi, G., R. Bellotti, V. Ghionna, M. Jamiolkowski, S. Marchetti, and E. Pasqualini, "Flat Plate Dilatometer Tests in Calibration Chambers," Use of In Situ Tests in Geotechnical Engineering, Geotechnical Special Publication No. 6, American Society of Civil Engineers, June 1986.

(24) Christian, J. T., and W. F. Swiger, "Statistics of Liquefaction and SPT Results," Journal of the Geotechnical Engineering Division, American Society of Civil Engineers, vol. 101, No. GT-11, 1975.

Items of Field Investigation

Region			Akita (Lagoon Hachiro)			Niigata		
Site No.			A	B	C	D	E	F
Location			Gomyoko bridge	Front levee	West levee	Kawagishi -cho	Showa Ohashi bridge left side	Showa Ohashi bridge right side
Occurrence of Liquefaction			yes	yes	no	yes	yes	no
Boring	No.1	(m)	0~20.0	0~20.0	0~20.0	0~20.0	0~20.0	0~20.0
	No.2	(m)	0~20.0	0~20.0	0~20.0	0~20.0	-	-
S.P.T. (JIS sampler)	No.1	(points)	10	10	10	10	10	10
	No.2	(points)	8	4	9	4	-	-
S.P.T. (ASTM sampler)	No.1	(points)	10	10	10	10	10	10
	No.2	(points)	8	4	8	4	-	-
Sand Sampling		(points)	5	5	2	7	-	-
Piezocone		(m)	0~9.7	0~20.0	0~12.7	0~20.0	0~18.0	0~10.5
Automatic Ram Sounding		(m)	0~14.4	0~20.0	0~20.0	0~20.0	0~20.0	0~20.0
Dutch Cone		(m)	0~6.2	0~11.8	0~6.2	0~10.4	0~12.0	0~6.2
Vibratory Cone		(m)	0~6.8	0~20.0	0~7.4	0~16.8	0~15.2	0~7.2
Swedish Sounding		(m)	0~12.0	0~15.0	0~15.0	0~20.0	0~15.5	0~1.0
Dynamic Cone Penetration Test		(m)	0~19.0	0~20.0	0~15.5	0~19.3	0~17.2	0~16.3
PS Logging		(m)	0~21.0	0~20.0	0~20.0	0~20.0	-	0~20.0
Magnetic Susceptibility Logging		(m)	-	8.0~15.0	-	1.5~1.8	3.4~21.2	3.5~20.0
Density Logging		(m)	0~20.0	3.0~15.8	1.0~20.5	0.5~20.5	0~21.4	3.0~20.1
Caliper Logging		(m)	0~20.8	-	0~20.5	0~20.6	0~20.9	0~20.8
Electric Logging		(m)	3.5~20.0	8.5~14.5	4.5~19.8	1.2~20.5	3.4~20.5	3.5~19.0
Classification Test		(points)	25	25	22	26	-	-
Cyclic Triaxial Test		(series)	3	3	1	4	-	-
Resonant Column Test and Cyclic Torsional Test		(series)	2	2	-	2	-	-

TABLE 1

SUMMARY OF SPT N160 CALCULATIONS - SITE A - HACHIRO GATA - WC 15+553

DEPTH m.	D50 mm.	MINUS #200 SIEVE %	N ASTM BPF	N LINER BPF	N JIS BPF	ROD ENERGY %	N60 BPF	VERT. STRESS TSF	CN	N160 BPF	FIELD CYCLIC STRESS RATIO	CYCLIC STRENGTH N160 METHOD
1.3					2	62	1.6	0.21	2.2	4	0.13	0.04
2.3	0.22	6	5	6		62	4.6	0.30	1.8	9	0.17	0.09
3.3	0.20	21			12	62	12.4	0.39	1.6	20	0.18	0.32
4.3	0.26	10	13	15.6		62	16.1	0.49	1.4	23	0.18	0.33
5.3	0.20	13			18	62	18.6	0.58	1.3	24	0.19	0.35
6.3	0.22	13	14	16.8		62	17.4	0.68	1.2	22	0.19	0.28
7.3	0.26	5			35	62	36.2	0.77	1.1	40	0.19	>.5
8.3	0.16	16	22	26.4		62	27.3	0.86	1.1	31	0.18	>.5
9.3	0.18	10			49	62	50.6	0.96	1	51	0.18	>.5
10.3	0.18	9	51	61.2		62	63.2	1.05	0.97	61	0.18	>.5
11.3	0.18	10			59	60	59	1.15	0.93	55	0.18	>.5
12.3	0.17	14	29	34.8		66	35.9	1.24	0.9	32	0.18	>.5
13.3	C				6	60	6	1.33			0.17	
14.3	C		5	6		62	6.2	1.43			0.17	
15.3	C				5	62	5.2	1.52			0.17	
16.3	C		7	8.4		62	8.7	1.62			0.17	
17.3	C				5	62	5.2	1.71			0.16	
18.3	C		6	7.2		62	7.4	1.80			0.16	
19.3	C				7	62	7.2	1.90			0.16	
20.3	C		10	12		62	12.4	1.99			0.15	

SUMMARY OF SPT N160 CALCULATIONS - SITE B - HACHIRO GATA - FD 6+900

DEPTH m.	D50 mm.	MINUS #200 SIEVE %	N ASTM BPF	N LINER BPF	N JIS BPF	ROD ENERGY %	N60 BPF	VERT. STRESS TSF	CN	N160 BPF	FIELD CYCLIC STRESS RATIO	CYCLIC STRENGTH N160 METHOD
1.3	0.28	12			12	76	11.4	0.23	2.10	24	0.12	0.32
2.3	0.28	11	3	3.6		76	3.6	0.32	1.80	6	0.15	0.10
3.3	0.40	3			10	76	12.7	0.42	1.60	20	0.16	0.22
4.3	0.20	5	5	6		76	7.6	0.51	1.40	11	0.17	0.12
5.3	0.24	3			7	76	8.9	0.60	1.30	12	0.18	0.13
6.3			6	7.2		76	9.1	0.70	1.20	11	0.18	0.12
7.3					12	76	15.2	0.79	1.10	17	0.18	0.18
8.3	0.22	6	10	12		76	15.2	0.89	1.10	17	0.18	0.18
9.3	0.24	5			12	76	15.2	0.98	1.00	15	0.18	0.17
10.3	0.23	7	9	10.8		76	13.7	1.07	0.96	13	0.18	0.16
11.3	0.28	5			10	70	11.7	1.17	0.92	11	0.17	0.12
12.3	0.30	1	10	12		78	15.6	1.26	0.89	14	0.17	0.16
13.3	0.28	6			10	73	12.2	1.36	0.86	11	0.17	0.12
14.3	C		5	6		84	8.4					
15.3	C				4	76	5.1					
16.3	C		3	3.6		76	4.6					
17.3	C				1	76	1.3					
18.3	C		2	2.4		76	3					
19.3	C				6	76	7.6					
20.3	C		3	3.6		76	4.6					

SUMMARY OF SPT N160 CALCULATIONS - SITE C - HACHIRO GATA - WC 0+580

DEPTH m.	D50 mm.	MINUS #200 SIEVE %	N ASTM BPF	N LINER BPF	N JIS BPF	ROD ENERGY %	N60 BPF	VERT. STRESS TSF	CN	N160 BPF	FIELD CYCLIC STRESS RATIO	CYCLIC STRENGTH N160 METHOD
1.3	0.36	1			2	72	1.8	0.26	1.98	4	0.11	0.06
2.3	0.28	2	4	4.8		72	4.5	0.44	1.5	7	0.11	0.08
3.3	0.28	3			4	72	4.8	0.56	1.34	6	0.12	0.06
4.3	0.28	3	16	19.2		72	23.6	0.65	1.24	29	0.13	>.5
5.3	0.28	2			15	72	18	0.75	1.16	21	0.14	0.23
6.3	0.23	5	14	16.8		72	20.2	0.84	1.09	22	0.15	0.26
7.3	0.22	4			22	72	26.4	0.93	1.03	27	0.15	0.32
8.3	0.19	4	17	20.4		72	24.5	1.03	0.99	24	0.15	0.28
9.3	0.16	4			28	72	33.6	1.12	0.94	32	0.15	>.5
10.3	0.15	6	39	46.8		72	56.2	1.22	0.91	51	0.16	>.5
11.3	0.15	8			25	70	29.2	1.31	0.87	25	0.16	0.28
12.3	0.17	6	33	39.6		69	45.5	1.40	0.84	38	0.16	>.5
13.3	0.15	4			30	72	36	1.50	0.82	29	0.16	>.5
14.3	0.18	8	20	24		72	28.8	1.59	0.79	23	0.15	0.27
15.3	0.13	18			35	74	43.2	1.69	0.77	33	0.15	>.5
16.3	0.18	4	26	31.2		69	35.9	1.78	0.75	27	0.15	0.35
17.3	0.11	17			17	71	20.1	1.87	0.73	14	0.15	0.20
18.3	0.11	22	22	26.4		70	30.8	1.97	0.71	22	0.15	>.5
19.3	0.11	12			20	77	25.7	2.06	0.7	18	0.14	0.24
20.3	0.11	15	23	27.6		75	34.5	2.16	0.68	24	0.14	>.5

SUMMARY OF SPT N160 CALCULATIONS - SITE D - KAWAGISHI-CHO - NIIGATA

DEPTH m.	D50 mm.	MINUS #200 SIEVE %	N ASTM BPF	N LINER BPF	N JIS BPF	ROD ENERGY %	N60 BPF	VERT. STRESS TSF	CN	N160 BPF	FIELD CYCLIC STRESS RATIO	CYCLIC STRENGTH N160 METHOD
1.3	0.32	3			11	64	8.8	0.24	2	18	0.11	0.27
2.3	0.36	4	8	9.6		64	7.7	0.33	1.7	13	0.14	0.21
3.3	0.36	2			6	64	6.4	0.42	1.5	10	0.15	0.11
4.3	0.40	2	4	4.8		64	5.1	0.52	1.4	7	0.16	0.07
5.3	0.36	4			6	64	6.4	0.61	1.3	8	0.16	0.08
6.3	0.42	3	7	8.4		64	8.96	0.71	1.2	11	0.17	0.12
7.3	0.34	3			10	64	10.7	0.80	1.1	12	0.17	0.13
8.3	0.18	12	7	8.4		64	8.96	0.89	1.06	10	0.17	0.13
9.3	0.34	3			8	64	8.5	0.99	1	9	0.16	0.10
10.3	0.41	1	9	10.8		64	11.5	1.08	0.96	11	0.16	0.13
11.3	0.27	1			8	59	7.9	1.18	0.92	7	0.16	0.07
12.3	0.28	3	8	9.6		63	10.2	1.27	0.89	9	0.16	0.10
13.3	0.43	2			8	64	8.5	1.36	0.85	7	0.16	0.07
14.3	0.27	2	9	10.8		64	11.5	1.46	0.83	10	0.16	0.13
15.3	0.27	4			17	66	18.7	1.55	0.8	15	0.16	0.17
16.3	0.26	4	15	18.6		63	19.2	1.65	0.78	15	0.15	0.17
17.3	0.26	4			25	62	25.8	1.74	0.76	20	0.15	0.22
18.3	0.25	13	21	25.2		64	26.7	1.83	0.74	20	0.15	0.28
19.3	0.22	6			35	68	39.7	1.93	0.72	29	0.15	>.5
20.3	0.26	6	29	34.8		66	37.1	2.02	0.7	26	0.14	0.39

SUMMARY OF SPT N160 CALCULATIONS - SITE E - SHOWA BRIDGE - NIIGATA

DEPTH m.	D50 mm.	MINUS #200 SIEVE %	N ASTM BPF	N LINER BPF	N JIS BPF	ROD ENERGY %	N60 BPF	VERT. STRESS TSF	CN	N160 BPF	FIELD CYCLIC STRESS RATIO	CYCLIC STRENGTH N160 METHOD
1.3	0.28	30			15	64	12	0.26	1.98	24	0.1	>.5
2.3	0.22	9	5	6		64	4.8	0.36	1.67	8	0.13	0.14
3.3	0.10	39			2	64	2.1	0.45	1.48	3	0.14	
4.3	0.25	5	6	7.2		64	7.7	0.55	1.35	10	0.15	0.12
5.3	0.29	2			9	64	9.6	0.64	1.25	12	0.16	0.13
6.3	0.52	3	11	13.2		64	14.1	0.74	1.16	16	0.16	0.17
7.3	0.40	1			12	64	12.8	0.83	1.09	14	0.16	0.15
8.3	0.42	3	11	13.2		64	14.1	0.93	1.04	15	0.16	0.16
9.3	0.40	3			10	64	10.7	1.02	0.99	11	0.16	0.12
10.3	0.38	5	12	14.4		64	15.4	1.11	0.95	15	0.16	0.16
11.3	0.41	4			10	64	10.7	1.21	0.91	10	0.16	0.11
12.3	0.41	6	8	9.6		64	10.2	1.30	0.87	9	0.16	0.10
13.3	0.30	3			39	64	41.6	1.40	0.84	35	0.16	>.5
14.3	0.30	4	24	28.8		64	30.7	1.49	0.82	25	0.15	0.32
15.3	0.25	4			27	64	28.8	1.59	0.79	23	0.15	0.27
16.3	0.26	6	27	32.4		64	34.6	1.68	0.77	27	0.15	0.36
17.3	0.30	3			36	64	38.4	1.77	0.75	29	0.15	0.40
18.3	0.28	5	19	22.8		64	24.3	1.87	0.73	18	0.15	0.20
19.3	0.22	4			25	64	26.6	1.96	0.71	19	0.14	0.21
20.3	0.20	8	31	37.4		64	39.7	2.06	0.69	27	0.14	0.40

SUMMARY OF SPT N160 CALCULATIONS - SITE F - SHOWA BRIDGE - NIIGATA

DEPTH m.	D50 mm.	MINUS #200 SIEVE %	N ASTM BPF	N LINER BPF	N JIS BPF	ROD ENERGY %	N60 BPF	VERT. STRESS TSF	CN	N160 BPF	FIELD CYCLIC STRESS RATIO	CYCLIC STRENGTH N160 METHOD
1.3	0.70	11			33	68	28	0.26	1.97	55	0.1	>.5
2.3	0.40	2	4	4.8		68	4.1	0.39	1.59	7	0.12	0.08
3.3	0.04	64			3	68	3.4	0.49	1.43	5	0.13	
4.3	0.01	94	0	0		68	0	0.58	1.31	0	0.14	
5.3	0.26	6			25	68	28.3	0.68	1.20	34	0.15	>.5
6.3	0.24	4	16	19		68	21.5	0.77	1.10	24	0.15	0.32
7.3	0.24	5			32	68	36.3	0.87	1.07	39	0.15	>.5
8.3	0.24	3	27	32.4		68	36.7	0.96	1.02	37	0.15	>.5
9.3	0.24	5			36	68	40.8	1.05	0.97	40	0.16	>.5
10.3	0.27	2	27	32.4		68	36.7	1.15	0.93	34	0.16	>.5
11.3	0.26	6			54	68	61.2	1.24	0.89	55	0.15	>.5
12.3	0.26	5	24	28.8		68	32.6	1.34	0.86	28	0.15	0.34
13.3	0.26	4			28	68	31.7	1.43	0.83	26	0.15	0.28
14.3	0.27	6	25	30		68	34	1.53	0.81	28	0.15	0.37
15.3	0.26	7			17	68	19.3	1.62	0.78	15	0.15	0.17
16.3	0.24	7	22	26.4		68	29.9	1.71	0.76	23	0.15	0.28
17.3	0.21	7			29	68	32.9	1.81	0.74	24	0.15	0.28
18.3	0.24	5	33	39.6		68	44.9	1.90	0.72	33	0.14	>.5
19.3	0.16	8			24	68	27.2	2.00	0.71	19	0.14	0.21
20.3	0.22	5	34	40.8		68	46.2	2.09	0.69	32	0.14	>.5

TABLE 3 SUMMARY OF CONE PENETRATION CALCULATIONS - ALL SITES

SITE	DEPTH m.	FIELD CYCLIC STRESS RATIO	SPT N160 STRENGTH	FRICTION RATIO %	MINUS NO.200 SIEVE %	D50 mm.	QC/N60 RATIO	QC1 AVG. n=0.5 TSF	CYCLIC STRENGTH QC1 METHOD	QC1 AVG. n=0.72 TSF	FSN SLEEVE FRICTION TSF	STATE PARAMETER
A	1.3	0.13	0.04	1.9			10	45	0.10	64	1.44	
A	2.3	0.14	0.09	1.2	6	0.22	4	44	0.11	58	0.70	-0.11
A	3.3	0.18	0.32	4.8	21	0.20	2	27	0.13	33	1.35	
A	4.3	0.18	0.33	1.0	10	0.26	3	60	0.17	71	1.70	-0.13
A	5.3	0.19	0.35	0.5	13	0.20	5	90	0.29	95	3.20	-0.18
B	1.3	0.12	0.32	1.5	12	0.28	5	121	>.5	169	1.57	
B	2.3	0.15	0.10	1.2	11	0.28	12	108	0.35	139		-0.20
B	3.3	0.16	0.22	1.1	3	0.40	5	90	0.20	109	2.15	-0.16
B	4.3	0.17	0.12	1.1	5	0.20	2	20	0.06	24	0.47	-0.06
B	5.3	0.17	0.13	0.6	3	0.24	2	27	0.06	30	0.20	-0.05
B	6.3	0.18	0.12	2.3			2	19	0.05	20	0.34	-0.04
B	7.3	0.18	0.18	1.5			3	44	0.11	48	0.82	-0.09
B	8.3	0.18	0.18	1.5	6	0.22	4	65	0.16	67	0.58	-0.11
B	9.3	0.18	0.17	1.6	5	0.24	2	28	0.08	29	0.42	-0.06
B	10.3	0.18	0.16	1.0	7	0.23	3	44	0.11	43	0.38	-0.08
B	11.3	0.18	0.12	1.0	5	0.28	5	54	0.14	52	0.63	-0.08
C	3.3	0.12	0.06	1.3	3	0.28	10	59	0.13	69	0.44	-0.11
C	4.3	0.13	>.5	1.7	3	0.28	3	97	0.21	109	2.18	-0.14
C	5.3	0.14	0.23	1.9	2	0.28	4	90	0.22	98	2.36	-0.11
C	6.3	0.15	0.26		5	0.23	5	120	0.33	127		-0.14
D	1.3	0.11	0.27	0.9	3	0.32	7	120	0.30	170	2.70	
D	2.3	0.14	0.21	0.3	4	0.36	10	129	0.33	169	1.64	-0.20
D	3.3	0.15	0.11	1.7	2	0.36	5	54	0.12	67	1.02	-0.12
D	4.3	0.16	0.07	1.4	2	0.40	6	45	0.10	53	0.58	-0.11
D	5.3	0.16	0.08	0.8	4	0.36	7	56	0.12	64	0.72	-0.12
D	6.3	0.16	0.12	2.2	3	0.42	5	51	0.11	56	1.69	-0.13
D	7.3	0.17	0.13	0.9	3	0.34	6	74	0.17	79	0.99	-0.13
D	8.3	0.17	0.13	1.9	12	0.18	5	46	0.16	48	0.56	-0.10
D	9.3	0.17	0.10	1.2	3	0.34	6	50	0.11	51	0.89	-0.09
D	10.3	0.16	0.13	0.6	1	0.41	6	63	0.13	63	0.31	-0.10
E	2.3	0.1	0.11	1.0	9	0.22	8	61	0.17	79	1.06	-0.13
E	3.3	0.14	NA	1.4	39	0.10	13	40	0.23	56	0.87	
E	4.3	0.15	0.12	1.0	5	0.25	4	41	0.12	47	0.48	-0.10
E	5.3	0.15	0.13	1.3	2	0.29	5	55	0.13	62	0.79	-0.12
E	6.3	0.16	0.17	1.4	3	0.52	4	59	0.11	64	1.06	-0.11
E	7.3	0.16	0.15	1.4	1	0.40	3	45	0.10	52	0.79	-0.09
E	8.3	0.16	0.16	1.3	3	0.42	4	64	0.12	67	0.79	-0.12
E	9.3	0.16	0.12	1.6	3	0.40	5	50	0.11	52	0.82	-0.10
E	10.3	0.16	0.16	2.1	5	0.38	4	50	0.11	49	0.55	-0.08
E	11.3	0.16	0.11	1.6	4	0.41	4	43	0.10	41	0.53	-0.08
F	2.3	0.12	0.08	2.2	2	0.40	15	102	0.23	129	3.35	
F	5.3	0.15	>.5	1.3	6	0.26	3	95	0.30	105	1.50	-0.15
F	6.3	0.15	0.28	1.3	4	0.24	6	141	>.5	150	1.70	

TABLE 4 SUMMARY OF FACTOR OF SAFETY AND STRENGTH DATA SHEET 1 OF 3

SITE	DEPTH m.	FIELD CYCLIC STRESS RATIO	N160 BPF	CYCLIC STRENGTH N160 METHOD	FS N160	CYCLIC STREGTH I&T METHOD	FS I&T	QC1 TSF	CYCLIC STRENGTH QC1 METHOD	FS QC1	VIBRO CONE D %	STRENGTH RL20 VIBRO CONE	STATE PARAMETER
A	2.3	0.17	9	0.09	0.5	0.18	1.1	44	0.11	0.6	0.70	0.32	-0.11
A	3.3	0.18	20	0.32	1.8	0.23	1.3	27	0.13	0.7	0.30	0.34	
A	4.3	0.18	23	0.33	1.8	0.23	1.3	60	0.17	0.9	0.20	0.35	-0.13
A	5.3	0.19	24	0.35	1.8	0.27	1.4	90	0.29	1.5	0.20	0.34	-0.18
A	6.3	0.19	22	0.28	1.5	0.23	1.2						
A	7.3	0.19	40	>.5		0.31	1.6						
A	8.3	0.18	31	>.5		0.28	1.6						
A	9.3	0.18	51	>.5		0.35	1.9						
A	10.3	0.18	61	>.5		0.36	2.0						
A	11.3	0.18	55	>.5		0.36	2.0						
A	12.3	0.18	32	>.5		0.29	1.6						
B	2.3	0.15	6	0.10	0.7	0.12	0.8	108	0.35	2.3	0.90	0.31	-0.2
B	3.3	0.16	20	0.22	1.4	0.17	1.1	90	0.20	1.3	0.50	0.32	-0.16
B	4.3	0.17	11	0.12	0.7	0.16	0.9	20	0.06	0.4	0.85	0.28	-0.06
B	5.3	0.18	12	0.13	0.7	0.16	0.9	27	0.06	0.3	0.80	0.27	-0.05
B	6.3	0.18	11	0.12	0.7	0.15	0.8	19	0.05	0.3	0.80	0.25	-0.04
B	7.3	0.18	17	0.18	1.0	0.19	1.1	44	0.11	0.6	0.40	0.29	-0.09
B	8.3	0.18	17	0.18	1.0	0.19	1.1	65	0.16	0.9	0.80	0.22	-0.11
B	9.3	0.18	15	0.17	0.9	0.18	1.0	28	0.08	0.4	0.70	0.22	-0.06
B	10.3	0.18	13	0.16	0.9	0.17	0.9	44	0.11	0.6	0.75	0.20	-0.08
B	11.3	0.17	11	0.12	0.7	0.15	0.9	54	0.14	0.8	0.75	0.20	-0.08
B	12.3	0.17	14	0.16	0.9	0.15	0.9				0.75	0.19	
B	13.3	0.17	11	0.12	0.7	0.14	0.8				0.75	0.18	
C	3.3	0.12	6	0.06	0.5	0.12	1.0	59	0.13	1.1	0.30	0.32	-0.11
C	4.3	0.13	29	>.5		0.22	1.7	97	0.21	1.6	-0.40	0.50	-0.14
C	5.3	0.14	21	0.23	1.6	0.2	1.4	90	0.22	1.6	0.10	0.35	-0.11
C	6.3	0.15	22	0.26	1.7	0.22	1.5	120	0.33	2.2	0.05	0.42	-0.14
C	7.3	0.15	27	0.32	2.1	0.24	1.6						
C	8.3	0.15	24	0.28	1.9	0.23	1.5						
C	9.3	0.15	32	>.5		0.27	1.8						
C	10.3	0.16	51	>.5		0.34	2.1						
C	11.3	0.16	25	0.28	1.8	0.26	1.6						
C	12.3	0.16	38	>.5		0.3	1.9						
C	13.3	0.16	29	>.5		0.26	1.6						
C	14.3	0.15	23	0.27	1.8	0.22	1.5						
C	15.3	0.15	33	>.5		0.28	1.9						
C	16.3	0.15	27	0.35	2.3	0.24	1.6						
C	17.3	0.15	14	0.20	1.3	0.22	1.5						
C	18.3	0.15	22	>.5		0.25	1.7						
C	19.3	0.14	18	0.24	1.7	0.21	1.5						
C	20.3	0.14	24	>.5			0.0						

SITE	DEPTH m.	FIELD CYCLIC STRESS RATIO	N160 BPF	CYCLIC STRENGTH N160 METHOD	FS N160	CYCLIC STRENGTH I&T METHOD	FS I&T	QC1 TSF	CYCLIC STRENGTH QC1 METHOD	FS QC1	VIBRO CONE D %	STRENGTH RL20 VIBRO CONE	STATE PARAMETER
D	2.3	0.14	13	0.21	1.5	0.17	1.2	129	0.33	2.4	1.00	0.31	-0.20
D	3.3	0.15	10	0.11	0.7	0.13	0.9	54	0.12	0.8	1.00	0.30	-0.12
D	4.3	0.16	7	0.07	0.4	0.11	0.7	45	0.10	0.6	0.90	0.28	-0.11
D	5.3	0.16	8	0.08	0.5	0.12	0.8	56	0.12	0.8	0.40	0.30	-0.12
D	6.3	0.16	11	0.12	0.8	0.13	0.8	51	0.11	0.7	0.80	0.25	-0.13
D	7.3	0.17	12	0.13	0.8	0.16	0.9	74	0.17	1.0	0.40	0.28	-0.13
D	8.3	0.17	10	0.13	0.8	0.17	1.0	46	0.16	0.9	0.30	0.30	-0.10
D	9.3	0.17	9	0.10	0.6	0.13	0.8	50	0.11	0.6	0.30	0.30	-0.09
D	10.3	0.16	11	0.13	0.8	0.12	0.8	63	0.13	0.8	0.10	0.38	-0.10
D	11.3	0.16	7	0.07	0.4	0.13	0.8				0.40	0.26	
D	12.3	0.16	9	0.10	0.6	0.14	0.9				0.20	0.33	
D	13.3	0.16	7	0.07	0.4	0.11	0.7				0.40	0.26	
D	14.3	0.16	10	0.13	0.8	0.15	0.9				0.10	0.39	
D	15.3	0.16	15	0.17	1.1	0.18	1.1				0.00	0.45	
D	16.3	0.15	15	0.17	1.1	0.17	1.1				0.10	0.40	
D	17.3	0.15	20	0.22	1.5	0.20	1.3						
D	18.3	0.15	20	0.28	1.9	0.20	1.3						
D	19.3	0.15	29	>.5		0.25	1.7						
D	20.3	0.14	26	0.39	2.8	0.22	1.6						
B	2.3	0.13	8	0.11	0.8	0.18	1.4	61	0.17	1.3	1.00	0.31	-0.13
B	4.3	0.15	10	0.12	0.8	0.16	1.1	41	0.12	0.8	1.00	0.27	-0.10
B	5.3	0.16	12	0.13	0.8	0.16	1.0	55	0.13	0.8	0.95	0.25	-0.12
B	6.3	0.16	16	0.17	1.1	0.14	0.9	59	0.11	0.7	0.90	0.24	-0.11
B	7.3	0.16	14	0.15	0.9	0.15	0.9	45	0.10	0.6	0.90	0.22	-0.09
B	8.3	0.16	15	0.16	1.0	0.15	0.9	64	0.12	0.8	0.90	0.19	-0.12
B	9.3	0.16	11	0.12	0.8	0.13	0.8	50	0.11	0.7	0.80	0.21	-0.10
B	10.3	0.16	15	0.16	1.0	0.15	0.9	50	0.11	0.7	0.75	0.20	-0.08
B	11.3	0.16	10	0.11	0.7	0.13	0.8	43	0.10	0.6	0.70	0.20	-0.08
B	12.3	0.16	9	0.10	0.6	0.12	0.8				0.60	0.21	
B	13.3	0.16	35	>.5		0.26	1.6				0.70	0.28	
B	14.3	0.15	25	0.32	2.1	0.17	1.1				0.40	0.26	
B	15.3	0.15	23	0.27	1.8	0.22	1.5						
B	16.3	0.15	27	0.36	2.4	0.23	1.5						
B	17.3	0.15	29	0.40	2.7	0.24	1.6						
B	18.3	0.15	18	0.20	1.3	0.18	1.2						
B	19.3	0.14	19	0.21	1.5	0.21	1.5						
B	20.3	0.14	27	0.40	2.9	0.25	1.8						

TABLE 4 SUMMARY OF FACTOR OF SAFETY AND STRENGTH DATA SHEET 3 OF 3

SITE	DEPTH m.	FIELD CYCLIC STRESS RATIO	N160 BPF	CYCLIC STRENGTH N160 METHOD	FS N160	CYCLIC STRENGTH I&T METHOD	FS I&T	QC1 TSF	CYCLIC STRENGTH QC1 METHOD	FS QC1	VIBRO CONE D %	STRENGTH RL20 VIBRO CONE	STATE PARAMETER
F	2.3	0.12	7	0.08	0.7	0.11	0.9	102	0.23	1.9	0.10	0.37	
F	5.3	0.15	34	>.5		0.26	1.7	95	0.30	2.0	0.25	0.32	-0.15
F	6.3	0.15	24	0.32	2.1	0.23	1.5	141	>.5				
F	7.3	0.15	39	>.5		0.28	1.9						
F	8.3	0.15	37	>.5		0.26	1.7						
F	9.3	0.16	40	>.5		0.29	1.8						
F	10.3	0.16	34	>.5		0.25	1.6						
F	11.3	0.15	55	>.5		0.31	2.1						
F	12.3	0.15	28	0.34	2.3	0.23	1.5						
F	13.3	0.15	26	0.28	1.9	0.22	1.5						
F	14.3	0.15	28	0.37	2.5	0.22	1.5						
F	15.3	0.15	15	0.17	1.1	0.18	1.2						
F	16.3	0.15	23	0.28	1.9	0.21	1.4						
F	17.3	0.15	24	0.28	1.9	0.23	1.5						
F	18.3	0.14	33	>.5		0.24	1.7						
F	19.3	0.14	19	0.21	1.5	0.22	1.6						
F	20.3	0.14	32	>.5		0.25	1.8						

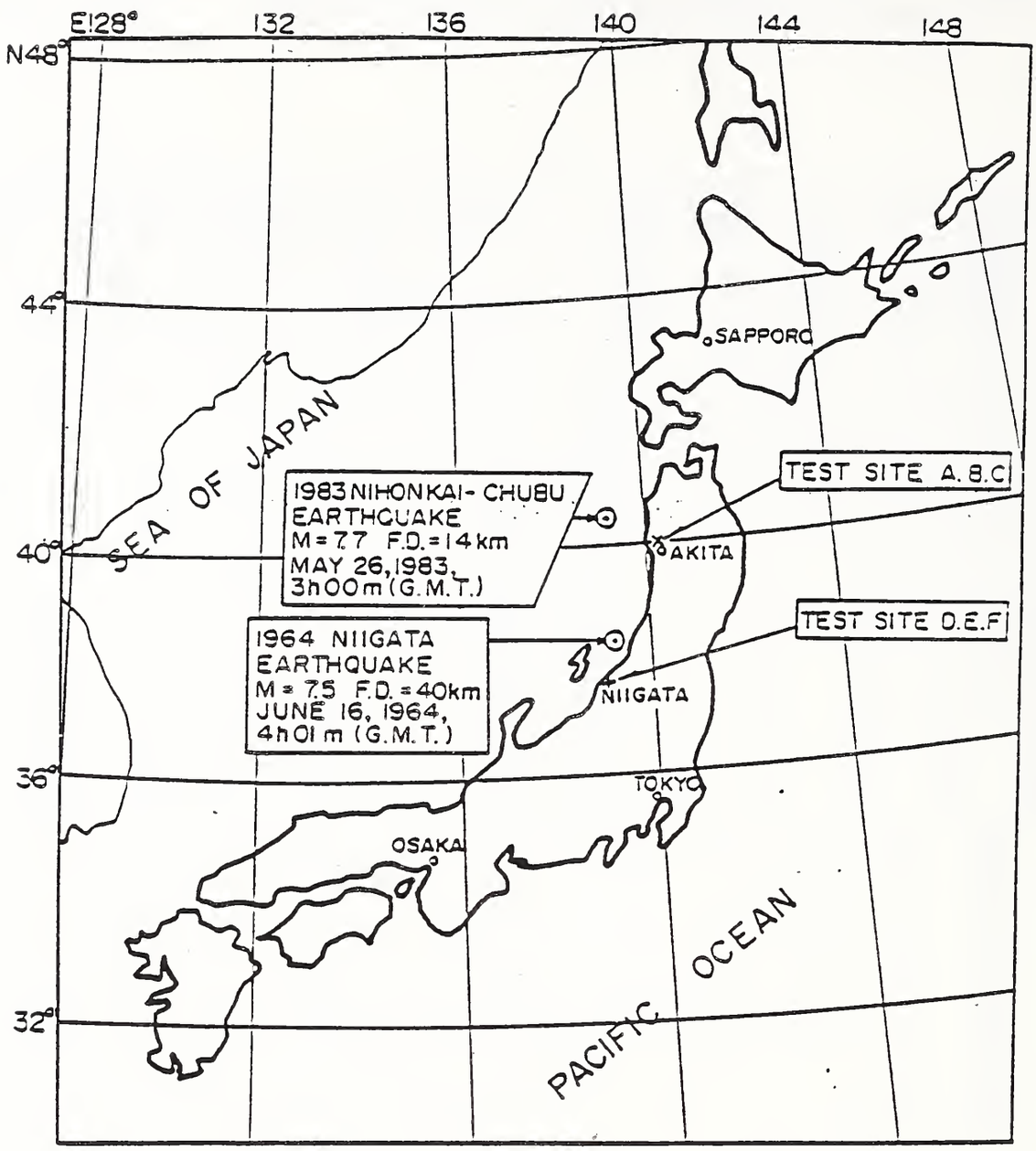

Figure 1 Location of test sites and the earthquake epicenters

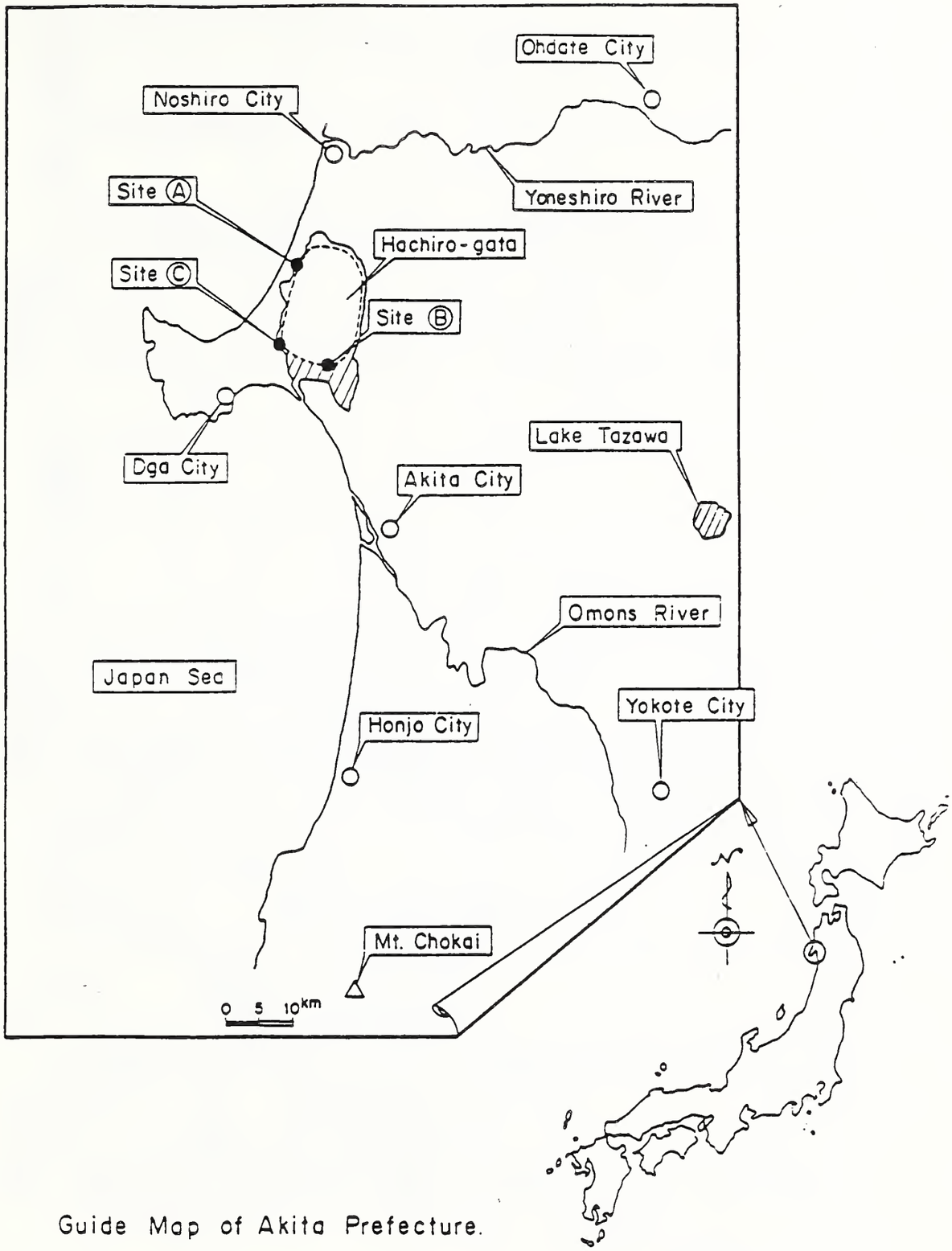

Guide Map of Akita Prefecture.

FIGURE 2

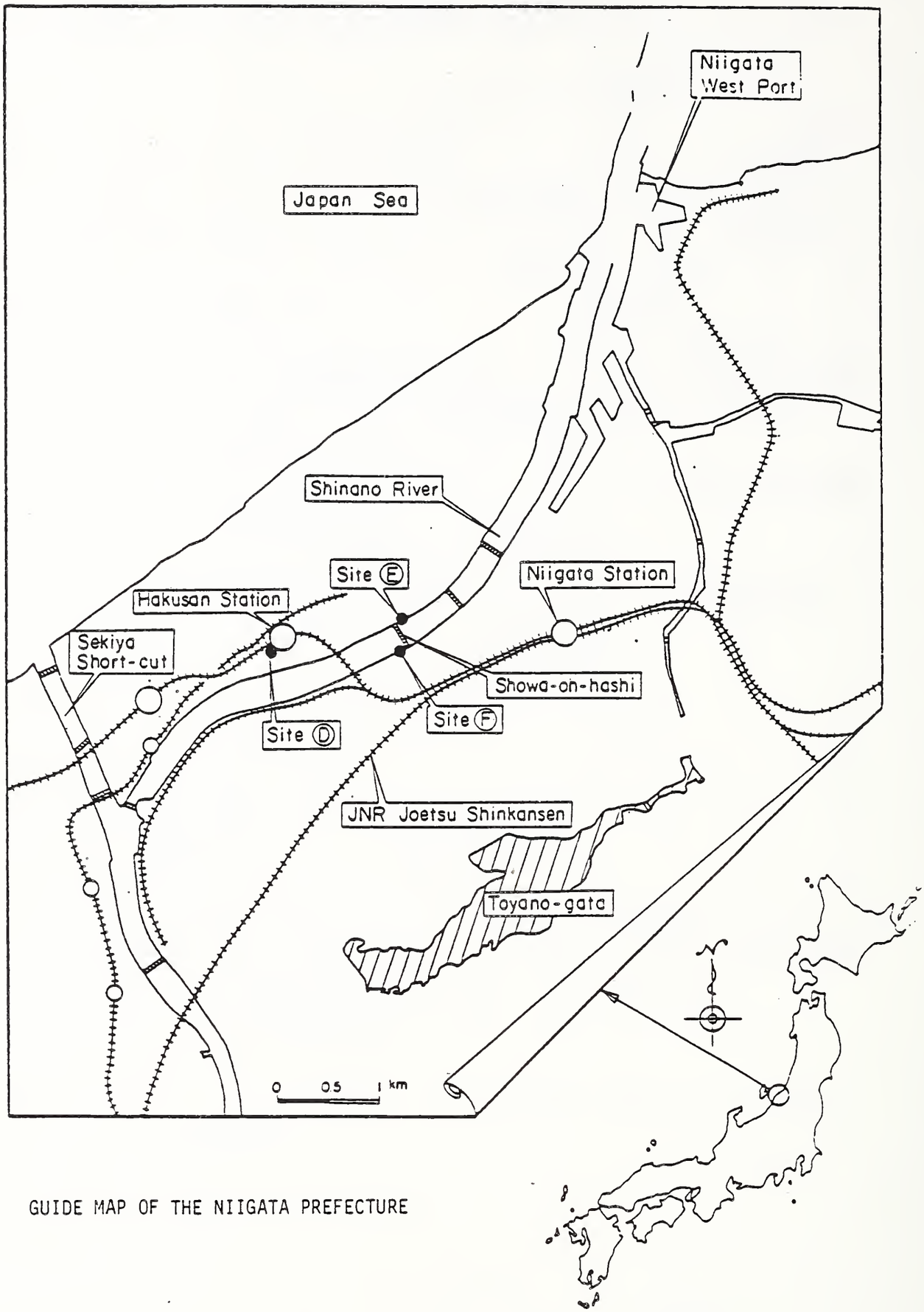

GUIDE MAP OF THE NIIGATA PREFECTURE

FIGURE 3

Soil properties and soil logs at test sites

FIGURE 4

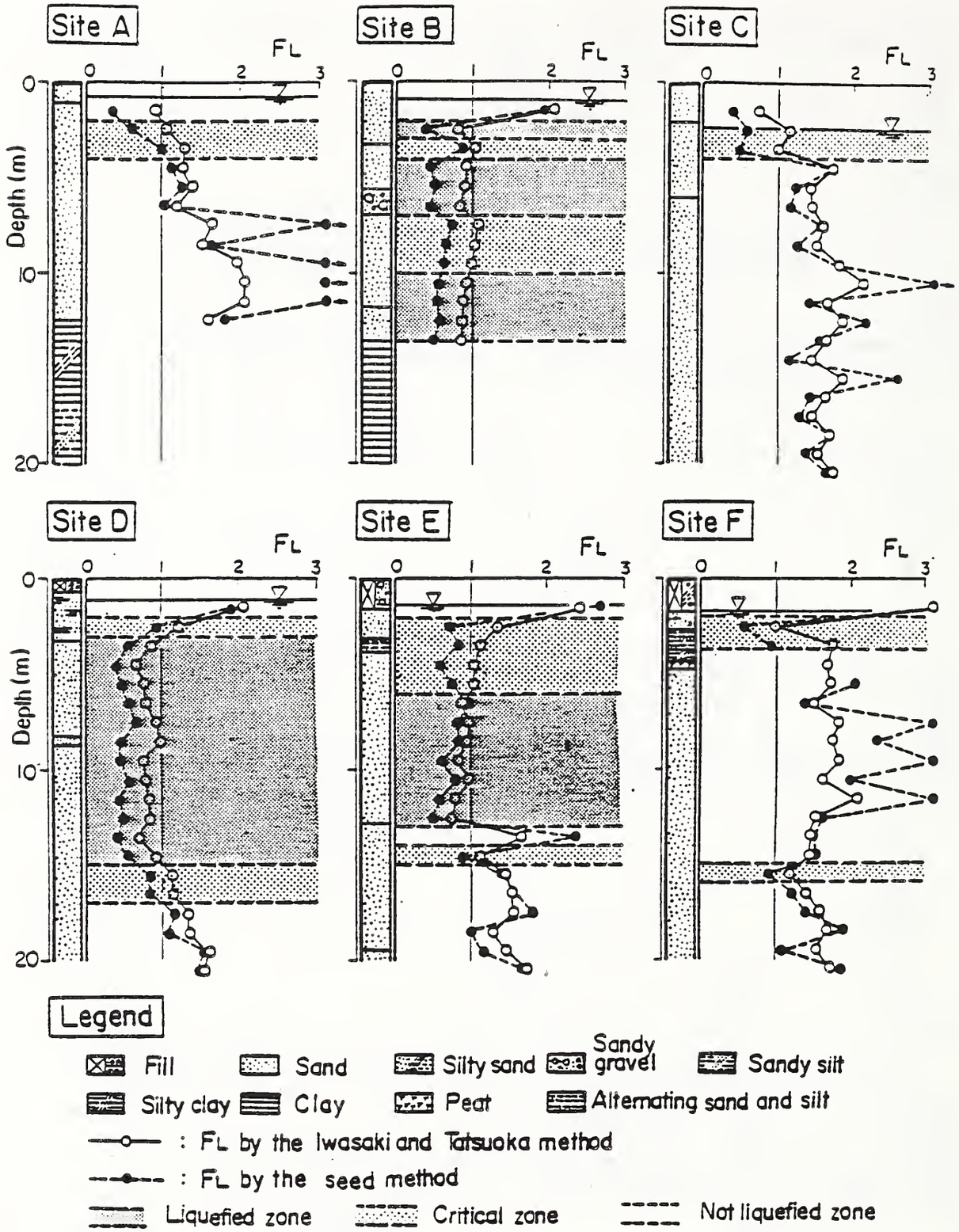

Comparision of F_L distribution by the Iwasaki and Tatsuokas' method and by the Seeds' method

FIGURE 5

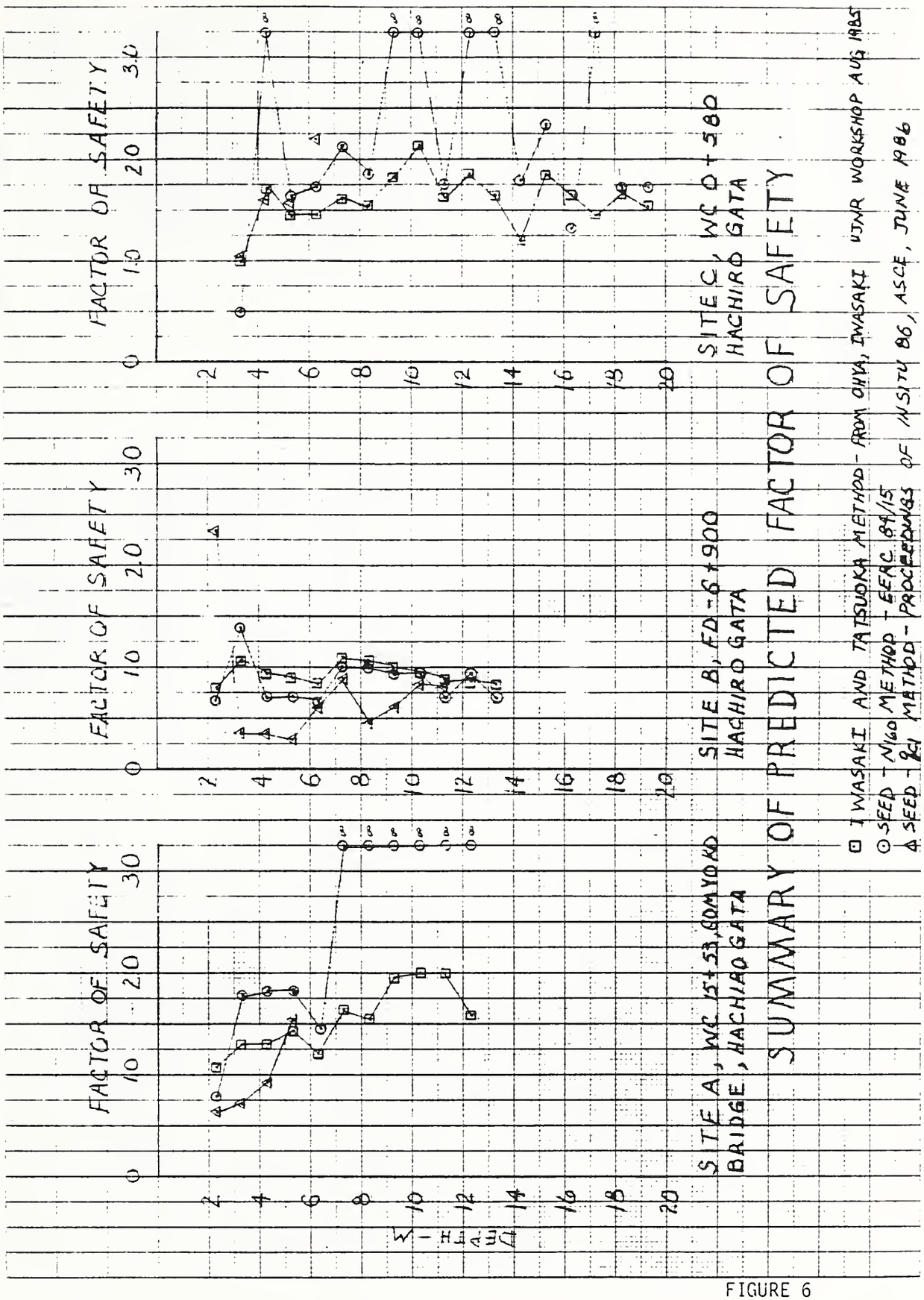

FIGURE 6

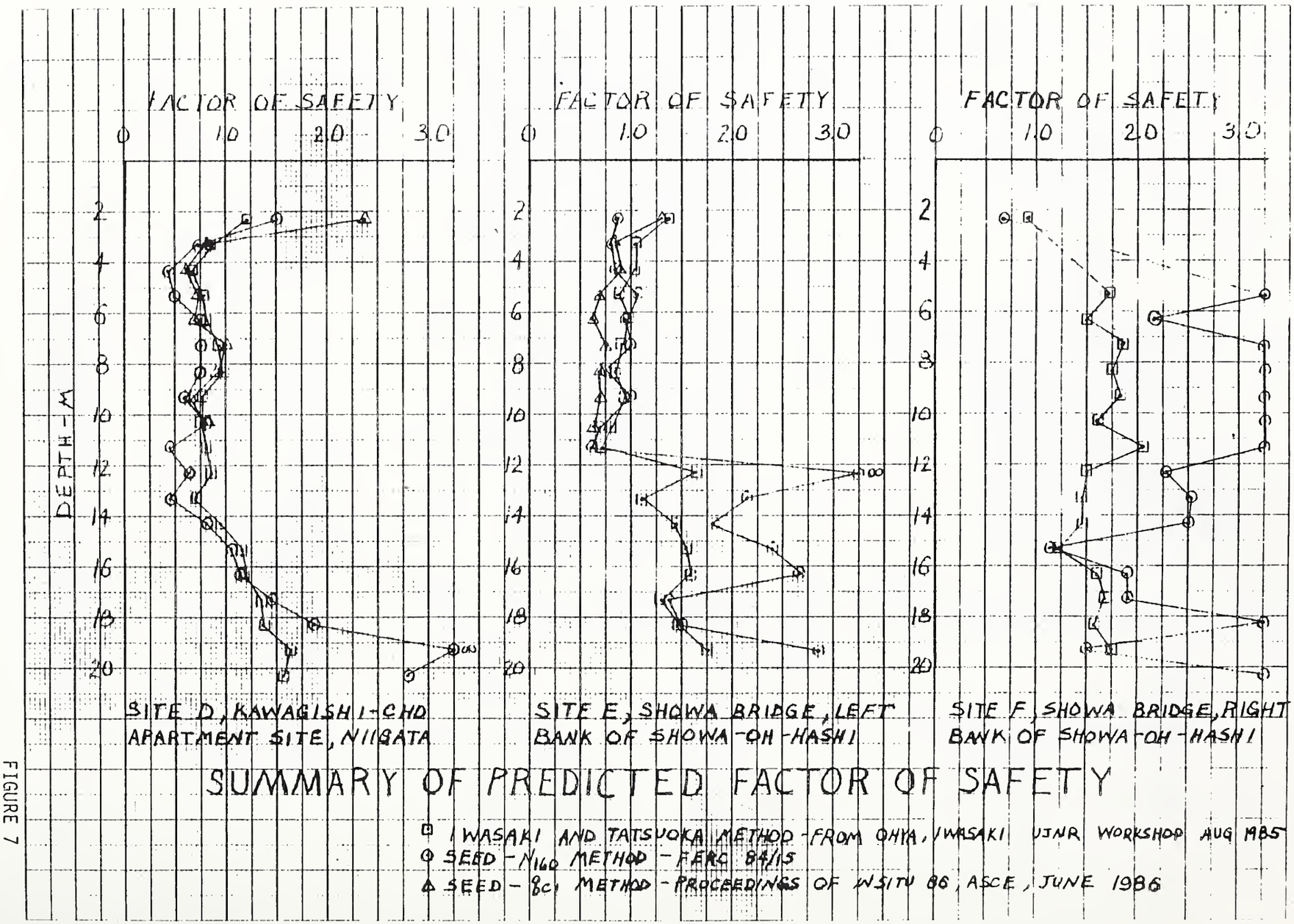

FIGURE 7

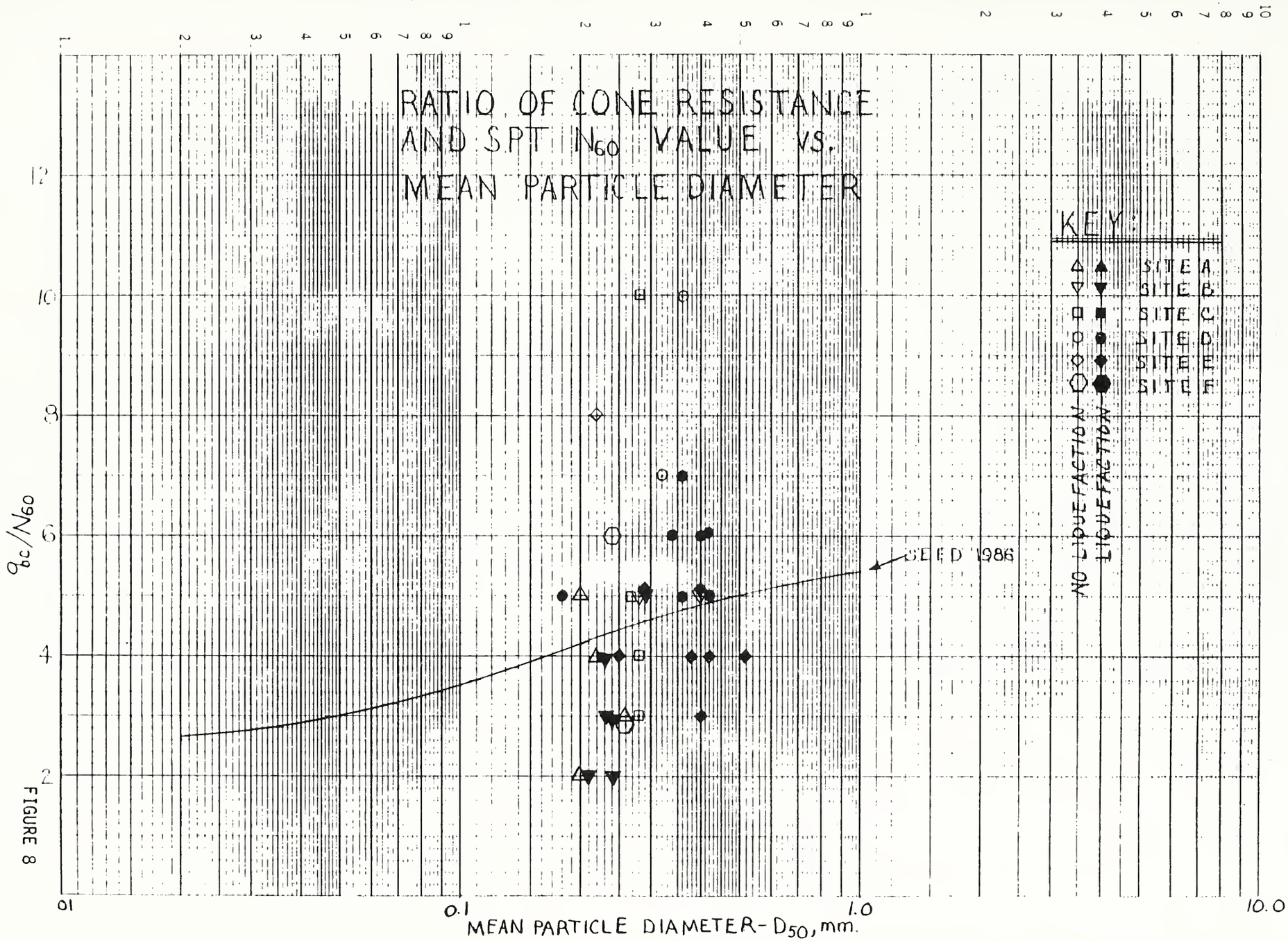

FIGURE 8

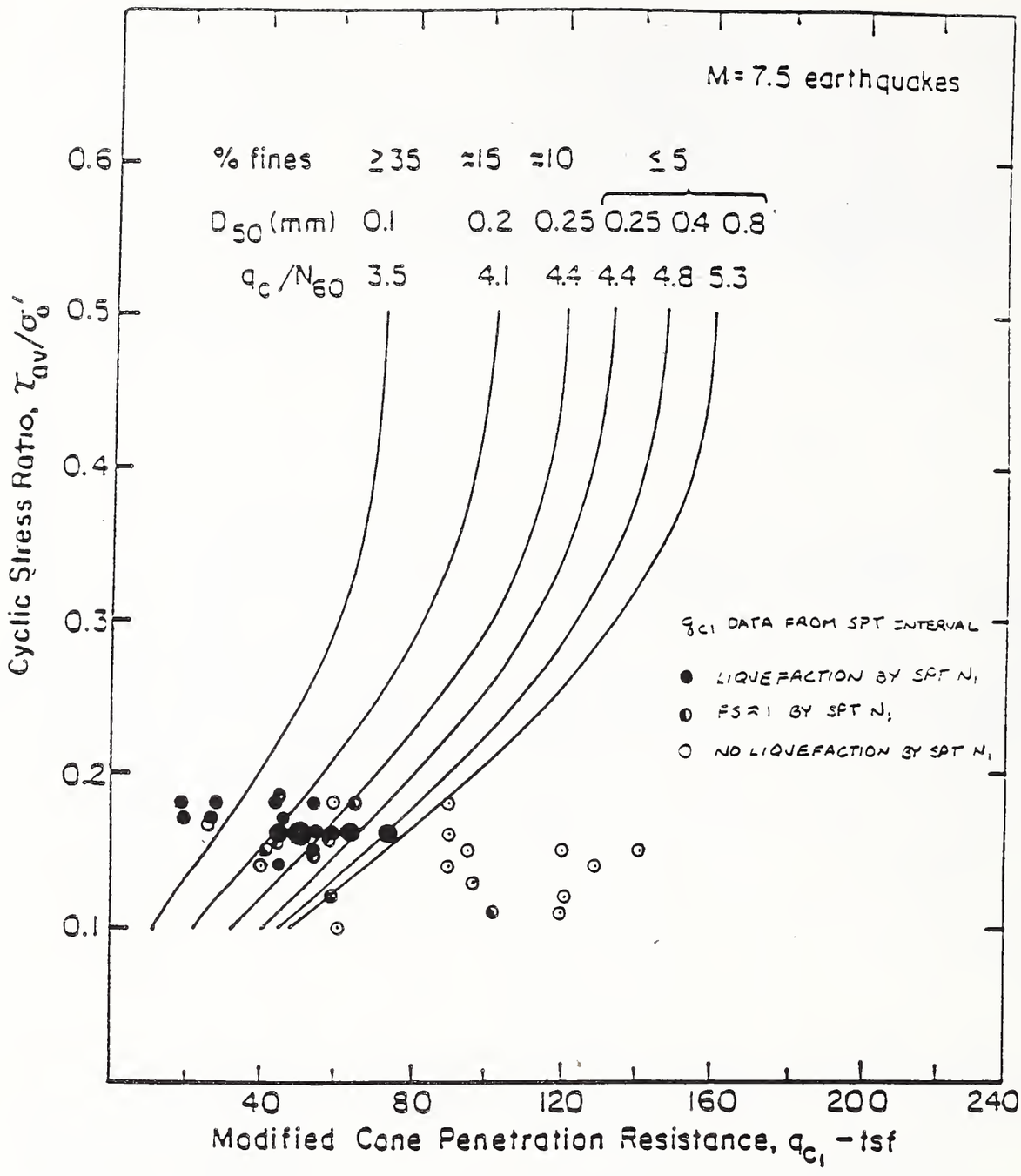

RELATIONSHIP BETWEEN STRESS RATIO CAUSING LIQUEFACTION AND CONE TIP RESISTANCE FOR SANDS AND SILTY SANDS - (SEED 1986)

SUMMARY OF DEPENDENT Qc1 DATA POINTS FROM THE 1983 US - JAPAN JOINT STUDY

FIGURE 9

SUMMARY OF NORMALIZED TIP AND SLEEVE FRICTION CPT DATA - 1983 US - JAPAN JOINT STUDY

ALL SITES

CPT SOIL CHARACTERIZATION CHART

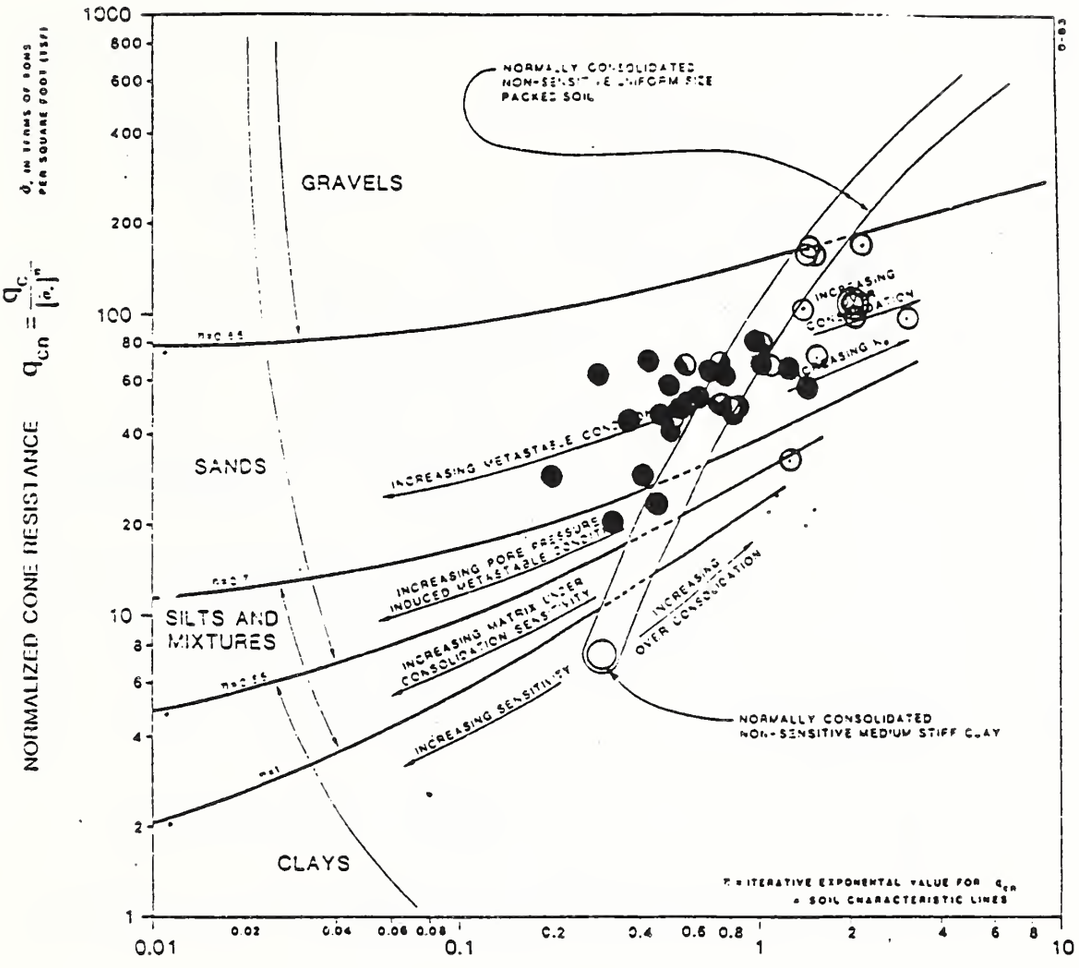

NORMALIZED SLEEVE FRICTION RESISTANCE $f_{sn} = \frac{f_s}{\sigma_v'}$

○ NO LIQUEFACTION
◐ CRITICAL FS=1.0
● LIQUEFACTION

} LIQUEFACTION FROM SPT N160 METHOD

FIGURE 10

SUMMARY OF NORMALIZED TIP AND SLEEVE FRICTION CPT DATA - SITE B - FD 6+900 - HACHIRO GATA

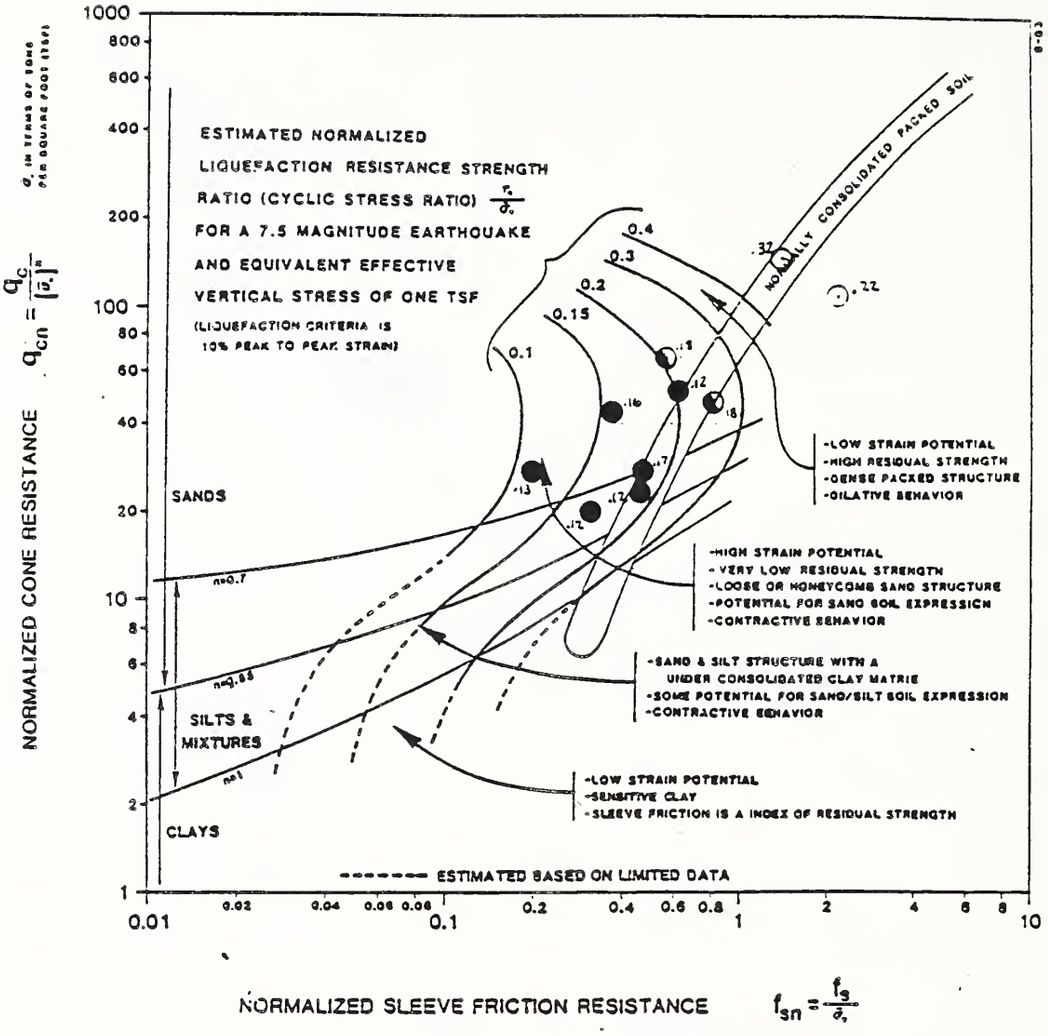

NO LIQUEFACTION
CRITICAL FS= 1.0
LIQUEFACTION

LIQUEFACTION OCCURRENCE FROM SPT N160 METHOD - NUMERAL BESIDE POINT IS ESTIMATED N160 STRENGTH

FIGURE 11

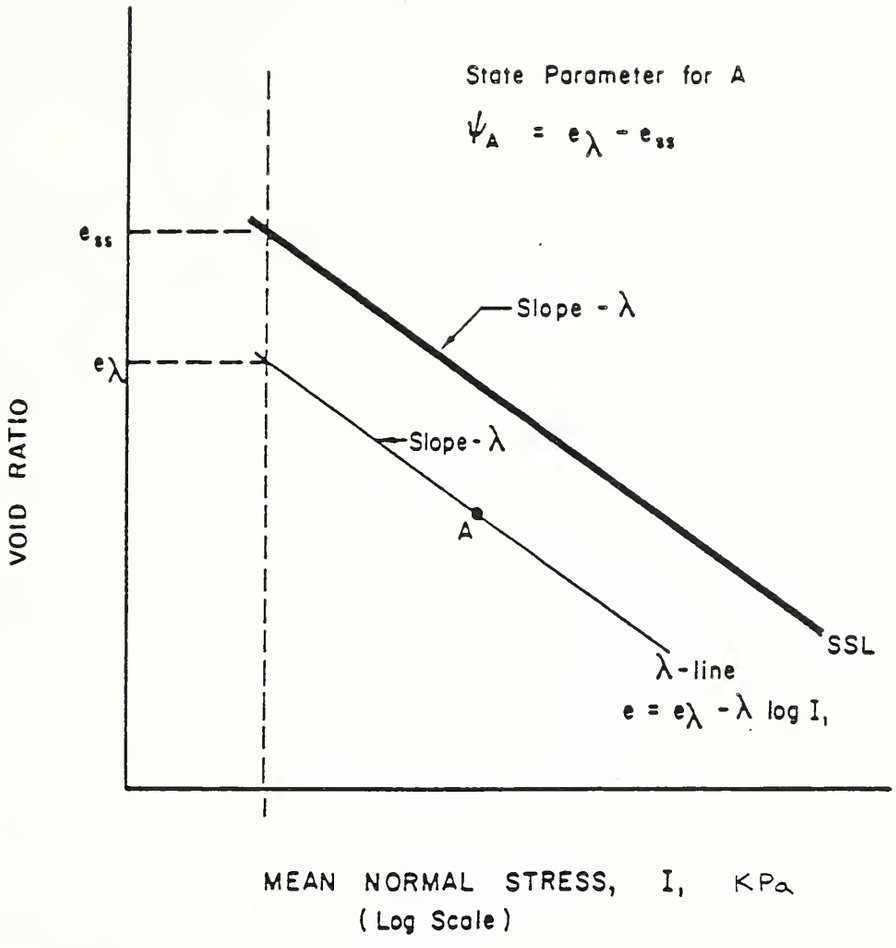

DEFINITION OF STATE PARAMETER ψ

FIGURE 12

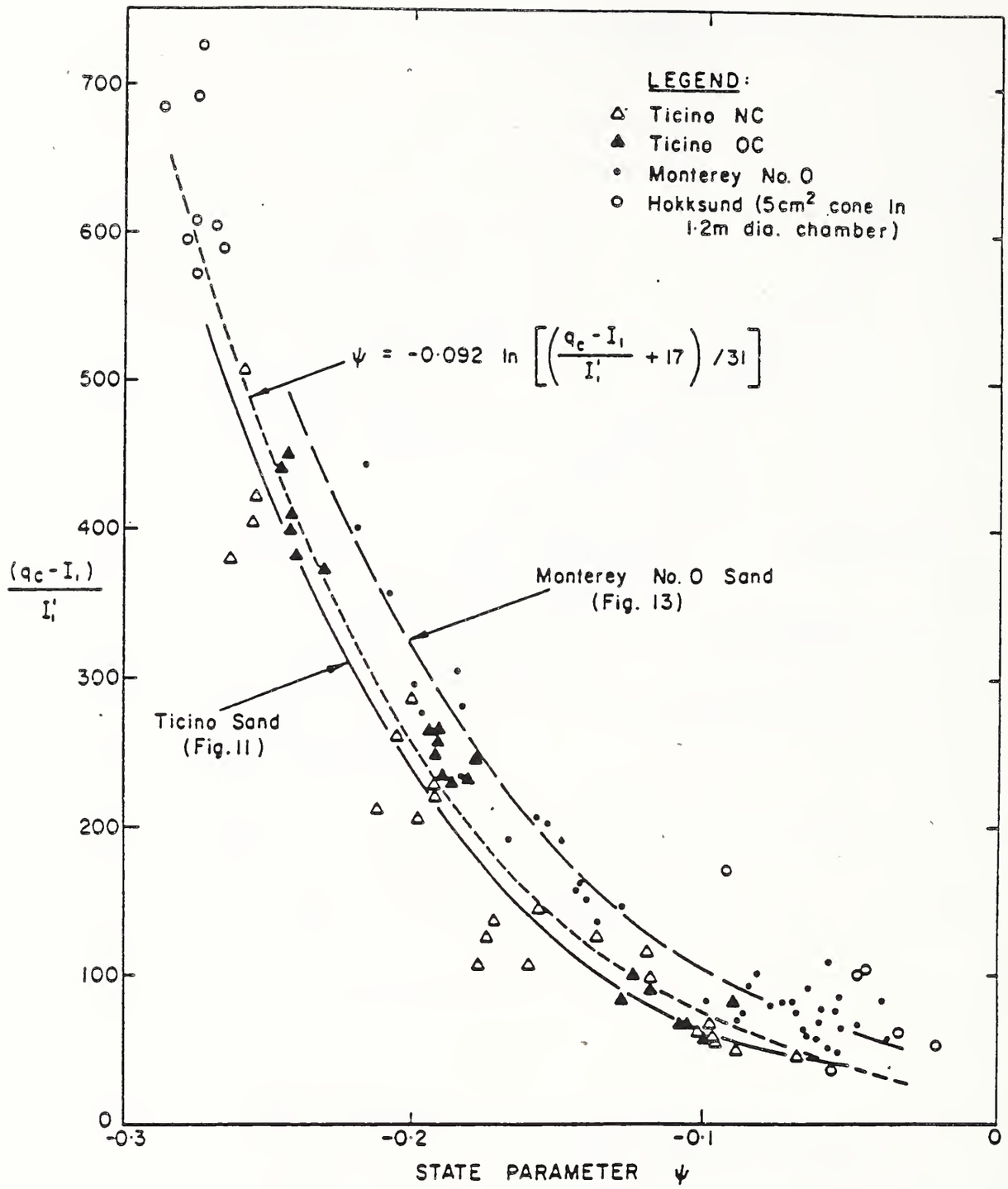

COMPARISON OF NORMALIZED CONE RESISTANCE STATE PARAMETER CORRELATIONS FOR HOKKSUN TICINO AND MONTEREY #0 SANDS

FIGURE 13

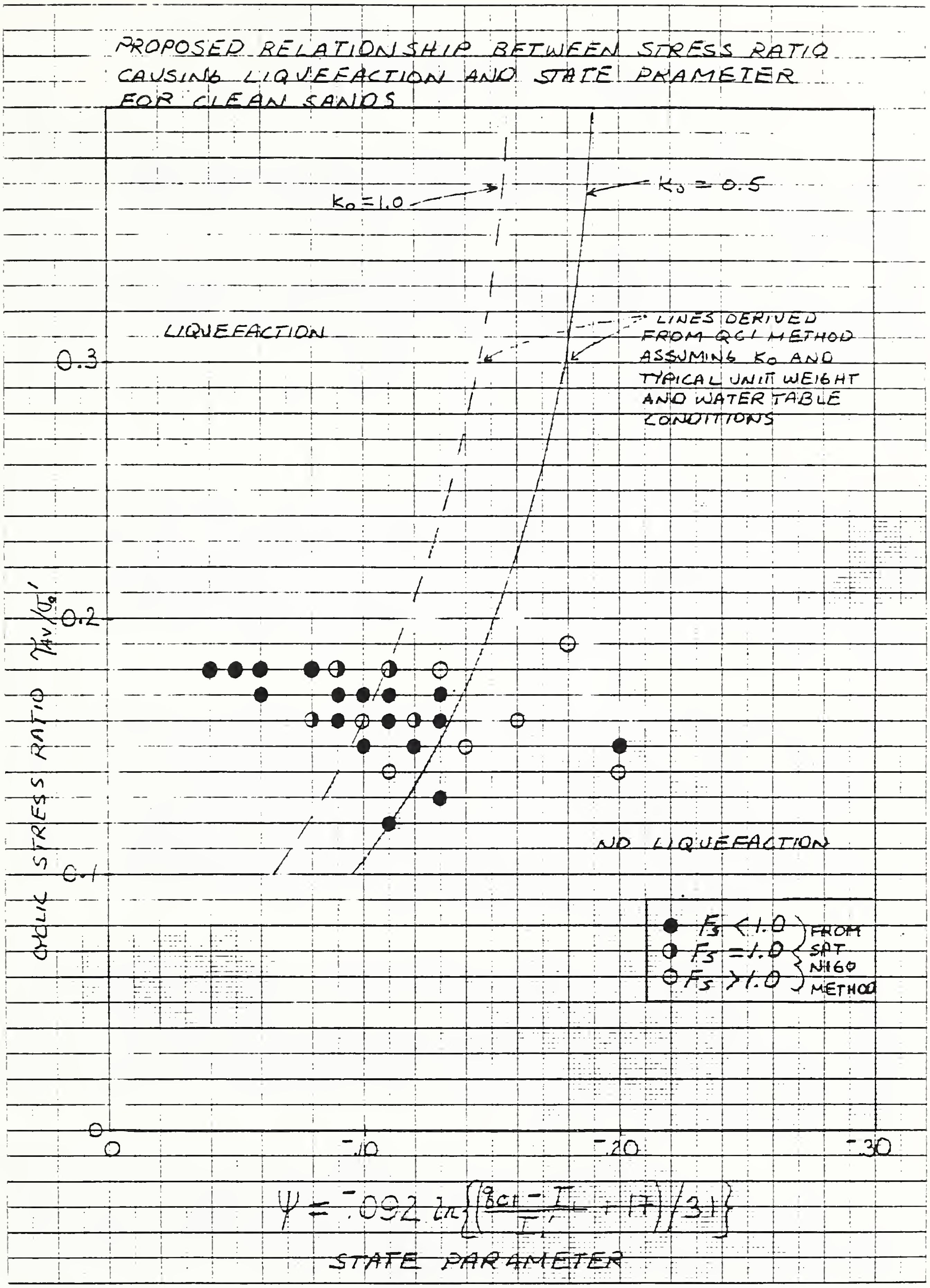
PROPOSED RELATIONSHIP BETWEEN STRESS RATIO CAUSING LIQUEFACTION AND STATE PRAMETER FOR CLEAN SANDS
Ko=1.0
Ko = 0.5
LIQUEFACTION
LINES DERIVED FROM QCI METHOD ASSUMING Ko AND TYPICAL UNIT WEIGHT AND WATER TABLE CONDITIONS
0.3
0.2
0.1
0
CYCLIC STRESS RATIO
NO LIQUEFACTION
Fs <1.0
Fs =1.0
Fs >1.0
FROM SPT N160 METHOD
0
-.10
-.20
-.30
STATE PARAMETER

FIGURE 14

FIGURE 15

GRAPHS OF RESULTS FROM DILATOMETER SOUNDING No.

Sounding location: SITE B , FD 6+920 ... B ... SAND LAGOON
Graphs plotted by: WW - JAF Date: ... 26 198...

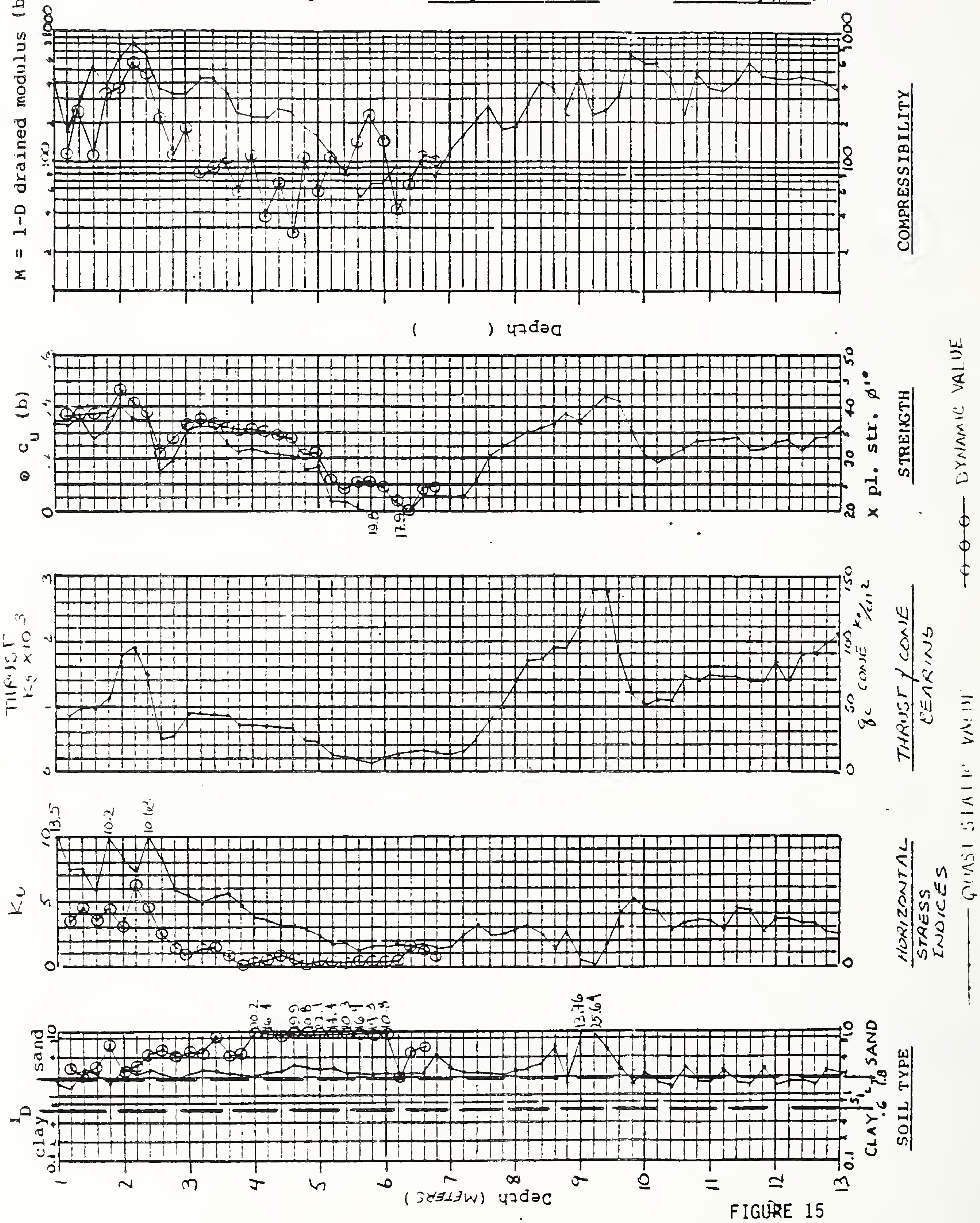

FIGURE 15

FIGURE 16

GRAPHS OF RESULTS FROM DILATOMETER SOUNDING No.

Sounding location: STATION W.: 13+620 24m N. & HACHIRO DATA [illegible]

Graphs plotted by: WW - JAF Date: MAR 26 19[illegible]

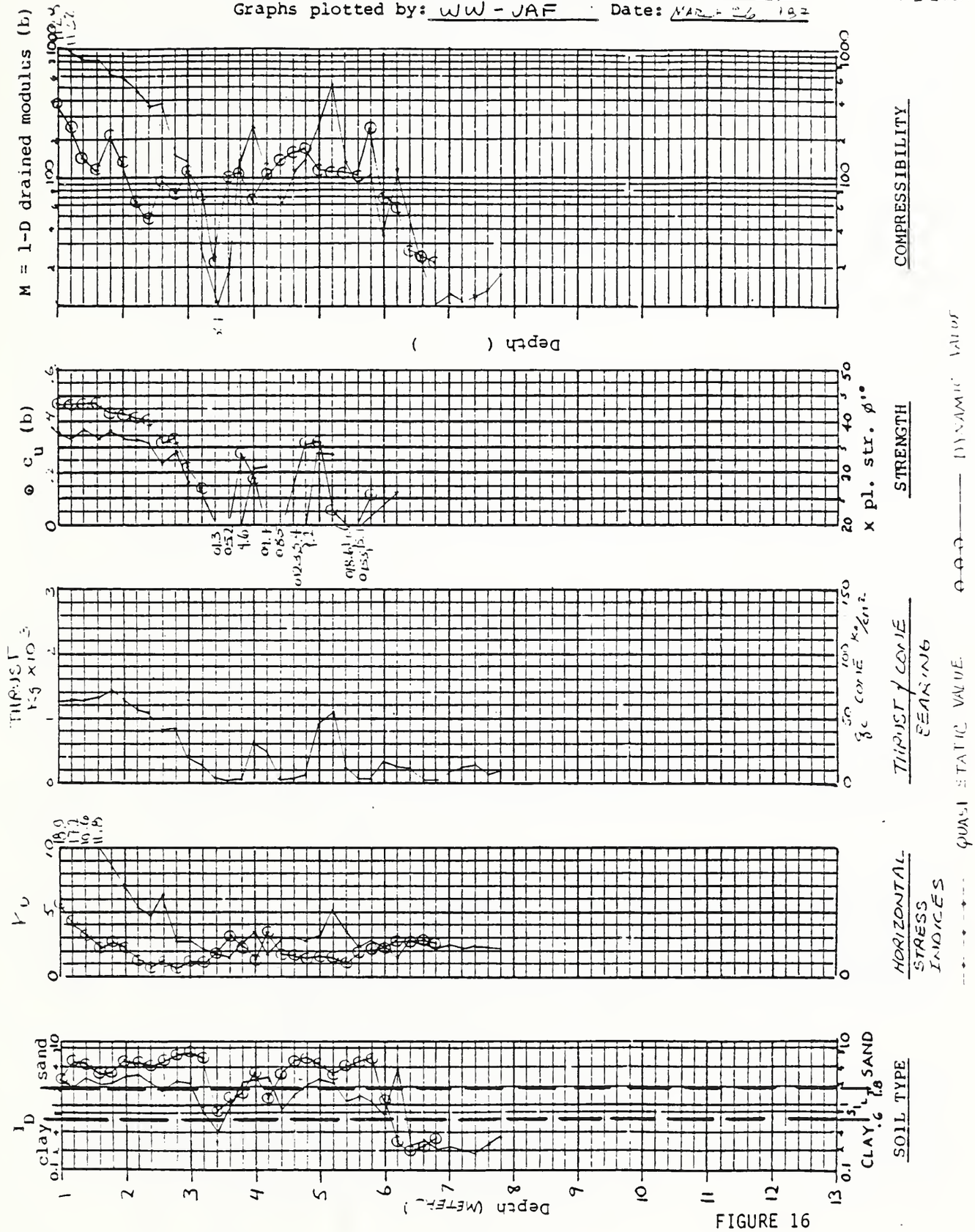

FIGURE 16

FIGURE 17

GRAPHS OF RESULTS FROM DILATOMETER SOUNDING No.

Sounding location: SITE C, STA W1 0+580 MAIN RD STA LAFFAN

Graphs plotted by: WW - JAF Date: [illegible]

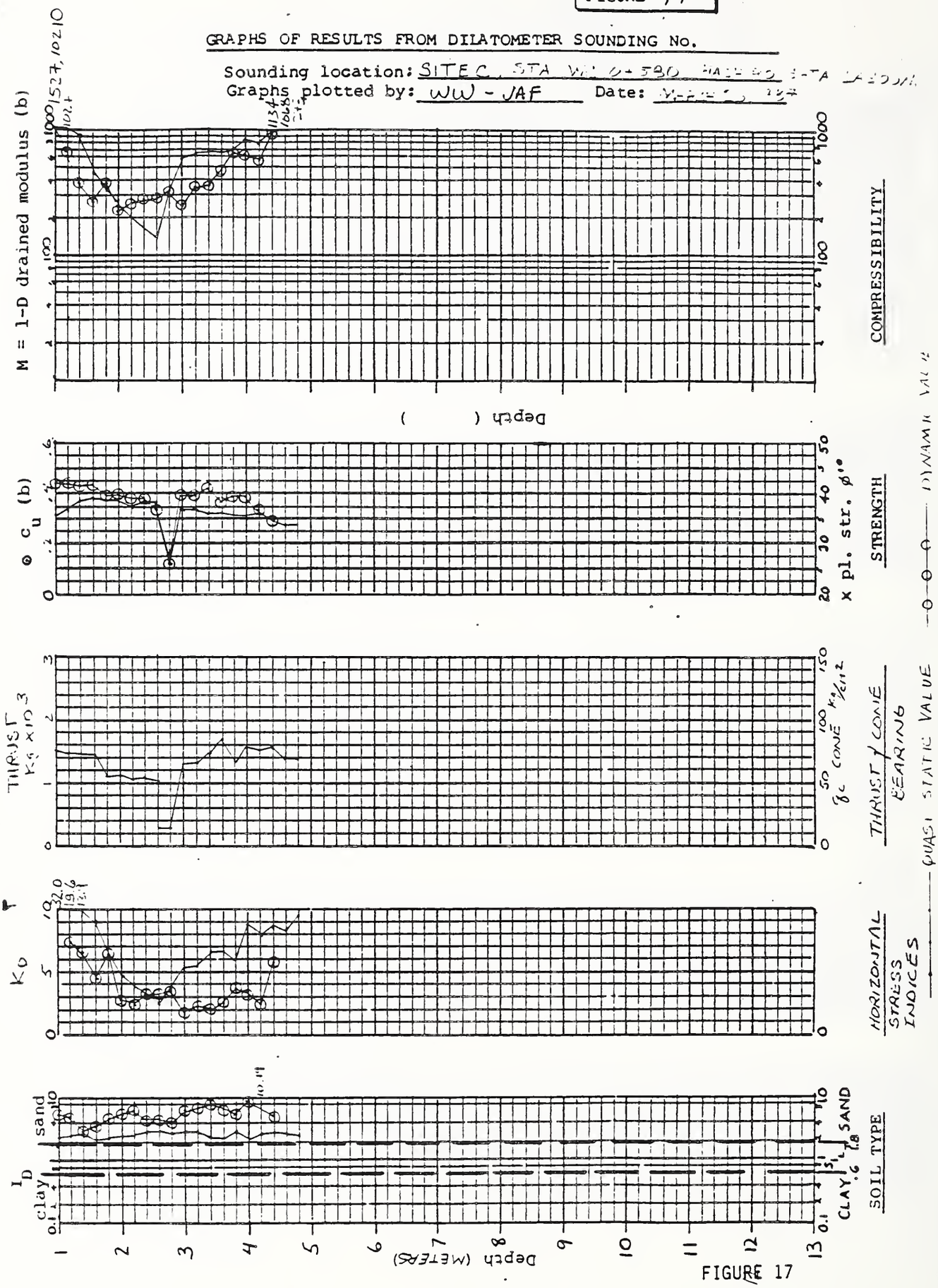

COMPARISON OF 1983 and 1986 QC1 VALUES -- SITE B - FD 6+900

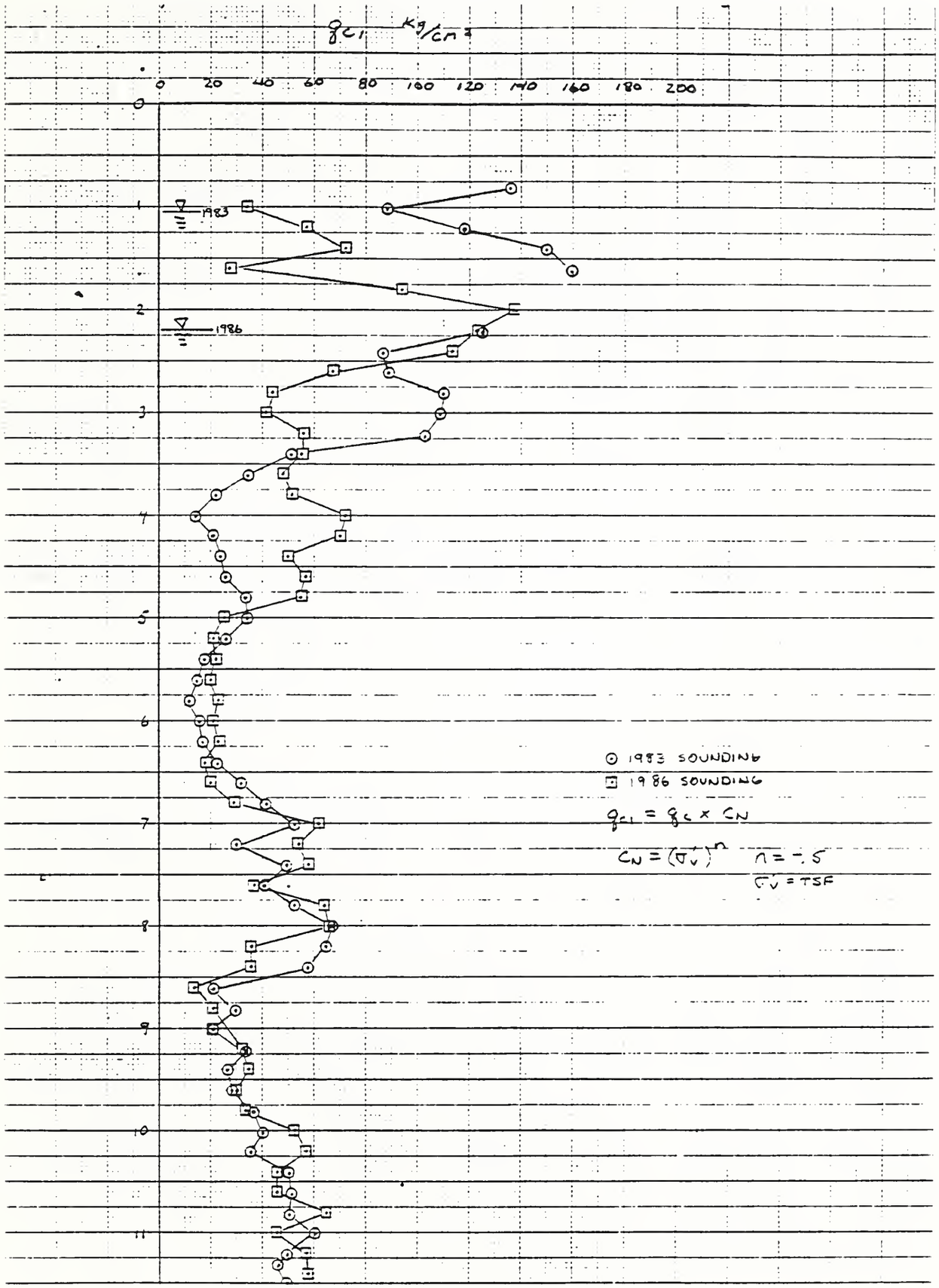

FIGURE 18

COMPARISON OF 1983 and 1983 QC1 VALUES - SITE C - WC 0+585

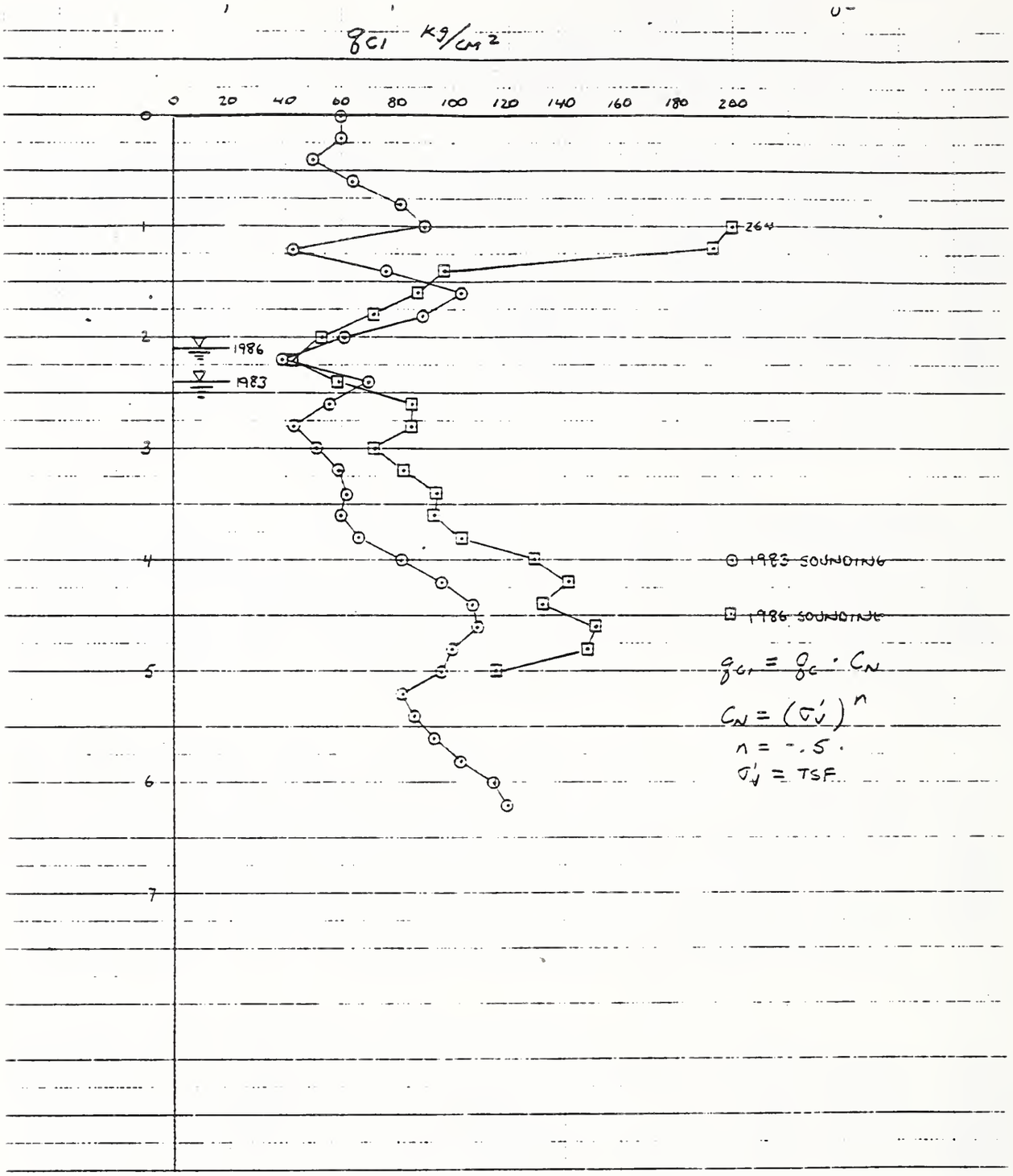

FIGURE 19

PROPOSED CORRELATION BETWEEN LIQUEFACTION RESISTANCE UNDER LEVEL GROUND CONDITIONS AND DILATOMETER HORIZONTAL STRESS INDEX

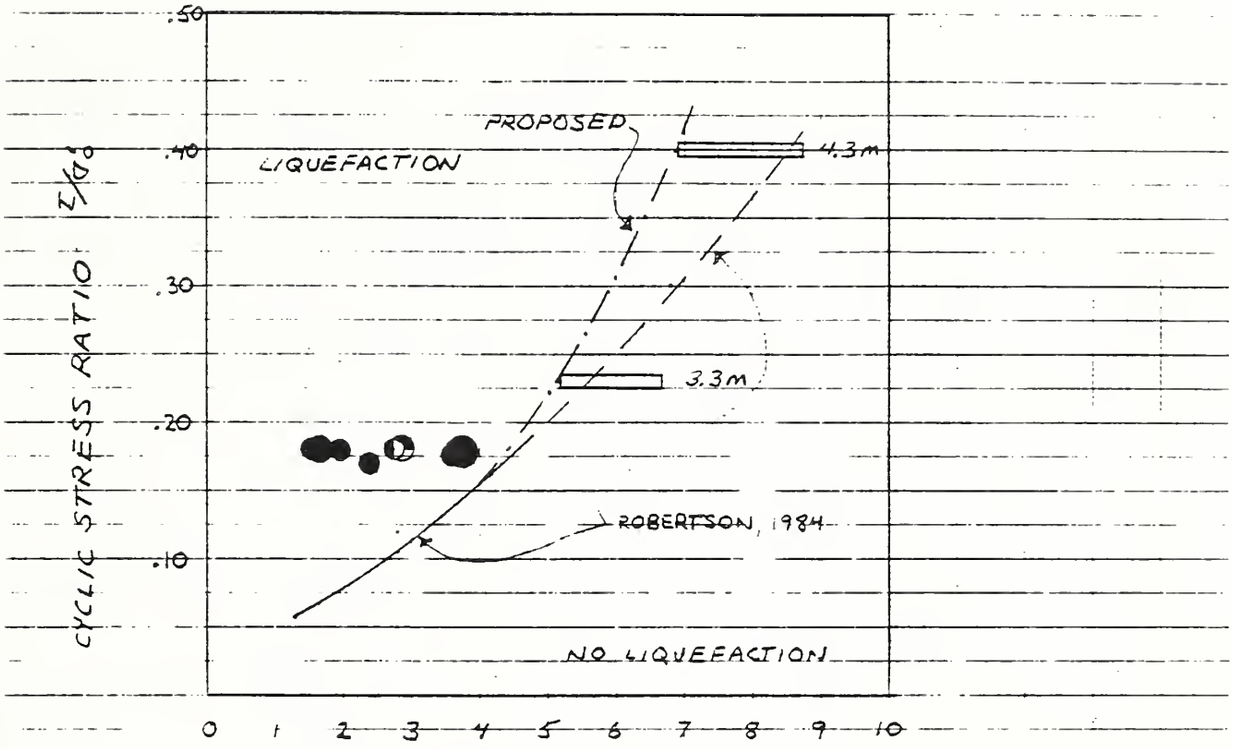

$K_D = (P_0 - u_0) / \sigma'_{vo}$

KEY: ● LIQUEFACTION
◐ CRITICAL FS ≈ 1.0
} FROM SITE B, AVERAGE K_D IN SPT INTERVAL, LIQUEFACTION OCCURRENCE FROM SPT N_{160}

▭ SITE C - ESTIMATED CYCLIC STRENGTH FROM 1986 CPT DATA USING QCI METHOD

FIGURE 20

COMPARISON OF VIBROCONE - PENETRATION AND CYCLIC STRENGTH FROM SPT N100 METHOD

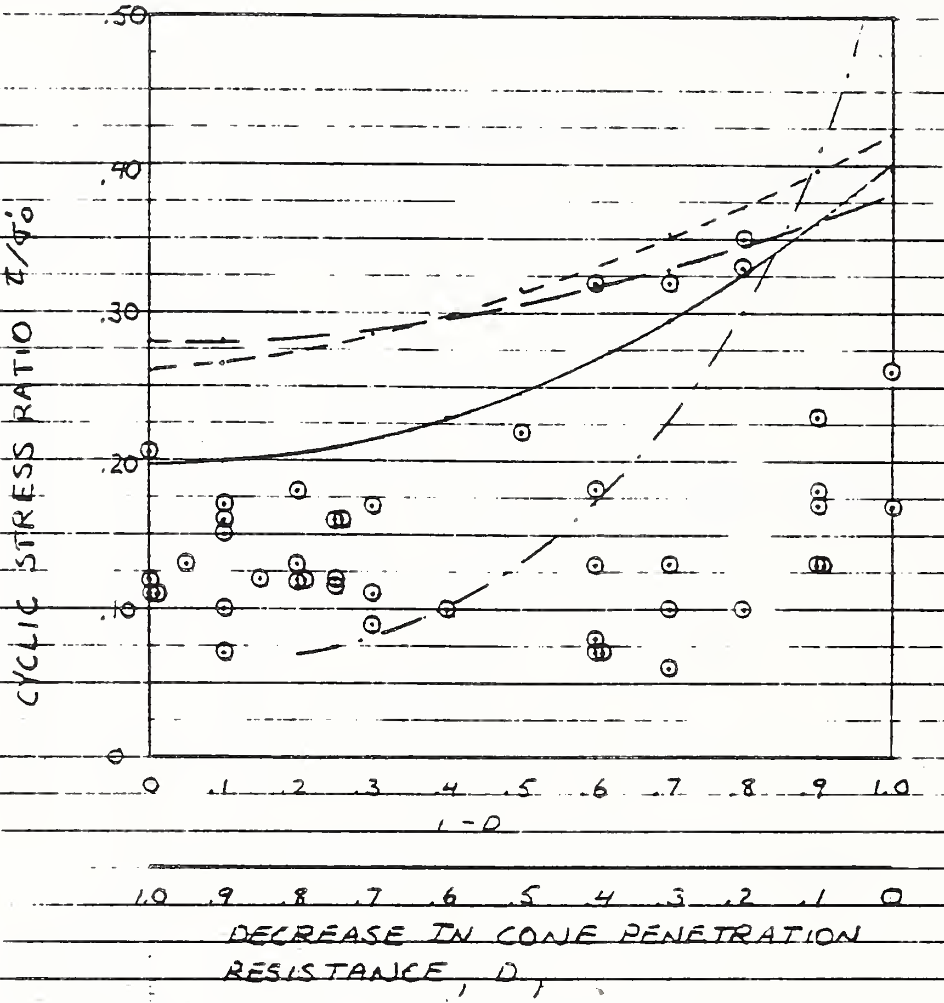

$$D = \frac{Q_{c\,STATIC} - Q_{c\,DYNAMIC}}{Q_{c\,STATIC}}$$

KEY: ⊙ D VALUE IN SPT INTERVAL AND CYCLIC STRENGTH FROM N160

——— $\sigma'_v = 1.0$ Kg/cm² }
— — $\sigma'_v = 0.5$ Kg/cm² } $\tau_{\ell 20} = \left[0.2\,\sigma_v'^{2}(1-D)^{2}\right] - \left(\frac{.1444}{\sigma'_v + .4}\right) + .3$ SASAKI 85'

- - - - $R_{L20} = 0.26 + 0.16\,(1-D)^{1.5}$ SASAKI 84'

— · — · — ANTICIPATED TREND

FIGURE 21

U.S.-Japan Coordinated Earthquake Research Program on Masonry Buildings, Seismic Behavior of Three-Story Full Scale Block Planar Frame Under Cyclic Lateral Loading

by

Shin Okamoto[*1], Yutaka Yamazaki[*2], Takashi Kaminosono[*3]

Masaomi Teshigawara[*4] and Hisahiro Hiraishi[*5]

ABSTRACT

In order to know the total behavior of structure which consists of reinforced masonry (RM) walls, RM beams, and reinforced concrete (RC) slabs, one reinforced clay block masonry specimen was tested under cyclic lateral loading. The specimen was a three story and two bay frame structure which was a part of a five story RM apartment house building. Loading applied to the specimen was planned so as to reproduce the same stress condition as that of the prototype apartment house building structure under the earthquake motion. Main purpose of this test is to get basic data for the design guideline of RM buildings and for a full-scale five story RM building structure which will be tested in 1987 at Building Research Institute, Tsukuba, JAPAN.

The objectives of this test, design procedure of the test specimen, loading method, and test results are presented and discussed in this paper. Conclusions obtained from this planar frame test are as follows;

1) The specimen showed larger shear capacity than that requested by the tentative design guideline.
2) The beams with short span should be designed to prevent from shear failure at small deflection by decreasing those depth or amount of reinforcement.
3) Joint steel arranged in the beam showed the effect on preventing the faceshell from falling down.
4) The specimen was still elastic and had only minute flexural cracks within the temporary shear stress level.
5) Short beam was forced into 1.6 to 2.0 times drift angle as long as story drift angle by long wall (Wall-A).
6) Transverse wall was effective totally on the strength at the maximum shear stress level.

KEY WORDS; Reinforced clay block masonry,
Walls, Beam, Transverse wall,
Reinforced concrete slab,
Full scale planar Frame,
Static lateral loading test

INTRODUCTION

U.S.-Japan Coordinated Research Program on Reinforced Masonry(RM) Building has been started since 1984[1]. The targets of Japanese side are not only to know behaviors of masonry elements and RM structures, but also to establish a design guideline of medium-rise RM buildings up to five stories. Structural elements of building such as walls, beams, and wall-beam subassemblages had been tested in 1985[2-6] and many useful informations concerning the structural behavior of elements were obtained. On the basis of those test results, a five story apartment house building was designed as a prototype building structure[7]. In order to know the total behavior of structure which consists of RM walls, RM beams, and reinforced concrete (RC) slabs, one reinforced clay block masonry specimen was tested in 1986 at Building Research Institute(BRI), Tsukuba, Japan. The specimen was a three story and two bay frame structure which was a part of a five story RM apartment house building. Loading applied to the specimen was planned so as to reproduce the same stress condition as that of the prototype apartment house building structure under the earthquake motion.

OBJECTIVES

Test on the three story reinforced clay block masonry frame was planned on the basis of the test results of RM walls, RM beams, and RM wall-beam subassemblages. Main objective of this test is to know the structural behaviors of a full-scale RM planar frame. And to know behaviors of structural elements which compose the test frame is also important objective. These elements are listed as follows;

1) wide wall with transverse wall
2) narrow wall
3) outer wall with varying axial load
4) short beam which depth or reinforcement is decreased
5) long beam
6) wall-beam joint panel
7) small openings in wall and wall-beam joint panel
8) special reinforcement(spiral reinforcement, joint steel)

Construction technique was also checked while the specimen was under construction. The test results

---

*1 Director,
Research Planning and Information Department,
Building Research Institute (BRI),
Ministry of Construction (MOC), JAPAN
Tatehara 1, Ohho, Tsukuba, Ibaraki 305, JAPAN
*2 Head, Large Scale Structure Testing Division,
Production Department, BRI, MOC, JAPAN
*3 Senior Research Engineer,
Large Scale Structure Testing Division
Production Department, BRI, MOC, JAPAN
*4 Research Engineer,
Large Scale Structure Testing Division
Production Department, BRI, MOC, JAPAN
*5 Head, StructureDivision,
Structural Engineering Department, BRI, MOC,
JAPAN

are considered to be helpful to establish the design guideline of buildings and to make a plan of the test of a full scale five story RM building structure which will be tested in 1987 at BRI.

SPECIMEN

Prototype Structure

A prototype structure of a five story apartment house building was designed using concrete block units in accordance with the tentative design guideline of RM buildings. The specimen described in this paper was a part of this prototype structure. Plan of the prototype structure is illustrated in Fig.1. Thickness of wall is 19cm(7.5inches). Ratios of total wall length to floor area of the structure are 15.2cm/m^2 (0.556inch/ft^2) in longitudinal direction (loading direction), and 18.4cm/m^2 (0.637 inch/ft^2) in transverse direction. A part of the Frame-Y3 was selected as the specimen, because the Frame-Y3 had various types of wall and beam. The tested portion is also shown in Fig.1.

Details of Specimen

Figure 2 shows plan, elevation, and reinforcement details of the specimen. The specimen constructed by reinforced clay block masonry was a three story structure and 2.8m (9.2feet) in each story height. There were three walls, those were 1) wide wall (Wall-A), 2) narrow wall (Wall-B), 3) outer wall (Wall-C). There were two spans. One span between Wall-A and Wall-B was short, and the other span between Wall-B and Wall-C was long. Therefore, the specimen had short beam (Beam-A) and long beam (Beam-B) with 2m(6.6ft) wide RC slab at each of the first and second stories. All of walls and beams were 19cm (7.5inches) in thickness. The specimen had a RC beam for loading at the top floor level. But dimensions and reinforcement details of the specimen was slightly different from those of the prototype structure, because of differences in the modulus of masonry units and some modification in details of the short beams. Walls and beams were as follows;

1) Wall-A was 3.8m(12.5ft) long and with 2m(6.6ft) transverse wall at the center of the wall.
2) Wall-B was 1.1m(3.6ft) long and with small openings.
3) Wall-C was 1.1m(3.6ft) long and with 2m(6.6ft) transverse wall at one edge of the wall.
4) Short beam(Beam-A) at the 1st story was 1.0m(3.3ft) span, 0.8m(2.6ft) depth, and with small flexural reinforcement. Short beam at the 2nd story 1.0m(3.3ft) span, 0.5m(1.64ft) depth, and with small flexural reinforcement.
5) Long beams(Beam-B) were 1.9m(6.2ft) span, and 0.8m(2.6ft) depth.

Small openings for piping were arranged in Wall-B and in joint panels of Wall-A and(Beam-A). Spiral reinforcing bars were placed around the flexural reinforcing bars at the bottom of the 1st story wall, where the flexural reinforcing bars were spliced, in order to prevent buckling and bond-slippage of reinforcing bars in early stage.

Material Properties

Concrete with small size aggregate which diameter was smaller than 10mm(0.4inch) was casted into walls and beams in order to get a good compactibility. Super plasticizer was also used for getting good compactibility. The value of slump became 25cm from 18cm by adding super plasticizer. Concrete with normal size aggregate, that was 25mm(1inch) was casted into slabs and loading beam. Prism compressive strength and compressive strength of slab concrete are tabulated in table 1 and 2. Six kinds of deformed reinforcing bar were used in the specimen. Those were 10mm diameter for slab, 13mm for shear reinforcement in walls and beams, 16mm for vertical reinforcement in walls and horizontal reinforcement in beams, 19mm for flexural reinforcement in walls and beams, and 22mm and 25mm for foundation and loading beam. Mechanical properties of reinforcing bars are listed in table 3.

DESIGN OF EXPERIMENT

Loading Method

Test setup is shown in Fig.3. Horizontal load was applied to the top of the Wall-A by four actuators. In pushing direction(negative loading), horizontal load would be distributed by loading beam, and in pulling direction(positive loading), that would be done by PC bars which were set in the loading block. This specimen was the model of lower three story parts of five story building. Vertical load were applied to the top of each wall by eight center hole jacks in order to adjust vertical stress at the bottom end of walls to that of walls in the five story building. Weight per unit floor area was assumed 1.2 ton per square meters(226lb/ft^2). Wall-A should be considered to locate the place where boundary beams were attached at the both ends. So vertical loading was controlled so that the vertical stress at the bottom of Wall-A was constant. Wall-B had also boundary beams at both sides. For this reason, the applying vertical load to Wall-B was kept constant. Outer wall (Wall-C) had boundary beams at its one side, so, varying axial load due to shear force of boundary beams would act on the Wall-C. The range of varying load to apply during this test was determined on the ultimate strength of upper beams which were supposed to be connected to the Wall-C in five story building. Overturning moments were adjusted to that of five story building subjected to external forces with Ai distribution. Figure 4 shows the horizontal loading hysteresis. Up to the mean shear stress of 10kg/cm^2(142.2psi) which was the value divided total horizontal load by wall area in loading direction; i.e.,11,343cm^2, experiment was controlled by the value of horizontal load. And after the drift angle of 2nd floor to basement exceeded 1.0×10^{-3}radian, experiment was controlled by the value of this drift angle of 2nd floor to basement.

Measurement

Horizontal and vertical load were measured by load cells which were attached to actuators and centerhole jacks. Horizontal and vertical

displacement were measured by strain gage type transducers which accuracy was from 30μstrain/mm to 1000μstrain/mm. Strain of reinforcements and concrete surface were measured by strain gages.

TEST RESULTS

Figure 5 and 6 show the crack pattern and the yielding stage of reinforcing bar at several shear stress levels or deformation levels respectively. In those figures deformation was described as the drift angle of 2nd floor to basement. Development of crack and yielding stage of reinforcing bars were as follows;

1) There were no cracks in the specimen up to the shear stress of 4kg/cm^2(56.9psi) that was considered as temporary design stress.
2) Up to the shear stress of 6kg/cm^2(85.3psi), flexural cracks occurred at the bottom of 1F and 2F Wall-A and at the end of 2F and 3F beams. Reinforcing bars at the 3F short beam and 2F, 3F slab close to Wall-A reached its yielding strain.
3) Flexural cracks of all beams and 3F Wall-C occurred till the shear stress of 8kg/cm^2(113.8psi).
4) Reinforcing bars at the bottom of Wall-A and short beam except for 2F lower part reached its yielding strain till the shear stress of 10kg/cm^2(142.2psi).
5) Shear cracks were observed at the 3F part of Wall-C and at the 2F short beam until the shear stress reached 12kg/cm^2(170.7psi). Up to this shear stress level, reinforcing bars at all beams except for 2F upper part of long beam reached those yielding strain. Reinforcing bars of Wall-A reached those yielding strain up to the bottom of 2nd floor slab. Reinforcing bars at the bottom of each story close to long beam in Wall-B and at the exterior part in Wall-C also yielded.
6) Until the drift angle of 2.5×10^{-3} radian, shear cracks at the 1F part of Wall-A, 3F short beam, at the 2F and the 3F part of long beam and at the joint panel zone occurred.
7) Until the drift angle of 5.0×10^{-3}radian, the 3F part of Wall-B failed in shear and vertical crack at the 3F and the 2F parts of Wall-C and the 1F part of Wall-A occurred along the flexural reinforcing bars. The reason of shear failure in Wall-B is considered that loading beam attached to the top of Wall-B restrained the rotation of Wall-B. Maximum horizontal load that was 176ton (15.5kg/cm^2=220.5psi) was recorded at this drift angle. On the yielding distribution of reinforcing bars, yielding hinges were made at the places that were the bottom of all walls, the end of all beams and both ends of the 2F part of Wall-B in negative direction. But in positive direction, yielding hinges were made at the both end of the 2F and the 3F part of Wall-C instead of at the long beams end close to Wall-C.
8) When the drift angle reached almost 10.0×10^{-3} radian, Wall-A failed in compression at its bottom part and 2F short beam failed in shear.
9) Over the drift angle of 10.0×10^{-3}radian and the faceshell or grout concrete in the 3F part of Wall-C, the 2F short beam, and the compressive failure zone of Wall-A fell down. But it was observed that joint steel arranged in half part of the 2F short beam prevented those faceshells from falling down.

The relationship of first story horizontal drift of Wall-A vs. horizontal load is shown in Fig.7. Until the mean shear stress was under 10kg/cm^2(142.2psi), the hysteresis loop showed almost such as elastic that had small hysteresis area and pointed to the same restoration force recorded before. From the drift angle of 2.5×10^{-3}radian the restoration force deteriorated with every repeated loading at the same drift angle. Maximum force was recorded at the drift angle of 5.0×10^{-3}radian. As above mentioned, from the drift angle of 5.0×10^{-3}radian to that of 10×10^{-3}radian the 2F beam with short span failed in shear and Wall-A failed in compression at its critical section, however, the restoration force of specimen kept the mean shear stress over 12kg/cm^2(170.7psi). This shear stress was almost the same level that was requested by the design guideline. In Fig.7, the analytical results of both static and dynamic are indicated. 7)

DISCUSSION OF TEST RESULTS

Horizontal Stiffness

Change of the story horizontal stiffness with increase of the first story drift angle is shown in Fig.8. The stiffness obtained from elastic analysis is also indicated in Fig.8. The stiffness obtained from elastic analysis agrees with those obtained from the test at the mean shear stress of 4kg/cm^2(56.9psi) which value was considered as temporary shear stress. Therefore, the specimen was still elastic within the temporary design force. In the case of the first and second stories, the decrease of the stiffness changes at the shear stress of 12 kg/cm^2(170.7psi). The reason is considered that the specimen yielded totally at this shear stress level. The decrease of the stiffness also changes, at the first story drift angle of 5×10^{-3}radian when the specimen indicated the maximum shear stress. The decrease of the stiffness of the third story started faster then those of the first and second stories, because cracks of loading beam occurred in early stage at slits of slabs.

Equivalent Damping Ratio

Change of the equivalent damping ratio obtained from the hysteresis loop of the specimen with increase of the first story drift angle is shown in Fig.9. The equivalent damping ratio was approximately in the range of 2% to 4% at the shear stress of 10kg/cm^2 when the first story angle was 0.73×10^{-3}radian. The equivalent damping ratio increased with increase of the first story drift angle. At the first story drift angle of 5×10^{-3} radian when the specimen indicated the maximum strength, the equivalent damping ratio increased up to the range of 10% to 25%.

Drift Angle of Beams

Drift angle of Beam-B, long beam between Wall-B and Wall-C, was almost equal to the story drift angle. On the other hand, drift angle of Beam-A, short beam between Wall-A and Wall-B, was 1.6 to

2.0 times as larger as the story drift angle. It is considered that Beam-A was forced into large deformation by the long wall(Wall-A).

Behavior of Wall-A

Figure 10 shows the deformation mode of Wall-A at several loading stages. It is evident that the deformation mode of Wall-A was flexural. Until the first story drift angle reached $5x10^{-3}$radian, Wall-A deformed only with the rotation at its bottom. The specimen reached its maximum strength when the first story drift angle was about $5x10^{-3}$ radian, and at that time third story of Wall-B failed in shear. After reaching maximum strength, the deformation mode of Wall-A changed; i.e., the Wall-A deformed in the third story more than in the other stories. In order to study the components of deformation, the strain distribution of reinforcing bar, (its location is shown in Fig.11(b)) and the curvature distribution of Wall-A are shown in Fig.11(d). The curvature at the lowest part of wall was very large. But those of other parts were very small. Tensile strain of the reinforcing bar was also very large, i.e., 1.5% at the first story drift angle of $1.2x10^{-3}$ radian ($12kg/cm^2$=170.7psi). The curvature at the lowest part of wall was $15x10^{-6}$(1/mm) and $50x10^{-5}$ (1/mm) at the drift angle of $2.5x10^{-5}$ radian and $5.0x10^{-3}$radian respectively. The relationship of the rotation angle due to this curvature vs. story drift angle is shown in Fig.11(c). Sixty percent of drift angle was represented by the rotation angle of the lowest part of wall at the drift angle of $5.0x10^{-3}$radian. This is match to the fact that the strain of reinforcing bar was not so large in upper part of wall. Because the compressive strain capacity of brick masonry was too small to let the tension bar be strain hardening range. It is seemed that the pulling out of reinforcing bar occurred at the first story drift angle of $1.6x10^{-3}$ radian. The lap joint was made at the critical section and this lap joint was reinforced by spiral bars, and the fixing length to foundation was 1 m. It is considered that reinforcing bar was pull out from foundation because of better fix characteristic in lap joint part. After pulling out of reinforcing bar, (A-3 in Fig.11(b)), the strain of reinforcing bars in inner part of wall and at the top edge of lap joint became larger.

Effect of Transverse Wall

Figure 11(a) shows the strain distribution of reinforcing bars. The strain was very large at the critical section. The reinforcing bar set in the edge of wall did not work so effectively up to the drift angle of $1.2x10^{-3}$ radian($12kg/cm^2$=170.7psi). This reinforcing bar, however, worked after the drift angle of $2.5x10^{-3}$ radian. It is observed that transverse wall of T-shape was effective totally from the drift angle of $0.73x10^{-3}$ radian($10kg/cm^2$), and the transverse wall of Cross-type did after $1.2x10^{-3}$ radian($12kg/cm^2$).

Analysis

On next three cases, maximum horizontal strength of this specimen was calculated on condition that the same shear force act on the every story of each three walls.

Case A: ignoring the effect of axial force of beams.

Case B: considering the effect of axial force of beams.

Case C: add the case B to the effect of hardening of beam reinforcing bars.

The effect of hardening was considered by the way that yielding strength of reinforcing bar was assumed to be 1.2 times as much as its natural yielding strength. In case B and Case C, it was supposed that axial load of beam acted only on loading beam(RF beam). The reason why the hardening of only beam reinforcing bars was considered in the case C was based on the fact that the test result did not show a large value of strain of the wall reinforcing bars(Fig.11(b)) as above mentioned. Results of analysis tabulates in Table 4. The results of analysis showed the smaller value than that of test results. The strength obtained by case C was smaller than test results by 40ton(23%) in pulling direction and 30 ton(17%) in pushing direction respectively. The shear failure of third story of Wall-B is considered to be one of the main reasons of the difference between analysis value and test results. The shear force carrying capacity of Wall-B was 29.6 ton. But shear strength capacity of the third story of Wall-B will be 52ton[2]. If the third story of Wall-B would carry this shear force(52ton), the maximum strength by case C would be over 156 ton in both direction, and the difference between test results and analysis(Case-C) would be within ten percent. More detailed and accurate analysis on ultimate strength of this test will be necessary, but this hand calculation shows followings.

1) The influence of axial load of beam due to the loading method did not observed on the total ultimate strength. But in order to know the influence to each member, more accurate analysis should be done.
2) It should be needed to evaluate the effect of failure of the third story of Wall-B on total strength capacity of the specimen.

CONCLUSIONS

Conclusions of the reinforced clay block three story planar frame test are as follows;

1) Shear stress at the drift angle of $10x10^{-3}$ radian was over the value that was requested by the tentative design guideline.
2) The beams with short span may be designed to prevent from shear failure at the small deflection range by decreasing those depth or amount of reinforcement.
3) Joint steel arranged in the beam with short span had the effect on preventing the faceshell from falling down.
4) The specimen was still elastic and had only minute flexural cracks within the temporary shear stress level.
5) Equivalents damping ratio increased approximately from three percent at low shear stress level to more than ten percent at maximum shear stress.
6) Short beam was forced into 1.6 to 2.0 times drift angle as long as story drift angle by

long wall (Wall-A).

7) In large deformation range, story drift angle was mainly represented by the rotation at the lowest part of wall.
8) Transverse wall was effective totally on the strength at the maximum shear stress level.
9) It should be needed to evaluate the effect of failure of the third story of Wall-B on total strength capacity of the specimen.

ACKNOWLEDGMENT

In carrying out the experiment described in this paper, the authors are pleased to acknowledge the considerable assistance of Messrs.

Kouji Saitoh: Nihon Renga Seizou Co.Ltd.,
Masanori Yokoshi: Matsumoto Renga Co.Ltd.,
Kiyoshi Ichijoh: Hokkaido Nozai Kougyo Co.Ltd.,
Tadao Sankawa: Nishitani Tougyo Co.Ltd.,
Masashi Yamamoto: Tobishima Corp. Co.Ltd.,
Hiroto Katoh, Hiroshi Isoishi: Building Research Institute,
Akio Nakaoka, Takaaki Nishi: Hasegawa Komuten Co.Ltd.,
Mototaka Matsuno: Hazamagumi Co.Ltd.,
Mitsuyasu Itou, Tatsunori Ryoh, Nobuhiko Yokoi, Nobuo Yokoyama: Kunishiro Taika Kougyo Co.Ltd.,
and
Mr. Kyle Woodward: UCSD, USA

The authors also would like to express their appreciation to TECCMAR, PROCMAR, and BLDCMAR members for their contribution to coordinate and to promote this U.S.-Japan research program.

REFERENCES

[1] S.Okamoto and J.Noland, "U.S.-Japan Coordinated Program on Masonry Research", Proceedings of the Third Conference on Dynamic Response of Structures, EM Div., ASCE, 1986, pp.55-70
[2] T.Okada, H.Hiraishi, T.kaminosono and M.Teshigawara, "Flexural Behavior of Reinforced Masonry Walls and Beams", Proceedings of the Third Conference on Dynamic Response of Structures, EM Div., ASCE, 1986, pp.481-488
[3] T.kaminosono, H.Isoishi, Y.Yamaguchi and R.Kawai, "Seismic Capacity of Reinforced Masonry Walls Including Effects of Axial Stress", Proceedings of the 4th Canadian Masonry Symposium, 1986, pp.163-173
[4] M.Fujisawa, T.Kawashima and Y.Yamaguchi, "Seismic Capacity of Reinforced Masonry Walls Effects of Shear Span Ratio", Proceeding of the 4th Canadian Masonry Symposium, 1986, pp.377-395
[5] M.Teshigawara, H.Isoishi and M.Yamamoto, "Seismic Behavior of Masonry Beams", Proceedings of the 4th Canadian Masonry Symposium, 1986, pp.759-773
[6] M.Teshigawara, H.Isoishi, A.Nakaoka and T.Terada, "Erect of Transverse Wall Attached to Reinforced Concrete Masonry Wall", Proceedings of the 4th Canadian Masonry Symposium, 1986, pp.774-782
[7] Y.Yamazaki and M.Teshigawara, "Earthquake Response of Five Story Reinforced Concrete Masonry Test Building," Proceedings of the Third Conference on Dynamic Response of Structures, EM Div., ASCE, 1986, pp.55-70

Table 1. Prism Compressive Strength

Story	Strength[kg/cm^2]
1 F	273
2 F	272
3 F	231

Young modulas is evaluated by Eq.1).
$E=2.1\times10^5\times\sqrt{F'm/200}$ --- Eq.1)
$E=239 ton/cm^2$

Table 2. Slab Concrete Compressive Strength

Story	Strength[kg/cm^2]
2 F	327
3 F	314
R F	319

Table 3. Mechanical Properties of Reinforcing Bars

Bar [mm]	Material [SD]	Area [cm^2]	Yield Stress [kg/mm^2]
10	30	0.71	39
13	30	1.27	37
16	35	1.99	39
19	35	2.87	40
22	35	3.87	41
25	35	5.07	40

Table 4. Results of Preliminary Analysis

Case	Load	Wall[ton]			Σ
		A	B	C	[ton]
A	+	81	23	10	114
	-	74	31	24	129
B	+	81	25	11	117
	-	78	35	26	139
C	+	103	37	15	155
	-	76	49	31	155

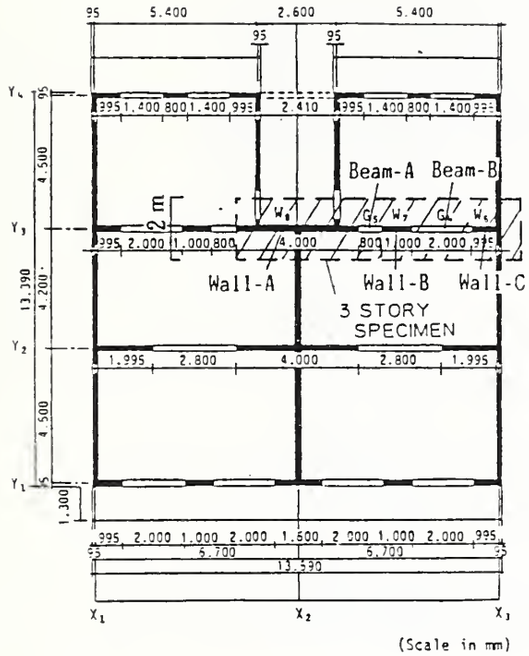

Fig.1. Plan of Prototype Building

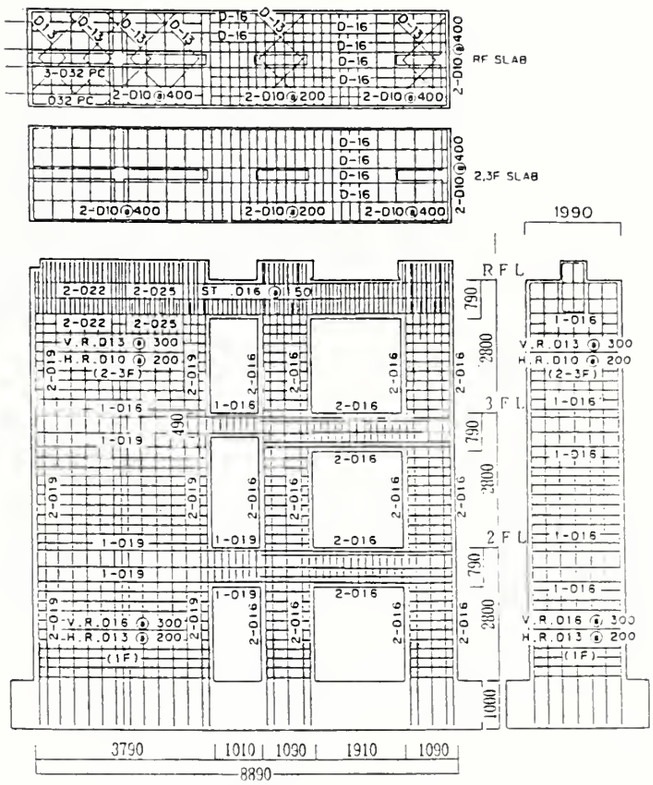

Fig. 2 a) Plan,Elevation,and Reinforcement of Test Specimens

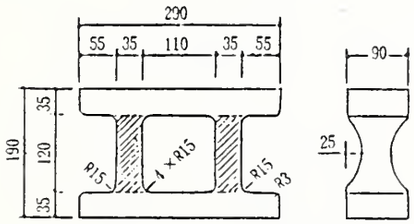

Fig. 2 b) Clay Brick Unit

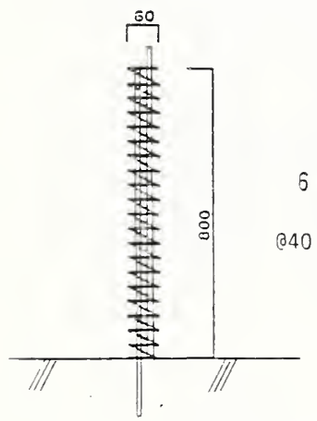

Fig. 2 c) Spiral Reinforcement

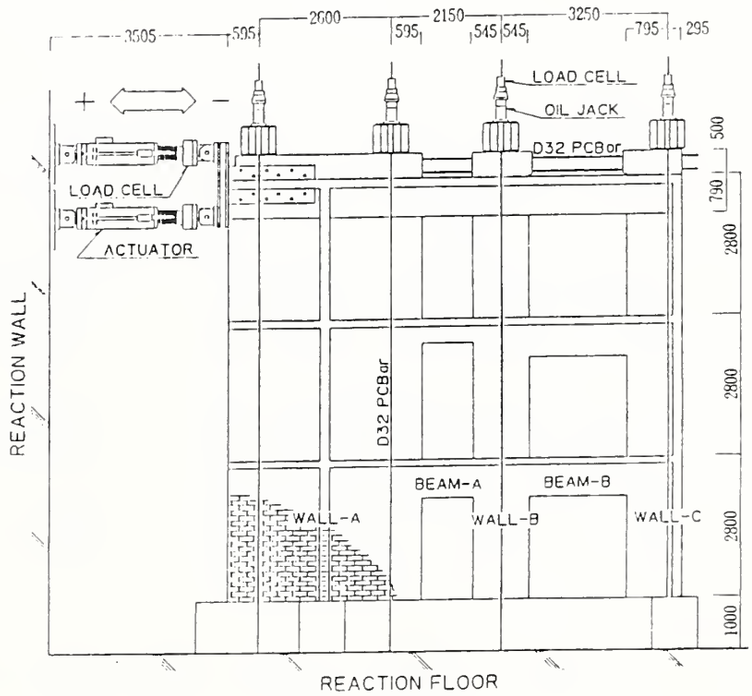

Fig. 3. Test Setup

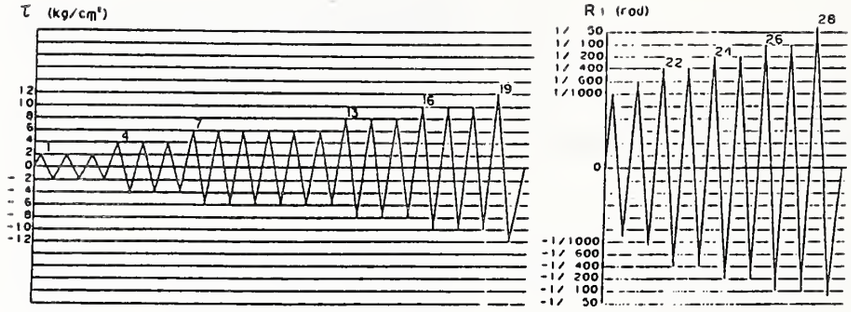

τ : Mean shear stress i.e. Q/sectional wall area in loading direction.
R1: The first story drift angle of Wall-A.

Fig. 4. Horizontal Loading Hysteresis

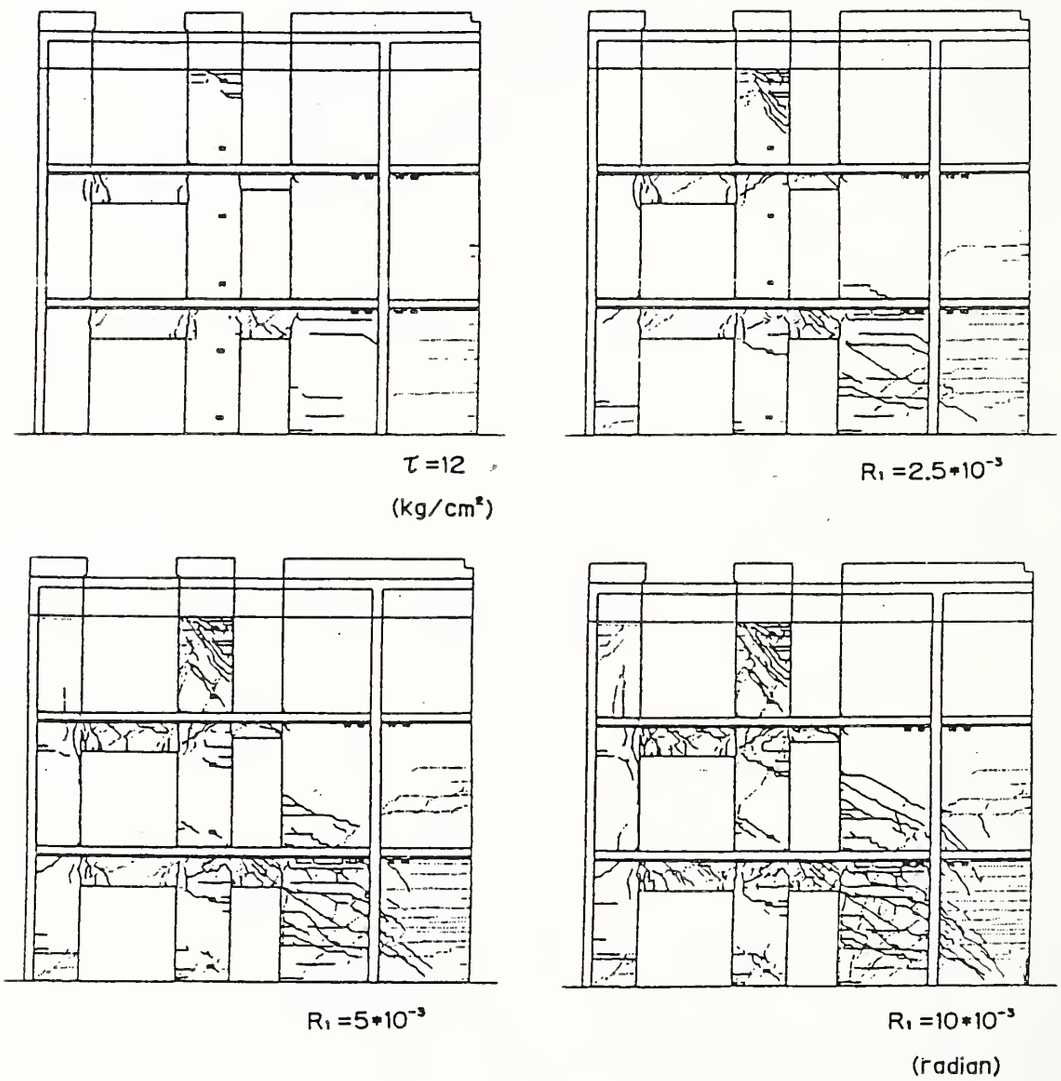

Fig. 5. Crack Pattern

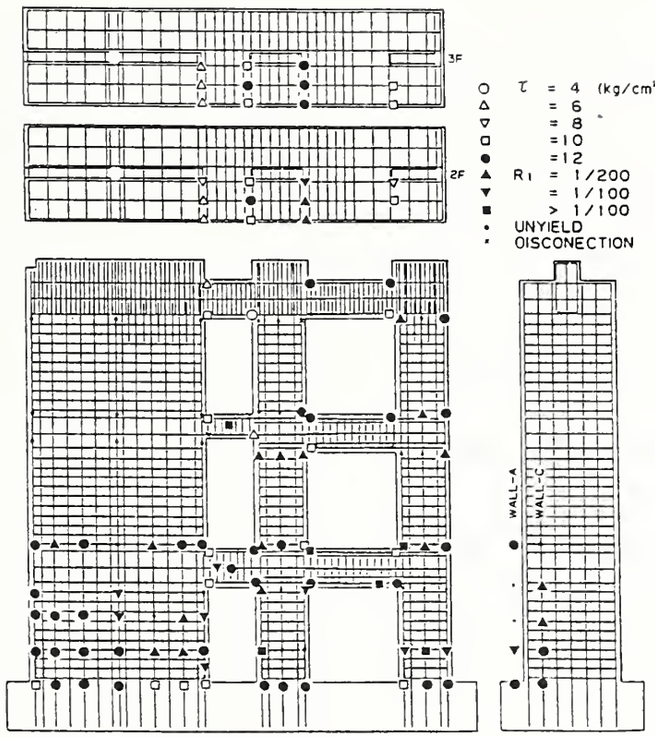

Fig. 6. Yielding Stage of Reinforcing Bars

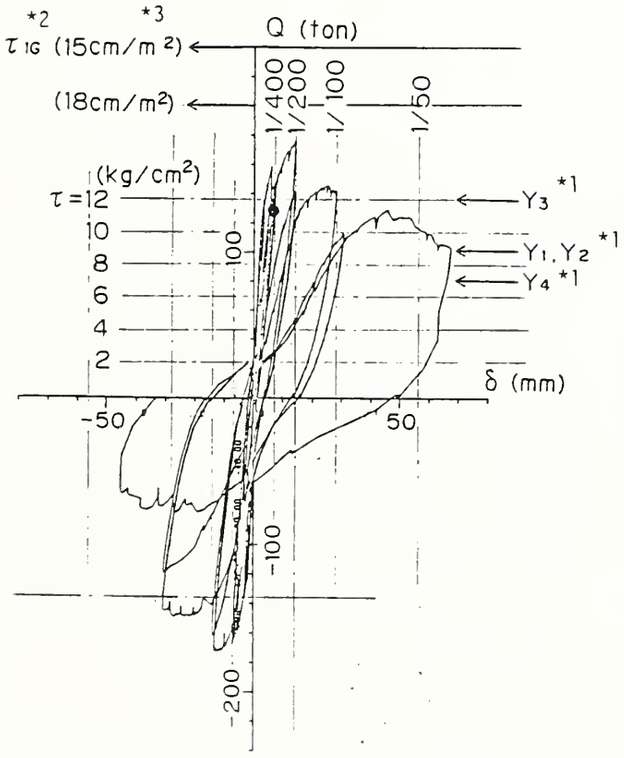

- Result of Earthquake Response Analysis
  Spring for sway was 2000 ton/cm.
  Ground Motion was "Hachinohe EW"
  which max acceleration was 450 Gal.

*1:mean shear stress at the ultimate stage obtain by static farame analysis

*2:mean shear stress of the first story when base shear corresponded to 1G.

*3: wall length ratio

Fig. 7. First Story Drift of Wall-A V.S. Lateral Force Relationship

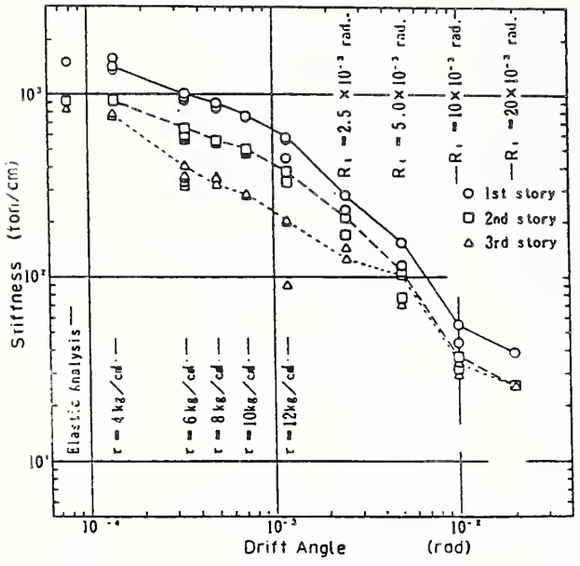

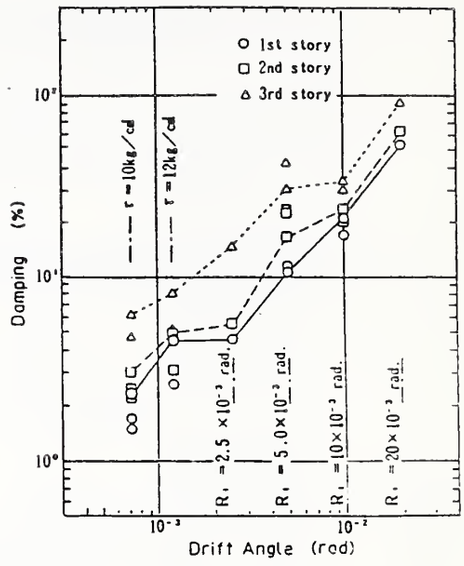

Line shows the first cycle of each loading stage

Fig. 8. Change of Story Stiffness

Fig. 9. Change of Equivalent Damping Ratio

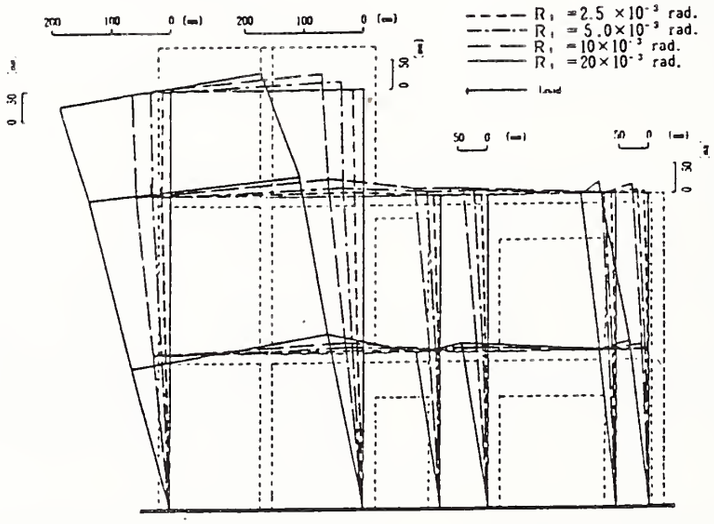

Fig. 10. Deformation Mode

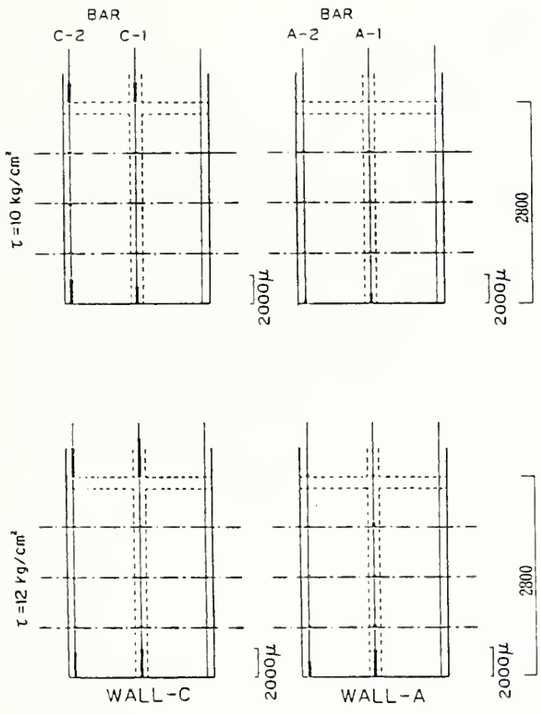

Fig. 11 a) Strain Distribution of Reinforcing Bars in Transeverse Wall

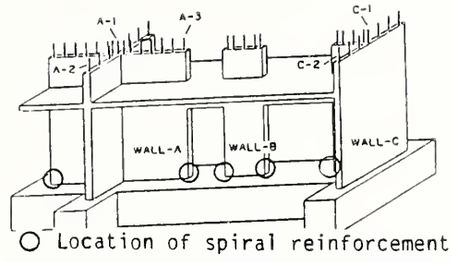

Fig. 11 b) Notation of Reinforcing Bars

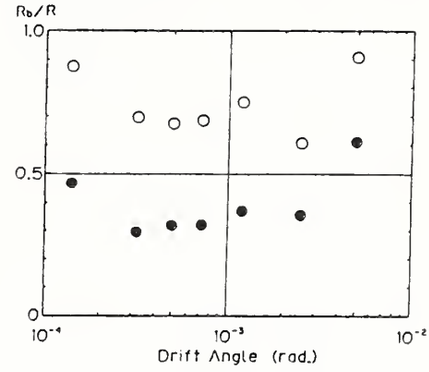

Fig. 11 c) Ratio of Flexural Drift to Story Drift

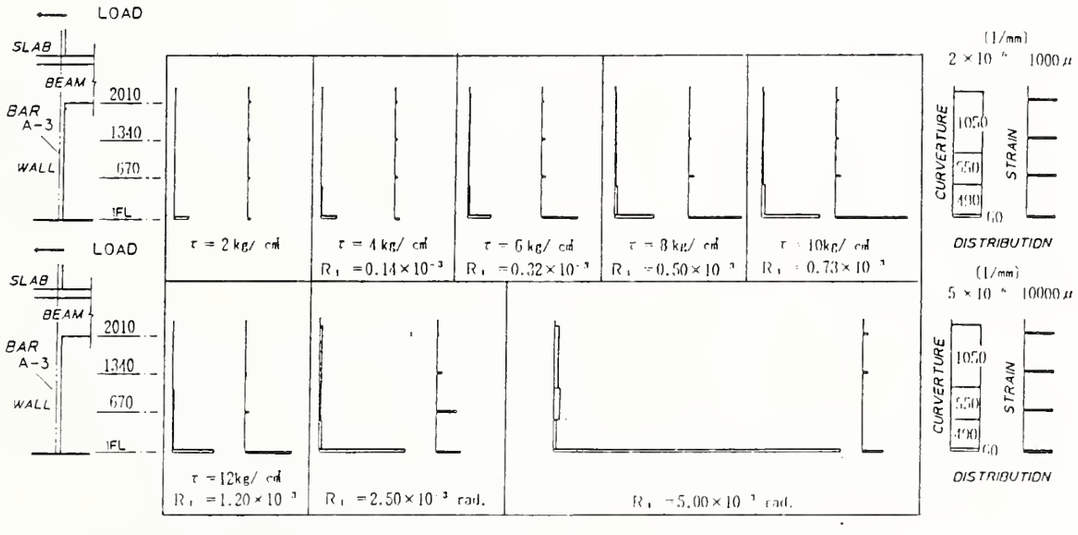

Fig. 11 d) Strain of Reinforcing Bars and Curvature Distribution (Wall-A)

U.S. Coordinated Program for Masonry Building Research—1986/87

by

James L. Noland[1]

ABSTRACT

The U.S. Coordinated Program for Masonry Building Research is an integrated set of twenty-five specific research tasks which address topics ranging from material properties to system behavior to design methodology. Work began in late 1985 and is currently in progress. Two new research tasks have been added to the program and the schedule has been slightly revised.

KEYWORDS: Masonry; Research; Tests; Structure; Design; Analysis

1. INTRODUCTION

The U.S. Coordinated Program for Masonry Building Research is the U.S. part of the third in a series of joint U.S.-Japan research projects conducted under the auspices of the UJNR Panel on Wind and Seismic Effects. This report is a brief review of the work and activities of the U.S. side during the period of May 1986 to May 1987.

2. OVERVIEW OF U.S. PROGRAM

A general description of the U.S. Coordinated Program for Masonry Building Research was presented at the UJNR meeting of May 1986. The essential ingredients of the program are repeated here for convenience.

2.1 Basic Concept

The U.S. program currently consists of twenty-five separate, but coordinated research tasks. Two additional research tasks were initiated in the period covered by this report, i.e., response of two-story reinforced concrete masonry walls to in-plane fully reversed lateral loads and shake table testing of three-story one-quarter scale reinforced concrete masonry buildings. A complete list of research tasks is presented in Table 1.

3.0 SCHEDULE

Task 1.1 was initiated in February 1985 and completed in August 1985 as a precursor to the majority of tasks which began in the fall of 1985.

The program schedule as of March 1987 is shown in Figure 1. It has not yet been revised to include new Task 3.1(c). Work on that task will begin in June 1987 and last for approximately two years.

Schedule revisions include:

1) a slight extension of Task 3.1(a)
2) a new start-date for Task 3.2(b)
3) a slight extension of Task 3.2(a)
4) a slight reduction of time for Task 3.2 (b1)
5) an advanced start-date and extended end-date for Task 4.2
6) an approximately 7 month extension of Tasks 5.1 and 5.2
7) a slight extension of Task 6.2
8) inclusion of new Task 7.1
9) a six month extension of Task 8.1
10) a six month postponement of both start and end dates of Task 8.1
11) a nine-month advance of the start date of the second phase of Task 9.1
12) a six-month postponement of Task 9.3
13) a six-month advance and a six-month extension of Task 9.4
14) a two-year advance and a six-month extension of Task 10.1
15) a six-month extension of Task 11.1

Note that the U.S. program now extends to January 1992.

4.0 ORGANIZATIONAL CHANGES

Gerald Dalrymple has replaced Alan Yorkdale on the Industry Observers and Industry Participation Panels. Mr. Dalrymple is a senior Engineer with the Brick Institute of America.

Dr. Charles Scribner of the NBS has replaced Dr. Leyendecker as liaison with UJNR.

[1] Atkinson-Noland & Associates, Inc., 2619 Spruce St.,

5.0 MEETINGS

In addition to numerous meetings within the U.S. of various subgroups of TCCMAR/U.S. the following major meetings have been held:

1) May 1986 - Hart, Kariotis, Ewing, Hamid and Noland met with Okamoto, Yamzaki, Teshigawara, Kaminosono, Baba and Senbu at BRI to review progress, data and experimental procedures.
2) July 1986 - Regular meeting of TCCMAR/U.S.
3) September 1986 - Special meeting of TCCMAR/U.S.
4) September 1986 - Second Joint U.S.-Japan Technical Meeting (JTCCMAR)
5) February 1987 - Regular meeting of TCCMAR/U.S.

The next meeting of TCCMAR/U.S. will be in August 1987 and the next JTCCMAR meeting will be in October 1987 in Japan.

6. PROGRESS

The approximate percentages of completion of the individual research tasks as of May 31, 1987 are as follows:

Task	Percent Complete
1.1	100
1.2(a)	40
1.2(b)	30
2.1	30
2.2	30
2.3	10
2.4	-0-
3.2(a)	35
3.2(b)	15
2.1(c)	-0-
3.2(a)	45
3.2(b1)	10
3.2(b2)	30
4.2	100
1/5.2	60
6.2	80
7.1	10
8.1	70
8.2	-0-
9.1	50
9.2	20
9.3	-0-
9.4	-0-
10.1	-0-
11.1	30

7.0 MISCELLANEOUS

7.1 Photogrammetry

Displacements at several times in the load histories of in-plane experimental specimens, i.e., shear walls and floor diaphragms are being obtained by photogrammetry. Those measurements will augment those obtained from strain gages and LVDTs.

7.2 Electronic Mail

Electronic mail has been used on a trial basis by several researchers to exchange messages. The system uses a VAX computer at the University of Illinois (courtesy of Dr. M. Sozen) as the "post office". This form of communication will be used by all of TCCMAR/U.S. in the near future.

8.0 RESEARCHERS EXCHANGE

Exchange of researchers between Japan and the United States is an important component of the joint research which fosters communication and understanding.

Dr. M. Teshigawara of BRI was the first exchange researcher. He spent approximately four months in the U.S. residing in Boulder, Colorado. In addition to monitoring the work at the University of Colorado, he visited several masonry-related organizations throughout the U.S..

Dr. K. Woodward of the University of California- San Diego spent two weeks in June 1986 at BRI. He was primarily interested in laboratory equipment and procedures used at BRI for large specimen tests.

Dr. O. Senbu of BRI spent one month in the U.S. in August-September 1986 observing the research work at the University of Colorado, participating in the Second JTCCMAR meeting in Keystone, Colorado and later visiting the researchers at the University of California in San Diego.

Dr. F. Seible of UCSD has applied for a Japanese government research grant for foreign researchers. If successful, he plans to be in residence at BRI during the last half of 1987.

9.0 CONCLUSIONS

The U.S. program is progressing well after a fitful start which unfortunately was well after the program in Japan started. Now that data is becoming available from the U.S. research, more frequent meetings of the U.S. researchers are planned and comparisons with Japanese results will be possible.

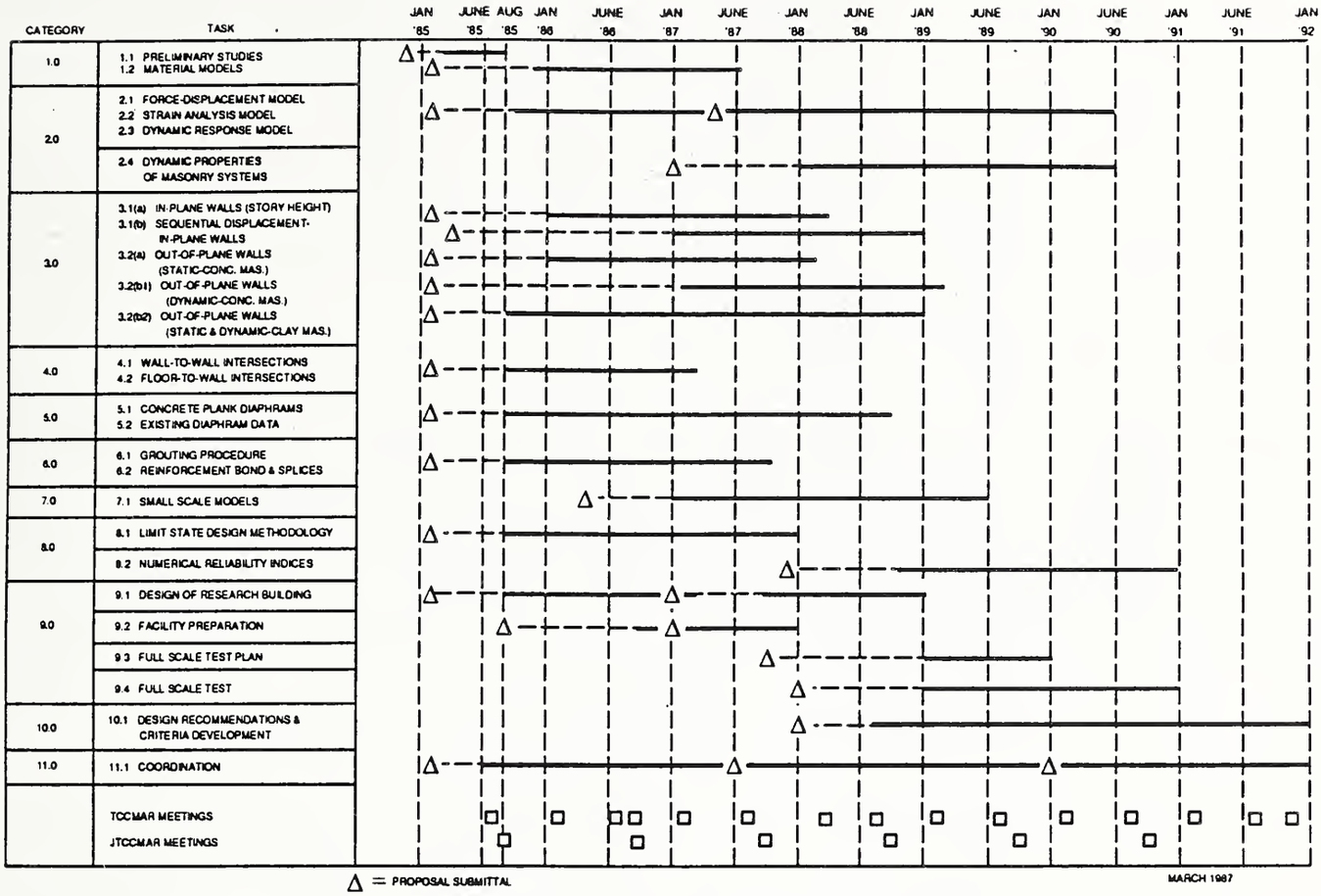

FIGURE 1 - U.S. PROGRAM SCHEDULE

Table 1
Research Tasks - U.S. Coordinated Program for Masonry Building Research

Category	Task	Task Title
1.0	1.1	Preliminary Material Studies
	1.2(a)	Material Models- Concrete Masonry
	1.2(b)	Material Models- Brick Masonry
2.0	2.1	Force-Displacement Models
	2.2	Finite Element Models
	2.3	Dynamic Response Models of Shear Walls
	2.4	Dynamic Properties of Masonry Systems
3.0	3.1(a)	In-Plane Walls, Story Height
	3.1(b)	Sequential Displacement - In-Plane Walls (3 story)
	3.1(c)	In-Plane Walls, Two Story
	3.2(a)	Out-of-Plane Walls (Static-Concrete Masonry)
	3.2(b1)	Out-of-Plane Walls (Dynamic-Concrete Masonry)
	3.2(b2)	Out-of-Plane Walls (Static & Dynamic - Clay Masonry)
4.0	4.1	Deleted
	4.2	Floor-to-Wall Intersections
5.0	5.1	Concrete Plank Floor Diaphragms- In-Plane Behavior
	5.2	Survey of Existing Diaphragm Data
6.0	6.1	Deleted
	6.2	Reinforcement Bond & Splices
7.0	7.1	Shake Table Studies of Scale Model Buildings
8.0	8.1	Limit State Design Methodology
	8.2	Numerical Reliability Indices
9.0	9.1	Design of Research Building
	9.2	Test Facility Preparation (for full-scale test)
	9.3	Full Scale Test Plan
	9.4	Full Scale Test
10.0	10.1	Design Recommendations & Criteria Development
11.0	11.1	Coordination

Manuscripts Authored for Panel Meeting But Not Presented Orally

Seismic Investigation and Improvement of Electrical Utility Systems

BY

Joseph V. Tyrrell, P.E.[1]

ABSTRACT

Electrical utility systems were investigated at naval bases location in areas of high seismic risk in the United States. Electrical systems within buildings as well as lifelines are addressed. The earthquake safety and reliability of commercially supplied power was not a part of the investigations although it is a key ingredient to performance after an earthquake.

1. INTRODUCTION

The Naval Facilities Engineering Command has been conducting earthquake safety investigations of naval shore facilities located in areas of high seismic risk. These investigations consist of identification of site hazards (faults, tsunami, etc.), establishing site response spectra based upon a site seismicity study, And investigation of lifelines and structures. The program involves 55 naval bases or activities and as of April 1987 is about 75% completed.

2. NATURE OF THE THREAT

Earthquake damage to electrical systems may result from electrical causes (short circuits, surges, overloads, etc.), structural failures (supports, housing, adjacent structures, etc.), site hazards (tsunami, liquefaction, etc.), and secondary effects such as fire. Prior to the San Fernando earthquake of 1971, little attention to earthquake design was given to electrical systems. After 1971, design codes were upgraded and some of the lessons learned about electrical systems were incorporated. Facilities constructed before 1973 warrant investigation and some that were constructed since may be deficient depending on the criteria used and the designer.

The typical naval base purchases most of its electric power from a commercial utility company, but has some on-base generating capacity. With regarded to manufactured electrical equipment, earthquake safe equipment is available for most items if specified. Because of the high rate of replacement of electrical equipment this aspect of the problem will diminish fairly rapidly in future years. The Navy specifications cover new equipment satisfactorily. For these reasons, an equipment replacement program does not seem to be necessary. However, many deficiencies in existing electrical systems do warrant attention including equipment supports and anchorage.

There appears to be no feasible way to complete prevent earthquake damage to a utility system. A large earthquake will very likely cause some disruption of electrical service regardless of the design code and criteria used. The chance of disruption can be minimized for specific facilities such as hospitals by use of standby emergency generators and special care in the details of the system. In a city or base wide system, redundancy and multiple sources will limit loss of power. Normal, good engineering practice provides reasonable protection for surviving system components in the event of a problem of an electrical nature. Present criteria for both structural and electrical design seems adequate, but there are no standards for performance the earthquake survivability of electrical systems.

The bulk of potential problems with existing electrical systems fall within the realm of structural engineering. Fortunately, structural criteria is available and design and analysis methods well known. However, even if all of the system components are structurally adequate, survivability is not assured because of the consequences of damage to structures housing the system or to adjacent structures.

Secondary losses may result from earthquake damage to an electrical utility. These include fire, injury from electric shock, release of hazardous materials, loss of production, and loss due of rescue and recovery being impeded by lack of power. Many transformers in use at naval bases contain PCB's, and could cause contamination. These transformers are being replaced but it take several years before the hazard is eliminated.

---

[1] Naval Facilities Engineering Command, Consultant in Earthquake Engineering

3. SITE HAZARDS

All facilities in active seismic areas are potentially subject to damage due to ground shaking. The motions induced in electrical systems may cause shorting and various degrees of damage due to swinging wires, displacements, and deflections in structures. It may also cause structural damage to the structures which are part of or adjacent to the system. Other site hazards are more localized and include faulting, liquefaction, soil slides and instability, tsunami or seiche, and the hazards resulting from adjacent facilities.

4. IDENTIFICATION OF HAZARDS

Base maps showing the roads and structures were useful in assessing in conjunction with discussions with local public works office personnel.. Utility maps show the power distribution system. The system layout can be checked against known or suspected site hazards. The need for redundancy, looping, or entry at additional points can be considered. In this connection the use and positioning of emergency generators is appropriate. If necessary, a follow-up investigation of site hazards is made.

A through examination of the system components is then made. The easiest and most effective technique was found to be a visual examination. Where major buildings are a part of the system, it is necessary to determine if a structural analysis is needed. The Navy has developed a method for rapid preliminary evaluation. It was found to be useful to employ a set of design guides for inspecting the components, determining mitigations, and estimating cost. Figures 1, 2, & 3 are typical examples. All costs are in 1975 dollars.

5. RESULTS OF INVESTIGATIONS

Problems with anchorage and bracing were common and found in many locations. Conductors running between two points rigidly anchored were found and differential movement would surely cause a break. Some structures, particularly older masonry buildings, were found to be inadequate. Typical conditions of system components are described below.

5.1. GENERATING PLANTS

The boilers and generators themselves were adequate, however, a few were not proper anchored. Ancillary equipment such as heat exchangers and condensate tanks were found to lack proper anchorage and sometimes needed bracing. Conductors and piping frequently were not detailed to accommodate differential displacements. Some piping supports did not provide any lateral resistance. About 50% of the buildings required some structural upgrading.

5.2. SUBSTATIONS

About 75% of the transformers and other equipment was unanchored and vulnerable to sliding or overturning. About 25% required bracing. A few dead end structures were found to be unstable.

5.3. UTILITY POLES

Most poles at the activities investigated were wood but some reinforced concrete or steel was found. The typical utility pole with one transformer is satisfactory; however, they vary in height and loading conditions. It is probably worthwhile to check a few. Some poles are utilized for multiple purposes including telephone lines and street lights. Others may have as many as four transformers mounted on them. Where there are heavy loads and/or changes in line direction, poles are sometimes guyed. An experienced structural engineer can tell when these conditions require analysis. In the past the Navy experienced some earthquake damage to poles on Guam.

5.4. STREET LIGHTS

Where street light poles were single purpose types, no problems were found. It may be prudent to check a typical unit.

5.5. SWITCHGEAR AND CONTROL PANELS

At least one third were found to be unanchored and most were unstable under earthquake loading and required bracing. As with many of the other deficiencies found, remedial measures were simple and inexpensive.

5.6. PUMPS AND PUMP MOTORS

Most were found to be adequately supported and secured; however, ancillary equipment and piping frequently needed improvement. Where vibration isolators are used under pumps or equipment, their effect must be considered and their anchorage checked. Lateral restraint is needed without interfering with the function of the isolator.

5.7. BATTERY RACKS

Racks are typically unanchored and batteries were sitting on shelves with no lip or restraint of any kind. Even a slight shake could cause disruption.

5.8. TELEPHONE EXCHANGES

Switchboards and distribution panels were usually anchored but found to require bracing at the top of the frames.

5.9. IN-BUILDING LIGHT FIXTURES

Several different types of fixtures were common. The support and mounting were the principle concerns. In general, chain hung fixtures and those on swivel pendants were satisfactory. Some were support by rigid pendants or light gage vertical members, or by light gage suspended ceiling supports. Most of these latter types were vulnerable and it was considered necessary to add safety chains from the fixture to a competent structural support above.

6. CONCLUSIONS

Existing electrical systems were found to be vulnerable to earthquake damage which would cause power outages and other damage. A great deal of improvement can be accomplished by simple, inexpensive measures such as anchorage, bracing, and reinforcement of supports. Certain major structures such as generating stations are vulnerable - especially older masonry buildings. Structural improvements of buildings may be simple and inexpensive (e.g. providing X bracing to a steel frame) or they may be complex and costly. In some cases it may be economical to rebuild rather than retrofit a structure.

Since it is not feasible to provide a completely earthquake proof system, it is necessary to plan and prepare for disaster recovery. Looping the system and providing more than one feed point are desirable steps in minimizing loss of power. The use of standby emergency generators should be considered. Flexible connections should be provided and slack allowed between rigidly anchored points. Dispersed and/or on-site water supply is desirable.

SEISMIC ZONE	EQUIPMENT WT. (KIPS)	NO. & DIAM. OF A.B. (INS.)	COST ESTIMATE $	UNIT COST $/KIP	MAX. H/L
1	200	4-3/4"	106	0.53	26.7
	150	4-5/8"	94	0.63	
	100	4-3/8"	69	0.69	
2	200	4- 1"	130	0.65	13.3
	150	4-7/8"	120	0.80	
	100	4-3/4"	106	1.06	
	50 & LESS	4-3/8"	69	1.38	
3	200	8- 1"	251	1.25	6.7
	150	6- 1"	189	1.26	
	100	4- 1"	130	1.30	
	50	4-3/4"	106	2.12	
	25 & LESS	4-3/8"	69	2.76	
4	200	8- 1¼"	305	1.52	4.4
	150	6- 1¼"	229	1.53	
	100	6- 1"	194	1.94	
	50	4-7/8"	130	2.60	
	25	4-5/8"	106	4.24	
	20	4-1/2"	95	4.75	
	15 & LESS	4-3/8"	81	5.40	

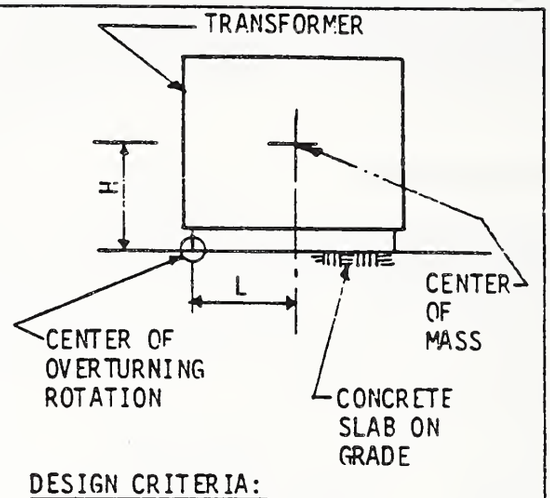

DESIGN CRITERIA:

P-355 EQUATION: 8-7-3, F= ZCW

$C = AC_S = 0.1 \times 1.5 = 0.15$

$C_S = 1.5$ (f_p SOIL = 6KSF)

MINIMUM CONNECTION TO BE 4 - 3/8" Ø ANCHOR BOLTS.

FOR TYPICAL BASE CONNECTION DETAILS SEE PLATE 1.

WHERE H/L EXCEEDS MAXIMUM INVESTIGATE OVERTURNING.

BASIS FOR WEIGHT/KVA CURVES:

#1. DISTRIBUTION TRANSFORMER

#2. SUBSTATION TRANSFORMER

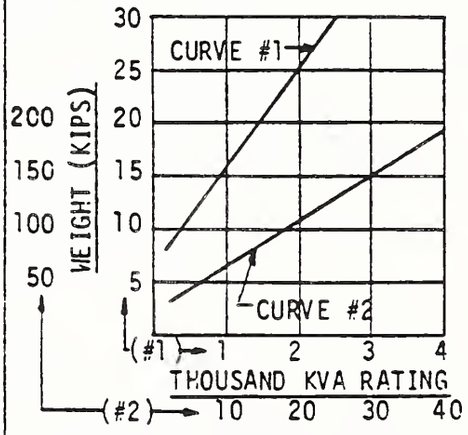

APPROXIMATE TYPICAL WEIGHT/KVA COMPARISON

COST/CONNECTION ESTIMATING DATA
TRANSFORMER ON GRADE

FIGURE 1

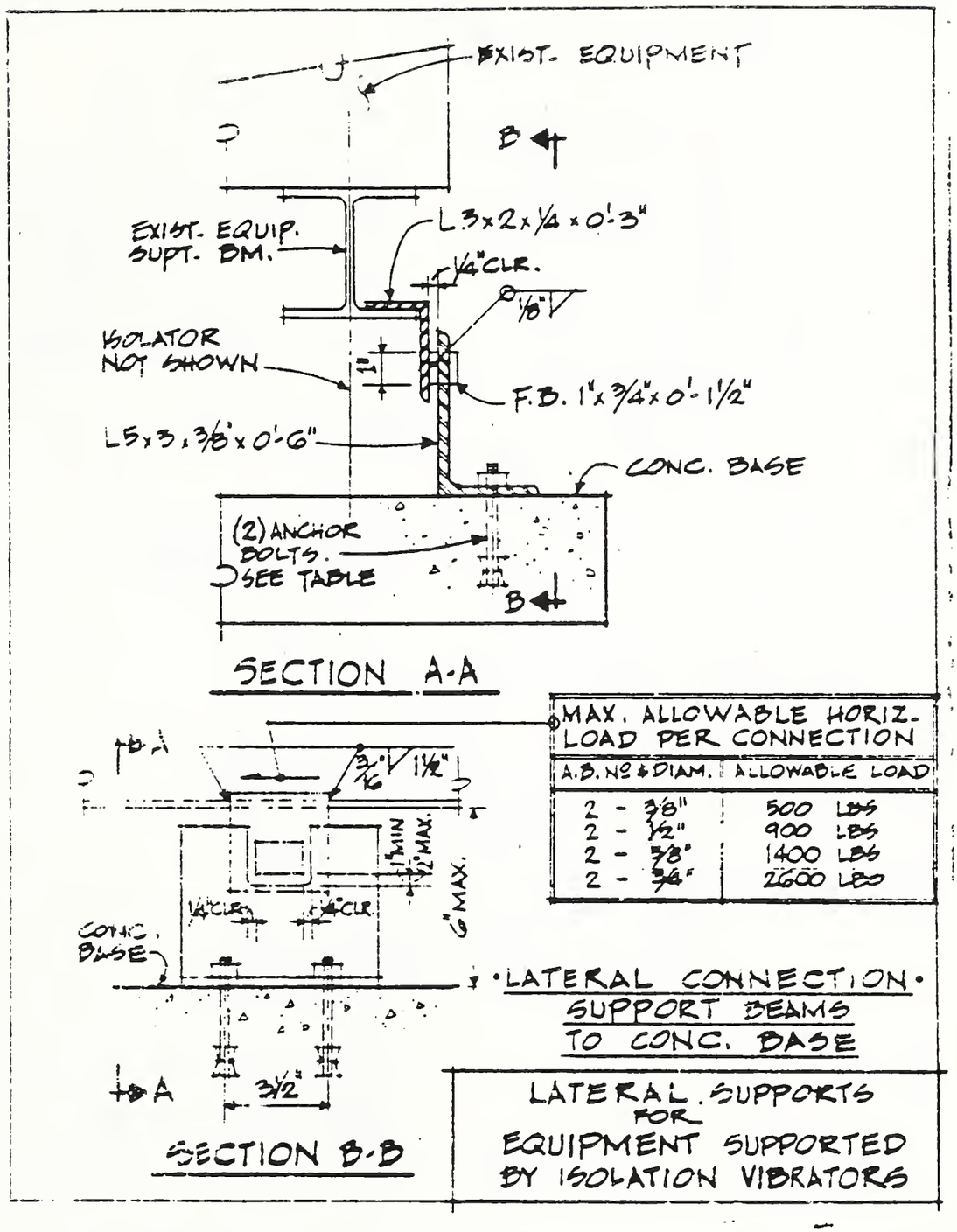
EXIST. EQUIPMENT
B
EXIST. EQUIP. SUPT. BM.
L 3x2x1/4 x 0'-3"
1/4" CLR.
1/8"
ISOLATOR NOT SHOWN
F.B. 1"x3/4"x 0'-1 1/2"
L 5x3x3/8"x 0'-6"
CONC. BASE
(2) ANCHOR BOLTS. SEE TABLE
B
SECTION A-A
MAX. ALLOWABLE HORIZ. LOAD PER CONNECTION
A.B. Nº & DIAM. | ALLOWABLE LOAD
2 - 3/8" | 500 LBS
2 - 1/2" | 900 LBS
2 - 5/8" | 1400 LBS
2 - 3/4" | 2600 LBS
3/16" 1 1/2"
1" MIN 2" MAX
6" MAX.
1/4" CLR.
1/4" CLR.
CONC. BASE
A
3 1/2"
SECTION B-B
•LATERAL CONNECTION•
SUPPORT BEAMS TO CONC. BASE
LATERAL SUPPORTS FOR EQUIPMENT SUPPORTED BY ISOLATION VIBRATORS

FIGURE 2

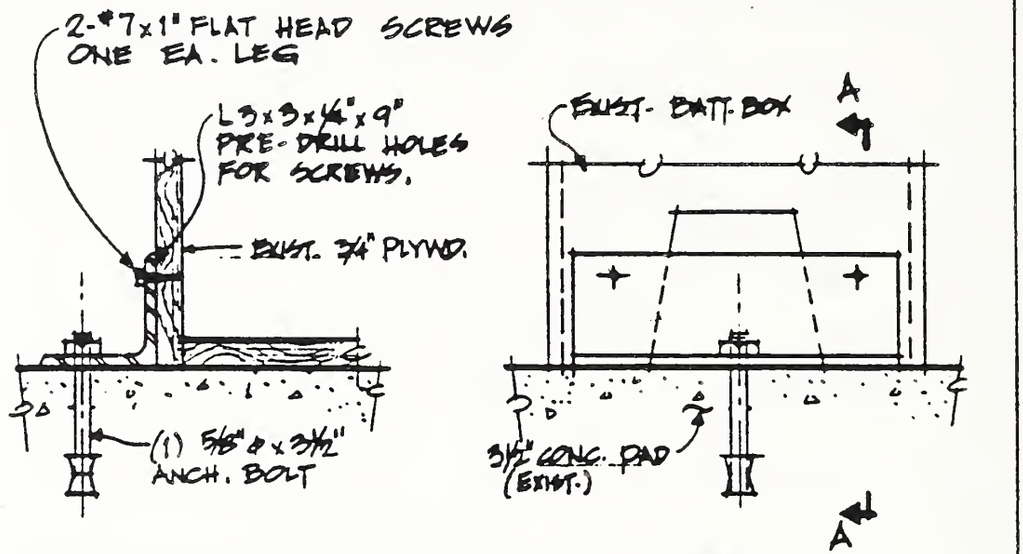

SECTION A-A

CONN. DETAIL
END VIEW

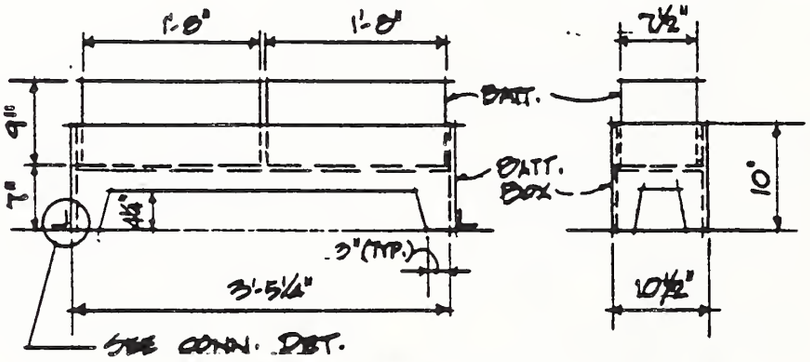

BATTERY BOX ELEVATIONS

BATTERY BOX
LATERAL CONN. DETAIL

FIGURE 3

Wind Tunnel Test on Behavior of Rooftiles under Strong Wind

BY

Hisashi Okada*1 and Tatsuo Murota*2

SUMMARY

A series of wind tunnel tests was conducted on the fluttering and scattering behavior of "hikkake-san-gawara", a hook type rooftiles, which are used widely for roofings of Japanese wooden dwellings. 1/20 scale models of two-storied dwellings of a rectangular plan and 1/20 miniature rooftile models made by brass cast were used for the test. The boundary layer realized in the wind tunnel corresponded to that on rural districts.

Following results were obtained:

(1) The spatial distribution of rooftile scattering was non-symmetric. Rooftiles on the right side roofs were susceptible to scattering.

(2) Locations of fastening in the customary tile-roofing works was effective to prevent rooftile scattering in strong winds of less than about 40m/s.

(3) Based on the consideration on the wind resistant mechanism in hikkake-san-gawara roofing system, the value of wind force coefficient for the first fluttering of rooftiles was obtained.

KEY WORDS: Wind Tunnel Test, Wind Resistant Mechanism of Rooftiles, Fluttering and Scattering of Rooftiles, Wind Force Coefficient

1. INTRODUCTION

Roofs of timber construction dwellings in Japan are mostly covered by clay tiles called as "hikkake-san-gawara" which are set on roof sheathings by hooking their upper edges to crosspieces nailed on sheathing boards. This type of rooftiles has often been damaged by strong winds. In order to prevent those damages, tile-roofing workmen fasten rooftiles with nails in some special locations known empirically.

In 1986 Building Research Institute was requested by Japan Clay-Tile Roofing Constructor Association to make wind tunnel tests to get information on the behavior of clay-tile roofings in winds and also on the effect of nail fastenings.

This paper describes the results of the wind tunnel tests.

2. DESCRIPTION OF WIND TUNNEL TESTS

2.1 Wind tunnel

The tests were conducted using the turbulent boundary layer wind tunnel of Building Research Institute, the dimensions and performance of which are listed in Table 1.

2.2 Similarity Law

2.2.1 Similarity of air flow

Mean wind velocity profiles in turbulent boundary layer can be described by the following equation.

$$U(Z)=\frac{U^*}{K}\ln\left(\frac{Z}{Zo}\right) \qquad (1)$$

in which, U(Z):mean wind velocity at the level Z
U* :friction velocity
K :Karman's constant
Zo :roughness parameter

In order to derive similarity for the mean wind velocity profile, the following similarity equation which is called "Jensen's similarity law" must be satisfied.

$$\left(\frac{Z}{Zo}\right)_p=\left(\frac{Z}{Zo}\right)_m \qquad (2)$$

in which, Z is height and/or length scale and suffix p and m refer to the quantity for full-scale and model, respectively.

Eq.(2) can be modified as follows:

$$\frac{(Z)m}{(Z)p}=\frac{(Zo)m}{(Zo)p} \qquad (3)$$

The term on the left hand side of eq.(3) is a geometric parameter related to the ratio of model scale to full-scale.

2.2.2 Similarity of forces on rooftiles

The wind force(F) which acts on a rooftile can be expressed as the product of velocity pressure(q), wind force coefficient(C) and area of rooftile(A).

$$F=C\cdot q\cdot A \qquad (4)$$

in which, $q=1/2\rho U^2$
ρ=air density
U=wind velocity

On the other hand, the force of resistance(R) against the removal of a rooftile which is not fastened to sheathing boards is approximately the same as the weight of the rooftile. The force(R) can be expressed as follows:

$$R=w\cdot A\cdot\cos\theta \qquad (5)$$

in which, w=weight of a roof tile per unit area
θ=pitch of roof

For the similitude of force, the following condition must be satisfied:

---

*1 Senior Research Officer, Building Aerodynamics Division, Structural Engineering Department, Building Research Institute, Ministry of Construction

*2 Director, Structural Engineering Department, ditto

$$(F/R)_p=(F/R)_m \quad (6)$$

Substituting eqs.(4) and (5) into eq.(6), the following equation can be obtained.

$$(\frac{U_p}{U_m})^2=(\frac{w_p}{w_m})^2 \quad (7)$$

This equation is very important to convert the wind velocity in wind tunnel tests into the one in full-scale phenomena.

2.3 MODELS

2.3.1 Dwelling Models

Two 1/20 scale models two-storied dwellings were used for wind tunnel tests. Gable and hip roofs of 4.5/10 pitch were selected to be tested as shown in Figs.1 and 2, respectively. Crosspieces are attached to roof surfaces in a direction parallel to the edge lines of eaves at a space of the effective length of rooftile as shown in Fig.4.

2.3.2 Roof-Tile Models

1/20 scale models of hikkake-san-gawara which are identified as clay rooftiles of JIS 53A were made by casting brass into moulds. A set of JIS 53A clay rooftiles includes rooftiles of 12 different shapes (Photo.1 and 2). The shape of rooftiles which are used most in number in tile roofing is shown in Fig.3. Here after we will call this rooftile as a common tile.

Common tiles are used at locations except ridges, verges and eaves. In this wind tunnel test, we casted 1496 and 1756 pieces of miniature rooftiles for a gable roof and a hip roof model, respectively. About 80%(gable roof) and 75%(hip roof) of them were common tiles.

Common tiles have small projections called "Hikkake" on upper edges of their under sides. This projection act as a hook on setting a common tile on crosspieces(Fig.4).

Figs.5 and 6 show rooftile arrangement for gable and hip roof, respectively. In case of actual tile-roofing works, rooftiles set along ridges or edges of roofs are not only hooked on crosspieces but also fastened by nails or copper wires. In the wind tunnel tests, two tile-fastening conditions were tested for comparison. One is the case similar to actual works stated above and the other is the case where all rooftiles are put on the sheathing without fastening. In the former case rooftiles fastened to the sheathing by adhesive tapes at places shown in Figs.5 and 6. Adhesive tape fastening was effective up to the wind speed of 40m/s at height of the roof ridge.

In Table 2 weights of miniature rooftiles are shown. The weight of a common tile was 1.22gw, which was 1/2,220 of the full-scale tile(2.7kgw). The value of w_p/w_m in eq.(7) was 5.55 for common tiles.

2.4 Test Series

Table 3 describes eighteen cases of the wind tunnel tests.

Wind directions were measured in such a way as shown in Figs.5 and 6.

In most cases the roof models was exposed to wind from a certain direction and the wind speed was increased step by step. On the other hand, in case of test No.8, 13 and 18, the roof model was rotated slowly and continuously on the turn-table and was exposed to wind of a constant speed, shown on the column "wind speed" in Table 3.

2.5 Wind Tunnel Flow

The wind tunnel flow was arranged to be similar to natural winds by arranging roughness blocks and spires set on the floor of wind tunnel. Mean wind velocity and turbulent intensity profiles of the wind tunnel flow at the site of roof models after arrangement are shown in Fig.7. The value of the roughness parameter Zo in the wind tunnel flow was about 1.3cm. It corresponds to 26cm in full-scale because the size reduction ratio of the model is 1/20. According to Table 4 the wind tunnel flow is similar to those on rural districts. Fig.8 shows power spectrum of turbulence at the height of 40cm above tunnel floor. This height corresponds to the level of roof ridges.

3.TEST RESULT

The behavior of rooftiles was observed at each step of wind speeds and recorded by video tape recorders. Locations of rooftiles which moved in wind are shown in Figs.10 to 25 with reference to the wind speeds. In these figures the movements of rooftiles are classified into two types;

1) fluttering: remarkable fluttering at or near the initial position. The distance of displacement is less than the width or breadth of a clay tile.

2) scattering: movement with the larger distance of displacement.

The values of wind speed in the figures correspond to those for full-scale phenomena at height of eaves and they mean that the movements of rooftiles shown there occurred at a wind speed less than the value in parentheses( ) or at a wind speed larger than one in ( ) and less than another without parentheses.

The minimum wind speed at which the first remarkable movement of a rooftile was observed in listed on Table 5 for each test.

The details of rooftile movements will be described in the following two sections, where the words "right-side roof" or "left side roof" will be used without noticing that they are seen from the windward.

3.1 Movement of rooftiles

1) In case of roofs with no fastened rooftiles

(1) Gable roof, wind direction 0° (Fig.10)

When the wind speed exceeded 25m/s, rooftiles near the edge of the windward verge began to flutter. Some of them scattered at

the wind speed more than 30m/s to leeward direction on the right-side roof surfaces and on the contrary to wind ward direction on the left-side roof surface. Tiles on the windward ridge were demolished at the same time.

The increase in the number of scattered tiles was more rapid on the right side roof surface, where most rooftiles in five or six rows near the eaves were blown off when the wind speed exceeded 40m/s.

(2) Gable roof, wind direction 90° (Fig.11)

Rooftiles in two rows on the windward eaves began to flutter when the wind speed exceeded 25m/s, and tiles in the first row scattered before the wind speed came to 30m/s. No other scattering was observed after that. At about 40m/s two rows of tiles on the windward right-side verge and a few rooftiles on the leeward left-side verge were blown off.

(3) Gable roof, wind direction -45° (Fig.12)

When the wind speed exceeded 30m/s, the first fluttering was observed along eaves and verge near the windward corner. The fluttering of eaves rooftiles extended leeward and all of them fluttered or a few of them scattered at 35m/s. No other scattering was observed until the wind speed became 40m/s after that. At 40m/s rooftiles on the ridge and rooftiles on the verge of leeward roof scattered.

(4) Gable roof, wind direction 45° (Fig.13)

When the wind speed exceeded 25m/s, fluttering occurred on rooftiles on the windward verge and eaves of a windward roof. At a little higher than 30m/s a row on windward eaves, a few row on the windward verge of the windward roof and a row on the windward verge of the leeward roof scattered. Area of scattering on the windward roof spread with the increase of wind speed and most of the windward rooftiles were blown off at 40m/s.

(5) Hip roof, wind direction 0° (Fig.14)

At a little higher than 25m/s, two rows of rooftiles near eaves on the windward roof began to flutter and the first row was blown off at about 30m/s. At a little lower than 35m/s, scattered rooftiles on windward eaves of the right-side roof parallel to the wind direction and also rooftiles on windward corner ridges.

Scatter of rooftiles of the right-side roof spread leeward with the increase of wind speed.

(6) Hip roof, wind direction 90° (Fig.15)

In this case the movement of rooftiles was similar to that in the preceding case.

(7) Hip roof, wind direction -45° (Fig.16)

At a wind speed of a little lower than 30m/s, two rows of rooftiles on eaves of the right-side windward roof began to flutter and they scattered soon after that. No other scattering occurred until 40m/s, when all the rooftiles of the right-side windward roof scattered suddenly. Several rooftiles on the left-side windward roof also scattered at the same time.

2) In case of roofs with fastened rooftiles

(1) In the tests No.10, 12, 15, 16 and 17

No remarkable movement of rooftiles was observed.

(2) Gable and hip roof, wind direction 0° (Figs.17, 21)

The first fluttering was observed at about 30m/s on rooftiles on the windward part of roofs parallel to the wind direction and a few of them scattered at a wind speed of a little lower than 40m/s.

(3) Gable roof, wind direction -45° (Fig.19)

At 35m/s a few rooftiles on the 2nd and 3rd row in the windward verge of the windward roof began to flutter, but they didn't scatter at a wind speed more than 40m/s. In this case rooftiles on the first row are fastened.

3.2 Non-symmetricity of scattering and effect of fastening

It will be noted that even if the shapes of right and left side roofs are symmetric, the areas of rooftile scattering on right and left side roofs are not symmetric. In general the area of scattering on the right side roof is far larger than that on the left side roof. The directions of scattering are also different on the right and left side roofs: on the right-side roof, rooftiles scattered leeward but on the left-side roof they scattered to the opposite direction.

The non-symmetric feature of scattering is considered to be caused by the non-symmetricity of tile-roofing works shown in Fig.9; the left and bottom edge of a rooftile are put on the adjacent tiles but the right and upper edge are put under another rooftiles.

Comparing the area of rooftile scattering shown in Figs.10 to 16 with those in Figs.17 to 22, the fastening is very effective for preventing scattering and fluttering of rooftiles. It is considered that the locations of fastening selected empirically in the customary roofing works will be effective to prevent scattering in strong winds of less than 40m/s.

3.3 Comparison of scattering in winds of fixed direction with that in winds of non-fixed direction

Figs.23 to 25 show the area of scattering after the test No.8, 13 and 18 in which the wind speed was constant but the wind direction changed continuously. The areas of scattering in these tests are generally larger than those in the tests for fixed wind direction. The difference is considered to be reasonable, because rooftiles in the test No.8, 13 and 18 were exposed to more extra wind effects than those in the other tests.

3.4 Force coefficient and wind resistant mechanism of rooftiles

Wind resistant mechanism of the "hikkake-san-gawara" roofing system can be modeled as shown in Fig.9, where forces f_i is sum of wind force, weight of a rooftile and fastening resistance if the tile is fastened.

Supposing that the i-th rooftile is

lifted by winds, force f_i must satisfy the equation:

$$f_i > (\frac{1}{3})f_{i+1} + (\frac{1}{3})^2 f_{i+2} + (\frac{1}{3})^3 f_{i+3} + \cdots \quad (8)$$

In general it is not unreasonable to suppose that the wind force acting on tile i is approximately the same as those acting on the adjacent tiles because the size of tiles is very small compared with that of roofs and the spatial change of wind pressure is not so large in a small area of roof surfaces.

Therefore, in the case that rooftiles are only hooked on crosspieces and not fastened to sheathings, force f_i can be supposed to be approximately equal to $f_{i+j}(j=1,2,3,\cdots)$. Then the eq.(8) can be simplified as $f_i > 0$. This condition leads to the wind force coefficient as follows:

$$C = \frac{W}{1/2\rho U^2 A} = \frac{W}{1/16 U^2 A} \quad (9)$$

where, W=weight of rooftile
A=effective area of a rooftile

If the (i+k)th rooftile is fastened and the sum of wind force and weight of rooftiles is the same for i-th and i+j(j=1,2,$\cdots$,k)th rooftiles, the fastening resistance F_f necessary for preventing the scatter of the i-th rooftile can be obtained as follows:

$$F_f > f_i\{1 - \sum_{j=1}^{k} (\frac{1}{3})^j\}/(1/3)^k \quad (10)$$

The first fluttering wind speeds of rooftiles obtained in the tests were approximately 25m/s in all cases. The corresponding wind force coefficient is obtained by eq.(9);

$$C = \frac{2.7kgw}{1/16 \times 25^2 \times (0.235 \times 0.265)} = 1.11 \quad (11)$$

where, 0.235=effective breadth of rooftiles in mm
0.265=effective length of rooftiles in mm

4. CONCLUSION

Model scale tests were carried out in a boundary layer wind tunnel on the behavior of "hikkake-san-gawara" roofing system. The following conclusion were obtained from the tests:

(1) The spatial distribution of rooftile scattering was non-symmetric. Rooftiles on the right side roofs were susceptible to scattering.

(2) The fastening of rooftiles was very effective for preventing scattering and fluttering of rooftiles. It is observed that the locations of fastening in the customary tile-roofing works was effective to prevent rooftile scattering in strong winds of less than about 40m/s.

(3) The wind resistant mechanism of hikkake-san-gawara was taken into consideration and the wind force coefficient for the first fluttering of rooftiles was obtained.

References

1) N. Frank and M. Jensen "Model-Scale Tests in Turbulent Wind, Part 1" , The Danish Technical Press,1963

2)J. Couhnian "Adiabatic Atmospheric Boundary Layer : A Review and Analysis of Data from the Period 1880-1972" ,Atmospheric Environment,Vol.9,Pergamon Press,1975

Table 1 Specifications of B.R.I Wind Tunnel for closed Göttingen type

Dimensions of Working Section(unit=mm)	3,000(breadth)×2,500(height) ×25,000(length)
Contraction Ratio	8:1
Range of wind velocity	0.5 to 24.4m/s

Table 2 Weight of Model Rooftiles

common tile	1.22gw	ridge tile (A)	0.79gw
eaves tile	1.35	ridge tile (B)	2.22
verge tile(left)	1.23	ridge tile (C)	0.81
verge tile(right)	1.26	corner tile (A)	1.83
ridge end tile(left)	2.08	corner tile (B)	1.42
ridge end tile(right)	3.24	corner tile (C)	1.59

Table 3 Test Series

No.	Roof Shape	Fastening	Wind Direction	Wind Speed
1	gable	none	0 degree	
2			90	
3			-45	
4			45	
5	hip	none	0	
6			90	
7			-45	
8			rotation	40m/s
9	gable	eaves	0	
10		ridge	90	
11		verge	-45	
12			45	
13			rotation	42m/s
14	hip	eaves	0	
15		ridge	90	
16		verge	-45	
17			45	
18			rotation	42m/s

Table 4 Value of Zo (unit=cm)[2)]

Terrain Type			
Smooth ice,mud, ,snow,sea	Moderately rough short grass ,grass/crops	Rough rural/woods ,woods	Very Rough Urban
0.001 to 2.0	0.1 to 20	100 to 150	100 to 400

Table 5 Wind speeds at which rooftiles start to flutter and scatter

Roof Shape and with or without fastening	Wind Direction	Wind Speed	
		Flutter	Scatter
Gable roof (without fastening)	0 degree	25m/s	31m/s
	90	27	29
	-45	32	34
	45	27	30
Gable roof (with fastening)	0	29	36
	90	48	48
	-45	33	>43
	45	39	>43
Hip roof (without fastening)	0	25	27
	90	27	27
	-45	29	32
Hip roof (with fastening)	0	34	38
	90	41	43
	-45	>41	>41
	45	>42	>42

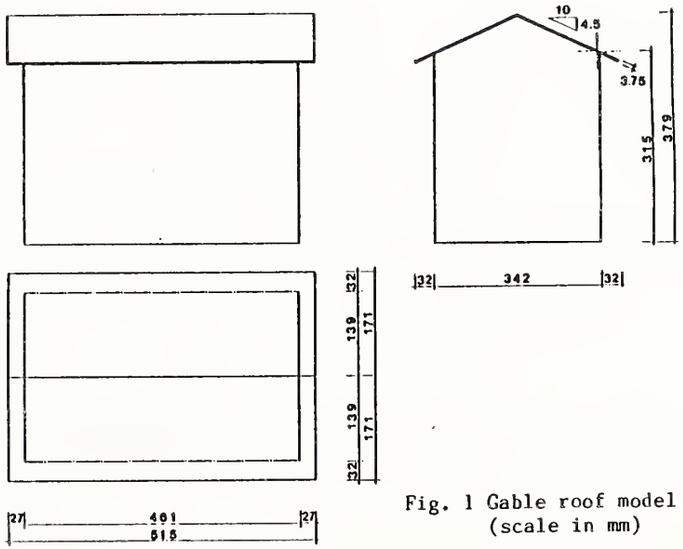

Fig. 1 Gable roof model
(scale in mm)

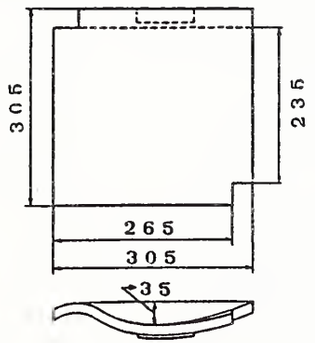

Fig. 3 Shape of JIS 53A
Hikkake-san-gawara
(scale in mm)

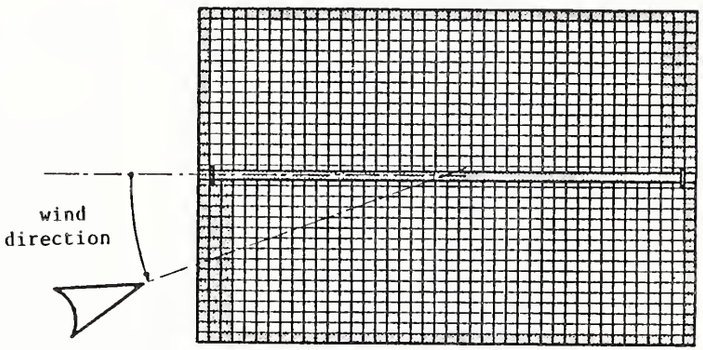

Fig. 5 Arrangement of rooftiles (Gable Roof)
(dotted rooftiles are fastened in cases
of tests on the effect of fastening)

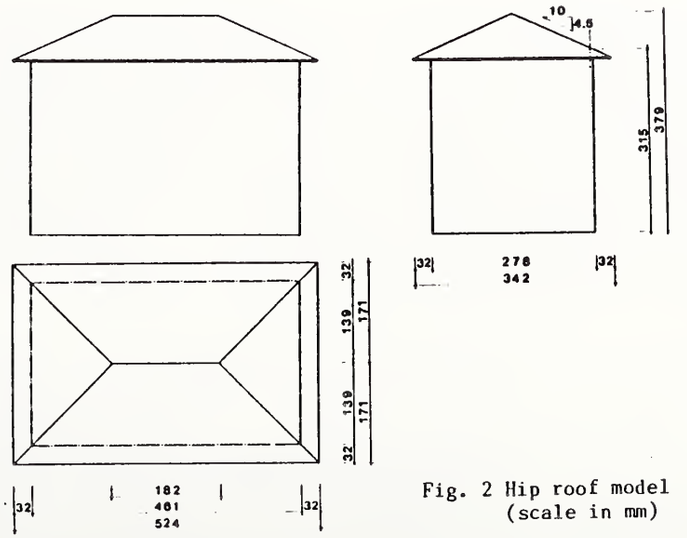

Fig. 2 Hip roof model
(scale in mm)

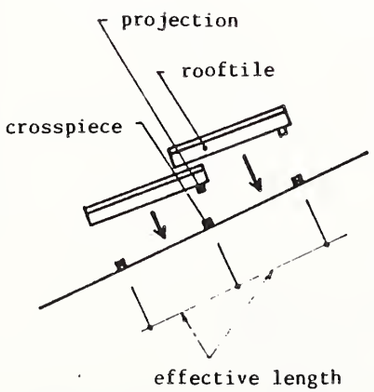

Fig. 4 Hooking mechanism of
rooftiles to crosspieces

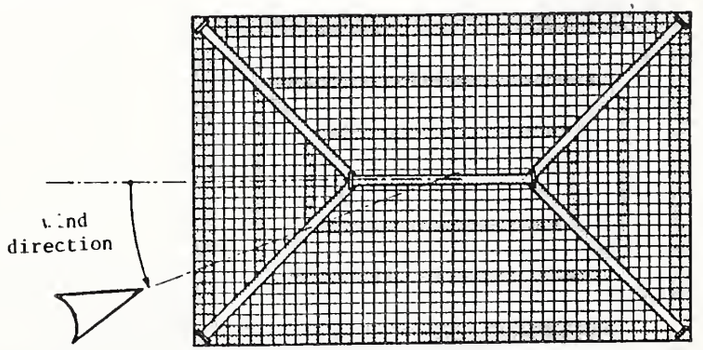

Fig. 6 Arrangement of rooftiles (Hip Roof)
(dotted rooftiles are fastened in cases
of tests on the effect of fastening)

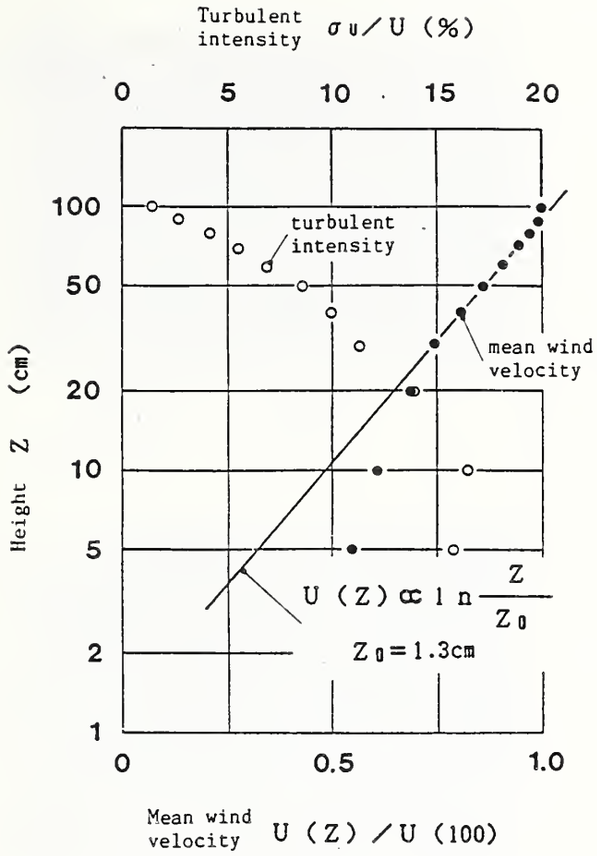

Fig.7 Mean wind velocity and turbulent intensity profile of wind tunnel flow

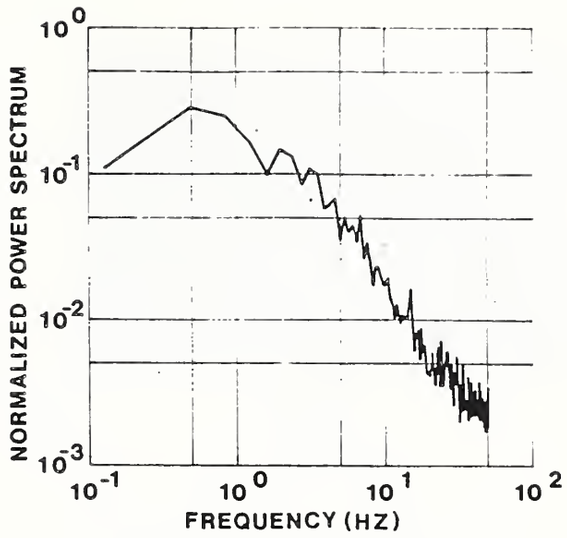

Fig.8 Power spectrum of turbulence of wind tunnel flow

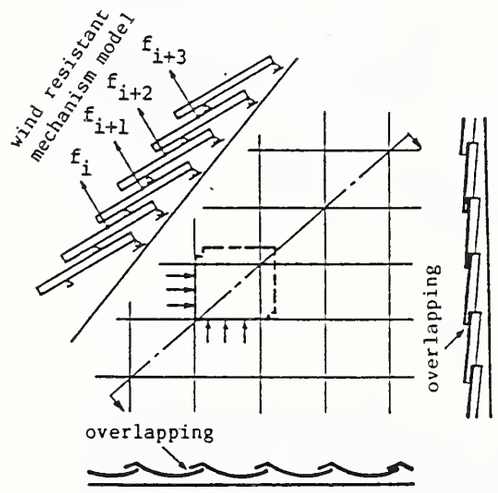

Fig. 9 Overlapping of rooftiles and wind resistant mechanism model

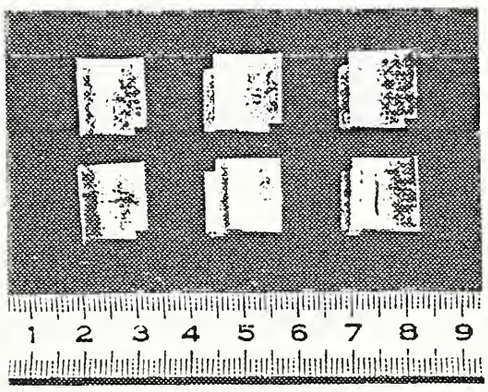

Photo.1 Shapes of miniature rooftiles (1)

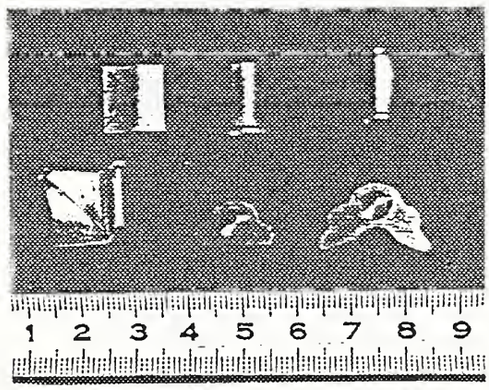

Photo.2 Shapes of miniature rooftiles (2)

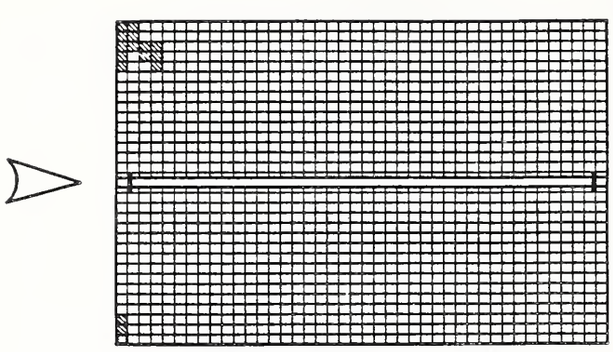

(a)U=27m/s
(25m/s)

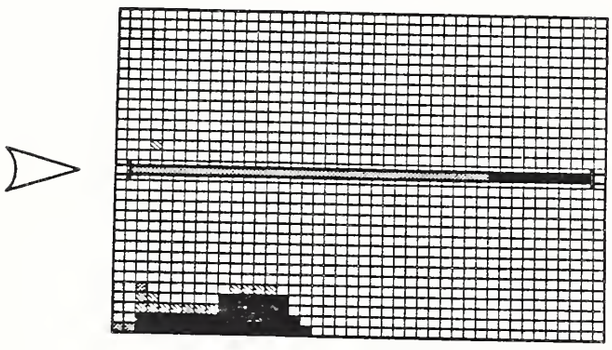

(b)U=34m/s
(32m/s)

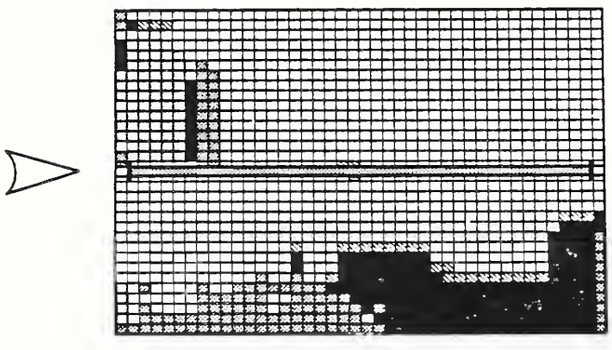

(c)U=41m/s
(40m/s)

Fig. 10 Distribution of movement of rooftiles
(Gable Roof without fastening
, Wind Direction =0 degree)

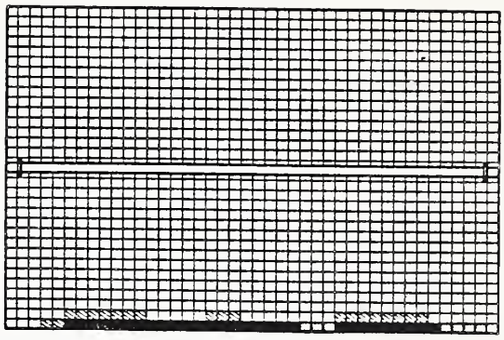

(a)U=29m/s
(27m/s)

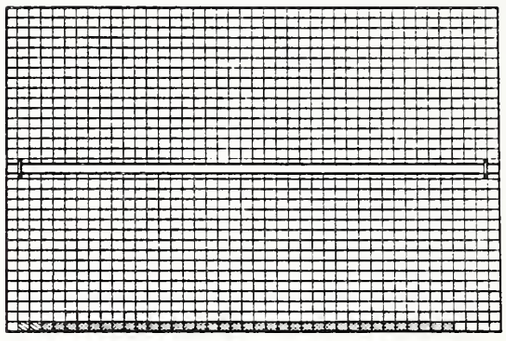

(b)U=34m/s
(32m/s)

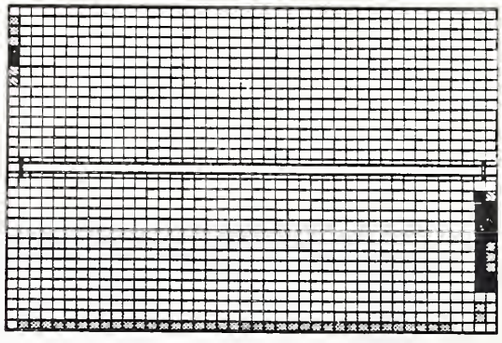

(c)U=41m/s
(40m/s)

Fig. 11 Distribution of movement of rooftiles
(Gable Roof without fastening
, Wind Direction =90 degree)

scattered in the preceding test but is not repaired

fluttered in the preceding steps

fluttered in this step

scattered in the preceding steps

scattered in this step

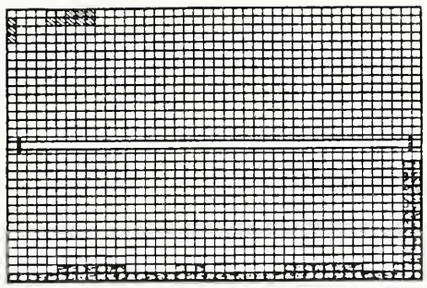

(a)U=32m/s
(30m/s)

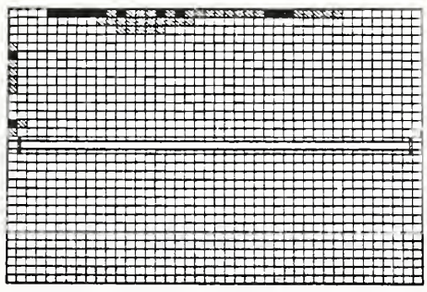

(b)U=34m/s
(32m/s)

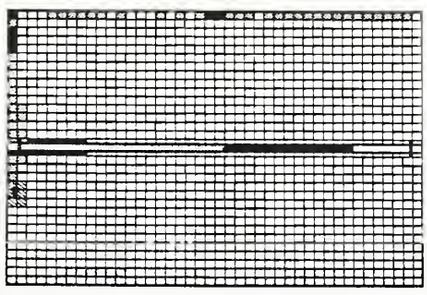

(c)U=40m/s
(38m/s)

Fig. 12 Distribution of movement of rooftiles
(Gable Roof without fastening
, Wind Direction =-45 degree)

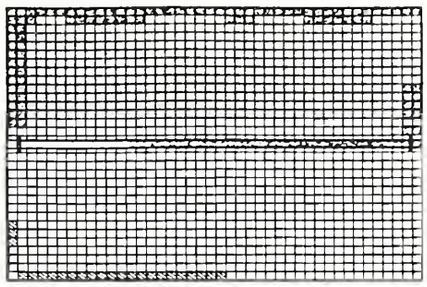

(a)U=29m/s
(27m/s)

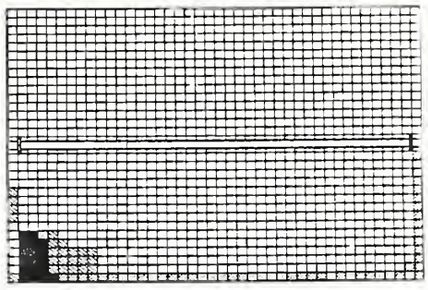

(b)U=34m/s
(32m/s)

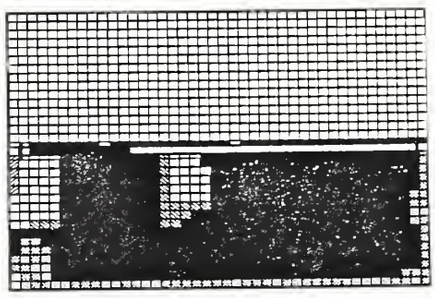

(c)U=38m/s
(36m/s)

Fig. 13 Distribution of movement of rooftiles
(Gable Roof without fastening
, Wind Direction =45 degree)

scattered in the preceding test but is not repaired

fluttered in the preceding steps

fluttered in this step

scattered in the preceding steps

scattered in this step

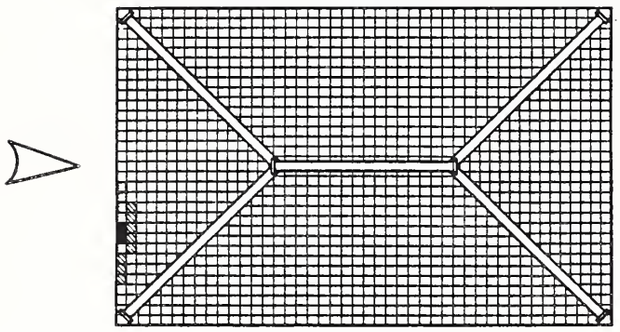

(a)U=27m/s
(25m/s)

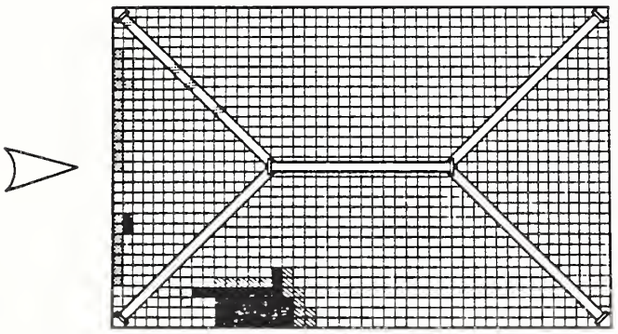

(b)U=34m/s
(32m/s)

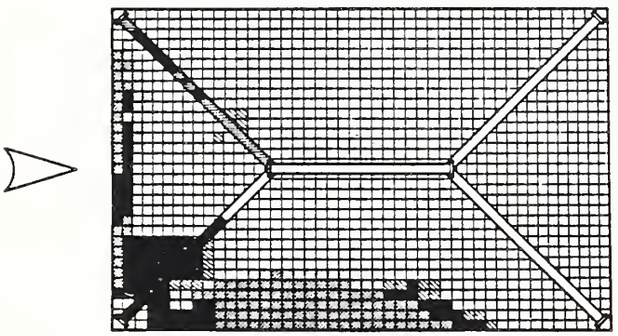

(c)U=38m/s
(36m/s)

Fig. 14 Distribution of movement of rooftiles
(Hip Roof without fastening
, Wind Direction =0 degree)

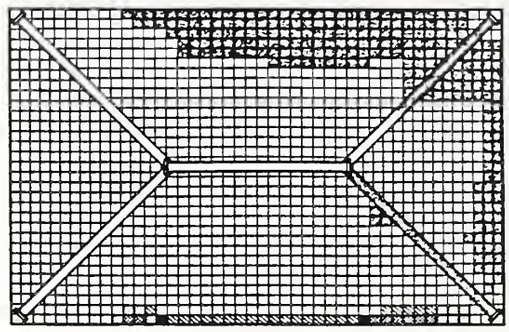

(a)U=29m/s
(27m/s)

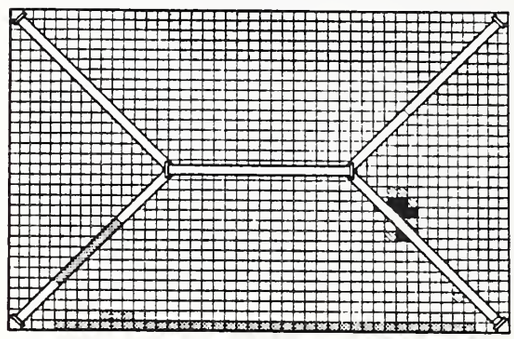

(b)U=34m/s
(32m/s)

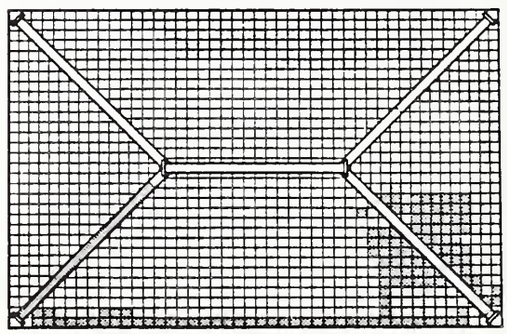

(c)U=40m/s
(38m/s)

Fig. 15 Distribution of movement of rooftiles
(Hip Roof without fastening
, Wind Direction =90 degree)

scattered in the preceding test but is not repaired

fluttered in the preceding steps

fluttered in this step

scattered in the preceding steps

scattered in this step

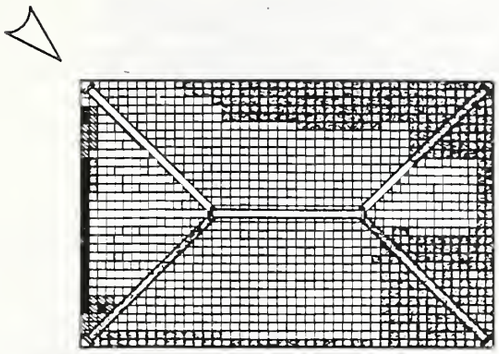

(a)U=32m/s
(29m/s)

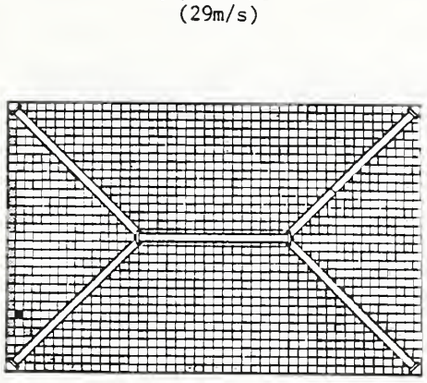

(b)U=34m/s
(32m/s)

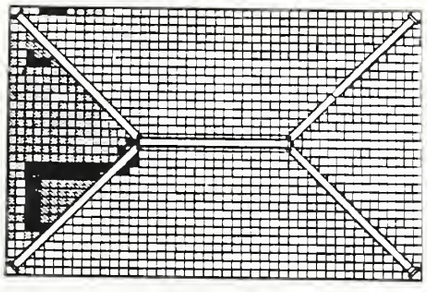

(c)U=40m/s
(38m/s)

Fig. 16 Distribution of movement of rooftiles
(Hip Roof without fastening
, Wind Direction =-45 degree)

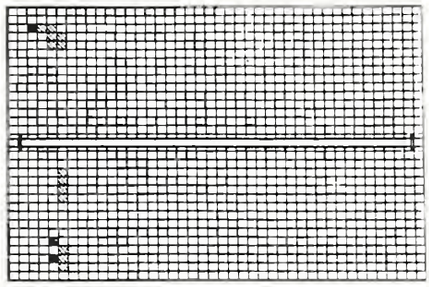

U=36m/s
(35m/s)

Fig. 17 Distribution of movement of rooftiles
(Gable Roof with fastening
, Wind Direction =0 degree)

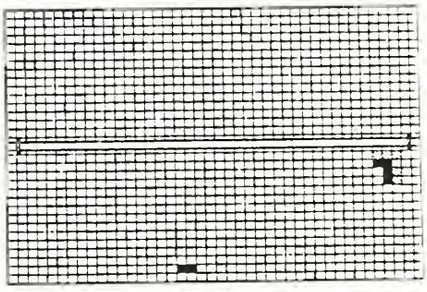

U=48m/s
(45m/s)

Fig. 18 Distribution of movement of rooftiles
(Gable Roof with fastening
, Wind Direction =90 degree)

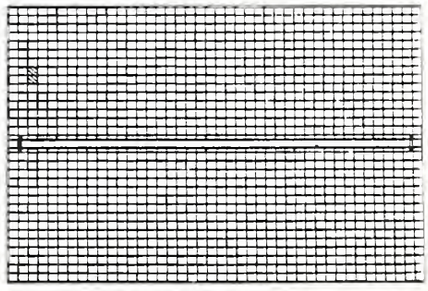

U=41m/s
(39m/s)

Fig. 19 Distribution of movement of rooftiles
(Gable Roof with fastening
, Wind Direction = -45 degree)

scattered in the preceding test but is not repaired

fluttered in the preceding steps

scattered in this step

scattered in the preceding steps

fluttered in this step

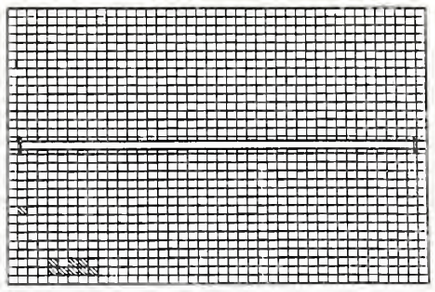

U=42m/s
(39m/s)

Fig. 20 Distribution of movement of rooftiles
(Gable Roof with fastening
, Wind Direction =45 degree)

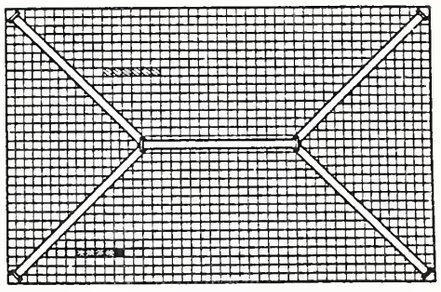

U=40m/s
(38m/s)

Fig. 21 Distribution of movement of rooftiles
(Hip Roof with fastening
, Wind Direction =0 degree)

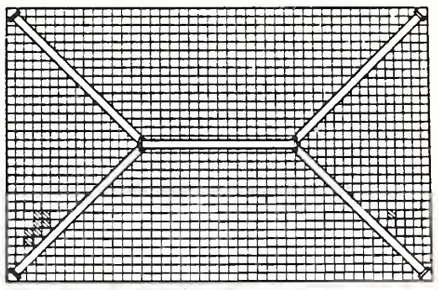

U=43m/s
(41m/s)

Fig. 22 Distribution of movement of rooftiles
(Hip Roof with fastening
, Wind Direction =90 degree)

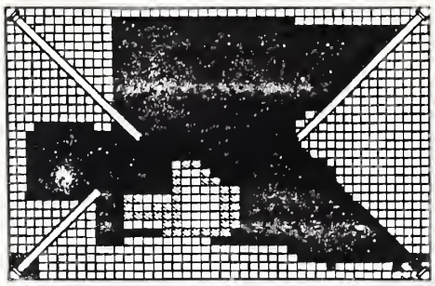

Fig. 23 Distribution of movement of rooftiles
(Gable Roof without fastening
, Rotation , U=40m/s)

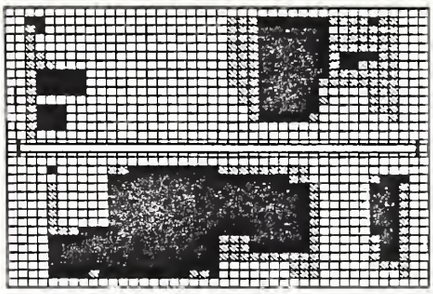

Fig. 24 Distribution of movement of rooftiles
(Gable Roof with fastening
, Rotation ,U=42m/s)

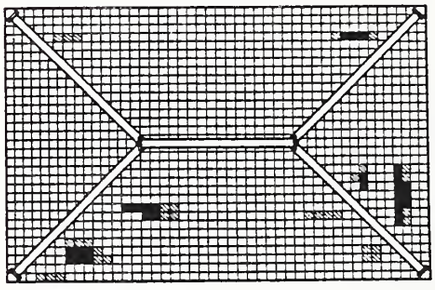

Fig. 25 Distribution of movement of rooftiles
(Hip Roof with fastening
, Rotation ,U=42m/s)

scattered in the preceding test but is not repaired

fluttered in the preceding steps

fluttered in this step

scattered in the preceding steps

scattered in this step

Seismic Microzonation Using Urban Ground Information

BY

Shinkichi Kishi[1], Toshikazu Morohoshi[2]
Keiichi Otani[3] and Hiroshi Takahashi[4]

ABSTRACT

The data of about 30,000 borehole records centering around the Metropolitan area has been stored in the database. The data were produced at the fundamental survey for construction of various structures. Regional distribution of the ground properties such as thickness of soft ground, vibrational characteristics of ground, liquefaction potential of sand layer, etc. are grasped from the database.
In addition, using the characteristics of earthquake motions in the basement and in the sedimentary layer estimated by the model constructed from the observed data at network of strong-motions including three deep boreholes, regional distribution of the size of surface ground motions were estimated.

KEY WORDS: Database, Urban ground, Borehole record, Microtremors, Ground motion, Seismic microzonation.

1. INTRODUCTION

Through the Niigata Earthquake in 1964 and the off-Tokachi Earthquake in 1968, because of the relations between the damage and the ground properties, development of the database system of borehole records in urban areas and development of its application methods for prediction of seismic damage have been conducted in NRCDP (National Research Center for Disaster Prevention). Some of the results are practically utilized in a few municipal authorities and at present the data of 20,000 borings in Tokyo metropolitan area and of 10,000 borings in Sizuoka prefecture are stored in the database[1].

On the otherhand, in NRCDP, a research project to estimate the average amplification characteristics of the thick sedimentary layer for the short period of S-waves in a specific region of the Metropolitan area has been under way using the data of accelerometers installed at the bottom of the deep boreholes in the pre-Tertiary basement and installed at the strong-motion observation points on the ground. A tentative estimation procedure were already proposed[2].

In this study a whole ground structure is divided into seismic basement and sedimentary layer, and furthermore the sedimentary layer is divided into engineering bedrock and surface ground. In this paper a method is described to estimate the regional distribution of the size of surface ground motions in the study area of eastern neighbor of Tokyo Metropolis against an assumed earthquake, using the amplification characteristics of engineering bedrock estimated from the above stated procedure and of surface ground estimated from the database and the observed data of microtremors.

2. SUMMARY OF THE DATABASE

The data of depth of layer, soil name, N-value, etc. on the borehole records mainly produced at the fundamental survey for construction of various structures are stored in the database. Location of boring was determined by the mesh with one side about 100 meter long.

2.1 Input System

The mnemonic code tables for non-numerical data, such as soil name and soil color, were designed in order to make the input work easier. A part of soil code is shown in Fig.1.
Recently two input works of coding and punching were put together by making most of the microcomputer system, and

[1]Head, Information Processing Labo. 4th Research Division, National Research Center for Disaster Prevention, Japan.
[2]Researcher, Infomation Processing Labo. 4th Research Division, NRCDP.
[3]Head, Earthquake Engineering Labo. 2nd Research Division, NRCDP, Japan.
[4]Director General, NRCDP, Japan.

as a result the time required in the work has been sharply shortened.

2.2 Accumulation System
Fig.2 shows how the boring data are arranged in computer. Each item is coded to binary type and packed in a word.
Retrieval by location index is basic in microzoning. The location of boring is given by the mesh with one side about 100 meter long. This mesh size is equal to the size of dividing side and length of the 1:25,000 topographic map, published by Geographical Survey Institute of Japan, into 100 equal parts, i.e. 4.5" in longitude and 3.0" in latitude, and is convenient to overlay with other information in practical use.
With the expansion of the area of accumulated data, geographical filing has been required. In the database, a unit file is constituted on the basis of the 25,000 topographic map.

2.3 Retrieval System
As a typical system there is a man-machine interaction system for the retrieval and display of the soil profile using XY-digitizer and CRT (Cathode Ray Tube). The system configuration is shown in Fig.3. In this system, soil profile at requested point or line on the map indicated by the input-pen is drawn on the CRT, as is shown in Fig.4. In the picture figures on the left signify the depth of layer and those on the right signify N-value.

3. OBSERVATION OF MICROTREMORS AND REGIONAL DISTRIBUTION OF VIBRATIONAL CHARACTERISTICS OF THE SURFACE GROUND

As a means to measure the vibrational characteristics of the surface ground, observation of microtremors were carried out at several tens of sites in the study area. While a method to output the regional distribution of vibrational characteristics of the ground from the database is described. Here we define the layer with N-value more than 50 as an engineering bedrock and presume the upper layer i.e. surface ground as a single layer of which elastic property is determined from the average of N-value.

3.1 Predominant Period of the Ground obtained from the Observation of Microtremors
The observation was carried out for 3-5 minutes at every point. Used apparatuses were 1Hz velocity horizontal component seismographs, amplifiers and data recorder. The most noiseless part for 10 seconds in the record were input to the spectrum analyser and a period which showed a maximum response was read as the predominant period of the ground.

3.2 A Formula to estimate Vs from N-value
In the observation point of micro-tremors, when we suppose the surface ground as a single layer, the velocity of S-wave Vs is obtained from the Law of quater wavelength

$$Vs=4H/T,$$

where H and T are the thickness and the predominant period of the layer, respectively.
On the other hand, calculating the average of N-value $\bar{N}$ in the surface ground from the borehole record of the observation point, and supposing a relation

$$Vs=a\bar{N}^{b},$$

and determining the coefficients by the method of least squares, we got a formula

$$Vs=92\bar{N}^{0.345}$$

3.3 Regional Distribution of the Vibrational Characteristics of the Ground
Predominant period of surface ground is estimated from the formula

$$T=4H/Vs,$$

where H and Vs are determined automatically from N-value on the borehole record in the database.
The above stated results are shown in Fig.5 with contours on the topographic map. Solid line and broken line show the contours of the predominant periods obtained from the observation and estimated from the database, respectively. Black dots show the observation points of microtremors with measured predominant periods(sec). Borehole records in Fig.4 are the data of the observation point A-D and each line on the right side sgnifies the boundary of surface ground and engineering bedrock.

In Fig.5, outlines of the contours of measured and estimated predominant periods coincide with each other. While the contours of 1 sec coincide well, the contour of measured period of 0.5 sec is seemed to lie on the contour of estimated period of 0.75 sec. On the other hand the boring data are densely distributed than the observation points of microtremors and therefore discordance between both contours are seen in the region where could not be interpolated by the measured data.

4. SEISMIC MICROZONATION

Seismic microzonation is to evaluate the characteristics of the earthquake motions in each mesh in the objective region as large as a municipality, considering the difference of erathquake motions due to the locality of the ground condition, and to apply the result to make the various kinds of maps predicting the seismic damage. In this study we divide a whole ground structure into seismic basement and sedimentary layer. The seismic basement is the pre-Tertiary layer and the sedimentary layer is a general term for Tertiary and Quaternary layer. Moreover we divide the sedimantary layer into engineering bedrock and surface ground. The surface ground is the alluvial layer with N-value less than 50 and the engineering bedrock is equivalent to Tokyo-Reki-So with N-value more than 50.

4.1 Characteristics of the Basement Motions

Characteristics of the basement motions is expressed by the zero-damped velocity response spectrum SVi(T;M,R) (gal·s) of the earthquake motions in the pre-Tertiary basement. This characteristics is given by the model

$$SVi(T;M,R)=10^{a(T)M-b(T)\log_{10}R+c(T)}$$

here M and R are the JMA magnitude and hypocentral distance in kilometers. The coefficients a, b and c are distinguished by the location of epicenter against the volcanic front of Japan. In this study the earthquakes were limited to the one whose epicenters were located out of the front.

4.2 Average Amplification Characteristics of the Sedimentary Layer

The average amplification characteristics of the sedimentary layer at the standard observation point on the ground is defined as follows,

$$\overline{G}(T)=\frac{1}{N}\sum_{n=1}^{N} SVo(T;Mn,Rn)/SVi(T;Mn,Rn)$$

where SVo(T;Mn,Rn) is the zero-damped velocity response spectrum obtained from the observed data on the ground for n'th earthquake (total N).

4.3 Average Amplification Characteristics of the Engineering Bedrock

The average amplification characteristics of the engineering bedrock toward the basement motions is given by dividing $\overline{G}(T)$ by Go(T) which signifies the amplification characteristics of the surface ground at the standard observation point

$$Ge(T)=\overline{G}(T)/Go(T)$$

In practice Ge(T) is given by the approximation

$$Ge(T)\approx\sum_{n} Kn\cdot(\log_{10}T)^{n}$$

where n=0~4, and the coefficients Kn are determined by the method of least squares.

Now the above stated characteristics were calculated for the data of 7 earthquakes[2] observed at the standard point (Urayasu city hall) between 1980 and 1984.

Fig.6 shows the estimated zero-damped velocity response spectra in the pre-Tertiary basement. Fig.7 shows the average amplification characteristics of the sedimentary layer at the standard observation point (broken line) and the amplification characteristics of the surface ground determined from N-value (solid line). Fig.8 shows the average amplification characteristics of the engineering bedrock toward the basement motions. While borehole record of the standard observation point is shown in Fig.9.

4.4 Characteristics of the Earthquake Motions at the Objective Point

The characteristics of the earthquake motions at m'th objective point in the study area is given in the zero-damped velocity response spectra

$$SVm(T;M,R)=Gm(T)\cdot Ge(T)\cdot SVi(T;M,R)$$

Where Gm(T) is the amplification characteristics of the surface ground at the objective point determined from the boring data. In this study, as a scale for microzonation to evaluate the earthquake motions, we adopt the spectral intensity ($gal \cdot s^2$) proposed by Housner

$$SIm=\int_{T_1}^{T_2} SVm(T;M,R)\,dT$$

This is not a momentary scale as a maximum acceleration but is more stable scale.

4.5 Estimation of Regional Distribution of Spectral Intensity

Although the spectral intensity is provided for the integral of zero-damped velocity response spectra from T_1=0.1s to T_2=2.5s, here we set T_1=0.15s because of the disturbance of Ge(T) in the short period range and T_2=4.0s in order to take account of the predominant vibration of the ground widely.
Here notice that the amplification characteristics of the surface ground at the objective points correspond to the velocity structure mentiond in the previous chapter, that is, a single layer with Vs determined by the average of N-value. And the Q-value and the density of the surface ground are uniformly given a value 10 and a value 1.65, respectively.

Fig.10 shows an example of the distribution of the spectral intensity of earthquake motions in the study area estimated through the procedures described in this paper. Magnitude and hypocentral distance of the assumed earthquake is respectively 7.0 and 100 km. Estimated spectral intensity is displayed in each mesh with the number corresponding to each rank of the intensity. Contours are drawn by hand for the intensity 200 and 240. Looking wholly at the figure a tendency is found that the spectral intensities become larger from northern region (the upper part) to southern reclaimed land (the lower part). The tendency appears similarly in the distribution of the predominant period of the surface ground in Fig.5 and generally speaking the tendency corresponds to the distribution of the thickness of soft ground.

The values of the spectral intensities displayed in Fig.10 show not only the regional relation on the surface, but also the result of amplification of earthquake motions from the basement to the surface in the absolute scale. In this connection, comparing that the spectral intensity distributed on the surface are about 200, that of the engineering bedrock was about 82 and that of the pre-Tertiary basement was about 17. Namely, the spectral intensity of the earthquake motion has been amplified 4 times between the pre-Tertiary basement and the engineering bedrock, 2.5 times between the engineering bedrock and the ground surface, and 10 times between the pre-Tertiary basement and the ground surface.

5. CONCLUDING REMARKS

The unique procedures of seismic microzonation synthesizing each technique developed in NRCDP, such as the model to estimate the characteristics of earthquake motions in the pre-Tertiary basement, the observation of strong-motions to estimate the amplification characteristics of the sedimentary layers and the database system of borehole records to evaluate the characteristics of earthquake motions on the ground at every 100 meter's meshes, may provide basic and useful data for the regional prediction of seismic damage.

REFFERENCES

1) S.Kishi: Apllication Method of Columnar Sections of Soil intended for the Prediction of Seismic Damage (in Japanese), Journal of the Japanese Society of Soil Mechanics and Foundation Engineering, Vol.22, No.3, pp.152-160, 1982.
2) K.Otani and S.Kinoshita: Spectral Characteristics of Ground Motion in the Tokyo Metropolitan Area, The 18th Joint Meeting U.S.-Japan Panel on Wind and Seismic Effects, 1986.

Soil Name	Card	MT	LP	CRT
Surface	SUR	0		
Humus	Y	1	Y	
Shell	Q	2	Q	
Pumice	P	3	P	
Boulder	B	4	B	
Gravel	G	5	O	
Sand gravel	DG	6	O.	
Sand	D	7	.	
Fine sand	F	8	.	
Medium sand	M	9	:	
Silt	T	10	-	
Clay	C	11	=	
Sandstone	DN	12	I.	
Siltstone	TN	13	I-	
Mudstone	MN	14	I=	

MT : Magnetic Tape
LP : Line Printer
CRT: Cathode Ray Tube

Fig.1 Table of soil code

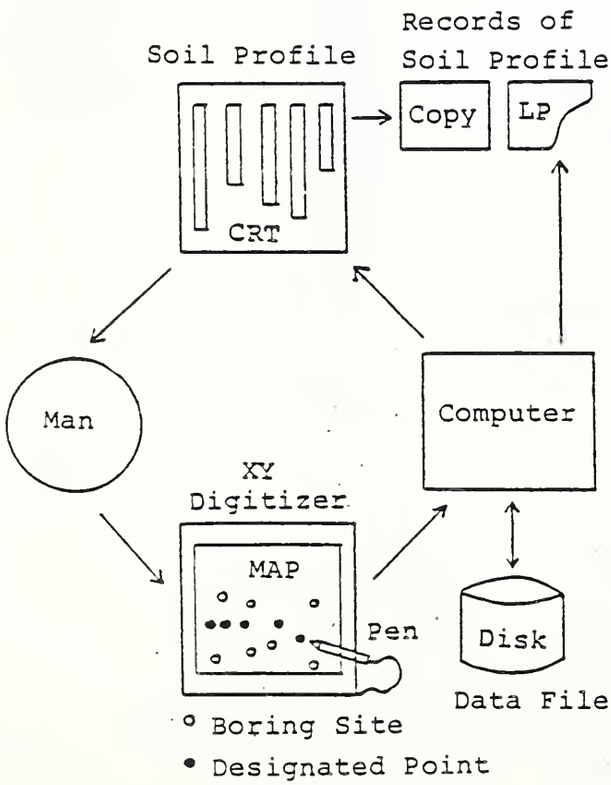

Fig.3 Man-machine interaction system

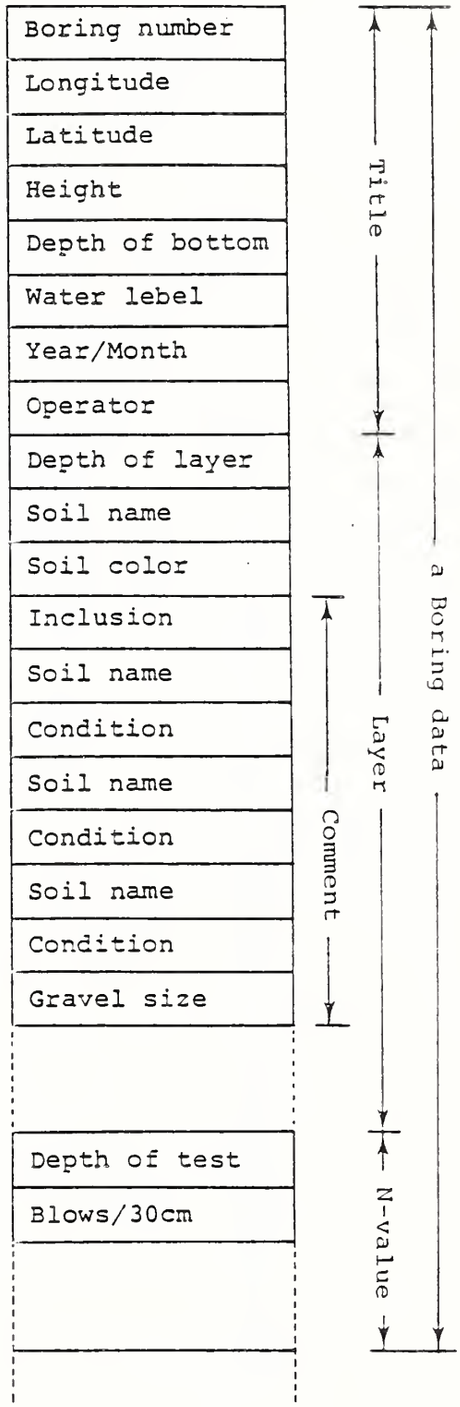

Fig.2 Data format in computer

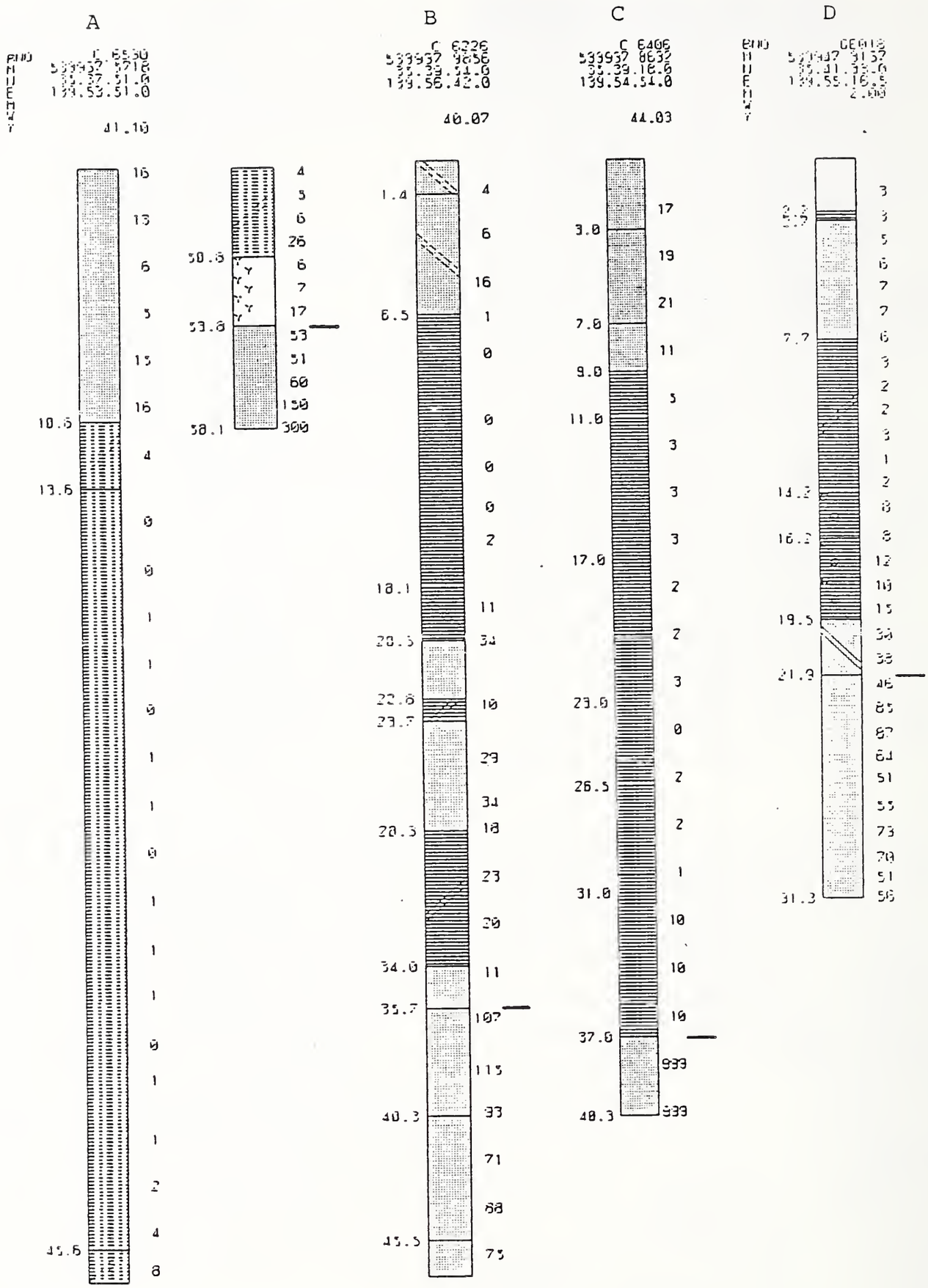

Fig.4 Columnar sections of soil at the observation points of microtremors

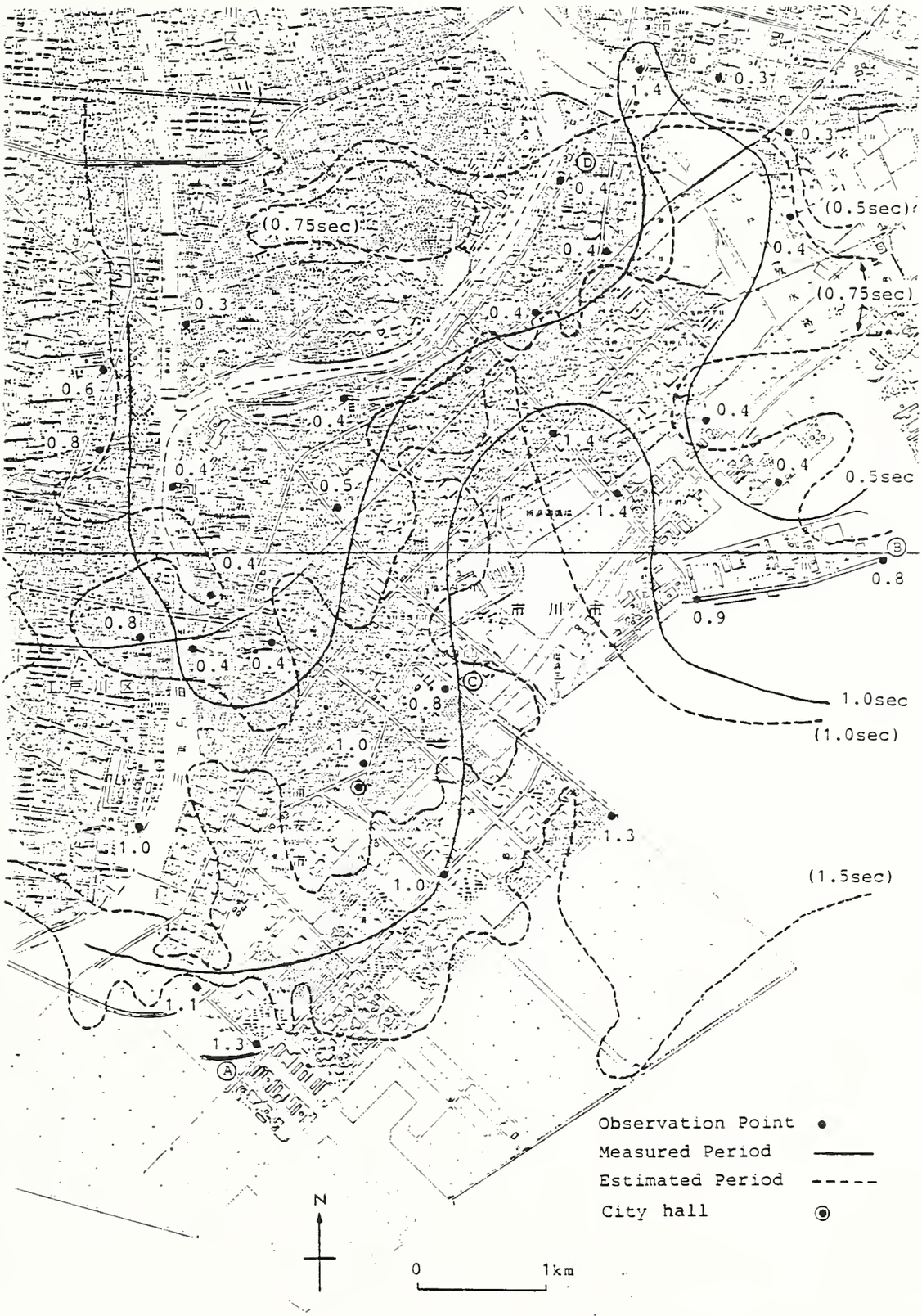

Fig.5 Predominant period of surface layer and observation points of microtremors (eastern neighbor of Tokyo)

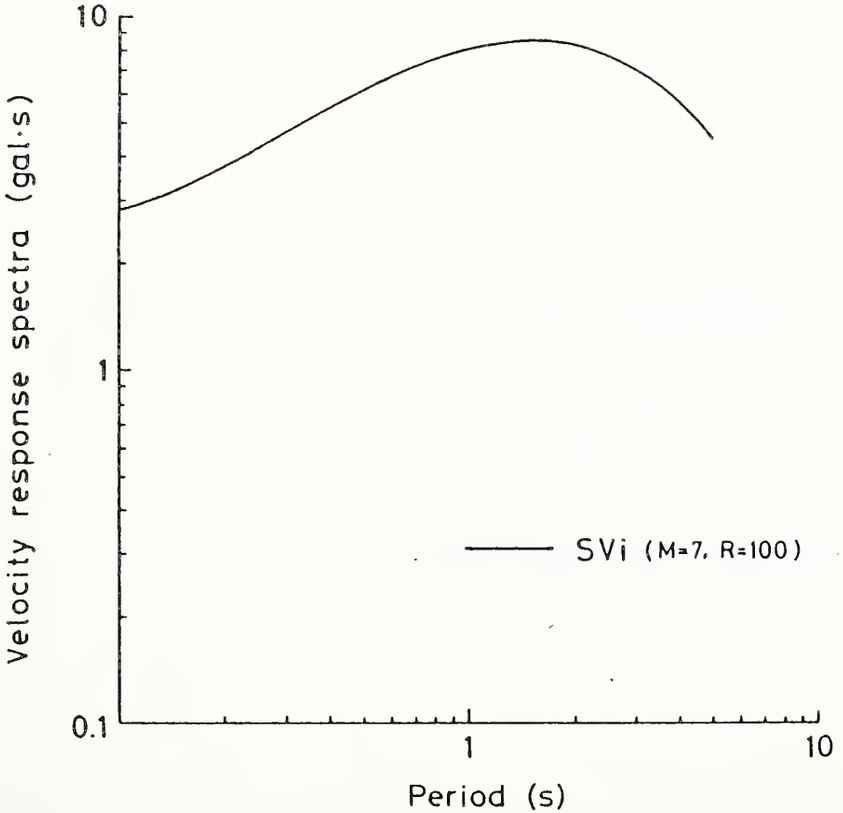

Fig.6 Estimated zero-damped velocity response spectra in the pre-Tertiary basement

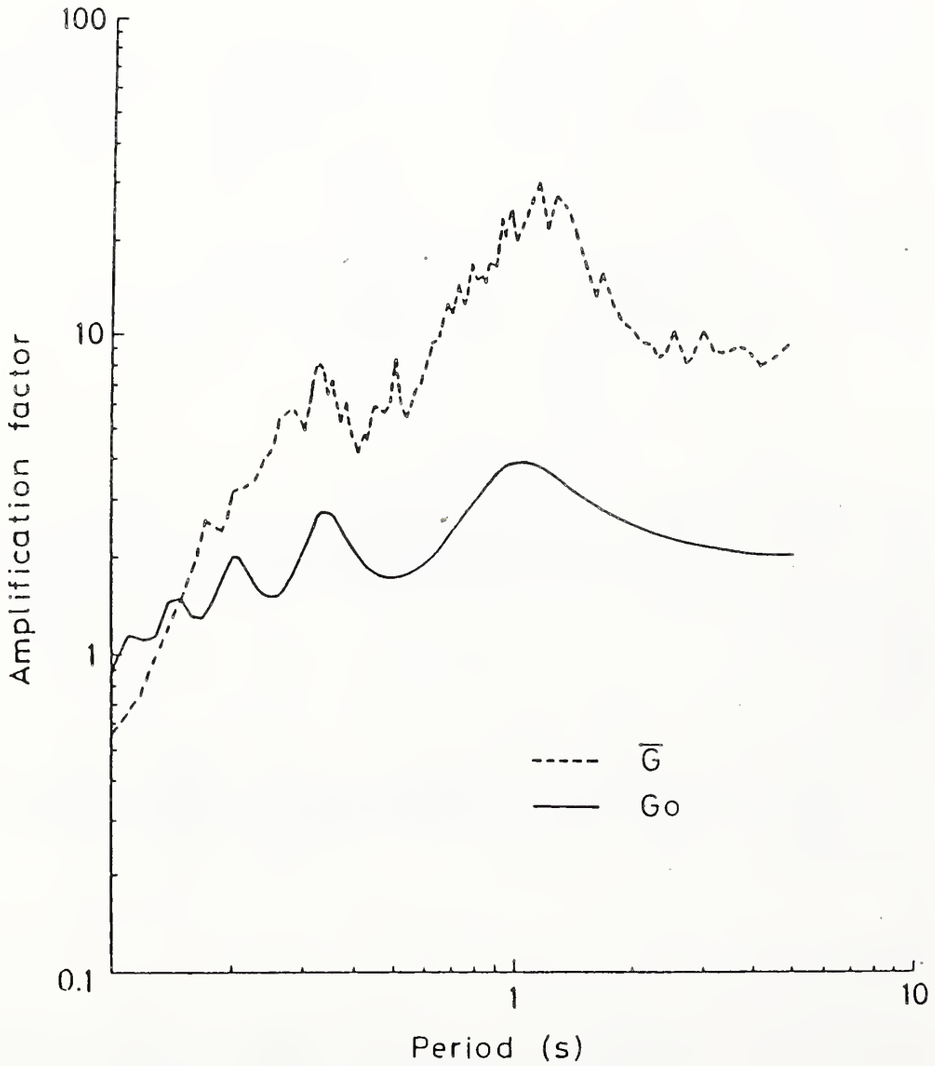

Fig.7 Average amplification characteristics of sedimentary layer and of surface layer at Urayasu city hall

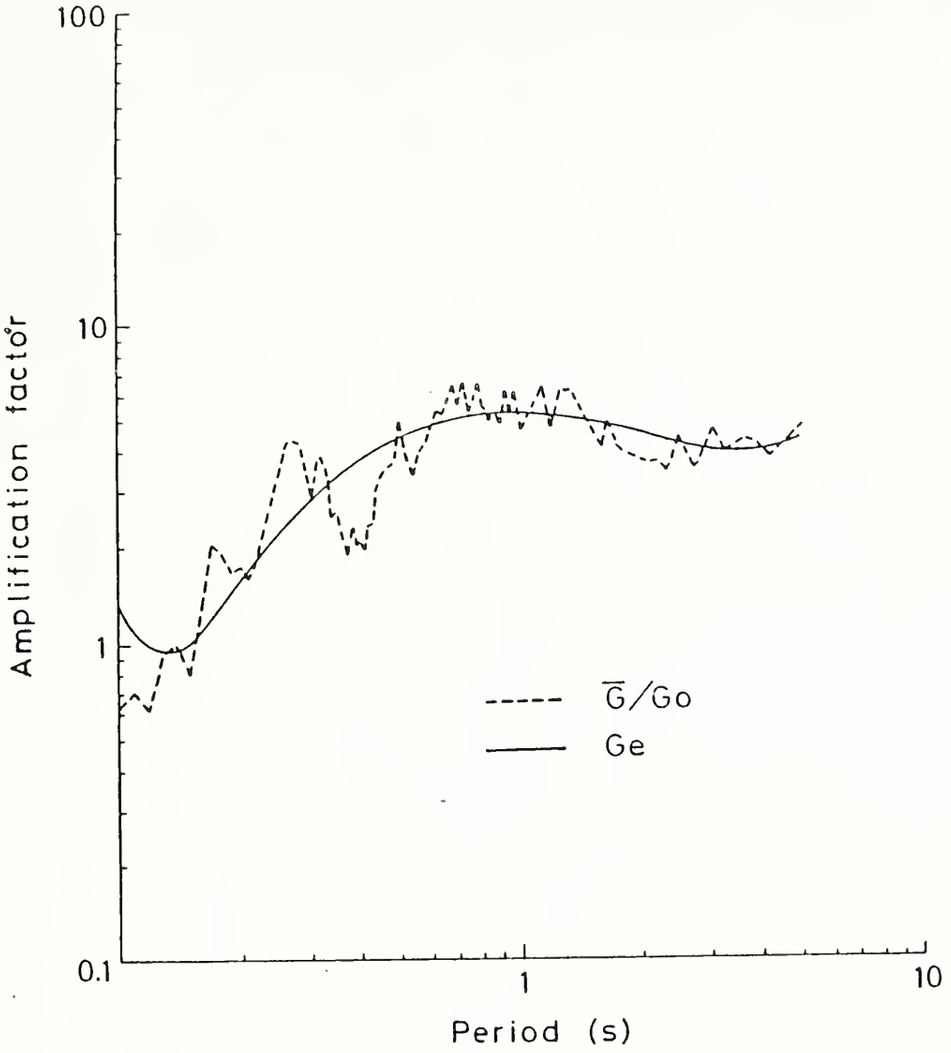

Fig.8 Average amplification characteristics of engineering bedrock

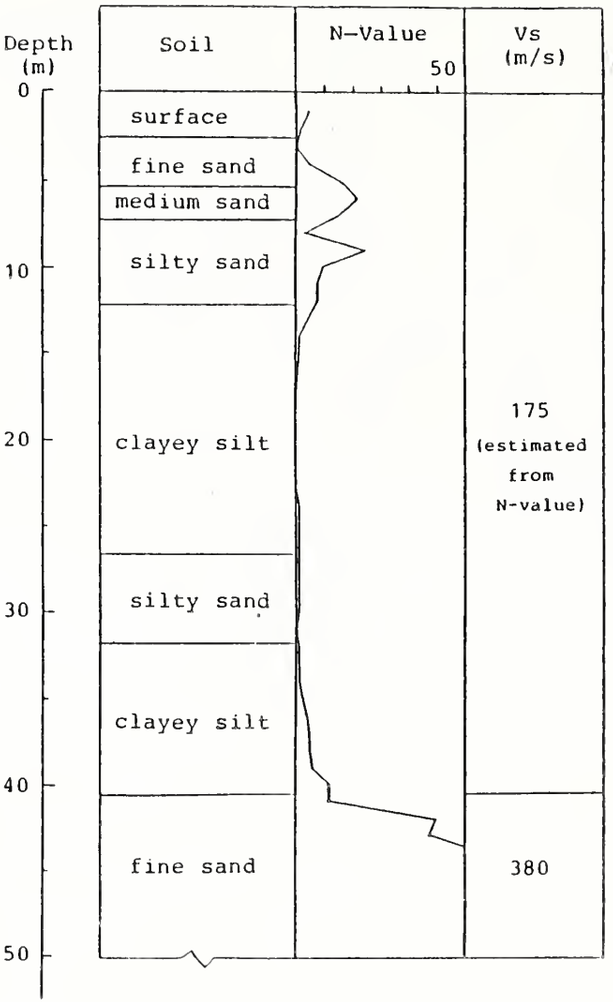

Fig.9 Soil profile at Urayasu city hall

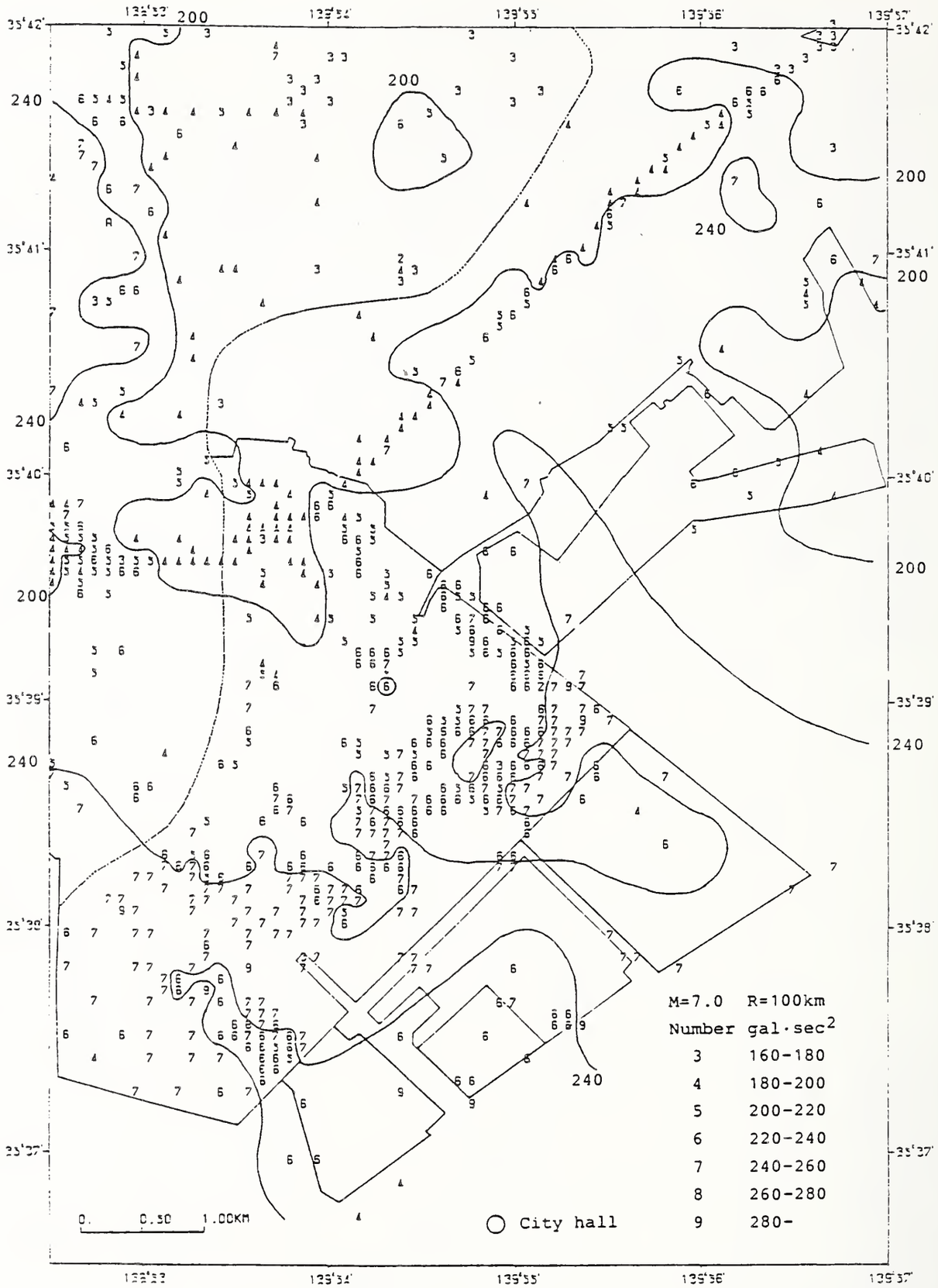

Fig.10 Regional distribution of spectral intensity

Simplified Evaluation Procedure of Seismic Stability of Embankments on Liquefiable Ground

by
Yasuyuki Koga[1] and Osamu Matsuo[2]

ABSTRACT

This paper presents a simplified procedure which evaluates the seismic stability of embankments constructed on sandy liquefiable ground without any complicated analysis. The procedure was made on the basis of 38 field data of the embankments which were damaged or not damaged by the earthquakes in Japan in the past several decades and the seismic stability analyses which were performed by the sliding method considering seismic force. The main concepts of the procedure are "critical N-value", "safety number" and "average safety number". The critical N-value was defined as an N-value of the ground which distinguish the seismic stability of embankment, the safety number as the ratio of the measured N-value to the critical N-value, and the average safety number as the average of the safety numbers calculated from the ground surface to a certain depth. The seismic stability of the embankment can finally be estimated by comparison of the minimum average safety number with unity.

Key words: seismic stability, embankment, liquefaction.

1. INTRODUCTION

The major earthquakes that occurred in the past several decades in Japan caused serious damages to many embankments on liquefiable sandy ground. With this background, it has recently become necessary that the seismic safety evaluation of earth structures such as river and road embankments be made. It is desirable that comprehensive stability analyses are applied to each embankment section on the basis of detailed soil data obtained from in-situ and laboratory tests. This is, however, almost impossible and impracticable from the viewpoint of cost performance because the total length of such embankments to be assessed is usually quite long. Therefore, it is required that a simplified procedure to evaluate the seismic stability of embankments be developed which can roughly select potentially dangerous sections of the whole embankments.

These kinds of procedures have been proposed to date by several official agencies in Japan[1]. However, it was considered from examinations that there is yet room for improvement in them on the mechanical rationality and the usability.

This paper presents a newly developed simplified procedure for seismic stability evaluation of embankments.

2. OUTLINE OF THE PROCEDURE

In this chapter, we will briefly describe a developing process and characteristics of the procedure in order to make it easy to comprehend.

Prior to developing the procedure, the authors considered the characteristics of the procedure as follows. It is expected that the procedure should be used to that the seismic stability can be evaluated using only soil data previously obtained, in order to evaluate point by point over a long embankment. On the other hand, it has been revealed that earthquake damages to river and road embankments is mainly due to the subsurface conditions.[2] Therefore, in order to expect the evaluation accuracy on the procedure, the subsurface field data are indispensable.

There are several types of methods of seismic stability evaluation of embankments as follows: (1) empirical method based on field performance data, (2) pseudo-static sliding surface method, and (3) method by dynamic response analysis.[1] Method (1) tends to be influenced by the field data which were used in producing the method, and not necessarily to correspond to mechanical rationality. On the contrary, methods (2) and (3) are not substantially appropriate as a "simplified method".

As a result of above consideration, the authors decided to make a simplified procedure which is a combination of methods (1) and (2) but not need a seismic stability analysis.

On the basis of the above mentioned considerations, the procedure was made according to the steps shown in Fig. 1. Firstly, details of the stability analysis method were determined so that it can distinguish failed and not failed embankments as much as possible, by applying the analysis method to them. Next, a comprehensive parametric study was performed on hypothetical embankment-ground models with various combinations of embankment-ground conditions and design seismicity. From this study, a "critical N-value" of sandy layer was summarized for various sandy soil types and design seismicity considered. This value can be used as a basic index to evaluate whether an embankment overlying on it is seismically stable or not. Then, the "average safety number"; a factor to directly evaluate the seismic stability of an embankment was proposed.

Finally, the evaluation procedure mentioned above was converted to a table for seismic stability evaluation of embankments in order to make it easy to use.

In conclusion, this procedure is such that all the required information are soil type and N-value of the subsurface ground and design seismicity.

3. DEVELOPMENT OF THE PROCEDURE

Developing process of the procedure will be described in the followings according to the flow chart shown in Fig. 1.

---

1 Head, Soil Dynamics Division, Construction Method and Equipment Department, Public Works Research Institute, Ministry of Construction, Japan.
2 Senior Research Engineer, Soil Dynamics Division, Construction Method and Equipment Department, Public Works Research Institute, Ministry of Construction, Japan.

3.1 Case Records of Seismically Damaged Embankments

Among case records of seismically damaged embankments during past earthquakes such records were collected that the damages were clearly described, the borings data and SPT-N-value data were obtained, and also the subsurface ground mainly consists of sandy soil.

Total number of the embankments was 38; 3 of the Niigata Earthquake of 1964, 14 of the Miyagi-ken-oki Earthquake of 1978, 21 of the Nihon-kai-chubu Earthquake of 1983.

They all were river embankments with a height of 2–7m, and settlements caused by earthquakes ranged from 0 to 2 m.

3.2 Seismic Stability Analysis

3.2.1 Description of Analysis

The circular sliding method considering seismic effect was used in the seismic stability analysis of the embankments. Modified-Fellenius method expressed by effective stress strength was adopted. In calculating a factor of safety, the effect of earthquake was taken into account in two ways. One is that seismic effect is considered as a seismic force (Eq.(1)), the other as a decrease of shear strength due to a generation of excess pore-water pressure in a sandy layer of the ground during earthquake (Eq.(2));

$$F_{s1}=\frac{\Sigma\{c'\cdot\ell+(W-u_0\cdot b)\cos\alpha\cdot\tan\phi'\}}{\Sigma(W\cdot\sin\alpha+k_h\cdot W\cdot y/R)} \quad \cdots\cdots (1)$$

$$F_{s2}=\frac{\Sigma\{c'\cdot\ell+\{W-(u_0+u_d)\cdot b\}\cos\alpha\cdot\tan\phi'\}}{\Sigma(W\cdot\sin\alpha)} \quad \cdots\cdots (2)$$

where,
- F_s : factor of safety
- c', ϕ' : effective stress shear strength parameters
- W : weight of slice
- u_0 : hydrostatic pressure
- u_d : excess pore-water pressure generated by cyclic shear stress during an earthquake
- k_h : horizontal seismic coefficient
- ℓ : length of sliding arc of slice
- b : width of slice
- α : angle of sliding arc to the horizontal plane
- y : vertical distance between the center of circle and the center of gravity of slice
- R : radius of sliding circle (see Fig. 2)

For each embankment two factors of safety were calculated by Eqs. (1) and (2), and the smaller one was finally adopted.

The procedure to compute the factor of safety is shown in Fig. 3. In the figure the following Meyerhof's formula was used to relate the N-value to the relative density D_r^* .

$$D_r^*=21\sqrt{N/(\sigma_v'+0.7)} \quad \cdots\cdots (3)$$

in which σ_v' is effective vertical stress in kgf/cm^2 .[3]

Mechanical and physical properties of sandy soils were assumed as in Table 1, and those of clayey soils were assumed as follows: unit weight $\gamma_t=1.5\ tf/m^3$, shear strength parameters $\phi=0°$ and $c_u=q_u/2=0.2+N/40$ (kgf/cm^2) (Ohsaki's formula). On the other hand, the properties of embankment material were given as $\gamma_t=1.8\ tf/m^3$, $c=2.0\ tf/m^2$ and $\phi=25°$ regardless of the soil type.

Seismic coefficient value k_h was determined from the maximum acceleration at ground surface, α_{smax} (gal), which were estimated based on the ground motion records taken in the neighborhood. It follows:

$$\left.\begin{aligned} k_s&=\alpha_{smax}/g\\ k_h&=0.65\times k_s\end{aligned}\right\} \quad \cdots\cdots (4)$$

where g is the acceleration of gravity (= 980 gals) and k_s is the peak (instant) seismic coefficient of ground surface.

To estimate the dynamic shear strength ratio, R, of the sandy soils, the two empirical methods, by the Specifications for Highway Bridges in Japan (SHB-method)[4] and by Tokimatsu and Yoshimi (T-Y-method)[5] were used. It is well known that for denser sand the former method estimates the ratio R smaller than the latter one. In addition, the excess pore-water pressure ratio u_d/σ_v' was given by

$$\left.\begin{aligned} u_d/\sigma_v'&=F_L^{-7} \quad (F_L\geqq 1)\\ u_d/\sigma_v'&=1 \quad (F_L<1)\end{aligned}\right\} \quad \cdots\cdots (5)$$

where F_L is the liquefaction resistance factor which is a ratio of the shear strength ratio R to the shear stress ratio during earthquake L.[6]

3.2.2 Results and Discussions

Fig. 4 shows the relationship between the factors of safety given by the analyses and the observed settlements for 38 embankments. Figs. (a) and (b) correspond to the SHB-method and the T-Y-method respectively.

In either method, there is a general tendency that the factor of safety F_s decreases as the settlement D increases, although the data plots are considerably scattered. When F_s is equal to F_{s2} (see Eq. (2)), the value F_s is small and it can be supposed that there would have been a build-up of pore-water pressure within the sand layer, possibly leading to the liquefaction. By comparing the data of $F_s=F_{s2}$ in the two figures it can be seen that the factors of safety in Fig. 4(a) are smaller than those in Fig. 4(b). It reflects that the SHB-method of Fig. 4(a) tends to estimate the dynamic shear strength ratio R smaller.

Now, let us examine quantitatively as to which method has resulted in a better agreement between the factors of safety and the settlements of the damaged embankments. It may well be approved to define "compatible" and "not-compatible" as shown in Fig. 5. In the figure the horizontal line, $D=D_0$ is supposed to divide data with significant damages and with insignificant or without damages. Therefore, D_0 may be called "critical settlement". Similarly, the vertical line, $F_s=F_{s0}$, in the figure is supposed to distinguish the two data groups appropriately; the value of F_{s0} may be called "critical factor of safety." It might be appropriate that the value of D_0 be determined from such engineering judgment as the maximum settlement under which the damaged embankment can keep its original function. On the other hand, the value of F_{s0} is usually assumed as $F_{s0}=1.0$ However, this is reasonable only if the seismic stability analysis method and parameters applied are considered as mechanically reasonable. Thus, we should not hold

that $F_{S0} = 1.0$ in this case, because the rationality of the analysis method described above has not been verified.

An index parameter expressed as Eq.(6) was used to evaluate and compare the degree of compatibility of the results as shown in Fig. 5.

$$I_C = \frac{N_A}{N_A + N_C} \times \frac{N_B}{N_B + N_D} \quad \cdots\cdots (6)$$

where, I_C = index parameter of compatibility,
N_i = number of data plotted in region i,
Subscript A,B,C,D = region shown in Fig. 5.

Parameter I_C is a function of F_{S0} and D_0, and the value of F_{S0} and D_0 were determined so that the value of I_C takes a maximum. The results are summarized in Table 2. It is seen from the table that the index parameter of compatibility I_C is larger in (b) compared with that in (a), where $D_0 = 20\,cm$ and $F_{S0} = 0.8$.

The resultant D_0-value of 20 cm is considered to be reasonable for river and road embankments as a safer value to keep their original functions. In addition, the resultant F_{S0}-value of 0.8 coincide well with a result by the authors[7] that the critical factor of safety computed by Eq.(2) is smaller than unity. Also shown in a right column of Table 2 is a percentage of compatibility P_C that is commonly used ans is given by:

$$P_C = \frac{N_A + N_B}{N_A + N_B + N_C + N_D} \quad \cdots\cdots (7)$$

In this case, this P_C was not directly used as a measure to compare the propriety of the two methods described above. It is because the case records studied herein are not necessarily a subset of the population by a random sampling but a subset which has a deviation towards the set of significantly damaged embankments. Therefore, it was presumed that, if we use Eq. (7) to compare the proprieties of the two methods, it might lead to a statistically wrong judgment. On the contrary Eq. (6) would lead to a correct judgment even in this case. In this point of view, it is concluded from the result shown in Table 2 that the T-Y-methos is more adequate than the SHB-method to evaluate the dynamic shear strength ratio R of sandy soil, and only the T-Y-method will be used below.

3.3 Critical N-value

In this part a "critical N-value" is proposed, which will be a basic factor to judge the seismic stability of an embankment by compared with a measure N-value of the sandy deposit at a depth. The critical N-value of the sandy deposit is determined corresponding to the soil type, the design earthquake intensity and the depth, and if a measured N-value is lower than the critical N-value the deposit is considered to make the overlying embankment seismically unsafe, and vice versa.

3.3.1 Model Studies

In order to make up the critical N-value, a set of model studies were performed with the hypothetical embankment-ground model illustrated in Fig. 6. The studies consisted of more than a hundred cases of seismic stability analyses with the model and various combinations of factors shown in Fig. 6 which are known to affect the seismic stability of embankment. From the model studies a set of critical N-values was compiled and its sensitivity to such factors was examined.

3.3.2 Results

Only the final result is described below as the process to derive the critical N-value was rather complicated. For the standard model with an embankment height of 4m and an ground water level of 1m below the surface as in Fig. 6, the critical N-value was given approximately as:

$$N_{Cr} = (3.03 + 0.37 \cdot z) \times \left(\frac{C \cdot k_S - D}{A \cdot k_S - B}\right)^2 \quad \cdots\cdots (8)$$

in which z is a depth from ground surface and A, B, C and D are constants relevant to soil type (exact values of the constants will be shown in Table 3).

Fig. 7 illustrates an example of the results. It is evident in the figure that the critical N-value increases with design seismicity k_h, depth z and coarser grained sandy soil. As for another factors, it was confirmed that as the embankment height and the depth of ground water level increases the critical N-value increases: however, they were not so sensitive as the above factors.

3.4 Average Safety Number

The critical N-value was derived from the above studies under the condition that the soil type of the ground was uniform over the whole depth. But the actual ground consists of various soil layers. Therefore, it is not necessarily easy to judge the seismic stability of an embankment only by comparing measured N-value and critical N-value at each depth. Fig. 8 illustrates this. In the case of (a) and (b) in the figure it is easy to judge as "safe" and "unsafe" respectively, because the measured N-values are greater or smaller than the critical N-values over the whole depth. On the other hand, it is difficult in the case of (c) to judge, although it is a common case. Thus, in order to enable to judge the seismic stability of an embankment in a quantitative manner even in such case as (c), an "average safety number" was contrived as a measure for judgment.

3.4.1 Definitions

The safety number N_s and the average safety number $\overline{N_s}$ were defined as:

$$N_s = N / N_{Cr} \quad \cdots\cdots (9)$$

$$\overline{N_s} = \left(\sum_{i=1}^{z} N_s\right) / z \quad \cdots\cdots (10)$$

3.4.2 Studies

A comprehensive studies were performed on how to determine the average safety number $\overline{N_s}$ as defined by Eq. (10), considering such factors as:

(1) The maximum of safety number N_s
(2) Safety number N_s of non-sandy soils such as silt and clay (; for such soils critical N-value ,Ncr, could not be determined because they are not susceptible to liquefaction)
(3) Depth within which the safety number is considered
(4) Corrections for the embankment height and the ground water level

The manners to calculate $\overline{N_S}$ were examined for 17 cases of combinations of these factors. Thus, the best way to calculate $\overline{N_S}$ so that $\overline{N_S}$ can represent a factor of safety computed by the stability analysis was found out. Comparisons of the cases were made based on Eq. (6).

3.4.3 Results

As a result, the best way to calculate $\overline{N_S}$ was given as follows:

(1) The value $\overline{N_S}$ should be calculated as an arithmetic mean of Ns of every 1m below water table up to the depth where $\overline{N_S}$ gets minimum. This is given by:

$$(\overline{N_S})_{min} = \min_{z} \left[\left(\sum_{i=1}^{z} N_S \right) / z \right] \quad \cdots\cdots\cdots\cdots (11)$$

(2) For silt or clay, $\overline{N_S}$ should be equal to 2.0 regardless of its N-value.

(3) The upper limit of $\overline{N_S}$ for sandy soil should be 3.0.

(4) By using $\overline{N_S}$ as calculated as above, the seismic stability of an embankment will be judged as follows:

$(\overline{N_S})_{min} < 0.8$: "unsafe"
$0.8 \leqq (\overline{N_S})_{min} < 1.0$: "possibly unsafe"
$1.0 \leqq (\overline{N_S})_{min}$: "safe"

Figs. 9 and 10 show the relationship between the average safety number and the factor of safety and that between the average safety number and the observed settlement, respectively. In both figures also shown is the percentage of compatibility P_C as calculated by Eq. (7). From these results it can be concluded that the average safety number calculated by the method described above is in good consistency with the factor of safety and the observed settlement from practical point of view.

4. SIMPLIFIED EVALUATION TABLE OF SEISMIC STABILITY OF EMBANKMENT

For the purpose of making it easy to apply the simplified method to evaluate the seismic stability of embankment described in the previous chapter, Table 3 was provided. This table is so designed that by filling in the banks in the order of the number we can automatically get the result. In addition, it whould be noted that the conditions of application described in the upper part of the table must be kept, which were duduced in the developing process of the method.

5. SUMMARY

A simplified procedure to evaluate the seismic stability of embankments was proposed on the basis of comprehensive seismic stability analyses of embankments that experienced severe earthquakes in the past. The procedure is such that the seismic stability can be evaluated by judging whether the minimum average safety number is greater or smaller than unity. Finally it was shown that the judgments by using the procedure agreed fairly well with the past field performance data.

References

1) Sasaki, Y., Koga, Y. and Taniguchi, E.: Earthquake resistant design of earth structures, Technical Note of Soil Dynamics Division No. 34, Soil Dynamics Division, Public Works Research Institute, April, 1984.
2) Public Works Research Institute: Report on the disaster caused by the Nihon-kai-chubu earthquake of 1983, Report of PWRI, Vol. 165, March, 1985 (in Japanese).
3) Meyerhof, G.G.: Discussion, Proc. 4th ICSMFE, Vol. 3, p. 110, 1957.
4) Japan Road Association: Specifications for Highway Bridges, Part V, Earthquake Resistant Design, pp 16~20 and pp. 69~75, May, 1980 (in Japanese).
5) Tokimatsu, K. and Yoshimi, Y.: Empirical correlation of soil liquefaction based on SPT N-value and fines content, Soils and Foundations, Vol. 23, No. 4, pp 56~74, JSSMFE, 1983.
6) Japan Road Association: Technical Guideline for Designing of Common Utility Duct, 1986 (in Japanese).
7) Koga, Y. and Matsuo, O.: Considerations on dynamic strengths of soil used in seismic stability analysis, Proceedings of the 21st Annual Convention of JSSMFE, pp. 867~870, June, 1986 (in Japanese).

Table 1 Properties for Sandy Soils

(a) Mechanical properties

SPT N-value	ϕ' (°)	c' (tf/m^2)
$N \leqq 10$	30	0
$10 < N \leqq 30$	35	0
$30 < N$	40	0

(b) Physical properties

Soil type	γ_t (tf/m^3)	γ_{sat} (tf/m^3)	D_{50} (mm)
Sandy silt	1.6	1.8	0.04
Fine grained sand	1.75	1.95	0.15
Medium sand	1.8	2.0	0.35
Coarse grained sand	1.8	2.0	0.6

Table 2 Summary of Compatibilities

Evaluation method of dynamic shear strength ratio R	Do (cm)	Fso	$\frac{N_A}{N_A+N_C}$	$\frac{N_B}{N_B+N_D}$	Ic *	Rc **
(a) "Specifications for Highway Bridges" method	30	0.2	$\frac{11}{11+10}$	$\frac{16}{16+1}$	0.49	0.71
(b) Tokimatsu-Yoshimi method	20	0.8	$\frac{11}{11+3}$	$\frac{16}{16+8}$	0.53	0.71

*) see Eq. (6), **) see Eq. (7)

Table 3 Table for Simplified Evaluation of Seismic Stability of Embankment on Sandy Deposit

Site:		
1 Max. Seismic Coef. Ks =	Embankment Hight H = (m)	Ground Water Depth Hw = (m)

≪ Conditions of Application ≫ (1) The ground mainly consists of sandy deposits.
(2) Max. seismic coefficient of ground surface, Ks, is 0.1 ~ 0.3.
(3) Embankment height, H, is 2 ~ 6m.
(4) Ground water level below ground surface, Hw, is 0 ~ 2m.

Depth from G.L. (m)	2 Depth from W.L. L (m)	3 Soil Type	4 Standardized Critical N-value (N_{cr})	5 Correction Factor	6 Corrected Critical N-value	7 Measured N-value (N)	8 Safety Number (Ns)	9 Average Safety Number ($\bar{N}s$)
1			3.4					
2			3.8					
3			4.1					
4			4.5					
5			4.9					
6			5.2					
7			5.6					
8			6.0					
9			6.4					
10			6.7					

≪ Remarks ≫ 1 $Ks = As_{max}/g$ (As_{max}: max. ground acc., g: acc. of gravity)
$Kh = 0.65 \times Ks$ (Kh: design seismic coefficient)
2 L is to be measured from the ground water level
3 Soil types and the corresponding mean grain size (D_{50}) are as follows:

Soil type	Clay, silt	Sandy silt	Silty fine-grained sand	Fine sand	Medium sand	Coarse sand
D_{50} (mm)	——	0.04	0.07	0.15	0.35	0.60

5 Correction factor

• Sandy silt	$: \left(\frac{65Ks - 10.3}{41Ks - 5.3}\right)^2 =$	
• Silty fine-grained sand	$: \left(\frac{72Ks - 10.4}{41Ks - 4.3}\right)^2 =$	
• Fine sand	$: \left(\frac{85Ks - 10.5}{41Ks - 2.7}\right)^2 =$	
• Medium sand	$: \left(\frac{138Ks - 6.3}{41Ks + 6.6}\right)^2 =$	
• Coarse sand	$: \left(\frac{244Ks - 1.7}{41Ks + 24.3}\right)^2 =$	

6 (Corrected Critical N-value) = (Standardized N-value) x (Correction Factor)
8 (Safety Number Ns) = (Measured N-value)/(Corrected Critical N-value).
For sandy soils, if calculated Ns is greater than 3.0, Ns should be equal to 3.0.
For clay and silt (except for sandy silt), Ns = 2.0
For depth above the ground water level, calculation of Ns is not needed.

9 $\bar{N}_s = \sum_{i=1}^{L} (N_s) \div L$

10 Minimum of average safety number : $\bar{N}_s' = \min_{L} (\bar{N}_s)$

10 Minimum of Average Safety Number	$\bar{N}_s'$	Judgment	Final Result
$\bar{N}_s' =$ ⇨	$\bar{N}_s' < 0.8$	Unstable	
	$0.8 \leqq \bar{N}_s' < 1.0$	Possibly unstable	
	$1.0 \leqq \bar{N}_s'$	Stable	

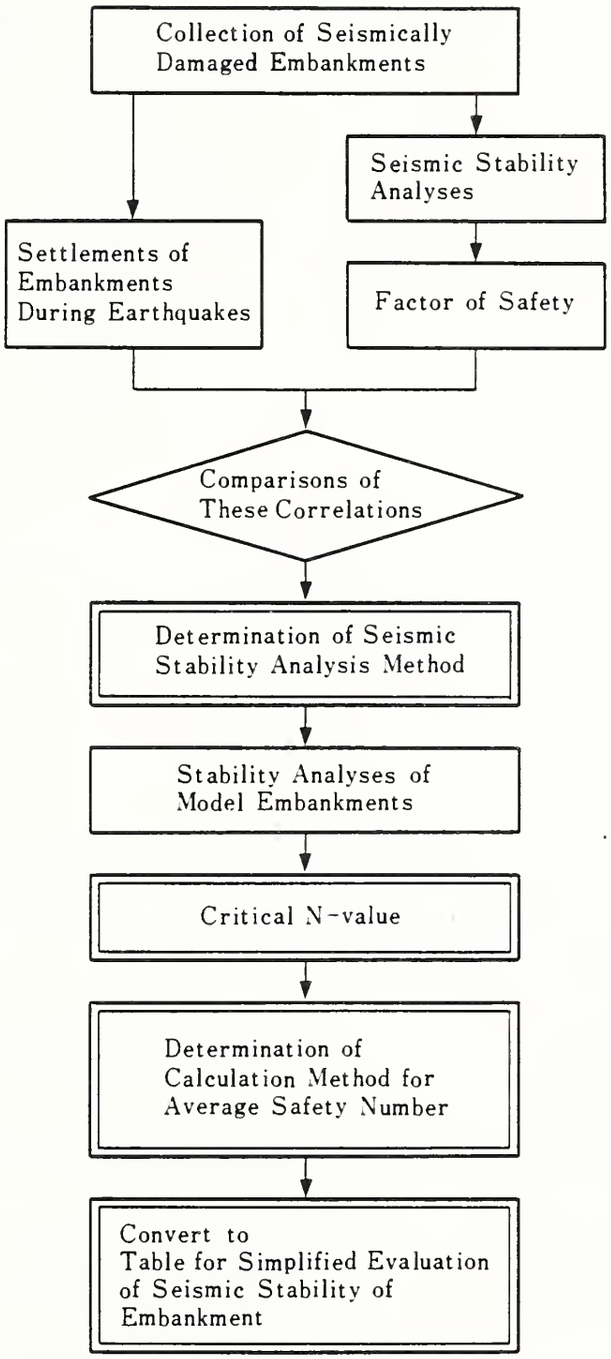

Fig. 1 Flow Chart of Producing Simplified Procedure to Evaluate Seismic Stability of Embankment

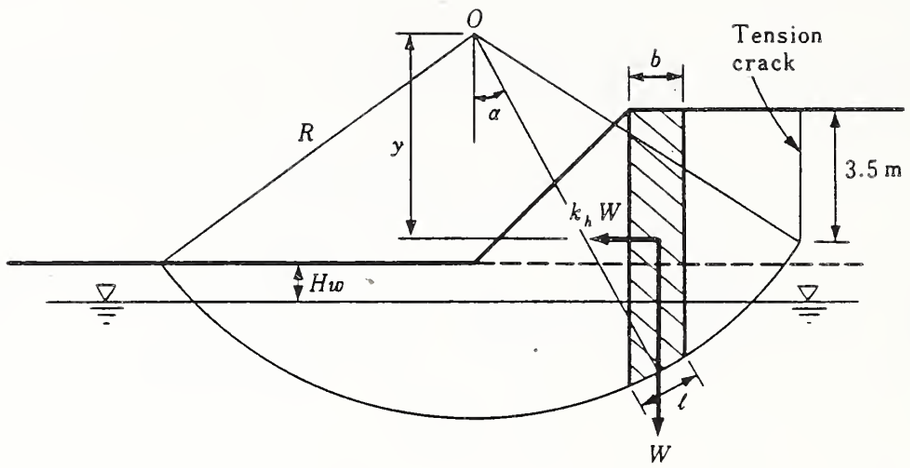

Fig. 2 Key Sketch for the Circular Sliding Method in the Seismic Stability Analysis

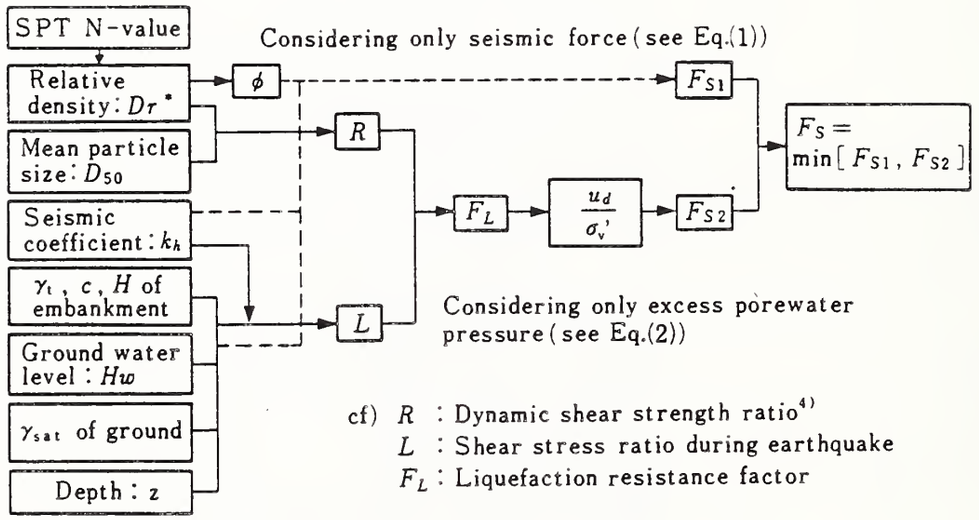

Fig. 3 Flow Chart to Compute Factor of Safety

(a) Dynamic shear strength ratio R of sandy soil evaluated by the "Specifications for Highway Bridges" method[4] was applied

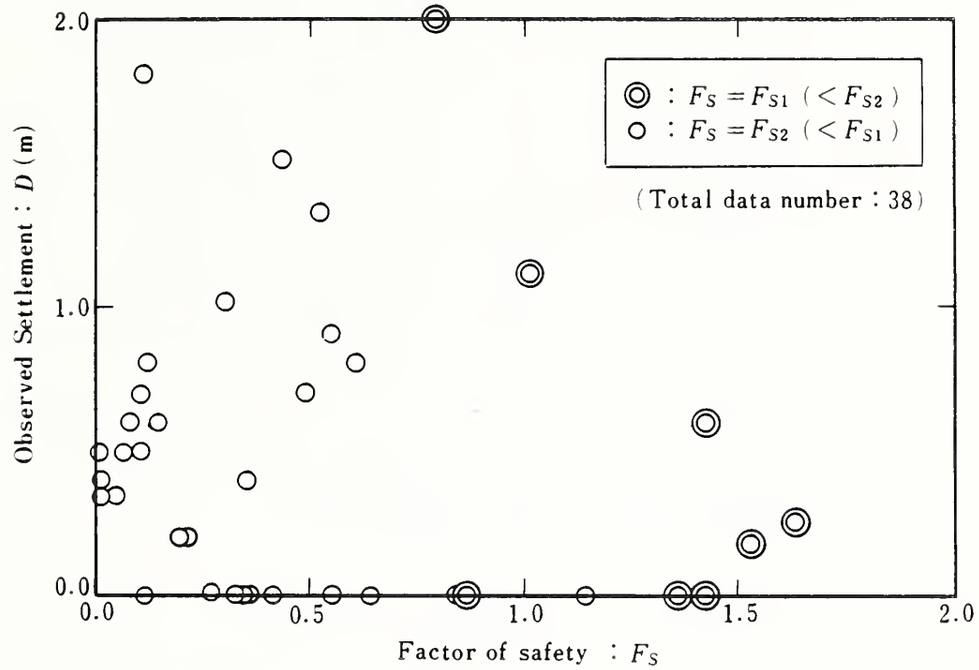

(b) Dynamic shear strength ratio R of sandy soil evaluated by the Tokimatsu-Yoshimi method[5] was applied

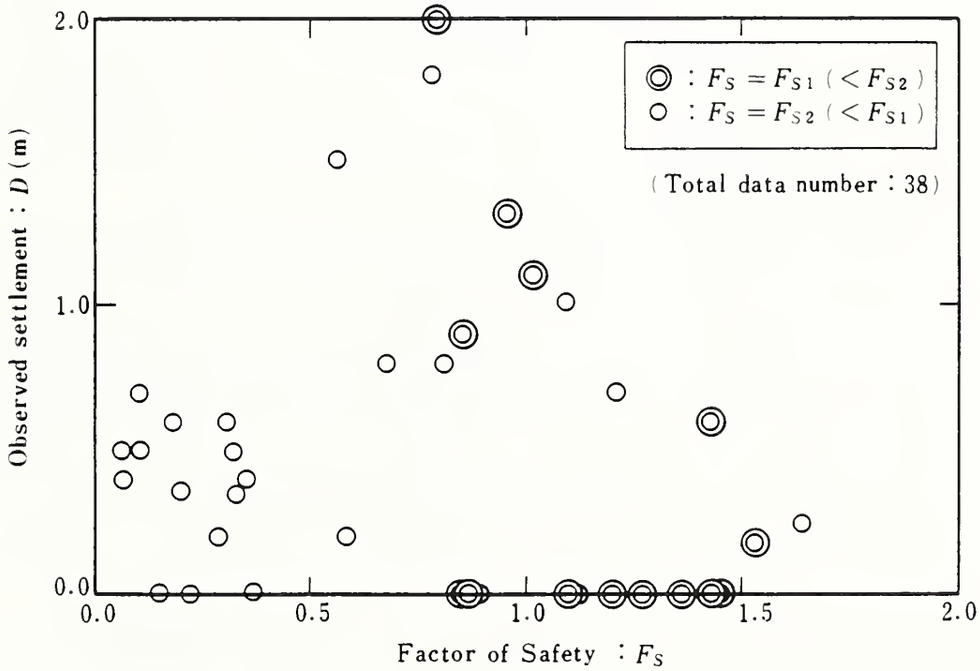

Fig. 4 Relationships Between Observed Settlements and Computed Factors of Safety

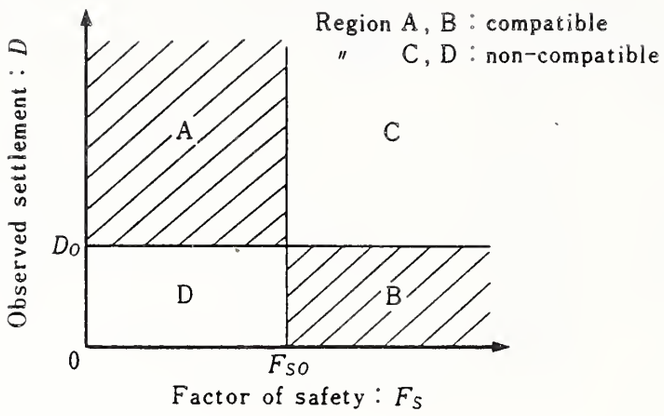

Fig. 5 Key Sketch for Evaluating Degree of Compatibility Between Observed Settlements and Factors of Safety

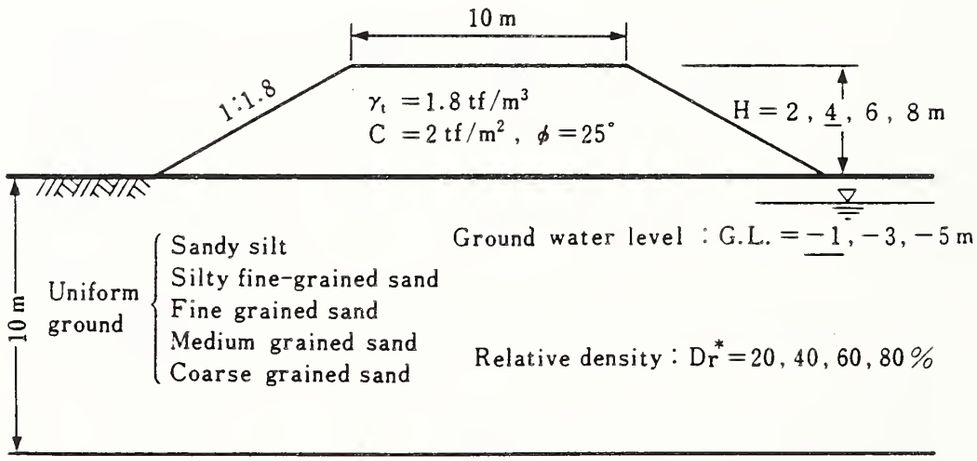

cf) The underlined indicates the standard value in a set of calculation.

Fig. 6 Hypothetical Analysis Model

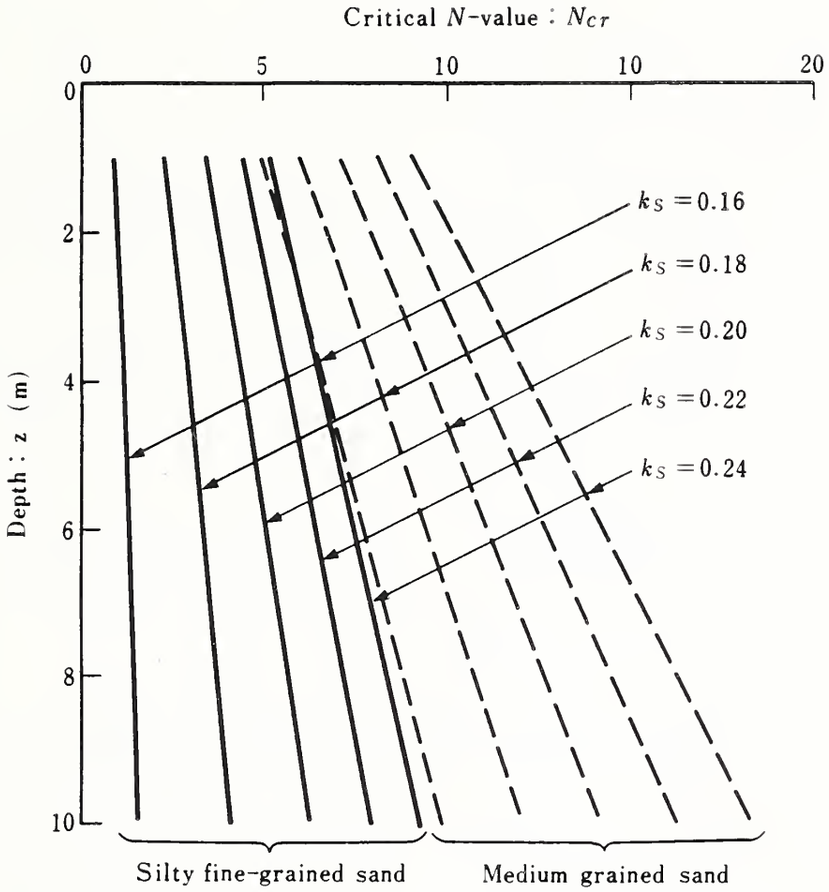

Fig. 7 Illustration of Critical N-value

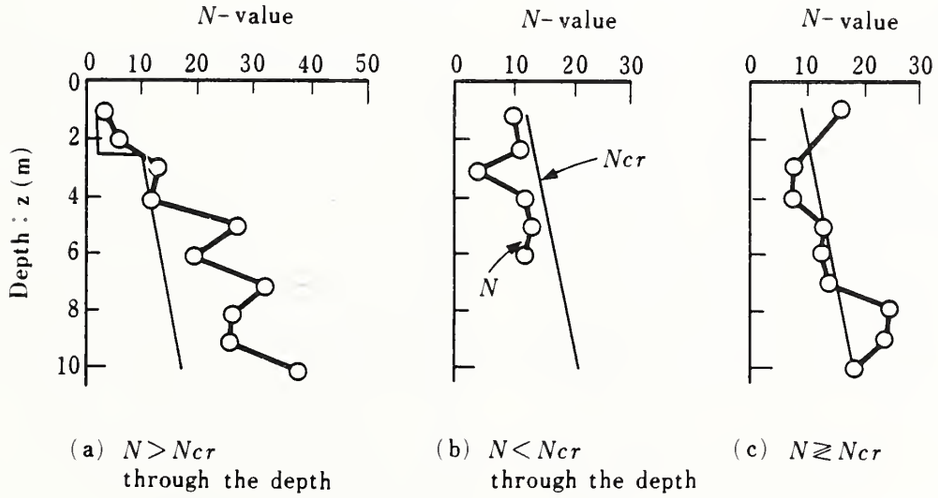

(a) $N > Ncr$ through the depth

(b) $N < Ncr$ through the depth

(c) $N \gtrless Ncr$

Fig. 8 Examples on Comparison of Observed and Critical N-value

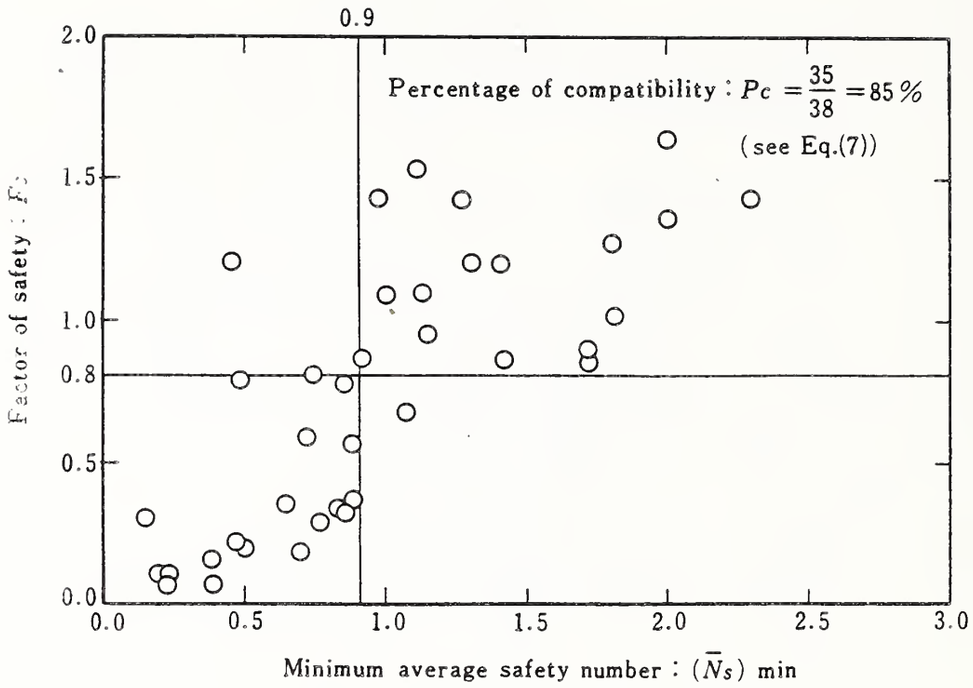

Fig. 9 Correlation Between Minimum Average Safety Number and Factor of Safety

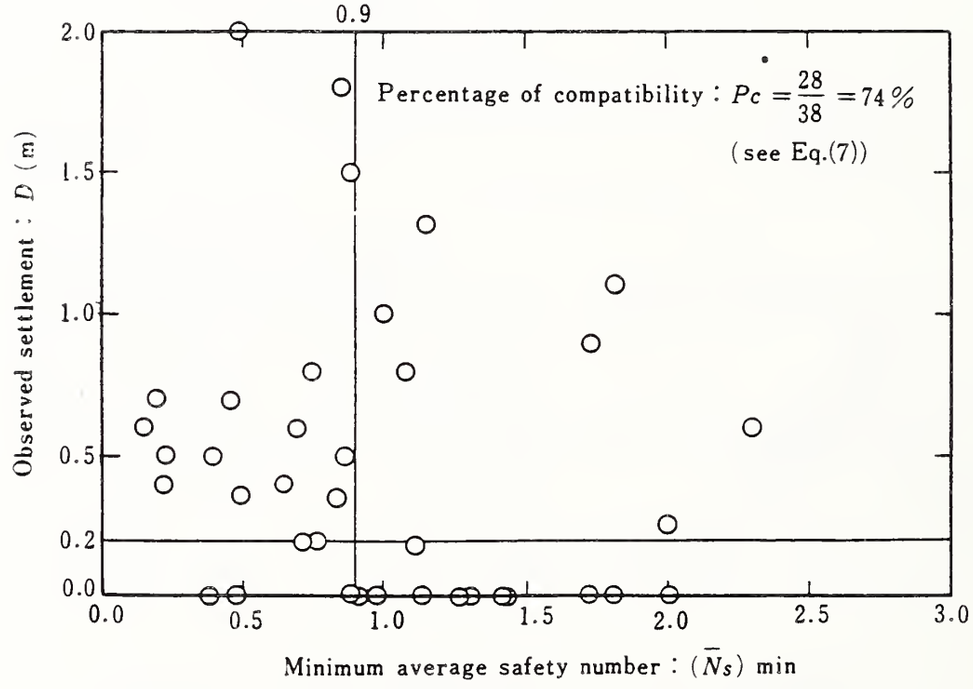

Fig. 10 Correlation Between Minimum Average Safety Number and Observed Settlement

Strong Motion Observation System of PWRI

Toshio IWASAKI*, Yasushi SASAKI** and Tetsuro KUWABARA***

SUMMARY

This report presents the Strong Motion Observation System of PWRI (Public Works Research Institute) as a continued report of the PWRI's Dense Instrument Array Observation System previously presented at the 18th Joint Meeting.

This report will cover the observation stations where PWRI is collecting data, data base system in which strong motion observation data collected up to now are recorded, digitizing method for analog records, and the situation of data utilization up to now.

KEY WORDS: Civil Engineering Structure, Earthquake Resistant Design, Strong Motion Observation, Strong Earthquake Motion Record, Data Base

1. INTRODUCTION

Strong motion accelerographs have been installed on civil engineering structures related to the Ministry of Construction at 291 places and the total number of accelerograph is 698 as of March, 1987. Strong motion earthquake records of 7,992 components from 669 earthquakes have been obtained after 1965 when the real strong motion observation was started. Among these records, 1,102 components have been digitized and being used for various kinds of analyses.

The strong motion observation means, in a narrow sense, the measurements of the vibration waveforms and amplitudes (normally acceleration) of strong earthquakes by means of strong motion accelerographs installed on the ground and structures and also the primary analyses of the characteristics of the magnitude of their acceleration amplitude and vibration period. In a broad sense, the strong motion observation will include secondary analyses in which correlations are examined among the earthquake motion characteristics such as the characteristics of magnitude of acceleration amplitude and vibration period obtained from primary analyses, the characteristics of earthquake mechanism including the magnitude of earthquake and focal depth, the propagation passage characteristics such as epicentral distance, topography and ground conditions, and the structural characteristics by type and scale of structures and by kind of structural materials. In a country like Japan where the earthquake activities are very vigorous, the strong motion observation will greatly contribute to the rationalization of the earthquake resistant design of civil engineering structures, to the safe and economical construction of ever-diversifying and scale-increasing structures and also to supply basic data for formulating earthquake disaster prevention measures by region and by topography and ground conditions.

This report will present PWRI's Strong Motion Observation System as a continued report of "Dense Instrument Array System by PWRI for Observing Strong Earthquake Motion" previously presented at the 18th Joint Meeting. This report will cover the observation stations where PWRI is collecting data, data base system in which strong motion observation data collected up to now are recorded, digitizing method for analog records, and the situation of data utilization up to now.

2. PROGRESS OF STRONG MOTION OBSERVATION BY THE MINISTRY OF CONSTRUCTION

The Strong Motion Observation by the Ministry of Construction is carried out by PWRI for civil engineering structures and also by Building Research Institute for buildings respectively. Fig. 1 shows the outline of PWRI's Strong Motion Observation System. As the strong motion observation for civil engineering structures, a SMAC-A type strong motion accelerograph was first installed at the Sarutani Dam within the jurisdiction of the Kinki Regional Construction Bureau in 1957. And the strong motion accelerographs were installed thereafter only at 10 places until 1963. However, the acceleration records obtained by a strong motion accelerograph installed in an apartment house in Niigata City were greatly useful for investigating the earthquake damages caused by the Niigata Earthquake occurred in June 1964. Thereafter, the necessity of strong motion observation was widely recognized by the public. Then, discussions were made between the river Bureau and Road Bureau of the Ministry of Construction and PWRI on the installation of accelerographs, and a plan for installing SMAC type strong motion accelerographs was formulated. This plan has been steadily carried out by the Ministry of Construction, Regional Construction Bureaus, Hokkaido Development Bureau, Public Corporations, local self-governing bodies, and PWRI. And Strong Motion Observation is being performed at 291 civil engineering facilities throughout the nation in March 1987.

*Dr. Eng., Director, Earthquake Disaster Prevention Department, PWRI, MOC
**Dr.Eng., Head, Ground Vibration Division, Earthquake Disaster Prevention Dept., PWRI, MOC
***Research Engineer, Ground Vibration Division, Earthquake Disaster Prevention Dept., PWRI, MOC

Fig. 2 shows the progress of the number of places where accelerographs were installed by type of facility. The number of places where accelerographs were installed increased after the Niigata Earthquake in 1964. In the decade from 1965 to 1975, the strong motion accelerographs were installed mainly on bridges among road facilities and more slowly on dams. In the decade from 1975 to 1985, the installation of strong motion accelerographs on road facilities was made more slowly compared to the previous decade, but the number of accelerographs installed on river facilities increased after the Miyagi-ken-oki Earthquake in 1978. In addition, after the establishment of the Construction Technology Evaluation System in 1981, "the Development of Newly Developed MOC Type Strong Motion Accelerograph for Measuring the Acceleration of Earthquake Motion" was carried out, and many MOC type strong motion accelerographs were installed on dam facilities and road facilities after 1982. After 1975, the average annual increase in the number of places where accelerographs were installed was 14 and the average annual increase in the number of accelerographs installed was 33.

3. PRESENT SITUATION OF STRONG MOTION OBSERVATION

3.1 Outline of Observation Stations

Table 1 shows the number of observation stations and the number of strong motion accelerographs (or number of components) by facility and by the type of accelerograph. And Fig. 3 shows the stations where the strong motion observation is being performed by road, river and dam facilities as of March 1987. Proportion of the observation stations by facility is 57% for road facilities, 12% for river facilities, 29% for dam facilities, and 2% for sewerage facilities. And the proportion of observation stations by type of strong motion accelerographs is 61% for SMAC type, 23% for electromagnetic type and 16% for MOC type.

3.2 Maintenance and Inspection of Strong Motion Accelerographs

Public Works Research Institute (PWRI) performs periodic inspection and calibration once a year for strong motion accelerographs installed by the Ministry of Construction and a part of strong motion accelerographs installed by prefectures. In FY 1986, PWRI inspected and calibrated 169 SMAC type strong motion accelerographs installed in 83 places, 186 components of electromagnetic type strong motion accelerographs installed in 22 places, and 33 MOC Type strong motion accelerographs installed in 13 places. By the adjustment and replacement of parts, it became possible to regain the normal conditions for more than 80% of SMAC type strong motion accelerographs. And among the main items of adjustment and replacement the replacements of consumables such as silica gel and batteries are more than 50%.

3.3 Digitization of Strong Motion Records

After the occurrence of an earthquake, the person in charge of strong motion observation at each observation station will confirm the presence of strong motion records and, if records have been obtained, will recover and mail the records to PWRI.

The records obtained from SMAC type strong motion accelerographs will be then digitized by the procedure shown in Fig. 4. The digitization is performed by reading the earthquake motion records and time records with a digitizer. Records made as digital values are subjected to Zero-Line correction, Arc correction and Time axis correction and then are turned into data with the intervals of 1/100 second. Then, the Fourier transformed data are applied to band-pass filters determined based on the accuracy of digitization and instrument character-istics. That is, if the acceleration record by strong motion accelerograph is $a_0(t)$, then its Fourier transform $F_0(f)$ can be given by

$$F_0(f) = \int_{-\infty}^{\infty} a_0(t) \cdot e^{-2\pi i f t} \cdot dt \qquad (3.1)$$

Then, corrected acceleration a(t) based on filter Fc(f) considering the accuracy of digitization and instrument characteristics of strong motion accelerograph can be given by the following formula:

$$a(t) = \int_{-\infty}^{\infty} F_0(f) \cdot F_c(f) \cdot e^{2\pi i f t} \cdot df \qquad (3.2)$$

where,

$$F_c(f) = \begin{cases} 0 \quad \cdots\cdots & 0 \le f < f_{ll} \\ \dfrac{f - f_{ll}}{f_{lu} - f_{ll}} \cdot \dfrac{\exp(i\,\phi(f))}{R(f)} \quad \cdots\cdots & f_{ll} \le f \le f_{lu} \\ \dfrac{\exp(i\,\phi(f))}{R(f)} \quad \cdots\cdots & f_{lu} \le f \le f_{ul} \\ \dfrac{f_{uu} - f}{f_{uu} - f_{ul}} \cdot \dfrac{\exp(i\,\phi(f))}{R(f)} \quad \cdots\cdots & f_{ul} \le f \le f_{uu} \\ 0 \quad \cdots\cdots & f > f_{uu} \end{cases} \qquad (3.3)$$

where, f_{lu} and f_{ul} are cut-off frequencies at low frequency side and high frequency side respectively, and f_{ll} and f_{uu} are the frequencies when the magnification of correction filter corresponding to f_{lu} and f_{ul} respectively becomes zero. Also, for correction factors $R(f)$ and $\phi(f)$ for amplitude and phase, the following equations are used by considering the effect of the air damper employed in SMAC type strong motion accelerograph working as spring.

$$R(f) = \frac{1 + (U/N)^2}{\sqrt{(1-U^2)^2 + \{(1-U^2)U/N + 2hU\}^2}} \qquad (3.4)$$

$$\phi(f) = \tan^{-1}\left[\frac{2hU}{(1-U^2)\{1+(U/N)^2\} + 2hU \cdot U/N}\right] \qquad (3.5)$$

In the above equations, $U = f / f_n$, $N = f_a / f_n$, f_n is the natural frequency of pendulum, and f_a is constant. Fig. 5 shows $1/R(f)$ and $\phi(f)$. $f_{1u} = 1/3$Hz and $f_{u1} = 12$Hz are used here as cut-off fruencies by taking account of the accuracy of digitization and the accuracy of strong motion accelerograph.

3.4 Present Situation of Strong Motion Observation Records

As stated previously, strong motion records of 7,992 components have been obtained from 669 earthquakes occurred after 1965 when the Strong Motion Observation was actually started, and 1,102 components of them have been digitized. Fig. 6 shows the annual progress of the number of recorded and digitized components and the number of earthquakes observed. In 1968, records were obtained from many earthquakes such as the Matsushiro Earthquake Swarm, Ebino Earthquake, Hyuganada Earthquake, and Tokachi-oki Earthquake. Also in 1978 and 1983, the number of earthquake records increased as a result of the occurrence of the Miyagi-ken-oki Earthquake and the Nihonkai-chubu Earthquake. After 1975, the annual average number of earthquakes observed is 20, from which 97 records or 291 components were obtained, and 16 records or 48 components of them were digitized.

Fig. 7 shows the number of record components classified by magnitude, epicentral distance and maximum acceleration for 1,007 components for which particular earthquakes were identified among 1,102 digitized components. From this figure, it can be known that 115 components, which is 52% of 223 components with the maximum acceleration of greater than 100 gal, were obtained at the places with the epicentral distance of less than 50 km where the magnitude was $5.0 \leq M \leq 6.9$ and that fewer records were obtained at the places with epicentral distance of less than 100 km where the magnitude was $M \geq 7.0$.

The largest maximum acceleration on the ground is 616 gal recorded by a SMAC-B2 type strong motion accelerograph installed on the ground near the Itajima Bridge with an epicentral distance of 20 km during an earthquake (M=6.6, D=20 km) occurred near the coast of the western part of Ehime Prefecture in 1986. And the largest maximum acceleration on the structure is 802 gal recorded by a SMAC-B2 type strong motion accelerograph installed on the pier of the Kaihoku Bridge with the epicentral distance of 85 km during the Miyagi Offshore Earthquake ((M=6.7, D=50 km) in February 1978.

Among these digitized records, the records larger than 30 gal on the ground and larger than 100 gal on the structure are published as Technical Note of PWRI and as of March 1987 12 volumes were issued.

4. STRONG MOTION OBSERVATION DATA BASE SYSTEM

4.1 Strong Motion Observation Data Base

Strong motion observation data is classified into three categories, data related to observation stations, data related to observed earthquakes and data related to strong motion records. And it is also classified into two categories based on data type, numerical or character data and figure data. For the purpose of retrieving these data quickly, Strong Motion Observation Data Base was developed in the Optical Disc Filing System (OLFIS) introduced by PWRI in FY 1985. This system is built in the large computer in PWRI, and numerical and character data are registered as relational data base, and data retrieval, addition and updating can be easily made by using software such as RDB1 (Relational Data Base System), ACE3 (End User Language) and OLFIS. Outline of OLFIS is shown in Fig. 8.

Strong Motion Observation Data Base comprises 7 kinds of numerical and character data tables and 4 kinds of graphic data. Various kinds of retrievals are possible for numerical and character data, and those shown in Fig. 7 in the foregoing Chapter are the results of retrieval with plural conditions attached to the Digitized Strong Motion Records Table and Earthquake Items Table. Data can be easily added to the data base from TSS terminal in the case of a small amount of data and by batch job using OLFIS software in the case of a large amount of data. And data update can be made on display of TSS terminal.

The following is outline of numerical and character tables.

1) Earthquake Items Table
   Earthquake items determined by Japan Meteorological Agency (J.M.A.), for which strong motion records were obtained, are registered.

2) Original Strong Motion Records Items Table
   Maximum acceleration values directly read out from strong motion records are registered.

3) Digitized Strong Motion Records Items Table
   Maximum acceleration values after digitized and corrected are registered.

4) A Large Amount of Acceleration Values Table
   All acceleration values after digitized and corrected are registered.

5) Strong Motion Observation Station Items Table
   Data such as strong motion accelerograph items and management body items at observation stations are registered.

6) J.M.A. Observation Station Items Table
   J.M.A. observation station items are

registered.

7) J.M.A. Seismic Intensity Table
J.M.A. seismic intensities, for the earthquake strong motion records were obtained, are registered.

4.2 Strong Motion Observation Data Retrieval and Graphic Processing System

Strong Motion Observation Data Retrieval and Graphic Processing System (SMDB86) was developed in order to retrieve data in Strong Motion Observation Data Base and to quickly and easily obtain list output and graphic output. Fig. 9 indicates the outline of the proces-sing system. This system is for producing graph and table outputs in interactive mode from graphic display terminals and has the following four functions:

1) Strong Motion Observation Station Retrieval and Plotting Module
This has the function of producing the location maps of strong motion observation stations and the lists of strong motion observation points near epicenter in order to identify observation stations near the epicenter and to confirm where to make contact after the occurrence of earthquake.

2) Prompt Report Preparation Module on Strong Motion Observation Records
This has the function of producing table of prompt Report on Strong-Motion Records, location figure of strong motion observation stations obtained records shown in Fig. 10 and figure of J.M.A. seismic intensity distribution. This module works about one week after the occurrence of earthquake by using seismic intensity in each area and the maximum value read out from strong motion records transmitted.

3) Primary Analysis Module for Strong Motion Records
This has the function of performing retrieval by earthquake or by observation station by using data in the strong motion observation data base.
a) Retrieval by earthquake No.
When an earthquake No. is input, the lists of earthquake, record, and observation station items can be obtained. In addition, location figure of strong motion observation stations obtained records, figure of J.M.A. seismic intensity distribution, figure of strong motion acceleration and figure of acceleration response spectrum ratio are prepared.
b) Retrieval by observation station No.
When an observation station No. is input, the lists of observation station, record and earthquake items can be obtained. In addition, figure of observed earthquake epicenters as shown in Fig. 11 can be obtained. Another function as same as the retrieval stated in Para. a) is also available.

4) Technical Note Table and Figure Preparation Module
This has the function of preparing the lists of earthquake, record and observation station items as well as location figure of strong motion observation stations obtained records, figure of J.M.A. seismic intensity distribution, figure of strong motion acceleration, figure of acceleration response spectrum ratio, and list of digitized and corrected acceleration values by means of batch job after the input of earthquake occurrence term or earthquake No.

5. Situation of Utilizing Strong Motion Records

Strong motion records, for which digitization and instrument correction were completed, are individually utilized for input earthquake motions during the design of civil engineering structures or examination of analysis method by comparing analyzed values to observed values or input earthquake motions during shaking table tests. Moreover, numerous strong motion records are being utilized for using by statistical analyses, the relations between maximum acceleration, duration of earthquake motions or repetition characteristics and magnitude of earthquake, epicentral distance or ground condition. Achievements obtained from the above are reflected upon "Specifications for High-way Bridges, Part V, Earthquake Resistant Design" and other various standards and guides. The following is some of the results obtained from statistical analyses.

5.1 Development of attenuation formula of maximum horizontal acceleration

Attenuation formulas by magnitude, epicentral distance and ground condition were determined by using 2@ 197 sets of horizontal acceleration records of strong motions which were observed at 67 strong motion observation stations (on the ground) located across the nation and operated by the Ministry of Construction and the Ministry of Transport.

$$\alpha_{max}^{n}=\begin{cases}987.4\times10^{0.216M}\\ 232.5\times10^{0.313M}\\ 403.8\times10^{0.265M}\end{cases}\times(\Delta+30)^{-1.218}\quad\begin{matrix}\text{(Group 1)}\\ \text{(Group 2)}\\ \text{(Group 3)}\end{matrix}$$
$$365.3\times10^{0.268M}\times(\Delta+30)^{-1.182}\quad\text{(All ground)}\qquad(5.1)$$

where,

a max: Presumed value of maximum horizontal acceleration (gal)
M : J.M.A. Mgnitude
Δ : Epicentral distance (km)
Group 1 : G.C. Group 1 set forth in "Specifications for High-way Bridges, Part V, Earthquake Resistant Design"

Group 2 : G.C. Group 2 & 3 set forth in "Earthquake Resistant Design"
Group 3 : G.C. Group 4 set forth in "Earthquake Resistant Design"

5.2 Development of attenuation formula of maximum vertical acceleration

Attenuation formulas by magnitude, epicentral distance and ground condition were obtained by using the vertical acceleration of strong motion records from 119 components observed at 53 observation points located across the nation and operated by the Ministry of Construction and the Ministry of Transport.

$$\alpha^{V}_{max} = \begin{cases} 117.0\times10^{0.268M} \\ 88.2\times10^{0.297M} \\ 13.5\times10^{0.402M} \\ 58.8\times10^{0.292M} \end{cases} \times(\Delta+30)^{-1.190} \times(\Delta+30)^{-1.116}$$

(Group 1) (Group 2) (Group 3) (All ground)

(5.2)

where, all the symbols are the same as equation (5.1)

5.3 Development of attenuation equation of acceleration response spectrum

It is known that the shape of acceleration response spectrum greatly varies depending on the kind of ground. Shown in Fig. 12 a) and b), the acceleration response spectrum ratio diagram of horizontal acceleration records obtained on the Ground Condition Group 1 (G.C. Group 1 set forth in Specifications for High-way Bridges) and Ground Condition Group 3 (G.C. Group 4 set forth in Specification for High-way Bridges). By using horizontal acceleration of 2@ 197 sets of strong motion records explained in Paragraph 5.1, PWRI has developed equations for estimating horizontal acceleration response spectrum by magnitude, epicentral distance, ground condition and natural period.

$$S_a(M,\Delta,T_k,GC_i,h=0.05) = \alpha(T_k,GC_i)\times10^{b(T_k,GC_i)\cdot M} \times(\Delta+30)^{-1.178} \quad (5.3)$$

where,

a(Tk, GCi), b(Tk, GCi): Coefficients each Natural Period and each Ground Condition
Sa : Estimated value of horizontal acceleration response spectrum (gal)
M : J.M.A. Magnitude
Δ : Epicentral distance (km)
GCi : Ground Condition (same as that of equation (5.1))

When estimating a response spectrum with the damping factor of other than 0.05, the following equation is used:

$$S_a(M,\Delta,T_k,GC_i,h) = S_a(M,\Delta,T_k,GC_i,h=0.05) \times \left[\frac{1.5}{40h+1}\right] \quad (5.4)$$

6. SUMMARY

Main items explained in the foregoing chapters will be summarized below.

1) Twenty-two years have passed after the real start of the Strong Motion Observation and, as of March 1987, observation by 698 strong motion accelerographs is being carried out at civil engineering facilities operated by the Ministry of Construction in 291 stations across the country.

2) After 1975, increases in the number of strong motion observation stations and in the number of strong motion accelerographs are respectively 14 and 33 in average per year.

3) Proportion of the number of observation station by facility to the whole is 57% for road facilities, 12% for river facilities, 29% for dam facilities and 2% for sewerage facilities. And the proportion of the number of accelerographs by type to the whole is 61% for SMAC type, 23% for electromagnetic type and 16% for newly developed MOC type.

4) In FY 1986, periodic inspection and calibration once a year were performed for 169 SMAC type strong motion accelerographs in 83 places, for 186 components of electromagnetic type strong motion accelerographs in 22 places and 33 MOC type strong motion accelerographs in 13 places.

5) From 1965 to December 1986, the records of 7,992 components were obtained from 669 earthquakes, and digitization was made for 1,102 components.

6) From annual average number of earthquakes of 20 after 1975, 97 records or 291 components have been obtained, and about 16% of them or 16 records or 48 components have been digitized.

7) Number of digitized strong motion records observed within the epicentral distance of 100 km of earthquakes with M≧7.0 is small.

8) The largest maximum horizontal acceleration on the ground is 616 gal, and on the structure is 802 gal.

9) Diversified data retrieval and graphic processing has become possible as a result of the arrangement of Strong Motion Observation Data Base and the development of Strong Motion Observation Data Retrieval and Graphic Processing System (SMDB86).

10) By utilizing the strong motion records, many research achievements have been realized such as the development of formulas for estimating the maximum acceleration and acceleration response spectrum.

ACKNOWLEDGMENT:

Persons in charge of strong motion observation who work in the Regional Construction Bureaus of the Ministry of Construction, Hokkaido Development Bureau, various Public Corporations, local self-governing bodies and so forth have greatly contributed to the strong motion observation. The authors would like to express here the deepest gratitude to these persons for their steady efforts made up to now.

REFERENCES:

Chapter 1
1) E. Kuribayashi, T. Iwasaki and S. Wakabayashi: Strong Motion Observation and the Utilization of Its Records (in Japanese), Civil Engineering Journal, Vol. 15, No.1, pp28-33, Jan. 1972.
Chapter 2
2) Public Works Research Institute, Ministry of Construction: Strong Motion Observation for Civil Engineering Structures (in Japanese), Technical Memorandum of Public Works Research Institute, No. 1847, July 1982.
Chapter 3
3) Public Works Research Institute, Ministry of Construction: Methods of Estimating Maximum Earthquake Motions and Earthquake Response Spectra (Part 4)--Re-examination of Attenuation Formulas for Maximum Acceleration, Velocity, Displacement, and Acceleration Response Spectrum--(in Japanese), Technical Memorandum of Public Works Research, No.1993, March 1983.
4) K. Kawashima, Y. Takagi and K. Aizawa: Accuracy of Digitization of Strong-Motion Records Obtained by SMAC-Accelerograph (in Japanese), Proc. of Japan Society Civil Engineers, No.323, pp67-75, 1982.
5) K. Kawashima, Y. Takagi and K. Aizawa: Procedure of Instrument Correction and Displacement Calculation for SMAC-B2 Accelerograph Records with Considering Accuracy of Digitization (in Japanese), Proc. of Japan Society Civil Engineers, No.325, pp35-44, 1982.
6) System Division, PWRI, Ministry of Construction: Manual of Optical Disc Filing System (in Japanese), June 1986
Chapter 5
3) Same as Paper 3) stated above.
7) Public Works Research Institute, Ministry of Construction: Methods of Estimating Maximum Earthquake Motions and Earthquake Response Spectra (part 5)--Development of Correction Formulas Based on Attenuation Constants for Earthquake Response Acceleration Spectra--(in Japanese), Technical Memorandum of Public Works Research Institute, No.2001, July 1983.
8) Public Works Research Institute, Ministry of Construction: Methods of Estimating Maximum Earthquake Motions and Earthquake Response Spectra (Part 6)--Attenuation Formulas for Maximum Vertical Acceleration and Acceleration Response Spectra--(in Japanese), Technical Memorandum of Public Works Research Institute, No. 2038, December 1983.

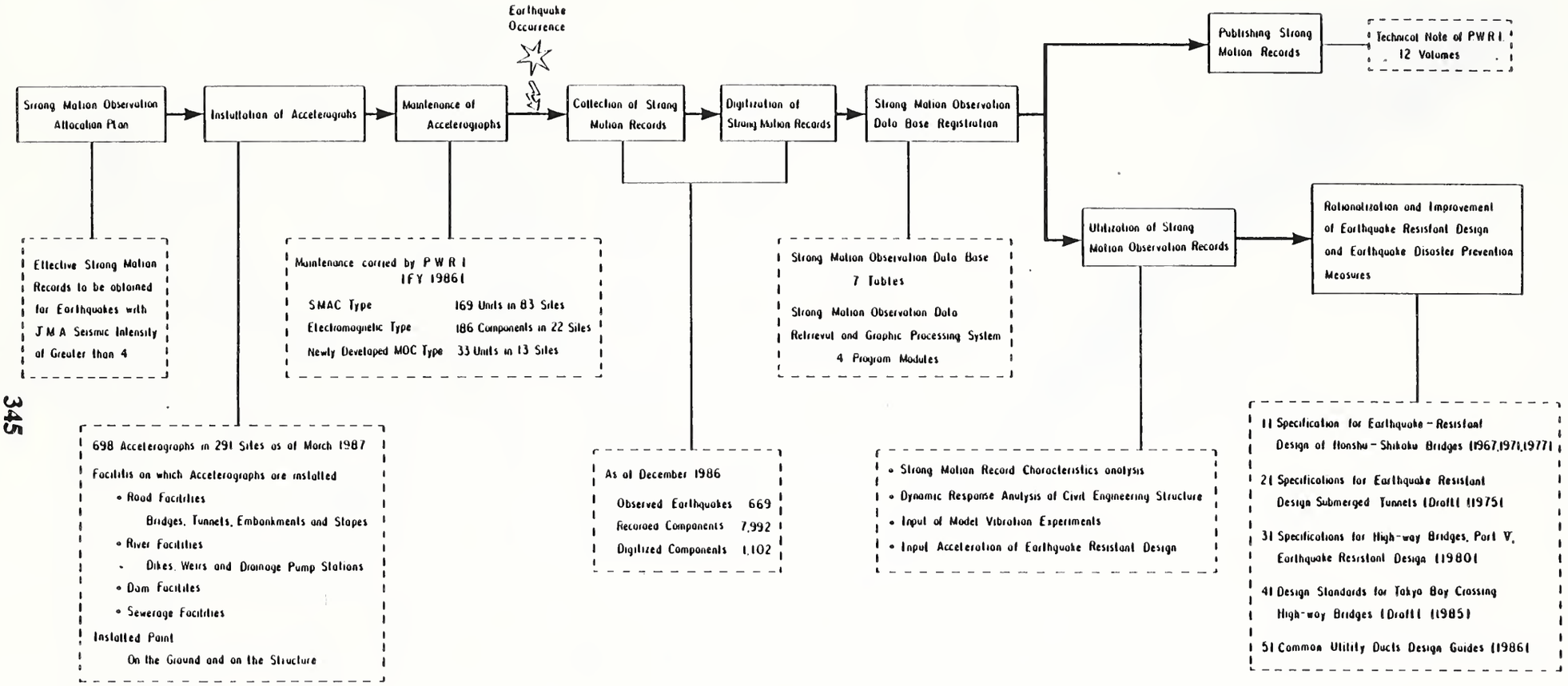

Fig. 1 Outline of Strong Motion Observation System in Public Works Research Institute

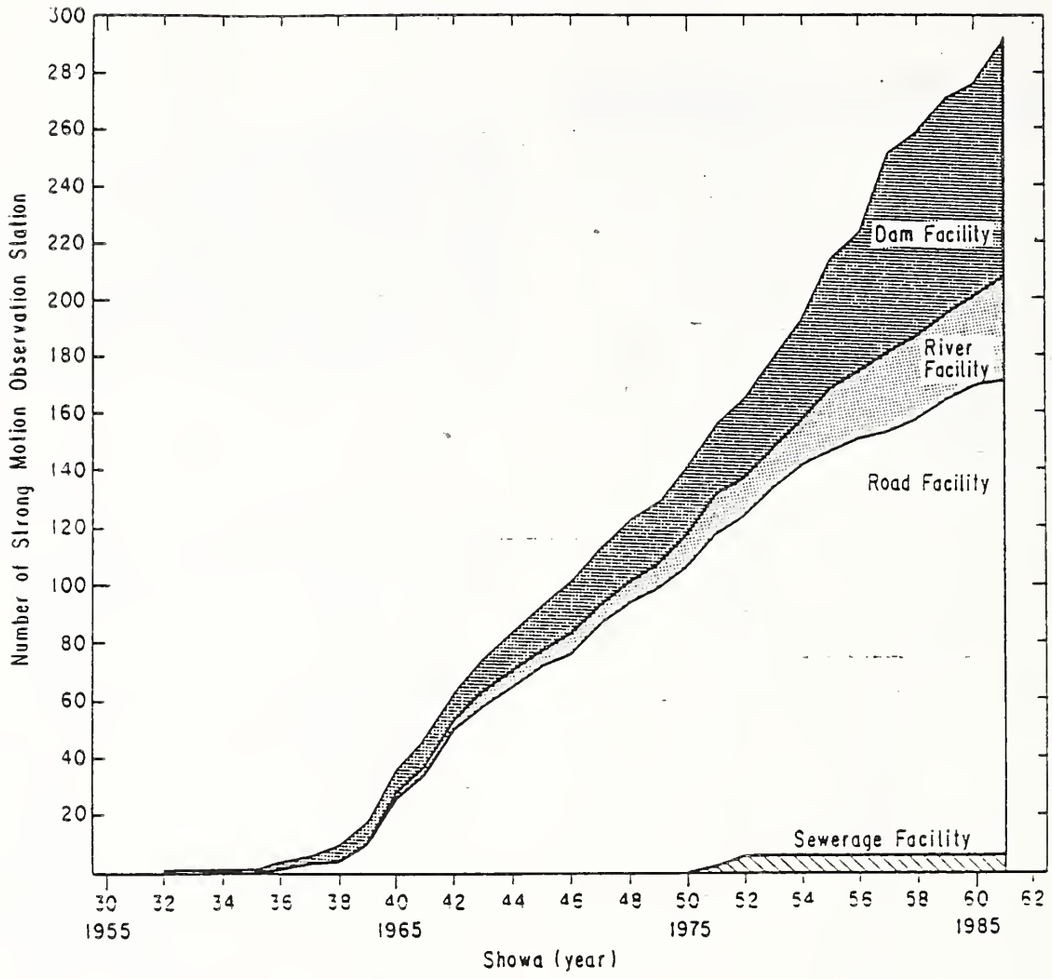

Fig. 2 Annual Transition of the Number of Strong Motion Observation Site for Each Facility

Table 1 Situation of Strong Motion Accelerograph Installation for Public Works Facilities

As of March 31, 1987

Facility	Number of Site	Accelerograph Type		
		SMAC Type Number of Site (Number of Accelerograph)	Electromagnetic Type Number of Site (Number of Component)	Newly Developed MOC Type Number of Site (Number of Accelerograph)
Road Facility (Bridge, Tunnel, Ground where Construction is arranged)	165	123 (242)	29 (365)	13 (53)
River Facility (Embankment, Weir, Flood Gate)	36	25 (50)	5 (37)	6 (14)
Dam Facility	84	24 (53)	32 (255)	28 (59)
Sewerage Facility (Pipe, Disposition Facility)	6	6 (13)	0	0
Total	291	178 (358)	66 (657)	47 (126)

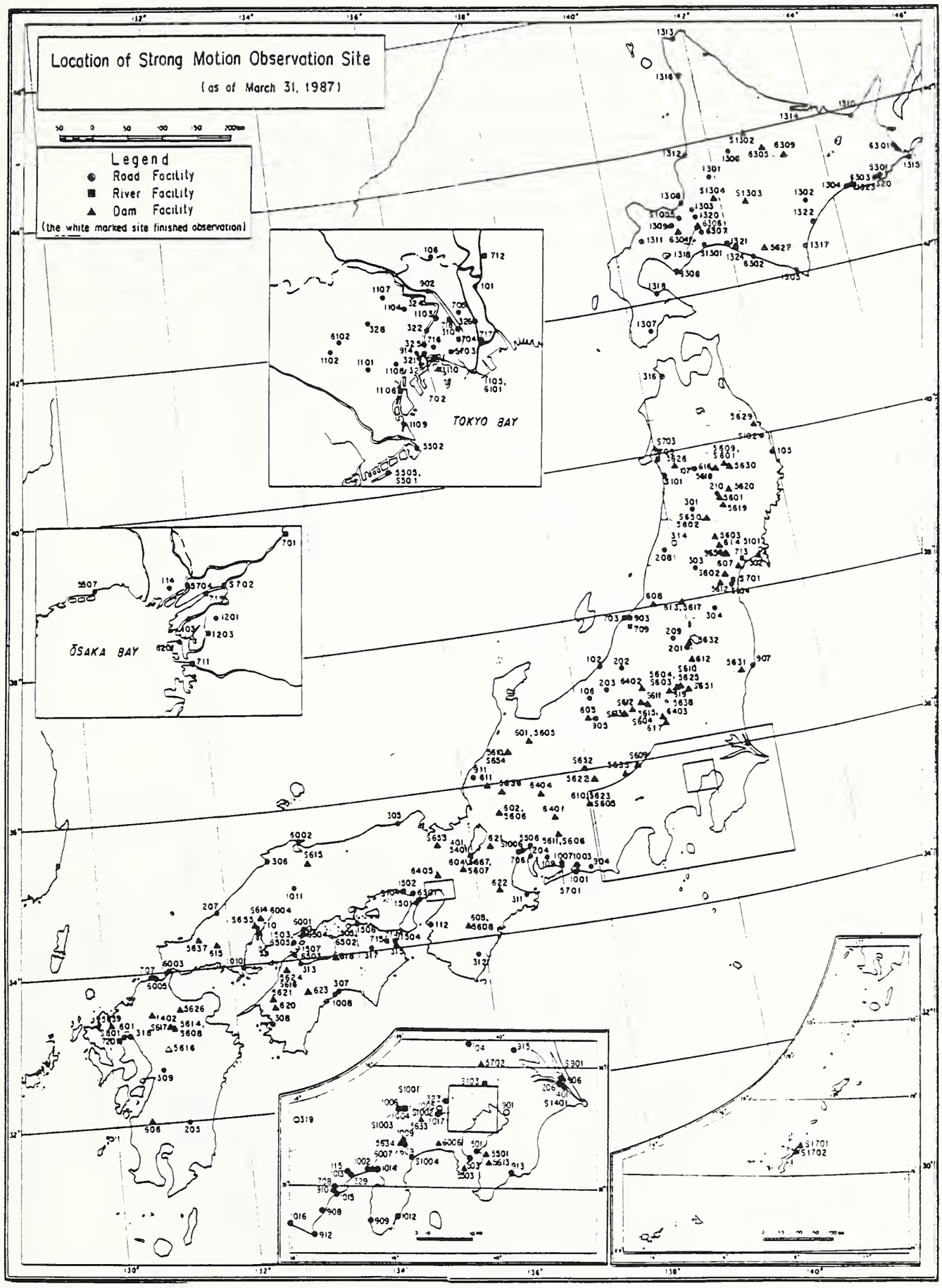

Note : the Number is P.W.R.I Station Number

Fig. 3 Location of Strong Motion Observation Site for Each Facility

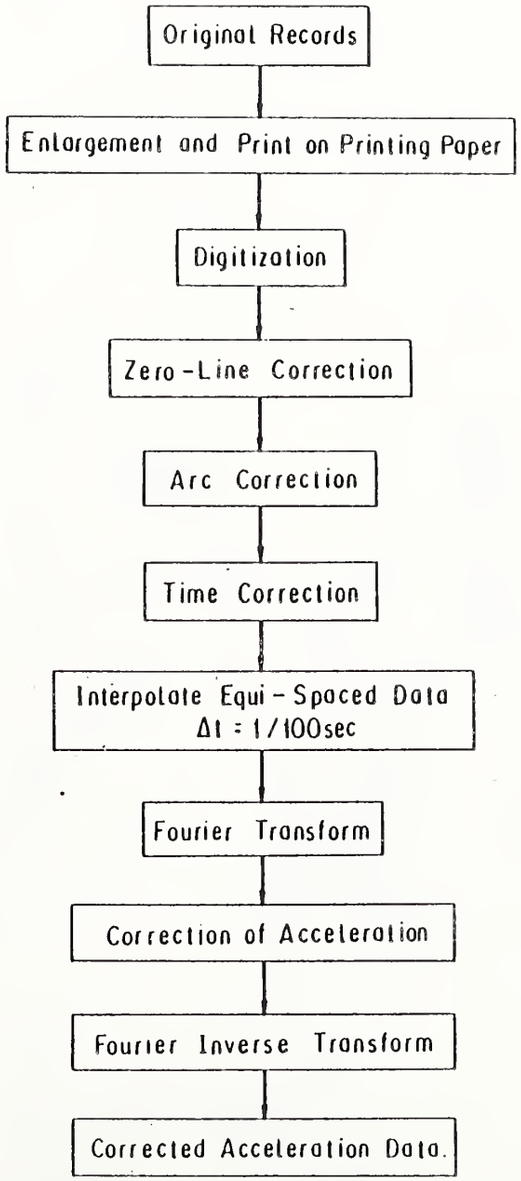

Fig. 4 Processing Flow of SMAC Type Accelerograph Records

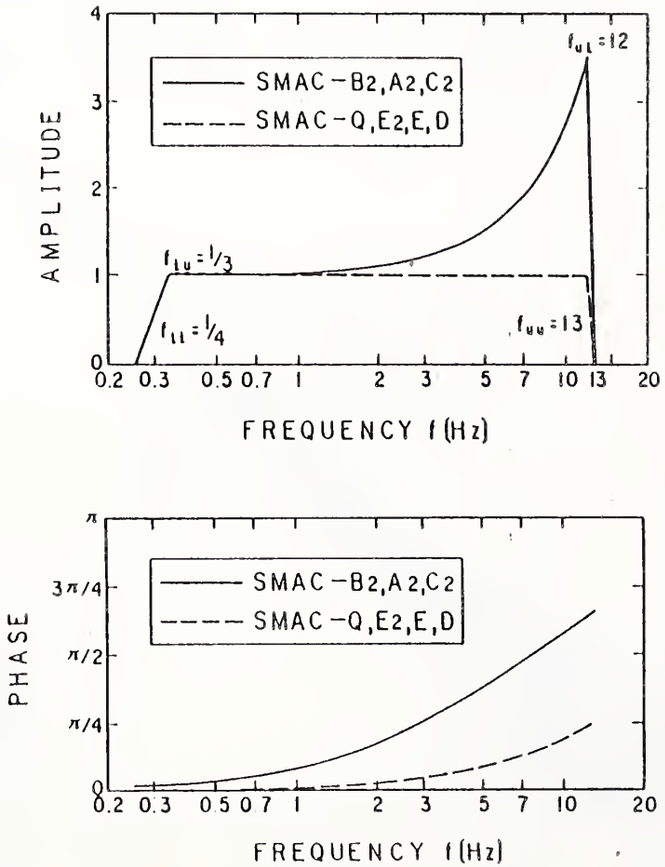

Fig. 5 Digitization of SMAC Type Accelerograph Records

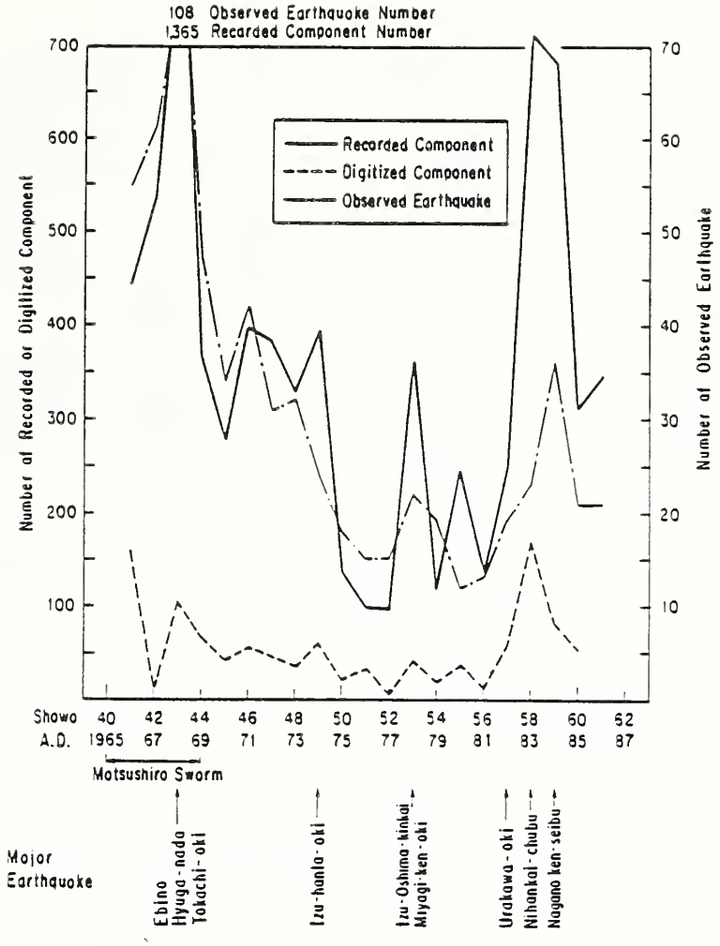

Fig. 6 Annual Transition of the Number of Recorded Component, Digitized Component and Observed Earthquake

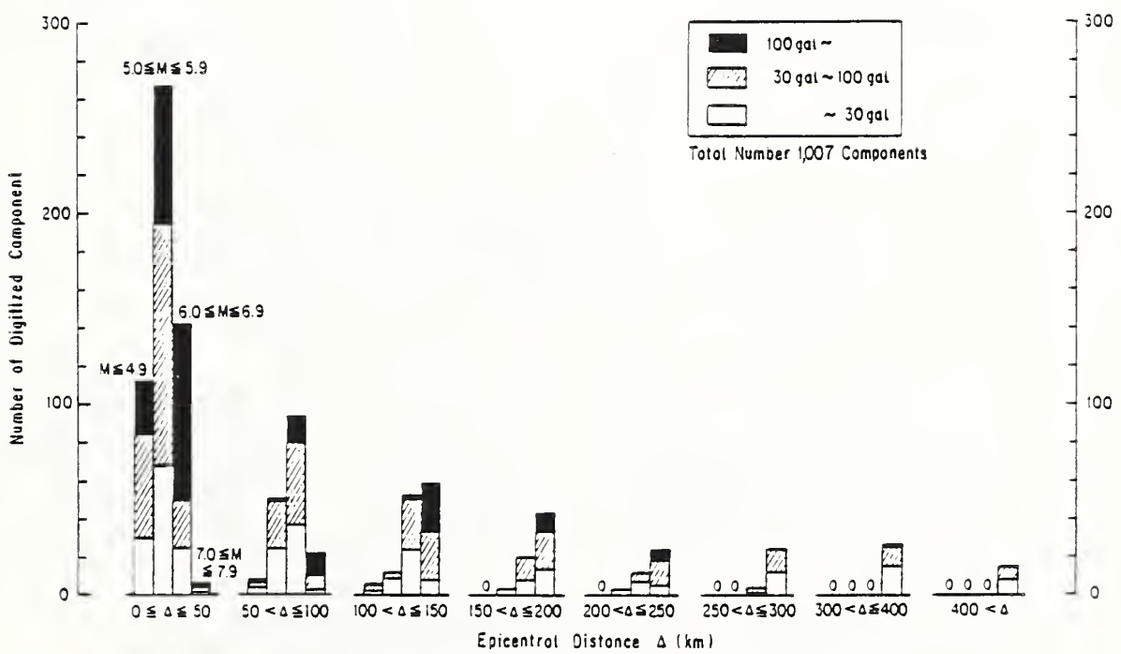

Fig. 7 Digitized Component Number Calssified by Earthquake Magnitude, Epicentral Distance and Maximum Acceleration

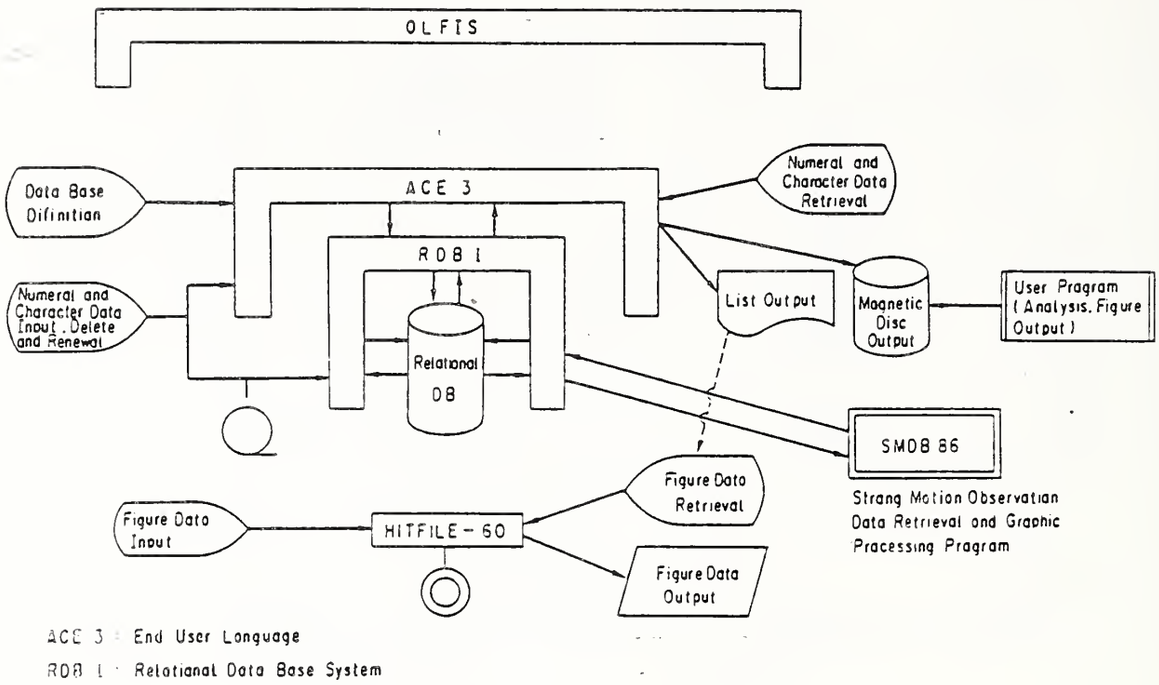

Fig. 8 Outline of Optical Disc Filing System (OLFIS)

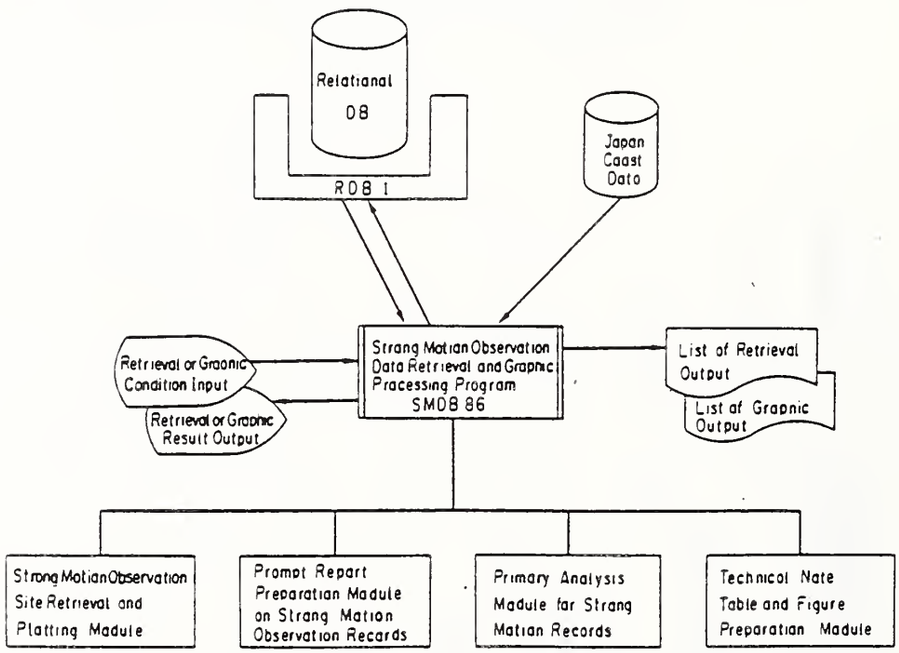

Fig. 9 Outline of Strong Motion Observation Data Retrieval and Graphic Processing System (SMDB 86)

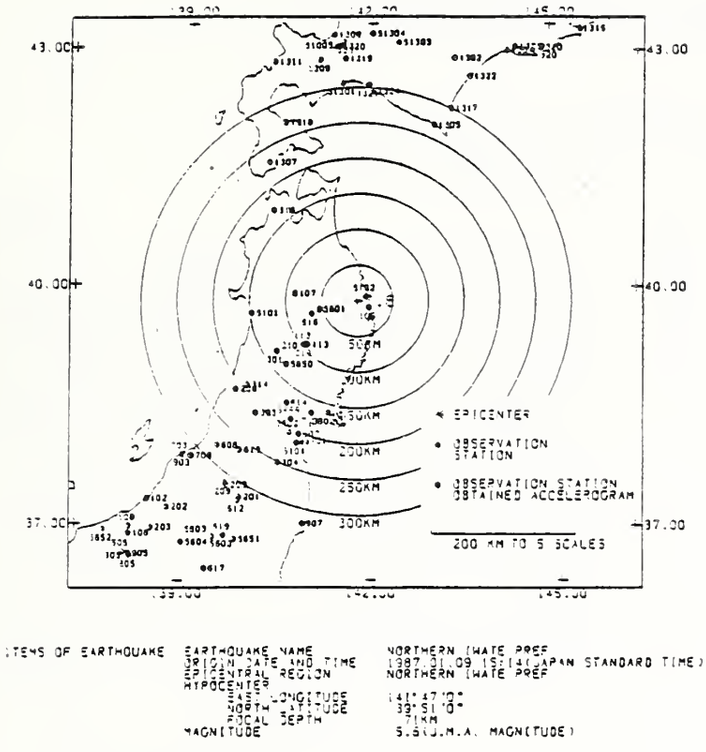

Fig. 10 Location Figure of Strong Motion Observation Stations Obtained Records

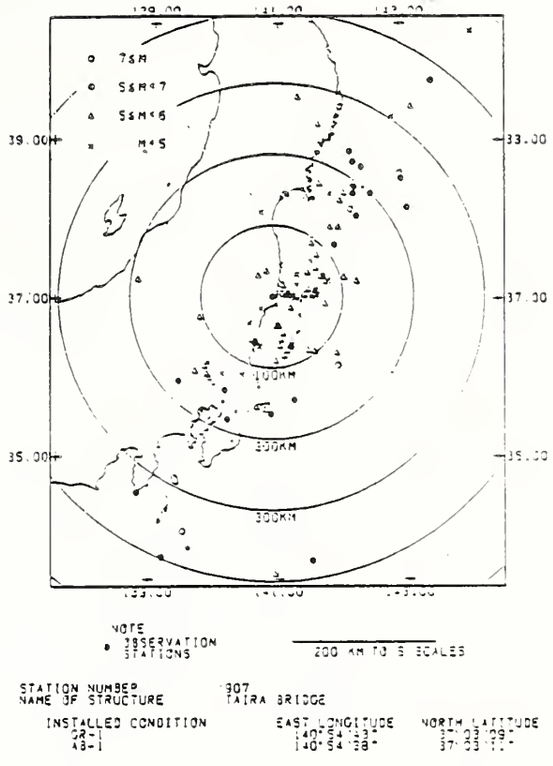

Fig. 11 Figure of Observed Earthquake Epicenters

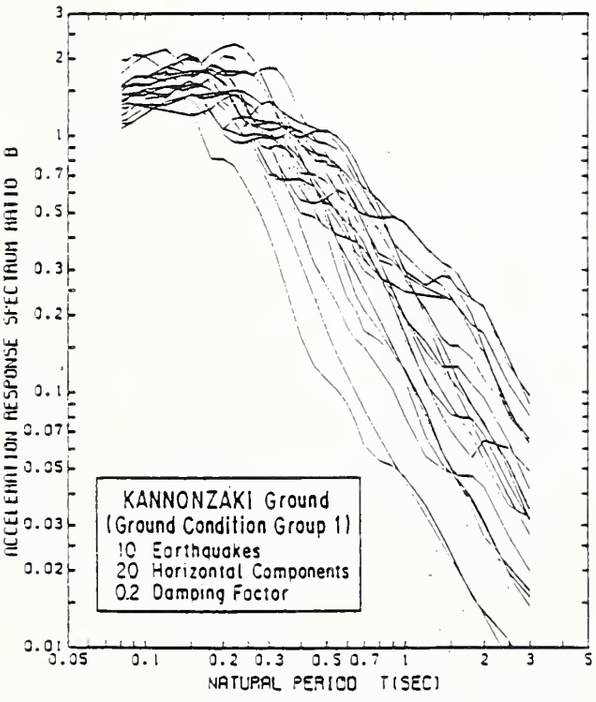

a) Ground Condition Group 1

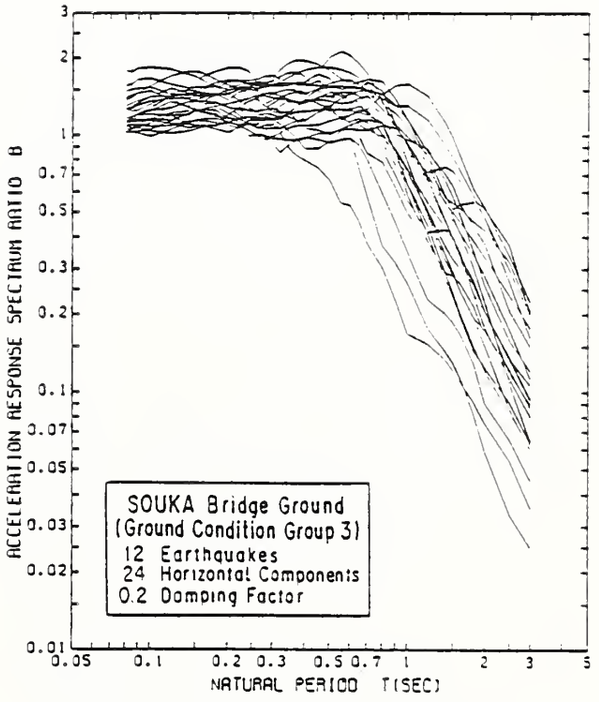

b) Ground Condition Group 3

Fig. 12 Characteristics of Acceleration Response Spectrum

Evaluation of Economical Losses Induced by the Nihonkai-Chubu Earthquake of 1983

By

Toshio Iwasaki[1], Kazuhiko Kawashima[2],
Naomi Obinata[3], and Takashi Kanoh[4]

ABSTRACT

Effect of earthquake are not restricted to damages of structures but it covers much larger aspects including economic effects. This paper presents a procedure proposed aiming to evaluate direct and indirect losses caused by an earthquake. The decrease of products was counted from three sources, i.e., decrease of products due to damage of facilities for production, due to damage of transportation facilities, and due to damage of materials and goods. Effect of investment for restoration was also considered in the analysis. Based on direct loss associated with these decrease of products, second spread effects were estimated through inter-industry relation analysis(input-output analysis).

The procedure was applied to the losses by the Nihonkai-chubu earthquake of 1983, and the estimated gross prefectural products agreed well with those actually developed after the earthquake. It was also concluded that further improvements are also needed to take account of actual economical activities immediately after the earthquake.

KEY WORDS: Indirect Losses, Economical Effects, Nihonkai-chubu Earthquake, Inter-industry Relation Analysis

1. INTRODUCTION

Damages induced by earthquakes have mostly been evaluated in terms of damages associated with failure of facilities and/or structures. Effects of earthqake are , however , not restricted to damages associated with failure of facilities but they cover much larger aspects including economic effects such as decrease of products due to suspension of production, decrease of consumption due to low social activities, etc. Losses associated with such effects are likely to be much larger than those counted only from failure of facilities. However, mechanism of economical losses induced by earthquakes is so complicated that little is known about these effects.

This paper presents a procedure proposed for aiming to evaluate direct and indirect losses caused by an earthquake as well as an example of application of the procedure for the Nihonkai-chubu, Japan, earthquake of 1983.

2. EFFECTS OF AN EARTHQUAKE ON ECONOMICAL LOSSES

When an earthquake developed damages at some of cities, towns and villages, the region within which damages took plase may be defined. Economical losses associated with that earthquake may then be evaluated on the basic of an amount of decrease of products within that region. When an amount of production $G_o(t)$ within the region after the earthquake can be defined, $G_o(t)$ may be evaluated as

$$G_o(t) = G_n(t) - G_d(t) + G_r(t) \qquad (1)$$

in which $G_n(t)$ represents products at the fiscal year of t within the region, which was supposedly achieved if the earthquake did not take place, and $G_d(t)$ and $G_r(t)$ represent a decrease of products within the region associated with the earthquake damages, and an increase of products within the region associated with investments for restoration, respectively.

Consequently, it may be possible to evaluate $G_o(t)$ provided appropriate evaluation of $G_n^o(t)$, $G_d(t)$ and $G_r(t)$ be made. It should be noted here that provided one prefecture can be regarded as the region within which economical losses are to be evaluated, the products $G_o(t)$ can be obtained in a form of gross prefectural products after a couple of years later than the earthquake. However the gross prefectural products only describes final products achieved in the prefecture at the specific fiscal year, and precise background informations on economical effects of earthquake can not be traced. Therefore it is required to develop appropriate analytical method with use of a relation presented by Eq.(1) for identifying economical effects of the earthquake. It should be noted that the accuracy of analytical model be checked by comparing products $G_o(t)$ predicted by Eq.(1) with the actual products determined statistically.

There are many aspects which can be regarded as effects induced by an earthquake, and economical effects may be classified as shown in Table 1, in which losses of facilities, properties, goods and materials can generally be evaluated by damage survey conducted by each body of the industry and regional

1) Dr. of Eng., Director, Earthquake Disaster Prevention Department, Public Works Research Institute, Ministry of Construction, Japan
2) Dr. of Eng., Head, Earthquake Engineering Division, Earthquake Disaster Prevention Department, Public Works Research Institute, Japan
3) Research Engineer, Earthquake Engineering Division, ditto
4) Assistant Research Engineer, Earthquake Engineering Division, ditto

government. Although surveys for secondary effects caused by spread of direct losses of facilities, properties, goods and materials are not generally made, they include ;

1)decrease of products due to damage of facilities for production
2)decrease of products due to damage of transportation facilities including transportation media
3)decrease of products due to damage of materials and goods

Therefore by appropriately evaluating the decrease of products induced by the above described three types of damages, economical effects of an earthquake may be identified in accordance with a flow chart shown in Fig.1. Reduction factor α, which represents a degree of reduction of products due to the earthquake, is defined for each industry as

$$\alpha = DP / PA \qquad (2)$$

in which DP and PA represent a decrease of products due to earthquake and total products supposedly developed if the earthquake did not take place, respectively.

3. EVALUATION METHOD FOR ECONOMICAL LOSSES INDUCED BY AN EARTHQUAKE

3.1 Evaluation Method for Decrease of Products Associated with Damage of Facilities for Production

Seismic damage of facilities and/or properties for production and sales, such as damages of factories, shops, machineries, public utilities, etc., induces a decrease and even suspension of production. Such a decrease of production and/or products was assumed here to be estimated by substituting products P_D^P actually developed after the earthquake from products P_A^P which were supposedly developed if the earthquake did not take place. It was also assumed here that the products P_D^P actually developed after the earthquake be evaluated from industrial structure models. The following two models were used for such purpose.

1) Production Function Model

An amount of products is generally specified by a number of labors and an amount of properties for production. Therefore, once an equation representing the products in terms of labor and facilities for production ,i.e., production function model, is formulated, the products developed after the earthquake may be evaluated by specifying the nummber of labors and the amount of facilities for production available after the earthquake. The Cobb-Douglas type equation in the form of Eq.(3) is sometimes used for such purpose,

$$Y = \alpha K^{\beta} L^{\gamma} \qquad (3)$$

in which, Y, K and L represent products, private capital stock, and number of labor, respectively, and α , β and γ represent constant to be determined by regression analysis. The amount of facilities for production was considered as the private capital stock for the analysis of products in this study.

When the facilities for production and the number of labor can be considered as independent, Eq.(3) is seperated into two independent functions as

$$Y = \alpha + \beta K \qquad (4)$$
$$Y = \alpha + \gamma K \qquad (5)$$

2) Unit Product Method

When the products per unit facilities for production or unit number of labor, which are designated here as a unit products, can be determined, the products after the earthquake may be evaluated by multiplying the unit products and facilities for production and/or number of labor available after the earthquake. Because unit products are generally time dependent, regression analysis was made to obtain the unit product at a specific fiscal year concerned.

The priority for selecting the products with use of the above-described procedures was assumed as an order of Eq.(3), Eq.(4)~Eq.(5) and unit products method.

3.2 Evaluation Method for Decrease of Products Associated with Damage of Transportation Facilities

Seismic damages of transportation facilities as well as transportation media cause a decrease of the products. Such a decrease of products was assumed here to be estimated as a decrease of trafic volumes which were defined as a differense between the trafic volumes supposedlly developed if the earthquake did not take place and those actually developed after the earthquake. The reduction factor was determined in accordance with Eq.(2).

3.3 Evaluation Method for Decrease of Products Associated with Damage of Materials and Goods

Decrease of products is also developed due to damages of materials and manufactured or partially manufactured goods for which the productions depend on.

It should be noted here that an amount of loss due to damage of materials and goods are generally determined for each industry by private or regional government bodies. Therefore, the reduction factor was obtained by dividing the loss due to damage of materials and goods by the products given in the inter-industry relations table (input-output table).

3.4 Evaluated Method of Decrease of Productions

Decrease of products was analyzed by the input-output analysis (analysis of inter-industry relations) with use of the reduction factors associated with damage of facilities for production, damage of transportation facilities, and damage of materials and goods. It should be noted here

that although the reduction factor of products can be estimated independently from the three types of damage, the products for i-th industry are, however, likely to be influenced by the most critical damage between the three damages. Therefore, decrease of products for the i-th industry ΔX_i may be evaluated as

$$\Delta X_i = X_i \times \max \left\{ \alpha_i^{\delta_1}, \alpha_i^{\delta_2}, \alpha_i^{\delta_3} \right\} \qquad (6)$$

in which $\alpha_i^{\delta_1}$, $\alpha_i^{\delta_2}$ and $\alpha_i^{\delta_3}$ represent the reduction factor of products associated with the damage of facilities for production, the damage of transportation facilities, and damage of materials and goods, respectively. X_i represents the supposed products of i-th industry unless the earthquake occured.

Besides such decrease of products, productions of other industries, which did not suffered damages but depend on the products of i-th industry, are also influenced. Such an effect is designated in this study as a first spread effect, and it was analyzed by an input-output analysis.

The input-output table has a form as shown in Table-2, in which I_i and X_i represent the i-th industry and the products of i-th industry, respectively. X_{ij}, f_i and V_i are the followings;

X_{ij} : products used from I_i to I_j, or amounts paid from I_i to I_j
f_i : final demand of I_i
V_i : value added of I_i

When an amount of α_i $(0 \leq \alpha_i \leq 1)$ of the products X_i of i-th industry became out of use due to earthquake damage, X_{ij}, f_i and V_i of the input-output table on i-th line change to $(1-\alpha_i)X_{ij}$, $(1-\alpha_i)f_i$ and $(1-\alpha_i)V_i$, respectively. It should be noted here that even if j-th industry did not suffere damages from the earthquake, the product of j-th industry decreases from X_j to $(1-\alpha_i)X_j$. Simiraly, when an amount of α_k $(0 \leq \alpha_k \leq 1)$ of the products X_k in k-th industry suffered damages, it also makes the products of j-th industry decrease from X_j to $(1-\alpha_k)X_j$. Therefore when the decreases of products arise in industries i and j simultaneously, both gives influences to the production of j-th industry. Although interactions of the decrease of products between various industries are significantly complex, it was assumed in this study that the decrease of products in j-th industry is specified by either I_i or I_j, which has larger reduction factor α. Therefore the decrease of products ΔX_j in j-th industry due to the first spread effect was estimated as

$$\Delta X_j = X_j \times \max \left(\alpha_i \mid X_{ij} \neq 0 \right) \qquad (7)$$

It should be noted here that such a decrease of products ΔX_j, then, decreases the values added such as commercial interests and salaries, i.e., ΔX_j was to be used to develop products in a form of consumption expenditure and capital formation if the earthquake did not occure. Such a effect due to decrease of products ΔX_j is designated in this study as a second spread effect. Determination of the second spread effect follows the procedure which will be described in 3.6.

3.5 Evaluation of Products Which was Supporsedly Developed If the Earthquake Did Not Take Place

Products, which was supporsedly developed unless the earthquake occured, were determined by a regression analysis of the products in the last several years before the earthquake.

3.6 Evaluation of Increase Due to Investment for Restoration

Repair and restoration after the earthquake accompany expenditures to purchase materials and goods for restoration. Such expenditures give positive impacts on various industries, which, in turn, develop the spread effects to the other industries. The spread effects caused by such chains were analyzed by the input-output analysis.

The input-output table presented in Table 2 may be written as

$$\underline{A}\,\underline{X} + \underline{F} = \underline{X} \qquad (8)$$

where, $\underline{A}$, $\underline{X}$ and $\underline{F}$ represent input coefficient matrix, output (products) vector and final demand vector, respectively. From Eq.(8), output vector $\underline{X}$ can be obtained as

$$\underline{X} = (\underline{I} - \underline{A})^{-1} \underline{F} \qquad (9)$$

in which I represents unit matrix, and $(\underline{I} - \underline{A})^{-1}$ is generally refered as the Leontief inverse matrix table. The procedure to calculate an increase due to investment associated with restoration consists of;

1) Evaluation of a first spread effect
   - ① Form final demand vector $\underline{F}$ by studying restoration investments
   - ② Calculate output (products) $\underline{X}$ developed by $\underline{F}$
   - ③ Calculate value added $\underline{X}^T\underline{V}$ by multiplying vector of ratio of value added $\underline{V}$ to $\underline{X}^T$
2) Evaluation of a second spread effect
   - ④ Determine final demand vector $\underline{F}$ associated with value added calculated by ③
   - ⑤ Calculate output (products) $\underline{X}$ developed by ④ with use of Eq.(9)
   - ⑥ Iterate ③, ④ and ⑤ until converge
3) Estimation of investment multiplier
   - ⑦ Calculate production inducement multiplier by dividing total products developed by the restoration investments
   - ⑧ Calculate income inducement multiplier by dividing total income inducement by the restoration investment
   - ⑨ Calculate tax by assuming tax ratio

4. APPLICATION TO THE NIHONKAI-CHUBU EARTHQUAKE OF 1983

4.1 Reduction of Products Due to Seismic Damages

Total amount of direct damage in the Akita prefacture due to the Nihonkai-chubu earthquake which occured in 1983 at sea bottom of Japan Sea with magnitude of 7.7 in Richter scale, was estimated as 148.2 billion yen in the nominal price of 1983, which is approximately 6.9% of the gross prefectural products of 2163.5 billion yen. Decrease of products in the Akita prefecture was estimated in accordance with the proposed procedure presented in the preceding chapter.

1) Decrease of products due to damage of facilities for production

Direct damages of the facilities and/or properties for production were estimated by private and regional government bodies after the earthquake, and the data for agriculture, forestry, fisheries, manufacturing industries, wholesale and retail were available. Among these damages, decrease of products associated with damages of forestry was disregarded in this analysis because of difficulty to evaluate products vs. properties relation.

Reduction factor of agricultural products was firstly estimated by formulating a production function model assuming the cultivated area as the private capital stock in Eq.(3). However, because accuraly of such a production function model for the agricultural products was poor, it was then decided to estimate the reduction factor from the unit product model, i.e., agricultural products per unit cultivated area was estimated by regressing the data between 1970 and 1981 as

$$U = 6.81 - 0.105 \times Y \quad (R=0.95) \quad (10)$$

in which U and Y represent the agricultural products per unit cultivated area in million yen, and year in Showa, respectively, and R represents a regression coefficient. Therefore, the agricultural products per unit cultivated area in 1983 (53 in Showa (fiscal year)) were estimated from Eq.(10) as

$$U_{58} = 6.81 - 0.105 \times 58 = 0.753 \quad (11)$$

On the other hand, total cultivated area in 1983 in the Akita prefecture was estimated as 162,329 ha, and the cultivated area of 3,139 ha was reported to be damaged by the Nihonkai-chubu earthquake. Therefore when it is assumed that the area which suffered damages by the earthquake could not be used for creating agricultural products in 1983 (58 in Showa), agricultural products at this year Y_{58} may be estimated as

$$\begin{aligned} Y_{58} &= U_{58} \times (162,329 - 3,139) \\ &= 0.753 \times 159,190 \\ &= 119,928 \text{ (million yen)}, \end{aligned} \quad (12)$$

The agricultural products YE_{58} which would possibly developed in 1983 (58 in Showa) unless the Nihonkai-chubu earthquake occured are also estimated as

$$\begin{aligned} YE_{58} &= U_{58} \times 162,329 \\ &= 0.753 \times 162,329 \\ &= 122,293 \text{ (million yen)} \end{aligned} \quad (13)$$

Therefore substituting Eqs.(12) and (13) into Eq.(2), one obtains the reduction factor a of agricultural products as

$$\alpha = \frac{YE_{58} - Y_{58}}{YE_{58}} = 1.9\ \%. \quad (14)$$

Fisheries facilities suffered severe damages by tsunami with an amount of 4,195 million yen. Because accuracy of production function models with use of Eqs.(3) ~ (5) taking account of number of fisher and fisheries capital was not sufficient, the reduction factor of fisheries products was estimated based on fisheries products per unit fisheries capital stock as 26.5 %.

For products of manufacturing industries, production function model was formulated from the data of 1982 (57 in Showa) as

$$Y = 8.03K^{0.519}L^{0.481} \quad (R = 0.87) \quad (15)$$

in which Y, K and L represent price of forwarding goods in million yen, fixed assets in million yen and number of labors, respectively. Because seperate regression analyses predicted K and L in 1983 as K = 179,939 million yen and L = 87,698 persons, the products of manufacturing industries YE58 which would supposedly achieved in 1983 (58 in Showa) if the earthquake did not take place may be estimated as

$$\begin{aligned} YE_{58} &= 8.03 \times 179,939^{0.519} \times 87,698^{0.481} \\ &= 1,022,741 \text{ (million yen)} \end{aligned} \quad (16)$$

On the other hand, damage on facilities of manufacturing industries, which suffered damages from the Nihonkai-chubu earthquake, was reported as 2,925 million yen. Therefore, the products of manufacturing industries Y_{58} in 1983 (58 in Showa) was estimated as

$$\begin{aligned} Y_{58} &= 8.03 \times (179,939-2,925)^{0.519} \times 87,698^{0.481} \\ &= 1,014,081 \text{ (million yen)} \end{aligned} \quad (17)$$

It should be noted in Eq.(17) that loss of number of labor due to death and/or injured was disregarded. The reduction factor was, then, estimated for manufacturing industries from Eq.(2) as

$$\alpha = \frac{YE_{58} - Y_{58}}{YE_{58}} = 0.85\ \%. \quad (18)$$

Reduction factor for wholesale and retail was estimated by formulating a production function model with use of the products and the capitals, in which capitals for wholesale and retail were estimated from capitals per unit number of employee.

The reduction factor of products associated with damage of facilities and/or properties for productions was thus estimated for each

industry as shown in Table 4. It should be noted here that Table 4 includes the reduction factor of products associated with damage of transportation facilities, materials and goods, which will be presented later.

2) Reduction factor of products associated with damage of transportation facilities

Restoration of road was made very quickly after the Nihonkai-chubu earthquake because the damage was relatively limited. Therefore, effect of road damage was disregarded here, and reduction factor of product was estimated only for railways and ports.

In the railways, decrease and suspention of transportation were developed at Oh-u Main-Line, Oga Line and Gonoh Line for 10 20 days, and this was reported to reach approximately 1.7 % of the annual total transportation for passengers. It should be noted, however, that because freight transportation was alternatively made by trucks instead of railway, effect of suspension and decrease of railway transportation is regarded practically limited. Therefore effects of railway damage were taken into account only for third industries by disregarding their effects for first and second industries. The reduction factor was assumed as 1.7 %.

Ports and harbours had suffered one of the most severe damages due to the Nihonkai-chubu earthquake, and it took one year and five months for their restoration.
Handling volume of the materials which depend on ship transportation such as crude oil, cement, heavy oil, petroleum goods was substantially decreased in the Akita prefecture. However, such a decrease of landing volume was not necessarily considered to bring direct decrease of products which depend on ship transportation; most of cement was landed at ports located in adjacent prefectures and transported to the Akita prefecture by trucks, heavy oil and petroleum goods were landed with use of exclusive wharves, which did not suffere damages, etc. Alternative transportation could not be made only for crude oil, which were used at the Tohoku Electric Power Station. Fig.2 shows landing volume of crude oil in the Akita prefecture, and it is seen that volume is only 450 thousands ton in 1983 (58 in Showa), which is approximately 45 % decrease as compared with the volume of 820 thousand tons which would supposedly expected if the earthquake did not take place. Therefore, it was assumed that damage of ports only developed an decrease of electricity with an amount of 45 %. It should be, however, noted that because shortage of electricity in the Akita prefecture was supplied from surrounding prefectures, decrease of products due to shortage of electricity was not developed. Therefore, the reduction factor of 45 % was considered only for production of electricity.

The reduction factor of products thus estimated is shown in Table 4.

3) Reduction factor of products associated with damage of materials and goods

Decrease of products associated with damage of materials and goods was evaluated for damage of agriculture, livestock, forestry, commerce and industry which were shown in Table 3. Dividing these decrease of products by amounts of products (output) of the input-output table, reduction factor of products was evaluated for each industry as shown in Table 4. It is seen in Table 4 that although the reduction factors are generally small, those for agriculture and commerce are appreciably larger than for other industries.

4) Critical reduction factor of products

The most critical reduction factor of products among the three types of damages, i.e., damage of facilities for production, transportation facilities, and materials and goods, was evaluated as shown in Table 4. It is apparent that the reduction factor was especially high for the ship transportation in the electricity industries (α = 45 %) and for fisheries (α = 26.3 %).

5) Analysis of decrease of products

The input-output table of the latest version of 1980 was used for input-output analysis to calculate decrease of products. It should be noted that the change of inter-industry structures developed between 1980 and 1983 (the Nihonkai-chubu earthquake of 1983) cannot be considered in this analysis. Large classifications with 14 categories and small classifications with 164 categories were used for input and output, respectively. It should be noted, however, that only for a category of transportation small classifications were used for input to identify ship transportation. Table 5 shows decreases of products predicted by the procedure described in the preceding chapter using the reduction factors presented in Table 4. The output was compiled into semi-large classifications with 31 categories. It is seen in Table 5 that total amount of decrease of products is predicted as 248.1 billion yen, which corresponds to approximately 1.7 times of the direct damage of 148.2 billion yen (refer to Table 3), and that the most significant decrease of products occured in service (95.4 billion yen) followed by electricity, gas and water industries (730 billion yen).

Then, the second spread effects were calculated. Table 6 summalizes the second spread effects thus calculated as well as the first spread effect and direct damages due to the Nihonkai-chubu earthquake. A ratio of the total damages caused by the earthquake to the gross prefectural products of the Akita prefecture was estimated as 11.0 % and 10.2 % on the bases of input-output table (I/O base) and value added, respectively.

4.2 Products Supposedly Developed Unless The Earthquake Occrued

Fig.3 shows variation of gross prefectural products between 1975 (50 in Showa) and

1982 (57 in Showa). The gross prefectural products Y at the year of y (in Showa) are obtained from regression analysis as

$$Y = -1,680,580 + 68,575 \times y \quad \text{(million yen)} \qquad (19)$$

Extrapolating the products with use of Eq.(19), one obtains the gross prefectural products in 1983 as 2296.8 billion yen.

4.3 Increase of Products due to Investment for Restoration

Increase of products due to investment for restoration was analyzed by the input-output analysis seperating the restorations of public works (44.3 billion yen) and those for housings (11.9 billion yen). It was found from the analysis that 22 billion yen of the total restoration of 44.3 billion yen for public works was paid to the industries, and that the rest (22.3 billion yen) was spent for value added. According to such investments, products of 89.2 billion yen were developed including the original investments, which, in turn, developed secondary spread effects. Including all these effects, it was found that the investment for restoration of public works developed products of 122.3 billion yen as well as value added of 40.9 billion yen.

The same analysis was made for the investments for restoration of housings (11.9 billion yen), and it was found that the investments developed products of 23.3 billion yen and secondary spread effects of 6.4 billion yen.

4.4 Effect of the Nihonkai-chubu Earthquake on Economy in the Akita Prefecture

Table 7 summalizes the decreases of products by the earthquake as well as the increase of products due to investments for restoration. It was predicted that the Nihonkai-chubu earthquake caused decrease of 87.5 billion yen on the basis of value added. Because the products supposedly developed unless the earthquake occured were estimated as 2296.8 billion yen in 4.2, it was considered that the gross prefectural products would be 2209.3 billion yen.

On the other hand, the gross prefectual products of the Akita prefecture in 1983 was reported in 1985. Table 8 compares the above-described predicted products with the actual products. It is seen in Table 8 that the gross prefectual products in 1983 was 227.3 billion yen, which is 63.5 billion yen larger than the above prediction. Precise comparisons depending on each industry are ;

1) When a ratio R is defined as the actual gross prefectual products divided by the predicted gross prefectual products, the ratio R takes a value between 0.89 and 1.22 excluding four industries, i.e., forestries(R = 1.46), minings(R = 1.43), electricity, gas and water(R = 0.58), and service and others(R = 0.78).

2) In case of fisheries industry, a decrease of products predicted as 27.1%, which is one of the most significant decrease of products, is fairly in good agreement with the actual decrease of 25.5%.

3) A ratio R is quite large in forestry and minings while it is very small in service. The reason for such discrepancies may be attributed to the fact that the products for these industries varied significantly between 1980 and 1983, i.e., although the latest version of input-output table of 1980 was used for the analysis of indirect losses of the Nihonkai-chubu earthquake of 1983, it does not consider changes of production structure developed between 1980 and 1983. It is considered that the products of forestry and minings had been decreasing between 1980 and 1983, while those of service had been increasing.

4) The actual products in electricity, gas and water industry are approximately two times larger than those predicted. This is regarded as a difference of assumption in this analysis that although the products of electricity was assumed to decrease in accordance with decrease of landing volume of crude oil at the port, actual products did not decrease because the electricity was supplied from a net-work covering the whole Tohoku region.

5. CONCLUDING REMARKS

For aiming to develop a complehensive procedure which considers socio-economic effects of earthquake from more wide views, proposed was a procedure which evaluates effect of earthquake on economic loss at a specific region, and applicability of the procedure was studied for the Nihonkai-chubu earthquake of 1983. The features and tentative conclusions deduced from this study are the followings.

1) To evaluate economical loss due to earthquake, proposed was a procedure which considers not only decrease of products with use of input-output analysis from three sources, i.e., damage of producing facilities, damage of transportation facilities, and damage of materials and goods, but increase of products associated with investment for restoration. This is an extention of the procedure, which is widely used to evaluate an positive effect for constructing public works, to seismic effects. The proposed procedure has, however, several limitations, such that it uses an input-output table which could only be used for economical activities at the normal time, it cannot be used to evaluate economical damage at a very limited area, etc., and further improvements are required.

2) Reduction factor of products, which is defined as the decrease of products due to the Nihonkai-chubu earthquake divided by the products supposedly developed if the earthquake did not take place, takes significantly high value of 45 % in ship transportation and of 26.3 % in fisheries as

compared with reduction factor in other industries such as 1.9 % in agriculture and 0.8 % in manufacturing industry. Reduction factor of products in road transportation was very limited. This is considered to be attributed from the fact that functions of ports had been suspended for a long time due to damage of the Akita port, and tsunami caused significant damage to marine facilities, while restoration of road facilities could be made promptly.

3) Although total direct damage in the Akita prefecture caused by the Nihonkai-chubu earthquake was 148.2 billion yen, decrease of products associated with such direct damages was estimated as 368.6 billion yen, which is 2.5 times larger than the total direct damages and consists of 248.1 billion yen by decrease of production, 112.2 billion yen by decrease of consumption and 8.3 billion yen by damage of materials and goods. Consequently, considering total direct damages of 148.2 billion yen and decrease of products of 368.6 billion yen, it is considered that the Nihonkai-chubu earthquake developed a loss of 508.5 billion yen in the Akita prefecture, which corresponds 11.0 % of the gross prefectural products of 4639.6 billion yen (I/O base products) in 1983.

4) Substituting increases of products developed by investment for restoration, the decreases of products in the Akita prefecture was estimated as 216.6 billion yen on the I/O base and 87.5 billion yen on the value added base. Consequently, because gross prefectural products in 1983, which was supposedly developed if the earthquake did not take place, was estimated as 2296.8 billion yen, the gross prefectural products actually developed in 1983 was predicted to be as 2209.3 billion yen. In comparison, actual gross prefectural products in 1983 were reported by the Akita prefecture as 2272.8 billion yen, which is 63.5 billion yen larger than the above prediction.

REFERENCE

1) Akita Prefecture : Record of the Nihonkai-chubu Earthquake of 1983, 1983
2) Kawashima, K., Obinata, N. and Kanoh, T. : Estimation of Socio-economic Damage induced by Earthquakes Part 1 Case Study for the 1983 Nihonkai-chubu Earthquake, Tecnhical Memorandum, No.2267, Public Works. Research Institute, Ministry of Construction, 1985
3) Katayama, T. and Moriyoshi, S. : Nihonkai-chubu Earthquake and Noshiro City Case Study of Effect of Earthquake on Regional Social Activities, Report NO.84-02(5), Institute of Industrial Science, University of Tokyo, 1984.
4) Kawashima, K., Obinata, N. and Kanoh, T. : Effects of Socio-economic Damage Induced by Earthquake A Case study for the 1983 Nihonkai-chubu Earthquake, Civil Engineering Journal, Vol.29-3, 1987.

Table-1 Classification of Earthquake Effects

Classification	Objective and/or Form of Damage	Effects of Loss and/or Damage
Human Life	Death, Injury	Loss of man power, Mental effects
Facilities for Living	House, Educational Facilities, Hospitals, etc.	Functional loss for Daily Human Activities
Facilities for Production	Cultivate Field, Non-Residential House (Factory, Shops), etc.	Decrease of Production, Loss of Products
Life-line Facilities	Electricity, Telecommunication, Gas, Water and Sewage, Trash	Decrease and/or Loss of Capability for Production
Transportation Facilities	Road, Bridge, Port, Rail-way	Decrease of Production due to Decrease of Transportation Capability for Material and Products
	. .	Decrease of Production due to Decrease of Transportation Capability for Passengers
Public Works Excluding Transportation Facilities	River, Sabo-works, Slope failure	Damage associated with Failure
Transportation Media	Trucks, Buses, Trains, Ships	Decrease of Production due to Decrease of Transportation Capability
Manufactured Goods, Partially Manufactured Goods	Loss of Manufactured and/or Partially Manufactured Goods	Decrease and/or Loss of Value of Goods, Decrease of Products due to Loss of Manufactured and/or Partially Manufacture Goods

Table-2 Inter-industry Relation Table(Input-output Table)

Sell \ Purchase		Intermediate Demand	Final Demand	Products
		I_1 I_2 ····· I_i ····· I_j ·····		
Intermediate Sales	I_1			
	I_2			
	:			
	I_i	····· X_{ii} ····· X_{ij} ·····	f_i	X_i
	:			
	I_j	····· X_{ji} ····· X_{jj} ·····	f_i	X_j
	:			
Value Added		····· v_i ····· v_j ·····		
Products		····· X_i ····· X_j ·····		

Table-3 Damages by the Nihonkai-chubu Earthquake of 1983 (million yen)

Type	Classification	Damage (million yen)
Damage of Facilities	Agricultural Facilities	24,477
	Fishery Port Facilities	1,486
	Marine Facilities	4,195
	Forestry Facilities	5,557
	Commercial Facilities	2,925
	Industrial Facilities	4,918
	Other Commercial and Industrial Facilities	2,263
	Public Works	59,253
	Other Public Works	3,958
	House	26,665
	Educational Facilities	1,733
Damage of Materials and Goods	Agriculture	2,411
	Livestock	7
	Forestry	400
	Commerce	1,344
	Industry	3,437
	Other Commerce and Industry	708
	Rail Ways	2,200
	Others	301
Total		148,238

Table-4 Reduction Factor of Products [%]

Classification		① Due to Damage of Facilities for Production	② Due to Damage of Transportation Facilities	③ Due to Damage of Materials and Goods	④ Most Critical Reduction Factor Between ①, ② and ③
1. Agriculture		1.93	0	0.79	1.93
2. Forestries		0	0	0.48	0.48
3. Fisheries		26.27	0	0	26.27
4. Mining		0	0	0	0
5. Manufacturing		0.85	0	0.12	0.85
6. Construction		0	0	0	0
7. Electricity, Gas, Water		0	0	0	0
8. Commercial		0.01	0	0.75	0.75
9. Finance and Insurance		0	0	0	0
10. Landed Estate		0	0	0	0
11. Transportation and Communication	Road	0	0	0	0
	Rail Way	0	1.7[1)]	0	1.7[1)]
	Ship	0	45.0[2)]	0	45.0[2)]
	Communication	0	0	0	0
12. Service		0	0	0	0
13. Official Business		0	0	0	0
14. Unclassificable		0	0	0	0

Note: 1) Only for products for third industry
2) Only for products for electricity

Table-5 Direct Loss due to Reduction of Products

Classification	① Original Products (billion yen)	② Reduction of Products (billion yen)	③ Decreasing Rate ②/① [%]
1. Cultivated Agriculture	253.6	4.9	1.93
2. Livestock	52.9	1.02	1.93
3. Forestry	82.8	1.04	1.25
4. Fisheries	11.5	3.02	26.27
5. Mining	91.6	0.78	0.85
6. Food	181.7	18.55	10.21
7. Texture and Clothes	100.5	1.81	1.80
8. Wood and Wooden Goods	236.8	2.36	1.00
9. Pulp and Paper	48.4	0.7	1.45
10. Printing and Publishing	20.2	0.17	0.85
11. Leather and Rubber Goods	1.3	0.02	1.64
12. Chemical Products	35.1	0.3	0.86
13. Petroleum and Coal Goods	43.5	0.42	0.97
14. Ceramics	47.6	0.4	0.85
15. Iron and Steel	13.9	0.12	0.85
16. Iron and Non-iron Goods	146.5	1.24	0.85
17. General Machinery	44.3	0.38	0.85
18. Electric Machinery	149.6	1.27	0.85
19. Transportation Machinery	62.9	0.53	0.85
20. Precision Machinery	14.8	0.13	0.84
21. Other Manufactures	12.6	3.31	26.27
22. Construction of Buildings	356.3	5.28	1.48
23. Construction of Public Works	246.9	4.77	1.93
24. Electricity, Gas, Water	193.0	73.02	37.82
25. Commerce	460.2	7.82	1.70
26. Finance and Insurance	114.5	1.95	1.70
27. Landed Estate	264.1	4.22	1.60
28. Transportation and Communication	307.5	5.23	1.70
29. Service	641.4	95.4	14.87
30. Official Business	145.2	7.32	5.04
31. Unclassificable	34.4	0.66	1.93
32. Total	4,415.6	248.14	5.62

Table-6 Predicted Reduction of Products due to the Nihonkai-chubu Earthquake of 1983

	Direct Damage (billion yen)	Damage Associated with Decrease of Products (billion yen)			Total Damage (billion yen)	Ratio to Gross Prefectural Products [%]
		Direct	Effect of Consumption (2nd Spread Effect)	Total		
I/O Base	148.2	248.1	112.2	360.3	508.5	11.4
Supplementary Value Base (Gross Prefectural Products Base)	73.2	120.6	39.9	160.5	233.9	10.2

Table-7 Effect of the Nihonkai-chubu Earthquake of 1983 on Economy of the Akita Prefecture

		I/O Base	Supplementaly Value Base
① Decrease of Products by the Earthquake (billion yen)	Damage of Materials and Goods	8.3 [1)]	4.1
	Direct Decrease associated with decrease of products	248.1	120.6
	Decrease of Consumption	112.2	39.9
	Total	368.6	164.6
② Increase of Products due to Investment for Restoration of Public Works (billion yen)	First Effect	89.2	51.4
	Second Effect	33.1	11.7
	Total	122.3	63.1
③ Increase of Products due to Investment for Restoration of Housing (billion yen)	First Effect	23.3	11.7
	Second Effect	6.4	2.3
	Total	29.7	14.0
Decrease of Products (① + ② + ③) (billion yen)		216.6	87.5
Ratio to Gross Prefectural Products (%)		4.7	3.8

Note: 1) Total of damage of products and goods presented in Table 3.

Table-8 Comparison of Predicted and Actual Products Developed in the Akita Prefecture in 1983 (Million yen in the price of 1983 fiscal year)

Classification	Prediction on Products of Akita Prefecture in 1983 Fiscal Year							
	Reduction of Products				⑤ Products Supposedly Developed Unless the Earthquake Occurred	⑥ Predicted Products ⑥=⑤-④	⑦ Actual Products Developed in 1983	Ratio ⑥/⑦
	① Decrease of Products due to Seismic Damage	② Increase of Products due to Investment for Restoration of Public Works	③ Increase of Products due to Investment for Restoration of Housings	④ Sub-total ①-②-③				
1. Agriculture	5,372	174	30	5,168	205,363	200,195	201,578	0.99
2. Forestries	1,743	435	275	1,033	46,248	45,215	30,904	1.46
3. Fisheries	1,899	27	6	1,866	7,320	5,454	5,193	1.05
4. Minings	1,396	1,458	184	-246	58,540	58,786	41,018	1.43
5. Manufacturing	10,391	2,902	721	6,768	341,085	334,317	322,208	1.04
6. Construction	7,845	45,670	10,039	-47,864	263,632	311,496	244,481	1.27
7. Electricity, Gas, Water	25,929	487	98	25,344	70,509	45,165	78,327	0.58
8. Commercial	14,421	2,701	554	11,166	333,730	322,564	334,056	0.97
9. Finance and Insurance	4,451	1,457	317	2,677	88,167	85,490	91,728	0.93
10. Landed Estate	4,471	627	144	3,700	232,495	228,795	226,156	1.01
11. Transportation and Communication	5,013	1,676	356	2,981	110,476	107,495	104,986	1.02
12. Service	81,612	5,563	1,220	74,829	539,195	464,366	592,214	0.78
Total	164,544	63,156	13,944	87,422	2,296,760	2,209,338	2,272,849	0.97

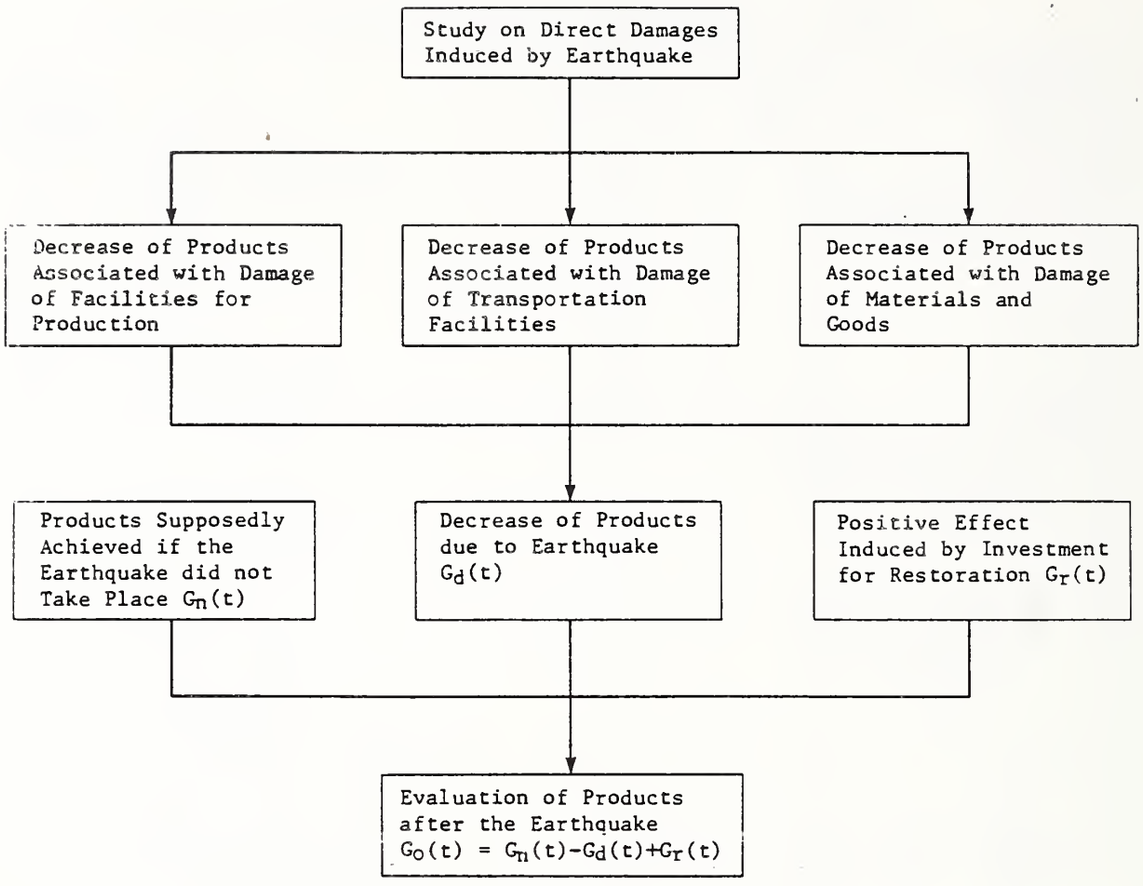

Fig.1 Evaluation of Economical Effects of Earthquake

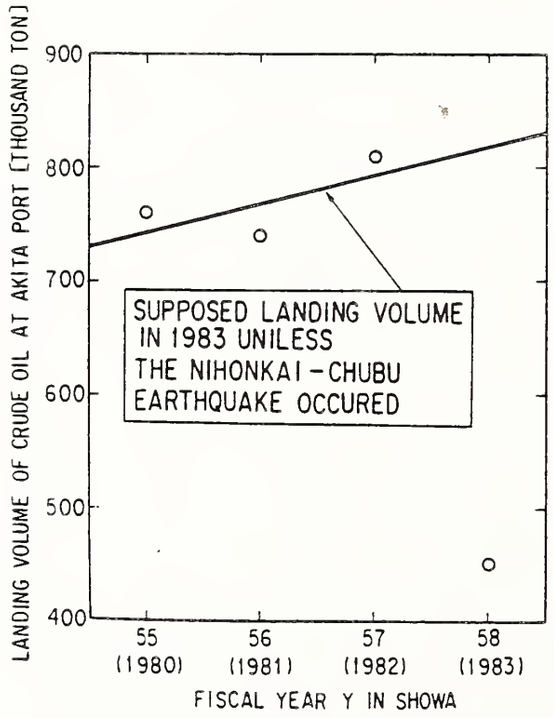

Fig.2 Variation of Landing Volume of Crude Oil at the Akita Port

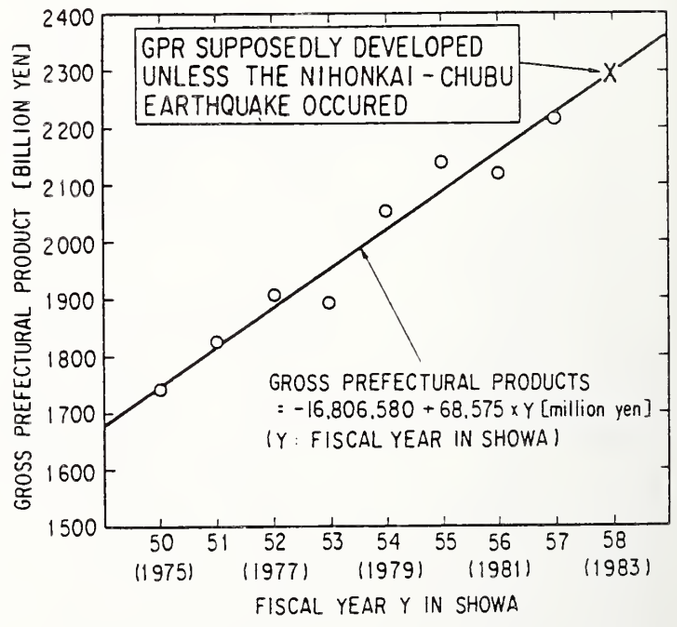

Fig.3 Variation of Gross Prefectural Products between 1975 and 1982

Analysis of Strong Motion Earthquake Records on January 9, 1987

by

Nobuyoshi Yamaguchi[1], Sadaiku Hattori[2], Shinsuke Nakata[3],
Hatsukazu Mizuno[4], Masanori Iiba[5]

ABSTRACT

Strong motion networks of Building Research Institute observed strong motions from the magnitude 6.6 Iwateken-Chubu (middle of Iwate Pref.) earthquake of January 9, 1987. Peak acceleration on the first basement of a building in Hachinohe city was 197 gals and 561 gals on the fifth floor.

A slight building damage occurred during this earthquake. The damaged building had a experience of a moderate damage during the 1968 Tokachi-Oki earthquake. The building had been repaired and strengthened after the 1968 earthquake, and it had damage again. BRI have installed accelerographs in another building beside the damaged building, and measured strong motions during this earthquake.

The analysis for these records clarifies the periods of them, and the behavior of the observed building. The building damage in 1968 and 1987 is examined. It is suggested the strengthening of the building after the 1968 earthquake is insufficient.

KEY WORDS : Strong motion record,
Earthquake input,
Seismic response of building,
Earthquake damage

1. INTRODUCTION

Building Research Institute have observed strong motions of the ground and buildings since 1957, in order to clarify building behavior and strong ground motions during severe earthquakes. For example, BRI succeeded liquefacted ground motions during the 1964 Niigata earthquake, and the world record building responses (1.06 G) during the 1978 Miyagiken-Oki earthquake. The object of this paper are to analyse strong motion records and to evaluate strengthening effects of a building based on the records.

2. EARTHQUAKE DATA AND OBSERVED RECORDS

Table 1 shows the earthquake data during the Iwateken-Chubu earthquake of January 9, 1987.[1)] Figure 1 shows isoseismal map of the earthquake.[2)] Table 2 summarized the observed records by BRI network.[3)] Although this earthquake was comparatively large among the earthquakes occurred in inland of Japan, the earthquake damage was slight on the whole due to its deep hypocentre.

3. OBSERVATION SITES

Photo 1 shows Atago junior high school in Miyako city which was the closest site to the epicentre among the BRI stations. The accelerograph of BRI was installed on the west end of the first floor in the school building. The site was cut for construction of the school, and its ground condition is fairly good.

Photo 2 presents Hachinohe city office which is 77.2 km apart from the epicentre. Hachinohe city office consists of the old city office completed in 1960, the annex building in 1969 and the new city office in 1980. The old city office and the annex building are jointed by expansion joints shown in photo 3. Photo 4 shows the annex building where the accelerographs were installed on the first basement and on the fifth floor. Figure 2 shows the soil profile of the site. The layers from the surface to - 9 m are consist of clay loam and sandy loam whose N values are less than 5. There are the layers of gravel in the depth of - 9 m whose N values are over 50.

4. DAMAGE OF THE 1968 EARTHQUAKE

It was reported the old city office in Hachinohe had been damaged during the 1968 Tokachi-Oki earthquake. Figures 3 - 5 show the damaged penthouse and frames. Figures 6 - 8 show plan views of the old city office and shear or bending damage of the columns in 1968. The old city office is reinforced concrete building supported by precast concrete piles (length: 9m, 5m with basement).[4)] The building was repaired and strengthened after the 1968 earthquake. The damaged penthouse was removed from the building, and walls for strengthening were installed around the east stairs of the building.

1: Geotechnical Engineering Division, Structural Engineering Department,Building Research Institute, Ministry of Construction, Japan
2: Dr. of Science, Special Senior Scientist, International Institute of Seismology and Earthquake Engineering, IISEE, BRI
3: Dr. of Eng. Head of Building Engineering Division, IISEE, BRI
4: Head of Housing Construction Division, Production Department, BRI
5: Research Engineer, Earthquake Information Division, IISEE, BRI

5. INSTRUMENTATION

The accelerograph was SMAC-M which includes three components of force balance type transducers and a FM recording system using magnetic cassette tapes. The records (* marked on table 2) were digitized every 1/200 or 1/100 seconds, and were made a tentative base line correction by least square fit method. The results are called uncorrected accelerograms. Table 2 summarized the maximum accelerations of them. But the values without * marks are calculated from the half length between positive and negative peak values. A final base line correction is carried out for the records of Hachinohe city office, and the velocities and displacements are calculated by the method of M.D. Trifunac.[5] Table 3 presents the cut-off and roll-off termination frequencies for the Ormsby filter used in the method.

6. ANALYSIS OF STRONG MOTIONS

Figure 9 - 11 show uncorrected accelerograms of Miyako 1F, Hachinohe B1F and 5F. Figure 12 - 16 show corrected accelerograms, velocities and displacements of Hachinohe B1F and 5F. Figure 17 - 22 show elastic response spectra of the records of Miyako 1F and Hachinohe B1F. Figure 23 - 25 show Fourier amplitude spectra of the records of Hachinohe 5F.

Figure 10 shows the maximum accelerations are on pulses, and a duration of the principle motion is about 10 seconds. Figure 18 shows frequency domain of EW components and periods of the motions are about 0.07 seconds (14 Hz) and 0.15 seconds (7 Hz). These periods are rather short among ground motions of typical buildings in Japan. The soil profile and short epicentral distances are considered to affect their characteristics. Although the maximum accelerations in Miyako were large, there was no remarkable damage around Miyako city because of their short periods.

Figure 21 shows the periods of EW component of Hachinohe B1F are around 0.16 - 1.0 seconds (1-6 Hz). Figures 12 - 13 show the maximum velocities of NS and EW components are about 10 kines, and a duration of the principle motion is about 10 seconds. Figure 23 presents the period of NS component of Hachinohe 5F is about 3 Hz and that of EW component is around 2 - 2.5 Hz. Figure 16 indicates the maximum velocity of EW component reaches about 38 kines, and the maximum displacement is about 3 cm. The results indicate the annex building deformed 1/500 of the height by adopting the assumption of fixed base. This deformation suggests structural damage of the annex building would not arise during this earthquake. In fact, any structural damage of the annex building is not observed.

7. DAMAGE OF BUILDING

The old city office in Hachinohe had damage of the fixed windows during this earthquake. The building have been jointed to the annex building with expansion joints. A glass glazing method of the old city office using stiffened putty material is consider to cause this window damage. The fixed windows of the annex building using PVC glazing channels had no damage during this earthquake.

The old city office also had slight structural damage in spite of strengthening after the 1968 earthquake. Photo 5 shows the column besides the courtyard, which had slight shear-bending damage due to the spandrel walls. Photo 6 presents the cracks on the walls which had been added for strengthening after the 1968 earthquake. Photo 7 shows the damage of expansion joints by the collusion of two buildings. Photo 8 indicates the repaired column by the injection of epoxy adhesive to the cracks.

8. CONCLUSIONS

Strong motions were observed beside the damaged building, Since a height of the damaged building is about 15 m, the natural periods of that will be about 0.3 seconds. The maximum response accelerations of the damaged building is evaluated 500 - 600 gals for EW direction and 300 - 400 gals for NS direction based on the response spectra of the ground motions. This result indicates the loads acting to the building are moderate. Since any structural damage is not observed around Hachinohe city except this case, it is considered this building needs more strengthening. Further inspections for this problem are required.

9. ACKNOWLEDGMENT

Strong motion observations in Miyako and Hachinohe are performed in cooperation with Atago junior high school of Miyako city and Hachinohe city office. The survey for the old city office in Hachinohe was assisted by the staff of Hachinohe city. The authors would like to express great thanks to them and Dr.Tetsuo Kubo and Mr.Hideo Tsukagoshi for making the programs of analysis.

REFERENCES

1). Announcement of Japan Meteorological Agency
2). The Mainichi News papers of Jan. 10 1987
3). 'Strong Motion Earthquake Observation News, the Earthquake of Jan. 9 1987 at the Middle of Iwate Pref.', Kenchiku Gijutsu No.427
4). 'The Reconnaissance Reports for the disasters of the Tokachi-Oki Earthquake of 1968', AIJ, Dec. 1968
5). M.D.Trifunac,'Low Frequency Digitization Errors and a New Method for Zero Baseline Correction of Strong-Motion Accelerograms', EERL 70-07, CIT

Table 1 Earthquake Data

Date & Time	Jan. 9 , 1987 15 : 14 (JST)
Location	Middle of IWATE Prefecture
Epicentre	39 51' N 141 47' E 71 km depth
Magnitude	6.6 (JMA)
Intensity	5 : Oh-funato, Morioka 4 : Hachinohe, Sakata, Ishinomaki, Sendai 3 : Mutsu, Aomori, Akita, Shinjo, Yamagata, Fukushima, Shirakawa, Onahama, Mito, Tokyo, Yokohama, Urakawa, Hiroo, Obihiro Kushiro

Table 2 Observation Results

Observation Sites				Max. Acceleration (gal)			
station	floor	instrument	Epicentral Distance	component			note
				NS	EW	UD	
MIYAKO Atago junior high school	1F	SMAC-M	27.6 km	186 (N03W)	388 (S87W)	219 (UP)	*
HACHINOHE City office	B1F	"	77.2	149 (S16E)	197 (N74E)	89 (UP)	*
"	5F	"	"	312 (N16W)	561 (S74W)	218 (UP)	*
SENDAI Tohoku univ.	1F	"	195.2	31 (N68W)	27 (S22W)	20 (UP)	
"	9F	"	"	103 (N68W)	80 (S22W)	35 (UP)	

Table 3 Cut-off & Roll-off Termination Frequency for filter

Record	L^fT	L^fC	H^fC	H^fT (HZ)
HACHINOHE B1F	0.05	0.1	25	27
" 5F	0.05	0.1	25	27

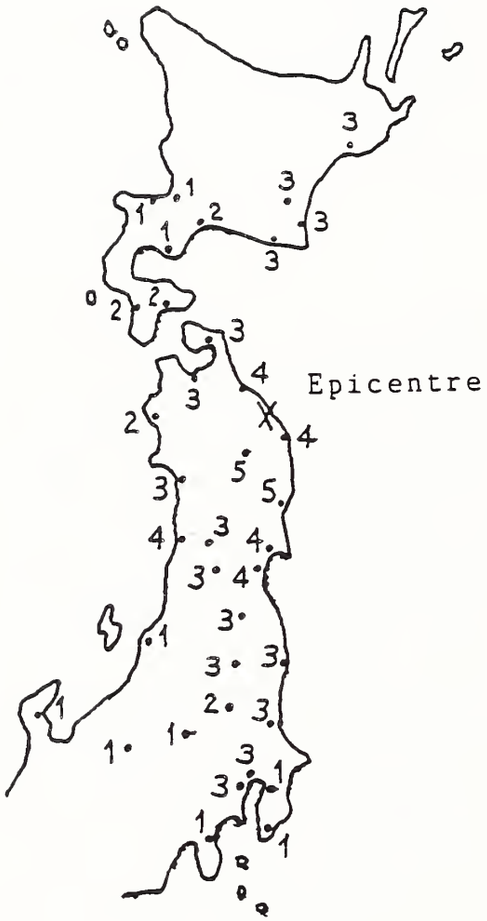

g. 1 Isoseismal Intensity Map

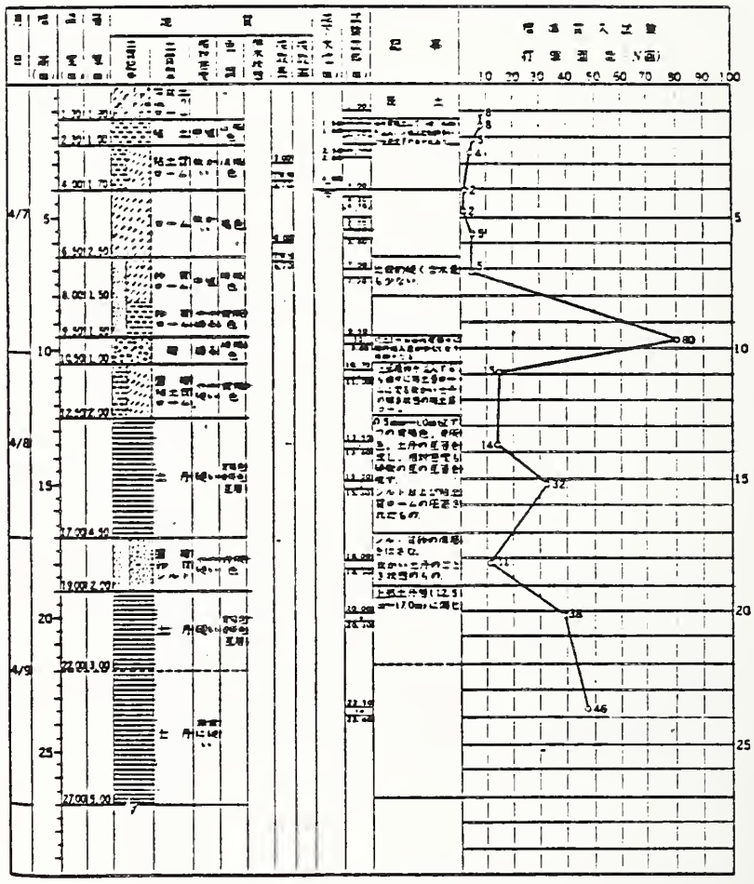

Fig. 2 Soil Profile by Boring

(HACHINOHE City office)

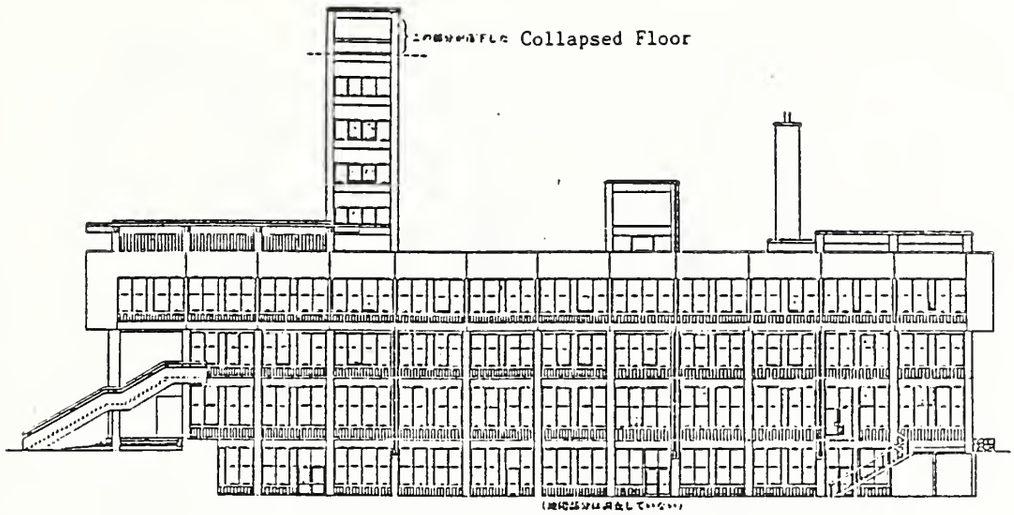

Fig. 3 North Side Elevation of Old City Office
and Damaged Windows in 1968 (Ref.4)

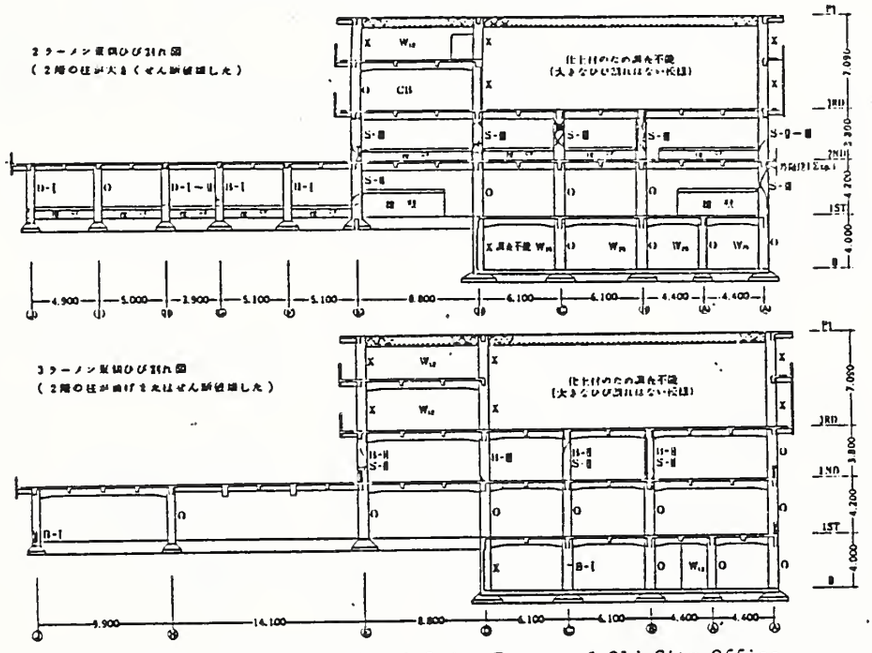

Fig. 4 Section of 2nd & 3rd - Frames of Old City Office
and the Damage of Columns in 1968 (Ref.4)

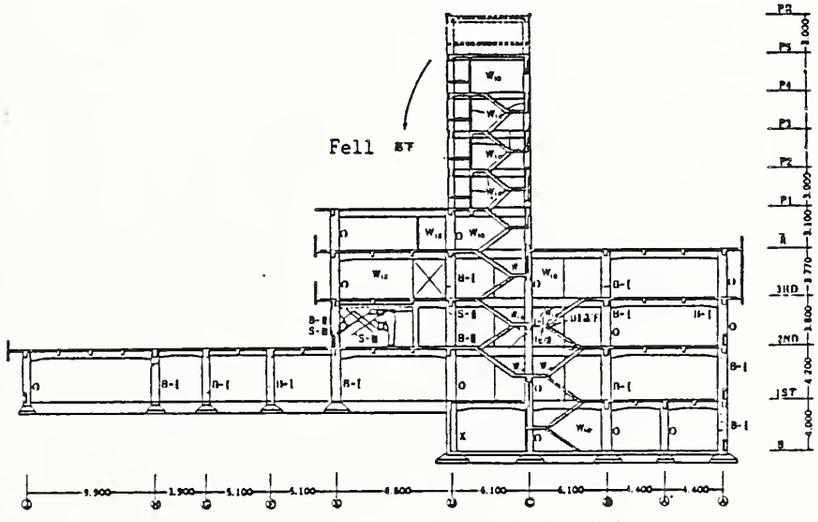

Fig. 5 Section of 4th-Frame of Old City Office
and the Damage of Columns in 1968 (Ref.4)

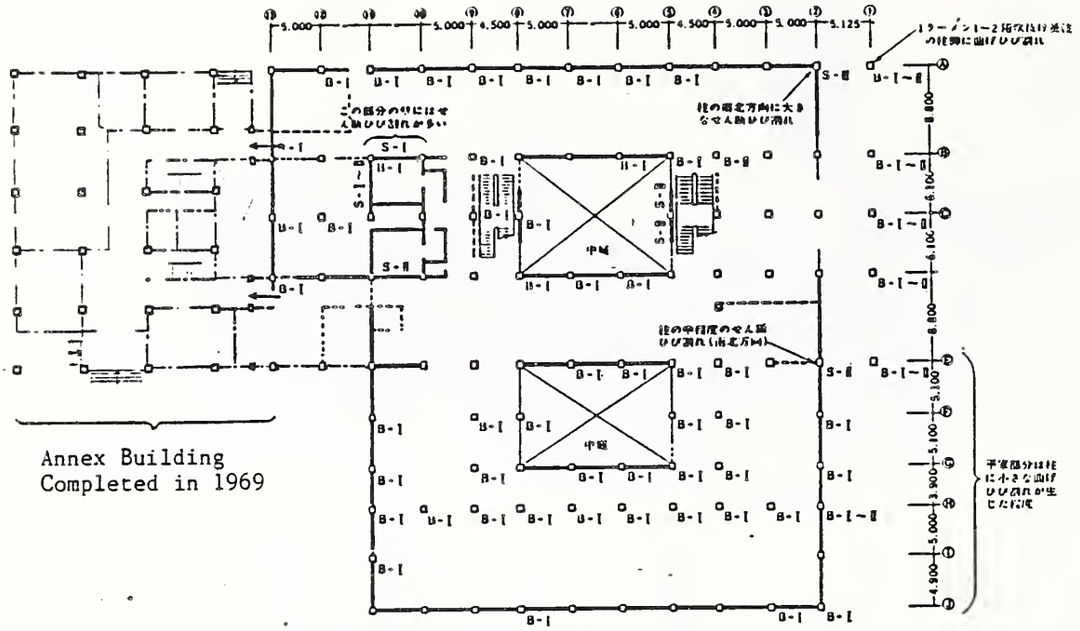

Fig. 6 1st Floor Plan of Old City Office and the Damage in 1968 (Ref.4)

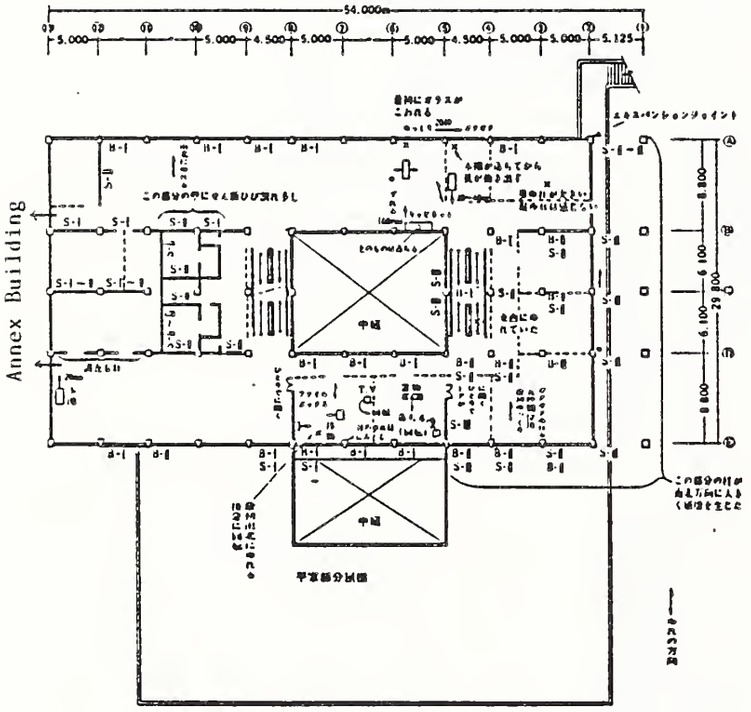

Fig. 7 Second Floor Plan of Old City Office and the Damage in 1968 (Ref.4)

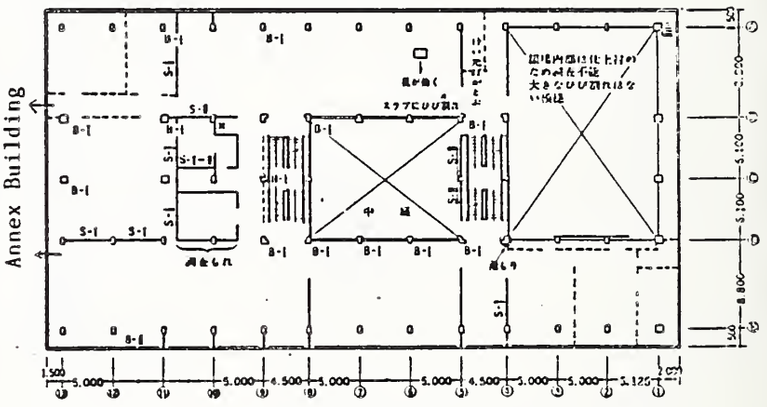

Fig. 8 Third Floor Plan of Old City Office and the Damage in 1968 (Ref.4)

----- Dotted lines show the added walles for strengthening after the 1968 earthquake.

code	damage
B-1	small bending cracks
B-2	large bending cracks
B-3	very large bending cracks
S-1	small shear cracks
S-2	large shear cracks
S-3	very large shear cracks

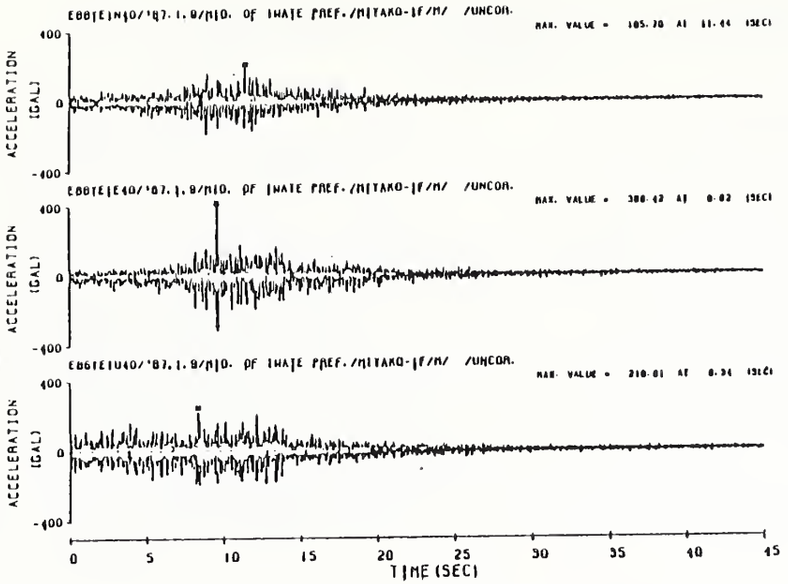

Fig. 9 Uncorrected Accelerograms of MIYAKO 1F

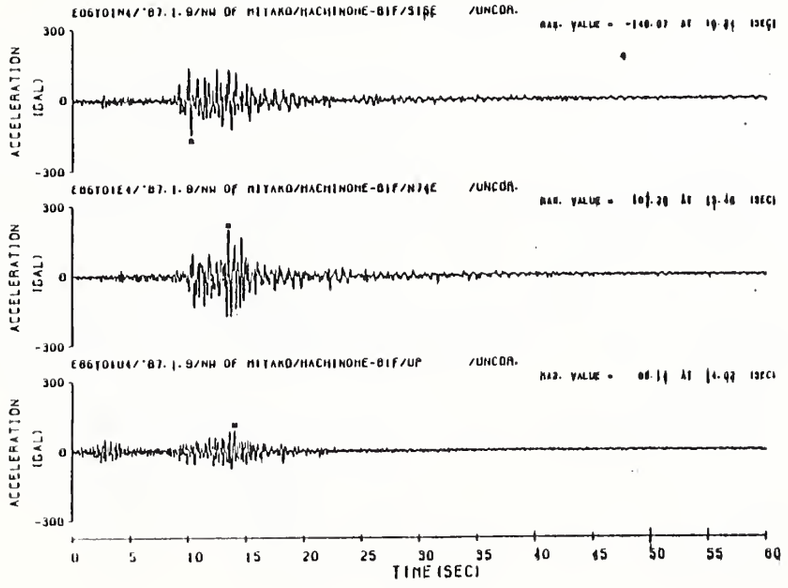

Fig. 10 Uncorrected Accelerograms of HACHINOHE B1F

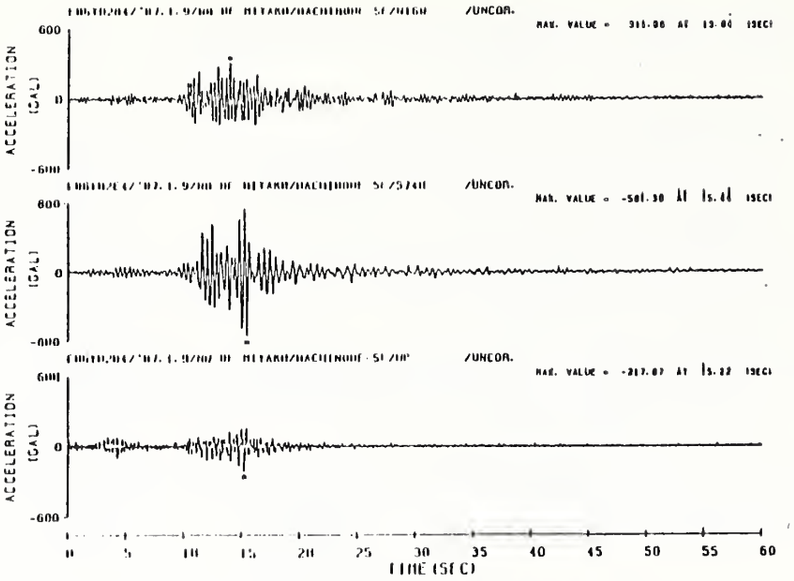

Fig. 11 Uncorrected Accelerograms of HACHINOHE 5F

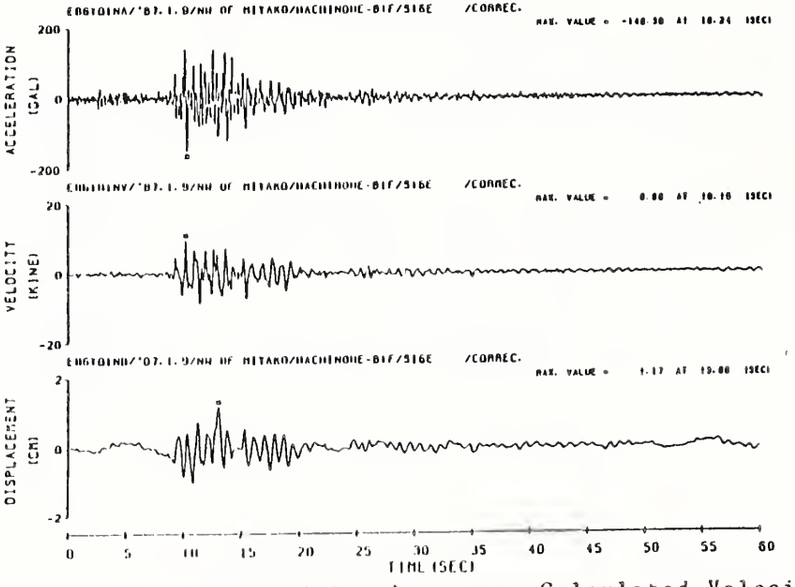

Fig. 12 Corrected Accelerogram, Calculated Velocity and Displacement of NS Component at HACHINOHE B1F

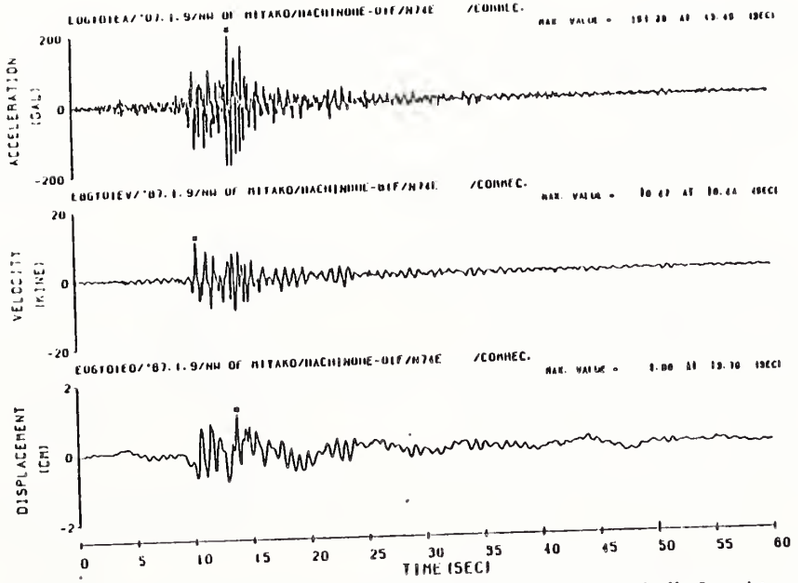

Fig. 13 Corrected Accelerogram, Calculated Velocity and Displacement of EW Component at HACHINOHE B1F

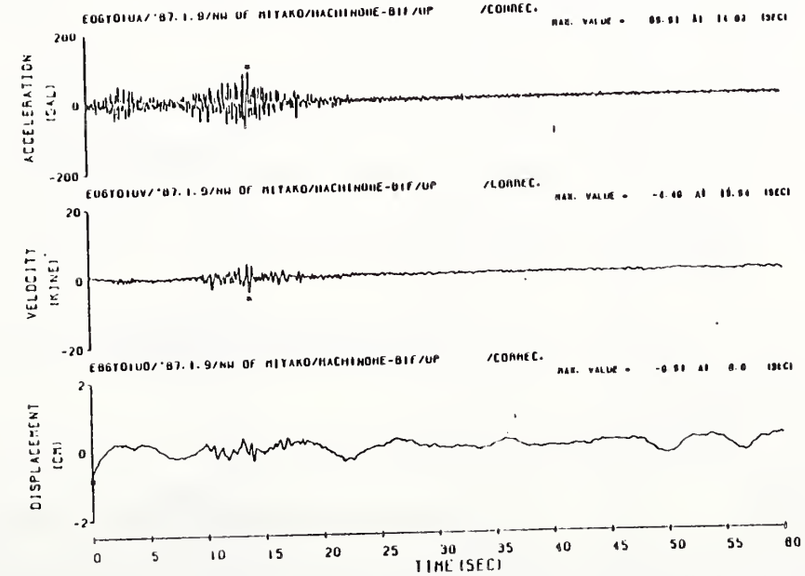

Fig. 14 Corrected Accelerogram, Calculated Velocity and Displacement of UD Component at HACHINOHE B1F

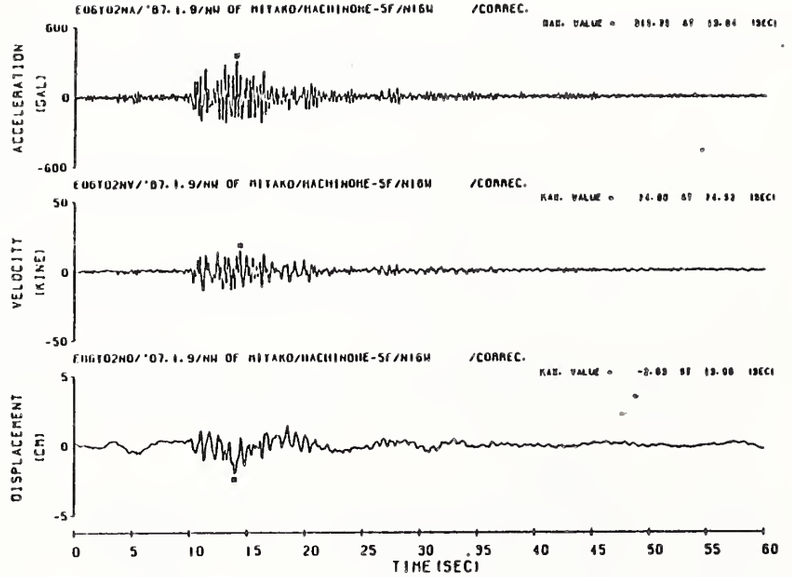

Fig. 15 Corrected Accelerogram, Calculated Velocity and Displacement of NS Component at HACHINOHE 5F

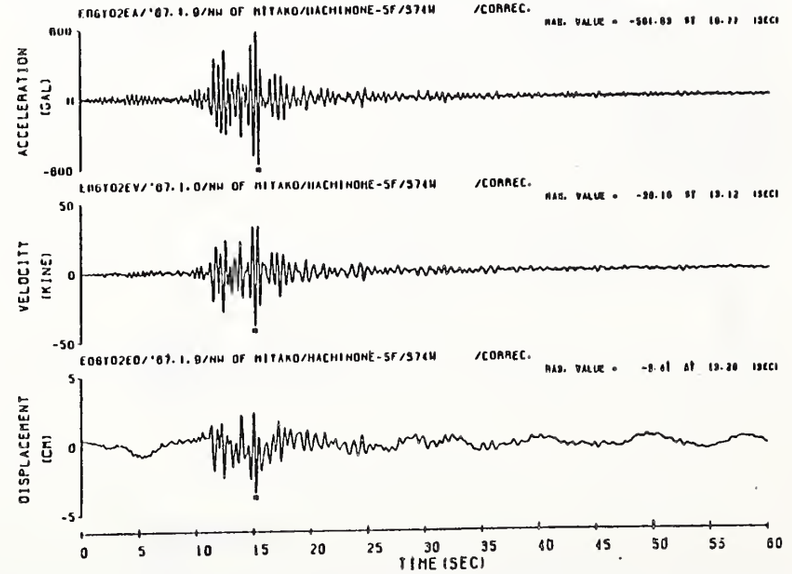

Fig. 16 Corrected Accelerogram, Calculated Velocity and Displacement of EW Component at HACHINOHE 5F

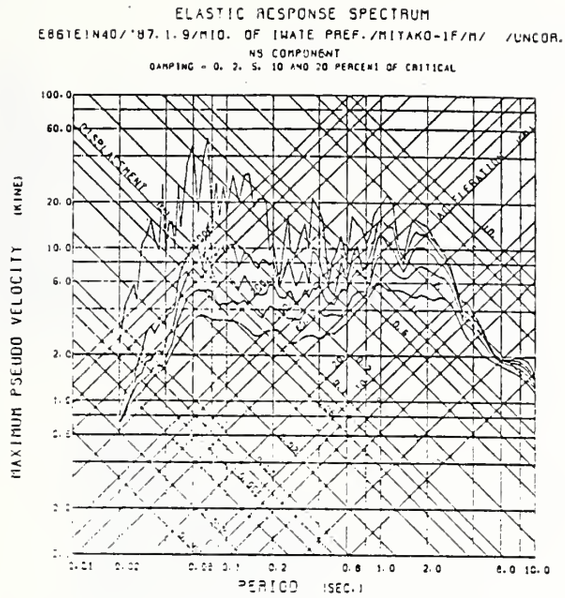

Fig. 17 Response Spectrum (NS, MIYAKO 1F)

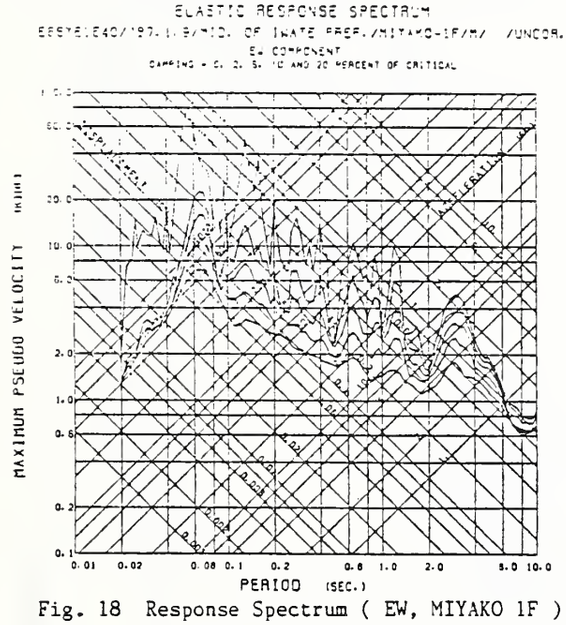

Fig. 18 Response Spectrum (EW, MIYAKO 1F)

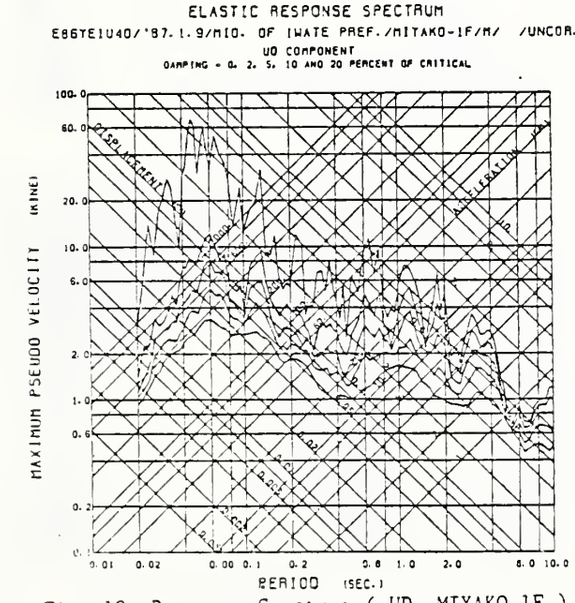

Fig. 19 Response Spectrum (UD, MIYAKO 1F)

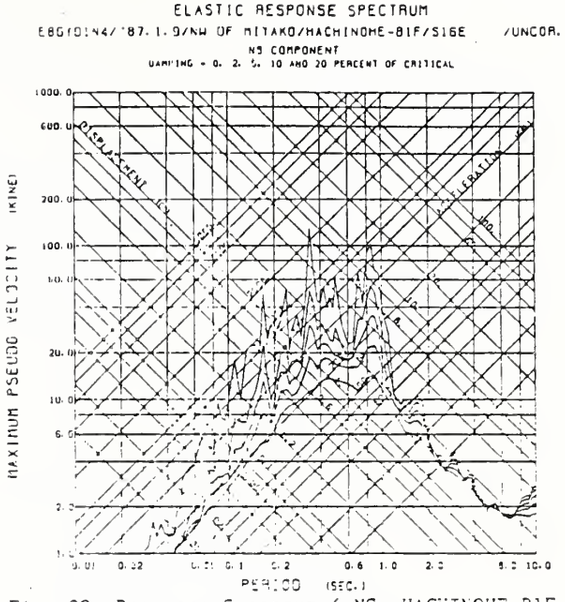

Fig. 20 Response Spectrum (NS, HACHINOHE B1F)

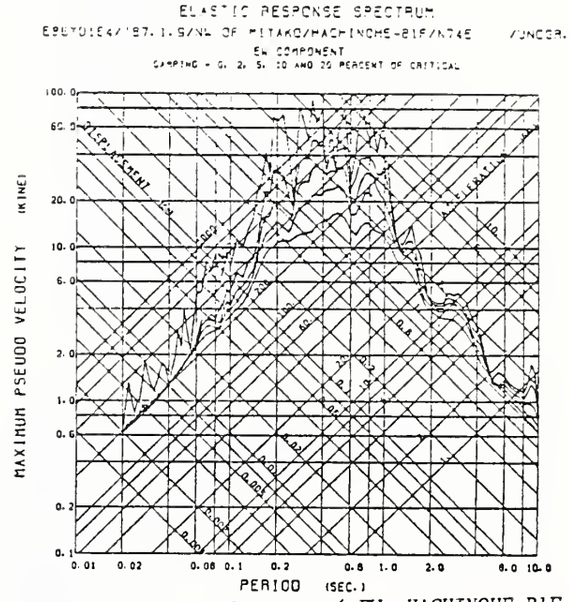

Fig. 21 Response Spectrum (EW, HACHINOHE B1F)

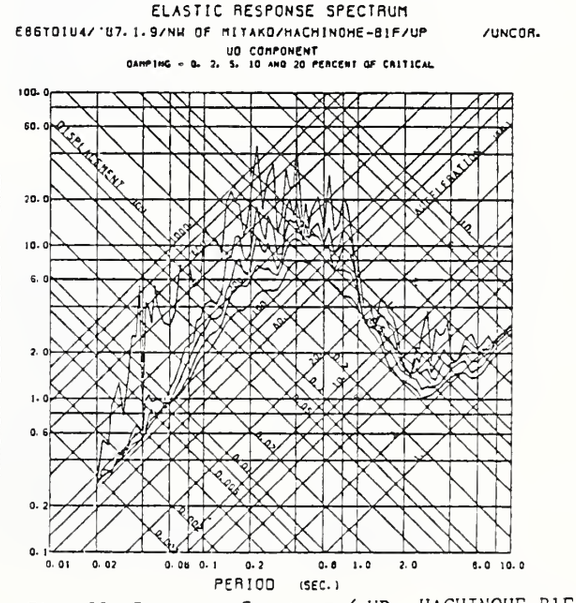

Fig. 22 Response Spectrum (UD, HACHINOHE B1F)

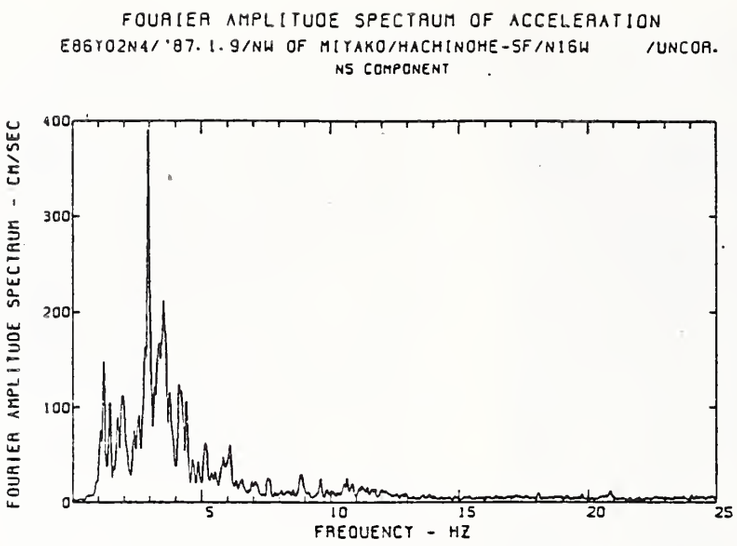

Fig. 23 Fourier Amplitude Spectrum of NS Comp. at HACHINOHE 5F

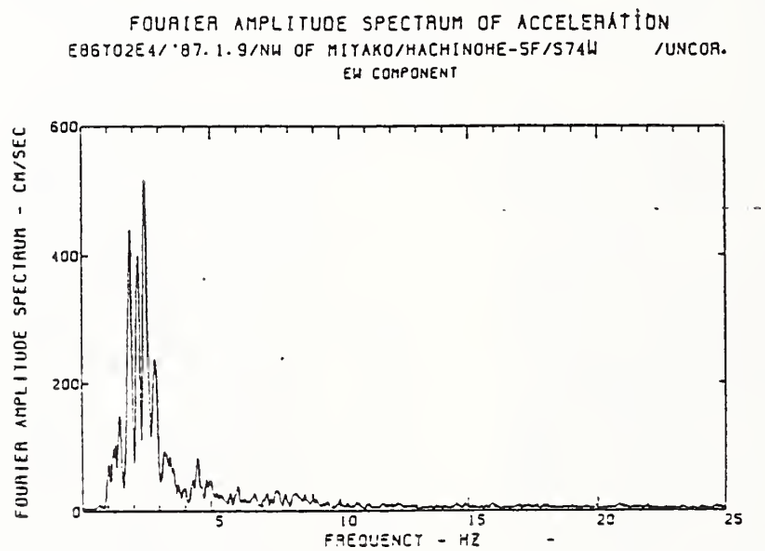

Fig. 24 Fourier Amplitude Spectrum of EW Comp. at HACHINOHE 5F

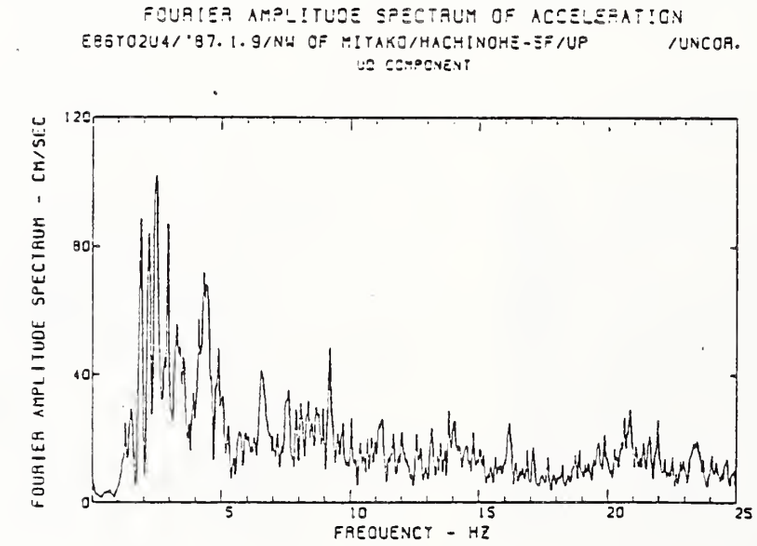

Fig. 25 Fourier Amplitude Spectrum of UD Comp. at HACHINOHE 5F

Photo 1 Atago Junior High School in MIYAKO

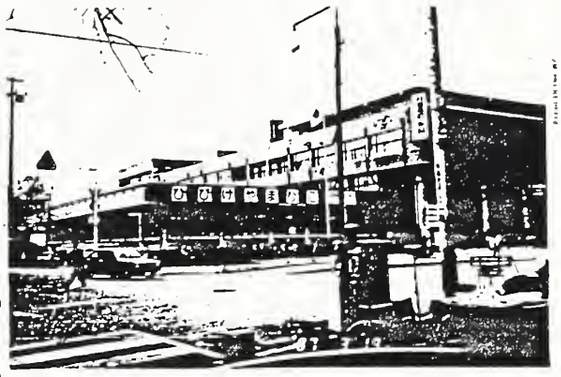

Photo 2 Old City Office in HACHINOHE (March, 1987)

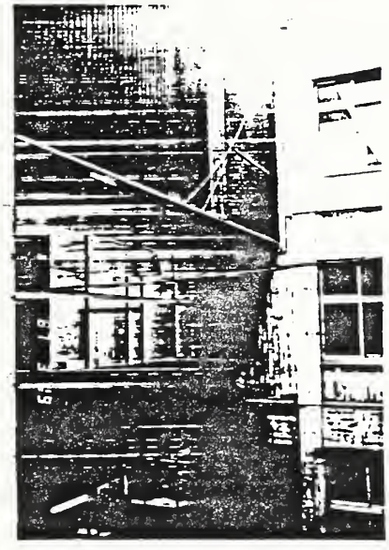

Photo 3 Expansion Joint between Old and Annex Building of City Office

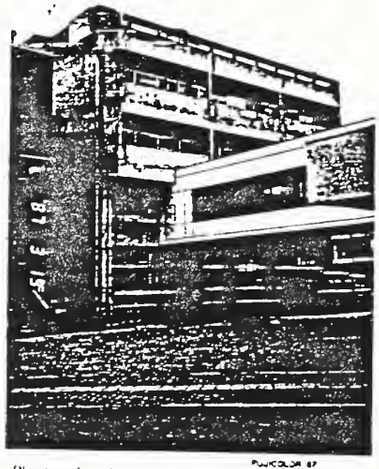

Photo 4 Annex Building of HACHINOHE City Office

Photo 5 Damage of Column by the Spandrel Walls during the Earthquake of 1987

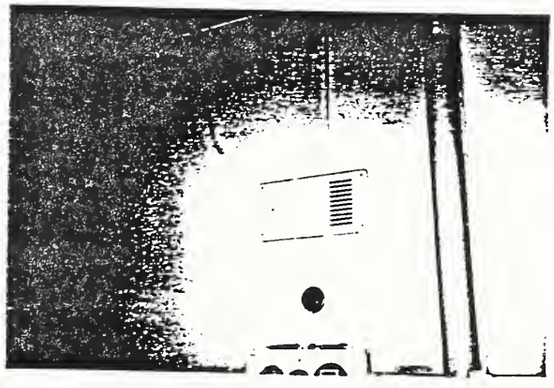

Photo 6 Damage of Walls during the Earthquke of 1987 (These walls are added after 1968)

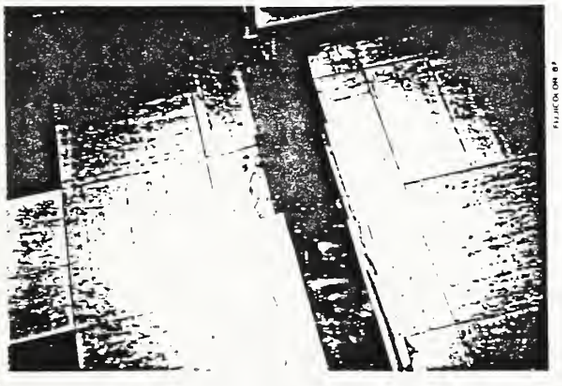

Photo 7 Damage of Expansion Joint by the Collision of Both Buildings during the Earthquke of 1987

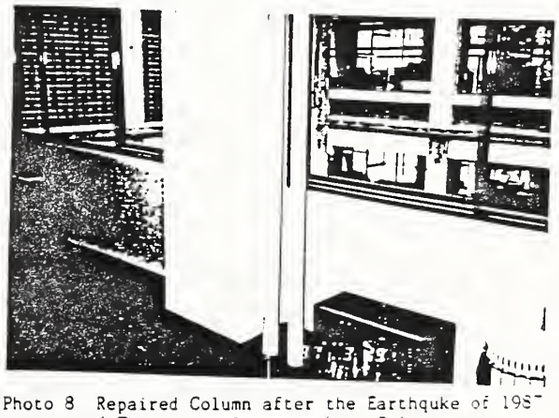

Photo 8 Repaired Column after the Earthquke of 1987 (The same column as photo 5)

Appendix:

Ten Task Committee Reports

Report of Task Committee on

(A) STRONG-MOTION INSTRUMENT ARRAYS AND DATA

Date: May 14, 1987

Place: Public Works Research Institute, Ministry of Construction
Toyosato-machi, Tsukuba-gun, Ibaraki-ken 305, Japan

Attendees:

Japan Side -	H. Tsuchida (Chairman)	(PHRI)
	S. Hattori	(BRI)
	M. Katsumata	(MRI)
	K. Ohtani	(NRCDP)
	Y. Sasaki	(PWRI)
	S. Noda	(PHRI)
	T. Kuwabara (Observer)	(PWRI)
	K. Tamura (Observer)	(PWRI)
U.S. Side -	A.G. Brady (Chairman)	(USGS)
	A.G. Franklin	(WES)
	R.R. Ledzian	(USBR)
	H. Meyers	(NOAA)

I. Activities and Principal Accomplishments to Date

1) Catalogs of strong-motion earthquake records observed both in the United States and Japan are being exchanged. U.S. data are published in the "Seismic Engineering Program Report," and the Japanese data are published in "Strong-Motion Earthquake Records in Japan." Many other publications were also exchanged.

2) Preparation was made for the workshop on strong-motion earthquake observation, which is expected to be held in August 1987. (See No. 10, following)

3) A progress report with ideas for consideration in a policy for international dissemination of strong-motion earthquake records has been prepared and presented to the Task Committee Meeting and, subsequently, to the Panel. (See No.12, following)

II. Future Programs

1. After an earthquake which has caused damage to structures or an earthquake during which maximum acceleration exceeding about 0.1g has been recorded, the task committee of the country where the earthquake has taken place will provide a list of the strong-motion earthquake records for the counterpart of the task committee. The list contains maximum component acceleration of each record. If there is such a list compiled by any organization, the list mentioned above may be replaced by it.

2. Every year the task committee will exchange catalogs of the strong-motion earthquake records during the previous year. The catalog contains maximum component accelerations and wave forms of major records. If there is such a catalog compiled by any organization, the catalog mentioned above may be replaced by it.

3 The Task Committee makes appropriate arrangements to provide digitizable copies of records when they are requested. In addition, arrangements will be made to provide information on the characteristics of the site, instrumentation, and structures at the locations where such records are obtained.

4. When the organizations taking part in the Panel publish reports on strong-motion earthquake records, these organizations will distribute copies of the reports to the other organizations of the Panel interested in them. The Task Committee exchanges lists of the organizations and their Panel representatives who wish to receive the reports.

5. The Task Committee will continue to exchange digitized data on all the major strong-motion earthquake records recovered in both countries, under the conditions mutually acceptable to the agencies involved in acquisition of the data.

6. The Task Committee will exchange technical information concerning seismometers and accelerometers to be developed, and the deployment and installation of instruments with emphasis on bore-hole instruments, and the design of seismic arrays.

7. The Task Committee plans to assist and cooperate, where possible, in the following areas:

   a. Assistance and cooperation with governmental organizations in other seismic areas, in order to promote high quality strong earthquake motion observations in all seismically active areas of the world.
   b. Assistance and cooperation with any international effort to record strong ground motion close to the source of a large magnitude shock.
   c. Exchange of scientists, engineers, and appropriate equipment in a timely fashion for observations following large earthquakes in either country. As the largest and most interesting aftershocks occur immediately following the main earthquake, recovery of the most useful aftershock data requires that the response to major earthquakes be initiated as rapidly as logistics permit.

8. The Task Committee feels the UJNR Panel on Wind and Seismic Effects should play a major cooperative role in the implementation of relevant parts of the Resolution of the International Workshop on Strong-Motion Earthquake Instrument Arrays held May 1978, in Honolulu, Hawaii. The exchange of complete information on all aspects of the program, as it develops particularly in Japan and the United States, will be carried out in the manner of our standard exchange when appropriate. Particularly with unique data from arrays, or deep bore-hole instruments in the U.S. and Japan, Task Committee Chairmen will retain the responsibility of relaying information on their existence and subsequently of transferring the digital data from such institutions as the USGS, CDMG, USC, and UCSD in the U.S.; and PWRI, BRI, PHRI, MRI, and NRCDP in Japan.

9. The Task Committee recommends collaborative studies involving strong-motion instrumentation and interpretation of resulting strong-motion data sets for purposes of earthquake hazard reduction.

10. The Task Committee will hold a workshop on Strong-Motion Earthquake Observation in the San Francisco area in August 1987. The details of the workshop program will be discussed between both Task-Committee chairmen and include array and network planning, recording instrumentation, digitizing hardware, and the digitization of representative records.

11. The Task Committee recognizes that another workshop on Processing of Seismic Strong Motion Records to be held in Vancouver in August 1987 is significantly relevant and would complement the Panel's Workshop. The Task Committee urges that Panel members contribute to this workshop.

12. The Panel discussed the occasional, but extended, unavailability of existing strong-motion data of engineering significance from very large earthquakes outside the U.S. and Japan. Based on input from the earthquake engineering data community, and guidance from the Panel on Wind and Seismic Effects, the Task Committee will draft a policy for international dissemination of strong-motion earthquake records for consideration by the Panel.

PROGRESS REPORT
WITH IDEAS FOR CONSIDERATION OF
A POLICY FOR INTERNATIONAL DISSEMINATION
OF
STRONG-MOTION EARTHQUAKE RECORDS

May 15, 1987

Task Committee on (A) Strong-Motion Instrument Arrays and Data
U.S.-Japan Panel on Wind and Seismic Effects, UJNR

1. Introduction

At the 18th Joint Panel Meeting held in May 1986, in Washington D. C., it was pointed out that some strong-motion records of significantly large earthquakes which had taken place in countries other than U.S. and Japan are still not available. It was also pointed out that there were many matters to be considered in establishing a dissemination rule which would be accepted by both the disseminating group and the users group. The Panel assigned the Task Committee-A to study this subject and propose a policy for for international dissemination of strong-motion earthquake records.

The Task Committee started its activity on this subject immediately after the 18th Joint Panel Meeting and has determined 1) necessary information and data to study the policy, 2) necessary considerations from viewpoints of the disseminators and the users, and 3) tentative contents of the final report. Then the task committee started to collect the data, the information, and the viewpoints.

This is a progress report to present the direction of the activity and achievement so far.

2. Tentative Contents of Final Report

The Task Committee-A determined tentatively the contents of the final report, included as an Appendix to this report. The Task Committee is presently engaged in collecting information and data and discussions to complete the report along the liues of the proposed contents.

3. Considerations for Establishing Policy

People related to strong-motion earthquake records can be divided into two groups. The first group consists of people engaged in the installation and operation of instruments, data processing, and dissemination of the records. This group will be called, tentatively in this report, the disseminators group. The other group consists of people who are using the records in practice or research. This group will be called the users

group. Some people may belong to both groups.

The conditions for record dissemination desired by the disseminators group may not harmonize with those of the users group. If the policy for the records dissemination fails to encourage the disseminators group or at least to be accepted by them, people of the group will be discouraged in continuing and expanding their efforts. This may cause contraction of the observation activity and as a result less opportunity for the users group to obtain the strong motion records of future earthquakes. On the other hand, if the policy considers too much the conditions requested by the disseminators group, people of the users group may meet inconveniences or impossibilities to obtain the records. This may cause inefficiency in utilizing the strong motion records and progress in earthquake engineering. Therefore, the policy should consider the conditions requested by the disseminators and users groups in appropriate balance.

The Task Committee is collecting the possible conditions from both groups and evaluating them. The conditions collected by this time are presented in the following subsections. The conditions are just "collected conditions" and are not "selected conditions for the policy." So, some of them may be contradictory to each other or overlapping each other, at this moment.

3.1 Conditions from Users' Viewpoint

The users hope that:

1) After an significantly large earthquake, the records are made available as many as possible and as soon as possible.

2) At least, the waveforms and the peak values are made available immediately after an significantly large earthquake.

3) Whether a field investigation team on seismic damage has had information or not on the ground motions which caused the damage makes big difference in fruitfulness of the investigation. Therefore, copies of the records are available to all the field investigation teams at an appropriate time.

4) For planning and design of restoration of damaged structures, the strong motion records are very important. High priority is given for such users.

5) Data bases of the strong motion earthquake records are provided and they can be accessed through the telephone cable.

6) When responsibility to the damage is questioned to the designer or the constructor, the strong motion earthquake record is very important information for the judgement. The record should be made availabe to the people in concern.

7) For assessing the possible aftershock of the largest magnitude to organize rescue activities and preparedness program, the strong motion earthquake record is very helpful.

8) Organizations such as World Data Center, NOAA is established.

9) Instrument characteristics are made available together with the strong motion earthquake records.

10) Information is attached to the record on the data processing details, such as procedures of the base-line correction, the instrument correction, the interpolation of data, etc.

3.2 Conditions from Disseminators' Viewpoint

The disseminators consider that:

1) Some of the strong motion networks are operated by researchers and their final tasks are to produce research reports which contribute to the scientific progress and to the practical application, not to disseminate the records. For such cases, the priority for the network operator to use the records for his research purpose has to be guaranteed. Otherwise, the records are made public after certain periods from the recovery. (Some researchers may analyze the records in a very similar way which the operator has had in his mind, when the operator is very busy to process and disseminate the records.)

2) Following case may happen. A researcher operator obtained some significant records and he analyzed and published a report. Then, he made his records public. However, he had intention to make some statistical analysis on all his records, when the records would reach at volume of his satisfaction. Unfortunately, other researchers made a similar statistical analysis and presented an empirical formula such as a magnitude-epicentral distance-peak acceleration relationship, while the record owner is waiting for additional records. The researcher operator lost opportunity to present his own formula although he has his own records.

3) Observation, processing, and dissemination of the strong motion records requires high knowledge and time consuming efforts of the disseminators. This effort of the high knowlegable people is not sufficiently respected by the users. The user's recognition on this point has to be improved for promoting the wide and quick circulation of the strong motion earthquake records.

4) The disseminators willingly make their records public at the

earliest possibility, if the priority for the researcher operator to make his report on his records and the disseminators' efforts are adequately recognized.

5) The disseminators wish to know all the users who used their records to ensure future information distributions such as correction of the records or the instrument characteristics.

6) The researcher operators are not working full time for the strong motion records. Their time is limited. Therefore, the records from the network operated by the researcher-operator can not be made public immediately. Strengthening of personnel and expenditure is essential.

7) Records of structural response should be made public after careful consideration. Some researchers who are not familiar with such structures may make an inadequate interpretation and judge the structure unsafe, although it will be judged safe by the researchers familiar with such structure. Inadequate interpretation and its public release may cause social problems. Before the public release, the agreement of the structure's owner should be confirmed.

8) Some researchers are applying corrections to the records obtained by others and making a data base. Even if such a case, the priority and recognition of the original records should be guaranteed.

9) Stronger requests to make the records public are made to the government agencies than to the private organizations. The records owned by private organizations are as useful as the government agencies. The request should be made equally to the government agencies and to the private organizations.

10) The users should give the original record owner credit for his effort in an appropriate way, such that the source of the records is clearly described in a reference list of the report.

Appendix

Task Committee Report on Policy for International Dissemination of Strong-Motion Earthquake Records

Contents (proposed)

4.2 Considerations from Network Operators' Viewpoint
4.3 Considerations to be included in the Policy
4.3.1 With respect to researchers engaged in observation, processing, and dissemination
4.3.2 Priority of record owners in making research reports

5. Proposed Policy

6. Problems for Further Study

Report of Task Committee on

(B) LARGE-SCALE TESTING PROGRAM

Date: May 13, 1987

Place: Public Works Research Institute, Ministry of Construction
Toyosato-machi, Tsukubagun, Ibarakiken,305 Japan

Attendees: Japan Side - K. Ohtani (Chairman) (NRCDP)
S. Noda (PHRI)
S. Okamoto (BRI)
H. Yamanouchi (BRI)
T. Murota (BRI)
Y. Yamazaki (Observer) (BRI)

U. S. Side - H. S. Lew (Chairman) (NBS)
R. J. Smith (COE)

I. Activities and Principal Accomplishments to Date

The main activities related to this task committee during the past year are as follows:

1. The Joint Technical Coordinating Committee on the Masonry Research (JTCCMAR) was held in Keystone, Colorado, in September, 1986. Coordinated research projects on masonry structures were discussed.

2. Active exchanges of U.S. and Japanese researchers have taken place under the Joint Program of Masonry Structures and have been very useful.

3. Testing of a full-scale three-story masonry planar frame was carried out at the BRI in 1986.

4. Construction of a full-scale five-story masonry building has been initiated at the BRI.

5. Research grants have been provided by the National Science Foundation to U.S. research institution. Currently 25 individual research projects are in progress and being coordinated by the U.S. TCCMAR.

II. Future Programs

The status of the U.S.-Japan Joint Program of Masonry Structures was reviewed. The Task Committee adopted the following resolutions:

1. To assure effective exchange of information on masonry structures, Task Committee recommends continuation and expansion of personnel exchange under the coordinated research program.

2. Task Committee discussed topics of future joint research projects. Task Committee will facilitate continued deliberation of the following topics between appropriate U.S. and Japan organizations.

   a. Seismic performance of precast concrete construction.
   b. Seismic performance of composite and mixed constructions.
   c. Application of high strength construction materials, such as concrete and steel, to structures in high seismic zones.
   d. Application of base isolation and controlled damping systems to critical structures located in high seismic and wind zones.

3. The Meeting of the Joint Technical Coordinating Committee on Steel Structures Research is scheduled to be held in Tokyo, July 1987 to summarize the Joint Research Project on steel structures.

4. The 3rd meeting of the Joint Technical Coordinating Committee on Masonry Research is scheduled for Fall, 1987 in Japan.

5. Testing of a full-scale five-story masonry building will begin at the BRI, November, 1987.

6. Task Committee (B), Large-Scale Testing Program and Task Committee (D), Evaluation of Performance of Structures should maintain closer liaison to facilitate the planning of instrumentation and analysis for full-scale test structures.

7. Exchange of information on large-scale testing facilities and large-scale testing programs should be encouraged.

Report of Task Committee on

(C) REPAIR AND RETROFIT OF EXISTING STRUCTURES

Date: May 14, 1987

Place: Public Works Research Institute, Ministry of Construction
Toyosato-machi, Tsukuba-gun, Ibaraki 305, Japan

Attendees: Japan Side - M. Hirosawa (Chairman) (BRI)
M. Shinohara (PWRI)
S. Nakata (Observer) (BRI)

U. S. Side - H.S. Lew (Temporary Chairman) (NBS)

I. Activities and Principal Accomplishments to Date

1. Both U.S. and Japan investigation teams provided technical assistance to repair and retrofit of structures damaged during the 1985 Mexico Earthquake, and related reports have been published.

2. Research grants have been provided by the National Science Foundation to U.S. institutes to carry out research projects on repair and retrofit technology.

3. Manual of Repair Methods for Civil Engineering Structures Damaged by Earthquakes was published by the Ministry of Construction.

4. The fourth workshop on repair and retrofit of structures was held on May 8 and 9, 1987 at the BRI. The outlines of the workshop and its conclusions are in Appendix.

5. Japanese side provided the U.S. side the Japanese handbook on repair and retrofit of reinforced concrete buildings.

II. Future Programs

1. Continue and expand the exchange of reports, books and special publications related to repair and retrofit of existing structures.

2. As a result of successful completion of the fourth workshop on repair and retrofit, the fifth workshop is proposed. Possible date might be in 1988 UJNR meeting to be held in U.S.

3. Compile information on specific projects such as evaluation of particular designs and cost of completed projects.

4. Devote increased attention to developing methods to assess nonstructural items in existing structures which could pose severe hazards and/or cause loss of service. Emphasis should be placed to develop methods for retrofit or repair of important nonstructural elements.

5. Carry out research to evaluate the potential structural benefits and relative economics of using base isolation and supplemental damping devices for retrofitting existing structures. Such devices may be of particular interest for historical or monumental structures in high seismic zone.

6. Maintain liaison with task committee D, "Evaluation of Performance of Structures" and J, "Wind and Earthquake Engineering for Transportation Systems" to exchange information relative to repair and retrofit.

Appendix

Workshop on Repair and Retrofit of Existing Structure
May 8-9, BRI

Activities

5 sessions- 18 presentations

General Discussion on issues

Concluding Remarks

1. Similarities of current techniques for repair and strengthening indicate the opportunities for fruitful exchange of ideas. Commonality of techniques and solutions make such exchange and coordination of activities particularly beneficial in the area of repair and strengthening activities.

2. Presentations emphasized concerns related to performance of elements and connections, need for quality control, cost of construction.

3. There appears to be a need in both countries to stimulate technical discussions on repair and strengthening. This workshop provided a means for initiating further discussions within each country and the desirability of similar joint meetings in the future.

Areas of future research activity

1. Most pressing need is for experimental verification of repair and strengthening techniques in the following areas.
   a) Use of new materials
   b) Development of innovative techniques
   c) Evaluation of foundation effects
   d) Influence of member response on overall structure response
   e) Implementation of analytical techniques calibrated from experimental results.

2. Need to continue efforts for common understanding of performance, design, and construction data. Documentation of data and exchange of information should be carried out to permit development of a data base in area of repair and strengthening.

3. There is a need for studies related to damage control for prevention of environment hazards and for maintenance of operations in existing structures.

4. Discussions between researchers and designers should be continued for maximum benefit from activities underway in each country.
   a) Benchmark structures could be used for comparison of techniques and design procedures.
   b) Typical methods used need to be discussed in detail.
   Examples - bracing systems, infill walls, jacketing columns. It is proposed that future workshops consider a particular topic in detail and prepare a state-of-the-art report for use by designers and researchers.

(D) EVALUATION OF STRUCTURAL PERFORMANCE

Date: May 14,1987

Place: Public Works Research Institute, Ministry of Construction
Toyosato-machi, Tsukuba-gun, Ibaraki 305, Japan

Attendees:

Japan Side -	S. Okamoto (Chairman)	(BRI)
	Y. Ishiyama	(BRI)
	M. Okahara	(PWRI)
	H. Yamanouchi	(BRI)
	Y. Yamazaki (Observer)	(BRI)
U. S. Side -	N.J. Raufaste (Temporary Chairman)	(NBS)
	R. J. Smith	(ARMY)
	R.N. White (Observer)	(Cornell Univ.)
	M. Miyahara (Observer)	(NSF, Tokyo)

I. Activities and Principal Accomplishments to Date

Task Committee D organized three U.S.-Japan workshops on the evaluation of the performance of existing buildings for resistance to earthquakes. The First Workshop on "Seismic Performance of Existing Buildings" was held in Japan in 1983. The Second Workshop was held in the U.S. in 1984. The Third and Final Workshop was held in Japan in 1985, and concentrated on comparisons of evaluations of benchmark structures and on updating information on methodologies by each country.

Comparisons reveal that the various methods are suitably accurate for the expected level of evaluation for buildings with good arrangement of lateral strength elements, and that a general idea of expected damage level can be estimated. However, additional evaluations are recommended to validate and improve the methods to make them more useful, especially for buildings of unusual geometry or with special secondary elements, and to include effects of soil- structure interaction.

The proceedings of the three workshops were published in three volumes* (1983, 1984, 1985) and were summarized in two papers: (1) "Performance of Existing Buildings: Results of Benchmark Structure Analyses Performed in U.S.-Japan Workshops", by R.N. White and P. Gergely, Proc. of Third ASCE EMD Conference on Dynamic Response of Structures, Los Angeles, April 1986, and (2) "Seismic Performance of Existing Buildings", by P. Gergely, R.N. White, and G.R. Fuller, Proc. of Third U.S. National Conference on Earthquake Engineering, Charleston, S.C., August 1986.

* Available from R.N. White, Cornell University, Ithaca, N.Y. 14853

A status report was presented on development of ATC-14 report, "Methods for Evaluating the Seismic Strength of Existing Buildings," and ATC-20, "Development of Procedures for Post-Earthquake Safety Evaluation of Buildings" was described.

Discussion concluded with a presentation on the status of various related projects, objectives, and possible future activities to be pursued.

II. Future Programs

The Task Committee reconfirmed its objectives and activities at the May 14, 1987 meeting and agreed to the following:

1. Encourage the continued exchange of literature, analyses, and research reports relative to assessment of seismic resistance of buildings.

2. Promote the dissemination of research findings to the other task committee chairmen and to the design and construction community.

3. Expand the catalog of benchmark existing buildings in each country that have been evaluated and instrumented.

4. Continue to evaluate other buildings in Japan, U.S. and other countries where data are available using Japanese and American methods of analysis including provisions of ATC-14.

5. Improve screening and evaluation methods for determination of seismic resistance of existing buildings, and identify research needs to improve evaluation technology.

6. Continue to plan joint activities with Task Committees B and C by encouraging summer meetings of the three chairmen in each country.

7. Participating government agencies in UJNR with missions in evaluating structural performance will be contacted by the Task Committee chairmen in both countries for continued support for the Task Committee activities.

Report of the Task Committee on

(E) NATURAL HAZARD ASSESSMENT AND MITIGATION THROUGH LAND USE PROGRAMS

Date: May 13, 1987

Place: Public Works Research Institute, Ministry of Construction, Toyosato-machi, Tsukuba-Gun, Ibaraki-ken, 305 Japan

Attendess: Japan Side - K. Kawashima (Chairman) (PWRI)
S. Hattori (BRI)
M. Nagaoka (GSI)
Y. Sugimura (BRI)
U. S. Side - A. G. Brady (Temporary Chairman) (USGS)
L.R.L. Wang
(Old Dominion University)

I. Activities and Principal Accomplishments to Date

1. The Gecgraphical Survey Institute (GSI) of Japan has been developing mapping procedures for natural hazard prediction.

The Public Works Research Institute (PWRI) of Japan has revised a procedure for assessing direct and indirect losses from earthquake disasters, and the direct and indirect losses were evaluated for the Miyagi-ken-oki eathquake of 1978 and the Nihon-kai chubu earthquake of 1983.

The Building Research Institute (BRI) of Japan is developing automatic computer programs for analyzing the expected ground intensity at an arbitrary site, and has made analyses on ground response characteristics.

The National Research Center for Disaster Prevention of Japan has been developing a seismic microzoning method using an urban ground database, and applying satellite remote sensing technology to natural disaster prevention.

2. The U.S. Geological Survey conducts a broad based program in natural hazards reduction. This program includes assessment of: (1) earthquake ground motion; (2) soil liquefaction potential; (3) landslide potential; and (4) earthquake economic losses.

3. Several papers pertaining to Task Committee (E) were included in the proceedings of the 19th Joint Panel Meeting:

a. Theme II "Earthquake Engineering"
b. Theme III "Storm Surge and Tsunamis"

II. Future Programs

1. Both sides will continue to exchange technical information on the following subjects:

a. Evaluation of seismic hazard and mapping procedures.
b. Evaluation of damage potential of structures, soil liquefaction potential and tsunami hazard.
c. Seismic response characteristics under various ground and topographic conditions.
d. Planning methodologies for earthquake disaster mitigation in large populated cities.
e. Evaluation of socio-economic losses from earthquake disasters.

2. Both sides will continue to promote coordinated research and exchange of specialists in natural hazard assessment and mitigation through land use programs.

3. The U.S. chairman will furnish to task committee members future reports on natural hazard assessment and mitigation through land use programs being coordinated or sponsored by the Federal Emergency Management Agency (FEMA), the Interagency Coordinating Committee of the National Earthquake Hazards Reduction Program (ICC/NEHRP), the U.S. Geological Survey (USGS), the National Science Foundation (NSF), the National Academy of Science (NAS) and National Academy of Engineering (NAE).

   The Japanese chairman will perform his similar responsibilities for reports from National Research Center for Disaster Prevention (NRCDP), Geographical Survey Institute (GSI), Public Works Research Institute (PWRI), Building Research Institute (BRI), and Port and Harbor Research Institute (PHRI).

4. Each member of the Task Committee shall provide to his chairman in time for a report at the 20th Joint Meeting in 1988, a one or two page description of his contributions to a projected workshop in May 1989. The contributions are to come from the subjects in paragraph II-1. above, and are to include an outline of research and expected results (in the form of publications, etc.) The two chairmen will compile these brief descriptions into a report to the Panel at the 20th Joint Meeting in May 1988.

Report of Task Committee on

(F) DISASTER PREVENTION METHODS FOR LIFELINE SYSTEMS

Date: May 14, 1987

Place: Public Works Research Institute, Ministry of Construction
Toyosato-machi, Tsukuba-gun, Ibaraki 305, Japan

Attendees: Japan Side - T. Iwasaki (Chairman) (PWRI)
K. Kawashima (PWRI)
H. Sugita (Observer) (PWRI)

U. S. Side - J. V. Tyrrell (Temporary Chairman) (NFEC)
L.R.L. Wang (Old Dominion University)
J.H. GATES (Cal Trans)

I. Activities and Principal Accomplishments to Date

1. In August, 1986 Task Committee Co-Chairman, Dr. T. Iwasaki (PWRI) attended the 3rd U.S. National Conference on Earthquake Engineering, Charleston, South Carolina. A planning conference was held during his visit and was attended by Dr. Iwasaki, Dr. S. C. Liu, Dr. Leon Wang, Dr. Masanobu Shinozuka, and others. The possibility of a U.S.-Japan Workshop on Lifeline Systems was discussed.

2. A technical report by PWRI entitled, "The Manual of Repair Methods for Civil Engineering Structures Damaged by Earthquakes (in Japanese)" was made available to NSF. In the Manual procedures of damage surveys and repair works for civil engineering structures including buried sewer pipelines are described. An outline of the results of this research project was introduced at the 18th UJNR Joint Meeting of the Panel on Wind and Seismic Effects. PWRI authorized NSF for its translation into English and for distribution to the U.S. professional community. Currently, the document is being considered for translation by NSF.

3. Complete copies of the Manual report (Japanese version) were distributed to concerned individuals of U.S. and Japan during the 19th UJNR Joint Meeting. To introduce the Manual training courses were held in Tokyo, Sendai, and Nagoya in April, 1987, in which about 1,000 practicing engineers participated.

4. PWRI is also conducting a dense instrument array measurement program at PWRI campus and in Shizuoka Prefecture to identify ground motions applicable to seismic design of buried pipeline structures. An outline of the dense instrument array program was presented at the 18th UJNR Joint Meeting.

The Ministry of Construction is promoting the construction of cable box systems (CAB systems) under urban highways, in order to move aerial cables (for electricity and telecommunication) into underground cable boxes, and has prepared Technical Standards for CAB Systems (Draft). In conjunction with these activities, PWRI has proposed a seismic design procedure of CAB Systems and conducted dynamic experiments for examining the seismic safety of CAB systems. An outline of the Technical Standards for CAB systems (Draft) and the dynamic experiments was reported during the 18th UJNR Joint Meeting.

5. In U.S., a study program to assess the design and operating standards for lifeline systems has been initiated by the Building Seismic Safety Council (BSSC) under the support of the Federal Emergency Managment Agency (FEMA), with the broad participation of ASCE members and other professionals. A workshop on abatement of earthquake hazards to lifelines was held in November, 1986 in Denver, Colorado, and the proceedings will be available and distributed soon.

6. NSF has continued the support of a number of research projects dealing with lifeline earthquake engineering. Among them, experimental results and analytical results were presented during the 19th UJNR Joint Meeting.

   The strong motion array project (SMART) and the soil response measurement project have been continuously operated and new data has been recorded. The data recorded from these projects is being continuously exchanged between the two countries.

II. Future Programs

1. The members of the Task Committee will facilitate the continued exchange for technical information and cooperation in research on specialized problems listed as follows:

   a. Survey reports of seismic damage to lifeline systems and seismic observation results
   b. Seismic design procedures for lifeline systems
   c. Procedures and instrumentation to detect and inspect damage and the behavior of lifeline structures during earthquakes
   d. Repair and retrofit methodology for lifeline systems
   e. Estimation of reliability of lifelines
   f. Management and public education on importance of lifeline systems
   g. Investigation of needs for large-scale testing of lifeline systems

2. It is recommended to continue U.S.-Japan coordinated research projcts on field observations and analyses on seismic behavior of buried pipelines, experiments and analyses on dynamic characteristics of joint behavior, effects of soil liquefaction on buried pipes, soil-buried pipes interaction, seismic reliability of lifeline systems, and seismic design methods. As for field observation, the Japan side will concentrate on seismic behavior of pipelines buried in soft soils and in boundary layers between hard and soft soils, whereas the U.S. side will focus on dynamic behavior of pipelines buried in and near active faults.

3. To promote U.S.-Japan coordinated research programs in earthquake resistance of lifeline facilities, it is recommended to plan a U.S.-Japan Workshop on lifeline earthquake enginering in 1989. Time, location and topics of this Workshop will be discussed between relevant individuals of both countries. The details of this Workshop will be finalized during the 20th UJNR Joint Meeting to be held in Washington, DC, in May 1988.

4. The Task Committee recognizes the importance and potential impact to the engineering practice of the Manual of Repair Methods for Civil Engineering Structures Damaged by Earthquakes (Draft) (in Japanese) prepared by PWRI, and recommends that the current translation of the document into English be given a high priority and the document be made available for wide distribution as soon as possible.

5. Drs. T. Iwasaki and K. Kawashima of PWRI and Dr. Leon Wang of Old Dominion University are proposing a joint research project on seismic component design, analysis and experimental observation of buried pipelines including the effects of pipe-structure interaction, and seismically induced soil liquefaction.

6. Dr. T.D. O'Rourke of Cornell University is visiting Japan in the beginning of June 1987 to discuss with Japanese experts a possible coordinated research project for studying the effects of large ground movements on buried pipelines.

Report of Task Committee on

(G) WIND CHARACTERISTICS AND STRUCTURAL RESPONSE

Date: May 14, 1987

Place: Public Works Research Institute, Ministry of Construction
Toyosato-machi, Tsukuba-gun, Ibaraki-ken 305, Japan

Attendees: Japan Side - K. Kurashige (Chairman) (MRI)
T. Fujitani (MRI)
T. Murota (BRI)
N. Narita (PWRI)
K. Yokoyama (PWRI)

U. S. Side - C.F. Galambos (Temporary Chairman)(FHWA)

I. Activities and Principal Accomplishments to Date

Noting that:

a. High winds frequently cause loss of life and extensive property damage.
b. The knowledge derived from the exchange of high wind date and information on wind effects can be useful in reducing loss of life and property damage,
c. Insufficient knowledge exists on the effects of high winds on structures and methods for modeling these effect, and
d. The needs for wind data for various applications and new projects are increasing.

The Task Committee carried out the following activities:

1. The following document was exchanged:

Report of Observation at the Meteorological Observation Tower, No.2, Meteorological Research Institute, Tsukuba Science City, Japan.

2. Measurements of high winds on 20 to 35m high towers at Kashima coast were completed on March, 1987. A new wind observation project is under preparation by Meteorological Research Institute at another coast near the point stated above.

3. National Science Foundation funded a study to obtain comprehensive measurements of surface pressures and internal pressures acting on a full-scale low-rise building situated in open terrain near Lubbock, Texas.

4. Concerning high wind effects, particular investigations continued in the U.S.A. on various projects, such as wind loading and strength prediction of glass cladding and wind loading and response of transmission towers.

5. Research needs were discussed as follows:

   a. Comparison of design methodology for wind resistance of structures in both countries.
   b. Comparison of wind tunnel test techniques using a common prototype to develop test models and techniques.
   c. Comparison of design philosophies, codes and practice in both countries.
   d. Better definition of the effect of internal pressure in buildings especially with large internal open spaces.
   e. Further development of actively controlled damping systems for full-scale buildings.
   f. Assessment of the influence of material deterioration on wind effects.
   g. Development of fundamental wind data in offshore areas.

II. Future Programs

1. Exchange observation reports of high winds.

2. Encourage interaction between meteorologists and engineers to identify the types of wind data required for future use in establishing extreme wind distributions; in determining wind loading on buildings and structures; in understanding the urban wind climate; and in considering design issues involved with the wind generation of energy.

3. Encourage the establishment of minimum requirements for the simulation of atmospheric boundary layers in wind tunnels and the exchange of boundary layer wind tunnel test results, including comparisons with corresponding full-scale situations.

4. Exchange information on criteria, techniques and instrumentation for structural modeling in boundary layer wind tunnels. Also encourage the exchange of information of measurements made on actual structures and on comparisons with predictions from wind tunnel studies of these structures.

5. Expand the exchange of engineers and meteorologists, and encourage the mutual use of available research facilities in the two countries.

6. Encourage the development of work plans for the pursuit of the research needs listed in I.5.

7. Plan a workshop in the coming year, with details to be worked out between the respective U.S. and Japanese Task Committee chairmen.

Report of Task Committee on

(H) SOIL BEHAVIOR AND STABILITY DURING EARTHQUAKES

Date: May 13, 1987

Place: Public Works Research Institute, Ministry of Construction
Toyosato-machi, Tsukuba-gun, Ibaraki 305, Japan

Attendees:

Japan Side -	Y. Sasaki (Chairman)	(PWRI)
	Y. Koga	(PWRI)
	H. Tsuchida	(PHRI)
	O. Matsuo (Observer)	(PWRI)
	H. Matsumoto (Observer)	(PWRI)
U. S. Side -	A. G. Franklin (Chairman)	(WES)
	R. R. Ledzian	(USBR)

I. Activities and Accomplishments to Date

1. Exchange of relevant documents on soil behavior during earthquakes was made throughout the year. During the Nineteenth Joint Meeting of the Panel, seven papers were submitted from the Japanese side and one paper was submitted from the U.S. side.

2. Under the auspices of the UJNR, the following researchers were exchanged between the U.S. and Japanese sides:

   a. Mr. Jeffrey A. Farrar of the USBR was hosted by the PWRI in October and November 1986.

   b. Mr. Takashi Tsuchida of the PHRI was hosted by WES from November 1985 to November 1986.

   c. Dr. Randall W. Jibson of the USGS was hosted by the PWRI from January 1987 to March 1987.

   d. Mr. Yoshitaka Hachiya of the PHRI is being hosted by the WES for one year beginning in March 1987.

II. Future Programs

1. Proceedings of the 1985 workshop on In-Situ Testing for Evaluation of Soil Liquefaction Susceptibility will be published.

2. The committee recommends that a workshop on remedial measures to mitigate or prevent damage due to liquefaction failures be held in conjunction with the twentieth Joint Meeting, as a first step in a future cooperative research program.

3. An exchange of available documents on current status and recently completed research concerning remedial measures to mitigate or prevent damage due to liquefaction will be made during the summer of 1987, in preparation for the recommended workshop. This exchange will be coordinated by the U.S. and Japanese chairmen.

4. When requested, the Task Committee will assist in arrangements for visits to earth embankments including fill dams and foundations which have been subjected to significant ground motions.

5. The Task Committee encourages the maximum exchange of information on the following areas of earthquake engineering which are currently of intense interest to both U.S. and Japanese engineers.

   a. Liquefaction potential of soils
   b. In-Situ testing methods for evaluation of soil liquefaction potential
   c. Seismic stability of embankment structures and natural slopes.
   d. Remedial treatment of embankments and foundations to improve seismic stability
   e. Seismically induced permanent displacements in earth structures
   f. Seismically induced settlements of soils and foundations
   g. Earthquake effects on semi-buried concrete structures
   h. Earthquake effects on retaining walls
   i. Centrifuge testing facilities and methods
   j. Laboratory testing of models of geotechnical structures
   k. Field performance data showing full-scale seismic response of earth dams

Report of Task Committee on

(I) STORM SURGE AND TSUNAMI

Date: May 13, 1987

Place: Public Works Research Institute, Ministry of Construction
Toyosato-machi, Tsukuba-gun, Ibaraki 305, Japan

Attendees;

Japan Side -	T. Uda (Chairman)	(PWRI)
	K. Tanimoto	(PHRI)
	K. Kurashige	(MRI)
	M. Okada (Observer)	(MRI)
U. S. Side -	H. Meyers (Temporary Chairman)	(NOAA)
	J. Tyrrell.	(NFEC)

I. Activities and Principal Accomplishements to Date

1. The U.S. and Japanese sides have continued to colaborate on tsunami propagation studies. Mr. Okada of MRI/JMA has used the bathymetric data received from NGDC/NOAA to produce preliminary propagation charts. These results were reported as part of the 19th Joint Meeting.

2. Mr. Okada has sent to NGDC/NOAA a copy of this computer model for tsunami propagation.

II. Future Programs

1. The Task Committee supports the continuation of exchange of data and information on Tsunami and Storm Surge. The Committee also supports exchange of researchers whenever possible.

2. The Task Committee recommends a Second Tsunami and Storm Surge Workshop to be held in U.S. in connection with the 20th Panel Meeting. Details of the workshop will be arranged by the Task Committee Chairmen with the approval of the Panel Chairmen. Specifically the workshop will address computational and experimental methods in tsunami and storm surge.

3. Mr. Okada will use his model and data to produce a Pacific-wide tsunami travel chart. This work is very valuable for the U.S. and other pacific countries because it will result in an improvement in tsunami warnings.

4. NEDL will test Mr. Okada's model and compare results with actual observations in the NOAA data base.

5. The U.S. side (NOAA) will give to the Japan side the report and documentation of the Storm Surge Model, SLOSH (Sea, Land, and Overland Surges from Hurricanes).

Report of Task Committee on

(J) WIND AND EARTHQUAKE ENGINEERING FOR TRANSPORTATION SYSTEMS

Date: May 13, 1987

Place: Public Works Research Institute, Ministry of Construction
Toyosato-machi, Tsukuba-gun, Ibaraki-ken 305,Japan

Attendees: Japan Side - H. Shinohara (Chairman) (PWRI)
T. Iwasaki (PWRI)
K. Yokoyama (PWRI)
H. Sato (Observer) (PWRI)

U. S. Side - C.F. Galambos (Chairman) (FHWA)
J. H Gates (State of California)

I. Activities and Principal Accomplishments to Date

The major accomplishments of Task Committee (J) during the past year were as follows:

1. Summaries of wind and earthquake research on bridges conducted by both countries were presented to the 19th Joint Meeting, and exchange of information was made.

2. The coordinated research study on the seismic performance of bridge piers and columns was begun in 1983, and the following experiments were conducted.

   a. Performance of reinforced concrete piers and columns subjected to dynamic cyclic loading
   b. Model tests on the failure of reinforced concrete piers
   c. Testing full-scale concrete columns and associated small-scale model tests
   d. Behavior of concrete filled steel tubes

3. Mr. Koichi Minosaku, researcher of Bridge Division, PWRI, MOC, is a guest researcher at the Center for Building Technology, NBS, U.S.A. for 10 months beginning in September, 1986, to perform cooperative experimental research on the seismic performance of bridge piers and columns. This assignment is a part of the personnel exchange program of the UJNR Panel.

4. The Third U.S.-Japan Bridge Workshop was held in Tsukuba Science City, in May 8-9, 1987 with cooperation from organizations concerned in both countries. Fourteen U.S. and thirty-three Japanese members participated in the workshop. Exchange of technical information was made and comprehensive discussion were held on future cooperative programs. The proceedings will be made and distributed to the participants of the both countries. Some of the subjects were:

a. Dynamic analysis of cable-stayed bridges
b. Reliability in bridge design
c. Earthquake resistant design of highway bridges and earthquake motion
d. Repair and retrofit of existing bridges
e. Wind resistant design of suspension bridges and cable-stayed bridges
f. Mitigation of vibration of highway bridges
g. Seismic behavior of RC bridge piers
h. Diaphram wall foundations

II. Future Programs

As a result of comprehensive discussions, the Task Committee (J) hereby resolves to carry forth with the following programs:

1. Continue with the coordinated experimental research study on the seismic performance of bridge piers and columns, and review the progress of the study at the intermediate stage.

2. Develop a coordinated research study, both theoretical and experimental, on the seismic, aeroelastic, and aerodynamic response of cable-supported bridges. Reciprocal wind tunnel testing for bridges should be made in the institutes concerned to evaluate and compare the wind tunnel testing methods. A specific proposal for the project is to be developed by the co-chairmen.

3. Encourage the continued exchange of information and research personnel through the Panel on Wind and Seismic Effects of UJNR.

4. The Task Committee endorses the initiation of a coordinated and expanded program of research on remedial measures to mitigate or prevent damage to existing bridges by the natural hazards of earthquakes and strong winds.

5. The Task Committee proposes the fourth Bridge Workshop to promote cooperative research on wind and seismic-resistant design of long span bridges, retrofit and strengthening of existing bridges. The Workshop will be held in U.S. in conjunction with the 20th Joint Meeting of the Panel in 1988. Details of the Workshop should be determined based on discussion between the Task Committee Chairmen. Emphasis of the workshop should be on practical applications. The workshop is to be followed by a technical tour.

6. Develop a coordinated research study to evaluate and compare the seismic design criteria for bridges used in Japan and the United States. Several bridges should be identified by each group. Bridges identified by one group should be redesigned for seismic loads only by other group using their particular seismic criteria. The study should identify the differences and similarities between the two seismic criteria and attempt to identify common areas of interest. A specific proposal for the project is to be developed by the co-chairmen.

NBS-114A (REV. 2-8C)

U.S. DEPT. OF COMM. BIBLIOGRAPHIC DATA SHEET (See instructions)	1. PUBLICATION OR REPORT NO. 88-3703	2. Performing Organ. Report No.	3. Publication Date JANUARY 1988

4. TITLE AND SUBTITLE

Wind and Seismic Effects--Proceedings of the 19th Joint Meeting of the U.S. - Japan Cooperative Program in Natural Resources Panel on Wind and Seismic Effects

5. AUTHOR(S)

Noel J. Raufaste, Editor

6. PERFORMING ORGANIZATION (If joint or other than NBS, see instructions)

NATIONAL BUREAU OF STANDARDS
U.S. DEPARTMENT OF COMMERCE
GAITHERSBURG, MD 20899

7. Contract/Grant No.

8. Type of Report & Period Covered

Final

9. SPONSORING ORGANIZATION NAME AND COMPLETE ADDRESS (Street, City, State, ZIP)

10. SUPPLEMENTARY NOTES

☐ Document describes a computer program; SF-185, FIPS Software Summary, is attached.

11. ABSTRACT (A 200-word or less factual summary of most significant information. If document includes a significant bibliography or literature survey, mention it here)

The Nineteenth Joint Meeting of the U.S.-Japan Panel on Wind and Seismic Effects was held at the Public Works Research Institute, Tsukuba, Japan, from May 12-15, 1987. This publication, the proceedings of the Joint Meeting, includes the program, list of members, panel resoulutions, Panel charter, task committee reports, and technical papers.

Subjects covered in the papers presented to the panel include: (1) wind engineering, (2) earthquake engineering, (3) storm surge and tsunami, (4) U.S. - Japan Cooperative Research Program, and (5) results of recent task committee workshops.

12. KEY WORDS (Six to twelve entries; alphabetical order; capitalize only proper names; and separate key words by semicolons)

accelerograph; codes; design criteria; disaster; earthquakes; earthquake hazards; geotechnical engineering; ground failure; liquefaction; pipeline; seismicity; solids; standards; structural engineering; structural response; tsunami; wind loads; winds

13. AVAILABILITY

☒ Unlimited

☐ For Official Distribution. Do Not Release to NTIS

☐ Order From Superintendent of Documents, U.S. Government Printing Office, Washington, D.C. 20402.

☒ Order From National Technical Information Service (NTIS), Springfield, VA. 22161

14. NO. OF PRINTED PAGES

427

15. Price

$36.95